frontiers | Research Topics

Omics-driven crop improvement for stress tolerance

Edited by
Weicong Qi, Jian Chen, Yi Han and Zhen Li

Published in
Frontiers in Plant Science

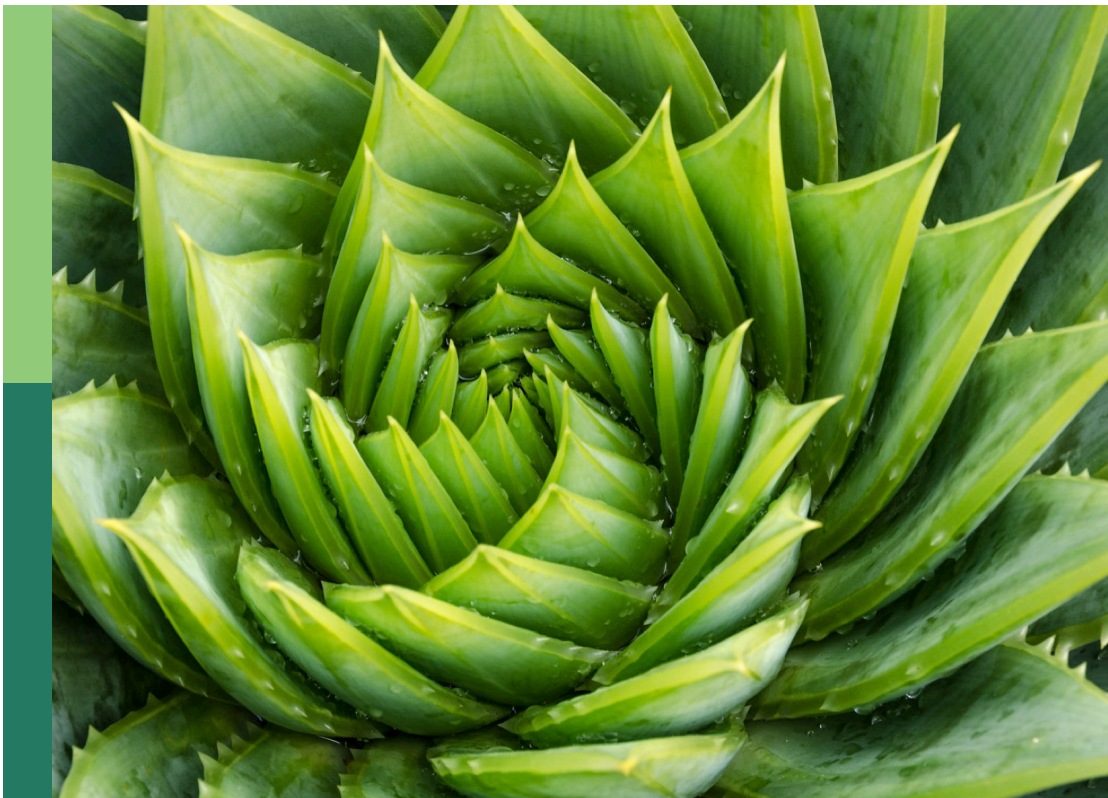

ISSN 1664-8714
ISBN 978-2-8325-2360-5
DOI 10.3389/978-2-8325-2360-5

About Frontiers

Frontiers is more than just an open access publisher of scholarly articles: it is a pioneering approach to the world of academia, radically improving the way scholarly research is managed. The grand vision of Frontiers is a world where all people have an equal opportunity to seek, share and generate knowledge. Frontiers provides immediate and permanent online open access to all its publications, but this alone is not enough to realize our grand goals.

Frontiers journal series

The Frontiers journal series is a multi-tier and interdisciplinary set of open-access, online journals, promising a paradigm shift from the current review, selection and dissemination processes in academic publishing. All Frontiers journals are driven by researchers for researchers; therefore, they constitute a service to the scholarly community. At the same time, the *Frontiers journal series* operates on a revolutionary invention, the tiered publishing system, initially addressing specific communities of scholars, and gradually climbing up to broader public understanding, thus serving the interests of the lay society, too.

Dedication to quality

Each Frontiers article is a landmark of the highest quality, thanks to genuinely collaborative interactions between authors and review editors, who include some of the world's best academicians. Research must be certified by peers before entering a stream of knowledge that may eventually reach the public - and shape society; therefore, Frontiers only applies the most rigorous and unbiased reviews. Frontiers revolutionizes research publishing by freely delivering the most outstanding research, evaluated with no bias from both the academic and social point of view. By applying the most advanced information technologies, Frontiers is catapulting scholarly publishing into a new generation.

What are Frontiers Research Topics?

Frontiers Research Topics are very popular trademarks of the *Frontiers journals series*: they are collections of at least ten articles, all centered on a particular subject. With their unique mix of varied contributions from Original Research to Review Articles, Frontiers Research Topics unify the most influential researchers, the latest key findings and historical advances in a hot research area.

Find out more on how to host your own Frontiers Research Topic or contribute to one as an author by contacting the Frontiers editorial office: frontiersin.org/about/contact

Omics-driven crop improvement for stress tolerance

Topic editors
Weicong Qi — Jiangsu Academy of Agricultural Sciences (JAAS), China
Jian Chen — Jiangsu University, China
Yi Han — Anhui Agricultural University, China
Zhen Li — Ghent University, Belgium

Topic coordinators
Xiaofeng Su — Institute of Biotechnology, Chinese Academy of Agricultural Sciences, China
Freddy, Kuok San Yeo — Universiti Malaysia Sarawak, Malaysia

Citation
Qi, W., Chen, J., Han, Y., Li, Z., eds. (2023). *Omics-driven crop improvement for stress tolerance.* Lausanne: Frontiers Media SA. doi: 10.3389/978-2-8325-2360-5

The authors declare that the research was conducted in the absence of any commercial or financial relationships that could be construed as a potential conflict of interest

Table of contents

frontiers | Frontiers in Plant Science

TYPE Editorial
PUBLISHED 21 April 2023
DOI 10.3389/fpls.2023.1172228

OPEN ACCESS

EDITED AND REVIEWED BY
Nunzio D'Agostino,
University of Naples Federico II, Italy

*CORRESPONDENCE
Weicong Qi
weicong_qi@163.com

SPECIALTY SECTION
This article was submitted to Plant Bioinformatics, a section of the journal Frontiers in Plant Science

RECEIVED 23 February 2023
ACCEPTED 23 March 2023
PUBLISHED 21 April 2023

CITATION
Qi W, Chen J, Han Y, Li Z, Su X and Yeo FKS (2023) Editorial: Omics-driven crop improvement for stress tolerance. *Front. Plant Sci.* 14:1172228. doi: 10.3389/fpls.2023.1172228

Editorial: Omics-driven crop improvement for stress tolerance

Weicong Qi[1,2]*, Jian Chen[3], Yi Han[4], Zhen Li[5], Xiaofeng Su[6] and Freddy Kuok San Yeo[7]

[1]Excellence and Innovation Center, Jiangsu Academy of Agricultural Sciences, Nanjing, China, [2]Key Laboratory of Saline-Alali Soil Improvement and Utilization (Coastal Saline-Alkali Lands), Ministry of Agriculture and Rural Affairs, Nanjing, China, [3]International Genome Center, Jiangsu University, Zhenjiang, China, [4]National Engineering Laboratory of Crop Stress Resistance Breeding, School of Life Sciences, Anhui Agricultural University, Hefei, China, [5]Vlaams Instituut voor Biotechnologie (VIB) Center for Plant Systems Biology, Department of Plant Biotechnology and Bioinformatics, Ghent University, Gent, Belgium, [6]Biotechnology Research Institute, Chinese Academy of Agricultural Sciences, Beijing, China, [7]Faculty of Resource Science and Technology Universiti Malaysia Sarawak (UNIMAS) Kota Samarahan, Sarawak, Malaysia

KEYWORDS

omics, transcriptomics, genomics, metabolomics, plant breeding, abiotic/biotic stress

Editorial on Research Topic
Omics-driven crop improvement for stress tolerance

Crop losses due to biotic and abiotic stresses are significant worldwide issues. According to a report of the Food and Agriculture Organization of the United Nations (FAO), an estimated 20-40% of global crop production is lost every year due to pests and diseases alone, while other environmental factors, like drought, floods, high salinity level in soil, and extreme temperatures contribute to the losses becoming even more severe. Crop yield stability and healthy growth under biotic and abiotic stresses have always been a major challenge for the plant/agricultural researchers. Crop resilience is an important trait, and it involves essential phenotypes that plant breeding researchers are concerned with. For instance, fusarium-head-blight resistance is highly desirable for breeding new wheat varieties nowadays. Therefore, improving stress tolerance becomes a major research direction in modern crop sciences.

Currently, the thriving omics technologies have revolutionized plant sciences because they facilitate researchers to comprehensively analyze biological processes from multiple dimensions and draw an atlas with more detailed overview of genomic and phenotypic profiles in different environmental conditions. These technologies include genomics, transcriptomics, proteomics, metabolomics, and phenomics, among others. Genomics allows researchers to sequence the entire genome of plants, which can reveal important genetic information relevant to stress-tolerance, yield potential, etc. Transcriptomics enables the identification of gene expression variation in specific tissues or their response to environment, stress, and stimulation. While proteomics provides insights into the nucleotide sequences translation and modification in various biological processes. Metabolomics could be engaged to study the complex network of biochemical reactions, chemical signals, specific metabolites accumulation, and so on. Phenomics enable constantly monitoring plant development traits, for instance, plant height, leaf size, as well as physiological characters like photosynthesis efficiency, nutrient absorption, water consumption, etc.

Omics technologies provide new opportunities for plant breeding and food development, which is enormously vital for the modern world facing challenges such as climate change, global warming, and population expansion. This research topic has welcomed research/review articles describing the application of omics technologies in crop sciences, and a total of 20 studies were collected. Most of the contributions employed genomics, transcriptomics, metabolomics, and other omics technologies to study various stress factors like drought, salt stress, fungi infection, nutrient starvation, as well as hormone and nanomaterial treatments, etc. All the investigations were carried out on crops such as quinoa (Luo et al.), rice (Liang et al.), potato (Qin et al.), strawberry (Chen et al.), orange (Duan et al.), tea (Hu et al.; Chen et al.), cotton (Lu et al.), ornamental crop rose (Liu et al.), and so on.

Quinoa (*Chenopodium quinoa* willd.) is a novel crop that gained popularity worldwide in the last decades and has been widely employed in the infant and healthy food market. Luo et al. investigated the long noncoding RNA (LncRNA) in transcriptomic data of quinoa under salt stress.

Chen et al. analyzed LncRNA in ripening strawberry fruit treated with Abscisic acid (ABA). ABA is a well-known hormone associated with plant stress tolerance and seed or fruit maturation. In their study, transposon-derived LncRNAs and ABA-responsive LncRNAs were identified, and critical metabolomic pathways involved in the ripening process of strawberry fruit were predicted.

Liu et al. conducted research on the resistance of rose petal to powdery mildew, which is caused by *Podosphera pannosa*, and could be devastating in postharvest process of the cut flower. Transcriptomic analysis indicated that ethylene is playing an important role in the infection process, and ethylene inhibitor treatment could alleviate the symptom of inoculation.

Yan et al. investigated calcium nutrition nanoagent applying to tomato, of which the result demonstrated the nanomaterial could rescue the plant from mosaic virus disease.

The contribution of Xu et al. indicated a histone deacetylase inhibitor could enhance rice immunity to rice blast. Based on ChIP-seq, ChIP-qPCR and transcriptome data, the mechanism was probed in depth.

Lu et al. examined the hormone and signaling pathways involved in *AmCBF1* transcription factor coding gene overexpression-induced dwarfism in cotton. With RNA sequencing, they identified *PP2C* gene could be relevant with AmCBF1 and mediating plant architecture. Their further yeast one-hybrid and dual-luciferase results validate this hypothesis.

Overall, current Research Topic demonstrates a collection of scientific studies on various crop plants and provides robust examples highlighting the importance of omics technologies in understanding plant stress responses. These results shed new light and greatly advanced our understanding of plant molecular biology. Hopefully, these results and data presented in the topic, will serve as valuable reference and dataset for researchers working on crop breeding purposes, agronomic trait improvement, food quality elevation, and sustainable agriculture development.

Author contributions

All authors listed have made a substantial, direct, and intellectual contribution to the work and approved it for publication.

Conflict of interest

The authors declare that the research was conducted in the absence of any commercial or financial relationships that could be construed as a potential conflict of interest.

Publisher's note

frontiers | Frontiers in Plant Science

ORIGINAL RESEARCH
published: 30 May 2022
doi: 10.3389/fpls.2022.914206

AmCBF1 Transcription Factor Regulates Plant Architecture by Repressing *GhPP2C1* or *GhPP2C2* in *Gossypium hirsutum*

*Junchao Lu[1,2], Lihua Wang[2], Qianqian Zhang[1,2], Caixia Ma[2,3], Xiaofeng Su[2], Hongmei Cheng[2] and Huiming Guo[2]**

[1]Zhengzhou Research Base, State Key Laboratory of Cotton Biology, School of Agricultural Sciences, Zhengzhou University, Zhengzhou, China, [2]Biotechnology Research Institute, Chinese Academy of Agricultural Sciences, Beijing, China, [3]College of Agriculture, Shanxi Agricultural University, Taigu, China

Dwarfism is a beneficial trait in many crops. Dwarf crops hold certain advantages over taller crops in lodging resistance, fertilizer tolerance, and yield. Overexpression of CBF/DREB transcription factors can lead to dwarfing in many plant species, but the molecular mechanism of plant dwarfing caused by overexpression of CBF/DREB in upland cotton (*Gossypium hirsutum*) remains unclear. In this study, we observed that overexpression of the *Ammopiptanthus mongolicus* AmCBF1 transcription factor in upland cotton R15 reduced plant height, whereas virus-induced gene silencing of *AmCBF1* in the derived dwarf lines L28 and L30 partially restored plant height. Five protein phosphatase (PP2C) genes (*GhPP2C1* to *GhPP2C5*) in cotton were identified by RNA-sequencing among genes differentially expressed in L28 or L30 in comparison with R15 and thus may play an important role in AmCBF1-regulated dwarfing in cotton. Gene expression analysis showed that the *GhPP2C* genes were down-regulated significantly in L28 and L30, and silencing of *GhPP2C1* or *GhPP2C2* in R15 inhibited the growth of cotton seedlings. Subcellular localization assays revealed that GhPP2C1 was localized to the cell membrane and nucleus, whereas GhPP2C2 was exclusively localized to the nucleus. Yeast one-hybrid and dual-luciferase assays showed that AmCBF1 was able to bind to the CRT/DRE elements of the upstream promoter of *GhPP2C1* or *GhPP2C2* and repress their expression. These findings provide insight into the mechanism of dwarfing and may contribute to the breeding of dwarf cultivars of upland cotton.

Keywords: cotton, transcription factor, *AmCBF1*, *GhPP2C*, plant architecture and plant height

OPEN ACCESS

Edited by:
Weicong Qi,
Jiangsu Academy of Agricultural Sciences (JAAS), China

Reviewed by:
Xiaoyang Ge,
Cotton Institute of the Chinese Academy of Agricultural Sciences, China
Zhikun Li,
Hebei Agricultural University, China

***Correspondence:**
Huiming Guo
guohuiming@caas.cn

Specialty section:
This article was submitted to Plant Bioinformatics, a section of the journal Frontiers in Plant Science

Received: *06 April 2022*
Accepted: *10 May 2022*
Published: *30 May 2022*

Citation:
Lu J, Wang L, Zhang Q, Ma C, Su X, Cheng H and Guo H (2022) AmCBF1 Transcription Factor Regulates Plant Architecture by Repressing GhPP2C1 or GhPP2C2 in Gossypium hirsutum. Front. Plant Sci. 13:914206. doi: 10.3389/fpls.2022.914206

INTRODUCTION

Dwarfism is a valuable agronomic trait, as it helps to improve the light use efficiency of the population and increases the ability of plants to resist an adverse external environment (Khush, 1999). In agricultural and horticultural crops, breeding for dwarfism is particularly important. Some tall crops have weak stalks and are susceptible to lodging, whereas dwarf crops have strong stalks and are resistant to lodging, highly fertilizer tolerant, and produce significantly

increased yields through reasonably dense planting. Dwarf and compact horticultural plants are increasingly popular with consumers because of their high ornamental value. In recent years, considerable progress has been made in screening and identifying genes associated with plant dwarfing. Phytohormone-related genes play an important role in causing dwarfing in plants (Hu et al., 2017; Li et al., 2018; Graeff et al., 2020). In addition, genes that affect plant cell wall synthesis, such as a mutation of the cellulose biosynthesis gene *CESA*, or regulation by transcription factors such as C-repeat binding factor/dehydration responsive element-binding factor (CBF/DREB) proteins, can cause dwarfing in plants (Xie et al., 2011). In cotton, the dwarf variety AS98 was detected in an introgressed line derived from an interspecific hybrid and exogenous application of gibberellic acid (GA_3) restores the plant height phenotype (Zhang et al., 2011; Jia et al., 2016). In the cotton *pag1* mutant, cell growth is disrupted, resulting in a dwarf phenotype and reduced fiber quality (Yang et al., 2014). The contents of indoleacetic acid and abscisic acid (ABA) are reduced in the Asian cotton dwarf *sd*^{a} mutant, and genetic analysis indicates that the dwarfism trait is controlled by a pair of recessive genes (Wu et al., 2009). The aforementioned studies indicate that utilization of a variety of dwarfing resources provides a means to increase cotton yield by changing the plant architecture.

The CBF proteins comprise a subfamily of the APETALA 2/ETHYLENE-RESPONSIVE FACTOR (AP2/ERF) family of transcription factors, also termed DREBs, which are involved in a range of processes during the plant life cycle (Agarwal et al., 2006). The CBF protein binds to the C-repeat/dehydration-responsive element (CRT/DRE) sequence in the promoter of downstream genes to regulate their expression, and enhances plant resistance to a variety of stresses, such as drought, freezing, and salinity (Baker et al., 1994; Yamaguchi-Shinozaki and Shinozaki, 1994; Dong et al., 2006). Overexpression of CBF transcription factors in diverse plants affects plant growth and leads to dwarfing, while affecting plant stress resistance. For example, overexpression of *AtDREB1A* or *OsDREB1A/2A* in *Arabidopsis* improves cold and drought tolerance, but growth of transgenic *Arabidopsis* is severely inhibited (Liu et al., 1998; Dubouzet et al., 2003). Similarly, overexpression of *OsDREB1A/1B* in rice (*Oryza sativa*) results in dwarfing (Ito et al., 2006). Interestingly, application of exogenous gibberellin (GA) partially restores the height of plants overexpressing *CBF*, suggesting that dwarfing caused by *CBF* overexpression may be due to GA deficiency (Hsieh et al., 2002). Overexpression of *DgDREB1B* in *Arabidopsis* leads to reduction in plant height and significant up-regulation of *GA2ox7* and GA-inactivating enzymes, suggesting that *DgDREB1B* may be involved in GA-mediated development in plants (Tong et al., 2009). Twenty-one *CBF* genes have been identified in the upland cotton (*Gossypium hirsutum*) genome and are categorized into four groups: GhCBF I, GhCBF II, GhCBF III, and GhCBF IV (Ma et al., 2014). Overexpression of *GhDREB1* in tobacco (*Nicotiana tabacum*) causes retarded growth and delays flowering (Shan et al., 2007). Recently, it was shown that overexpression of *GhDREB1B* in upland cotton results in significant reduction in plant height, shorter branch lengths, and reduced branch angles (Ji et al., 2021). These results confirm that overexpression of CBF/DREB transcription factors can lead to plant dwarfing, but the specific mechanism of dwarfing remains to be studied.

Post-translational modification of proteins plays an important role in plant developmental processes. Among these modifications, protein phosphorylation/dephosphorylation plays a role at various stages of plant growth and development by regulating protein activity and participating in the transmission of a number of signals in plants (Schweighofer et al., 2007; Fuchs et al., 2013; Singh et al., 2016). This reversible protein phosphorylation is achieved through the activities of the enzyme pair protein kinase and protein phosphatase. Depending on the catalytic substrate, protein phosphatases are mainly divided into protein tyrosine phosphatases and protein serine/threonine phosphatases (Xin et al., 2021). Protein phosphatase 2C (PP2C) comprises a class of protein serine/threonine phosphatases and is a monomeric enzyme (Zhang et al., 2022). In plants, PP2C is less conserved at the N terminus and more conserved at the C terminus, which confers PP2C with functional diversity (Ingebritsen and Cohen, 1983; Hubbard and Cohen, 1993; Bork et al., 1996). A recognized mechanism of action is that PP2C participates in the ABA signaling pathway. In this signaling mechanism, PP2Cs bind to SnRK2, resulting in the loss of SnRK2 phosphokinase activity and the inability of downstream substrates to be phosphorylated (Soon et al., 2012). In the presence of ABA, the ABA receptor PYR/PYL/RCAR binds to PP2C and SnRK2 is released, phosphorylating downstream transcription factors, such as ABA-responsive element-binding factors, and further activating the expression of certain downstream genes (Miyazono et al., 2009; Cutler et al., 2010; Hubbard et al., 2010; Rodrigues et al., 2013; Zhu, 2016).

The function of *PP2C* genes is closely associated with processes such as signal transduction, growth and development, hormone regulation, and oxidative stress (Gaits et al., 1997; Rodriguez, 1998; Kerk et al., 2002; Schweighofer et al., 2004). Nine and 10 subgroup A PP2C members have been identified in *Arabidopsis* and rice, respectively, of which most play a negative regulatory role in ABA signaling (Saez et al., 2004; Kuhn et al., 2006; Nishimura et al., 2007; Bhaskara et al., 2012; He et al., 2014; Née et al., 2017; Miao et al., 2018). Overexpression of *OsPP108* in *Arabidopsis* enhances plant tolerance to salt and drought stress, and reduces ABA sensitivity (Singh et al., 2015). Overexpression of *OsPP2C09* in rice results in rapid growth and increases individual plant yield, whereas its mutant reduces plant height and yield (Miao et al., 2020). A lack of *SlPP2C3* expression in tomato (*Solanum lycopersicum*) not only affects plant growth, but also accelerates the onset of fruit ripening and affects fruit gloss by altering the outer epidermal structure (Liang et al., 2021). Genome-wide identification of PP2C family members detected 87, 99, 147, and 181 *PP2C* genes in *Gossypium arboreum*, *Gossypium raimondii*, *Gossypium barbadense*, and *G. hirsutum*, respectively. Among these genes, the 181 PP2Cs in *G. hirsutum* were roughly divided into 12 subgroups; the transcription of some of these *PP2C* genes was induced by high temperature, low temperature, drought, or high salt stress separately, suggesting that *PP2C*

genes play a crucial role in abiotic stress response in cotton (Shazadee et al., 2019). However, the relationship between *PP2C* genes and a dwarf phenotype in upland cotton has not been examined.

Cotton, which is among the world's most important oilseed and textile crops, plays an important role in global agricultural and industrial production. With technological developments, mechanized harvesting of cotton is increasingly important and dwarf cotton is a major breeding target on account of the compact plant height and suitability for machine harvesting. Although dwarf cotton varieties have various advantages, there are still relatively few dwarf cotton varieties on the market today. Therefore, development of new cotton varieties showing stable inheritance of dwarfism is a matter of urgency. Although a number of dwarfing-related genes have been identified, little information is available on their biological functions, especially the molecular mechanisms that regulate cotton growth and development.

In our previous work, *Ammopiptanthus mongolicus AmCBF1* was overexpressed in the upland cotton line R15 to evaluate its function in abiotic stress response. We observed that overexpression of *AmCBF1* increased the resistance of cotton to low temperature and drought stress, and decreased the plant height. In the present study, we further confirmed the relationship between *AmCBF1* and the dwarf phenotype in cotton. Five down-regulated *GhPP2C* (*GhPP2C1-GhPP2C5*) genes were identified among differentially expressed genes by RNA-Seq and AmCBF1 transcription factors could negatively regulate the expression of *GhPP2C1* or *GhPP2C2*. These results will help to understand the molecular mechanism of cotton dwarf and provide theoretical basis for cotton dwarf breeding.

MATERIALS AND METHODS

Plant Materials and Growing Conditions

Transgenic dwarf cotton lines (L28 and L30), transgene recipient (R15), and tobacco (*Nicotiana benthamiana*) plants were grown in pots containing nutrient soil in a greenhouse (25 ± 3°C, 50% relative humidity, and 16 h light/8 h dark cycle). In addition, R15, L28, and L30 were grown in the field (39°36′10.3"N, 116°36′07.3″E). Cotton and tobacco plants at different growth stages were selected for subsequent experiments.

Quantitative Real-Time PCR

Total RNA was extracted from cotton leaves using an RNA extraction kit (Tiangen Biotech, Beijing, China). The RNA concentration was measured using a NanoDrop 2000 spectrophotometer (Thermo Fisher Scientific, Waltham, MA, United States). Purified RNA (>1 μg) treated with gDNase was reverse transcribed with HiScript III RT SuperMix for qPCR (+gDNA wiper; Vazyme Biotech, Nanjing, China) to generate the first-strand cDNA. Gene expression levels were analyzed with an ABI ViiA™ 7 Real-Time PCR System (Applied Biosystems, Waltham, MA, United States) and ChamQ Universal SYBR qPCR Master Mix (Vazyme Biotech). The quantitative real-time PCR (qRT-PCR) protocol was as follows: 40 cycles at 95°C for 30 s, 95°C for 10 s, 60°C for 30 s, and 72°C for 15 s. Relative expression levels were calculated using the $2^{-\Delta\Delta Ct}$ method. Primers were designed using PRIMER PREMIER 5 (Premier Biosoft, Palo Alto, CA, United States). The cotton *ubq* gene (Gh_D13G1489) was used as an internal control.

Virus-Induced Gene Silencing

Virus-induced gene silencing (VIGS) is an approach widely used to study gene function and functional genomics in a variety of plants (Becker and Lange, 2010). We performed a VIGS experiment to test if plant height was partly restored after silencing *AmCBF1* in L28 or L30. The *AmCBF1* fragment was amplified and inserted into the pTRV2 vector digested with the *Xba*I and *Kpn*I restriction enzymes. The plasmids pTRV1, pTRV2, pTRV2-*AmCBF1*, and pTRV2-*CLA1* were transferred to *Agrobacterium tumefaciens* strain GV3101 receptor cells by electroshock and incubated overnight in LB liquid medium supplemented with 50 mg L^{-1} kanamycin, 50 mg L^{-1} rifampicin, 10 mM MES, and 20 mM acetosyringone at 28°C on a shaker at 200 rpm. The *Agrobacterium* cells were collected by centrifugation and suspended in permeate [containing 10 mM $MgCl_2$, 10 mM MES (pH 5.6), and 20 μM acetyleugenone] to optical density (OD_{600}) = 1.2. After incubation at room temperature for 3 h in the dark, the suspensions containing the pTRV2, pTRV2-*AmCBF1*, or pTRV2-*CLA1* plasmids were mixed with pTRV1 suspension (1:1, *v*/*v*) respectively. Cotton seedlings with well-grown, fully expanded cotyledons were selected and a small wound was made on the lower surface of the cotyledons with a syringe needle. Silencing of the *CLA1* gene in R15 was used as a positive control to produce an albino phenotype in cotton. The injected cotton plants were cultured in the dark for 24 h, then for 4 weeks under a 16 h light/8 h dark cycle at 23°C and 50% relative humidity. Total RNA was extracted from young cotton leaves and qRT-PCR was performed to detect the relative expression level of *AmCBF1*. In addition, based on sequence alignment of *GhPP2C1*, *GhPP2C2*, and *GhPP2C3*, we designed specific VIGS fragments and qRT-PCR detection fragments (**Supplementary Figure 3**). The *GhPP2C1*, *GhPP2C2*, or *GhPP2C3* genes were silenced in R15 by VIGS to investigate whether the genes affect the height of cotton plants. Fragments for silencing *GhPP2C1*, *GhPP2C2*, and *GhPP2C3* were amplified from R15 cotton cDNA using specific primers and inserted into the *Xba*I and *Kpn*I double-cleaved pTRV2 vector using seamless cloning. The specific experimental method was based on the gene silencing analysis of *AmCBF1*. The primers used for VIGS vector construction and qRT-PCR detection are listed in **Supplementary Table 1**.

Scanning Electron Microscopy

To investigate whether overexpression of *AmCBF1* affects the morphology and size of cotton leaf cells, the upper epidermis of cotton seedling leaves was observed by scanning electron microscopy. The fourth true leaf of cotton seedlings was washed three times with deionized water and fixed with 2.5% glutaraldehyde at 4°C for more than 8 h. After dehydration, the fixed samples were dried in a CO_2 critical-point desiccator

for approximately 2 h. The samples were observed under a scanning electron microscope (Hitachi SU-8010, Tokyo, Japan) and photographed.

RNA-Sequencing Analysis

Total RNA extracted from fresh seedlings of R15, L28, and L30 was subjected to transcriptome sequencing by Libaijia Biologicals (Beijing, China). Two biological replicates of each material were designated R15R1, R15R2, L28R1, L28R2, L30R1, and L30R2. Quantification of gene expression levels was expressed as fragments per kilobase of transcript per million fragments mapped (FPKM). The fold change is the ratio of expression between the two samples, and the false discovery rate (FDR) is a value obtained by correcting for the difference in significance *p*-value (*p*-value). Fold change ≥ 2 and FDR < 0.01 were used as the screening criteria. The Benjamini–Hochberg correction method was used to correct the *p*-value obtained from the original hypothesis test to avoid the problem of false positives. Finally, the FDR was adopted as the crucial index for screening differentially expressed genes (DEGs). Twelve DEGs involved in different metabolic pathways were randomly selected to verify the transcriptome data. The selected genes, designated Q1–Q12, are listed in **Supplementary Table 2**.

Phylogenetic Analysis

The amino acid sequence of all PP2C proteins of upland cotton were downloaded from the Cotton Functional Genomics Database (cottonFGD).[1] Sequences of the PP2C proteins of *Arabidopsis* were downloaded from The Arabidopsis Information Resource database (TAIR).[2] Phylogenetic analyses were conducted using the neighbor-joining method implemented in the MEGA 7.0 software.

Subcellular Localization

The full-length coding regions (without the termination codon) of *GhPP2C1*, *GhPP2C2*, and *GhPP2C3* were inserted into the pCambia1302 vector carrying the green fluorescent protein (GFP) gene. The plasmids 1302, 1302-GhPP2C1, 1302-GhPP2C2, and 1302-GhPP2C3 were transferred into *A. tumefaciens* strain EHA105 using the freeze–thaw method, and incubated in LB liquid medium supplemented with 50 mg L^{-1} kanamycin and 50 mg L^{-1} rifampicin for 16 h at 28°C on a shaker at 200 rpm. The *Agrobacterium* cells were centrifuged at 3,000 × *g* using a High-speed Micro Centrifuge and the supernatant was discarded. The sediment was resuspended in MMA solution [containing 10 mM $MgCl_2$, 10 mM MES (pH 5.6), and 150 μM acetyleugenone] to $OD_{600} = 1.2$ and incubated at room temperature for 3 h in the dark. Healthy tobacco leaves were selected and the suspension was gently injected into the lower surface of the leaves with a syringe. Injection of GFP alone was used as a control, and H2B-mCherry was used as a nucleolus marker. After incubation for 16 h in the dark at 21°C, the leaves were incubated in the light for 8 h. Two days after injection, the fluorescence signal was observed using a LSM 700 confocal microscope (Zeiss, Oberkochen, Germany). The primers used for construction of the transient expression vectors are listed in **Supplementary Table 1**.

Yeast One-Hybrid assay

Three or two predicted CRT/DRE (A/GCCC/GAC) elements were identified in the 3 kb promoter regions upstream of the *GhPP2C1* or *GhPP2C2* genes, and designated P1, P2, P3, P4, and P5, respectively. A Y1H analysis was conducted to verify whether AmCBF1 is capable of interacting with the corresponding *cis*-elements in the upstream promoters of *GhPP2C1* and *GhPP2C2*. The full-length coding sequence of *AmCBF1* was amplified using specific primers and inserted into the pGADT7 vector digested with *Eco*RI and *Bam*HI to generate the prey plasmid. The 2,049 bp or 882 bp promoter region containing all CRT/DRE elements of *GhPP2C1* or *GhPP2C2* was separately cloned and inserted into the pAbAi vector digested with *Kpn*I and *Sal*I to generate the bait plasmid. In addition, separate forward and reverse complementary oligonucleotide strands were synthesized for P1, P2, P3, P4, and P5, annealed to generate promoter DNA fragments containing the CRT/DRE elements, and inserted into the pAbAi bait vector. The bait plasmid was transformed into the yeast strain Y1H Gold by *Bstb*I digestion using the EX-Yeast Transformation Kit (Zhuangmeng Bio, Beijing, China). The linearized bait plasmid was homologously integrated with the yeast Y1H Gold genome to generate a decoy reporter yeast strain, which was tested using an aureobasidin A (AbA) inhibition assay and Matchmaker Insert Check PCR Mix 1 (Clontech Laboratories, Inc., Palo Alto, CA, United States) to identify positive strains. The prey plasmids were then transformed into the bait reporter strains to verify DNA–protein interactions. The transformed cells were cultured on SD/−Leu/−Ura medium incubated for 3 days at 30°C. Positive strains were identified using the pGADT7 universal primer. Subsequently, yeast cells at different dilutions (1:10, 1:100, and 1:1,000) were cultured on SD/−Leu/−Ura medium supplemented with different concentration of AbA (0, 200, or 400 ng ml^{-1}). The pGADT7 vector was used as a negative control. The primers used in this experiment are listed in **Supplementary Table 1**.

Dual-Luciferase Analysis

The full-length coding sequence of *AmCBF1* was inserted by seamless cloning into the *Nco*I monozyme-cleaved pCambia1302 vector to generate the effector plasmids. A short truncated fragment of the promoter containing different numbers of CRT/DRE elements upstream of the ATG start codon for *GhPP2C1* or *GhPP2C2* was inserted by seamless cloning into the pGreenII 0800-LUC vector to generate GhPP2C1 Pro:LUC, C1:LUC, C2:LUC, GhPP2C2 Pro:LUC, and C3:LUC reporter plasmids. The recombinant plasmid and the negative control plasmid were introduced into *Agrobacterium* EHA105 (pSoup-p19) competent cells using the freeze–thaw method, inoculated in LB liquid medium supplemented with 50 mg L^{-1} kanamycin and 50 mg L^{-1} rifampicin, and incubated at 28°C on a shaker at 200 rpm to $OD_{600} = 1.0$. The *Agrobacterium* cells were

[1]https://cottonfgd.org/
[2]https://www.arabidopsis.org/

centrifuged at 3,000 × *g* for 10 min. The supernatant was discarded and the *Agrobacterium* cells were suspended in permeate [containing 10 mM $MgCl_2$, 10 mM MES (pH 5.6), and 150 μM acetosyringone] to $OD_{600} = 1.2$ and incubated for 3 h at room temperature in the dark. The suspensions were mixed (1:1, *v*/*v*) and injected into the lower surface of the tobacco leaves using a needleless syringe and incubated for 48–60 h under a 16 h light/8 h dark cycle at 23°C and 50% relative humidity. D-Luciferin potassium salt (10 μM) was sprayed onto the tobacco leaves and then imaged using the LB985 Night SHADE fluorescence imaging system (Berthold Technologies, Bad Wildbad, Germany). The dual LUC activity of the different samples was determined using a GloMax 20/20 luminometer (Promega, Madison, WI, United States) and the Dual-Luciferase Reporter Assay System (Promega) in accordance with the manufacturer's instructions. The primers used in this experiment are listed in **Supplementary Table 1**.

Statistical Analysis

Statistical analyses were performed with the SPSS 22.0 software (IBM, Armonk, NY, United States). Values were the means ± SE deviations. Comparisons between groups were performed using one-way ANOVA followed by Duncan's multiple comparisons. For all comparisons, significant at $p < 0.05$ and highly significant at $p < 0.01$ were considered statistically significant.

RESULTS

AmCBF1 Is Closely Associated With Plant Height

The plant height of upland cotton overexpressing *AmCBF1* was significantly reduced in both the greenhouse and the field. During the growth period, the plant height of L28 and L30 decreased by approximately 33 and 35% compared with that of R15 (**Supplementary Figure 2**). In the VIGS experiment, silencing of the cotton *CLA1* gene in R15 was used as a positive control (**Figure 1A**). Silencing of *AmCBF1* in L28 or L30 reduced the expression of *AmCBF1* by approximately 75 and 85%, and the plant height was partly restored to 70.5 and 81.3% of that of R15, respectively (**Figures 1A–C**). The plant height of VIGS lines may be depending on the silencing efficiency of *AmCBF1*. These results indicated that overexpression of *AmCBF1* was crucial for dwarfing in the cotton lines.

AmCBF1 Negatively Regulates the Size of Cotton Leaf Epidermal Cells

The epidermal cells were observed with a scanning electron microscope. The epidermal cells of true leaves of L28 and L30 were smaller than those of R15, and the cells were more tightly packed. After silencing of *AmCBF1* in L28 and L30, the epidermal cells of true leaves tended to enlarge, and partially recovered the size and morphology of the epidermal cells of R15 (**Figure 1D**). Statistical analysis indicated that the size of epidermal cells in L28 and L30 decreased by approximately 40 and 45% compared with that of R15, and the size of epidermal cells was recovered by approximately 25 and 35%, respectively, after silencing of *AmCBF1* (**Figure 1E**). Overexpression of *AmCBF1* led to reduction in the size of leaf epidermal cells, which suggested that the dwarfing mechanism in cotton may be regulated by AmCBF1.

RNA-Seq Analysis

To identify the regulatory pathway for AmCBF1-regulated plant dwarfing, we investigated the DEGs in R15, L28, and L30 in response to *AmCBF1* overexpression by RNA-seq. Cluster analysis of the DEGs demonstrated that the number of down-regulated genes affected by overexpression of *AmCBF1* was generally higher in L28 and L30 than in R15 (**Figure 2A**). A Venn diagram indicated that 780 DEGs were shared between R15 and L28, of which 309 were up-regulated and 471 were down-regulated in L28. There were 3,899 DEGs in common between R15 and L30, of which 1,424 were up-regulated and 2,475 were down-regulated in L30. Among these DEGs, 384 DEGs were common to L28 and L30 compared with R15 (**Figure 2B**). Analysis of Kyoto Encyclopedia of Genes and Genomes (KEGG) pathway enrichment revealed that the DEGs were mainly enriched in phytohormone signaling, DNA replication, starch and sucrose metabolism, carbon metabolism, and amino acid biosynthesis (**Figure 2C**). Subsequently, 12 DEGs from different metabolic pathways were randomly selected to verify the results of transcriptome sequencing, which suggested the RNA-seq results were reliable (**Figure 2D**). Notably, five *GhPP2C* genes were down-regulated in the transcriptome data (**Supplementary Figure 1**). These genes are important intermediate receptors in ABA signal transduction.

Phylogenetic Analyses of Upland Cotton PP2C Family Members

Eighty PP2C family members have been identified in *Arabidopsis*, which are classified into 12 subgroups (Fuchs et al., 2013). To clarify the phylogenetic relationships of PP2C family members in upland cotton, the keyword "protein phosphatase 2C" was used as the query term in a search of the cottonFGD database. A total of 265 PP2C family members from the upland cotton genome were retrieved. Phylogenetic analysis showed that the upland cotton PP2Cs could be divided into 12 subgroups (A–L; **Figure 3A**). Among these subgroups, 39 PP2C family members were present in subgroup A and may be involved in ABA signaling. Interestingly, four GhPP2C proteins (GhPP2C1–GhPP2C4) belonged to subgroup A of the PP2C family. Among these proteins, GhPP2C1, GhPP2C2, and GhPP2C3 were most closely related to AtHAI1/2/3 and AtAHG3 in *Arabidopsis* (**Figure 3B**).

Expression Analyses and Subcellular Localization of GhPP2Cs

The expression levels of *GhPP2C1–GhPP2C4* were analyzed by qRT-PCR in three cotton materials (R15, L28, and L30). The expression levels were significantly lower in L28 compared with those in R15, and were extremely significantly decreased in L30. Compared with R15, the expression of these genes

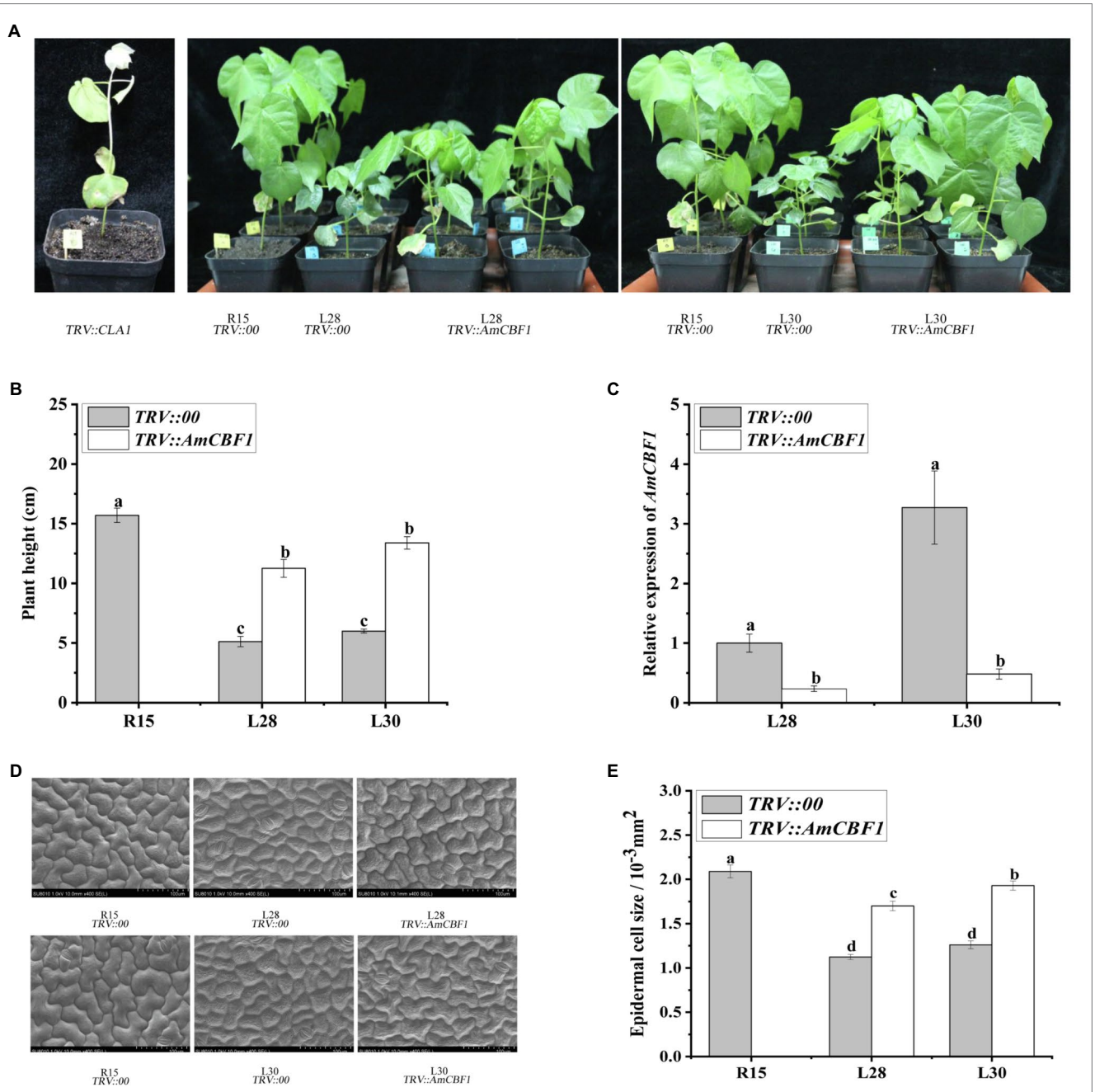

FIGURE 1 | Cotton phenotypes and leaf epithelial cells observed before and after silencing of *AmCBF1* by VIGS. **(A)** Phenotype of cotton after *AmCBF1* silencing. TRV::*CLA1*, albino phenotype, positive control; TRV::*AmCBF1*, *AmCBF1* silencing in L28 and L30. **(B)** Cotton plant height after *AmCBF1* silencing. **(C)** Relative expression of *AmCBF1* in cotton leaves after *AmCBF1* silencing. **(D,E)** Scanning electron micrographs and size of the upper epidermal cells of true leaves. Error bars indicate the standard error ($n = 3$ biological replicates). Different lower-case letters above bars indicate a significant difference at $p < 0.05$ as determined using Duncan's multiple range test.

decreased by approximately 40–80% in L28 and 60–90% in L30 (**Figure 4A**). These results implied that the expression of these *GhPP2C* genes was negatively correlated with expression of AmCBF1.

To investigate the subcellular localization of the GhPP2C proteins, we first predicted the subcellular localization using the CELLO 2.5 online tool.[3] The results predicted that GhPP2C1–GhPP2C3 were localized in the nucleus, whereas GhPP2C4 was localized in the chloroplast. Combined with the phylogenetic analysis, the subcellular localization of GhPP2C1–GhPP2C3

[3]http://cello.life.nctu.edu.tw/

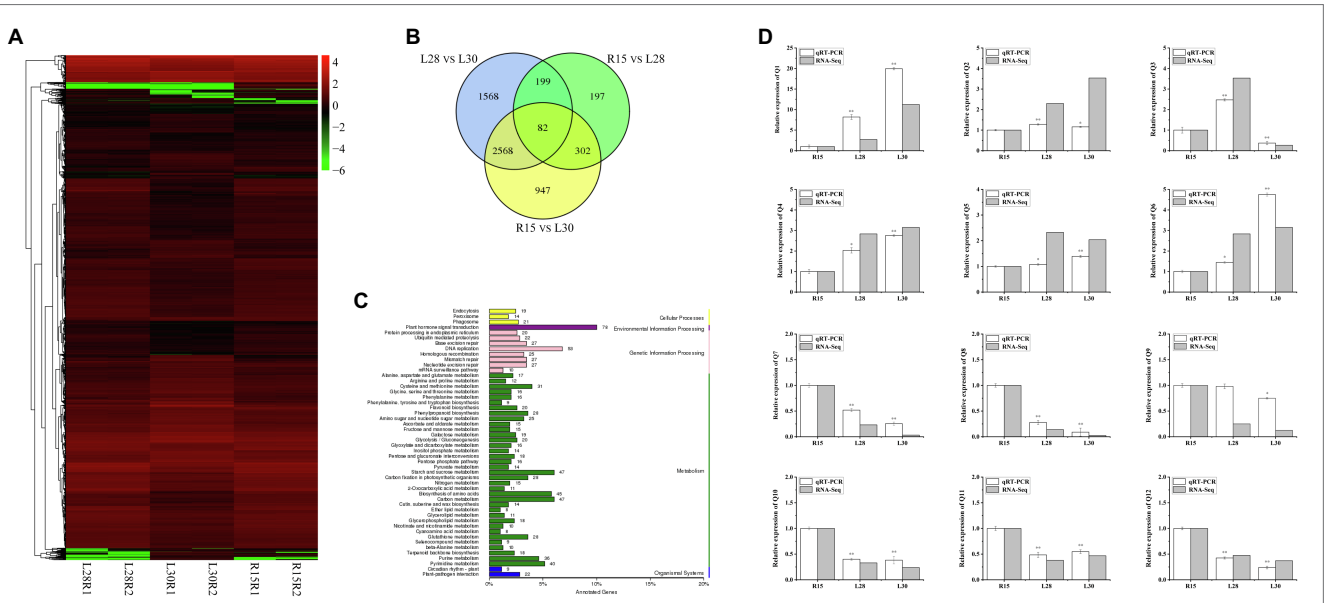

FIGURE 2 | RNA-seq analysis of cotton R15, L28, and L30 seedlings. **(A)** Cluster diagram of expression patterns of all differentially expressed genes (DEGs). The horizontal axis represents the clustering results for the R15, L28, and L30 materials, and the vertical axis represents the clustering of the DEGs. Each column represents one sample of the plant materials and each row represents a different gene. The color indicates the log (FPKM +1) expression level of the gene in the sample. **(B)** Venn diagram of DEGs. Each circle in the plot represents a differential grouping, and the intersection of the circles represents the common DEGs, with the corresponding number of genes identified in the set. **(C)** KEGG classification plot of DEGs. The vertical axis is the name of the KEGG metabolic pathway, and the horizontal axis is the number of genes annotated to the pathway as a proportion of the total number of genes annotated. The value beside each bar is the number of genes annotated for each pathway. **(D)** Expression patterns of 12 genes in R15, L28, and L30 determined by RNA-seq and qRT-PCR analyses. Error bars indicate the standard error ($n = 3$ biological replicates). $^*p < 0.05$, $^{**}p < 0.01$ (Student's t-test).

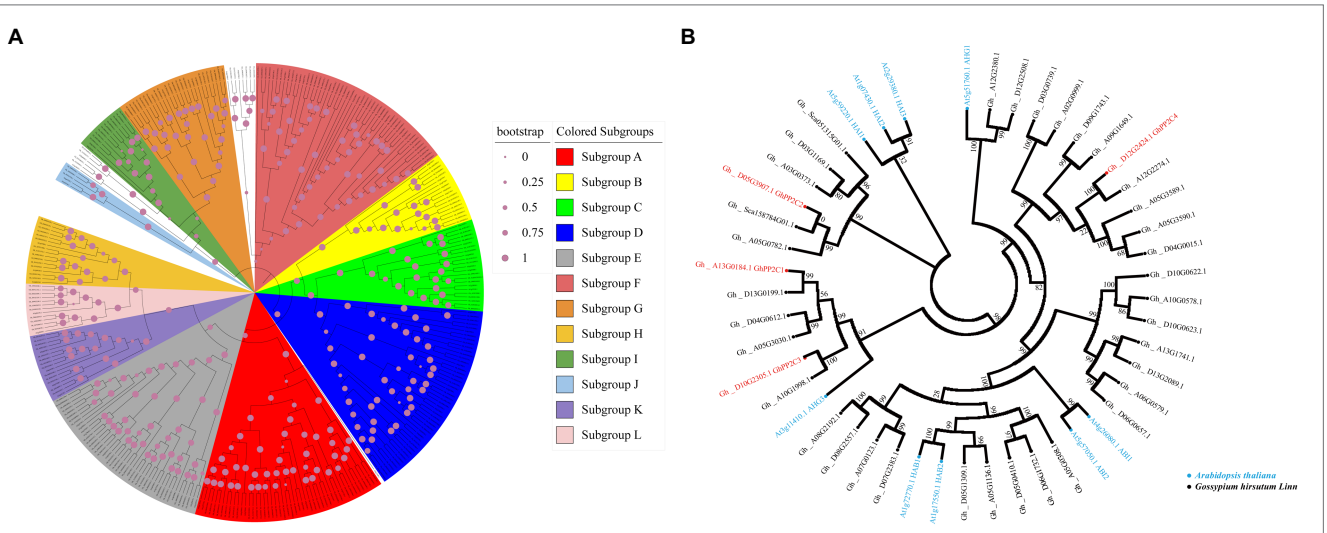

FIGURE 3 | Phylogenetic relationships among PP2C family members. **(A)** Phylogenetic tree for PP2C family members of upland cotton and *Arabidopsis*. Sequences for PP2C family members of *Arabidopsis* were obtained from TAIR (http://www.arabidopsis.org). Subgroups A–L are as delimited in a previous study (Fuchs et al., 2013). Different subgroups are indicated by different colors. **(B)** Phylogenetic tree for subgroup A PP2C family members of upland cotton and *Arabidopsis*. Blue and black indicate *Arabidopsis* and upland cotton, respectively; red indicates the four *GhPP2C* genes detected in the transcriptome data. The evolutionary tree was constructed using the neighbor-joining method with MEGA7. The values at the nodes are bootstrap support percentages ($n = 1{,}000$ replicates).

was further verified by fusion expression with GFP. The fluorescence signal of the GhPP2C1-GFP fusion protein was localized to the cell membrane and nucleus, whereas the GFP signal of the GhPP2C2-GFP and GhPP2C3-GFP fusion proteins was localized to the nucleus (**Figure 4B**). The 1302-GFP protein was used as a control.

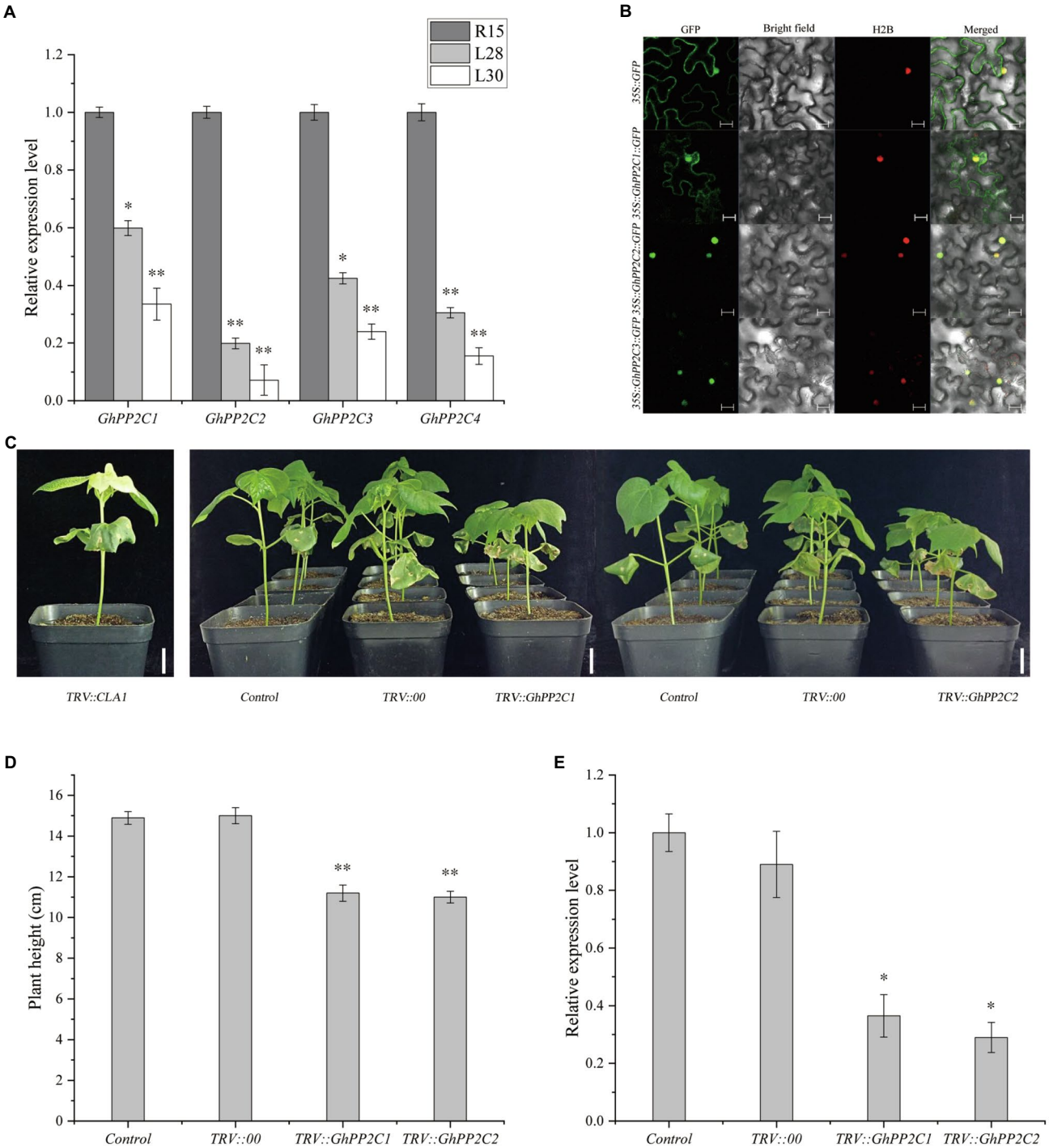

FIGURE 4 | Preliminary analysis of *GhPP2C* gene functions. **(A)** Expression of four *GhPP2C* genes in cotton R15, L28, and L30 seedlings. **(B)** Subcellular localization of GhPP2C proteins. Fluorescence of GhPP2C1-GFP, GhPP2C2-GFP, and GhPP2C3-GFP fusion proteins and GFP (negative control) was detected at 488 nm by confocal microscopy with H2B-mCherry as the nucleolus marker; images were merged (Merged). Scale bar = 20 μm. **(C)** Plant phenotype after VIGS silencing of *GhPP2C1* or *GhPP2C2* in R15. TRV::*CLA1*, albino phenotype, positive control; Control, not treated; TRV::00, empty vector control. Scale bar = 2 cm. **(D)** Plant height after silencing of *GhPP2C1* and *GhPP2C2*. **(E)** Gene expression assay after silencing of G*hPP2C1* or *GhPP2C2*. Error bars indicate the standard error ($n = 3$ biological replicates). $^{*}p < 0.05$, $^{**}p < 0.01$ (Student's *t*-test).

Silencing of *GhPP2C* Genes Reduces Plant Height

To further explore the function of *GhPP2C1–GhPP2C3* in regulating plant height, we separately silenced these genes in R15 using VIGS and observed whether the plant phenotype was altered. Silencing of *GhPP2C1* or *GhPP2C2* resulted in a significant decrease in growth rate, and the plant height was reduced by approximately 25% compared with that of the control (**Figures 4C,D**). The qRT-PCR analysis indicated that the relative expression level of these two genes was significantly decreased (by approximately 65 and 70%) in gene-silenced plants than in the control (**Figure 4E**). These results suggested that *GhPP2C* played a vital role in regulating cotton plant height. Silencing of *GhPP2C3* did not cause a significant change in phenotype, so no further studies were conducted on this gene (data not shown). TRV2::*CLA1* was used as a positive control (**Figure 4C**).

AmCBF1 Binds Directly to the CRT/DRE Elements in the *GhPP2C* Promoter

Overexpression of *AmCBF1* led to down-regulation in the expression level of *GhPP2C* genes, whereas silencing of the *GhPP2C* genes resulted in decreased plant height. These results suggested that there may be a regulatory relationship between AmCBF1 and GhPP2C proteins. The 3 kb promoter sequence upstream of *GhPP2C1* or *GhPP2C2* was further analyzed. Three or two CRT/DRE (A/GCCC/GAC) elements were identified and designated P1, P2, and P3 (upstream elements of *GhPP2C1*), and P4 and P5 (upstream elements of *GhPP2C2*; **Figure 5A**). A Y1H assay was conducted to verify whether AmCBF1 could bind to the promoter DNA fragments containing CRT/DRE elements. The yeast strains containing pGADT7 were unable to grow on SD/−Leu/−Ura medium supplemented with 400 ng ml^{-1} AbA, whereas the yeast strains harboring pGADT7-AmCBF1 were able to grow on this medium. Thus, AmCBF1 could directly bind to the CRT/DRE element in the promoter of *GhPP2C1* (containing P1, P2, and P3) or *GhPP2C2* (containing P4 and P5; **Figure 5B**). The binding properties between P1–P5 and AmCBF1 were also verified separately by means of a Y1H assay (**Supplementary Figure 4A**).

AmCBF1 Represses Transcription of *GhPP2C1* or *GhPP2C2*

To verify how AmCBF1 regulates the transcription of *GhPP2C1* or *GhPP2C2*, a dual-luciferase assay was performed in tobacco. The relevant vectors were constructed (**Figure 5C**; **Supplementary Figure 4B**). When the suspension containing the

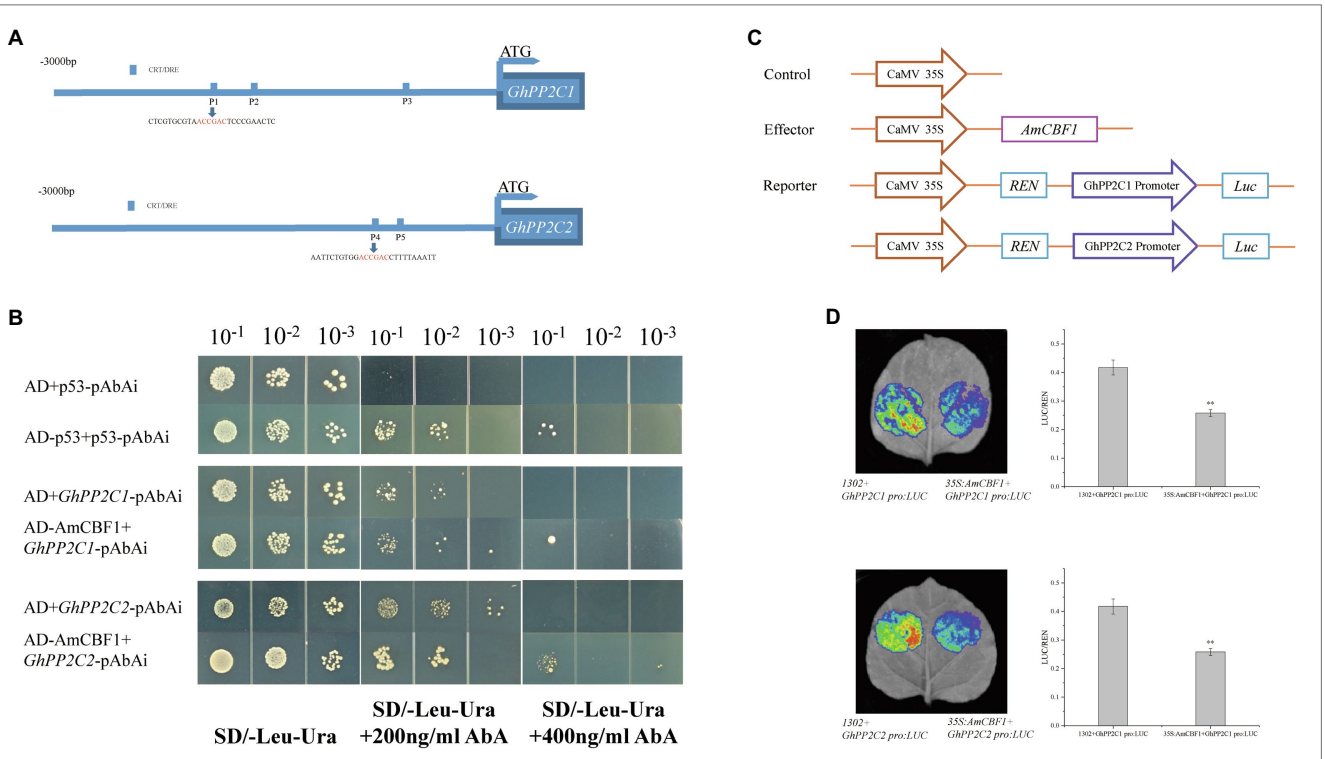

FIGURE 5 | AmCBF1 transcription factor inhibition of the expression of *GhPP2C1* and *GhPP2C2*. **(A)** Schematic diagram of the CRT/DRE binding element in the 3,000 bp promoter upstream of the ATG start codon of *GhPP2C1* and *GhPP2C2*. **(B)** Yeast one-hybrid analysis showing binding of AmCBF1 to the promoter sequence of *GhPP2C1* or *GhPP2C2*. Yeast cells were cultured at serial dilutions of 1:10, 1:100, and 1:1,000 on SD/−Leu/−Ura medium supplemented with or lacking 400 ng ml^{-1} aureobasidin A. The pGADT7 vector was used as a negative control. **(C)** Schematic diagram of vector construction of the reporter and effector plasmids for transient transcriptional activity assays in tobacco. REN, *Renilla* luciferase; LUC, firefly luciferase. **(D)** Tobacco leaf live-imaging observations. Red indicates the strongest fluorescence signal intensity. Luciferase activity was normalized to the respective REN activity and expressed as relative expression. Error bars indicate the standard error ($n = 3$ biological replicates). $^{**}p < 0.01$ (Student's *t*-test).

reporter plasmid GhPP2C1 Pro:LUC, C1:LUC, C2:LUC, GhPP2C2 Pro:LUC or C3:LUC were, respectively, mixed with the suspension containing the effector plasmid 35S:AmCBF1 to inject tobacco, the LUC luminescence intensity was significantly reduced and the relative LUC/*Renilla* luciferase (REN) activity was significantly lower than that of the control (decreased by approximately 30–45%; **Figure 5D**; **Supplementary Figure 4C**). These results further suggested that AmCBF1 may act as a transcriptional repressor and inhibits the expression of *GhPP2C1* or *GhPP2C2*.

DISCUSSION

Plant architecture strongly influences the fiber quality and yield of cotton. New cotton varieties with a dwarf and compact growth phenotype not only perform well in terms of lodging resistance and photosynthetic efficiency, but also are suitable for mechanical harvesting to reduce labor costs (Bednarz et al., 2005; Dai et al., 2015). Overexpression of CBF/DREB transcription factors in a variety of plant species, including *Arabidopsis*, tobacco, tomato, and cotton, can lead to dwarfing (Zhang et al., 2004; Zhou et al., 2014, 2017; Ji et al., 2021). In the present study, L28 and L30 overexpressing *AmCBF1* both showed a dwarf phenotype in the greenhouse and in the field (**Supplementary Figure 2**). When *AmCBF1* expression in L28 and L30 was inhibited by VIGS, the plant height was partially recovered (**Figures 1A,B**). This result was consistent with previous research that silencing of *GhDREB1B* in the AS98 cotton mutant exhibited partial restoration to normal plant height (Ji et al., 2021). At the cellular level, the upper epidermal cells were observed by scanning electron microscopy before and after *AmCBF1* silencing. In addition to the change in size of epidermal cells, it was noteworthy that the epidermal cells were more tightly packed in L28 and L30 than in R15. The surface of the epidermal cells in L28 and L30 was less smooth than in R15, even after *AmCBF1* silencing, and this phenotype was not visibly restored (**Figure 1D**). We speculated that *AmCBF1* overexpression may affect the expression of genes associated with cell morphological structure, which leads to this change in cell morphology. Thus, the relationship between AmCBF1 and cell morphology requires further study.

To further investigate the genetic pathway of AmCBF1-regulated plant dwarfing, RNA-seq of R15, L28, and L30 seedlings was performed, and the genes differentially expressed in L28 or L30 in comparison with R15 were identified. Cluster analysis of the expression patterns of all DEGs revealed that most DEGs were significantly down-regulated in the overexpressed material, and more DEGs were down-regulated in L30 than in L28 (**Figure 2A**). A Venn diagram provided a visual representation of the number of DEGs common in the different materials (**Figure 2B**). However, the number of DEGs between R15 and L28 was 780, while 3,899 DEGs were found between R15 and L30. The possible reason for the huge differences in the number of DEGs may be due to the different insertion site of *AmCBF1*. A similar study revealed that in upland cotton overexpressing *DREB1B*, the number of up-regulated and down-regulated DEGs was approximately equal (Ji et al., 2021). We speculated that the difference in findings between these two studies was due to the different genes overexpressed in cotton or differences in the growth and development status of cotton seedlings used in transcriptome sequencing. The KEGG enrichment analysis of the DEGs revealed that most of the DEGs were enriched in phytohormone signaling pathways, and several genes were enriched in starch and sucrose metabolism, amino acid biosynthesis, carbon metabolism, and lignin biosynthesis pathways (**Figure 2C**). This result suggested that phytohormones may play an important role in plant dwarfing and was similar to the findings of previous reports (Chen et al., 2021; Sun et al., 2021).

Among the DEGs enriched in phytohormone signaling pathways, four *GhPP2C* genes were down-regulated. The function of *PP2C* genes has been widely studied in diverse plant species, such as *Arabidopsis*, rice, tomato, maize (*Zea mays*), and pepper (*Capsicum annuum*; Kerk et al., 2002; Singh et al., 2010; Kim et al., 2014; Wei and Pan, 2014; Liang et al., 2021). However, few studies have investigated the function of *PP2C* genes in cotton. In the present study, we analyzed the evolutionary relationships of PP2C family members in upland cotton and 265 putative *PP2C* genes were identified from the cottonFGD database. This result contrasted with a previous study in which 181 *PP2C* genes were identified in upland cotton (Shazadee et al., 2019). The difference might be due to the different cotton databases accessed or differences in retrieval methods. The 265 *GhPP2C* genes were classified into 12 subgroups of which 39 genes were classified in subgroup A. Interestingly, four of the five down-regulated *GhPP2C* genes identified by RNA-seq belonged to subgroup A. Among these genes, *GhPP2C1–GhPP2C3* were closely related to *AtHAI1/2/3* and *AtAHG3* (**Figure 3B**). Subcellular localization analysis revealed that GhPP2C1 was localized to the nucleus and cell membrane, whereas GhPP2C2 and GhPP2C3 were localized to the nucleus (**Figure 4B**). It has previously been reported that PP2C proteins are localized in the cytoplasm (Amir Hossain et al., 2018). The aforementioned results indicate that PP2C proteins may be localized in different subcellular locations to perform different functions. In the present study, silencing of *GhPP2C1* or *GhPP2C2* resulted in dwarfing (**Figure 4C**). Their functions in regulating plant height may be similar to those of *AtPP2CF1* (in *Arabidopsis*), *OsPP2C09* (in rice), and *SlPP2C3* (in tomato; Sugimoto et al., 2014).

Members of the CBF/DREB transcription factor subfamily interact with genes containing CRT/DRE elements in the promoter and either activate or repress gene expression (Magome et al., 2008; Tsutsui et al., 2009; Kuang et al., 2017; Zhou et al., 2017). The target genes of CBF/DREB transcription factors were significantly enriched in phytohormone signaling pathways, especially the ABA signaling pathway (Song et al., 2021). Whether *GhPP2C* genes are directly regulated by AmCBF1 and are involved in dwarfing in upland cotton has not been reported previously. In the present study, the upstream 3 kb promoter of *GhPP2C1* or *GhPP2C2* was analyzed. The Y1H assay verified that AmCBF1 was capable of binding to the CRT/DRE element in the promoter of *GhPP2C1* or *GhPP2C2* (**Figure 5B**; **Supplementary Figure 4A**). The dual-luciferase assay indicated that AmCBF1 directly inhibited transcription of *GhPP2C1* or *GhPP2C2* by binding to the CRT/DRE element in the promoter (**Figure 5D**; **Supplementary Figures 4B,C**).

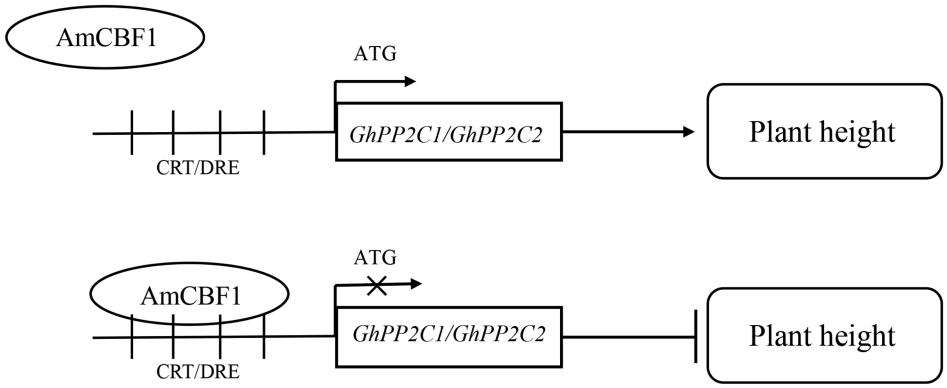

FIGURE 6 | Schematic diagram of a working model for AmCBF1 regulation of *GhPP2C* genes. The transcription factor AmCBF1 inhibits expression of *GhPP2C* genes and negatively regulates the growth of upland cotton seedlings by binding to CRT/DRE elements. Bar, inhibition.

To our knowledge, the present study is the first to report that CBF-like transcription factors are involved in dwarfing of upland cotton by regulating the expression of *GhPP2C* genes.

There is increasing evidence that *PP2C* genes of subgroup A are crucial negative regulators of the ABA signaling pathway, and show distinct expression patterns and subcellular localization in plants (Saez et al., 2004; Nishimura et al., 2007; Umezawa et al., 2009; Zhang et al., 2012). Abscisic acid may exert various inhibitory effects in plant growth (Sharp and Lenoble, 2002; Chen et al., 2006; Zhao et al., 2015; Wang et al., 2018). The ABA–PYR/PYL/RCAR–PP2C complex is an important ternary complex that initiates signal transduction and activates the expression of downstream genes in the classical ABA signaling pathway (Hao et al., 2011; Antoni et al., 2012; Bhaskara et al., 2012; Chen et al., 2016). It is well known that GA and ABA have antagonistic effects in plants, jointly maintain the dynamic balance of plant hormones, and play roles in the growth and development of plants (Yoshida et al., 2014; Liu and Hou, 2018; Shu et al., 2018; Song et al., 2021; Tuan et al., 2021). Based on these findings and the present results, we hypothesized that AmCBF1 overexpression may affect ABA signaling by down-regulating the expression of *GhPP2C1* or *GhPP2C2*, thereby leading to cotton dwarfing by disrupting the balance of ABA and GA.

CONCLUSION

Overexpression of the AmCBF1 transcription factor in upland cotton affected plant growth. *GhPP2C1* and *GhPP2C2* were identified among the DEGs detected by RNA-seq, and silencing of these two genes caused a dwarf phenotype in upland cotton. We verified that AmCBF1 could bind to CRT/DRE elements and negatively regulate the expression of *GhPP2C* genes, thereby regulating plant height. Based on these findings, we propose a molecular model for coordinated regulation of plant height by AmCBF1 and *GhPP2C* genes (**Figure 6**). The present findings expand our knowledge of the regulatory mechanism of dwarfing in cotton, and might contribute to the molecular breeding of cotton cultivars with a dwarf phenotype.

DATA AVAILABILITY STATEMENT

The datasets presented in this study can be found in online repositories. The transcriptome sequencing data can be found in the NCBI database under accession no. PRJNA791756.

AUTHOR CONTRIBUTIONS

HG designed the experiments. JL and LW performed the experiments. JL and LW performed the data analysis. QZ, CM, XS, and HC provided valuable suggestions on the research design and improvement of the manuscript. JL and HG wrote the manuscript. All authors read and approved the final manuscript.

FUNDING

This work was supported by Central Public-interest Scientific Institution Basal Research Fund (nos. Y2022PT22 and Y2022ZK25).

ACKNOWLEDGMENTS

We thank Robert McKenzie, PhD, from Liwen Bianji (Edanz; www.liwenbianji.cn) for editing the English text of a draft of this manuscript. We thank the research team of Jianmin Wan, Institute of Crop Science, Chinese Academy of Agricultural Sciences, for providing the dual-luciferase plasmids. We thank the research team of Zhiying Ma, Hebei Agricultural University, for providing the VIGS related plasmids.

SUPPLEMENTARY MATERIAL

The Supplementary Material for this article can be found online at: https://www.frontiersin.org/articles/10.3389/fpls.2022.914206/full#supplementary-material

REFERENCES

Agarwal, P. K., Agarwal, P., Reddy, M. K., and Sopory, S. K. (2006). Role of DREB transcription factors in abiotic and biotic stress tolerance in plants. *Plant Cell Rep.* 25, 1263–1274. doi: 10.1007/s00299-006-0204-8

Amir Hossain, M., Ahn, C.-H., Lee, I. S., Jeon, J.-S., An, G., and Park, P. B. (2018). Isolation of a novel protein phosphatase2C in rice and its response to gibberellin. *Biochem. Biophys. Res. Commun.* 503, 1987–1992. doi: 10.1016/j.bbrc.2018.07.146

Antoni, R., Gonzalez-Guzman, M., Rodriguez, L., Rodrigues, A., Pizzio, G. A., and Rodriguez, P. L. (2012). Selective inhibition of clade A phosphatases type 2C by PYR/PYL/RCAR abscisic acid aeceptors. *Plant Physiol.* 158, 970–980. doi: 10.1104/pp.111.188623

Baker, S. S., Wilhelm, K. S., and Thomashow, M. F. (1994). The 5′-region of *Arabidopsis thaliana* cor15a has cis-acting elements that confer cold-, drought- and ABA-regulated gene expression. *Plant Mol. Biol.* 24, 701–713. doi: 10.1007/BF00029852

Becker, A., and Lange, M. (2010). VIGS – genomics goes functional. *Trends Plant Sci.* 15, 1–4. doi: 10.1016/j.tplants.2009.09.002

Bednarz, C. W., Shurley, W. D., Anthony, W. S., and Nichols, R. L. (2005). Yield, quality, and profitability of cotton produced at varying plant densities. *Agron. J.* 97, 235–240. doi: 10.2134/agronj2005.0235a

Bhaskara, G. B., Nguyen, T. T., and Verslues, P. E. (2012). Unique drought resistance functions of the highly ABA-induced clade A protein phosphatase 2Cs. *Plant Physiol.* 160, 379–395. doi: 10.1104/pp.112.202408

Bork, P., Brown, N. P., Hegyi, H., and Schultz, J. (1996). The protein phosphatase 2C (PP2C) superfamily: detection of bacterial homologues. *Protein Sci.* 5, 1421–1425. doi: 10.1002/pro.5560050720

Chen, P., Sun, Y.-F., Kai, W.-B., Liang, B., Zhang, Y.-S., Zhai, X.-W., et al. (2016). Interactions of ABA signaling core components (SlPYLs, SlPP2Cs, and SlSnRK2s) in tomato (*Solanum lycopersicon*). *J. Plant Physiol.* 205, 67–74. doi: 10.1016/j.jplph.2016.07.016

Chen, L., Yang, H., Fang, Y., Guo, W., Chen, H., Zhang, X., et al. (2021). Overexpression of GmMYB14 improves high-density yield and drought tolerance of soybean through regulating plant architecture mediated by the brassinosteroid pathway. *Plant Biotechnol. J.* 19, 702–716. doi: 10.1111/pbi.13496

Chen, C.-W., Yang, Y.-W., Lur, H.-S., Tsai, Y.-G., and Chang, M.-C. (2006). A novel function of abscisic acid in the regulation of rice (*Oryza sativa* L.) root growth and development. *Plant Cell Physiol.* 47, 1–13. doi: 10.1093/pcp/pci216

Cutler, S. R., Rodriguez, P. L., Finkelstein, R. R., and Abrams, S. R. (2010). Abscisic acid: emergence of a core signaling network. *Annu. Rev. Plant Biol.* 61, 651–679. doi: 10.1146/annurev-arplant-042809-112122

Dai, J., Li, W., Tang, W., Zhang, D., Li, Z., Lu, H., et al. (2015). Manipulation of dry matter accumulation and partitioning with plant density in relation to yield stability of cotton under intensive management. *Field Crop Res.* 180, 207–215. doi: 10.1016/j.fcr.2015.06.008

Dong, C.-H., Agarwal, M., Zhang, Y., Xie, Q., and Zhu, J.-K. (2006). The negative regulator of plant cold responses, HOS1, is a RING E3 ligase that mediates the ubiquitination and degradation of ICE1. *Proc. Natl. Acad. Sci. U. S. A.* 103, 8281–8286. doi: 10.1073/pnas.0602874103

Dubouzet, J. G., Sakuma, Y., Ito, Y., Kasuga, M., Dubouzet, E. G., Miura, S., et al. (2003). OsDREB genes in rice, *Oryza sativa* L., encode transcription activators that function in drought-, high-salt- and cold-responsive gene expression. *Plant J.* 33, 751–763. doi: 10.1046/j.1365-313X.2003.01661.x

Fuchs, S., Grill, E., Meskiene, I., and Schweighofer, A. (2013). Type 2C protein phosphatases in plants. *FEBS J.* 280, 681–693. doi: 10.1111/j.1742-4658.2012.08670.x

Gaits, F., Shiozaki, K., and Russell, P. (1997). Protein phosphatase 2C acts independently of stress-activated kinase cascade to regulate the stress response in fission yeast. *J. Biol. Chem.* 272, 17873–17879. doi: 10.1074/jbc.272.28.17873

Graeff, M., Rana, S., Marhava, P., Moret, B., and Hardtke, C. S. (2020). Local and systemic effects of brassinosteroid perception in developing phloem. *Curr. Biol.* 30, 1626.e3–1638.e3. doi: 10.1016/j.cub.2020.02.029

Hao, Q., Yin, P., Li, W., Wang, L., Yan, C., Lin, Z., et al. (2011). The molecular basis of ABA-independent inhibition of PP2Cs by a subclass of PYL proteins. *Mol. Cell* 42, 662–672. doi: 10.1016/j.molcel.2011.05.011

He, Y., Hao, Q., Li, W., Chuangye, Y., Yan, N., and Yin, P. (2014). Identification and characterization of ABA receptors in *Oryza sativa*. *PLoS One* 9:e95246. doi: 10.1371/journal.pone.0095246

Hsieh, T.-H., Lee, J.-T., Yang, P.-T., Chiu, L.-H., Charng, Y.-Y., Wang, Y.-C., et al. (2002). Heterology expression of the *Arabidopsis* C-repeat/dehydration response element binding factor 1 gene confers elevated tolerance to chilling and oxidative stresses in transgenic tomato. *Plant Physiol.* 129, 1086–1094. doi: 10.1104/pp.003442

Hu, Y.-X., Tao, Y.-B., and Xu, Z.-F. (2017). Overexpression of Jatropha gibberellin 2-oxidase 6 (JcGA2ox6) induces dwarfism and smaller leaves, flowers and fruits in *Arabidopsis* and *Jatropha*. *Front. Plant Sci.* 8:2103. doi: 10.3389/fpls.2017.02103

Hubbard, M. J., and Cohen, P. (1993). On target with a new mechanism for the regulation of protein phosphorylation. *Trends Biochem. Sci.* 18, 172–177. doi: 10.1016/0968-0004(93)90109-Z

Hubbard, K. E., Nishimura, N., Hitomi, K., Getzoff, E. D., and Schroeder, J. I. (2010). Early abscisic acid signal transduction mechanisms: newly discovered components and newly emerging questions. *Genes Dev.* 24, 1695–1708. doi: 10.1101/gad.1953910

Ingebritsen, T. S., and Cohen, P. (1983). Protein phosphatases: properties and pole in cellular regulation. *Science* 221, 331–338. doi: 10.1126/science.6306765

Ito, Y., Katsura, K., Maruyama, K., Taji, T., Kobayashi, M., Seki, M., et al. (2006). Functional analysis of rice DREB1/CBF-type transcription factors involved in cold-responsive gene expression in transgenic rice. *Plant Cell Physiol.* 47, 141–153. doi: 10.1093/pcp/pci230

Ji, G., Liang, C., Cai, Y., Pan, Z., Meng, Z., Li, Y., et al. (2021). A copy number variant at the HPDA-D12 locus confers compact plant architecture in cotton. *New Phytol.* 229, 2091–2103. doi: 10.1111/nph.17059

Jia, Y., Ding, Y., Shi, Y., Zhang, X., Gong, Z., and Yang, S. (2016). The cbfs triple mutants reveal the essential functions of CBFs in cold acclimation and allow the definition of CBF regulons in *Arabidopsis*. *New Phytol.* 212, 345–353. doi: 10.1111/nph.14088

Kerk, D., Bulgrien, J., Smith, D. W., Barsam, B., Veretnik, S., and Gribskov, M. (2002). The complement of protein phosphatase catalytic subunits encoded in the genome of *Arabidopsis*. *Plant Physiol.* 129, 908–925. doi: 10.1104/pp.004002

Khush, G. S. (1999). Green revolution: preparing for the 21st century. *Genome* 42, 646–655. doi: 10.1139/g99-044

Kim, S., Park, M., Yeom, S.-I., Kim, Y.-M., Lee, J. M., Lee, H.-A., et al. (2014). Genome sequence of the hot pepper provides insights into the evolution of pungency in *Capsicum* species. *Nat. Genet.* 46, 270–278. doi: 10.1038/ng.2877

Kuang, J.-F., Chen, J.-Y., Liu, X.-C., Han, Y.-C., Xiao, Y.-Y., Shan, W., et al. (2017). The transcriptional regulatory network mediated by banana (*Musa acuminata*) dehydration-responsive element binding (MaDREB) transcription factors in fruit ripening. *New Phytol.* 214, 762–781. doi: 10.1111/nph.14389

Kuhn, J. M., Boisson-Dernier, A. L., Dizon, M. B., Maktabi, M. H., and Schroeder, J. I. (2006). The protein phosphatase AtPP2CA negatively regulates abscisic acid signal transduction in *Arabidopsis*, and effects of abh1 on AtPP2CA mRNA. *Plant Physiol.* 140, 127–139. doi: 10.1104/pp.105.070318

Li, Z., Zhang, X., Zhao, Y., Li, Y., Zhang, G., Peng, Z., et al. (2018). Enhancing auxin accumulation in maize root tips improves root growth and dwarfs plant height. *Plant Biotechnol. J.* 16, 86–99. doi: 10.1111/pbi.12751

Liang, B., Sun, Y., Wang, J., Zheng, Y., Zhang, W., Xu, Y., et al. (2021). Tomato protein phosphatase 2C influences the onset of fruit ripening and fruit glossiness. *J. Exp. Bot.* 72, 2403–2418. doi: 10.1093/jxb/eraa593

Liu, X., and Hou, X. (2018). Antagonistic regulation of ABA and GA in metabolism and signaling pathways. *Front. Plant Sci.* 9:251. doi: 10.3389/fpls.2018.00251

Liu, Q., Kasuga, M., Sakuma, Y., Abe, H., Miura, S., Yamaguchi-Shinozaki, K., et al. (1998). Two transcription factors, DREB1 and DREB2, with an EREBP/AP2 DNA binding domain separate two cellular signal transduction pathways in drought- and low-temperature-responsive gene expression, respectively, in *Arabidopsis*. *Plant Cell* 10, 1391–1406. doi: 10.1105/tpc.10.8.1391

Ma, L. F., Zhang, J. M., Huang, G. Q., Li, Y., Li, X. B., and Zheng, Y. (2014). Molecular characterization of cotton C-repeat/dehydration-responsive element binding factor genes that are involved in response to cold stress. *Mol. Biol. Rep.* 41, 4369–4379. doi: 10.1007/s11033-014-3308-1

Magome, H., Yamaguchi, S., Hanada, A., Kamiya, Y., and Oda, K. (2008). The DDF1 transcriptional activator upregulates expression of a gibberellin-deactivating gene, GA2ox7, under high-salinity stress in *Arabidopsis*. *Plant J.* 56, 613–626. doi: 10.1111/j.1365-313X.2008.03627.x

Miao, J., Li, X., Li, X., Tan, W., You, A., Wu, S., et al. (2020). OsPP2C09, a negative regulatory factor in abscisic acid signalling, plays an essential role in balancing plant growth and drought tolerance in rice. *New Phytol.* 227, 1417–1433. doi: 10.1111/nph.16670

Miao, C., Xiao, L., Hua, K., Zou, C., Zhao, Y., Bressan, R. A., et al. (2018). Mutations in a subfamily of abscisic acid receptor genes promote rice growth and productivity. *Proc. Natl. Acad. Sci. U. S. A.* 115, 6058–6063. doi: 10.1073/pnas.1804774115

Miyazono, K.-I., Miyakawa, T., Sawano, Y., Kubota, K., Kang, H.-J., Asano, A., et al. (2009). Structural basis of abscisic acid signalling. *Nature* 462, 609–614. doi: 10.1038/nature08583

Née, G., Kramer, K., Nakabayashi, K., Yuan, B., Xiang, Y., Miatton, E., et al. (2017). DELAY OF GERMINATION1 requires PP2C phosphatases of the ABA signalling pathway to control seed dormancy. *Nat. Commun.* 8:72. doi: 10.1038/s41467-017-00113-6

Nishimura, N., Yoshida, T., Kitahata, N., Asami, T., Shinozaki, K., and Hirayama, T. (2007). ABA-hypersensitive Germination1 encodes a protein phosphatase 2C, an essential component of abscisic acid signaling in *Arabidopsis* seed. *Plant J.* 50, 935–949. doi: 10.1111/j.1365-313X.2007.03107.x

Rodrigues, A., Adamo, M., Crozet, P., Margalha, L., Confraria, A., Martinho, C., et al. (2013). ABI1 and PP2CA phosphatases are negative regulators of Snf1-related protein kinase1 signaling in *Arabidopsis*. *Plant Cell* 25, 3871–3884. doi: 10.1105/tpc.113.114066

Rodriguez, P. L. (1998). Protein phosphatase 2C (PP2C) function in higher plants. *Plant Mol. Biol.* 38, 919–927. doi: 10.1023/A:1006054607850

Saez, A., Apostolova, N., Gonzalez-Guzman, M., Gonzalez-Garcia, M. P., Nicolas, C., Lorenzo, O., et al. (2004). Gain-of-function and loss-of-function phenotypes of the protein phosphatase 2C HAB1 reveal its role as a negative regulator of abscisic acid signalling. *Plant J.* 37, 354–369. doi: 10.1046/j.1365-313X.2003.01966.x

Schweighofer, A., Hirt, H., and Meskiene, I. (2004). Plant PP2C phosphatases: emerging functions in stress signaling. *Trends Plant Sci.* 9, 236–243. doi: 10.1016/j.tplants.2004.03.007

Schweighofer, A., Kazanaviciute, V., Scheikl, E., Teige, M., Doczi, R., Hirt, H., et al. (2007). The PP2C-type phosphatase AP2C1, which negatively regulates MPK4 and MPK6, modulates innate immunity, jasmonic acid, and ethylene levels in *Arabidopsis*. *Plant Cell* 19, 2213–2224. doi: 10.1105/tpc.106.049585

Shan, D.-P., Huang, J.-G., Yang, Y.-T., Guo, Y.-H., Wu, C.-A., Yang, G.-D., et al. (2007). Cotton GhDREB1 increases plant tolerance to low temperature and is negatively regulated by gibberellic acid. *New Phytol.* 176, 70–81. doi: 10.1111/j.1469-8137.2007.02160.x

Sharp, R., and Lenoble, M. (2002). ABA, ethylene and the control of shoot and root growth under water stress. *J. Exp. Bot.* 53, 33–37. doi: 10.1093/jxb/53.366.33

Shazadee, H., Khan, N., Wang, J., Wang, C., Zeng, J., Huang, Z., et al. (2019). Identification and expression profiling of protein phosphatases (PP2C) gene family in *Gossypium hirsutum L. Int. J. Mol. Sci.* 20:1395. doi: 10.3390/ijms20061395

Shu, K., Zhou, W., and Yang, W. (2018). APETALA 2-domain-containing transcription factors: focusing on abscisic acid and gibberellins antagonism. *New Phytol.* 217, 977–983. doi: 10.1111/nph.14880

Singh, A., Giri, J., Kapoor, S., Tyagi, A. K., and Pandey, G. K. (2010). Protein phosphatase complement in rice: genome-wide identification and transcriptional analysis under abiotic stress conditions and reproductive development. *BMC Genomics* 11:435. doi: 10.1186/1471-2164-11-435

Singh, A., Jha, S., Bagri, J., and Pandey, G. (2015). ABA inducible rice protein phosphatase 2C confers ABA insensitivity and abiotic stress tolerance in *Arabidopsis*. *PLoS One* 10:e0125168. doi: 10.1371/journal.pone.0125168

Singh, A., Pandey, A., Srivastava, A. K., Tran, L.-S. P., and Pandey, G. K. (2016). Plant protein phosphatases 2C: from genomic diversity to functional multiplicity and importance in stress management. *Crit. Rev. Biotechnol.* 36, 1023–1035. doi: 10.3109/07388551.2015.1083941

Song, Y., Zhang, X., Li, M., Yang, H., Fu, D., Lv, J., et al. (2021). The direct targets of CBFs: in cold stress response and beyond. *J. Integr. Plant Biol.* 63, 1874–1887. doi: 10.1111/jipb.13161

Soon, F.-F., Ng, L.-M., Zhou, X. E., West Graham, M., Kovach, A., Tan, M. H. E., et al. (2012). Molecular mimicry regulates ABA signaling by SnRK2 kinases and PP2C phosphatases. *Science* 335, 85–88. doi: 10.1126/science.1215106

Sugimoto, H., Kondo, S., Tanaka, T., Imamura, C., Muramoto, N., Hattori, E., et al. (2014). Overexpression of a novel *Arabidopsis* PP2C isoform, AtPP2CF1, enhances plant biomass production by increasing inflorescence stem growth. *J. Exp. Bot.* 65, 5385–5400. doi: 10.1093/jxb/eru297

Sun, Q., Xie, Y., Li, H., Liu, J., Geng, R., Wang, P., et al. (2021). Cotton GhBRC1 regulates branching, flowering, and growth by integrating multiple hormone pathways. *Crop J.* 10, 75–87. doi: 10.1016/j.cj.2021.01.007

Tong, Z., Hong, B., Yang, Y., Li, Q., Ma, N., Ma, C., et al. (2009). Overexpression of two chrysanthemum DgDREB1 group genes causing delayed flowering or dwarfism in *Arabidopsis*. *Plant Mol. Biol.* 71, 115–129. doi: 10.1007/s11103-009-9513-y

Tsutsui, T., Kato, W., Asada, Y., Sako, K., Sato, T., Sonoda, Y., et al. (2009). DEAR1, a transcriptional repressor of DREB protein that mediates plant defense and freezing stress responses in *Arabidopsis*. *J. Plant Res.* 122, 633–643. doi: 10.1007/s10265-009-0252-6

Tuan, P. A., Nguyen, T.-N., Jordan, M. C., and Ayele, B. T. (2021). A shift in abscisic acid/gibberellin balance underlies retention of dormancy induced by seed development temperature. *Plant Cell Environ.* 44, 2230–2244. doi: 10.1111/pce.13963

Umezawa, T., Sugiyama, N., Mizoguchi, M., Hayashi, S., Myouga, F., Yamaguchi-Shinozaki, K., et al. (2009). Type 2C protein phosphatases directly regulate abscisic acid-activated protein kinases in *Arabidopsis*. *Proc. Natl. Acad. Sci. U. S. A.* 106, 17588–17593. doi: 10.1073/pnas.0907095106

Wang, P., Zhao, Y., Li, Z., Hsu, C.-C., Liu, X., Fu, L., et al. (2018). Reciprocal regulation of the TOR kinase and ABA receptor balances plant growth and stress response. *Mol. Cell* 69, 100.e6–112.e6. doi: 10.1016/j.molcel.2017.12.002

Wei, K., and Pan, S. (2014). Maize protein phosphatase gene family: identification and molecular characterization. *BMC Genomics* 15:773. doi: 10.1186/1471-2164-15-773

Wu, C., Zhou, B., and Zhang, T. (2009). Isolation and characterization of a sterile-dwarf mutant in Asian cotton (*Gossypium arboreum* L.). *J. Genet. Genomics* 36, 343–353. doi: 10.1016/S1673-8527(08)60123-X

Xie, L., Yang, C., and Wang, X. (2011). Brassinosteroids can regulate cellulose biosynthesis by controlling the expression of CESA genes in *Arabidopsis*. *J. Exp. Bot.* 62, 4495–4506. doi: 10.1093/jxb/err164

Xin, J., Li, C., Ning, K., Qin, Y., Shang, J.-X., and Sun, Y. (2021). AtPFA-DSP3, an atypical dual-specificity protein tyrosine phosphatase, affects salt stress response by modulating MPK3 and MPK6 activity. *Plant Cell Environ.* 44, 1534–1548. doi: 10.1111/pce.14002

Yamaguchi-Shinozaki, K., and Shinozaki, K. (1994). A novel cis-acting element in an *Arabidopsis* gene is involved in responsiveness to drought, low-temperature, or high-salt stress. *Plant Cell* 6, 251–264. doi: 10.1105/tpc.6.2.251

Yang, Z., Zhang, C., Yang, X., Liu, K., Wu, Z., Zhang, X., et al. (2014). PAG1, a cotton brassinosteroid catabolism gene, modulates fiber elongation. *New Phytol.* 203, 437–448. doi: 10.1111/nph.12824

Yoshida, T., Mogami, J., and Yamaguchi-Shinozaki, K. (2014). ABA-dependent and ABA-independent signaling in response to osmotic stress in plants. *Curr. Opin. Plant Biol.* 21, 133–139. doi: 10.1016/j.pbi.2014.07.009

Zhang, X., Fowler, S. G., Cheng, H., Lou, Y., Rhee, S. Y., Stockinger, E. J., et al. (2004). Freezing-sensitive tomato has a functional CBF cold response pathway, but a CBF regulon that differs from that of freezing-tolerant *Arabidopsis*. *Plant J.* 39, 905–919. doi: 10.1111/j.1365-313X.2004.02176.x

Zhang, C., Sun, J.-L., Jia, Y.-H., Wang, J., Xu, Z.-J., and Du, X.-M. (2011). Morphological characters, inheritance and response to exogenous hormones of a cotton super-dwarf mutant of *Gossypium hirsutum*. *Plant Breed.* 130, 67–72. doi: 10.1111/j.1439-0523.2009.01759.x

Zhang, K., Xia, X., Zhang, Y., and Gan, S.-S. (2012). An ABA-regulated and Golgi-localized protein phosphatase controls water loss during leaf senescence in *Arabidopsis*. *Plant J.* 69, 667–678. doi: 10.1111/j.1365-313X.2011.04821.x

Zhang, P., Yuan, Z., Wei, L., Qiu, X., Wang, G., Liu, Z., et al. (2022). Overexpression of ZmPP2C55 positively enhances tolerance to drought stress in transgenic maize plants. *Plant Sci.* 314:111127. doi: 10.1016/j.plantsci.2021.111127

Zhao, S., Wu, Y., He, Y., Wang, Y., Xiao, J., Li, L., et al. (2015). RopGEF2 is involved in ABA-suppression of seed germination and post-germination growth of *Arabidopsis*. *Plant J.* 84, 886–899. doi: 10.1111/tpj.13046

Zhou, M., Chen, H., Wei, D., Ma, H., and Lin, J. (2017). *Arabidopsis* CBF3 and DELLAs positively regulate each other in response to low temperature. *Sci. Rep.* 7:39819. doi: 10.1038/srep39819

Zhou, M., Xu, M., Wu, L., Shen, C., Ma, H., and Lin, J. (2014). CbCBF from *Capsella bursa-pastoris* enhances cold tolerance and restrains growth in *Nicotiana tabacum* by antagonizing with gibberellin and affecting cell cycle signaling. *Plant Mol. Biol.* 85, 259–275. doi: 10.1007/s11103-014-0181-1

Zhu, J. K. (2016). Abiotic stress signaling and responses in plants. *Cell* 167, 313–324. doi: 10.1016/j.cell.2016.08.029

Conflict of Interest: The authors declare that the research was conducted in the absence of any commercial or financial relationships that could be construed as a potential conflict of interest.

Publisher's Note: All claims expressed in this article are solely those of the authors and do not necessarily represent those of their affiliated organizations, or those of the publisher, the editors and the reviewers. Any product that may be evaluated in this article, or claim that may be made by its manufacturer, is not guaranteed or endorsed by the publisher.

frontiers | Frontiers in Plant Science

ORIGINAL RESEARCH
published: 16 June 2022
doi: 10.3389/fpls.2022.915569

Transcriptome Profiling of Transposon-Derived Long Non-coding RNAs Response to Hormone in Strawberry Fruit Development

Xi Chen[1,2†], Chengdong Wang[3†], Bing He[4], Zifan Wan[1,2], Yukun Zhao[1,2], Fengqin Hu[4] and Yuanda Lv[4*]*

[1] School of Agronomy and Horticulture, Jiangsu Vocational College of Agriculture and Forest, Jurong, China, [2] Engineering and Technical Center for Modern Horticulture, Jurong, China, [3] Key Laboratory of Tobacco Biology and Processing, Ministry of Agriculture, Tobacco Research Institute of Chinese Academy of Agricultural Sciences, Qingdao, China, [4] Excellence and Innovation Center, Jiangsu Academy of Agricultural Sciences, Nanjing, China

OPEN ACCESS

Edited by:
Jian Chen,
Jiangsu University, China

Reviewed by:
Xiaofeng Su,
Biotechnology Research Institute (CAAS), China
Na Zhao,
Nanjing Agricultural University, China
Aasim Majeed,
Institute of Himalayan Bioresource Technology (CSIR), India

***Correspondence:**
Fengqin Hu
Fengqinhu2008@126.com
Yuanda Lv
Lyd0527@126.com

[†] These authors have contributed equally to this work

Specialty section:
This article was submitted to Plant Bioinformatics, a section of the journal Frontiers in Plant Science

Received: 08 April 2022
Accepted: 02 May 2022
Published: 16 June 2022

Citation:
Chen X, Wang C, He B, Wan Z, Zhao Y, Hu F and Lv Y (2022) Transcriptome Profiling of Transposon-Derived Long Non-coding RNAs Response to Hormone in Strawberry Fruit Development. Front. Plant Sci. 13:915569. doi: 10.3389/fpls.2022.915569

Strawberry is an economically grown horticulture crop required for fruit consumption. The ripening of its fruit is a complex biological process regulated by various hormones. Abscisic acid (ABA) is a critical phytohormone involved in fruit ripening. However, little is known about the long non-coding RNAs (LncRNAs), especially transposon-derived LncRNA (TE-lncRNA), response to hormones during fruit ripening in octoploid strawberry. In the study, the transcriptome data of developing strawberry fruits treated with ABA and its inhibitor Nordihydroguaiaretic acid (NGDA) were analyzed to identify responsive LncRNAs and coding genes. A total of 14,552 LncRNAs were identified, including 8,617 transposon-derived LncRNAs (TE-LncRNAs), 412 LncRNAs (282 TE-LncRNAs), and 382 ABA-sensitive LncRNAs (231 TE-LncRNAs). Additionally, a weighted co-expression network analysis constructed 27 modules containing coding RNAs and LncRNAs. Seven modules, including "MEdarkorange" and "MElightyellow" were significantly correlated with ABA/NDGA treatments, resulting in 247 hub genes, including 21 transcription factors and 22 LncRNAs (15 TE-LncRNAs). Gene ontology enrichment analysis further revealed that ABA/NDGA-responsive modules, including LncRNAs, were associated with various metabolic pathways involved in strawberry fruit development and ripening, including lipid metabolism, organic acid metabolism, and phenylpropanoid metabolism. The current study identifies many high-confidence LncRNAs in strawberry, with a percentage of them being ABA pathway-specific and 22 hub-responsive LncRNAs, providing new insight into strawberry or other Rosaceae crop fruit ripening.

Keywords: long non-coding RNA, transposon, strawberry, fruit ripening, ABA

INTRODUCTION

Strawberry (*Fragaria* × *ananassa*) is an octoploid *Rosaceae* species that is a vital horticultural crop grown worldwide (Edger et al., 2019). It was first cultivated and developed in France, where it has remained popular for more than a century due to its juicy, sweaty texture and pleasant aroma (Darrow, 1966). Strawberry fruit is prevalent in almost all the food markets in every corner around

the world, and it is also an essential feedstock for producing jelly jam, and biscuits. Although strawberries cannot cope under harsh growth conditions or many abiotic stress factors, greenhouse or artificial climate chambers provide a favorable environment for its harvesting (Khoshnevisan et al., 2013). Therefore, strawberry is a non-climacteric fruit (Given et al., 1988) that has been widely cultured in many countries, and in some areas, it has even become the most important crop for local farmers (Lieten, 2005; Antunes and Peres, 2013; Zhang et al., 2014). The fruit is the most valuable part of this economic crop, and as a result, the scientific research on strawberry fruit development is significantly meaningful and economically beneficial (Wang et al., 2017). Thus, it has emerged as a significant scientific study subject in strawberry breeding and botany research.

Angiosperm plants have conserved mechanisms for developing fruits and regulating fruit ripening (Forlani et al., 2019). To date, there are some key gene encoding proteins that regulate this progression that has been discovered to be conserved in structure and function across different plant species such as *NACs* (Mitsuda and Ohme-Takagi, 2008; Xu et al., 2021), *YABBY* (Dinneny et al., 2005), and *AGAMOUS* (Itkin et al., 2009) families, etc. Fruit development and ripening have been shown to be influenced by the phytohormones, auxin, gibberellic acid (GA), abscisic acid (ABA), jasmonic acid (JA), and cytokinin (CK), as well as brassinosteroids (BR) and ethylene (ET) (Chen et al., 2020). Auxin and cytokines were the primary regulators of cell division and tissue expansion in the carpel during the early stages of fruit development, respectively (Pattison and Catalá, 2012). Later on, ABA and ethylene were also found to play central regulatory roles in the process of climacteric-fruit ripening, with ABA playing a role in the process of non-climacteric-fruit ripening (Chen et al., 2020). Strawberry is a typical non-climacteric fruit. Through the study on the diploid strawberry (landwood, *F. vessa*), it was found that auxin and gibberellic acid could activate the expression of a gene (FveCYP707A4a) encoding cytochrome P450 monooxygenase, which is a key enzyme in the bio-degradation of ABA during the fruit development process (Liao et al., 2018). On the other hand, ABA has the potential to activate the *FveNCED* gene, which encodes the rate-limiting enzyme of ABA biosynthesis, and this activity would be enhanced during the ripening stage of the fruit.

Many studies have been conducted to determine how the expression of coding genes changes during the ripening of strawberry fruits, and the results have revealed the presence of many important coding genes. However, LncRNA, especially transposon-derived LncRNAs (TE-LncRNA), is still not fully understood or even illustrated. After the introduction of new generation sequencing technology, the high-through transcriptome analysis has facilitated the discovery of LncRNA greatly (Lv et al., 2019; Chen et al., 2022; Liang et al., 2022). Recently, LnRNAs were predicted and verified in the transcriptome of *F. vesca* fruit in altering stages (Kang and Liu, 2015). Later, functional LnRNAs that could regulate *F. vesca* (diploid strawberry) fruit ripening were identified (Tang et al., 2021). These results implied that the LnRNAs are involved in the ripening process, which remains largely unknown.

In the study, we systemically identified LncRNAs response to exogenous ABA and NDGA under the developing fruit of octoploid strawberry (*F. ananassa*). The responsive LncRNAs and differentially expressed genes were analyzed and then linked into modules using the weighted co-expression network method. According to the findings of this study, the LnRNA profile of the octoploid strawberry was determined, as well as the transcriptomic deviation induced by the exogenous hormone, both in coding RNAs and in LncRNAs.

MATERIALS AND METHODS

Plant Materials and Growth Conditions

Octoploid strawberry cultivar 'Toyonoka' was cultivated in a greenhouse with photoperiod and temperatures of 14-h light, 25°C /10-h dark, 20°C as described by Li et al. (2019). Fruits of 2-week after anthesis were injected with 150 μl of exogenous ABA (1 μM) solution when the CK is of mock injection with distilled water. Fruits were collected 5 days after the injection and immediately deep-frozen with liquid nitrogen for further qRT-PCR validation. Three independent biological replicates for each condition were performed. The germplasm was acquired from the USDA-ARS National Plant Germplasm System (NPGS) with permission for scientific research. Detailed information on the variety could be found at npgsweb.ars-grin.gov (accession: PI616632).

RNA-Seq Data Processing and Transcript Assembly

As mentioned in Li et al. (2019), RNA-seq files were obtained and uncompressed from the SRA database (Accession: PRJNA338879) (Li et al., 2019). Fastp v0.20.0 (Chen et al., 2018) was used to clean the raw data, which contained sequencing adapters, low-quality bases, and too short reads (50 bp). Cleaned data was then mapped to the *Fragaria* × *ananassa* Camarosa genome (v1.0.a2)[1] using STAR v2.7.9a (Dobin and Gingeras, 2016) with two-pass mode. The aligned reads were then assembled with the known transcript annotation (v1.0.a2) (Liu et al., 2021) by reference annotation-based transcript (RABT) assembly algorithm and generated a combined GTF-formatted annotated file using StringTie v2.1.5 (Pertea et al., 2016). Finally, the expression abundance of transcripts was quantified as counts with the above-updated annotation using featureCounts (Liao et al., 2014) and then normalized as the fragments per kilobase of transcript per million fragments mapped (FPKM) value by a custom script.[2] For downstream gene expression analysis, only

[1] www.rosaceae.org

[2] https://github.com/Lyd0527/RNAnorm

transcripts with an FPKM > 1 in at least three samples were considered.

Computational Prediction and Transposon Annotation of Long Non-coding RNAs

To identify potential LncRNAs, a strict computational strategy was performed as described by Lv et al. (2019). First, all transcript sequences were extracted by gffread v0.12.2 program (Geo and Mihaela, 2020). Secondly, we employed three tools, including CPC2 and PLncPRO, to predict the coding potential of every transcript. Swissport and Pfam protein databases were selected for PLncPRO program. Default parameters were then performed CPC2 and PLncPRO. Finally, non-coding transcripts larger than 200 bp, with an FPKM > 1 and joint from two tools were considered candidate LncRNAs for further analysis. Additionally, the EDTA program was used to annotate transposon elements (TE) in octoploid strawberries (Ou et al., 2019). Coding sequences of octoploid strawberry were employed to purge gene sequences in the TE library. To avoid overmasking, coordinates specified compared with known gene position were also whitelisted from TE annotation. RepeatModeler (Flynn et al., 2020) is used to salvage some TEs such as SINE and LINE types left by structure-based scans.

Differential Gene Expression Analysis

With the combined transcript annotation, DESeq2 (Love et al., 2014) was used to perform pairwise comparisons between conditional samples to find differentially expressed genes (DEGs). The following criteria were used to determine whether transcripts, including coding and non-coding RNAs, were differentially expressed: (I) the log2 fold change had to be greater than 1 and (II) the adjusted *p*-value from DESeq2 analysis had to be less than 0.05.

Co-expression Network Analysis

To link the coding and non-coding RNAs, the WGCNA tool was used to generate a weighted co-expression network using the above count matrix under ABA and NDGA conditions (Pei et al., 2017). The DESeq2 package standardized the raw count expression matrix (Love et al., 2014). Co-expression correlation between coding and non-coding RNAs was then calculated using Pearson correlation with $r^2 \geq 0.85$. The normalized expression data from coding and non-coding RNAs were extracted to construct an unsigned co-expression network using the WGCNA package with a soft threshold = 10 (Pei et al., 2017). Module assignment of coding and non-coding RNAs was identified using Topological Overlap Matrix (TOM). Besides, additionally, correlations between modules and treatments were evaluated, and transcripts from modules with significant correlations were retrieved and displayed using the Cytoscape software (Saito et al., 2012). Furthermore, hub genes were defined as those with a module-trait correlation value greater than 0.8 and membership within modules greater than 0.8.

Gene Ontology Enrichment Analysis

To infer the potential biological function of LncRNAs, coding transcripts in modules related to different were then performed for Gene Ontology (GO) enrichment analysis using the agriGO v2.0 toolkit (Tian et al., 2017). Significantly, over-represented GO terms were detected *via* Fisher's exact test, and multi-test adjustment was made using the Yekutieli (FDR under dependency) method with a cutoff of FDR < 0.05. GO enriched results were combined and visualized by clusterProfiler (Yu et al., 2012).

RNA Extraction and qRT-PCR Analysis

Total RNA was extracted using the RNAprep Pure Plant Kit (Tiangen, China) and cDNA was synthesized using PrimeScript RT Master Mix (Takara, Japan) according to kit instructions. PCR reactions were performed on the LightCycler 96 Real-Time PCR System (Roche, United States) using the SYBR Premix DimerEraser kit (Takara, Japan). Each PCR reaction was repeated three times, and relative expression levels of transcripts were calculated using the comparative Ct ($\Delta\Delta$Ct) method. qRT-PCR primers were designed using Beacon Designer 8 software and can be found in **Supplementary Table 9**.

RESULTS

Updated Genome Annotation Based on RNA-Seqs Under Treatments

Fourteen RNAseq datasets from octoploid strawberry ripening fruit with treatments of phytohormone ABA and its inhibitor nordihydroguaiaretic acid (Li et al., 2019) were cleaned, mapped, and assembled with the RABT method. A total of 162,558 transcripts with 109,126 loci combined with known annotated transcripts were finally generated (**Supplementary Table 1**). By comparing with known annotation by gffcompare program (Geo and Mihaela, 2020), 3,595 novel transcripts were identified and located in the intergenic regions; 75.32% (122,445, " = ") transcripts were matched with the annotated genes perfectly; 14.84% (24,119, j) matching multiple exons with at least one junction connected; 1.60% (2,596, n) transcripts retained part of the intron; 0.16% (255) retained all the introns. There were also 2.21% (3,595, u) matching the intergenic region, and only 0.01% (24) transcripts were found to be located within the reference intron (**Figure 1A** and **Supplementary Table 1**).

Identification and Characterization of Potential Long Non-coding RNAs

CPC2 and PLncPRO programs were used to identify potential LncRNAs from these candidate transcripts. Two state-of-the-art programs were engaged in proofreading the predicted LncRNAs. A total of 14,552 transcripts were identified as LncRNA (**Supplementary Table 2**). Only 1,029 LncRNA overlapped with known LncRNAs predicted by Edger et al. (2019). The distribution of the predicted LncRNA on octoploid strawberry chromosomes is shown in **Figure 1B**. Their FPKM

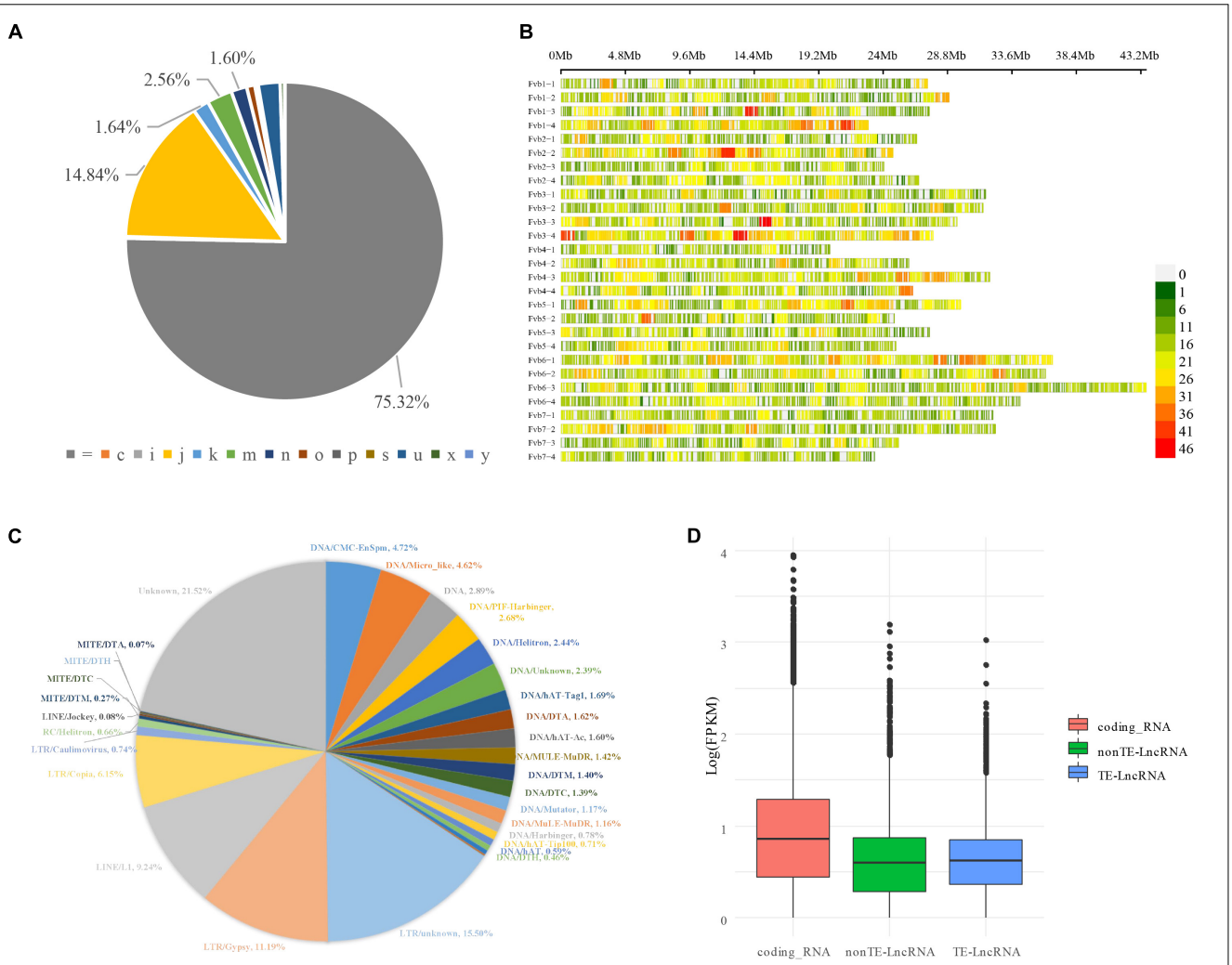

FIGURE 1 | LncRNAs mining, identification, and expression level evaluation in strawberry developing fruit. **(A)** LncRNA distribution on the strawberry genome. The LncRNA distribution and density are demonstrated by the physical positions of chromosomes and coloration. The window wide is 1 M. **(B)** The result of StringTie analysis. The transcripts were categorified by StringTie software into different groups in different colors and marked with characters and symbols. For example, " = " complete as the reference transcript, exact match of intron cutoff; "i" fully contained within a reference intron; "u" intergenic or unknown. **(C)** Identifying transposon elements derived LncRNAs. **(D)** The Expression level evaluation on LncRNAs, TE-LncRNAs, and coding genes.

value is highly varied in developing fruit. The transcripts with an FPKM value of more than 1 were deemed high-confidence stress-responsive transcripts. There hence were the transcriptions of 3,684 high-confidence expressed LncRNA detected in the study. Simultaneously, a total of 725 novel coding genes such as transposase-derived proteins FHY3/FAR1 (MSTRG.787, MSTRG.13323, MSTRG.39595, MSTRG.52515) were identified in developing fruit. By further annotating with transposon elements, we found 59.2% (8,617 of 14,552) LncRNAs were derived from transposon elements (TEs), and 2,074 with FPKM $\geq$ 1 were considered as high-confidence TE-LncRNAs (**Supplementary Table 3**). According to the TE family classification, the majority of TE-LncRNAs (530, 6.10%) were from the Copia family, followed by Gypsy (964, 11.1%) (**Figure 1C**). The details of TE annotation and TE-LncRNAs of the whole genome can be found in **Supplementary Table 3**. Besides, LncRNAs, especially TE-LncRNAs, showed a relatively lower expression level than coding genes, consistent with previous studies (**Figure 1D**; Lv et al., 2019).

Abscisic Acid—and NDGA- Responsive Long Non-coding RNAs and Coding Genes

According to the expression profile, differentially expressed genes were further analyzed by DESeq2. The results showed that ABA- and NDGA- treatment had significantly influenced the expression of LncRNAs and coding genes. In the ABA treatment, at 5- and 8- days after chemical injection, in comparison with control, there were 60/117 and 233/325 TE-LncRNA/LncRNAs, and 1,169 and 1,417 coding genes differentially expressed, respectively. Simultaneously, NDGA treatment at 5- and 8- days

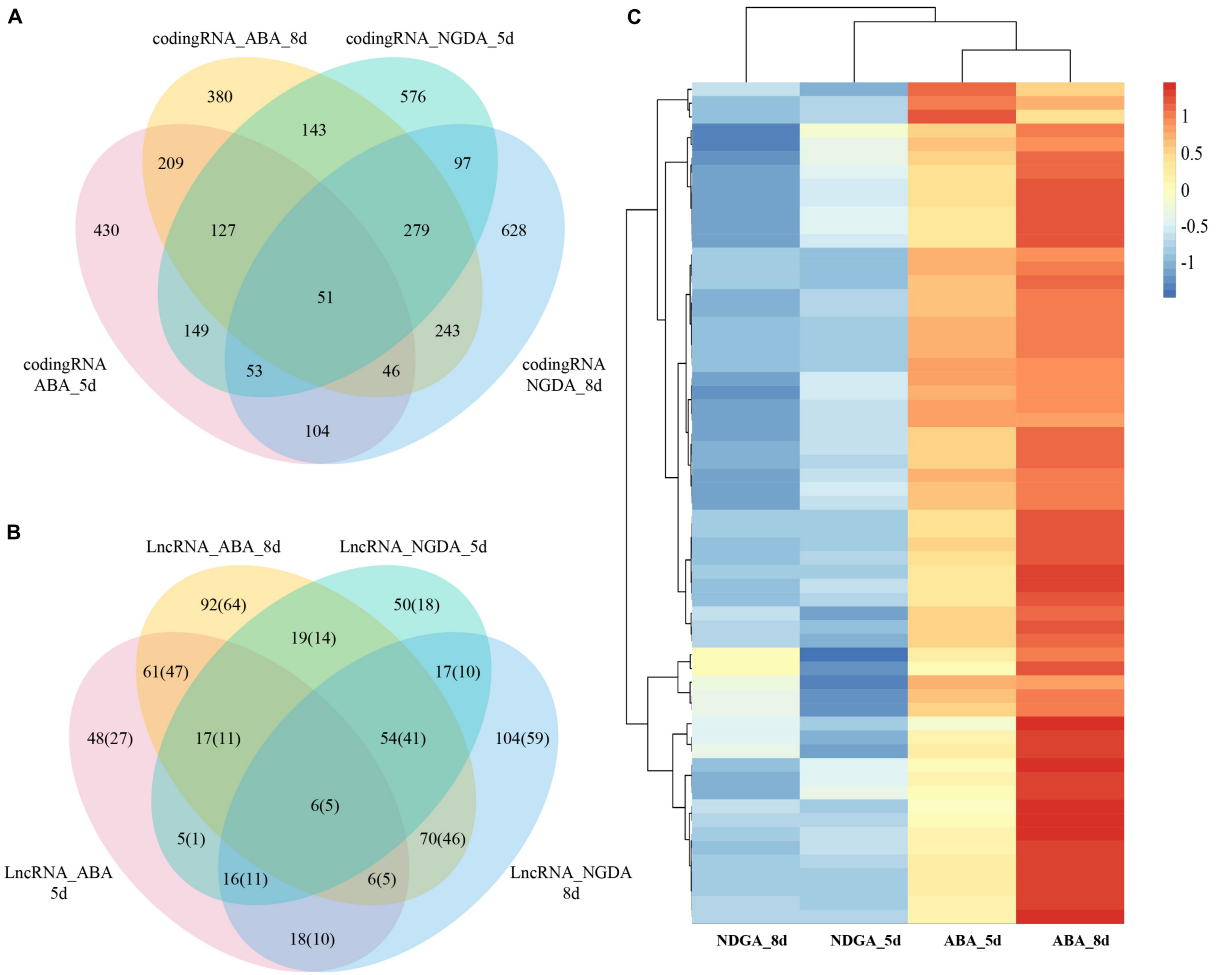

FIGURE 2 | The Venn diagrams of 5- and 8-day ABA treatment and 5- and 8-day NGDA treatment. **(A)** The differentially expressed coding RNAs of ABA and NGDA treatment, and overlap between 5- and 8-day; **(B)** the differentially expressed LncRNAs of ABA and NGDA treatment, and overlap between 5- and 8-day; **(C)** the heatmap of the common ABA-responsive LncRNAs between ABA_5d and ABA_8d treatments.

after injection, compared with control, there were 111/184 and 187/291 TE-LncRNA/LncRNAs, and 1,475 and 1,501 coding genes differentially expressed, respectively. As shown in VENN graphics (**Figures 2A,B** and **Supplementary Table 4**), for ABA, between 5- and 8-day, there were 90 LncRNAs (67 TE-LncRNAs) and 433 coding genes overlapped; between NDGA, 5- and 8-day, 93 LncRNAs (66 TE-LncRNAs) and 480 coding genes overlapped, respectively. Compared with NDGA treatment, 61 LncRNA (47 TE-LncRNAs) showed specific-responsive under ABA treatment across 5th and 8th day (**Figure 2C** and **Supplementary Table 4**).

Co-expression Network of the Differentially Expressed Long Non-coding RNA

Predicting the biological role of LncRNAs in plant development and abiotic and biotic stresses remains a challenge. To investigate the potential functions of these ABA and NGDA treatment responsive LncRNAs, a well-developed computational algorithm WGCNA was employed to generate the weighted co-expression network based on the correlation between the expressing variation of LncRNAs and coding RNAs. The significantly correlated LncRNAs and coding genes were further constructed into the weighted co-expression network, from which a total of 27 modules were generated (**Figure 3A** and **Supplementary Table 5**). Furthermore, the correlation between the different modules, and the treatments, was also calculated. The correlation between the part of the modules is demonstrated by the heatmap and the dendrogram shown in **Figure 3B**. The heatmap in **Figure 3C** showed the correlation between a part of the modules with the treatments. In the figure, it was apparent that part of the modules positively correlated with the treatment, while the other part of them was negative.

In total, seven modules, including "MEdarkorange," "MElightyellow," "MEblack," "MEturquoise," "MEgrey60," "MElightyellow," and "MElightgreen" were significantly correlated with ABA/NDGA treatments, of which 247 hub genes including 21 transcription factors and 22 LncRNAs

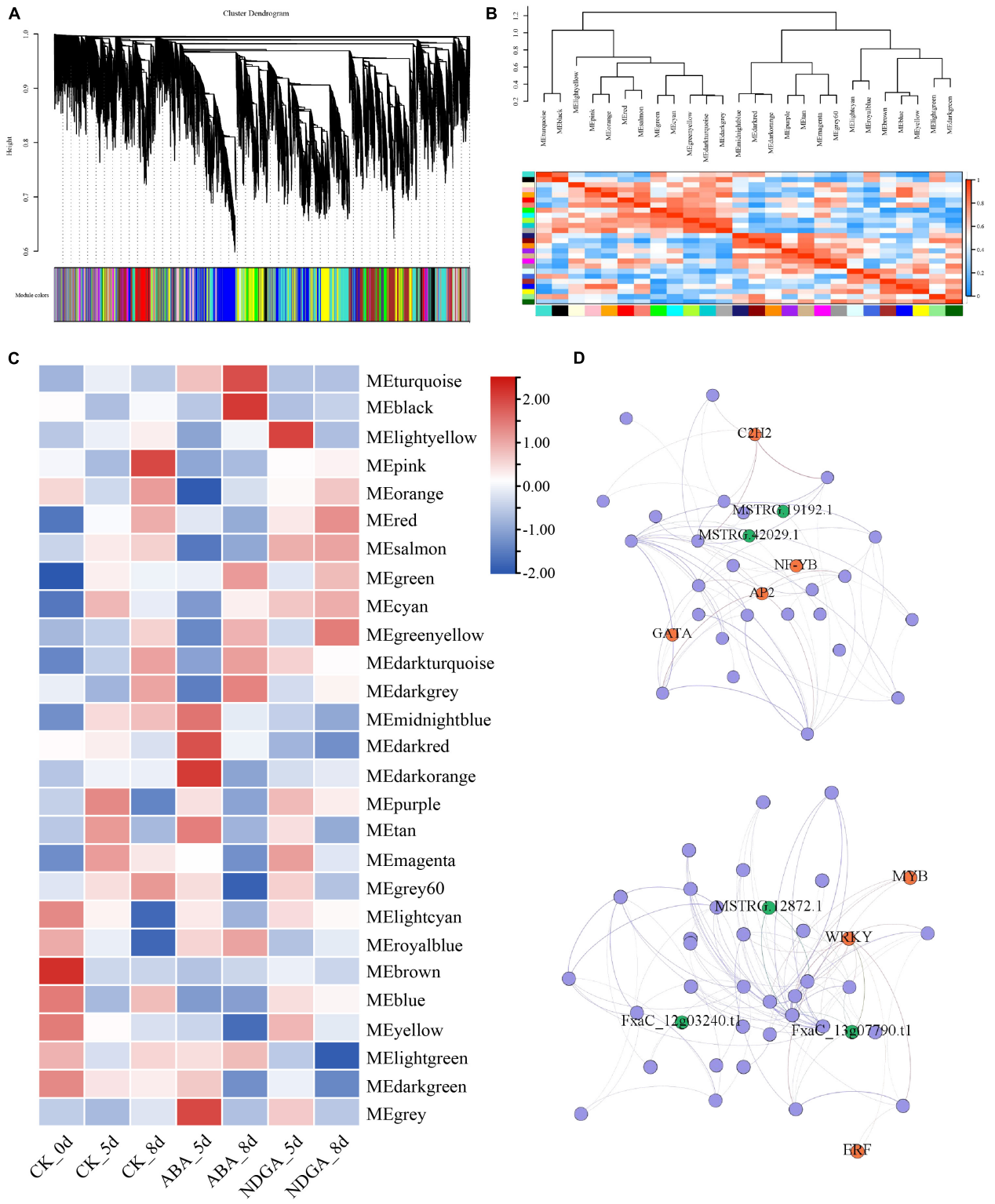

FIGURE 3 | The co-expression network was constructed according to the differentially expressed LncRNAs and coding genes. **(A)** The clustering dendrogram with dissimilarity based on the topological overlap, together with assigned module colors; **(B)** the heatmap of correlation within co-expression modules; **(C)** the heatmap of correlation between co-expression modules and the treatments; **(D)** network illustration of co-expression module "MEdarkorange" and "MEblack." The spots represent the node genes, which have high intramodular connectivities. Transcription factors are marked as orange, and the spots in blue are LncRNAs.

(15 TE-LncRNAs) were further identified (**Figure 3C** and **Supplementary Tables 5**, **6**). For example, the modules "MEdarkorange" and "MElightyellow" showed the highest correlation with treatment ABA 5-day and NGDA 5-day, respectively (**Figures 3C,D**). The module "MEdarkorange" was constructed with 8 LncRNAs (4 TE-LncRNAs) and 54 coding genes (4 transcription factors). As shown in **Figure 3D**, the upper illustration demonstrated the regulation network of MEdarkorange. There were four TF coding genes (C2H2, NF-YB, AP2, and GATA) and LncRNAs (MSTRG19192.1 and MSTRG42029.1) playing a critical hub role in regulating the eigengenes. The lower one was the network of MElightyellow, which had the highest correlation with NGDA 5-day. There was 148 genes contained in this module, three TF coding genes (MYB, WRKY, and ERF), and five LncRNAs played an important hub role.

Gene Ontology Enrichment

The coding eigengenes in stress-responsive modules were analyzed by AgriGO V2 (Tian et al., 2017) to assign the enrichment. The coding eigengenes were selected from the module with the highest correlation with the treatment, and they were marked. The GO enrichment was demonstrated in **Figure 4** and **Supplementary Table 7**. All of the treatments triggered the plant's response to abiotic stimulus (GO:0009628) and response to chemicals (GO:0042221). The result also showed that there were several pathways relevant to fruit development enriched because of NGDA treatment for 8 days, such as small molecule biosynthetic process (GO: 0044283), organic acid metabolic process (GO: 0006082), small molecule metabolic process (GO:0044281), phenylpropanoid metabolic process (GO:0009698), and response to disaccharide (GO:0034285). The ABA and NGDA treatment could also influence the pathways concerned with light (GO:0009416, GO:0009644) and photosynthesis (GO:0009765). On the other hand, multiple pathways by which plant response to abiotic stress was significantly enriched, including response to heat (GO:0009408), response to water deprivation (GO:0009414), response to water (GO:0009415), response to osmotic stress (GO:0006970), etc.

Evolutionary Conservation Analysis of Long Non-coding RNAs

The evolutionary conservation of identified octoploid strawberry LncRNAs was investigated among three related Rosaceae species: *Prunus salicina* (plum), *Malus domestica* (apple), and *Potentilla micrantha*. The homology analysis of 14,552 LncRNAs was carried out by Megablast with *E*-value $\leq$ 1e-10. As a result (**Supplementary Table 8**), 477(3.28%), 488(3.35%), and 3,760(25.8%) LncRNAs showed similarity with *P. salicina* (plum), *M. domestica* (apple), and *P. micrantha* genome. Besides, 268 LncRNAs were common among three species. These results suggested that the homology of LncRNAs was relatively consistent with phylogenetic distance and had lower conservation compared with coding RNAs.

qRT-PCR Validation of the Long Non-coding RNA

To validate the reliability of ABA-responsive LncRNAs, we performed an ABA-treatment experiment on strawberries (see section "Materials and Methods"), and their RNA was extracted. We then subjected the samples to quantitative real-time PCR (qRT-PCR) to compare expression changes between replicated control and ABA-treated. We randomly selected 12 representative long non-coding transcripts. All LncRNAs were significantly up-regulated under ABA treatment based on qRT-PCR (**Figure 5**), which showed a high degree of consistency between RNA-Seq and qRT-PCR (**Figure 5** and **Supplementary Table 9**).

DISCUSSION

In the study, the transcriptome data of strawberry developing fruit with exogenous ABA and its inhibitor NGDA treatment were assessed for LncRNA mining and further conjoint analysis of gene co-expression network and gene ontology with coding RNAs. We discovered 14,552 LncRNAs and 3,595 novel transcripts using the transcriptome dataset, including some previously unidentified functional genes such as FHY3/FAR1. FHY3 is a transcription factor that plays an essential role in the response of plants to light and in photomorphogenesis. *FHY3* gene is derived from a part of the transposon sequence (transposase coding gene) (Tang et al., 2012). Compared with the previous LncRNA identification on diploid strawberry, *F. vesca* and octoploid strawberry (Kang and Liu, 2015; Edger et al., 2019), we first identified hormone-responsive LncRNAs and further inferred their potential biological function by weight-coexpression network construction.

Besides, we further discovered that 8,617 transposon-derived LncRNAs (TE-LncRNAs) are derived from transposable elements (transposon) in the genome. The transposon is a DNA sequence that can move or copy itself to a different position in the genome. It has a vital role in evolution because it can change a cell's genetic identity and the size the genome (Lisch, 2013). Moreover, in the process of evolution, transposons could vary and transform into sequences with other biological functions, such as miRNA or LncRNA. More than half of the identified LncRNAs derived from TE in this study. The result implied that TE might play an essential role in strawberry genome polyploidization and transmission. Only a few reports about strawberry transposon prediction emerged (Edger et al., 2019). Hence the function of transposon and transposon-derived genes need to be analyzed intensively in future studies.

The present study also investigated how exogenous ABA and its inhibitor influence the LncRNAs expression in the strawberry fruit ripening process. A total of 412 LncRNAs (282 TE-LncRNA) and 382 LncRNAs (231 TE-LncRNA) were identified with significantly differential expression responding to ABA and inhibitor (NGDA), respectively. The co-expression

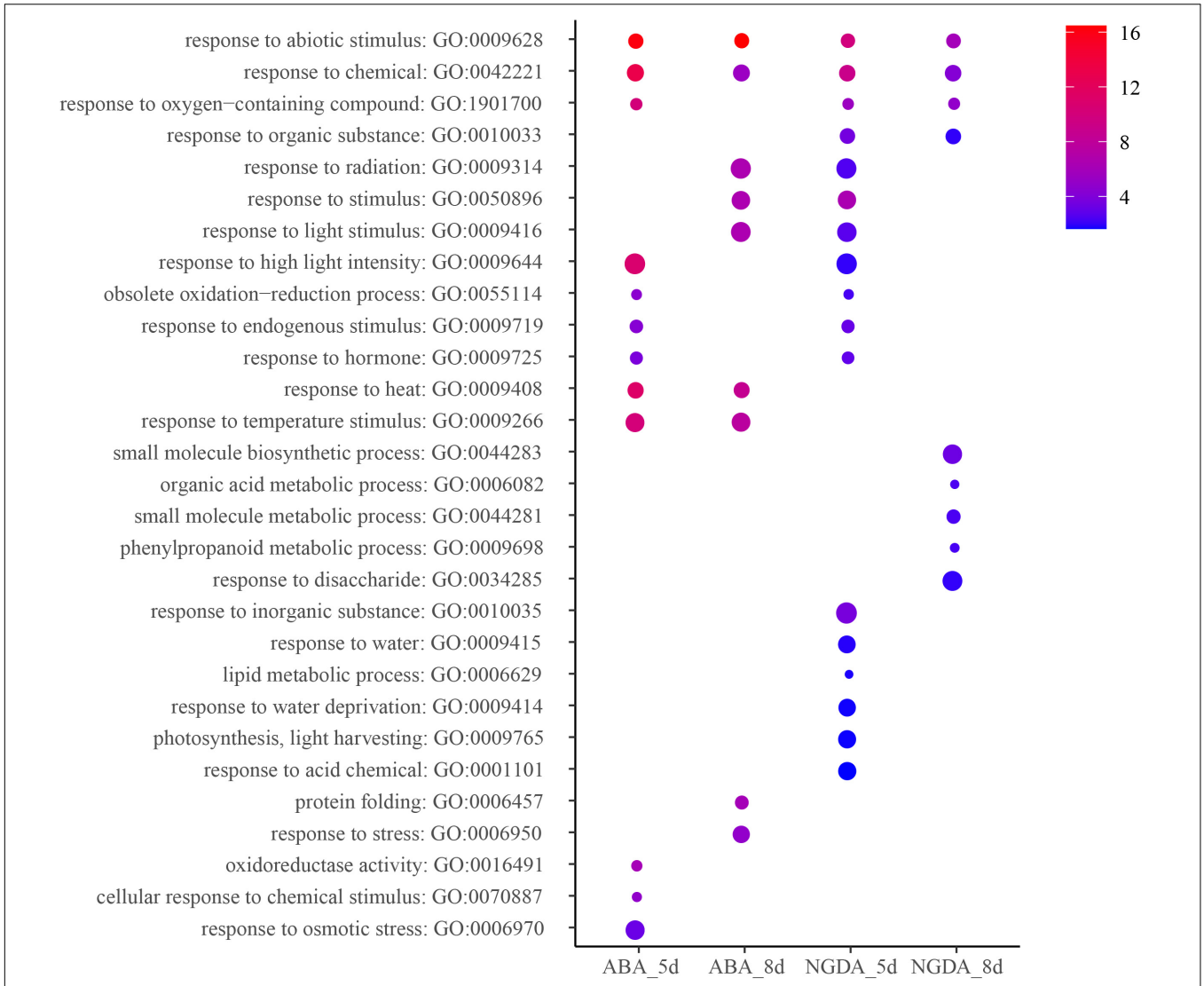

FIGURE 4 | Gene ontology analysis of ABA/NDGA responsive modules. The heat map scale reflects the significant level of enrichment of GO terms. The red showed the most significant enrichment in statistics. Size of spot represents transcript numbers of terms.

network analysis had 27 modules constructed, all of them containing LncRNAs and coding genes. This result implied that ABA regulates strawberry fruit ripening *via* a complicated mechanism with intensive interaction and cooperation between LncRNAs and coding genes. As reported by Liao et al. (2018) in diploid strawberry (*F. vesca*) the homeostasis is controlled by the expression of *FveCYP707A4a* (cytochrome P450 monooxygenase). Cytochrome P450 monooxygenase is the key enzyme of ABA degradation. There were five homologous of FveCYP707A4a identified: FxaC_7g36210.t1, FxaC_5g00020.t1, FxaC_5g36690.t1, FxaC_8g11790.t1, and FxaC_6g40060.t1. The expression levels of FxaC_7g36210.t1 and FxaC_5g00020.t1 increased 5 days after ABA injection, but FxaC_5g00020.t1 was downregulated at ABA 8-day. FxaC_7g36210.t1 belonged to the module "MEtan," which correlated with ABA 5-day and had 697 members. There were 52 LncRNAs in "MEtan" module when TE-LncRNA MSTRG.27422.1 played an important node in the network. On the other hand, gene FxaC_9g05310.t1 encoding an isoform of cytochrome P450 monooxygenase, its expression level was significantly induced at ABA 5- and 8-day. This gene belonged to module "MEblack" which had the highest association with ABA 8-day. This module had 1,684 members, among which 126 LncRNA were included. LncRNAs such as FxaC_14g11020, MSTRG.5872.1, and MSTRG.5719.1 were significant nodes in this network. The upregulated expression level of cytochrome P450 monooxygenase coding genes was possibly induced by the ABA injection, which disturbed the ABA homeostasis.

Interestingly, the expression level of ABA1s and NCDEs was elevated after exogenous ABA injection, but not NGDA. ABA1 (zeaxanthin epoxidase) and NCDE (9-cis-epoxycarotenoid dioxygenase) are critical enzymes of the endogenous ABA biosynthesis pathway. This phenomenon implied that the

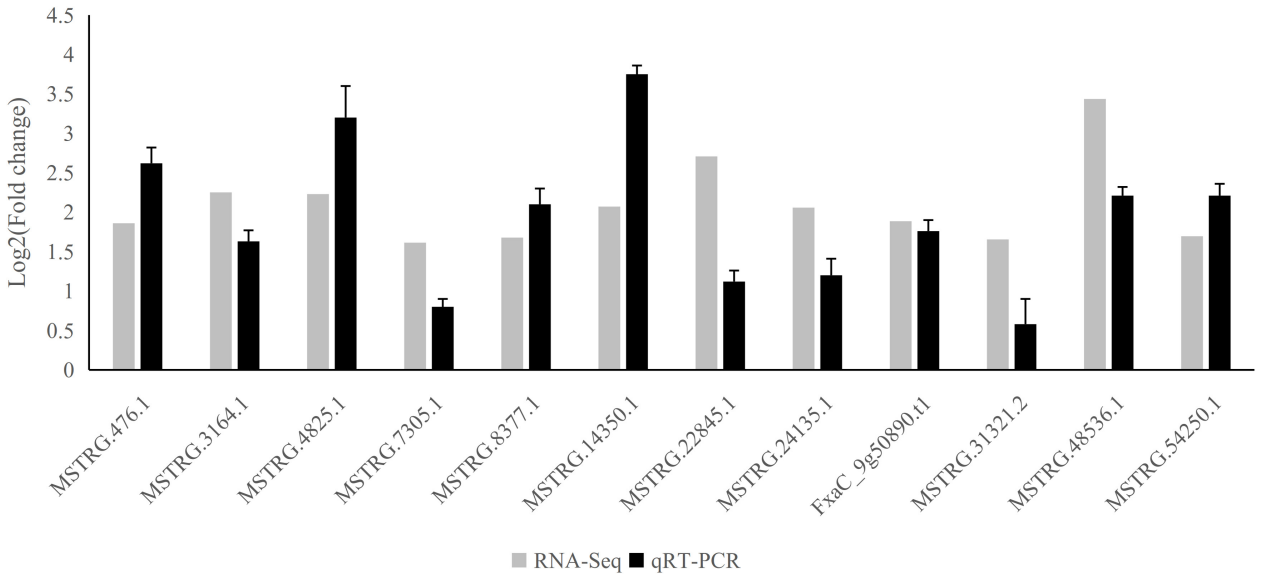

FIGURE 5 | qRT-PCR validation of differentially expressed lncRNAs. The qRT-PCR histogram for each locus represents the mean ± standard error (SE) of three independent biological replicates, and the qRT-PCR was compared to fold-change data inferred from RNAseq data.

exogenous ABA injection might improve the endogenous ABA biosynthesis, accelerating the ripening process.

The gene ontology analysis performed in the study did not cover all the differentially expressed LncRNAs and coding genes but selected those in the modules with the highest association with the treatments. The result was quite remarkable. First, the exogenous hormone and inhibitor injection induced the gene expression responding to chemicals, which was understandable. Furthermore, all the treatments also induced the response process to abiotic stimulus. It might also indicate the general influence of exogenous chemical injection and collateral damage. ABA is an essential hormone regulating plants tolerant to abiotic and biotic stress (Lee and Luan, 2012; Danquah et al., 2014). It is well known that ABA induces the closure of stoma to reduce evaporation (Hsu et al., 2021; Movahedi et al., 2021). Hence in the GO analysis at ABA treatment, the module contained genes responding to heat and temperature. This result implied those genes involved in stress tolerance might play some roles in the fruit-ripening process as well. Some studies reported that ABA could downregulate photosynthesis (Leng et al., 2021; Park et al., 2021), and in the analysis, the pathways of response to light (stimulus and intensity) were significantly enriched. It is well-known that light could induce the fruit ripening, hence present result showed ABA and its corresponding genes and LncRNAs could be a part of the mechanism. Furthermore, this experimental phenomenon indicated that the exogenous hormone injection had induced and activated the massive number of genes of multiple pathways; those involved in the fruit ripening process and or even more genes activated were relevant to stress-tolerance relevant pathways.

Comparing with exogenous ABA and NDGA treatment could reveal the transcriptome profile variation when the endogenous ABA level decrease in the ripening fruit. NDGA is also an exogenous chemical. It can effectively inhibit 9-cis-Epoxycarotenoid dioxygenase, the key enzyme of ABA biosynthesis (Han et al., 2004). Therefore, compared with CK, the NDGA-treated fruit ought to have a lower ABA level, which would delay its ripening progress. It could explain the GO analysis result of NGDA treatment showing the biochemical pathways of organic acid metabolism (Hwang et al., 2019), phenylpropanoid metabolism (Crizel et al., 2020; Pott et al., 2020), small molecule metabolism, response to disaccharides and lipid metabolism significant enriched. The hypothesis is that NDGA treatment decreases the ABA level in the developing fruit, and affects its nutrient compound biosynthesis and deposition, including organic acid, sugar, lipids (aroma), phenylpropanoid, and other small molecules. On the other hand, the photosynthesis, light-harvesting, response to light density pathways, etc., were also enriched in the gene-network module of NDGA treatment. We deduced that it could be a partial result of the delayed fruit ripening (green fruit) and postponed the fruit-color transmission (Warner et al., 2021).

CONCLUSION

In the study, the transcriptomic data of octoploid strawberry developing fruit treated with exogenous ABA and its inhibitor NDGA were used for LncRNA mining and co-expression analysis. The result provides a massive amount of LncRNA, especially transposon-derived LncRNA (TE-LncRNA) in strawberries, and identified those expressed in fruit and the part which was ABA-responsive, potential fruit ripening, and abiotic stress relevant. The LncRNAs and the co-expression modules would serve as promising references and databasess for further

studies on fruit ripening in strawberries or other Rosaceae crops, and ABA signal pathways.

DATA AVAILABILITY STATEMENT

Publicly available datasets were analyzed in this study. RNA-seq data under treatments can be found in the publicly accessible NCBI Sequence Read Archive (SRA) Database under the accession number PRJNA338879.

AUTHOR CONTRIBUTIONS

YL and FH designed the study. XC, CW, BH, ZW, and YZ collected plant materials, performed the experiments, and carried out the data analyses. XC, FH, and YL wrote the manuscript. All authors have read and approved the final version of this manuscript.

FUNDING

This study was sponsored by the Natural Science Foundation of Jiangsu Province (BK20191224), supported project of Jiangsu Vocational College of Agriculture and Forest (2019kj005), Second Batch of National Vocational Education Teacher and Teaching Innovation Team Project (ZH2021100201), and Blue Project of Jiangsu Province.

SUPPLEMENTARY MATERIAL

The Supplementary Material for this article can be found online at: https://www.frontiersin.org/articles/10.3389/fpls.2022.915569/full#supplementary-material

Supplementary Table 1 | Updated annotation based on RNA-Seq of ABA/NDGA treatments.

Supplementary Table 2 | The detail of potential LncRNAs.

Supplementary Table 3 | The information of transposon-derived LncRNAs.

Supplementary Table 4 | Differentially expressed LncRNAs.

Supplementary Table 5 | Modules of co-expression network and their correlation with treatments.

Supplementary Table 6 | Genes from modules and their correlation with treatments.

Supplementary Table 7 | GO (Gene Ontology) enrichment result.

Supplementary Table 8 | Conservation of LncRNA among three related species.

Supplementary Table 9 | qRT-PCR primers.

REFERENCES

Antunes, L. E. C., and Peres, N. A. (2013). Strawberry production in Brazil and South America. *Int. J. Fruit Sci.* 13, 156–161.

Chen, S., Zhou, Y., Chen, Y., and Gu, J. (2018). fastp: an ultra-fast all-in-one FASTQ preprocessor. *Bioinformatics* 34, i884–i890. doi: 10.1093/bioinformatics/bty560

Chen, T., Qin, G., and Tian, S. (2020). Regulatory network of fruit ripening: current understanding and future challenges. *New Phytol.* 228, 1219–1226. doi: 10.1111/nph.16822

Chen, X., Meng, L., He, B., Qi, W., Jia, L., Xu, N., et al. (2022). Comprehensive transcriptome analysis uncovers hub long non-coding rnas regulating potassium use efficiency in *Nicotiana tabacum*. *Front. Plant Sci.* 13:777308. doi: 10.3389/fpls.2022.777308

Crizel, R., Perin, E., Siebeneichler, T., Borowski, J., Messias, R., Rombaldi, C., et al. (2020). Abscisic acid and stress induced by salt: effect on the phenylpropanoid, L-ascorbic acid and abscisic acid metabolism of strawberry fruits. *Plant Physiol. Biochem.* 152, 211–220. doi: 10.1016/j.plaphy.2020.05.003

Danquah, A., de Zelicourt, A., Colcombet, J., and Hirt, H. (2014). The role of ABA and MAPK signaling pathways in plant abiotic stress responses. *Biotechnol. Adv.* 32, 40–52. doi: 10.1016/j.biotechadv.2013.09.006

Darrow, G. M. (1966). *The Strawberry. History, Breeding and Physiology*. New York, NY: Holt, Rinehart and Winston.

Dinneny, J. R., Weigel, D., and Yanofsky, M. F. (2005). A genetic framework for fruit patterning in *Arabidopsis thaliana*. *Development* 132, 4687–4696. doi: 10.1242/dev.02062

Dobin, A., and Gingeras, T. R. (2016). "Optimizing RNA-Seq mapping with STAR," in *Data Mining Techniques for the Life Sciences*, eds O. Carugo and F. Eisenhaber (Berlin: Springer), 245–262. doi: 10.1007/978-1-4939-3572-7_13

Edger, P. P., Poorten, T. J., VanBuren, R., Hardigan, M. A., Colle, M., McKain, M. R., et al. (2019). Origin and evolution of the octoploid strawberry genome. *Nat. Genet.* 51, 541–547.

Flynn, J. M., Hubley, R., Goubert, C., Rosen, J., Clark, A. G., Feschotte, C., et al. (2020). RepeatModeler2 for automated genomic discovery of transposable element families. *Proc. Natl. Acad. Sci. U.S.A.* 117, 9451–9457. doi: 10.1073/pnas.1921046117

Forlani, S., Masiero, S., and Mizzotti, C. (2019). Fruit ripening: the role of hormones, cell wall modifications, and their relationship with pathogens. *J. Exp. Bot.* 70, 2993–3006. doi: 10.1093/jxb/erz112

Geo, P., and Mihaela, P. (2020). GFF Utilities: GffRead and GffCompare. *F1000Research* 9:304. doi: 10.12688/f1000research.23297.2

Given, N., Venis, M., and Gierson, D. (1988). Hormonal regulation of ripening in the strawberry, a non-climacteric fruit. *Planta* 174, 402–406. doi: 10.1007/BF00959527

Han, S. Y., Kitahata, N., Saito, T., Kobayashi, M., Shinozaki, K., Yoshida, S., et al. (2004). A new lead compound for abscisic acid biosynthesis inhibitors targeting 9-cis-epoxycarotenoid dioxygenase. *Bioorgan. Med. Chem. Lett.* 14, 3033–3036. doi: 10.1016/j.bmcl.2004.04.035

Hsu, P. K., Dubeaux, G., Takahashi, Y., and Schroeder, J. I. (2021). Signaling mechanisms in abscisic acid-mediated stomatal closure. *Plant J.* 105, 307–321. doi: 10.1111/tpj.15067

Hwang, H., Kim, Y.-J., and Shin, Y. (2019). Influence of ripening stage and cultivar on physicochemical properties, sugar and organic acid profiles, and antioxidant compositions of strawberries. *Food Sci. Biotechnol.* 28, 1659–1667. doi: 10.1007/s10068-019-00610-y

Itkin, M., Seybold, H., Breitel, D., Rogachev, I., Meir, S., and Aharoni, A. (2009). TOMATO AGAMOUS-LIKE 1 is a component of the fruit ripening regulatory network. *Plant J.* 60, 1081–1095. doi: 10.1111/j.1365-313X.2009.04064.x

Kang, C., and Liu, Z. (2015). Global identification and analysis of long non-coding RNAs in diploid strawberry *Fragaria vesca* during flower and fruit development. *BMC Genom.* 16:815. doi: 10.1186/s12864-015-2014-2

Khoshnevisan, B., Rafiee, S., and Mousazadeh, H. (2013). Environmental impact assessment of open field and greenhouse strawberry production. *Eur. J. Agron.* 50, 29–37. doi: 10.1016/j.jenvman.2017.03.090

Lee, S. C., and Luan, S. (2012). ABA signal transduction at the crossroad of biotic and abiotic stress responses. *Plant Cell Environ.* 35, 53–60. doi: 10.1111/j.1365-3040.2011.02426.x

Leng, Y., Li, Y., Ma, Y.-H., He, L.-F., and Li, S.-W. (2021). Abscisic acid modulates differential physiological and biochemical responses of roots, stems, and leaves in mung bean seedlings to cadmium stress. *Environ. Sci. Pollut. Res.* 28, 6030–6043.

Li, D., Mou, W., Xia, R., Li, L., Zawora, C., Ying, T., et al. (2019). Integrated analysis of high-throughput sequencing data shows abscisic acid-responsive genes and miRNAs in strawberry receptacle fruit ripening. *Hortic. Res.* 6, 1–13. doi: 10.1038/s41438-018-0100-8

Liang, W., Hu, F., Qi, W., Zhao, C., Chen, T., Wang, C., et al. (2022). Comprehensive transcriptome analysis of gs3 near-isogenic lines during panicle development in rice (*Oryza sativa* L.). *Front. Genet.* 13:857143. doi: 10.3389/fgene.2022.857143

Liao, X., Li, M., Liu, B., Yan, M., Yu, X., Zi, H., et al. (2018). Interlinked regulatory loops of ABA catabolism and biosynthesis coordinate fruit growth and ripening in woodland strawberry. *Proc. Natl. Acad. Sci. U.S.A.* 115, E11542–E11550. doi: 10.1073/pnas.1812575115

Liao, Y., Smyth, G. K., and Shi, W. (2014). featureCounts: an efficient general purpose program for assigning sequence reads to genomic features. *Bioinformatics* 30, 923–930. doi: 10.1093/bioinformatics/btt656

Lieten, P. (2005). Strawberry production in central Europe, International. *J. Fruit Sci.* 5, 91–105.

Lisch, D. (2013). How important are transposons for plant evolution? *Nat. Rev. Genet.* 14, 49–61. doi: 10.1038/nrg3374

Liu, T., Li, M., Liu, Z., Ai, X., and Li, Y. (2021). Reannotation of the cultivated strawberry genome and establishment of a strawberry genome database. *Hortic. Res.* 8, 1–9. doi: 10.1038/s41438-021-00476-4

Love, M. I., Huber, W., and Anders, S. (2014). Moderated estimation of fold change and dispersion for RNA-seq data with DESeq2. *Genome Biol.* 15, 1–21. doi: 10.1186/s13059-014-0550-8

Lv, Y., Hu, F., Zhou, Y., Wu, F., and Gaut, B. S. (2019). Maize transposable elements contribute to long non-coding RNAs that are regulatory hubs for abiotic stress response. *BMC Genomics* 20:864. doi: 10.1186/s12864-019-6245-5

Mitsuda, N., and Ohme-Takagi, M. (2008). NAC transcription factors NST1 and NST3 regulate pod shattering in a partially redundant manner by promoting secondary wall formation after the establishment of tissue identity. *Plant J.* 56, 768–778. doi: 10.1111/j.1365-313X.2008.03633.x

Movahedi, M., Zoulias, N., Casson, S. A., Sun, P., Liang, Y.-K., Hetherington, A. M., et al. (2021). Stomatal responses to carbon dioxide and light require abscisic acid catabolism in *Arabidopsis*. *Interface Focus* 11:20200036. doi: 10.1098/rsfs.2020.0036

Ou, S., Su, W., Liao, Y., Chougule, K., Agda, J. R., Hellinga, A. J., et al. (2019). Benchmarking transposable element annotation methods for creation of a streamlined, comprehensive pipeline. *Genome Biol.* 20, 1–18.

Park, S.-H., Lee, B.-R., Al Mamun, M., Bae, D.-W., and Kim, T.-H. (2021). Characterization of salicylic acid-and abscisic acid-mediated photosynthesis, Ca^{2+} and H_2O_2 accumulation in two distinct phases of drought stress intensity in *Brassica napus*. *Environ. Exp. Bot.* 186:104434.

Pattison, R. J., and Catalá, C. (2012). Evaluating auxin distribution in tomato (*Solanum lycopersicum*) through an analysis of the PIN and AUX/LAX gene families. *Plant J.* 70, 585–598. doi: 10.1111/j.1365-313X.2011.04895.x

Pei, G., Chen, L., and Zhang, W. (2017). WGCNA application to proteomic and metabolomic data analysis. *Methods Enzymol.* 585, 135–158. doi: 10.1016/bs.mie.2016.09.016

Pertea, M., Kim, D., Pertea, G. M., Leek, J. T., and Salzberg, S. L. (2016). Transcript-level expression analysis of RNA-seq experiments with HISAT, StringTie and Ballgown. *Nat. Protoc.* 11:1650. doi: 10.1038/nprot.2016.095

Pott, D. M., Vallarino, J. G., Cruz-Rus, E., Willmitzer, L., Sánchez-Sevilla, J. F., Amaya, I., et al. (2020). Genetic analysis of phenylpropanoids and antioxidant capacity in strawberry fruit reveals mQTL hotspots and candidate genes. *Sci. Rep.* 10, 1–15. doi: 10.1038/s41598-020-76946-x

Saito, R., Smoot, M. E., Ono, K., Ruscheinski, J., Wang, P.-L., Lotia, S., et al. (2012). A travel guide to *Cytoscape plugins*. *Nat. Methods* 9:1069. doi: 10.1038/nmeth.2212

Tang, W., Wang, W., Chen, D., Ji, Q., Jing, Y., Wang, H., et al. (2012). Transposase-derived proteins FHY3/FAR1 interact with PHYTOCHROME-INTERACTING FACTOR1 to regulate chlorophyll biosynthesis by modulating HEMB1 during deetiolation in *Arabidopsis*. *Plant Cell* 24, 1984–2000. doi: 10.1105/tpc.112.097022

Tang, Y., Qu, Z., Lei, J., He, R., Adelson, D. L., Zhu, Y., et al. (2021). The long noncoding RNA FRILAIR regulates strawberry fruit ripening by functioning as a noncanonical target mimic. *PLoS Genet.* 17:e1009461. doi: 10.1371/journal.pgen.1009461

Tian, T., Liu, Y., Yan, H., You, Q., Yi, X., Du, Z., et al. (2017). agriGO v2.0: a GO analysis toolkit for the agricultural community, 2017 update. *Nucleic Acids Res.* 45, W122–W129. doi: 10.1093/nar/gkx382

Wang, Y., Zhang, J., Cui, W., Guan, C., Mao, W., and Zhang, Z. (2017). Improvement in fruit quality by overexpressing miR399a in woodland strawberry. *J. Agric. Food Chem.* 65, 7361–7370. doi: 10.1021/acs.jafc.7b01687

Warner, R., Wu, B. S., MacPherson, S., and Lefsrud, M. (2021). A review of strawberry photobiology and fruit flavonoids in controlled environments. *Front. Plant Sci.* 12:611893. doi: 10.3389/fpls.2021.611893

Xu, N., Meng, L., Song, L., Li, X., Du, S., Hu, F., et al. (2021). Identification and characterization of secondary wall-associated nac genes and their involvement in hormonal responses in tobacco (*Nicotiana tabacum*). *Front. Plant Sci.* 12:712254. doi: 10.3389/fpls.2021.712254

Yu, G., Wang, L.-G., Han, Y., and He, Q.-Y. (2012). clusterProfiler: an R package for comparing biological themes among gene clusters. *OMICS* 16, 284–287. doi: 10.1089/omi.2011.0118

Zhang, C., Shi, J. Y., Zhu, L. P., Li, C. L., and Wang, Q. G. (2014). Cooperative effects of hydrogen sulfide and nitric oxide on delaying softening and decay of strawberry. *Int. J. Agric. Biol. Eng.* 7, 114–122.

Conflict of Interest: The authors declare that the research was conducted in the absence of any commercial or financial relationships that could be construed as a potential conflict of interest.

Publisher's Note: All claims expressed in this article are solely those of the authors and do not necessarily represent those of their affiliated organizations, or those of the publisher, the editors and the reviewers. Any product that may be evaluated in this article, or claim that may be made by its manufacturer, is not guaranteed or endorsed by the publisher.

frontiers | Frontiers in Plant Science

TYPE Original Research
PUBLISHED 01 August 2022
DOI 10.3389/fpls.2022.932926

OPEN ACCESS

EDITED BY
Weicong Qi,
Jiangsu Academy of Agricultural Sciences (JAAS), China

REVIEWED BY
Shuai Li,
Qingdao Agricultural University, China
Sonia Balyan,
University of Delhi South Campus, India

*CORRESPONDENCE
Renying Zhuo
zhuory@gmail.com
Xiaohua Yao
yaoxh168@163.com

SPECIALTY SECTION
This article was submitted to Plant Bioinformatics, a section of the journal Frontiers in Plant Science

RECEIVED 30 April 2022
ACCEPTED 11 July 2022
PUBLISHED 01 August 2022

CITATION
Chen J, Han X, Ye S, Liu L, Yang B, Cao Y, Zhuo R and Yao X (2022) Integration of small RNA, degradome, and transcriptome sequencing data illustrates the mechanism of low phosphorus adaptation in *Camellia oleifera*. *Front. Plant Sci.* 13:932926. doi: 10.3389/fpls.2022.932926

Integration of small RNA, degradome, and transcriptome sequencing data illustrates the mechanism of low phosphorus adaptation in *Camellia oleifera*

Juanjuan Chen[1,2,3], Xiaojiao Han[1,2], Sicheng Ye[1,2], Linxiu Liu[1,2], Bingbing Yang[1,2], Yongqing Cao[1,2], Renying Zhuo[1,2]* and Xiaohua Yao[1,2]*

[1]State Key Laboratory of Tree Genetics and Breeding, Chinese Academy of Forestry, Hangzhou, China, [2]Key Laboratory of Tree Breeding of Zhejiang Province, Research Institute of Subtropical Forestry, Chinese Academy of Forestry, Hangzhou, China, [3]Forestry Faculty, Nanjing Forestry University, Nanjing, China

Phosphorus (P) is an indispensable macronutrient for plant growth and development, and it is involved in various cellular biological activities in plants. *Camellia oleifera* is a unique high-quality woody oil plant that grows in the hills and mountains of southern China. However, the available P content is deficient in southern woodland soil. Until now, few studies focused on the regulatory functions of microRNAs (miRNAs) and their target genes under low inorganic phosphate (Pi) stress. In this study, we integrated small RNA, degradome, and transcriptome sequencing data to investigate the mechanism of low Pi adaptation in *C. oleifera*. We identified 40,689 unigenes and 386 miRNAs by the deep sequencing technology and divided the miRNAs into four different groups. We found 32 miRNAs which were differentially expressed under low Pi treatment. A total of 414 target genes of 108 miRNAs were verified by degradome sequencing. Gene ontology (GO) functional analysis of target genes found that they were related to the signal response to the stimulus and transporter activity, indicating that they may respond to low Pi stress. The integrated analysis revealed that 31 miRNA–target pairs had negatively correlated expression patterns. A co-expression regulatory network was established based on the profiles of differentially expressed genes. In total, three hub genes (*ARF22*, *WRKY53*, and *SCL6*), which were the targets of differentially expressed miRNAs, were discovered. Our results showed that integrated analyses of the small RNA, degradome, and transcriptome sequencing data provided a valuable basis for investigating low Pi in *C. oleifera* and offer new perspectives on the mechanism of low Pi tolerance in woody oil plants.

KEYWORDS

***Camellia oleifera*, low phosphorus stress, integration analysis, miRNA, co-expression network**

Introduction

Phosphorus (P) is an indispensable macronutrient required for plant growth and development and is involved in energy transfer, metabolic regulation, protein activation, and other cellular biological activities in plants (Wang Y. et al., 2021; Wang Z. et al., 2021; Navarro and Munné-Bosch, 2022). Inorganic phosphate (Pi) in soil exists mainly in the form of organophosphate compounds and inorganic Pi (HPO_4^{2-} and $H_2PO_4^-$) (Lidbury et al., 2022). Although some soils contain high levels of Pi, the low solubility and high adherence of Pi in soil lead to a lack of available Pi, which is one of the factors that limits crop yield (Crombez et al., 2019). To maintain high crop production, an excessive amount of phosphate fertilizer is often applied to the soil, leading to severe water eutrophication (Conley et al., 2009; Johnston et al., 2014). Moreover, the already insufficient phosphate rock resources are declining and speculated to deplete within 50–100 years (Cordell et al., 2009).

Plants maintain cellular Pi homeostasis by coordinating Pi acquisition, storage, translocation, and remobilization (Fan X. et al., 2021; Jia et al., 2021; Wang Z. et al., 2021). In response to low Pi environments, plants produce various Pi starvation responses to survive. The Pi starvation response is modulated by gene regulatory networks that involve hundreds of Pi transporters and Pi starvation-induced genes (Rubio et al., 2001; He et al., 2015; Wang F. et al., 2018). Pi starvation-induced genes include transcription factors, signal molecules, and other upstream regulators. In *Arabidopsis*, nine phosphate transport 1 (*Pht1*) genes were involved in the absorption of Pi from the soil and the redistribution of Pi in plants (Smith et al., 2003). Phosphate starvation response 1 (*AtPHR1*) and other related transcription factors play vital roles in regulating the Pi starvation response. In the presence of Pi, SYG1/PHO81/XPR1 (*SPX1*) shows high binding affinity to *PHR1*, which inhibits the interaction of *PHR1* with its conserved P1BS motif. However, in the absence of Pi, the binding affinity of *SPX1* to *PHR1* is reduced, allowing the PHR1–P1BS interaction and subsequent induction of transcription to take place (Liu N. et al., 2018; Li et al., 2021). For example, in rice (*Oryza sativa*), *OsSPX1* and *OsSPX2* interact with *OsPHR2* and repress the activity of *OsPHR2* in a similar way to that in *Arabidopsis* (Wang et al., 2014; Tyagi et al., 2021). The phosphorus-responsive transcription factors *OsPHR1/2/3* are located in the core of the mycorrhizal symbiotic transcription regulatory network in plants under Pi starvation (Shi et al., 2021).

Recently, Pi starvation-induced genes, mainly those that encode signaling molecules and transcription factors, have been studied extensively in *Arabidopsis* and rice (Sun et al., 2012; Wang Q. et al., 2018). MicroRNAs (miRNAs) have also been shown to play crucial roles in regulating the Pi starvation response at the posttranscription level (Li et al., 2010; Wang S. et al., 2021). A large number of differentially expressed miRNAs involved in the response to low Pi stress have been identified by using small RNA (sRNA) sequencing. In soybean (*Glycine max*), 36 differentially expressed miRNAs involved in the response to Pi starvation were identified (Xu et al., 2013). In poplar (*Populus tomentosa*), three novel and 65 known miRNAs were found to respond dynamically to Pi fluctuations, and *miR167*, *miR171*, *miR394*, and *miR857* participated in low Pi stress response (Bao et al., 2019). The functions of miRNAs in the response to Pi starvation have also been investigated. In *Arabidopsis*, *miRNA399* was the first shown to regulate the Pi stress response. The expression of *miRNA399* was upregulated when Pi was deficient and decreased quickly when Pi was sufficient (Fujii et al., 2005). Subsequently, six *miRNA399* genes (*miRNA399A–F*) in *Arabidopsis* were found to be induced differently under low Pi stress, and three genes (phosphate transporter 1;7, DEAD box, and ubiquitin E2 conjugase) were predicted to be regulated by *miRNA399*, but only ubiquitin E2 conjugase (*UBC24*) was confirmed to be a target (Allen et al., 2005). In *miRNA399*-overexpressed *Arabidopsis* lines, the expression level of *UBC24* mRNA was reduced significantly (Pegler et al., 2021). Several conserved miRNA families and some novel miRNAs have also been shown to respond to Pi starvation in various plant species. In wheat (*Triticum aestivum*), *TaemiR408* was shown to be of great importance for adaptation to Pi starvation, and its overexpression in tobacco (*Nicotiana tabacum*) increased Pi accumulation upon Pi deprivation by improving Pi absorption (Bai et al., 2018). In Pi-deprived plants, *TamiR1139* overexpression in wheat enhanced the phenotype, biomass, photosynthesis, and Pi acquisition, which suggested that *TamiR1139* was vital in plant Pi starvation tolerance by transcriptionally regulating the target genes and modulating the Pi stress–defense processes (Liu Z. et al., 2018). In *alfalfa* (*Medicago sativa*), under Pi deficiency, the expression of *miR399* and *miR398* was upregulated and the expression of *miR159*, *miR156*, *miR171*, *miR160*, and *miR2111* was downregulated (Li et al., 2018). In the woody tree *Betula luminifera*, the functions of *miR395*, *miR397*, *miR169*, and *miR399* in response to Pi starvation were hypothesized to affect downstream biological processes (Zhang et al., 2021). In brief, the functions of Pi-responsive miRNAs have been studied mainly in herbaceous plants. Many of these miRNAs are species-specific and regulate biological processes by binding to their target genes.

Camellia oleifera is a unique high-quality woody oil plant that grows in the hills and mountains of southern China and has a long history of cultivation and consumption. Tea oil is a high-quality edible oil rich in nutrients. The unsaturated fatty acid content of the oil is approximately 80%, and it is easily absorbed and digested by the human body, thus giving it the name "Oriental Olive Oil [*sic*]" (Shi et al., 2020). Suitable distribution areas of *C. oleifera* have red, yellow, or yellow-brown soil with pH values of 4.5–6.5; however, mineral nutrient deficiencies are common in these areas (Li et al., 2019). Pi deficiency reduces *C. oleifera* biomass and Pi accumulation and also affects germination and fruiting (Wu et al., 2019).

Until now, research on the adaptation of *C. oleifera* to low Pi has focused on the physiological aspects, and few reports focused on miRNAs (Zhou et al., 2020; Sun et al., 2021). The molecular mechanism of low Pi adaptation in *C. oleifera* requires further investigation to explain its resistance to low Pi. In this study, we aimed to identify miRNAs and their target genes that respond to under low Pi stress in the *C. oleifera*. For this, we combined the sRNA, degradome, and transcriptome sequencing data and generated an integrated resource for recognizing pivotal regulatory miRNA–target gene interactions in plants under low Pi stress. Our results will provide genetic resources for cultivating improved *C. oleifera* varieties that can adapt to low Pi environments and also provide a theoretical foundation for further alleviating the problems of Pi deficiency and environmental pollution.

Materials and methods

Plant materials and low phosphate stress treatment

Camellia oleifera "changlin166" cuttings (semi-lignified shoots and approximately 20 cm long) were collected from the Dongfanghong Forestry Farm in Jinhua City, Zhejiang Province, China, in June 2019. The cuttings from one single genotype were asexually propagated and cultivated and then grown in an artificial climate culture room under controlled conditions (25–28°C, 16-h light, 8-h dark). The experiment was performed in March 2021. First, individual plastic pots (19 × 11 cm) were filled with sand and placed in a climate chamber. Before beginning the treatment, the seedlings were irrigated every 3 days with a 1/2-strength Hoagland nutrient solution (Coolaber, China). Then, similarly developed plants were treated as follows: (1) control, 1/2-strength phosphorus-free Hoagland nutrient solution supplemented with 1 mM KH_2PO_4 and (2) low Pi treatment, 1/2-strength phosphorus-free Hoagland nutrient solution plus 5 μM KH_2PO_4. The pH of the nutrient solution was adjusted to 5.8 ± 0.1 by adding diluted HCl or NaOH. Then, 30 uniformly developed plants were divided into five groups, and a completely randomized block design with three replicates was used. Their roots were sampled at CK (control), 1, 3, 7, and 30 days, respectively. Fine powder (100 mg dry weight) was digested in a mixture of 5 mL 98% H_2SO_4 and 1 mL H_2O_2, and the P content was determined spectrophotometrically at 700 nm based on the molybdenum blue method (Sun et al., 2012). ATPase activity in the roots was analyzed using the modified p-nitrophenyl phosphate (NPP) method (Liu et al., 2004). Samples from the same batch were used for small RNA, transcriptome, and degradome high-throughput sequencing.

All collected root samples were frozen quickly in liquid nitrogen and stored at –80°C. Total RNA was extracted using the Total RNA Purification Kit (NORGEN, Thorold, ON, Canada). The RNA was treated with DNase I (Takara, Dalian, China) to remove any genomic DNA contamination. The integrity and concentration of RNA were measured by denaturing 1.2% (p/v) agarose gel electrophoresis and using a 2100 Bioanalyzer (Agilent Technologies, Santa Clara, CA, United States), respectively. The RNA concentrations of *C. oleifera* were 305.24–610.30 ng·μL^{-1}. Each sample had an RNA integrity number > 8.0.

To construct cDNA libraries for transcriptome sequencing, the mRNA was obtained from the total RNA using Oligo (dT) magnetic beads and fragmented. First-strand cDNA was synthesized using six random hexamer primers and reverse transcriptase. Second-strand cDNA was synthesized using second-strand buffer, DNA polymerase I, RNase H, and RNase-free deionized water. This was followed by end-repairing of the double-stranded cDNA, and an "A" residue was added to the 3′ end. Then, specific sequencing adapters were attached to both ends of the DNA fragments. The ligated cDNA fragments were purified by gel-tipping (generally, 200 500-bp-long fragments are recovered), and high-fidelity enzymes were used to amplify the sequencing libraries. For sequencing libraries, quality control of raw data, adapters, and trimers and cleanup of low-quality reads were performed by FastQC software. The final products were loaded onto an Illumina HiSeq^{TM} 2500 platform for transcriptome sequencing.

For sRNA sequencing, RNA was isolated from three replicates at five time periods and used to construct 15 sRNA libraries. Gel separation technology was used to collect 18- to 30-nt or 18- to 40-nt fragments in the samples, and adapters were ligated to their 5′ and 3′ ends. The fragments were used for cDNA synthesis, followed by PCR amplification and single-strand separation. The obtained single-stranded cDNA will be circularized and digested. The final products were sequenced on an Illumina HiSeq^{TM} 2500 platform.

Library construction was performed as described previously (German et al., 2008). Raw reads (single-end; 50 bp) with adapter or primer contamination were removed using Trimmomatic V0.35 (Bolger et al., 2014) to obtain clean degradome reads, which were then mapped to the *C. oleifera* transcriptome sequencing data.

Analysis of transcriptome sequencing data

To ensure that the reads were of high enough quality, the low-quality raw sequencing data were removed and clean reads were obtained. Trinity[1] with default parameters was used to evaluate the unigene sets obtained by assembling clean reads.

1 http://trinityrnaseq.github.io/

Then, the unigenes were searched against the NCBI non-redundant (nr[2]), Kyoto Encyclopedia of Genes and Genomes (KEGG[3]), and Gene Ontology (GO[4]) databases to obtain protein functional annotations and metabolic pathway information (Ünlü et al., 2021). Using the assembled unigenes as the reference, the reads in each sample were mapped to the reference sequences to obtain the read coverage of each unigene in each sample, and then the fragments per kilobase of exon model per million mapped fragments (FPKM) normalization formula was applied to normalize the number of enriched fragments. Differentially expressed genes (DEGs) were identified between the different samples using DE-Seq software (Kvam et al., 2012). A gene was considered to be differentially expressed with $|\log2(\text{foldchange})| > 1$ and $p\text{-value} \leq 0.05$.

Analysis of the sRNA sequencing data

Adapters, low-quality sequences, regions of low complexity, and common RNA families (tRNA, rRNA, snRNA, and snoRNA) were removed using RFam.[5] Clean and unique reads were aligned to the miRBase database (v22.0)[6] using BLAST to identify known miRNAs (Ling et al., 2014). The parameters for known and novel miRNAs and their precursor structure identification were referenced by Axtell and Meyers (2018). The sRNA sequencing data from 15 samples have been deposited in the NCBI SRA database[7] under accession numbers SRR18672953–SRR18672967. Differentially expressed miRNAs with $|\log2(\text{foldchange})| > 1$ and adjusted p-values < 0.05 were selected for further analysis.

Analysis of degradome sequencing data

Adapter and low-quality sequences obtained by sequencing using the Illumina HiSeq^{TM} 2500 platform were removed, and the adaptor and the clean reads were compared with the assembled unigene reference sequences to obtain the degraded mRNA fragments. Then, miRNA–mRNA degradation sites were analyzed using CleaveLand 4.0[8] (Addo-Quaye et al., 2009). The target genes were divided into five categories (0, 1, 2, 3, and 4) based on their transcript abundance levels. The predicted target genes were searched against the NCBI nr and nt databases and Swiss-Prot to annotate them. The candidate target genes were functionally annotated by GO and KEGG enrichment analyses.

cDNA and miRNA syntheses and analyses of gene transcription levels

In total, eight miRNA–target genes were randomly selected for fluorescent qPCR analysis. Reverse transcription was performed using an Mir-X^{TM} miRNA First Strand Synthesis Kit (Takara, Dalian, China) and a PrimeScript^{TM} RT Master Mix (Perfect Real Time) Kit (Takara, Dalian, China) according to the manufacturers' instructions. The expression levels of the miRNAs and their target genes were determined using an Mir-X miRNA qRT-PCR TB Green® Kit (Takara, Dalian, China) and TB Green® Premix Ex Taq^{TM} II (Tli RNaseH Plus) (Takara, Dalian, China), respectively, on a 7300 Real-Time PCR System (Applied Biosystems, CA, United States). Each sample was run in triplicate. The expression levels of the mRNAs and miRNAs were normalized to 18S rRNA and GAPDH, respectively (Zhou et al., 2013), and were calculated using the $2^{-\Delta\Delta Ct}$ method (Livak and Schmittgen, 2001). The primers for miRNAs and their target genes are listed in **Supplementary Table 1**.

Co-expression network construction

Weighted gene co-expression network analysis (WGCNA) is the systematic biology method for analyzing the correlation patterns among differentially expressed genes across different samples (DiLeo et al., 2011; de Jong et al., 2012). A co-expression network analysis package is freely available at: https://horvath.genetics.ucla.edu/html/CoexpressionNetwork/Rpackages/WGCNA (Langfelder and Horvath, 2008). In brief, the expression profiles of all expressed genes under Pi stress conditions were used to construct a co-expression network. A matrix of pairwise correlation coefficients was used to construct a weighted adjacency matrix that contains pairwise connection strengths using the soft threshold method (power = 6) (de Jong et al., 2012). Rank clustering was performed based on the similarity between genes, and then, the genes with consistent expression in the gene cluster tree are partitioned into the same module (Zhang and Horvath, 2005). Each module is represented by a color, and gene expression profiles were summarized for each module using module signature genes. The gene expression profiles of each module were summarized by the module eigengene and defined as the first principal component of the module expression levels. The targets of differentially expressed miRNAs were selected as hub genes. To display the hub genes, we used Cytoscape software (v3.9.1)[9] to produce a gene regulatory network diagram based

2 https://www.ncbi.nlm.nih.gov/refseq/about/non-redundantproteins/

3 https://www.genome.jp/kegg/

4 http://geneontology.org/

5 http://rfam.janelia.org

6 http://www.mirbase.org/

7 https://www.ncbi.nlm.nih.gov/sra/?term=

8 https://github.com/MikeAxtell/CleaveLand4

9 https://cytoscape.org/download.html

on the data obtained from the transcriptome and degradome analyses (Zhang et al., 2020). Genes with the same or similar functions were classified into one group by GO annotation.

Results

Phosphate deprivation alters physiological characteristics

After 30 days of Pi starvation, the root/shoot ratio was increased significantly in roots, and the Pi content in shoots was decreased significantly. However, ATPase activity in roots increased significantly under Pi deprivation. The seedlings of *C. oleifera* showed attenuated growth and increased root biomass after 30 days of Pi starvation (**Figure 1**).

Transcriptome sequencing in *Camellia oleifera* roots under low phosphate treatments

Transcriptome libraries were constructed using the extracted total RNA, and 29,389,514 assembled bases were generated. After removing low-quality reads, the remaining high-quality reads were assembled into 40,689 unigenes. Details of the transcriptome sequencing of *C. oleifera* are shown in **Table 1**. The unigenes were annotated by sequence alignments to a number of different databases. The BLASTX results identified 27,027 unigenes that were homologs of sequences in the nr database. A total of 23,423 and 18,713 genes were annotated with enriched GO terms and KEGG pathways, respectively. In the low Pi treatment groups, 2,787, 1,657, 1,413, and 4,548 genes were upregulated and 2,666, 1,845, 2,189, and 3,929 genes were downregulated at 1, 3, 7, and 30 days, respectively, compared with their expression levels in the corresponding control groups, and 1,586 differentially expressed mRNAs were common to all the time periods (**Supplementary Figure 1**). The heatmap of the gene expression level (top 3,000 genes with large expression variation) is shown in **Supplementary Figure 2**. The FPKM of all unigenes is shown in **Supplementary Table 2**.

Sequencing and identification of known and novel miRNAs

An overview of the obtained raw and clean sequences is given in **Supplementary Table 3**, and the 18- to 25-nt-long sequences obtained after deleting low-quality sequences are listed in **Supplementary Table 4**. The number distribution of the sRNAs is shown in **Supplementary Figure 3**. The length of *C. oleifera* sRNAs was 18–24 nt long, and the 21-nt sRNAs

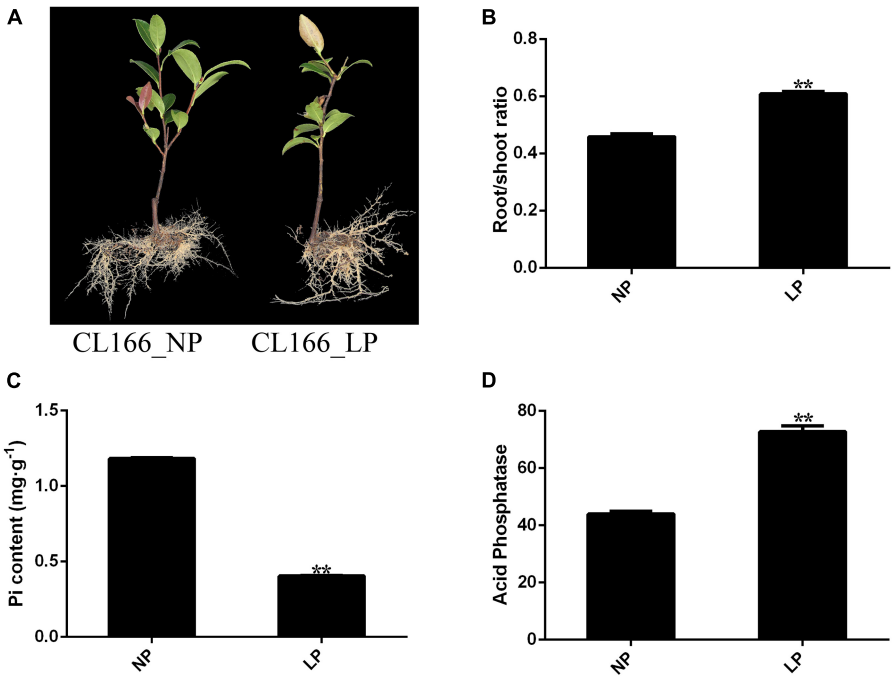

FIGURE 1
(A) Changes in phenotype. **(B)** Root/shoot ratio. **(C)** Pi content. **(D)** Acid phosphate. Bars indicate means ± SE (n = 4). P-values were obtained from t-tests between LP and NP condition. $^{**}P < 0.01$.

TABLE 1 Summary of Illumina transcriptome sequencing for *Camellia oleifera*.

Species	*C. oleifera*
Total assembled bases	29,389,514
Number of genes	40,689
N50 length (bp)	1,045
GC (%)	42.57
GO	23,423
KEGG	18,713
Pfam	20,259
swissprot	19,315
EggNOG	26,203
NR	27,027

were the most abundant in all 15 libraries. A total of 386 miRNAs were found and divided into four separate groups (Figure 2). A total of 214 pre-miRNAs had the highest degree of similarity with 275 known unique mature miRNAs in 63 miRNA families (Supplementary Figure 4), which had a high degree of similarity compared to other known miRNAs. A total of 70 pre-miRNAs corresponding to 68 mature miRNAs were recognized as novel miRNAs (Supplementary Table 5). Among them, miRNAs of a length of 21 nt made up 38.99% of the known miRNAs, and miRNAs of a length of 24 nt made up 45.59% of the novel miRNAs (Supplementary Table 6). The free energy (dG) and minimum folding free energy index (MFEI) of predicted pre-miRNAs ranged from −17.1 to −93.4 kcal/mol and from 0.9 to 1.7 kcal/mol, respectively (Supplementary Table 7). These characteristics maintain the stability of the hairpin structures of the pre-miRNAs.

miRNAs that respond to low phosphate in *Camellia oleifera* roots

To identify miRNAs involved in the response to Pi deficiency, the expression levels of miRNAs in the five time periods were analyzed and compared. A total of 32 miRNAs

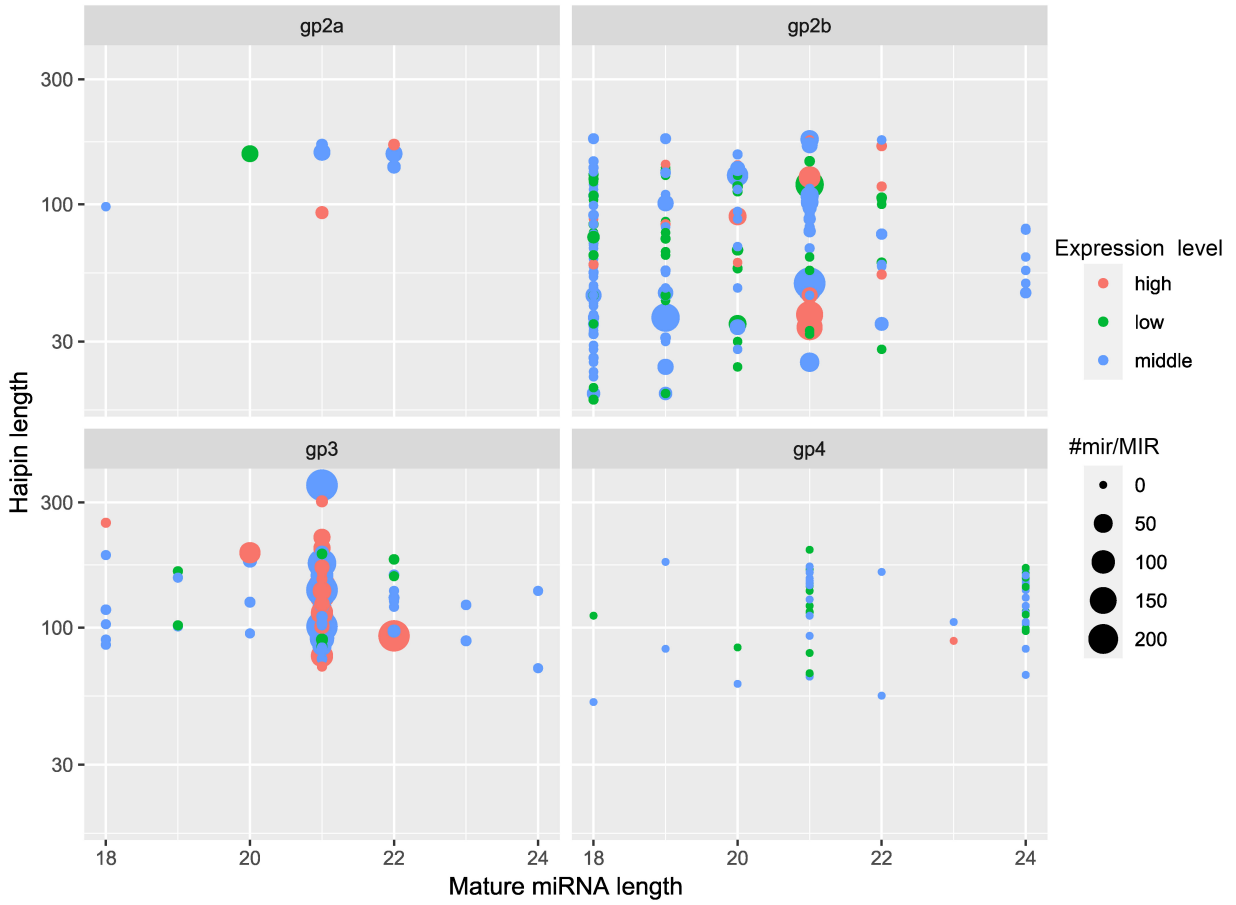

FIGURE 2
Summary of the classification of the four identified groups of miRNAs in *C. oleifera*. Counts MIRb, the counts of miRNAs from miRBase; expression level, low indicates < 10; middle indicates > 10 but less than average; high indicates over average.

($p < 0.05$) showed differential expression patterns; among them, 29 were known miRNAs and three were novel miRNAs. A heatmap of differentially expressed miRNAs is shown in Figure 3A. Some members of the same miRNA families had similar expression patterns. For example, two miRNA167s and three miRNA393 were significantly upregulated after low Pi stress for 7 days, and two of the novel miRNAs (*PC-3p-24651_983* and *PC-5p-174389_91*) were upregulated, and one (*PC-3p-132795_129*) was downregulated (Figure 3A). We counted the distribution of 32 differential miRNAs between the control and treatments groups (Figure 3B). The largest number (17) of upregulated miRNAs was found after low Pi treatment for 1 day, and five miRNAs were significantly downregulated after low Pi treatment for 3 days compared with their expression levels in the corresponding controls (Figure 3B). These findings indicate that the duration of the low Pi treatment may have a short-run effect on the miRNA expression levels.

Prediction of the target genes of the known and novel miRNAs by degradome sequencing

The degradome sequencing generated 61,520,868 raw reads, representing 19,066,404 unique reads from the mixed degradome pool. After removing the low-quality reads and the reads that lacked the adapters, 58,817,780 (95.61% of all reads) sequences were successfully mapped to the 40,689 unigenes. The candidate target genes were divided into five categories, namely, 0, 1, 2, 3, and 4, based on the abundance of degradation sites and transcripts (Addo-Quaye et al., 2009). To select the most credible genes for analysis, we set the alignment score ≤ 4 and category ≤ 2 and obtained 52, 2, and 360 target genes in categories 0, 1, and 2, respectively (Supplementary Table 8). Among the novel miRNAs, 13 miRNAs targeted 21 different genes. In order to predict their authenticity, the target sites of miRNAs and their targets were aligned by psRNATarget[10] in Supplementary Table 9 (Dai and Zhao, 2011). In addition, t-plots were also constructed to show the cleavage sites for each miRNA–mRNA pair (Supplementary Figure 6).

A total of 414 target genes for 108 miRNAs were identified from the mixed degradome sequencing data; of the 414 target genes, 51 of the miRNAs were predicted to regulate a single gene and 56 of the miRNAs were predicted to regulate two or more genes (Supplementary Table 8). Target genes of 14 novel miRNAs were also obtained by degradome sequencing; eight of them were predicted to regulate a single gene and six novel miRNAs were predicted to regulate two or more genes (Table 2). The length distribution of the novel miRNAs was similar to that of the known miRNAs. We also found that the expression levels of different miRNAs in the same family were different.

10 https://www.zhaolab.org/psRNATarget/analysis?function=3

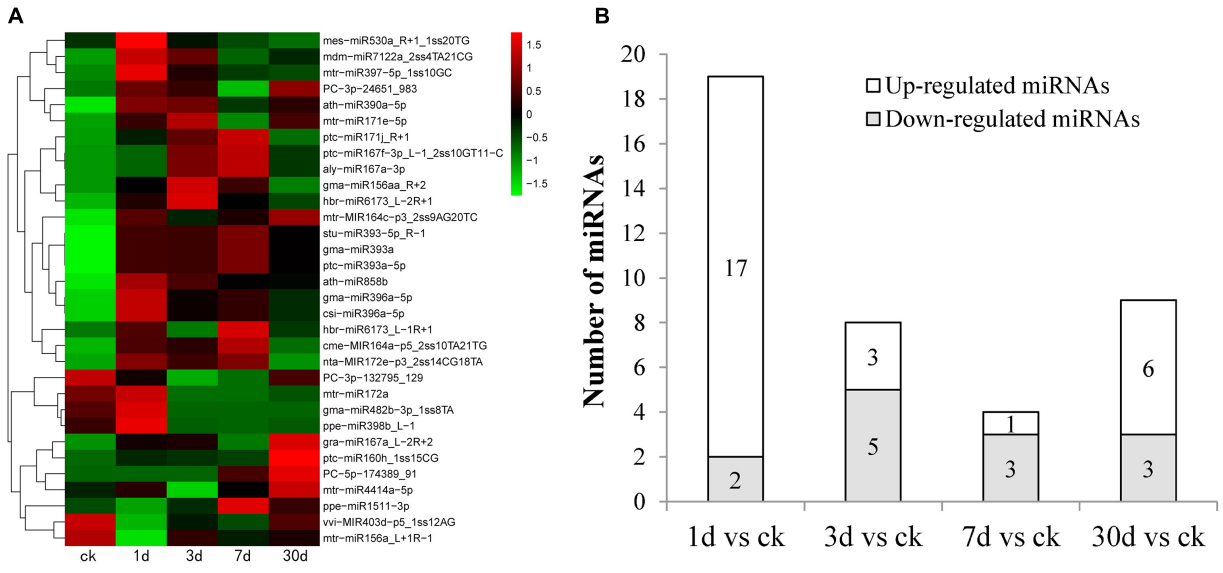

FIGURE 3
Phosphorus (Pi) deficiency and miRNAs in *C. oleifera*. **(A)** Differential expressed miRNAs in five different low Pi treatment durations (CK, 1, 3, 7, and 30 days) by miRNAs hierarchical clustering. Red indicates higher levels of miRNAs and green indicates lower levels of miRNAs. The names of the samples are shown at the bottom. The original expression values of the miRNAs were normalized using Z-score normalization. The absolute signal intensity ranges from −1.5 to +1.5, with corresponding color changes from green to red. **(B)** The number of differentially expressed miRNAs under Pi deficiency compared with the control.

TABLE 2 Target genes of 14 novel miRNAs and their functional annotation.

Small RNA	Targets	Alignment score	Cleavage site	Category	Target annotation	Biological process
PC-3p-100894_182	TRINITY_DN30301_c0_g3	4	823	2	LRR receptor-like serine/threonine-protein kinase	Protein kinase activity
PC-3p-132795_129	TRINITY_DN33563_c0_g5	4	297	2	Unknown	Nucleic acid binding
PC-3p-132795_129	TRINITY_DN35456_c0_g2	4	747	2	Calcineurin-binding protein like	–
PC-3p-18140_1384	TRINITY_DN31490_c2_g1	3.5	25	2	Unknown	–
PC-3p-27079_883	TRINITY_DN42730_c0_g2	3	17	2	Unknown	–
PC-3p-30509_767	TRINITY_DN42730_c0_g2	2.5	26	2	Unknown	–
PC-3p-346339_35	TRINITY_DN33230_c0_g2	3	870	2	Branched-chain-amino-acid aminotransferase	–
PC-3p-346339_35	TRINITY_DN42258_c0_g3	4	413	2	Ankyrin repeat-containing protein	Signal transduction
PC-3p-41728_531	TRINITY_DN28460_c0_g1	4	439	2	U3 small nucleolar ribonucleoprotein protein MPP10	Small-subunit processome
PC-3p-41728_531	TRINITY_DN34544_c0_g6	3.5	1733	0	Glycerol-3-phosphate transporter 1 like	Transmembrane transport
PC-3p-41728_531	TRINITY_DN38304_c0_g1	3.5	755	2	Zeaxanthin epoxidase	Secondary metabolite biosynthetic process
PC-3p-44318_495	TRINITY_DN40647_c2_g5	3	71	2	Unknown	–
PC-3p-44318_495	TRINITY_DN42805_c2_g2	4	582	2	Methyl-CpG-binding domain-containing protein	Regulation of transcription
PC-3p-459616_23	TRINITY_DN38590_c0_g4	3	431	2	Hypothetical protein MANES_08G157000	Regulation of transcription
PC-3p-545895_17	TRINITY_DN34459_c0_g1	3.5	144	2	Proteasome subunit alpha type-2-A	Proteasome activity
PC-3p-545895_17	TRINITY_DN45451_c1_g1	3	344	2	Unknown	–
PC-3p-545895_17	TRINITY_DN46149_c1_g4	4	411	2	Unknown	–
PC-3p-66331_303	TRINITY_DN30968_c2_g4	4	101	2	Unknown	–
PC-3p-66331_303	TRINITY_DN44551_c1_g4	4	211	2	AMP deaminese	AMP deaminase activity
PC-3p-90001_209	TRINITY_DN42730_c0_g2	3	15	2	Unknown	–
PC-5p-115327_154	TRINITY_DN24873_c3_g4	2	94	2	Unknown	–
PC-5p-182503_85	TRINITY_DN34544_c0_g6	4	1742	2	Glycerol-3-phosphate transporter 1 like	Transmembrane transport

These results suggest that different miRNAs may have different mechanisms adapted to Pi deficiency in *C. oleifera* roots.

Annotation and enrichment analysis of the target genes for miRNAs

The 414 target genes were annotated with terms under the three main GO categories: biological process, cellular component, and molecular function. The enriched terms were visualized using REVIGO software (Liu et al., 2015) and plotted (**Figure 4**). Under biological processes, the plant hormone signaling pathways (GO:0009873 ethylene-activated signaling pathway, GO:0009734 auxin-activated signaling pathway, and GO:0009738 abscisic acid-activated signaling pathway) and their response to the stimulus (GO:2000306 positive regulation of photomorphogenesis, GO:0048768 root hair cell tip growth, and GO:0071281 cellular response to iron ion) were enriched, which are consistent with the current understanding of Pi deficiency. Under the cellular component, the nucleus and membrane components were the most enriched term. Under molecular function, DNA binding was the most enriched term, and enzymatic activities (GO:0004842 ubiquitin protein transferase activity, GO:0046522 S-methyl-5-thioribose kinase activity, and GO:0004721 phosphoprotein phosphatase activity) were also enriched, which suggests that these enzymes may play essential roles under low Pi conditions.

The top 20 most enriched KEGG pathways are shown in **Figure 4B**. Among them, biosynthesis of secondary metabolites (ko01110) and plant hormone signal transduction (ko04075)

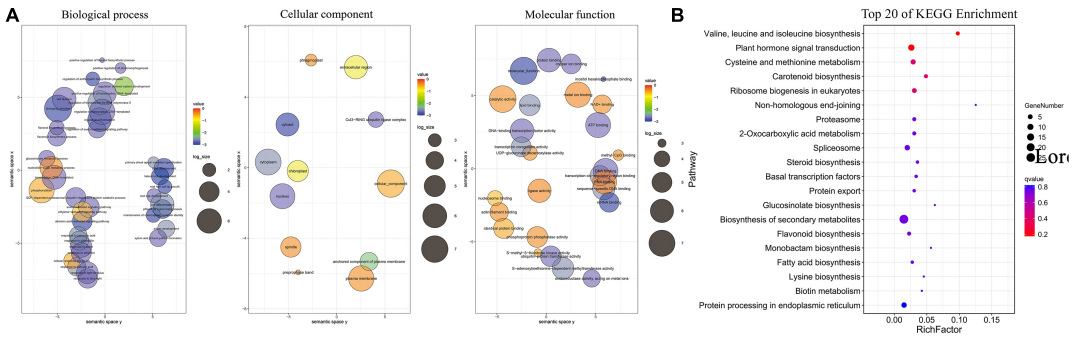

FIGURE 4
Gene ontology (GO) and Kyoto Encyclopedia of Genes and Genomes (KEGG) functional classification of identified target genes. **(A)** GO enrichment analysis for targets of DE miRNAs under conditions of phosphate (Pi) starvation. **(B)** KEGG Enrichment Analysis for Targets of DE miRNAs under conditions of Pi starvation.

were the most enriched pathways, which is consistent with GO enrichment results. Plant hormones, such as auxin, salicylic acid, jasmonic acid, ethylene, and gibberellin, are known to be involved in the response to Pi deficiency.

Correlation analysis of the expression profiles of the miRNAs and their target genes

To investigate changes in the whole transcriptome of *C. oleifera* roots under different Pi treatments, the assembled unigenes were used to analyze the differentially expressed genes. In a survey, 48 genes were the targets of 33 miRNAs, which responded to low Pi tolerance (Table 3), and 31 of the miRNA–target genes were negatively correlated with the absolute value of the negative correlation coefficient greater than 0.5 (Figure 5). For example, *ptc-miR160h_1ss15CG* was significantly downregulated and its target auxin response factor 22 (*ARF22*, TRINITY_ DN39928_c3_g4) was significantly upregulated and *mtr-miR171d* was upregulated and its target *SCL6* (Scarecrow-like protein, TRINITY_DN38636_c0_g1) was downregulated under Pi deficiency.

A RT-qPCR analysis was conducted to verify the expression profile of eight key miRNA–target pairs. The results showed that the expression trends of the eight miRNAs and target genes were similar to those obtained by deep sequencing (Figure 6). The expression levels of the eight miRNA–target pairs were confirmed to be negatively correlated. For example, *mtr-miR160a* and *ptc-miR160h_1ss15CG* were upregulated and then downregulated at the longer time periods, and their target genes showed significant opposite expression patterns. These results suggest that transcription of the target mRNAs may be repressed by the corresponding miRNAs (Figure 6). These results suggest that transcription of the target miRNAs may be repressed by the corresponding miRNAs (Figure 6).

Gene co-expression network analysis

After removing unexpressed and lowly expressed genes, we identified 34 gene co-expression modules that contained 40,689 unigenes (Supplementary Figure 5). We constructed a co-expression regulatory network based on different modules (Figure 7). To explore the network connections for the target genes, we focused on three of the differentially expressed target genes (*ARF22*, *ptc-miR160h_1ss15CG* target gene; *WRKY53*, *mtr-miR2592ao-p5_2ss1AT18TC* target gene; and *SCL6*, *mtr-miR171d* target gene), which were hub genes, which may play important roles in low Pi stress. A complete list of the module assignments for the three hub genes is provided in Supplementary Table 10. In the network, the three hub genes *ARF22*, *WRKY53*, and *SCL6* are directly connected with 735, 46, and 272 edge genes, respectively. These hub genes will provide a foundation for future studies.

We also created a subnetwork containing 390 genes that were annotated with six GO terms related to the response to stimulus, signaling, binding, catalytic activity, biological process, and transporter activity (Figure 7); 94, 44, and 20 of these genes were annotated in the response to stimulus, signaling, and transporter activity terms, respectively (Supplementary Table 11). In the subnetwork, there were three signaling-related transcription factors as hub genes that may be involved in Pi uptake, transport, and homeostasis, and four transporter-related members of the ABC family also may promote Pi uptake and transport. When plants experience Pi deficiency, phosphate transporter and vacuolar H^+ pyrophosphatase together maintain Pi balance.

Discussion

Camellia oleifera is a woody oil plant that grows in southern China. It is frequently exposed to low Pi availability in red

TABLE 3 Pi deficiency expressed miRNAs and their targets.

miRNA family	miRNA name	Targets	Annotation
miR160	ahy-miR160-5p_L+1_1ss16AT	TRINITY_DN37578_c1_g1	Auxin response factor 10
		TRINITY_DN39928_c3_g4	Auxin response factor like
	ptc-miR160h_1ss15CG	TRINITY_DN37578_c1_g1	Auxin response factor 10
		TRINITY_DN39928_c3_g4	Auxin response factor like
	mtr-miR160a	TRINITY_DN37578_c1_g3	Auxin response factor like
miR4248	aly-MIR4248b-p3_2ss8TC18AC	TRINITY_DN31971_c2_g3	Pumilio 1 like
		TRINITY_DN39965_c1_g1	Mediator of RNA polymerase II transcription subunit 26c
		TRINITY_DN44758_c0_g1	MKI67 FHA domain-interacting nucleolar phosphoprotein
miR399	aqc-miR399	TRINITY_DN34998_c0_g3	Ubiquitin-conjugating enzyme E2 24
	mtr-miR399c	TRINITY_DN25615_c1_g4	–
miR171	mtr-miR171d	TRINITY_DN23484_c2_g1	Scarecrow-like protein 15
		TRINITY_DN27835_c0_g1	Scarecrow-like protein
	ptc-miR171j_R+1	TRINITY_DN35708_c0_g1	Zinc finger SWIM domain-containing protein
	mtr-miR171e-5p	TRINITY_DN43082_c0_g1	PREDICTED: mitochondrial outer membrane protein porin of 34 kDa
	gma-miR171k-3p_2ss11CT19AT	TRINITY_DN38636_c0_g1	Scarecrow-like protein
		TRINITY_DN38636_c0_g5	Scarecrow-like protein 6
miR2592	mtr-MIR2592ao-p5_2ss1AT18TC	TRINITY_DN26826_c0_g2	PREDICTED: uncharacterized protein LOC100245641
		TRINITY_DN26936_c0_g1	WRKY transcription factor
		TRINITY_DN44535_c0_g3	Sucrose phosphate phosphatase
	mtr-MIR2592ay-p5_2ss6AG17CG_2	TRINITY_DN35276_c4_g2	Transcription termination factor like
		TRINITY_DN39805_c0_g1	7-deoxyloganetin glucosyltransferase-like isoform X1
	mtr-MIR2592bj-p5_2ss12TC19AT	TRINITY_DN35421_c0_g1	Eukaryotic translation initiation factor 4B3 like
miR408	mtr-miR408-3p_L-1R-1	TRINITY_DN27457_c0_g1	Ethylene-responsive transcription factor RAP2-3-like isoform X2
		TRINITY_DN31259_c0_g3	Flavanone 3-hydroxylase
	mtr-miR408-3p_L-1R-2	TRINITY_DN26569_c0_g2	Copper-transporting ATPase
		TRINITY_DN32565_c0_g9	Basic blue protein
	mtr-MIR408-p3_1ss13CT	TRINITY_DN32465_c1_g6	Unknown
		TRINITY_DN35836_c1_g2	Transcription factor bHLH83
	stu-miR408b-3p	TRINITY_DN26662_c1_g5	Unknown
miR172	gma-miR172a	TRINITY_DN40809_c0_g1	Ethylene-responsive transcription factor like isoform 2
	gma-miR172b-5p_L-1R+2	TRINITY_DN32888_c2_g5	LMBR1 domain-containing protein 2 A like
	stu-miR172a-3p	TRINITY_DN28507_c2_g5	Ethylene-responsive transcription factor RAP2-7 like
	vvi-MIR172d-p5_2ss7GT17CT	TRINITY_DN25739_c0_g1	Ribosome biogenesis regulatory protein, partial
	mtr-miR172a	TRINITY_DN41667_c0_g2	Ethylene-responsive transcription factor RAP2-7 like
miR169	ppe-MIR169i-p3_1ss17GT	TRINITY_DN38370_c1_g6	General transcription factor 3C polypeptide like
	ppe-MIR169i-p3_2ss1CT19GT	TRINITY_DN41819_c0_g4	Transcription factor HHO3-like
	ppe-MIR169i-p5_1ss16GT	TRINITY_DN26297_c0_g2	ABC transporter C family member 3 like, partial
	ptc-MIR169o-p5_2ss1AC17TC	TRINITY_DN44254_c0_g1	Unknown
miR156	ptc-miR156a_L+1	TRINITY_DN32530_c0_g1	Squamosa promoter-binding-like protein
	ptc-MIR156l-p3_2ss4TC17TA	TRINITY_DN41932_c0_g3	Transcription elongation factor like
	mtr-miR156a_L+1R-1	TRINITY_DN40091_c1_g7	Squamosa promoter-binding-like protein
miR472	ath-MIR472-p3_2ss6TG18AG	TRINITY_DN37745_c0_g2	F-box/FBD/LRR-repeat protein
miR858b	ath-miR858b	TRINITY_DN31256_c0_g4	Myb-related protein
		TRINITY_DN31679_c2_g2	Transcription factor MYB5e
		TRINITY_DN42660_c1_g4	Transcription factor MYB5b
Novel miRNA	PC-3p-346339_35	TRINITY_DN33230_c0_g2	Branched-chain-amino-acid aminotransferase
		TRINITY_DN42258_c0_g3	Ankyrin repeat-containing protein
	PC-3p-41728_531	TRINITY_DN28460_c0_g1	U3 small nucleolar ribonucleoprotein protein MPP10
		TRINITY_DN34544_c0_g6	Glycerol-3-phosphate transporter 1 like
		TRINITY_DN38304_c0_g1	Zeaxanthin epoxidase
	PC-5p-182503_85	TRINITY_DN34544_c0_g6	Glycerol-3-phosphate transporter 1 like

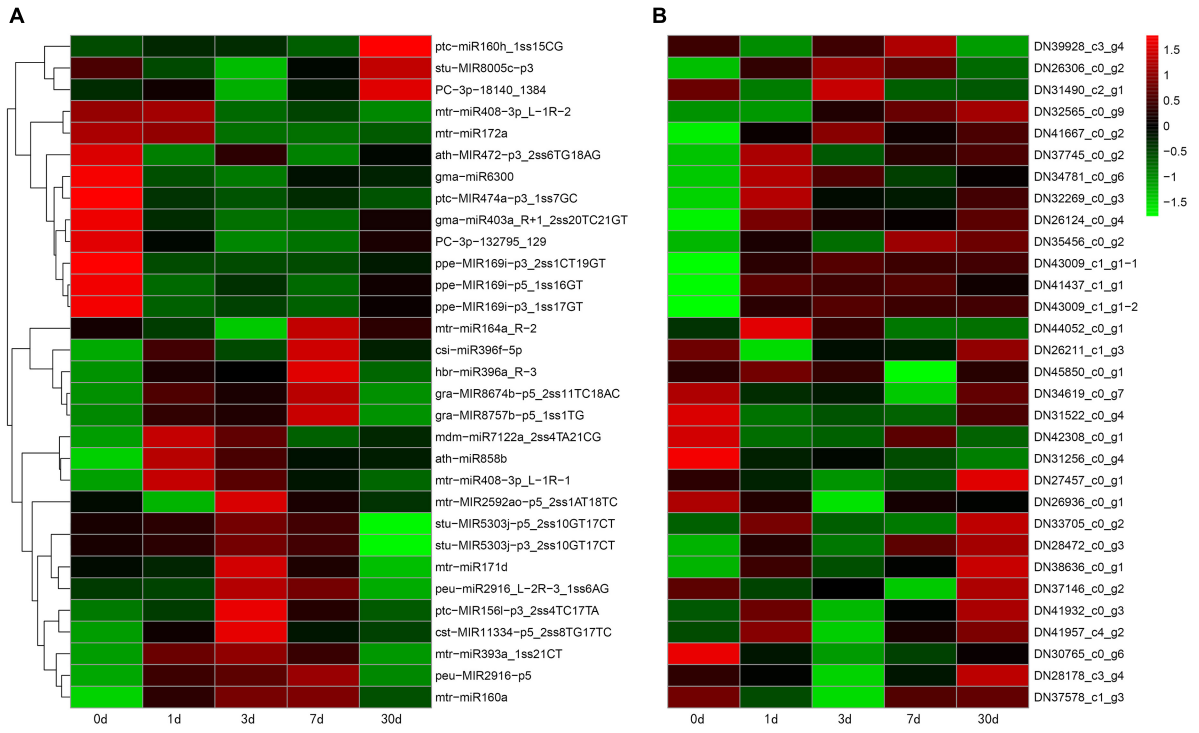

FIGURE 5
Combined view of expression levels between differentially expressed miRNAs **(A)** and their target genes **(B)** in *C. oleifera* at five different Pi treatment durations. The original expression values of miRNAs and their target genes were normalized by Z-score normalization.

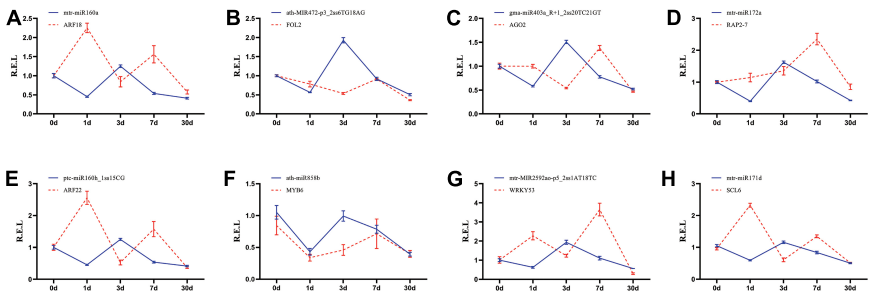

FIGURE 6
Expression correlation between miRNAs and their targets at five different Pi treatment durations. **(A)** *mtr-miR160a/ARF18*; **(B)** *athMIR472p3_2ss6TG18AG/FOL2*; **(C)** *gmamiR403a_R + 1_2ss20TC21GT/AGO2*; **(D)** mtr-miR172a/RAP2-7; **(E)** ptc-miR160h_1ss15CG/ARF22; **(F)** *ath-miR858b/MYB6*; **(G)** *mtr-MIR2592ao-p5_2ss1AT18TC/WRKY53*; **(H)** *mtr-miR171d/SCL6*; The blue and red lines indicate miRNAs and the target abundance, respectively, based on the RT-qPCR results.

soils and has evolved a suite of adaptive mechanisms to cope with conditions of Pi deficiency. Understanding the potential molecular mechanisms is essential for screening germplasm resources resistant to low Pi. The regulation of plant resistance to nutritional deficiency by the miRNA–target gene interactions has been described in several herb plants. However, the molecular mechanisms underlying the responses of woody plants to Pi deficiency are poorly understood. In this study, we performed an integrated analysis to investigate the regulatory network in the roots of *C. oleifera* under Pi deficiency based on miRNA, degradome, and transcriptome sequencing data. Our results showed that the genes targeted by miRNAs play important roles in response to Pi deficiency in the roots. Although our findings provide some understanding of the low Pi adaptation mechanisms, many more studies are needed to gain a comprehensive understanding of the miRNA–target genes of Pi deficiency.

miRNAs have been studied in many plants, but very few studies have been conducted on plants in the family *Theaceae*, which includes *C. oleifera*. In this study, the transcriptome

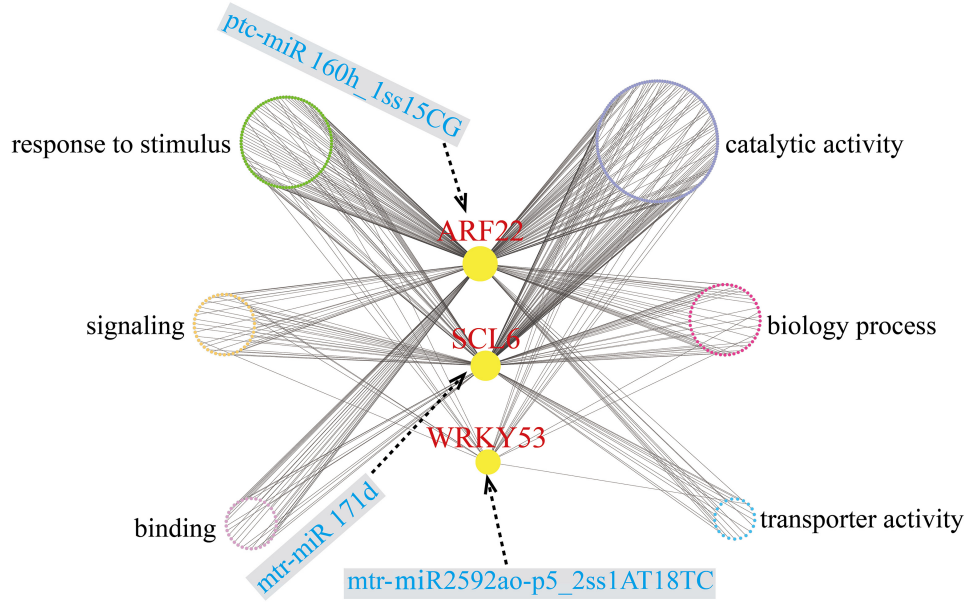

FIGURE 7
Co-expression subnetwork of *ARF22*, *WRKY53*, and *SCL6*. Red-colored letter denotes key hub gene; blue-colored letter denotes key miRNA; six different colored circles represent six different categories.

sequences of *C. oleifera* were used as reference sequences for the miRNA and the degradome sequencing analysis. The relationship between miRNAs and target genes was obtained by degradome sequencing. Then, the miRNA–target gene network regulation map showed that the regulation of multiple target genes could be regulated by one miRNA and that one target gene could be regulated by multiple miRNAs. A total of 386 miRNAs were identified and divided into four groups (**Figure 2**), out of which 284 of them were highly confident miRNAs. Only 14% of them were relatively highly expressed, confirming that high-throughput sequencing can identify miRNAs with low expression levels in plants. The length of mature miRNAs was 18–24 nt (**Supplementary Figure 3**), which is consistent with previous results in plants such as alfalfa (Li et al., 2018), wheat (Bai et al., 2018), *Betula luminifera* (Zhang et al., 2021), poplar (*Populus tomentosa*) (Bao et al., 2019), and pine (*Pinus massoniana*) (Fan F. et al., 2021).

We identified 32 differentially expressed miRNAs (29 conserved and 3 novel miRNAs) under low Pi stress (**Figure 3A**). Different members of the same miRNA family had similar expression levels; for example, three *miR393* and two *miR171* family members were significantly upregulated under low-Pi conditions. Similar phenomena were also found in other species. In *Arabidopsis*, *miR393s* play important roles in the root system architecture of Pi deficiency and nitrogen deprivation (Vidal et al., 2010). In *Populus tomentosa*, the expression of *miRNA171e* decreased after 24 h of Pi deficiency and then increased dramatically when Piwas supplied (Bao et al., 2019). In maize (*Zea mays*), under low Pi stress, members of the miR393 family were differentially expressed in the leaves and roots (Gupta et al., 2017). In *Medicago truncatula*, *miR171h* is involved in integrating nutrient homeostasis by regulating the expression of *NSP2* during arbuscular mycorrhizal and root nodule symbiosis (Hofferek et al., 2014). Therefore, *miR393* and *miR171* show different expression patterns in response to low Pi in different plants. In our study, we found two miR167 and two miR396 family members that were significantly upregulated by Pi deficiency. In maize, members of the miR396 family were differentially expressed by Pi starvation, *zma-miR396a* expression was continuously suppressed by Pi starvation, *miR396c* expression was slightly increased during the early phase of low Pi stress, and *zma-miR396d* was significantly upregulated in maize leaves (Nie et al., 2016). We also found two miR156 family members that showed contrary expression patterns in *C. oleifera* roots. *miR156* is a highly conserved miRNA that plays key roles in many biological processes, including developmental and metabolic regulation, immune response, and abiotic stress. In *Arabidopsis*, members of the miR156 family responded to phosphate deprivation and played a potential role in phosphate homeostasis (Hsieh, 2010). Together, these results indicate that miRNAs have diverse functions in plants, and the complex mechanisms need to be further explored in future studies.

We used the transcriptome sequences as reference sequences and analyzed the correlation between miRNAs and their target genes by degradome sequencing. Many target transcripts were identified for the known and novel miRNAs (Han et al., 2016). Mature miRNAs regulate their target

mRNAs by forming an miRNA-induced silencing complex that cleaves miRNA or inhibits its translation, thereby negatively regulating the target genes (Sun et al., 2019). miRNAs are known to be involved in abiotic and biotic stresses in plants, and miRNAs can be expressed to act on target genes under abiotic stresses (Cui et al., 2020; Li and Yu, 2021; Ma et al., 2021). We identified 414 genes that were predicted to be targeted by 108 corresponding miRNAs by degradome sequencing (**Supplementary Table 8**). We also identified 30 differentially expressed target genes that were targeted by 31 miRNAs, and most of these miRNA–target gene pairs had opposite expression patterns (**Figure 4**), including *ptc-miR160h_1ss15CG*, which was significantly downregulated under Pi deficiency, whereas its target gene *ARF22* (TRINITY_DN39928_c3_g4) was significantly upregulated. However, in *Arabidopsis*, *miR160* and its target genes *ARF16*, *ARF10*, and *ARF17* regulate hypocotyl elongation in a light, brassinazole (BRZ, a BR biosynthesis inhibitor), or paclobutrazol (PAC, a GA biosynthesis inhibitor)-dependent manner (Dai et al., 2021). This finding also indicates that the same miRNA can regulate different target gene pairs and play different roles in different plants.

miR399 is responsive to Pi starvation and plays important regulatory roles in Pi homeostasis (Pegler et al., 2020, 2021; Peng et al., 2021). In our study, two miR399 members, *miR399* and *miR399c*, which regulated six and 11 mRNAs, respectively, were detected by the analysis of our degradome sequencing data (**Supplementary Table 12**). However, *miR399* and *miR399c* were not differentially expressed miRNAs, suggesting that *C. oleifera* may have evolved some other miRNAs in response to low Pi stress. In addition, *miR827* was absent in the present sRNA libraries; the possible reason is the lack of its precursor sequence in the draft genome, which led to the loss of *miR827* during evolution or the failed match during sRNA library construction. Similar phenomena were observed in *B. luminifera* and *C. papaya*, in which the *miR827* locus was lost during evolution (Lin et al., 2018; Zhang et al., 2021).

There are 199 miRNA-target genes whose expression levels are negatively correlated (**Supplementary Table 13**). Overall, three transcription factors as hub genes, *ARF22*, *WRKY53*, and *SCL6*, may play pivotal roles in the regulation of low Pi-responsive genes through a co-expression regulatory network and are critical mediators in regulating various abiotic stresses (Wang X. et al., 2021). In durum wheat (*Triticum turgidum* subsp. *Durum*), *ttu-miR160* was upregulated, and its target *ARF22* was significantly downregulated in roots under chronic and short-term nitrogen stress (Zuluaga et al., 2018). In rice, several miR160s were downregulated in roots and shoots under heat stress (Sailaja et al., 2014). In our study, *ARF22* was targeted by *ptc-miR160h_1ss15CG*, and *ptc-miR160h_1ss15CG* was slightly downregulated at the early stage and increased dramatically after 30 days under low Pi stress, whereas *ARF22* showed opposite expression patterns (**Figure 6**). *WRKY53* is involved in a complicated transcription factor signaling network that regulates senescence-specific gene expression and may participate in signal transduction in *Arabidopsis* (Miao et al., 2004). Several other WRKY family members were reported to be involved in the low Pi response, such as in an *OsWRKY74*-overexpressing plant that showed significantly enhanced tolerance to Pi starvation, whereas RNAi lines of *OsWRKY74* were sensitive to Pi starvation (Dai et al., 2016). In soybean, *WRKY46* showed an opposite expression pattern to that of *OsWRKY74*. The *GmWRKY46*-overexpressed plants were more sensitive to low Pi stress than the controls, whereas RNAi lines of *GmWRKY46* had significantly enhanced Pi deficiency tolerance (Liu et al., 2022). Previous studies showed that *miR171c*-targeted *SCL6* plays an important role in the control of shoot branch production in *Arabidopsis* (Wang et al., 2010). In soybean, the *miR171–SCL6* pair regulated rhizobium symbiosis (Hossain et al., 2019). We found that the *miR171d–SCL6* pair may respond to low Pi availability. We consider that these three hub genes and the miRNAs that target them may have major roles in the response to Pi deficiency in *C. oleifera* roots. However, the specific regulatory mechanism needs to be further verified.

Conclusion

In the study, we performed an integrated analysis of sRNA, degradome, and transcriptome sequencing data and generated a well-rounded resource centered on identifying key regulatory miRNA–target gene pairs that respond to low Pi stress. A total of 40,689 unigenes and 386 miRNAs were identified, and 32 significantly differentially expressed miRNAs were detected. The edge genes of the target hub genes for the low Pi-responsive miRNAs were involved in transporter activity, the response to the stimulus, catalytic activity, signaling, binding, and biological processes. Furthermore, 30 differentially expressed target genes of 31 differentially expressed miRNAs were identified by a concordant analysis of the expression patterns of the miRNA–target gene pairs. A total of 390 co-expressed genes formed a co-expression regulatory subnetwork in which three hub target genes, *ARF22*, *WRKY53*, and *SCL6*, which may play key roles in controlling transcriptomic regulation in response to low Pi stress, were identified. Our results provided a comprehensive understanding of Pi deficiency in *C. oleifera* and will help explain miRNA-mediated molecular mechanisms associated with plant responses to low Pi stress.

Data availability statement

The original contributions presented in the study are included in the article and **Supplementary material**. Transcriptome raw reads sequence data are available through the NCBI Sequence Read Archive (BioProject: PRJNA792896; BioSample: SAMN24471059; SRA Accession Number: SRR17365487-SRR17365501, 15 samples). Degradome

raw reads sequence data are available through the NCBI Sequence Read Archive (BioProject: PRJNA795525; BioSample: SAMN24731130; SAMN24471059; SRA Accession Number SRR17494566). Small RNA raw reads sequence data are available through the NCBI Sequence Read Archive (BioProject: PRJNA824141; BioSample: SAMN27393800; SRA Accession Number: SRR18672953-SRR18672967, 15 samples).

Author contributions

JC and XY conceived this project. JC and XH designed experiments and interpreted the results. JC wrote the manuscript. XH provided technical guidance for the experiment. SY, LL, BY, and YC performed the experiments and analyzed the data. RZ and XY provided experimental materials and funds. All authors read and approved the submission of this manuscript.

Funding

This study was supported by the National Key R&D Program of China (2019YFD1001602).

Conflict of interest

The authors declare that the research was conducted in the absence of any commercial or financial relationships that could be construed as a potential conflict of interest.

Publisher's note

All claims expressed in this article are solely those of the authors and do not necessarily represent those of their affiliated organizations, or those of the publisher, the editors and the reviewers. Any product that may be evaluated in this article, or claim that may be made by its manufacturer, is not guaranteed or endorsed by the publisher.

Supplementary material

The Supplementary Material for this article can be found online at: https://www.frontiersin.org/articles/10.3389/fpls.2022.932926/full#supplementary-material

References

Addo-Quaye, C., Miller, W., and Axtell, M. J. (2009). CleaveLand: A pipeline for using degradome data to find cleaved small RNA targets. *Bioinformatics* 25, 130–131. doi: 10.1093/bioinformatics/btn604

Allen, E., Xie, Z., Gustafson, A. M., and Carrington, J. C. (2005). microRNA-directed phasing during trans-acting siRNA biogenesis in plants. *Cell* 121, 207–221. doi: 10.1016/j.cell.2005.04.004

Axtell, M. J., and Meyers, B. C. (2018). Revisiting criteria for plant microRNA annotation in the era of big data. *Plant Cell* 30, 272–284. doi: 10.1105/tpc.17.00851

Bai, Q., Wang, X., Chen, X., Shi, G., Liu, Z., Guo, C., et al. (2018). Wheat miRNA TaemiR408 acts as an essential mediator in plant tolerance to Pi deprivation and salt stress via modulating stress-associated physiological processes. *Front. Plant Sci.* 9:499. doi: 10.3389/fpls.2018.00499

Bao, H., Chen, H., Chen, M., Xu, H., Huo, X., Xu, Q., et al. (2019). Transcriptome-wide identification and characterization of microRNAs responsive to phosphate starvation in *Populus tomentosa*. *Funct. Integr. Genom.* 19, 953–972. doi: 10.1007/s10142-019-00692-1

Bolger, A. M., Marc, L., and Bjoern, U. (2014). Trimmomatic: A flexible trimmer for Illumina sequence data. *Bioinformatics* 30, 2114–2120. doi: 10.1093/bioinformatics/btu170

Conley, D. J., Paerl, H. W., Howarth, R. W., Boesch, D. F., Seitzinger, S. P., Havens, K. E., et al. (2009). Controlling eutrophication: Nitrogen and phosphorus. *Science* 323, 1014–1015. doi: 10.1126/science.1167755

Cordell, D., Drangert, J. O., and White, S. (2009). The story of phosphorus: Global food security and food for thought. *Glob. Environ. Change* 19, 292–305. doi: 10.1016/j.gloenvcha.2008.10.009

Crombez, H., Motte, H., and Beeckman, T. (2019). Tackling plant phosphate starvation by the roots. *Dev. Cell* 48, 599–615. doi: 10.1016/j.devcel.2019.01.002

Cui, C., Wang, J. J., Zhao, J. H., Fang, Y. Y., He, X. F., Guo, H. S., et al. (2020). A *Brassica* miRNA regulates plant growth and immunity through distinct modes of action. *Mol. Plant* 13, 231–245. doi: 10.1016/j.molp.2019.11.010

Dai, X., and Zhao, P. X. (2011). psRNATarget: A plant small RNA target analysis server. *Nucleic Acids Res.* 39:W155–W159. doi: 10.1093/nar/gkr319

Dai, X., Lu, Q., Wang, J., Wang, L., Xiang, F., and Liu, Z. (2021). MiR160 and its target genes ARF10, ARF16 and ARF17 modulate hypocotyl elongation in a light, BRZ, or PAC-dependent manner in *Arabidopsis*: MiR160 promotes hypocotyl elongation. *Plant Sci.* 303:110686. doi: 10.1016/j.plantsci.2020.110686

Dai, X., Wang, Y., and Zhang, W. H. (2016). OsWRKY74, a WRKY transcription factor, modulates tolerance to phosphate starvation in rice. *J. Exp. Bot.* 67, 947–960. doi: 10.1093/jxb/erv515

de Jong, S., Boks, M. P., Fuller, T. F., Strengman, E., Janson, E., de Kovel, C. G., et al. (2012). A gene co-expression network in whole blood of schizophrenia patients is independent of antipsychotic-use and enriched for brain-expressed genes. *PLoS One* 7:e39498. doi: 10.1371/journal.pone.0039498

DiLeo, M. V., Strahan, G. D., den Bakker, M., and Hoekenga, O. A. (2011). Weighted correlation network analysis (WGCNA) applied to the tomato fruit metabolome. *PLoS One* 6:e26683. doi: 10.1371/journal.pone.0026683

Fan, F., Shang, X., Ding, G., Zhou, Z., and Tan, J. (2021). Integrated mRNA and miRNA expression analyses of *Pinus massoniana* roots and shoots in long-term response to phosphate deficiency. *J. Plant Growth Regul.* 1–18. doi: 10.1007/s00344-021-10486-0

Fan, X., Zhou, X., Chen, H., Tang, M., and Xie, X. (2021). Cross-talks between macro-and micronutrient uptake and signaling in plants. *Front. Plant Sci.* 12:663477. doi: 10.3389/fpls.2021.663477

Fujii, H., Chiou, T. J., Lin, S. I., Aung, K., and Zhu, J. K. (2005). A miRNA involved in phosphate-starvation response in *Arabidopsis*. *Curr. Biol.* 15, 2038–2043. doi: 10.1016/j.cub.2005.10.016

German, M. A., Pillay, M., Jeong, D. H., Hetawal, A., Luo, S., Janardhanan, P., et al. (2008). Global identification of microRNA-target RNA pairs by parallel analysis of RNA ends. *Nat. Biotechnol.* 26, 941–946. doi: 10.1038/nbt1417

Gupta, S., Kumari, M., Kumar, H., and Varadwaj, P. K. (2017). Genome-wide analysis of miRNAs and Tasi-RNAs in *Zea mays* in response to phosphate deficiency. *Funct. Integr. Genom.* 17, 335–351. doi: 10.1007/s10142-016-0538-4

Han, X., Yin, H., Song, X., Zhang, Y., Liu, M., Sang, J., et al. (2016). Integration of small RNA s, degradome and transcriptome sequencing in hyperaccumulator *Sedum alfredii* uncovers a complex regulatory network and provides insights into cadmium phytoremediation. *Plant Biotechnol. J.* 14, 1470–1483. doi: 10.1111/pbi.12512

He, C., Liu, H., Su, S., Lu, Y., Luo, B., Nie, Z., et al. (2015). Genome-wide identification of candidate phosphate starvation responsive genes and the development of intron length polymorphism markers in maize. *Plant Breed.* 134, 11–16. doi: 10.1111/pbr.12230

Hofferek, V., Mendrinna, A., Gaude, N., Krajinski, F., and Devers, E. A. (2014). MiR171h restricts root symbioses and shows like its target *NSP2* a complex transcriptional regulation in *Medicago truncatula*. *BMC Plant Biol.* 14:199. doi: 10.1186/s12870-014-0199-1

Hossain, M. S., Hoang, N. T., Yan, Z., Tóth, K., Meyers, B. C., and Stacey, G. (2019). Characterization of the spatial and temporal expression of two soybean miRNAs identifies SCL6 as a novel regulator of soybean nodulation. *Front. Plant Sci.* 10:475. doi: 10.3389/fpls.2019.00475

Hsieh, L. C. (2010). Uncovering small RNA-mediated responses to phosphate deficiency in *Arabidopsis* by deep sequencing. *Plant Physiol.* 151, 2120–2132. doi: 10.1104/pp.109.147280

Jia, X., Wang, L., Zeng, H., and Yi, K. (2021). Insights of intracellular/intercellular phosphate transport and signaling in unicellular green algae and multicellular land plants. *New Phytol.* 232, 1566–1571. doi: 10.1111/nph.17716

Johnston, A., Poulton, P. R., Fixen, P. E., and Curtin, D. (2014). Chapter Five-Phosphorus : Its efficient use in agriculture. *Adv. Agron.* 123, 177–228. doi: 10.1016/B978-0-12-420225-2.00005-4

Kvam, V. M., Liu, P., and Si, Y. (2012). A comparison of statistical methods for detecting differentially expressed genes from RNA-seq data. *Am. J. Bot.* 99, 248–256. doi: 10.3732/ajb.1100340

Langfelder, P., and Horvath, S. (2008). WGCNA: An R package for weighted correlation network analysis. *BMC Bioinform.* 9:559. doi: 10.1186/1471-2105-9-559

Li, A., Hu, B., and Chu, C. (2021). Epigenetic regulation of nitrogen and phosphorus responses in plants. *J. Plant Physiol.* 258:153363. doi: 10.1016/j.jplph.2021.153363

Li, J., Wu, Z., and Yuan, J. (2019). Impact of agro-farming activities on microbial diversity of acidic red soils in a *Camellia Oleifera* Forest. *Rev. Bras. Cienc. Solo* 43:0190044. doi: 10.1590/18069657rbcs20190044

Li, M., and Yu, B. (2021). Recent advances in the regulation of plant miRNA biogenesis. *RNA Biol.* 18, 2087–2096. doi: 10.1080/15476286.2021.1899491

Li, M., Xia, Y., Gu, Y., Zhang, K., Lang, Q., Chen, L., et al. (2010). MicroRNAome of porcine pre-and postnatal development. *PLos One* 5:e11541. doi: 10.1371/journal.pone.0011541

Li, Z., Xu, H., Li, Y., Wan, X., Ma, Z., Cao, J., et al. (2018). Analysis of physiological and miRNA responses to Pi deficiency in *alfalfa* (*Medicago sativa L.*). *Plant Mol. Biol.* 96, 473–492. doi: 10.1007/s11103-018-0711-3

Lidbury, I. D., Scanlan, D. J., Murphy, A. R., Christie-Oleza, J. A., Aguilo-Ferretjans, M. M., Hitchcock, A., et al. (2022). A widely distributed phosphate-insensitive phosphatase presents a route for rapid organophosphorus remineralization in the biosphere. *Proc. Natl. Acad. Sci. U.S.A.* 119:e2118122119. doi: 10.1073/pnas.2118122119

Lin, W. Y., Lin, Y. Y., Chiang, S. F., Syu, C., Hsieh, L. C., and Chiou, T. J. (2018). Evolution of micro RNA 827 targeting in the plant kingdom. *New Phytol.* 217, 1712–1725.

Ling, Y.-H., Ren, C.-H., Guo, X.-F., Xu, L.-N., Huang, Y.-F., Luo, J.-C., et al. (2014). Identification and characterization of microRNAs in the ovaries of multiple and uniparous goats (*Capra hircus*) during follicular phase. *BMC Genom.* 15:339. doi: 10.1186/1471-2164-15-339

Liu, N., Shang, W., Li, C., Jia, L., Wang, X., Xing, G., et al. (2018). Evolution of the SPX gene family in plants and its role in the response mechanism to phosphorus stress. *Open Biol.* 8:170231. doi: 10.1098/rsob.170231

Liu, Q., Zhou, Z., Wei, Y., Shen, D., Feng, Z., and Hong, S. (2015). Genome-wide identification of differentially expressed genes associated with the high yielding of oleoresin in secondary xylem of Masson pine (*Pinus massoniana Lamb*) by transcriptomic analysis. *PLos One* 10:e0132624. doi: 10.1371/journal.pone.0132624

Liu, X., Yang, Y., Wang, R., Cui, R., Xu, H., Sun, C., et al. (2022). GmWRKY46, a WRKY transcription factor, negatively regulates phosphorus tolerance primarily through modifying root morphology in soybean. *Plant Sci.* 315:111148. doi: 10.1016/j.plantsci.2021.111148

Liu, Y., Mi, G., Chen, F., Zhang, J., and Zhang, F. (2004). Rhizosphere effect and root growth of two maize (*Zea mays* L.) genotypes with contrasting P efficiency at low P availability. *Plant Sci.* 167, 217–223.

Liu, Z., Wang, X., Chen, X., Shi, G., Bai, Q., and Xiao, K. (2018). TaMIR1139: A wheat miRNA responsive to Pi-starvation, acts a critical mediator in modulating plant tolerance to Pi deprivation. *Plant Cell Rep.* 37, 1293–1309. doi: 10.1007/s00299-018-2313-6

Livak, K. J., and Schmittgen, T. D. (2001). Analysis of relative gene expression data using real-time quantitative PCR and the $2^{-\Delta\Delta Ct}$ method. *Methods* 25, 402–408.

Ma, X., Denyer, T., Javelle, M., Feller, A., and Timmermans, M. C. (2021). Genome-wide analysis of plant miRNA action clarifies levels of regulatory dynamics across developmental contexts. *Genome Res.* 31, 811–822. doi: 10.1101/gr.270918.120

Miao, Y., Laun, T., Zimmermann, P., and Zentgraf, U. (2004). Targets of the WRKY53 transcription factor and its role during leaf senescence in *Arabidopsis*. *Plant Mol. Biol.* 55, 853–867. doi: 10.1007/s11103-004-2142-6

Navarro, M., and Munné-Bosch, S. (2022). Reduced phosphate availability improves tomato quality through hormonal modulation in developing fruits. *J. Plant Growth Regul.* 41, 153–162. doi: 10.1007/s00344-020-10290-2

Nie, Z., Ren, Z., Wang, L., Su, S., Wei, X., Zhang, X., et al. (2016). Genome-wide identification of microRNAs responding to early stages of phosphate deficiency in maize. *Physiol. Plant.* 157, 161–174. doi: 10.1111/ppl.12409

Pegler, J. L., Nguyen, D. Q., Oultram, J. M. J., Grof, C. P. L., and Eamens, A. L. (2021). Molecular manipulation of the miR396 and miR399 expression modules alters the response of *Arabidopsis thaliana* to phosphate stress. *Plants* 10:2570. doi: 10.3390/plants10122570

Pegler, J. L., Oultram, J. M., Grof, C. P., and Eamens, A. L. (2020). Molecular manipulation of the miR399/PHO2 expression module alters the salt stress response of *Arabidopsis thaliana*. *Plants* 10:73. doi: 10.3390/plants10010073

Peng, K., Tian, Y., Sun, X., Song, C., Ren, Z., Bao, Y., et al. (2021). Tae-miR399-UBC24 module enhances freezing tolerance in winter wheat via a CBF signaling pathway. *J. Agric. Food Chem.* 69, 13398–13415. doi: 10.1021/acs.jafc.1c04316

Rubio, V., Linhares, F., Solano, R., Martín, A. C., Iglesias, J., Leyva, A., et al. (2001). A conserved MYB transcription factor involved in phosphate starvation signaling both in vascular plants and in unicellular algae. *Genes Dev.* 15, 2122–2133. doi: 10.1101/gad.204401

Sailaja, B., Voleti, S., Subrahmanyam, D., Sarla, N., Prasanth, V. V., Bhadana, V., et al. (2014). Prediction and expression analysis of miRNAs associated with heat stress in *Oryza sativa*. *Rice Sci.* 21, 3–12. doi: 10.1016/S1672-6308(13)60164-X

Shi, J., Zhao, B., Zheng, S., Zhang, X., Wang, X., Dong, W., et al. (2021). A phosphate starvation response-centered network regulates mycorrhizal symbiosis. *Cell* 184:5527–5540.e18. doi: 10.1016/j.cell.2021.09.030

Shi, T., Wu, G., Jin, Q., and Wang, X. (2020). *Camellia* oil authentication: A comparative analysis and recent analytical techniques developed for its assessment. A review. *Trends Food Sci. Technol.* 97, 88–99. doi: 10.1016/j.tifs.2020.01.005

Smith, F. W., Mudge, S. R., Rae, A. L., and Glassop, D. (2003). Phosphate transport in plants. *Plant Soil* 248, 71–83. doi: 10.1023/A:1022376332180

Sun, Q., Liu, Y., Tang, Y., Zhang, P., Tong, Y., He, G., et al. (2021). The composition and phosphate-solubilizing capability of phosphate-solubilizing bacteria in the rhizosphere of wild *Camellia oleifera* in mountain Lushan. *Am. J. Agric. For.* 9:141.

Sun, S., Gu, M., Cao, Y., Huang, X., Zhang, X., Ai, P., et al. (2012). A constitutive expressed phosphate transporter, OsPht1; 1, modulates phosphate uptake and translocation in phosphate-replete rice. *Plant Physiol.* 159, 1571–1581. doi: 10.1104/pp.112.196345

Sun, X., Lin, L., and Sui, N. (2019). Regulation mechanism of microRNA in plant response to abiotic stress and breeding. *Mol. Biol. Rep.* 46, 1447–1457. doi: 10.1007/s11033-018-4511-2

Tyagi, W., Nongbri, E. N., and Rai, M. (2021). "Chapter 11 – Harnessing tolerance to low phosphorus in rice: Recent progress and future perspectives," in *Molecular breeding for rice abiotic stress tolerance and nutritional quality*, eds M. A. Hossain, L. Hassan, K. M. Ifterkharuddaula, A. Kumar, and R. Henry

(Hoboken, NJ: John Wiley & Sons, Ltd.), 215–233. doi: 10.1002/9781119633174.ch11

Ünlü, E. S., Kaya, Ö, Eker, I., and Gürel, E. (2021). Sequencing, de novo assembly and annotation of Digitalis ferruginea subsp. schischkinii transcriptome. *Mol. Biol. Rep.* 48, 127–137. doi: 10.1007/s11033-020-05982-7

Vidal, E. A., Araus, V., Lu, C., Parry, G., Green, P. J., Coruzzi, G. M., et al. (2010). Nitrate-responsive miR393/AFB3 regulatory module controls root system architecture in *Arabidopsis thaliana*. *Proc. Natl. Acad. Sci. U.S.A.* 107, 4477–4482. doi: 10.1073/pnas.0909571107

Wang, F., Deng, M., Xu, J., Zhu, X., and Mao, C. (2018). Molecular mechanisms of phosphate transport and signaling in higher plants. *Semin. Cell Dev. Biol.* 74, 114–122.

Wang, L., Mai, Y. X., Zhang, Y. C., Luo, Q., and Yang, H. Q. (2010). MicroRNA171c-targeted SCL6-II, SCL6-III, and SCL6-IV genes regulate shoot branching in *Arabidopsis*. *Mol. Plant* 3, 794–806. doi: 10.1093/mp/ssq042

Wang, Q., Kang, Y. S., Alowaifeer, A., Shi, K., Fan, X., Wang, L., et al. (2018). Phosphate starvation response controls genes required to synthesize the phosphate analog arsenate. *Environ. Microbiol.* 20, 1782–1793. doi: 10.1111/1462-2920.14108

Wang, S., Liu, L., Mi, X., Zhao, S., An, Y., Xia, X., et al. (2021). Multi-omics analysis to visualize the dynamic roles of defense genes in the response of tea plants to gray blight. *Plant J.* 106, 862–875. doi: 10.1111/tpj.15203

Wang, X., Niu, Y., and Zheng, Y. (2021). Multiple functions of MYB transcription factors in abiotic stress responses. *Int. J. Mol. Sci.* 22:6125. doi: 10.3390/ijms22116125

Wang, Y., Wang, F., Lu, H., Liu, Y., and Mao, C. (2021). Phosphate uptake and transport in plants: An elaborate regulatory system. *Plant Cell Physiol.* 62, 564–572. doi: 10.1093/pcp/pcab011

Wang, Z., Kuo, H. F., and Chiou, T. J. (2021). Intracellular phosphate sensing and regulation of phosphate transport systems in plants. *Plant Physiol.* 187, 2043–2055. doi: 10.1093/plphys/kiab343

Wang, Z., Ruan, W., Shi, J., Zhang, L., Xiang, D., Yang, C., et al. (2014). Rice SPX1 and SPX2 inhibit phosphate starvation responses through interacting with PHR2 in a phosphate-dependent manner. *Proc. Natl. Acad. Sci. U. S. A.* 111, 14953–14958. doi: 10.1073/pnas.1404680111

Wu, F., Li, J., Chen, Y., Zhang, L., Zhang, Y., Wang, S., et al. (2019). Effects of phosphate solubilizing bacteria on the growth, photosynthesis, and nutrient uptake of *Camellia oleifera* abel. *Forests* 10:348. doi: 10.3390/f10040348

Xu, F., Liu, Q., Chen, L., Kuang, J., Walk, T., Wang, J., et al. (2013). Genome-wide identification of soybean microRNAs and their targets reveals their organ-specificity and responses to phosphate starvation. *BMC Genom.* 14:66. doi: 10.1186/1471-2164-14-66

Zhang, B., and Horvath, S. (2005). A general framework for weighted gene co-expression network analysis. *Stat. Appl. Genet. Mol.* 4, Article17. doi: 10.2202/1544-6115.1128

Zhang, J., Lin, Y., Wu, F., Zhang, Y., Cheng, L., Huang, M., et al. (2021). Profiling of microRNAs and their targets in roots and shoots reveals a potential miRNA-mediated interaction network in response to phosphate deficiency in the forestry tree *Betula luminifera*. *Front. Genet.* 12:38. doi: 10.3389/fgene.2021.552454

Zhang, J., Miao, H., Xie, B., Wang, J., Jia, C., Zhang, J., et al. (2020). Genomic and transcriptional analysis of banana ovate family proteins reveals their relationship with fruit development and ripening. *Biochem. Genet.* 58, 412–429. doi: 10.1007/s10528-020-09951-4

Zhou, C., Lin, P., Yao, X., Wang, K., Chang, J., and Han, X. (2013). Selection of reference genes for quantitative real-time PCR in six oil-tea *camellia* based on RNA-seq. *Mol. Biol.* 47, 836–851.

Zhou, J., Lu, M., Zhang, C., Qu, X., Liu, Y., Yang, J., et al. (2020). Isolation and functional characterisation of the PHT1 gene encoding a high-affinity phosphate transporter in *Camellia oleifera*. *J. Hortic. Sci. Biotechnol.* 95, 553–564. doi: 10.1080/14620316.2019.1703562

Zuluaga, D. L., Liuzzi, V., Curci, P. L., and Sonnante, G. (2018). MicroRNAs in durum wheat seedlings under chronic and short-term nitrogen stress. *Funct. Integr. Genom.* 18, 645–657. doi: 10.1007/s10142-018-0619-7

frontiers | Frontiers in Plant Science

TYPE Original Research
PUBLISHED 09 August 2022
DOI 10.3389/fpls.2022.986365

OPEN ACCESS

EDITED BY
Jian Chen,
Jiangsu University, China

REVIEWED BY
Zheng Zheng,
South China Agricultural University, China
Shimin Fu,
United States Department of Agriculture (USDA), United States

*CORRESPONDENCE
Min-Li Bao
minlibao_bob@163.com

†These authors have contributed equally to this work

SPECIALTY SECTION
This article was submitted to Plant Bioinformatics, a section of the journal Frontiers in Plant Science

RECEIVED 05 July 2022
ACCEPTED 21 July 2022
PUBLISHED 09 August 2022

CITATION
Duan S, Xu Z, Li X-Y, Liao P, Qin H-K, Mao Y-P, Dai W-S, Ma H-J and Bao M-L (2022) Dodder-transmitted mobile systemic signals activate a salt-stress response characterized by a transcriptome change in *Citrus sinensis*. *Front. Plant Sci.* 13:986365. doi: 10.3389/fpls.2022.986365

Dodder-transmitted mobile systemic signals activate a salt-stress response characterized by a transcriptome change in *Citrus sinensis*

Shuo Duan[1†], Zhou Xu[1†], Xin-Yu Li[1], Ping Liao[1], Hong-Kun Qin[1], Ya-Ping Mao[1], Wen-Shan Dai[1], Hai-Jie Ma[2] and Min-Li Bao[1*]

[1]China-USA Citrus Huanglongbing Joint Laboratory, National Navel Orange Engineering Research Center, Gannan Normal University, Ganzhou, China, [2]College of Horticulture Science, Zhejiang A&F University, Hangzhou, Zhejiang, China

Citrus is an essential horticultural fruit whose yield and quality are affected by salinity all over the world. The recognition and adaptive regulation of citrus against salt stress are important areas for cultivar improvement, but the vascular system signal transduction mechanism of the plant response to salt stress remains elusive. In this study, we constructed a dodder (*Cuscuta spp.*) linked Hamlin sweet orange (*Citrus sinensis*) plant community in which deliver a vascular signal through the dodder in response to salt stress. RNA-seq technology was used to analyze the gene expression profile of citrus leaves after salt treatment. The results showed that a vascular signal was transmitted to a dodder-linked host plant, triggering a transcriptional response to salt stress. However, the phenotypic and transudative ability of the dodder changed after 24 h. The salt treatment group (Group S) and the dodder-linked group (Group D) respectively contained 1,472 and 557 differentially expressed genes (DEGs). 454 of which were common to both groups. The results of our analysis revealed that the gene expression categories in Group D represented a highly consistent trend compared to the group S plants, indicating that the dodder-bridged vascular signals activated the stress-response of citrus leaves for transcriptomic reconfiguration. The KEGG pathway database and an analysis of key drivers revealed that phenylpropanoid biosynthesis, photosynthesis-antenna proteins, starch and sucrose metabolism, plant hormone signal transduction, circadian rhythm, and MAPK signaling pathways were significantly enriched as the critical genes during salt stress. A systemic signal in the dodder-bridged host significantly regulated abiotic stress-related secondary metabolic pathways, including those for phenylpropanoids, lignin, and lignans. The physiological indexes of photosynthetic intensity, respiration, and attractiveness among

communities supported the transcriptional changes. Thus, our results indicate that salt stress-induced vascular system signals can be transmitted through the vascular system of a dodder linking citrus plants, revealing the genetic regulation and physiological changes of citrus leaves responding to plant stress signal transmission.

KEYWORDS

mobile systemic signals, salt-stress, dodder (*Cuscuta chinensis*), dodder-transmitted, transcriptome change

Introduction

A abiotic and biotic stresses including drought, low temperature, diseases, pests, and salinity, significantly affect plants during their lifespan (Golldack et al., 2014; Pandey et al., 2017; Zhang et al., 2022). Salinity is one of the most prevalent abiotic stressors that threatens agricultural production. Plants subjected to salt stress can suffer restricted growth due to reduced photosynthesis and damaged cellular structures (Chaves et al., 2009). Chronic salt stress is widespread and decreases the growth and yield of all crops.

Citrus is the most economically important horticultural type of fruit worldwide. However, salt stress adversely affects its yield and fruit quality. Salt induces osmotic stress and ionic toxicity in plants, resulting in stomatal closure, which in turn reduces photosynthesis and transpiration (Arif et al., 2020). Salt stress can also cause nutritional disorders, oxidative stress, membrane effects and other secondary effects such as tissue disorder, and metabolic imbalance; these physiological changes often lead to plant growth inhibition and even death. Thus, improving the salt tolerance of citrus can reduce economic losses and increase the cultivation area, including locations with saline-alkaline soil. The plant plasma membrane is affected by salinity, because the lipid bilayer becomes more fluid, consequently inducing a Ca^{2+} influx into the cytoplasm (Mahajan and Tuteja, 2005). Orderly amplification by Ca^{2+} signaling cascades (e.g., CMLs, CAMs, and CBLs) and MAPK cascades further regulates the expression of a series of salt stress response genes (Xie et al., 2017). Experimental data show that salinity can negatively affect critical plant cellular pathways, such as photosynthesis (Chaves et al., 2009), plant hormone signal transduction, MAPK signaling, circadian rhythm, etc.

Salt hypersensitivity (SOS) genes, reactive oxygen species (ROS), WRKYs, glutathione peroxidase (Avsian-Kretchmer et al., 2004; Xie et al., 2018; Pardo-Hernandez et al., 2020), and plant hormones play essential roles in mediating plant responses to ionic and osmotic stresses (Dai et al., 2018; Liu et al., 2022; Primo-Capella et al., 2022; Yacoubi et al., 2022), which possibly could help to improve tolerance to salt stress. However, the cellular pathways involved in the plant response to salt stress are still being explored. Plants usually react to stressful situations and improve their defensive ability by retaining and sustaining memories of the stress, allowing for stronger or faster responses to repeated instances of stress (Sharma et al., 2022). However, plant adaptation to environmental stress requires short and long term intercellular, inter-tissue, and inter-organ communication mediated by different signaling systems. Many studies of transcriptional changes (Peng et al., 2014; Tan et al., 2015; Robertson et al., 2017; Lee et al., 2021; Nivedita et al., 2021) have identified various plant tissue responses to salt stress, but an analysis of transcriptional changes triggered by a stress-induced vascular signal system in woody plants has not been done.

Dodder (*Cuscuta spp.*) is a vine plant with a parasitic stem without leaves and roots. It uses a unique organ, the haustorium (Yoshida et al., 2016), to attach to and penetrate the host's stem tissue forming a connection between the xylem and phloem and the host's vascular system (Shimizu and Aoki, 2019). The dodder parasitizes the plant host and steals nutrients and water from its vascular system, and exchanges a variety of molecules with it, including proteins, mRNAs, and small RNAs (Liu et al., 2020; Shen et al., 2020; Song et al., 2022). Research has revealed that systemic vascular signals can be delivered to another parasitized plant host through the dodder-bridged stem, which induces a response due to a biotic or abiotic stressor in the other host (Qin et al., 2019; Li et al., 2020; Zhang et al., 2021; Song et al., 2022). For example, salt treatment of one cucumber plant can prime the salt stress tolerance of another dodder-linked host and induce physiological and biochemical changes, including changes in the proline content, stomatal conductance, and the photosynthetic rate (Li et al., 2020). Signal transduction through the dodder can induce transcriptome and methylation changes in a host in a cucumber with a nitrogen deficiency, but not the response of the dodder with a nitrogen deficiency (Zhang et al., 2021). A biotic stress signal resulting from a pest attack, can also activate the dodder and cucumber defense responses. For instance, an aphid (*Myzus persicae*) feeding on the dodder can induce a systemic defense response in soybean, leading to increased host resistance to the insect (Song et al., 2022). The dodder stems often establish bridge links to multiple adjacent plants, establishing a plant community, i.e., a group of plants

which consists of a single dodder and two or more host plants. Within these clusters, the dodder can likely transfer systemic molecular signals among the host plants. Further research has shown that many mRNAs, portable proteins, and microRNAs are transferred among the host plants, the dodder, and pests (Liu et al., 2020). Studies have also found that the dodder delivered mature proteins instead of mRNA from the host plant and still maintained the activity of mobile proteins. For instance, the FT protein synthesized by the host, not the dodder's own, delivered into the dodder's vascular system can interact with FD transcription factors to promote dodder self-flowering (Shen et al., 2020). The mobile system signal plays a critical role in triggering the response to biotic or abiotic stress and regulating growth and development. However, it is difficult to extract and analyze vascular system signals or inter-plants. A dodder-mediated signal analysis method provides an essential tool for this puzzle.

The research on dodder-mediated herbaceous plants is well developed, but similar research on woody plants with respect to salt stress is still lacking. Previous studies provide evidence for salinity-triggered transcriptomic profiling in citrus (Tan et al., 2015; Xie et al., 2017). However, no vascular system signal studies with citrus have been reported. Therefore, in this study, we analyzed the transcriptome profiles of salt-treated and dodder bridge-linked citrus plants. The transcriptional changes and reconfiguration in dodder-linked citrus leaves could reveal the abiotic-induced systemic signals of citrus plants, providing new insight and methods vis-à-vis dodder-mediated plant-plant interactions in woody plants.

Materials and methods

Plant materials preparation

The Hamlin sweet oranges (*Citrus sinensis* (L.) Osbeck) used in this study were kept in a greenhouse at the National Navel Orange Engineering Research Center, Gannan Normal University, Ganzhou, Jiangxi, China (with a 16-h light and 8-h dark photoperiod, a 25/18°C temperature cycle, at 50% humidity). Citrus plants (approximately 2 years old) were further cultured in modified Hoagland solution (MHS) (#NS10205, Coolaber, China). The dodders were germinated and used to parasitize periwinkle (*Catharanthus roseus* (L.) *G. Don*) to form stock. Periwinkle twined with dodder stocks were moved next to a citrus plant to parasitize the citrus stem. To understand the response and adaptation of the dodder to the stress signal *via* mobile signal mediation, a citrus community was constructed using hydroculture and dodder parasitism for subsequent transcriptional data analysis. The citrus was cultured in a Hoagland culture solution (#NS1011, Coolaber, China), and the adjacent plants were connected by a dodder to construct the citrus-dodder-citrus experimental sets (**Figure 1A**). Once infested with dodders, the citrus plants were transferred to a 500 mL conical flask containing MHS liquid medium. Citrus communities link-bridged with dodders were constructed by culturing two or more plants next to each other. For approximately 30 days, all community members solidly infested by dodders were used for salinity treatment experiments. Then one of the citrus community plants was infiltrated with 500 mM NaCl in Hoagland medium for phenotype observation and continuous sample collection (**Figure 1B**). Subsequently, two-time points [12 and 24 h post immersion in the salt solution (hpi)] were chosen for transcriptional analysis. The experimental groups were designed as follows: the salinity-treated groups of sweet orange seedlings, as group S, and the dodder bridge-linked experimental group of sweet oranges, as group D, no salinity-treated groups of sweet orange seedlings, as mock.

RNA extraction, reverse transcription, and illumina sequencing

Leaf samples were collected, frozen in liquid nitrogen, and stored at −80°C until RNA extraction was carried out. RNA extraction was performed on all plant tissues using an RNA isolation kit (#DR0409050, Easy-Do, China). The absorbance ratio was determined *via* a Nanodrop spectrophotometer (NanoDrop Technologies, Wilmington, United States) to assess the RNA quality and concentration. RNA samples (OD260/280 > 2.0 and OD260/230 > 2.0) were used for further analysis. The first-strand cDNA was synthesized from RNA samples using an RNA reverse transcription kit (#RR047A, Takara, Japan) according to the manufacturer's instructions. The resultant cDNA was purified and enriched by PCR to produce the final cDNA libraries. The libraries were sequenced on an Illumina Hiseq 2000 platform, and 100 bp paired-end reads were generated for transcriptome sequencing.

Analysis pipeline

Clean data and count numbers of the RNA sequencing libraries were assessed and summarized using the transcriptional analysis website Dr. Tom.[1] The statistical number of genes in different TPM (Transcripts Per Kilobase of exon model per Million mapped reads) ranges for each sample was assessed for three ranges (TPM ≤ 1, TPM 1 –10, TPM ≥ 10) (**Supplementary Figure 1**). After alignment, the mapping rate statistics and the distribution of reads on the reference sequence were used to determine whether the alignment result passed a second QC. A gene quantification analysis and other analyses based on gene expression (i.e., principal component, correlation, differential gene screening) were then carried out, and a significant enrichment analysis of gene ontology

1 https://biosys.bgi.com/

10.3389/fpls.2022.986365

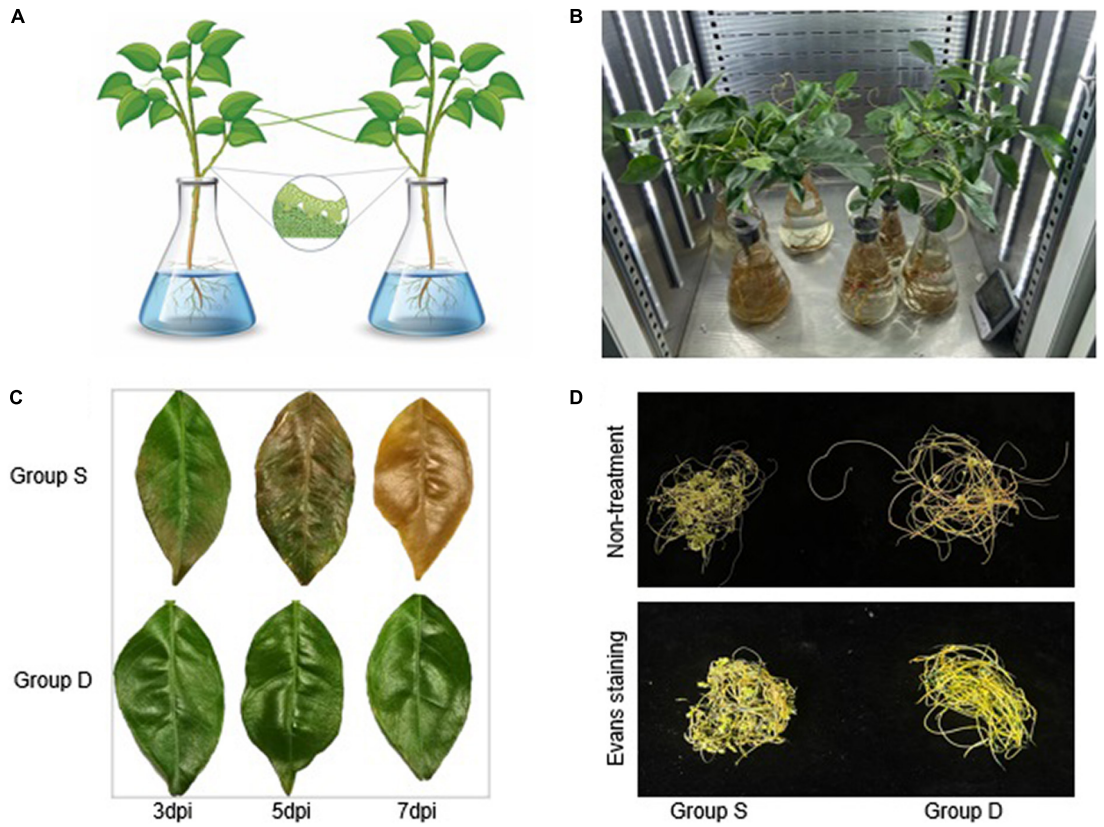

FIGURE 1
Experimental setup in this study. **(A)** Schematic of the experimental design for citrus-dodder-citrus community. **(B)** Group D, Group S, Mock, and the control group were set up in the growth chamber for phenotypes observation. The control group was mock-treated, while in group S, the citrus was treated with 500 mM NaCl. **(C)** The experimental groups citrus leaves for electrolyte leakage to monitor the cell viability during salinity treatment. **(D)** The dodder phenotypic observation in Groups S and D at 72 hpi.

(GO) functions for the DEGs among the screened samples, a significance enrichment pathway analysis, clustering, protein interaction networks, and transcription factors, and a more in-depth mining analysis were performed.

Categorization of differentially expressed genes

The RNA-seq data was loaded into the software with a filter of FDR < 0.05, The Q-value was obtained by correction of the P-value (the function of Q-value ≤ 0.05 was regarded as a significant enrichment). For the MapMan analysis, all gene IDs were transferred into the corresponding citrus microarray library. The pathways were visualized in the context of built-in Citrus AFFY mapping, and a Wilcoxon rank-sum test implemented in MapMan was used to extract the item number in each BIN and return a BIN whose gene members showed significantly different gene expression. To analyze GO term enrichment of differentially expressed genes, SEA was performed online through the agriGO program, a GO analysis tool kit for the agricultural community.[2] Briefly, the differentially expressed gene probe identification numbers were first uploaded into agriGO; then, the Citrus Affymetrix Genome Array was selected as the reference. Statistical P-values were calculated with the Fisher multiple-test adjustment using the Yekutieli (FDR under dependency) method. Venn diagrams were generated using an online program, Draw Venn Diagram.[3]

Quantitative reverse transcription-polymerase china reaction analyses

All primers used for quantitative reverse transcription-polymerase china reaction (qRT-PCR) in various experiments were designed on the website[4] using the following parameters:

2 http://systemsbiology.cau.edu.cn/agriGOv2/index.php
3 https://www.vandepeerlab.org/
4 https://www.idtdna.com/Primerquest/Home/Index

melting temperatures between 60 and 64°C, oligo lengths of 18–30 bp, a GC contents of 40%–60% and an amplicon sizes between 70 and 150 bp. An ABI QuantStudio5 Real-time PCR system (#A28139, Thermofisher, United States) was used to perform qRT-PCR using a 2 × SYBR Green qPCR Mix (#SL2690, Coolaber, Beijing, China). Each reaction was run in a 10-μL reaction system containing 2-μL of template cDNA, 5-μL of SYBR Green qPCR mix, and a final primer concentration of 300 nm. All reactions were performed under the following conditions: 30 s at 95°C and 40 cycles of 5 s each at 95°C and 30 s at 60°C in 96-well optical reaction plates (#4346907, applied biosystems, United States). A melting curve was generated from 60 to 95°C at the end of the reaction. The gene expression levels in all samples were determined by the number of cycles (Ct) required for the amplification-related fluorescence to reach a specific threshold detection level. The raw Ct value was analyzed using QuantStudio^{TM} design and analysis software v1.4.1. The $2^{-\Delta\Delta Ct}$ method was applied for relative quantification. Each experiment was repeated twice, and contained three replicates. The endogenous housekeeping gene was GAPDH (glyceraldehyde 3-phosphate dehydrogenase) (NCBI: LOC102614495) and the gene-specific primer sequences and information are listed (**Supplementary Table 6**).

Electrolyte leakage determination

Five citrus leaves were collected from each experimental plants. All leaves were wiped, rinsed with ddH_2O three times, and then soaked in 30 mL of ddH_2O. After immersion in a 37°C incubator with shaken at 200 rpm for 24 h, the electrolyte leakage value (L_t) of leaves was measured using a conductometer (#DDSJ-308F, INESA, Shanghai, China). The total electrical conductivity (L_0) was obtained after the same samples were heated in a water bath at 90°C for 2 h. The relative electrolyte leakage (L) was calculated using the formula:

$$L = L_t/L_0 \times 100\%.$$

Evans blue assay

Five citrus leaves were soaked into ddH_2O and then immersed in a 37°C incubator shaken at 200 rpm for 12 h. All leaves were immersed in a 0.5% (w/v) Evans blue solution (#SL7200, Coolaber, Beijing, China) for 24 h at room temperature. Each leaf was rinsed extensively with ddH_2O and photographed. Then the leaves were immersed in an ethanol series (95–25%) with an 8 h interval between concentrations, and photographed again.

Statistical data analysis

Statistical analysis was performed with the Prism 9 software (Graphpad, United States). All numerical data were expressed as mean ± standard deviation (SD) unless specified. The *P*-values and statistical analysis methods are indicated. One/two-way ANOVA analyses were processed with corresponding subsequent multiple comparison tests to meet the data analysis requirement with the Tukey test (95% confidence interval) using GraphPad Prism 9 ($^{**}p \leq 0.05$, $^{***}p \leq 0.001$, $^{****}p \leq 0.0001$, ns $P > 0.05$).

Result

Experimental design and phenotypic observation

A citrus community for subsequent transcriptional data analysis was constructed using hydroculture and dodder parasitism. One of the citrus community plants was then infiltrated in a Hoagland medium with 500 mM NaCl for phenotypic observation and continual sample collection (**Figure 1B**). The phenotypic observation results showed that the haustoria of the dodder easily separated from the stems of the group S at 48 hpi. The dodder parasitized on the stem of group S evidenced a weakly salt-stressed phenotype at 72 hpi, while the dodder linked to the stem of group D grew normally (**Figure 1D**). The leaves of the orange plant in the group S showed fallen, wilting, greenness, or necrotic salt stress-related phenotypes at 7 days post-treatment, while the leaves of the group D did not show any abnormal phenotypes. The photosynthetic intensity of the leaves of the experimental groups was measured every 2 h. To monitor the cell viability during the salt treatment, we determined the electrolyte leakage to the leaves and dodders in the experimental groups at 7 days post-treatment. The results showed that the leaves from group S were heavy, but those from group D were barely damaged (**Figure 1C**). The ion leakage from the leaves of group S ranged from 67 to 72.13%, approximately 70.47% higher than in the leaves of group D. Interestingly, the dodder parasite associated with group S showed apparent growth retardation, evidencing a weak salt-stress phenotype compared with the dodder parasite associated with group D. However, the dodder parasite associated with group S showed similar cell viability to the dodder parasite associated with group D during the leakage detection experiment. The Evans blue staining assay revealed that the linked dodder in both experimental groups retained complete cell vitality during salt stress.

RNA-seq quality statistics

In order to analyze the transcriptional changes in sweet orange leaves in response to salt stress, the leaves of group S and the dodder were collected for transcriptome analysis at 0 h, 12 h, and 24 h post salt treatment.

In this study, The NCBI Reference Genome Version Csi_valencia_1.0[5] was employed. Eighteen samples were sequenced using the DNBSEQ platform (sequencing length PE150), with an average yield of 6.74 Gb data per sample (**Supplementary Table 1**). We used HISAT to align the clean reads to the reference genome. We aligned the clean reads to the reference genes using Bowtie2 to obtain the alignment result (**Supplementary Table 2**). The average alignment ratio of the sample comparison genome was 88.09%, which was comparative. The average alignment of the gene sets was 77.47%, and 22,465 genes were detected. The coverage of the transcripts of each sample in this project based on the alignment results is shown (**Supplementary Figure 2**). A boxplot of an expression quantity analysis combined with a sequencing saturation analysis depicted the distribution of gene expression levels in each sample. The dispersal degree of the data distribution was stable and equal (**Supplementary Figure 2**), revealing that sequencing data met the experimental requirements. Additionally, a density map analysis showed a parallel trend of gene abundance in the samples as the expression level changed, reflecting that the interval of the gene expression concentration among samples were similar (**Supplementary Figure 3**).

A principal component analysis (PCA) is a multivariate statistical analysis method that reduces multiple variables to a small number of independent variables (principal components) by reducing the dimensionality while retaining as much of the original information as possible. Our quality analysis revealed that the filtering and mapping read of the RNA-seq data represent an acceptable sequencing standard among the different samples, allowing a PCA and Heatmap analysis using Pearson correlation coefficients to be applied. The PCA facilitated the identification of outlier samples and the discrimination of sample clusters with high similarity, revealed the variance among each group and indicated that group D was similar to group C at 12hpi (**Supplementary Figure 4**). The Pearson correlation coefficients for all gene expressions between each samples pair were subsequently calculated, and these coefficients were plotted as a heatmap (**Supplementary Figure 5**). A Heatmap of the expression profiles of the DEGs (Filtered with $|\log2FC| \geq 1.58$, $Q\text{-value} \leq 0.05$) was used to validate RNA-Seq data obtained from both experimental groups (424 genes were defined after the *t*-test) (**Supplementary Figure 6**). Results showed that the correlation heatmap results were consistent with the PCA and showed better homogeneity within experimental groups, which indicated that the read number and quality were sufficient for further analysis.

Dynamic transcriptome response of citrus and dodder to salt stress

Quantification of transcript abundance using standardized TPM helped us compare mRNA levels among samples. The genes with a cutoff $|\log2FC| \geq 1.58$ and $Q\text{-value} \leq 0.05$ were defined as DEGs. A total of 1,472 (472 up-regulated, 1,000 down-regulated) and 1,904 (981 up-regulated, 923 down-regulated) DEGs at 12 hpi and 24 hpi were identified in the salt group, and 557 (74 up-regulated, 483 down-regulated) and 59 (19 up-regulated, 40 downregulated) genes were identified in group D at 12 hpi and 24 hpi. Groups S and D shared 424 DEGs at 12 hpi, accounting for 76.12% of the total DEGs in group D, indicating a high correlation and cooperativity in a weighted correlation network analysis (**Supplementary Figure 7**). After 24 h, group S showed more obvious expression patterns related to salt stress than at other time points, and more obvious differences in the regulation of gene expression (**Figure 2**). Interestingly, the gene expression of the Group D showed an obvious adaptation to salt stress, and the regulation of gene expression was consistent with the initial gene expression pattern.

Despite the overlapping genes, a dramatic difference was observed in the transcriptional profiles at 12 hpi and 24 hpi. At 12 hpi, 424 DEGs were found in the group S and D transcriptomes (**Figure 3B**). However, at 24 hpi, the number of DEGs in the salt stress group and the Group D decreased to 29. There were only 59 DEGs in Group D at 24hpi, while there were 1,904 DEGs in group S. The overlapping differentially expressed genes at the two-time points were compared using a Venn diagram analysis (**Figure 3A**). Four

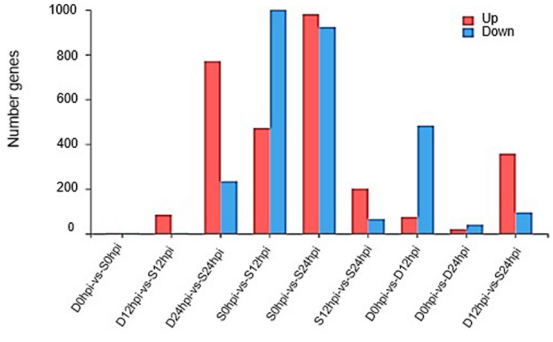

FIGURE 2
Changes in gene expression profile. The DEGs numbers of up-regulated and down-regulated genes among groups S and D at different time points are summarized.

5 https://www.ncbi.nlm.nih.gov/assembly/GCF_000317415.1

genes were found to be regulated at all three-time points: the two down-regulated genes were the small heat shock protein (LOC102608585), and a zinc-transporting ATPase HMA3(LOC102625788), and the two up-regulated genes were the late embryogenesis abundant protein(LOC102616716) and an amino acid transporter AVT1C(LOC102623467), respectively (Figure 3A). The results showed no similarity of the transcriptional changes between the two groups after 24 h, but the gene expression changes were evident in the leaves of group S. In contrast, the gene expression of group D was consistent with that of the 0 hpi group, indicating that the leaves of group D had adapted to the early salt stress signal. A combination of a volcano plot and a correlation analysis at 12 hpi indicated the most of the DEGs identified in the group S and group D at 12 hpi showed a consistent, similar gene expression trend (Figures 3B,C,D), indicating that the system signal triggered by salt in the root of group D was transmitted through the dodder and citrus vascular tissue and induced transcriptional changes in the leaves of group D. Therefore, 12 hpi is the critical time for analyzing the stress-signal transduction transcriptional regulation in the following contents.

Signaling pathways are involved in salt stress

To compare the DEGs at 12 hpi and 24 hpi, we analyzed the citrus genes whose mRNA levels were altered in response to salt

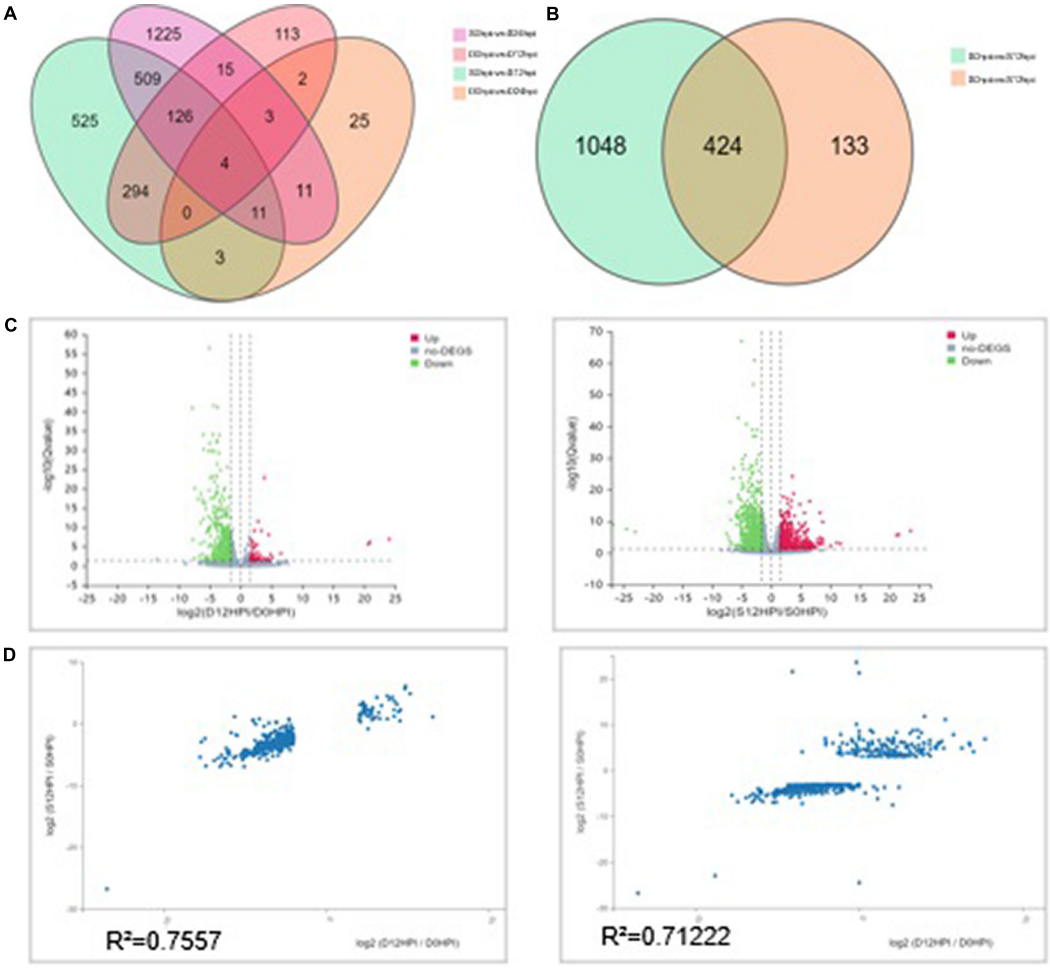

FIGURE 3
Differentially expressed genes (DEGs) analysis among groups at different time points. **(A)** Venn diagram showing the relationship between the differentially expressed genes at 12 and 24 hpi, respectively. The values in each circle represent the number of genes. The cut-off value of log2 fold changes for up-regulated and down-regulated gene/protein was ±1.58. **(B)** The Venn diagram distribution of DEGs in groups S and D at 12hpi. **(C)** Volcano plot of DEGs signals in groups S (left) and D (right). The scatter in the figure represents each gene; green genes are down-regulated, red genes are up-regulated, and gray genes are not differentially expressed. The vertical axis indicates the *P*-value (−log 10 value), | log2FC| ≥ 1.58 were applied for the cut-off value. **(D)** Correlation between the DEGs (| log2FC| ≥ 1.58) of groups S (left) and D (right) at 12hpi. The value represents 557 DEGs in group D (Left) and 1,472 in group S (Right). The regression line and Pearson's correlation coefficient are shown.

stress in group S and group D. We further assigned the DEGs to functional categories according to their similarity to genes with known functions in plants using two separate software packages: the MapMan software and the web-based singular enrichment analysis (SEA) tool in the AgriGO software (see text footnote 2). According to the AgriGO-SEA interpretation, the enrichment or over-representation of a category was assessed with a significantly (FDR < 0.05) higher percentage in all of the DGEs than in the overall percentage in the total expressed sequence tag. At 12 hpi, the downregulated genes in group S were enriched for photosynthesis, response to stimulus, cellular nitrogen compound metabolic process, and pigment metabolic process. Interestingly, compared to group S, the DEGs of group D at 12hpi showed similar enrichment for photosynthesis and response to stimulus. At 12 hpi, the singular enrichment analysis of significant terms of DEGs in group S revealed that the categories of "response to the stimulus" (FDR:0.00042, GO:0050896), "response to biotic stimulus" (FDR:0.00027, GO:0009628), "cellular response to stimulus" (FDR:0.041, GO:0051716) and "response to stress" (FDR:0.023, GO:0006950) were the significant terms. In group D, "response to stimulus" (FDR:0.029, GO:0050896) was the only significant term under the analysis (**Supplementary Figure 8**). The singular enrichment analysis of cellular components in groups S and D was consistently localized in the photosynthetic membrane, photosystem I, Photosystem II, plastid, and chloroplasts (**Supplementary Figure 9**).

We then used AgriGO-SEA to interpret this time-based comparison, which illustrated that most of the differentially expressed gene-enriched categories at 12 hpi were consistent with a comparison of groups S and D with respect to biological process cellular components. The AgriGo analysis results indicated that significantly down-regulated gene expression was enriched for photosystem I and photosystem I thylakoids, photorespiration, and the Calvin cycle in the chloroplasts of group S. Compared with group S, only photosystem II was affected in group D during salt stress (**Supplementary Figure 10**). A Wilcoxon rank-sum test of the cellular response overview revealed that biotic stress, abiotic stress, and development were highly enriched in DEGs of both groups at 12 hpi.

Gene ontology term enrichment with respect to the salt stress-response

A GO analysis was performed on the DEGs at 12 hpi between group S and group D, including "main metabolic process," "nitrogen compound metabolism process," and "cellular macromolecular biosynthesis process." The second GO class enrichment statistics are for the 424 DEGs in group D and group S at 12 hpi (Filtered with $|\log2FC| \geq 1.58$, Q-value ≤ 0.05). The results showed that KEGG pathways, such as phenobarbitone biosynthesis, photosynthesis, carbon fixation in the photosynthetic organization, circadian rhythm, and carbon metabolism, were enriched, suggesting that these pathways may be involved in the signal regulation of early system responses in plants (**Figure 4**). A KEGG pathway relationship network analysis showed the main significantly up-regulated categories were related to phenylpropanoid biosynthesis, photosynthesis-antenna protein, starch and sucrose metabolism, amino nucleotide sugar, plant hormone signal transduction, circadian rhythm, and the MAPK signaling pathway in both group S and group D (**Figure 5**).

According to the GO annotation classification, the phyper function in the R software was used to perform an enrichment analysis and calculate the P-value. When comparing the up-and downregulated genes in both group S and group D at different

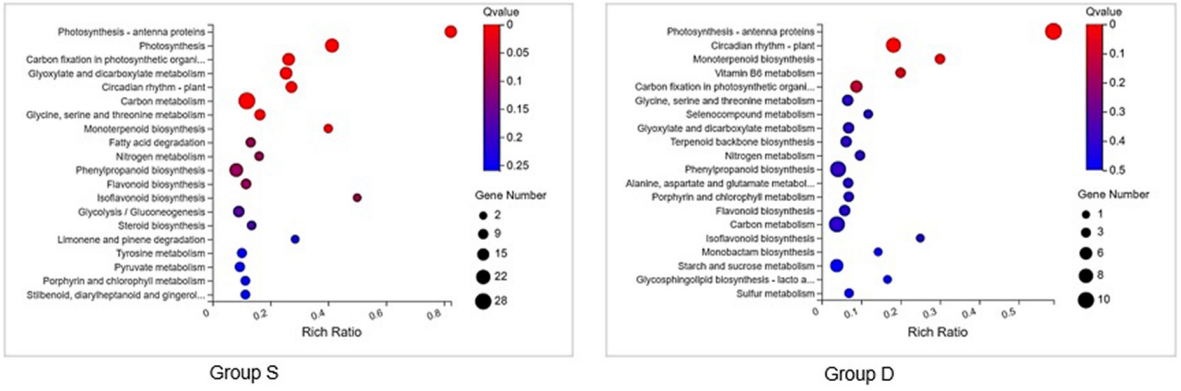

FIGURE 4
KEGG pathway enrichment scatters plot of experimental groups at 12hpi. Top 20 enriched pathways of KEGG metabolism pathway categories of DEGs in groups S (left) and D (right). The vertical axis represents the pathname, and the horizontal axis represents the path factor corresponding to the Rich factor. The color of the point represents the size of the q-value. The number of differential genes included in each pathway is expressed by the point's size. (The smaller the Q-value, the closer the color is to the red color).

A

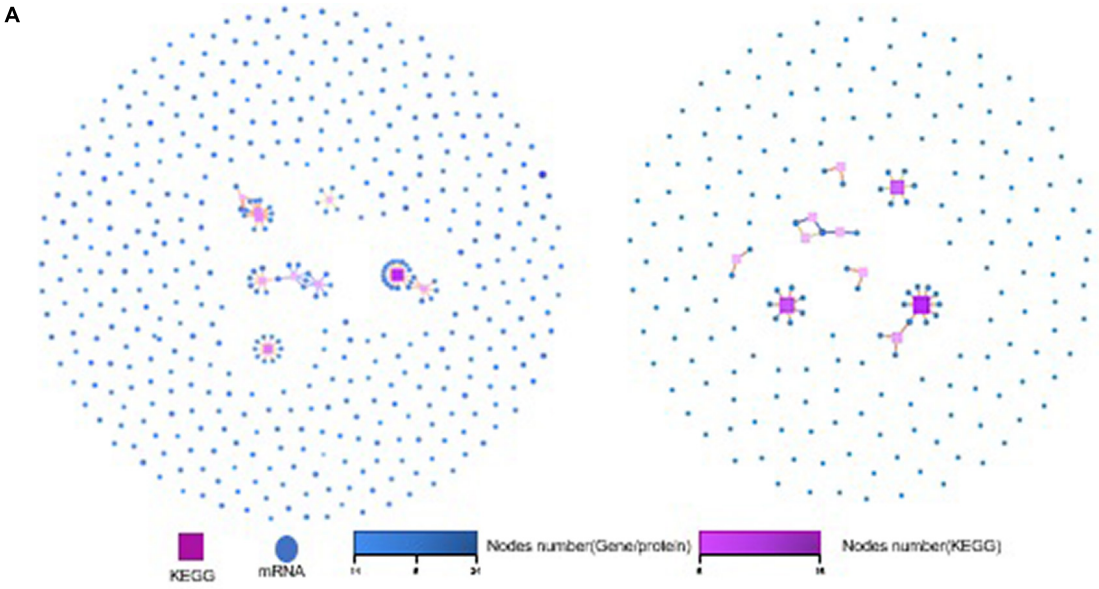

B

	Group S/12hpi	Group D/12hpi
Phenylpropanoid biosynthesis	16	9
Photosynthesis - antenna proteins	10	7
Starch and sucrose metabolism	7	6
Amino sugar and nucleotide sugar	7	3
Plant hormone signal transduction	7	2
Circadian rhythm	6	2
MAPK signaling pathway	6	2

FIGURE 5
KEGG pathway relationship network analysis and same nodes comparison between experimental groups at 12hpi. **(A)** The KEGG pathways of the selected genes are ranked by the number of genes on the pathway, and the top 10 pathways with the most significant number of genes were displayed in Group S (left) and Group D (right), respectively. Different shapes represent different content (nodes); the box represents KEGG Pathway, and the circle represents mRNA. Both color and size indicate the number of genes or transcripts connected to the node. The darker the color, the size of the box, the line with a different color represents the different path classification, and red represents cellular processes. **(B)** The nodes gene between groups S and D at 12hpi in KEGG pathway relationship networks.

time points, we found that the biological process categories of photosynthesis, light-harvesting, protein-chromophore linkage, and response to light stimulus were enriched for all of the down-regulated genes in both group D and group S at 12 hpi, and no significant enrichment categories were found for all up-regulated genes in both groups (**Supplementary Table 3**). We found that the molecular function categories of chlorophyll-binding, channel activity, water channel activity, and oxidoreductase activity were enriched in both groups. No significant enrichment in up-regulated genes was found in either group (**Supplementary Figure 11**). Consistent with the number of identified DEGs, a Pearson correlation analysis based on the TPM values of all DEGs also showed significant differences in expression between the transcriptomes of the different leaf samples at 24 hpi, but no significant enrichment of biological processes or pathways. However, the DEGs in group S and group D were enriched in several processes at 12 hpi, including "metabolic process," "cell process," and "stress response." The cellular component categories enriched in all down-regulated genes of group D are plastoglobule, plastid, photosystem, thylakoid, chloroplast, chloroplast thylakoid membrane, photosystem II, an integral membrane component,

and chloroplast envelope, which is consistent with the down-regulated genes enriched in group S.

The set of key driver salt stress-responsive genes

The key driver gene analysis (KDA) was employed in this study to predict the node genes through the PPI relationship, which can help in understanding the regulatory relationship with the altered gene set and can regulate the main gene/protein at 12 hpi (Filtered with $|\log2FC| \geq 1.58$, Q-value ≤ 0.05). Filtering the results showed that 10 key driver genes and 147 linked genes were predicted in group S, and 10 key driver genes and 171 linked genes in group D (**Supplementary Figure 12**). The most node genes were highlighted in chloroplasts and regulated the binding/catalytic activity functions on chlorophyll-binding (GO:0016168), phosphatase activity (GO:0016791), phosphoglycolate phosphatase activity (GO:0008967), fructose 1,6-bisphosphate 1-phosphatase activity (GO:0042132), magnesium-protoporphyrin IX monomethyl ester (oxidative) cyclase activity (GO:0048529) and ribulose-bisphosphate carboxylase activity (GO:0016984). The KEGG network and KDA analysis indicated that node genes are consistent with the biological photosynthesis process, which hinted that critical biological processes are regulated by the vascular signal triggered by salt treatment in *C. sinensis*.

Stress-related secondary metabolism pathway induced by the dodder-delivered signals

Phenylpropanoids have been reported to play an essential role in plant adaptation against salt stress. The Phenylpropanoid pathway transforms phenolics, flavonoids, anthocyanins, and lignin, and it can help the plant adapt to abiotic stress. The chemical structures of phenylpropanoids can facilitate the degradation of reactive oxygen species by reducing free radicals. A MapMan Wilcoxon Rank Sum analysis found that the significantly regulated genes were involved in stress, the photosystem, secondary metabolism, hormone metabolism, TCA, and fermentation in group D. The significantly regulated categories included the photosystem, stress, protein, tetrapyrrole synthesis, and major CHO metabolism in group S. We visually assessed the differentially expressed genes in a MapMan pathway, which revealed that the categories phenylpropanoids, lignin, and lignans contained remarkably more regulated genes than other secondary metabolism pathways in both groups (**Figure 6**). Therefore, the activation of the phenylpropanoid genes is concomitant with the detection of stress in plants. In both groups, the phenylpropanoids synthesis process was significantly and comprehensively changed during salt stress at 12 hpi.

Quantitative reverse transcription-polymerase reaction verification

Our previous analysis suggested that vascular system signals can be triggered from the rootS of group S, then transmitted *via* the dodder stem and delivered into the leaves of group D in 12 h. The transcriptional level in the leaves of group D showed a consistent change with group S at 12 hpi but became different at 24 hpi. Therefore, qRT-PCR was used to validate the RNA-seq data and our hypothesis. A total of 14 overlapping DEGs between two experimental groups at 12 hpi, overlaying DEGs were selected from the RNA-seq data, based on the KDA and the pathway network analysis results (**Supplementary Table 4**). The qRT-PCR results showed a similar trend in the gene expression pattern and abundance with the RNA-Seq data (**Figure 7**), which further confirmed the reliability of the RNA-seq data and the above analysis results.

Discussion

A dodder connects to the vascular tissue of a host plant through the haustoria, which not only absorbs nutrients but also transmits systemic signaling molecules between separate hosts. The dodder has long been used in citrus research and is a critical vector for studing the spread and expansion of the most important bacterial disease of citrus, the citrus huanglongbing (HLB) pathogen (Zhou et al., 2007; Duan et al., 2008). However, there is no precedent for the application of a dodder in signal transmission between citrus plants. Using a dodder as a signal transduction bridge between herbacula hosts, has recently become an essential tool to study signal transduction in herbacula with respect to abiotic/biotic stress. In this study, the dodder was used to study the transcriptional signaling system of plants with respect to salt stress on a separate host, the woody plant- *C. sinensis*, which not only indicated that dodder could transmit the salt stress signals over a long distance but also showed that the signal-regulated transcriptional changes were induced in dodder bridge-linked hosts. Our results suggest that a regulatory role for signals in citrus in response to salt stress and provide a reliable experimental system for woody plants to respond to various stress responses. Previous research (Li et al., 2020) revealed that the Na^{2+} ion was not delivered through the vascular system of the dodder or the host plant. Therefore, it was the salt particles themselves that caused the salt stress phenotype in the dodder, rather than systemic vascular signals generated after salt stress in sweet orange. The stress signal can be transferred to the vascular tissue of orange through the stem

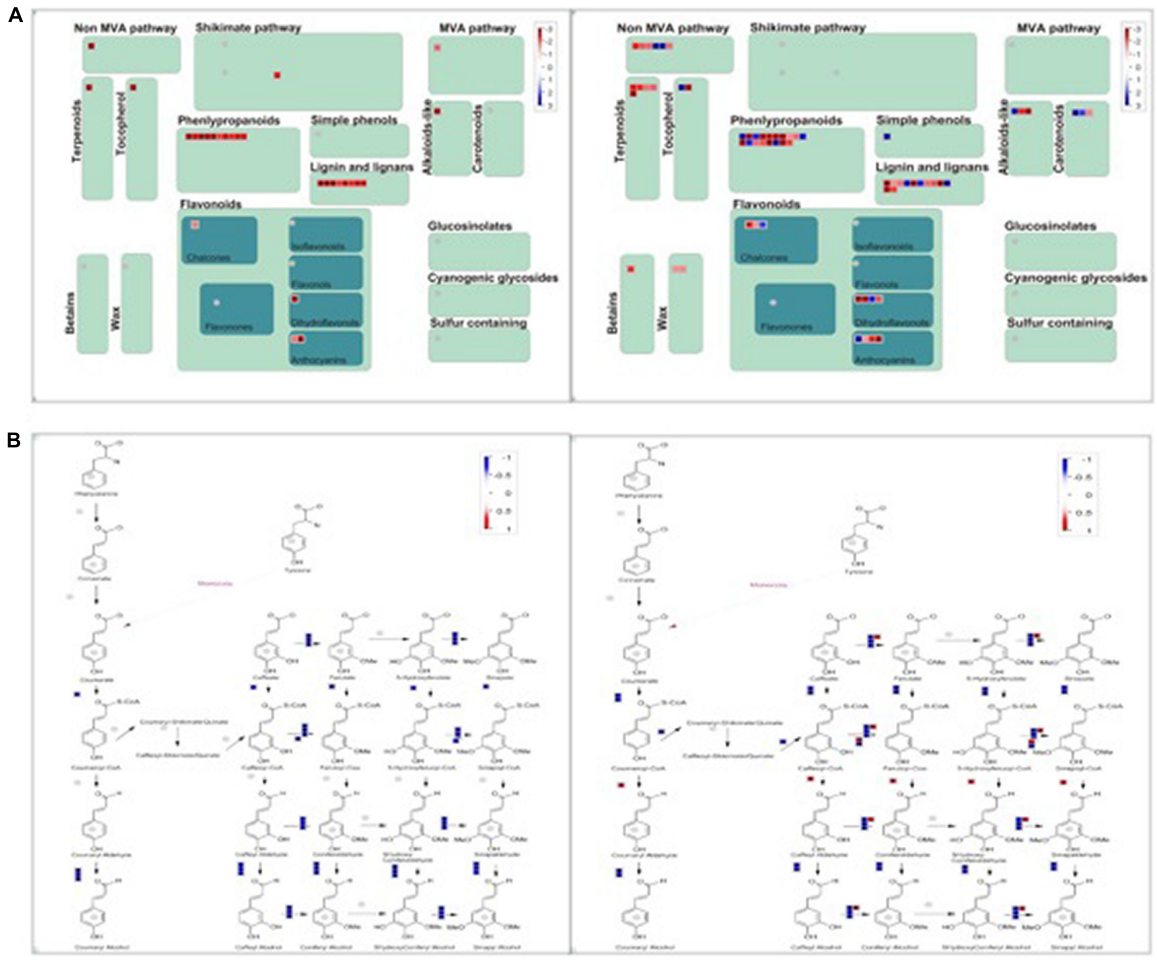

FIGURE 6
MapMan-based visualization of the transcripts involved in "secondary metabolism" in experimental groups (a). **(A)** The secondary metabolism pathway compares groups S (left) and D (right) at 12hpi. Functional subBINs shown in red or blue indicate up/down-regulation, respectively. **(B)** All DEGs involved in the pathway of phenylpropanoids in both groups S (left) and D (right) at 12 hpi. **(B)** The DEGs are involved in the Phenylpropanoids synthesis Pathway.

of the dodder, subsequently inducing a transcriptional response to salt stress signal.

A KEGG enrichment analysis revealed that photosynthesis, emergency response, and rhythm genes were significantly enriched. In addition, using a MapMan analysis, we found that the phenylpropanoid, lignin, and lignan pathways were significantly regulated in both groups. Phenylpropanoid compounds play an essential role in plant adaptation to different environmental conditions. Abiotic stress usually stimulates the phenylpropanoid pathway as evidenced by increases in phenols, flavonoids, anthocyanins, and lignin. These compounds protect plants from diseases or pests. The phenylpropanoid chemical structure can reduce reactive oxygen species by reducing free radicals. Therefore, the activation of the phenylpropanoid gene concomitant with stress induction in plants. Understanding the regulation of the phenylpropanoid pathway might be used to improve cultivation of crops, even under limiting stress conditions. Light, temperature, drought, and salt are stressors that activate the amphetamine gene. In recent years, microRNAs have been shown to regulate the phenylpropanoid genes, and synthetic microRNAs can also be used to regulate the expression of the phenylpropanoid genes. In addition, lignin biosynthesis genes play an essential role in plant adaptation to extreme salt stress. A metabolic analysis of a suspension cell culture of Arabidopsis thaliana root adapted to high salt stress showed that the lignin content increased and the cell wall became thickened. The regulation of the secondary metabolic pathway presents the appearance of salt tolerance and adaption characteristics in all experimental groups, which revealed an early salt stress response triggered by vascular system signal in citrus and provided new insight for improving plant stress resistance.

A dodder may transmit various stress-induced signals between host plants, changing the interaction or adaptation

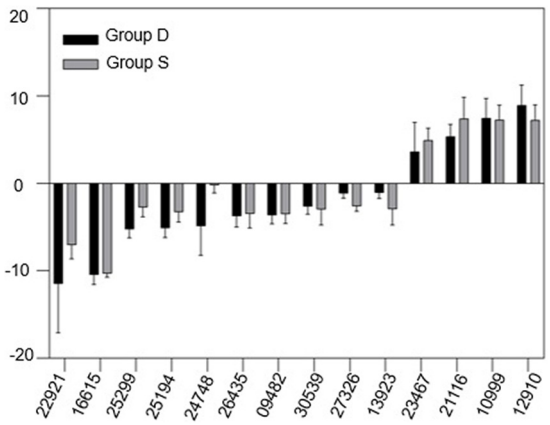

FIGURE 7
Gene expression change between group D and S. mRNA samples were extracted from the leaves of both experimental groups at 12hpi. The housekeeping gene GAPDH was used as an endogenous control. Each value represents three replicates mean ± standard deviation (SD).

mode between the host plants and the environment. This study suggests that a dodder can form a "telephone wire" to convey stress response between woody citrus plants under saline conditions. This study is significant to our understanding of the periodic signals of stress and provides a theoretical basis for an agricultural understanding of the early response regulation of *C. sinensis* to salt stress. Additionally, this study provides a theoretical timepoint of the system's signal generation and transmission characteristics in response to stress in the group S plants. Furthermore, the transcriptional change triggered by dodder-mediated mobile signal has been proposed, which helped understand the vascular stress-induced vascular signals at an early stage in woody plant. The other potential application of this study lies in the related research of citrus bacterial diseases (e.g., citrus bacterial canker disease and HLB). HLB is a devastating citrus disease caused by the phloem-colonizing bacterium "*Candidatus* Liberibacter asiaticus" (CLas). As a phloem-restricted bacteria, the citrus HLB pathogens can not be cultured *in vitro*, and its pathogenic mechanism is not clearly understood. A dodder can transmit the HLB pathogens from an infected to a healthy tree, which suggests that the dodder has potential for significant application in the study of pathogenic mechanism of citrus HLB. Recently, HLB has been considered as a pathogen-triggered immune disease, suggesting a new research direction for HLB studies, such as vascular signal transduction in and related triggering of an immune response (Ma et al., 2022). The dodder has not been used as a tool for signal transduction in woody plants because an effective model for its use has not been constructed. This study established a salt-mediated vascular signal transport system among a citrus-dodder-citrus community and a corresponding transcriptome change, which will provide an experimental basis for subsequent studies of citrus bacterial diseases.

Data availability statement

The original contributions presented in this study are publicly available. This data can be found here: NCBI, PRJNA839513.

Author contributions

SD and M-LB: conceptualization. SD, M-LB, and ZX: writing – original draft preparation. H-JM and W-SD: writing – review and editing. SD: supervision and project administration. ZX: transcriptome analysis. X-YL, PL, M-LB, and SD: experiment. H-KQ: plants maintenance. All authors have read and agreed to the published version of the manuscript.

Funding

This work was financially supported by the National Natural Science Foundation of China (32002021), the Major Science and Technology R&D Program of Jiangxi Province (20194ABC28007), the National Key R&D Program of China (2021YFD1400805), and Key R&D Projects of Jiangxi (20171ACF60022).

Conflict of interest

The authors declare that the research was conducted in the absence of any commercial or financial relationships that could be construed as a potential conflict of interest.

Publisher's note

All claims expressed in this article are solely those of the authors and do not necessarily represent those of their affiliated organizations, or those of the publisher, the editors and the reviewers. Any product that may be evaluated in this article, or claim that may be made by its manufacturer, is not guaranteed or endorsed by the publisher.

Supplementary material

The Supplementary Material for this article can be found online at: https://www.frontiersin.org/articles/10.3389/fpls.2022.986365/full#supplementary-material

References

Arif, Y., Singh, P., Siddiqui, H., Bajguz, A., and Hayat, S. (2020). Salinity induced physiological and biochemical changes in plants: an omic approach towards salt stress tolerance. *Plant Physiol. Biochem.* 156, 64–77. doi: 10.1016/j.plaphy.2020.08.042

Avsian-Kretchmer, O., Gueta-Dahan, Y., Lev-Yadun, S., Gollop, R., Ben-Hayyim, G., et al. (2004). The salt-stress signal transduction pathway that activates the gpx1 promoter is mediated by intracellular H2O2, different from the pathway induced by extracellular H2O2. *Plant Physiol.* 135, 1685–96. doi: 10.1104/pp.104.041921

Chaves, M., Flexas, J., and Pinheiro, C. (2009). Photosynthesis under drought and salt stress: regulation mechanisms from whole plant to cell. *Ann. Bot.* 103, 551–60. doi: 10.1093/aob/mcn125

Dai, W., Wang, M., Gong, X., and Liu, J. (2018). The transcription factor FcWRKY40 of Fortunella crassifolia functions positively in salt tolerance through modulation of ion homeostasis and proline biosynthesis by directly regulating SOS2 and P5CS1 homologs. *New Phytol.* 219, 972–89. doi: 10.1111/nph.15240

Duan, Y. P., Gottwald, T., Zhou, L. J., and Gabriel, D. W. (2008). First Report of dodder transmission of '*Candidatus* Liberibacter asiaticus' to tomato (*Lycopersicon esculentum*). *Plant Dis.* 92:831. doi: 10.1094/PDIS-92-5-0831C

Golldack, D., Li, C., Mohan, H., and Probst, N. (2014). Tolerance to drought and salt stress in plants: unraveling the signaling networks. *Front. Plant. Sci.* 5:151. doi: 10.3389/fpls.2014.00151

Lee, C., Chung, C. T., Hong, W. J., Lee, Y. S., Lee, J. H., Koh, H. J., et al. (2021). Transcriptional changes in the developing rice seeds under salt stress suggest targets for manipulating seed quality. *Front. Plant Sci.* 12:748273. doi: 10.3389/fpls.2021.748273

Li, S., Zhang, J., Liu, H., Liu, N., Shen, G., Zhuang, H., et al. (2020). Dodder-transmitted mobile signals prime host plants for enhanced salt tolerance. *J. Exp. Bot.* 71, 1171–84. doi: 10.1093/jxb/erz481

Liu, N., Shen, G., Xu, Y., Liu, H., Zhang, J., Li, S., et al. (2020). Extensive inter-plant protein transfer between *cuscuta* parasites and their host plants. *Mol. Plant.* 13, 573–85. doi: 10.1016/j.molp.2019.12.002

Liu, W. C., Song, R. F., Zheng, S. Q., Li, T., Zhang, B. L., Gao, X., et al. (2022). Coordination of plant growth and abiotic stress responses by Tryptophan Synthase beta Subunit1 through modulating tryptophan and ABA homeostasis in Arabidopsis. *Mol. Plant* 2022:9. doi: 10.1016/j.molp.2022.04.009

Ma, W., Pang, Z., Huang, X., Xu, J., Pandey, S. S., Li, J., et al. (2022). Citrus Huanglongbing is a pathogen-triggered immune disease that can be mitigated with antioxidants and gibberellin. *Nat. Commun.* 13:529. doi: 10.1038/s41467-022-28189-9

Mahajan, S., and Tuteja, N. (2005). Cold, salinity and drought stresses: an overview. *Arch. Biochem. Biophys.* 444, 139–58. doi: 10.1016/j.abb.2005.10.018

Nivedita, R. A., Ramchiary, N., and Abdin, M. Z. (2021). A high-throughput RNA-Seq approach to elucidate the transcriptional response of Piriformospora indica to high salt stress. *Sci. Rep.* 11:4129. doi: 10.1038/s41598-021-82136-0

Pandey, P., Irulappan, V., Bagavathiannan, M. V., and Senthil-Kumar, M. (2017). Impact of combined abiotic and biotic stresses on plant growth and avenues for crop improvement by exploiting physio-morphological traits. *Front. Plant. Sci.* 8:537. doi: 10.3389/fpls.2017.00537

Pardo-Hernandez, M., Lopez-Delacalle, M., and Rivero, R. M. (2020). ROS and NO regulation by melatonin under abiotic stress in plants. *Antioxidants* 9:9111078. doi: 10.3390/antiox9111078

Peng, Z., He, S., Gong, W., Sun, J., Pan, Z., Xu, F., et al. (2014). Comprehensive analysis of differentially expressed genes and transcriptional regulation induced by salt stress in two contrasting cotton genotypes. *BMC Genom.* 15:760. doi: 10.1186/1471-2164-15-760

Primo-Capella, A., Forner-Giner, M. A., Martinez-Cuenca, M. R., and Terol, J. (2022). Comparative transcriptomic analyses of citrus cold-resistant vs. sensitive rootstocks might suggest a relevant role of ABA signaling in triggering cold scion adaption. *BMC Plant Biol.* 22:209. doi: 10.1186/s12870-022-03578-w

Qin, Y., Zhang, J., Hettenhausen, C., Liu, H., Li, S., Shen, G., et al. (2019). The host jasmonic acid pathway regulates the transcriptomic changes of dodder and host plant under the scenario of caterpillar feeding on dodder. *BMC Plant Biol.* 19:540. doi: 10.1186/s12870-019-2161-8

Robertson, L. S., Galbraith, H. S., Iwanowicz, D., Blakeslee, C. J., Cornman, R. S., et al. (2017). RNA sequencing analysis of transcriptional change in the freshwater mussel Elliptio complanata after environmentally relevant sodium chloride exposure. *Environ. Toxicol. Chem.* 36, 2352–66. doi: 10.1002/etc.3774

Sharma, M., Kumar, P., Verma, V., Sharma, R., Bhargava, B., Irfan, M., et al. (2022). Understanding plant stress memory response for abiotic stress resilience: molecular insights and prospects. *Plant Physiol. Biochem.* 179, 10–24. doi: 10.1016/j.plaphy.2022.03.004

Shen, G., Liu, N., Zhang, J., Wu, J. Q., et al. (2020). Cuscuta australis (dodder) parasite eavesdrops on the host plants' FT signals to flower. *Proc. Natl. Acad. Sci. U S A.* 117, 23125–30. doi: 10.1073/pnas.2009445117

Shimizu, K., and Aoki, K. (2019). Development of parasitic organs of a stem holoparasitic plant in genus *cuscuta*. *Front. Plant Sci.* 10:1435. doi: 10.3389/fpls.2019.01435

Song, J., Bian, J., Xue, N., Xu, Y., Wu, J. Q., et al. (2022). Inter-species mRNA transfer among green peach aphids, dodder parasites, and cucumber host plants. *Plant Divers.* 44, 1–10. doi: 10.1016/j.pld.2021.03.004

Tan, F. Q., Tu, H., Liang, W. J., Long, J. M., Wu, X. M., Zhang, H. Y., et al. (2015). Comparative metabolic and transcriptional analysis of a doubled diploid and its diploid citrus rootstock (*C. junos* cv. Ziyang xiangcheng) suggests its potential value for stress resistance improvement. *BMC Plant Biol.* 15:89. doi: 10.1186/s12870-015-0450-4

Xie, R., Pan, X., Zhang, J., Ma, Y., He, S., Zheng, Y., et al. (2018). Effect of salt-stress on gene expression in citrus roots revealed by RNA-seq. *Funct. Integr. Genomics* 18, 155–73. doi: 10.1007/s10142-017-0582-8

Xie, R., Zhang, J., Ma, Y., Pan, X., Dong, C., Pang, S., et al. (2017). Combined analysis of mRNA and miRNA identifies dehydration and salinity responsive key molecular players in citrus roots. *Sci. Rep.* 7:42094. doi: 10.1038/srep42094

Yacoubi, I., Gadaleta, A., Mathlouthi, N., et al. (2022). Abscisic acid-stress-ripening genes involved in plant response to high salinity and water deficit in durum and common wheat. *Front. Plant Sci.* 13:789701. doi: 10.3389/fpls.2022.789701

Yoshida, S., Cui, S., Ichihashi, Y., Shirasu, K., et al. (2016). The Haustorium, a specialized invasive organ in parasitic plants. *Annu. Rev. Plant Biol.* 67, 643–67. doi: 10.1146/annurev-arplant-043015-111702

Zhang, H., Zhu, J., Gong, Z., and Zhu, J. (2022). Abiotic stress responses in plants. *Nat. Rev. Genet.* 23, 104–19. doi: 10.1038/s41576-021-00413-0

Zhang, J., Xu, Y., Xie, J., Zhuang, H., Liu, H., Shen, G., et al. (2021). Parasite dodder enables transfer of bidirectional systemic nitrogen signals between host plants. *Plant Physiol.* 185, 1395–410. doi: 10.1093/plphys/kiaa004

Zhou, L. J., Gabriel, D. W., Duan, Y. P., Halbert, S. E., and Dixon, W. N. (2007). First report of dodder transmission of Huanglongbing from naturally infected murraya paniculata to citrus. *Plant Dis.* 91:227. doi: 10.1094/PDIS-91-2-0227B

frontiers | Frontiers in Plant Science

TYPE Review
PUBLISHED 07 September 2022
DOI 10.3389/fpls.2022.995746

OPEN ACCESS

EDITED BY
Weicong Qi,
Jiangsu Academy of Agricultural Sciences (JAAS), China

REVIEWED BY
Baoxing Song,
Peking University, China
Xueqing Geng,
Shanghai Jiao Tong University, China

*CORRESPONDENCE
Degang Zhao
dgzhao@gzu.edu.cn
Xin Xie
ippxiexin@163.com

SPECIALTY SECTION
This article was submitted to Plant Bioinformatics, a section of the journal Frontiers in Plant Science

RECEIVED 16 July 2022
ACCEPTED 15 August 2022
PUBLISHED 07 September 2022

CITATION
Fang Y, Jiang J, Hou X, Guo J, Li X, Zhao D and Xie X (2022) Plant protein-coding gene families: Their origin and evolution.
Front. Plant Sci. 13:995746.
doi: 10.3389/fpls.2022.995746

Plant protein-coding gene families: Their origin and evolution

Yuanpeng Fang[1], Junmei Jiang[2], Xiaolong Hou[1], Jiyuan Guo[3], Xiangyang Li[2], Degang Zhao[4,5]* and Xin Xie[1,5]*

[1]Key Laboratory of Agricultural Microbiology, College of Agriculture, Guizhou University, Guiyang, China, [2]State Key Laboratory Breeding Base of Green Pesticide and Agricultural Bioengineering, Key Laboratory of Green Pesticide and Agricultural Bioengineering, Ministry of Education, Guizhou University, Guiyang, China, [3]Department of Resources and Environment, Moutai Institute, Zunyi, China, [4]Key Laboratory of Mountain Plant Resources Protection and Germplasm Innovation, Ministry of Education, College of Life Sciences, Institute of Agricultural Bioengineering, Guizhou University, Guiyang, China, [5]Guizhou Conservation Technology Application Engineering Research Center, Guizhou Institute of Prataculture/Guizhou Institute of Biotechnology/Guizhou Academy of Agricultural Sciences, Guiyang, China

Steady advances in genome sequencing methods have provided valuable insights into the evolutionary processes of several gene families in plants. At the core of plant biodiversity is an extensive genetic diversity with functional divergence and expansion of genes across gene families, representing unique phenomena. The evolution of gene families underpins the evolutionary history and development of plants and is the subject of this review. We discuss the implications of the molecular evolution of gene families in plants, as well as the potential contributions, challenges, and strategies associated with investigating phenotypic alterations to explain the origin of plants and their tolerance to environmental stresses.

KEYWORDS

plant evolution, gene families, molecular evolution, gene duplication, gene loss

Introduction

The driving force underlying biological evolution is environmental selection. The criteria for plant diversification include marked interspecific phenotypic and genetic differences, which can be accompanied by marked reproductive isolation. However, by its very nature, plant evolution is a process wherein variations occur based on the presence, composition, and number of genes (Lafon-Placette et al., 2016). Interestingly, throughout this process, several important evolutionary mechanisms have dominated. These mechanisms include changes in drought resistance and oxygen uptake due to adaptation of plants to life on land ("landing"), formation of root and vascular structures, and evolution of metabolites in response to stress hazards. Additionally, co-evolution of floral structures has occurred in parallel with insects, leading to the co-evolution of insect mouthparts and floral diversity. Indeed, selected traits are often closely associated

with the generation, development, and functional specialization of specific gene families (Gramzow et al., 2010; Cheng et al., 2019; Nikolov et al., 2019).

Horizontal gene transfer (HGT) may contribute to the adaptation of plants to life on land (Cheng et al., 2019), and has been documented in various gene families (Preston and Hileman, 2013; Shao et al., 2019). Moreover, several gene families are associated with repeated events, including tandem replication, fragment replication, wide-genome duplication (WGD), and transposable replication, leading to significant functional or phenotypic differences among plants (Wang et al., 2019, 2020; Schilling et al., 2020). For example, transposable replication often results in the formation of pseudogenes, while other types of replications cause a rapid expansion of plant genomes, leading to severe functional redundancy and increased functional differentiation in plant gene families. The presence of these redundant genes leads to a more complex adaptive system that drives plant-gene-phenotype-environment interactions, resulting in sub functionalization or *de novo* functionalization of these genes. This enables a coordinated and robust molecular network of environmental regulation in plants (Duplais et al., 2020; Man et al., 2020; Schilling et al., 2020).

A gene family is a group of genes with a common origin that encode proteins with similar structural properties and biochemical functions. Several key gene families, including *MADS* (Mcml Agamous Deficiens Srf-box domain gene family), *CYP* (Cytochrome P450 protein family), and *HSP* (Heat Shock Protein family), are core promoters of plant metabolism and flower formation (Ng and Yanofsky, 2001; Nelson and Werck-Reichhart, 2011; Bondino et al., 2012). For example, in the "ABCDE" model of flower development, the *MADS-box* genes are divided into two groups, namely, *M-type_MADS* and *MIKC_MADS*, with the latter considered to be the main contributor to flower development (Airoldi and Davies, 2012; Theissen et al., 2016; Hsu et al., 2021). In addition, evolutionary studies suggest extensive functional differentiation within these gene families and subfamilies. For example, the *CYP* gene family can be divided into two groups: type A-encoding genes, which encode oxygenases acting in pathways for the synthesis of plant-specific metabolites, including many chemosensory substances and drug components, and non-type A-encoding genes, which encode oxygenases required for the synthesis of more basic plant metabolites, such as endogenous plant hormones and essential metabolites (Ng and Yanofsky, 2001; Nelson and Werck-Reichhart, 2011; Airoldi and Davies, 2012; Theissen et al., 2016; Hsu et al., 2021; Su et al., 2021). Knowledge of the functional roles of plant gene families is vital to our understanding of plant evolution.

However, due to the richness of species and the associated wide range of gene families, the evolution of most gene families is poorly documented. This limits our in-depth exploration of plant origin and differentiation, as well as the application of molecular genetics. Therefore, evolutionary studies have taken a more comprehensive, multispecies approach.

Plant evolution

The evolution of plants from primitive plant ancestors has been largely simplified to red algae to green algae (basic green plants), mosses (basic land plants), ferns (basic vascular plants), gymnosperms (basic seed plants), and angiosperms. During this process, the phenotypes and genotypes of algae, mosses, ferns, and seed plants varied considerably. At the phenotypic level, selection of characteristics, such as plant type, leaf shape, and floral organs, is influenced by animal behavior, human activities, as well as climatic factors, leading to broad phenotypic diversity (**Figure 1**). At the genotypic level, abundant genetic changes such as WGD, tandem repeats, transposition, gene loss, and parallel gene transfer contribute significantly to the diversity of protein-coding plant genes and selective responses to the environment (Gramzow et al., 2010; Preston and Hileman, 2013; Cheng et al., 2019; Nikolov et al., 2019; Shao et al., 2019; Schilling et al., 2020).

Although the origin of terrestrial plants remains controversial, Cheng et al. (2019) reported that land plants might have originated from two Zygnematophyceae species, namely, *Spirogloea muscicola* and *Mesotaenium endlicherianum*. Cheng et al. (2019) and Liang et al. (2020) further reported that two species from outside the Streptophytina—*Mesostigma viride* and *Chlorokybus atmophyticus*—may represent the most primitive branches of terrestrialized plants. Further, genomic analysis identified Prasinodermaphyta as a potential new phylum between the green and red algal phyla (Li et al., 2020). Meanwhile, molecular analyses have revealed that mosses originated approximately 908–680 million years ago (Mya), suggesting that the origin of land plants occurred earlier than the Ordovician (Sun et al., 2021). Additionally, comparison of the genomes of magnolias indicates that Magnoliids and monocotyledons form a unique monophyletic group that may appear earlier than either the monocotyledon or the Austrobaileyales, Nymphaeales, and Amborellales (ANA) branches (Dong et al., 2021).

Based on genomic and transcriptomic analysis of representative bryophytes (including liverworts, hornworts, and mosses), Gao et al. (2020) noted that polyploidy was common in bryophytes. Polyploidization events occurred in bryophyte ancestors before differentiation, as well as within Funarioideae ancestors, and Buxbaumiidae, Diphysciidae, Timmiidae, and Funariidae branches. Schneider et al. (2017) found that polyploidization plays an important role in fern diversity. In fact, several instances of polyploidization contributed to the diversity of Asplenium plants, with ploidy

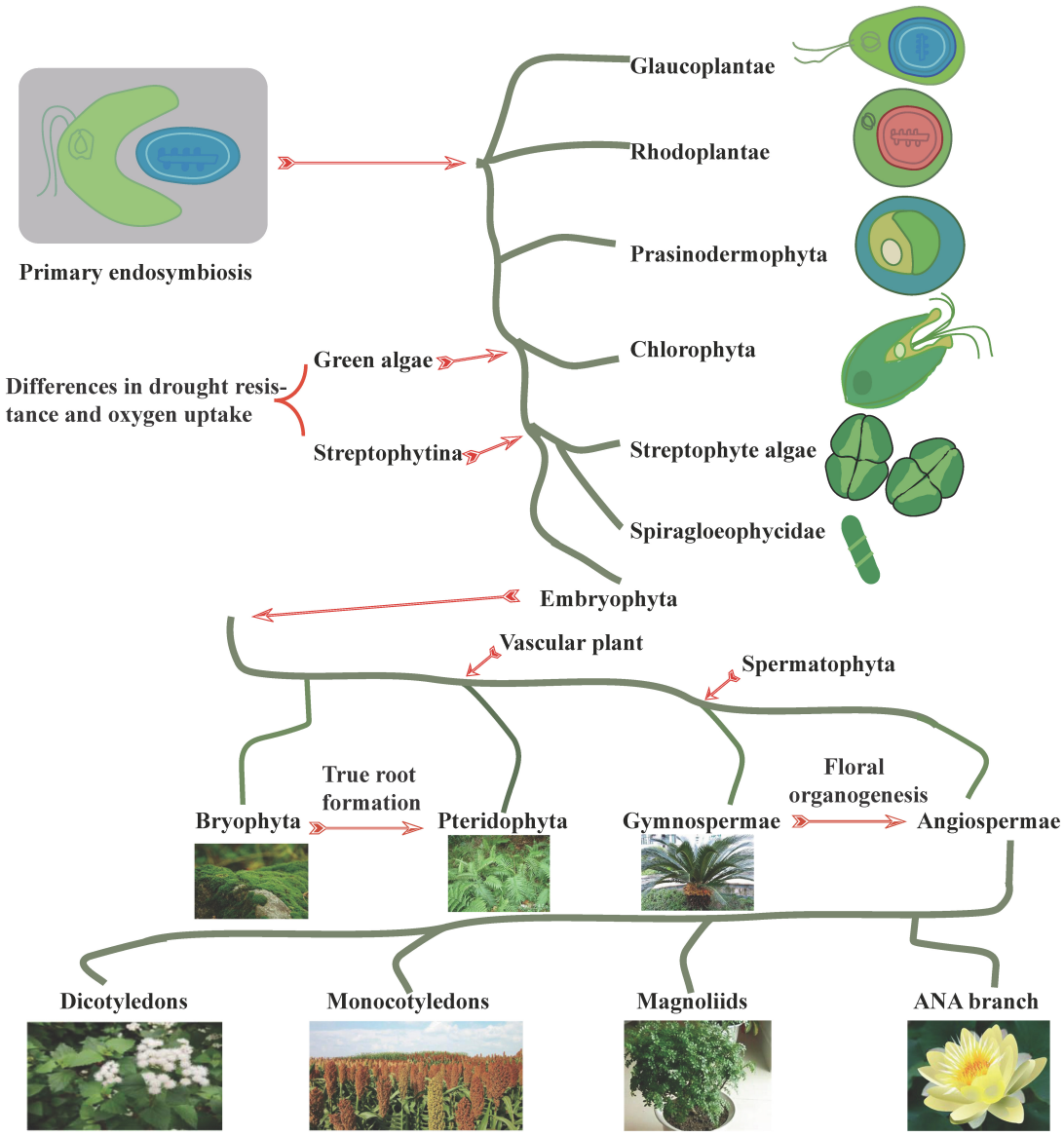

FIGURE 1
Plant evolution. The symbiosis of dinoflagellate protists with cyanobacteria prompted the occurrence of phytoplanktonic communities, with diverse phytoplanktonic taxa (including plants, green algae, red algae, and cryptophytes) arising through biological adaptation to the environment. At the origin of green algae and Streptophytina, significant differences in drought and oxygen stress tolerance developed to facilitate terrestrialization. During the process of adaptation to the environment, certain taxa underwent unique adaptations in root, flower, and other related phenotypes, which in turn ensured the dominance of the widely distributed angiosperms.

levels of 2* and 4* being the most common. Meanwhile, two of the oldest polyploidization events were reported in seed plants (192 Mya) and angiosperms (319 Mya), during which genome multiplication was a hallmark of the evolution of angiosperms from gymnosperms (Schneider et al., 2017). In basal angiosperms, the ANA branch of camphor and water lily genomes indicates a polyploidization event in the water lily ancestor (Zhang et al., 2019). Similarly, magnolia genomes indicate that one polyploidization event occurred during their ancestry, while two additional polyploidization events occurred in Lauraceae. Wang et al. (2019) and Zhang L. S. et al. (2020) systematically organized the abundant polyploidy of angiosperms and confirmed that monocotyledonous plants from the Gramineae (100–110 Mya) and Lemnaceae (115–125 Mya) families are highly polyploid. Specifically, the orders Poales and Arecales appear to have had one polyploidization event, whereas plantains arose from three polyploidization events over a short period. Indeed, dicotyledonous plants are usually paleohexaploid (gamma triplication; 115–130 Mya), including Malvaceae,

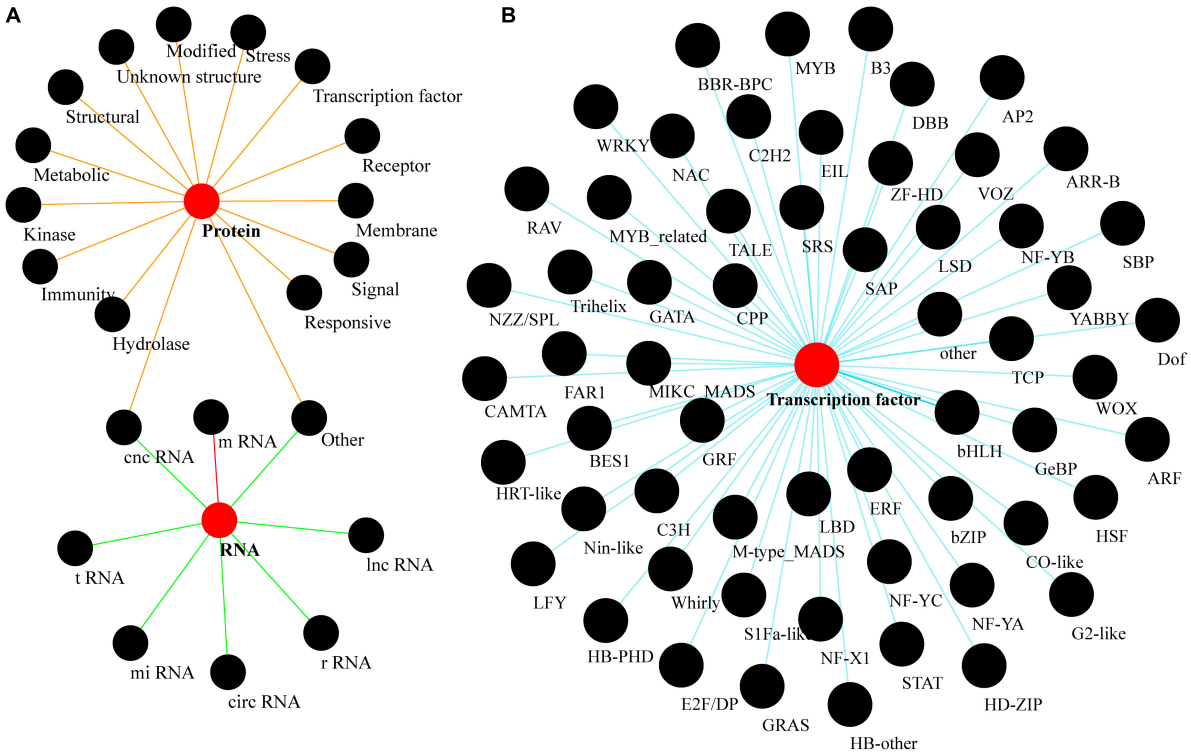

FIGURE 2
Plant gene families. **(A)** A brief classification of gene families found in plants. **(B)** A rich taxonomy of plant transcription factors. tRNA is an RNA composed of 76–90 nucleotides that carry amino acids into the ribosome and synthesize proteins under the guidance of mRNA; lnc RNA is a class of non-coding RNA molecules longer than 200 nt; mi RNA is a class of endogenous, small RNAs of about 20–24 nucleotides in length; circ RNA is a class of RNAs that do not have a 5′ terminal cap and 3′ terminal poly(A) tail, and are covalently bonded to form a loop structure; they are a class of non-coding RNA molecules that are found in living organisms. cnc RNA (coding and non-coding RNA) is a family of functional genes that can be differentially sheared in a variable manner, resulting in both short peptides or small molecular weight proteins and untranslatable functional RNAs (e.g., lnc RNA, mi RNA, etc.).

Brassicaceae, Cucurbitaceae, and Leguminosae, all of which originated following multiple ploidy events (Wang et al., 2019). Importantly, abundant gene duplications have also been reported in the genomes of other angiosperms, including sugarcane, kiwifruit, and tea tree (Vilela et al., 2017; Wang et al., 2018).

Overview of plant gene families

A plant gene family refers to a group of genes with related functions that are generated by gene duplication from a single-copy gene source in an ancestor, and retain similar sequence and structure (Li et al., 2022). Gene families can be associated with repeated events, such as tandem replication, fragment replication, WGD, or transposable replication, based on the scope of replication, size of the replicated region, and influence of transposons (Airoldi and Davies, 2012; Su et al., 2021). Transposable replication is one such event that often leads to formation of pseudogenes, while other types of replications cause a rapid expansion of plant genomes, leading to severe functional redundancy and increased functional differentiation within plant gene families (Schilling et al., 2020; Yu et al., 2020).

Plant genomes include protein-coding and non-coding RNA (ncRNA) gene families (Song et al., 2021; Li et al., 2022). Gene families encoding ncRNA can be further subdivided into those encoding lncRNA (long non-coding RNA), miRNA (micro RNA), rRNA (ribosomal RNA), tRNA (transfer RNA), and circRNA (circular RNA), and will not be further discussed here. Protein-coding gene families can also be broadly classified by the function of the proteins they encode, including receptors, kinases, epigenetic modification, structural, and transcription factors (TFs) (**Figure 2A**). However, these classifications are not unique; gene families can also be divided into several categories depending upon the classification criteria, such as classifications based on function, structural features, or the pathways involved. Hence, the class of chloroplast transporters TOC-TIC can be classified as either membrane proteins or structural proteins, whereas G-protein-coupled signal receptors can be classified as either membranes

or receptor proteins. Many gene families within plant genomes are unique to plants, including more than 57 families of TFs, e.g., the TEOSINTE BRANCHED 1/CYCLOIDEA/PROLIFERATING CELL FACTOR (*TCP*), and SQUAMOSA PROMOTER-BINDING PROTEIN (*SBP*) families (**Figure 2B**; Reeves and Olmstead, 2003; Yang et al., 2008; Preston and Hileman, 2013; Jin et al., 2017; Wu et al., 2017).

Evolution of gene families in plants

Evolution of resistance gene families

Resistance genes are groups of genes encoding proteins required for tolerance or immunity during plant adaptation to adverse external stress. Multiple environmental stresses have driven the molecular selection of these genes. Resistance gene clusters such as the *NBS-LRR* family are large and exhibit a high degree of functional differentiation (Shao et al., 2019). *HSP* and *sHSP* encode important heat-responsive proteins and molecular chaperones, and the copy number of *sHSPs* is significantly increased in polyploid plants with multiple branches. Genes from different subclasses may have diversified in function (Bondino et al., 2012). In contrast, the molecular chaperone gene *PFDN,* which displays only marginal differences between different groups, is expanded in polyploid plants such as soybean (Cao et al., 2016). Furthermore, the number of chilling injury-related gene (*CRG*) family members in Cruciferae is affected by polyploidy (Song et al., 2020). On the other hand, evolution of the *AOX* gene family is primarily mediated by intron/exon loss or gain, and fragment deletion, although gene loss and duplication, as well as tandem blocking, also play essential roles in the origin and maintenance of the family (Pu et al., 2015; **Tables 1**, **2**; **Figure 3**).

Natural selection often drives the evolution of disease resistance-related genes to establish functional differentiation between these genes, with various external hazards leading to the vast expansion of the genes. For example, there are many structural variations in the leucine-rich repeat receptor-like kinase (*LRR-RLK)* gene family (Man et al., 2020). The resistance I genes from the *NBS-LRR* superfamily originated from Chlorophyta (green algae) and were classified into five categories according to their structural characteristics [Chlorophyta: RNL; Charophyta: CNL; Embryophyta (land plants): TNL, HNL, and PNL] (Shao et al., 2019). *NLR* genes (*CNL*, *TNL*) are clearly classified as being found in Solanaceae species; however, their prevalence varies markedly, with few reported within the genome of tomato plants and many more in those of potatoes and peppers (Borrelli et al., 2018). Another example is offered by the evolution of the *AGO* gene family, which encodes proteins associated with antiviral activity. This family may have experienced 133–143 repeat events and 272–299 loss events, including five major repeats. Specifically, the differentiation of green algae may have formed four major branches (I: 1/10, II: 5, III: 4/6/8/9, IV: 2/3/7) of the *AGO* gene family (Singh et al., 2015). Similarly, the *DRB* gene family is divided into two branches based on differences in the number of double-stranded RNA binding motifs (dsRBM); the number of DRB proteins also varies among different species (Clavel et al., 2016). The plant *RDR* (RNA-dependent RNA enzyme) family originated from copies of three monophyletic genes, *RDR*α, *RDR*β, and *RDR*γ, and was dependent on species divergence (Zong et al., 2009). Plant *DCL* (Dicer-like), however, followed the evolutionary traces of early plant evolution through independent replication, remodeling its RNA binding pocket in response to virus resistance (Mukherjee et al., 2013). Finally, expansion of the *TLP* gene family in green algae (1), mosses (6), and angiosperms (>20), may be based on tandem and segmental duplication events (Cao et al., 2016; **Tables 1**, **2**; **Figure 3**).

Evolution of transcription factor gene families

Transcription factors function as regulatory elements of various plant processes, including growth, the stress response, and reproduction (Yang et al., 2008; Lian et al., 2014; Zhao et al., 2014; Finet et al., 2016; Vasco et al., 2016; Feng et al., 2017; Wu et al., 2017; Naramoto et al., 2020). Due to the rich evolutionary history of plants, TF gene families tend to have more members and a higher degree of functional differentiation compared with structural protein-related coding genes (Finet et al., 2016). In particular, the *AHL* gene family, which is related to plant growth and development, may have evolved from the fusion of algal PPC structural proteins and AT-hook motifs, and is thought to have originated in bryophytes. This family can be divided into three groups (A: I; B: II, III), with a high degree of gene loss and numerous duplication events throughout evolution (Zhao et al., 2014). The *WOX* gene family, which is involved in cell division, originated in green algae and is primarily divided into nine classes (WOX1/2, WOX5/7, WOX3, WOX4, WOX6, WOX11/12, WOX13, and WUS) with WOX13 being recognized as the oldest branch. Indeed, WOX genes exhibit significant variation in their motifs and number of members throughout their evolutionary process (Lian et al., 2014). CPP-like genes, which are associated with plant development, are divided into four branches: Gene deletion and species-specific amplification have been important in expanding this gene family, while positive selection has served as the primary evolutionary driving force (Yang et al., 2008).

TABLE 1 Structural analysis of plant protein-coding gene families.

Gene family	Abbreviation	Major function	Domain	References
Metabolic enzymes				
Cytochrome P450	*CYP/P450*	Monooxygenation activity	P450	Su et al., 2021
12-oxo-phytodienoate acid reductase	*OPR*	Jasmonic acid biosynthesis	Unknown	Guo et al., 2016
3-hydroxy-3-methylglutaryl Coenzyme A Reductase	*HMGR*	Terpene synthesis	PF00368	Li et al., 2014
Aconitase	*ACO*	Catalyzes the Isomerization of citrate to isocitrate	ACO	Wang et al., 2016
3-ketoacyl-coa synthase	*KCS*	Very long-chain fatty acids (VLCFAS) synthesis	ACP synthase III C and like	Guo et al., 2016
Antiviral gene cluster				
Leucine-rich repeats Receptor-like protein kinases	LRR-RLK	Perceptual signaling and phosphorylation	LRR and RLK	Man et al., 2020
Argonaute	*AGO*	Antiviral activity	PAZ and Piwi	Singh et al., 2015
Double stranded RNA binding protein	*DRB*	Antiviral activity	DSRM	Clavel et al., 2016
Thaumatin-like protein	*TLP*	Plant disease resistance	TLP	Cao et al., 2016
Nucleotide-binding leucine-rich repeat	*NLR*	Plant disease resistance	NB-ARC	Borrelli et al., 2018
Nucleotide binding site leucine-rich repeat	*NBS-LRR*	Plant disease resistance	LRR and NBS	Shao et al., 2019
Transcription factor cluster				
\	*MADS*	Flower development	MADS	Gramzow et al., 2010
AT-hook Motif Nuclear Localized	*AHL*	Organ development and bulky	AT-hook and PPC	Zhao et al., 2014
Arabidopsis LSH1 and Oryza G1	*ALOG*	Regulate reproductive growth	Unknown	Naramoto et al., 2020
Auxin/Indole Acetic Acid and Auxin Response Factor	*Aux/IAA*	Auxin response	Aux/IAA	Wu et al., 2017
Cysteine-rich polycomb-like protein	*CPP-like*	Development of reproductive organs	CXC	Yang et al., 2008
Wuschel-related	*WOX*	Regulating cell division and differentiation	WOX	Lian et al., 2014
Class III Homeodomain-Zine finger protein	*C3HDZ*	Leaf growth	HD-ZIP	Vasco et al., 2016
\	*YABBY*	Leaf growth	YABBY	Finet et al., 2016
\	*3R-MYB*	Drought and development	3 MYB	Feng et al., 2017
Anti-stress gene cluster				
Small heat shock protein/alpha-crystallin	*sHSP/Cry*	Molecular chaperone	HSP20	Bondino et al., 2012
Prefoldin	*PFDN*	Molecular chaperone	Prefoldin	Cao, 2016
Cold-related genes	*CRG*	Cold-related	Unknown	Song et al., 2020
Alternative oxidase	*AOX*	Ubiquinol to reduce oxygen to water	Unknown	Pu et al., 2015
Structural composition or organogenesis gene cluster				
SH3 and BAR domain-containing protein	*SH3P*	The Plant Cell Division and Autophagy	BAR domain	Forero and Cvrckova, 2019
Hairy meristem	*HAM*	Meristem formation	GRAS	Geng et al., 2021
Cellulose synthase	*CesA*	Cellulose synthesis	Cellulose_synt, Glycos_transf_2 and Glyco_trans_2_3	Little et al., 2018
Flowering locus t/terminal flower 1	*FT/TFLl*	Flower development	Unknown	Jin et al., 2021
Myosin	*Myo*	Actin system	Unknown	Peremyslov et al., 2011

(Continued)

TABLE 1 (Continued)

Gene family	Abbreviation	Major function	Domain	References
Alternative splicing modulators nuclear speckle rna-binding proteins	*NSR/RBP*	Gene expression	Unknown	Lucero et al., 2020
Cyclin	*Cyc*	Cycle control	Cyclin_N and Cyclin_C	Boscolo-Galazzo et al., 2021
OVATE family protein	*OFP*	Fruit shape regulation	OVATE	Liu et al., 2014
Aquaporins	*AQP*	Water inflow and cycle control	Unknown	Hussain et al., 2020
Dynein light chain	*DLC*	Dynein complexes	4 helix and 4 sheet	Cao et al., 2017
Psbp protein	*PsbP*	Oxygen-evolving complex (OEC)	I and II	Ifuku et al., 2008
Signal-mediated gene clusters				
Calcineurin B-Like and CBL-Interacting Protein Kinase	*CBL/CIPK*	Ca^{2+} signal	CBL/CIPK/C2	Zhang X. X. et al., 2020
Calcium-dependent protein kinase and CDPK-related kinase	*CDPK/CRK*	Ca^{2+} signal	CDPK/CRK/C2	Xiao et al., 2017
Glycerol-3-phosphate acyltransferase	*GPAT*	Phospholipid signal	acyltransferase	Waschburger et al., 2018
Phosphatidyl ethanolamine binding protein	*PEBP/MFT-like*	Phospholipid signal	Unknown	Hedman et al., 2009; Karlgren et al., 2011
Rapid alkalization factor	*RALF*	PH rise induction	Unknown	Cao and Shi, 2012
Auxin response factor	*ARF*	Auxin signal transduction	ARF	Finet et al., 2013
Cyclic nucleotide-gated ion channel	*CNGC*	Calcium signal transduction	CNB	Saand et al., 2015
C-terminally encoded peptide	*CEP*	Small secreted peptide signals	CEP	Ogilvie et al., 2014
Poly(A)-binding protein	*PAB*	Promoting mrna integrity and protein synthesis	PABP	Gallie and Liu, 2014
Supply of nutrients or ions gene clusters				
Vacuolar iron transporter	*VIT*	Iron sensing and transport	VIT	Cao, 2019
Ferritin	*Fer*	Iron sensing and transport	Unknown	Strozycki et al., 2010
H+-ppase	*VP*	Proton-translocating pyrophosphatase	TM1-16	Zhang Y. M. et al., 2020
Phosphate 1	*PHO*	Inorganic phosphate (Pi) sensing and transport	SPX, EXS	He et al., 2013
Cobalamin-independent methionine synthase	*CIMS*	Cobalamin-independent methionine synthase	Unknown	Rody and de Oliveira, 2018
Hydrolase gene clusters				
B-amylase	*BAM*	Glucan hydrolytic	Unknown	Thalmann et al., 2019
Sucrose synthase	*SUS*	Sugar hydrolysis	Unknown	Xu et al., 2019
Apparent components gene clusters				
Histone methyltransferases	*HMT*	Methylation process	Unknown	Zhao et al., 2018
F-box	*FBP*	Ubiquitylation process	F-box	Navarro-Quezada et al., 2013

Major function indicates the most important functional role of gene families; domain refers to a conserved region of a protein sequence that may be related to the functional site of the protein. Some gene families are marked with a domain labeled "Unknown" to denote that a specific model of their overall structure is not currently known, and the methods available for further discovery of new sequences can only rely on the appropriate "blast p" homology search. For such proteins, a larger scale phylogenetic exploration may be useful to infer and resolve their function and structure.

The *SPL/SBP* family mainly includes nine subbranches, among which there are obvious evolutionary differences; their formation may be completed before the differentiation of the angiosperms (Preston and Hileman, 2013). The nine evolutionary branches, namely, *SPL* evolutionary branch-I, evolutionary branch-II, evolutionary branch-IV, evolutionary branch-V, evolutionary branch-VI, evolutionary branch-VII, evolutionary branch-VIII, and evolutionary branch-IX, are characterized by differences in function and altered mi RNA regulatory differences (Preston and Hileman, 2013). The *TCP* gene family consists of two main classes (classes I and II, i.e.: the CIN and CYC/TB1 evolutionary branches) (Liu et al., 2019). Among them, all land plants have CIN evolutionary branch *TCP* genes, while CYC evolutionary branch genes are only found in true dicotyledons and monocotyledons (Liu et al., 2019). In addition, the rapid expansion of the *TCP* gene family is consistent with a polyploidy trend in land plants, with fewer tandem duplication events (Liu et al., 2019). *3R-MYB* is a regulatory TF associated with drought-resistance and development. Its structure is progressively more complex in different species groups, in conjunction with a gradual increase in the number of gene family members,

TABLE 2 Evolutionary events of plant protein-coding gene families.

Gene family	Numbers	Coverage	Copy event	Contribution to genome-wide repeating events	Stage of event	References
Metabolic enzymes						
CYP/P450	251	Unknown	Order level and below level	B_1	Unknown	Su et al., 2021
OPR	6	A_1, 11	Order level and below level	B_1	Chlorophyta, unknown	Li et al., 2009
HMGR	2	A_1, 20	Species level	B_1	Moss, unknown	Li et al., 2014
ACO	3	A_2, 12	Species level	B_1	Unknown	Wang et al., 2016
KCS	11	A_1, 28	Order level and below level	B_1	Chlorophyta, unknown	Li et al., 2009
Antiviral						
LRR-RLK	225	A_2, 9	Species level	B_1	Unknown	Man et al., 2020
AGO	10	A_1, 30	Order level and below level	B_1	Chlorophyta, unknown	Singh et al., 2015
DRB	7	A_5, 15	Species level	B_1	Unknown	Clavel et al., 2016
TLP	24	A_1, 6	Order level and below level	B_1	Chlorophyta, unknown	Cao et al., 2016
NLR	144	A_5, 3	Species level	B_1	Unknown	Borrelli et al., 2018
NBS-LRR	204	A_0, 79	Order level and below level	B_1	Chlorophyta, unknown	Shao et al., 2019
Transcription factors						
MADS	43	A_0, Unknown	Order level and below level	B_1	Earlier, MRCA	Gramzow et al., 2010
AHL	29	A_1, 19	Order level and below level	B_1	Moss, unknown	Zhao et al., 2014
ALOG	10	A_1, 9	Order level and below level	B_1	Chlorophyta, ALOS1	Naramoto et al., 2020
Aux/IAA	29	A_1, 17	Order level and below level	B_1	Moss, unknown	Wu et al., 2017
CPP-like	8	A_4, 2	Unknown	B_0	Unknown	Yang et al., 2008
WOX	16	A_0, 50	Order level and below level	B_1	Chlorophyta, unknown	Lian et al., 2014
C3HDZ	5	A_1, 32	Order level and below level	B_1	Chlorophyta, unknown	Vasco et al., 2016
YABBY	6	A_3, 50	Species level	B_1	Unknown	Finet et al., 2016
3R-MYB	5	A_1, 65	Order level and below level	B_1	Chlorophyta, unknown	Feng et al., 2017
Anti-stress						
sHSP/Cry	27	A_4, 17	Species level	B_1	Unknown	Bondino et al., 2012
PFDN	9	A_1, 14	Family level	B1	Chlorophyta, unknown	Cao et al., 2016
CRG	420	A_2, 21	Species level	B1	Unknown	Song et al., 2020
AOX	5	A_1, Unknown	Order level and below level	B_1	Charophyta, *AOX1* and *AOX2*	Pu et al., 2015
Structural composition or organogenesis						
SH3P	3	A_1, 20	Family level of angiosperms	B_0	Charophyta, *SH3P1*	Lucero et al., 2020
HAM	3	A_1, 42	Order level and below level	B_1	Moss, unknown	Liu et al., 2014
CesA	26	A_4, 46	Order level and below level	B_1	Charophyta, unknown	Guo et al., 2016
FT/TFLl	6	A_1, Unknown	Order level and below level	B_1	Charophyta, MFT-like	Forero and Cvrckova, 2019
Myo	17	A_1, 12	Order level and below level	B_0	Charophyta, *myo-xi (a)*	Cao et al., 2017
NSR/RBP	2	A_5, 7	Species level	B_1	Unknown	Hussain et al., 2020
Cyc	50	A_1, 10	Order level and below level	B_1	Chlorophyta, unknown	Ifuku et al., 2008
OFP	19	A_1, 19	Species level	B_1	Moss, unknown	Jin et al., 2021
AQP	35	A_1, 24	Order level and below level	B_1	Chlorophyta, *lips*	Peremyslov et al., 2011
DLC	6	A_1, 15	Order level and below level	B_1	Chlorophyta, *DLC-VIII*	Boscolo-Galazzo et al., 2021
PsbP	2	Unknown	Unknown	B_0	Unknown	Little et al., 2018
Signal transduction						
CBL/CIPK	14/35	A_2, 18	Order level and below level	B_1	Unknown	Xiao et al., 2017
CDPK/CRK	34/8	A_3, 6	Family level	B_1	Unknown	Cao and Shi, 2012
GPAT	10	A_1, 39	Order level and below level	B_1	Chlorophyta, *GPAT* and *GPAT9*	Karlgren et al., 2011
PEBP	6	A_3, 106	Order level and below level	B_1	Unknown	Hedman et al., 2009; Zhang X. X. et al., 2020

(Continued)

TABLE 2 (Continued)

Gene family	Numbers	Coverage	Copy event	Contribution to genome-wide repeating events	Stage of event	References
RALF	33	A_4, 4	Family level	B_1	Unknown	Finet et al., 2013
ARF	23	A_2, 21	Unknown	B_0	Unknown	Saand et al., 2015
CNGC	20	A_4, 15	Unknown	B_0	Unknown	Ogilvie et al., 2014
CEP	12	A_3, 106	Order level and below level	B_1	Unknown	Gallie and Liu, 2014
PAB	8	A_1, 54	Unknown	B_1	Unknown	Geng et al., 2021
Supply of nutrients or ions						
VIT	6	A_1, 14	Angiosperms	B_0	Unknown	Strozycki et al., 2010
Fer	4	A_0, 16	Order level and below level	B_0	Unknown	Zhang Y. M. et al., 2020
VP	3	A_0, 27	Order level and below level	B_1	Rhodoplantae and Chlorophyta, unknown	He et al., 2013
PHO	9	A_1, 32	Order level and below level	B_1	Chlorophyta, unknown	Geng et al., 2021
CIMS	3	A_1, 35	Species level	B_1	Chlorophyta, unknown	Cao, 2019
Hydrolases						
BAM	10	A_0, 136	Order level and below level	B_1	Unknown	Rody and de Oliveira, 2018
SUS	6	A_4, 16	Species level	B_1	Unknown	Thalmann et al., 2019
Other components						
HMT	3	A_2, 29	Unknown	B_0	Unknown	Xu et al., 2019
FBP	211	A_1, 34	Order level and below level	B_1	Chlorophyta, unknown	Zhao et al., 2018

A0, Archaeplastida populations; A1, green plant population; A2, land plant population; A3, seed plant population; A4, angiosperm population; A5, dicotyledonous plant population. For the contributions made to the genome-wide repeat events (such as paleopolyploidization and WGD), B0 indicates that no effect was observed or had been studied, and BN indicates an effect caused by N repeats. The copy event refers to the level of replication events that impact copy number.

forming three branches (A, B, and C3) in angiosperms (Feng et al., 2017). The family of *ALOG* genes, which regulate reproductive growth, originated in green algae and expanded significantly in angiosperms (Naramoto et al., 2020). The *YABBY* and *C3HDZ* gene families, associated with leaf growth, have evolved in stages of biological evolution and their molecular structures have given rise to several major branches with different molecular classes exerting unique effects on leaf development (Finet et al., 2016; Vasco et al., 2016).

Moreover, the *MADS* and *AUX/IAA* gene families originated in early land plants (mosses) and expanded to encompass multiple gene sub-family classes that have shown rich functional differentiation with multiple rounds of evolutionary events (Theissen et al., 2016; Wu et al., 2017). Specifically, the MADS domains in plants originated from the transformation of topoisomerase IIA subunit A (*TOPOIIA-A*) into *MRCA* and the latter's subsequent modification to SRF-like and MEF2-like MADS-box genes. Furthermore, in angiosperms, type II *MADS-box* genes mediate major evolutionary innovations in plant flowers, ovules and fruits, whereas the formation of the *Mγ* and interacting *Mα* genes (*Mα**) of type I *MADS-box* can be traced back to the angiosperm ancestor and may be related to its heterodimeric function in angiosperm-specific embryonic trophoblast endosperm tissue (Qiu and Claudia, 2021). This evolutionary process was affected by various events, including replication and functional differentiation, resulting in the functional diversity of their regulatory properties (Ng and Yanofsky, 2001; Gramzow et al., 2010; Airoldi and Davies, 2012; Theissen et al., 2016; Schilling et al., 2020; Hsu et al., 2021; **Tables 1**, **2**; **Figure 3**).

Evolution of metabolic enzyme gene families

Metabolites are a direct manifestation of plant physiology. Highly specific biochemical processes that produce various metabolites have driven the formation and functional specialization of metabolic gene clusters (Duplais et al., 2020). Studies investigating the recurring events that led to the development of plant metabolic enzyme gene clusters have revealed a close relationship among the different metabolites (Duplais et al., 2020). The *CYP/P450* gene family of mono-oxygenases is highly abundant in angiosperms, possibly due to multiple repeated events (polyploidy, tandem replication, and fragment repeat). They can be divided into two categories, A-type (e.g., CYP71) and non-A-type (e.g., CYP51, CYP72, CYP74, CYP85, CYP86, CYP97, CYP710,

CYP711, CYP727, and CYP746), with CYP51 and CYP97 potentially representing the oldest clades (Su et al., 2021). The *ACO* gene families associated with respiration were almost lost early in the evolutionary path; however, they subsequently expanded and currently exist as large, functionally distinct subclasses (Wang et al., 2016; **Tables 1**, **2**; **Figure 3**).

The *OPR* gene family of jasmonic acid biosynthesis-related enzymes doubled in number during the evolution of algae to land plants and further expanded *via* polyploidization and tandem duplication events. This gene family comprises seven categories. All *OPR* genes from green algae form subclade VII, subclade VI (present only in lower land plants), and subclade II (present in all land plants except the gymnosperm *Picea sitchensis*); subclade I is composed of gymnosperm and angiosperm sequences. Only monocotyledon sequences comprise subbranches III, IV, and V. The *OPR* gene family is particularly abundant in rice and sorghum (13 genes) (Li et al., 2009).

The *HMGR* gene family is associated with terpene biosynthesis and originated from bryophytes. It has only expanded in maize, soybean, cotton, and poplar, with each species containing five *HMGR* genes (sporophyte-specific branch, monocotyledon-specific branch HMGR III/IV, and dicotyledon-specific branch HMGR I/II) with different conserved sequences (Li et al., 2014).

The *KCS* gene family, which is involved in ultra-long-chain fatty acid synthesis, is divided into five main sub-clades (A, B, C, D, and E) with the number of genes in this family gradually increasing from one in algae to eleven in angiosperms, and with an apparent trend in the expansion of related polyploid species (Little et al., 2018).

Evolution of protein families associated with plant cell structure

Proteins with roles in cell wall formation and other aspects of cell structure are important for plant morphogenesis and can have basic enzymatic reactions. These proteins tend to have a low probability of gene loss, but they can accumulate a high degree of functional differentiation throughout a long evolutionary process, as observed within the *CesA* family of cellulose synthases (Little et al., 2018). The *PSBP* gene, encoding the light-harvesting protein complex PSII, only exists in the green plants of polymorphic biological groups that consist of few members with obvious structural differences (Ifuku et al., 2008). Cell cycle-related *Cyc* genes are divided into ten branches, most of which existed before green algae and became widely expanded during the transition to angiosperms (Boscolo-Galazzo et al., 2021). *DLC* genes associated with the dynein system are derived from *DLC*-VIII genes of green algae. With the gradual expansion of *DLC* genes along the evolutionary path, each plant type produced unique molecules (e.g., algae: DLC-VIII, bryophyte: DLC-VII, fern: DLC-IV, monocotyledon: DLC-I/II, dicotyledon: II/V), with a common branch in seed plants (DLC-VI) (Cao et al., 2017). The actin-associated *Myo* gene produces Myo-XI (A) in green algae and gradually extends into ten branches (Peremyslov et al., 2011). The aquaporin-encoding gene *AQP* developed from the *LIPS* type gene in green algae and gradually diverged into eight significantly different *AQP* genes (GIPS, LIPS, HIPS, XIPS, SIPS, PIPS, TIPS, and NIPS) in various plants, including soybean, upland cotton, and oilseed rape (Hussain et al., 2020). The RNA splice component *NSR/RBP* was slightly extended in soybean but contained differences in its conserved motifs (Lucero et al., 2020; **Tables 1**, **2**; **Figure 3**).

The *SH3P* gene family, associated with cell plate formation, may have originated from the SH3P1-like ancestor of Charophyta and gradually expanded during the transition to mosses and angiosperms (Forero and Cvrckova, 2019). The cellulose synthase superfamily *CesA*, associated with cell wall formation, developed several branches among different species (CSLA and its developed branches CSLC and CESA, CSLB/H and its developed branches CSLF, CSLJ/M, CSLG, and CSLE). Moreover, the different subfamilies exhibit obvious selection for sugar synthesis. For example, certain members of the CSLJ subfamily may mediate (1, 3;1, 4)-β-glucan biosynthesis (Little et al., 2018). The *FT*/*TFLL* gene family, associated with flowering time, developed from *MFT-like* in angiosperms and contains several members (6) (Jin et al., 2021). The *OFP* gene family, associated with fruit shape, may have originated from the ancestors of land plants. Different species have varying numbers of these genes, which have been divided into 11 classes, due to numerous copy-number loss events (Liu et al., 2014). *HAM* gene families associated with tissue formation were generated from bryophytes and exhibit several molecular differences among different plant classes, where each family formed one branch. These gene families expanded in seed plants and ultimately evolved into two angiosperm branches (Type-I and Type-II) (Geng et al., 2021; **Tables 1**, **2**; **Figure 3**).

Evolution of signal transduction gene families

Studies on signal transduction-related gene families showed that the number of *PAB* gene families, which are involved in promoting mRNA stability and protein translation, varies significantly among different groups. These gene families are divided into three groups (Class I: PAB1/PAB3/PAB5, Class II: PAB2/PAB4/PAB8, and Class III: PAB6/PAB7); however, their individual evolutionary routes remain unknown (Gallie and Liu, 2014). In seed plants, small peptide signal-related *CEP* gene families may have significantly expanded *via* WGD, especially in the Gramineae and Solanaceae (Ogilvie et al., 2014). The *CNGC* gene family, which act in calcium-gating, are

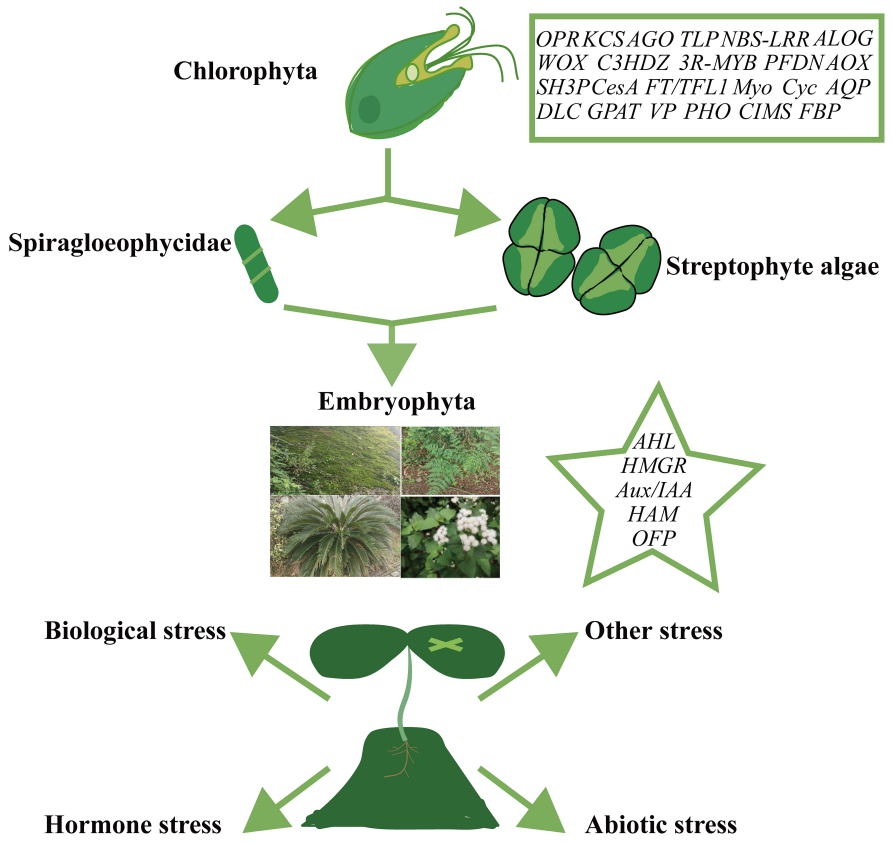

FIGURE 3
Origin and expansion of plant gene families. Gene families in boxes representing their origin in green algae or earlier. Families include OPR (12-oxo-phytodienoate acid reductase), KCS (3-ketoacyl-coa synthase), AGO (Argonaute), TLP (thaumatin-like protein), NBS-LRR (nucleotide binding site leucine-rich repeat), ALOG (Arabidopsis LSH1 and Oryza G1), WOX (WUSCHEL-related), C3HDZ (class III homeodomain-zinc finger protein), 3R-MYB, PFDN (prefoldin), AOX (alternative oxidase), SH3P (SH3 and BAR domain-containing protein), CesA (cellulose synthase), FT/TFL1 (flowering locus t/terminal flower 1), Myo (myosin), Cyc (cyclin), AQP (aquaporins), DLC (dynein light chain), GPAT (glycerol-3-phosphate acyltransferase), VP (vacuolar-type H+-pyrophosphatase), PHO (phosphate 1), CIMS (cobalamin-independent methionine synthase), and FBP (F-box). Gene families listed in the star may have contributed to the development of Streptophyte algae or functional innovations in the plant community, and include AHL (AT-hook motif nuclear localized), HMGR (3-hydroxy-3-methylglutaryl coenzyme A reductase), Aux/IAA (auxin/indole acetic acid and auxin response factor), HAM (hairy meristem), and OFP (OVATE family protein).

divided into five classes (Groups I, II, III, IVA, and IVB), and the number of members within each class varies considerably (Saand et al., 2015). Auxin response factors are classified into three classes and seven groups (Class A: ARF5/7, ARF6/8; Class B: ARF1, ARF2, ARF3/4, ARF9; and Class C: ARF10/16/17) and were formed through the evolution of three bryophyte proteins (Finet et al., 2013). The alkalization factor *RALF* genes are divided into ten classes and may have developed from two primitive ancestors (Cao and Shi, 2012; **Tables 1**, **2**; **Figure 3**).

The number of *CBL*, *CIPK*, *CDPK*, and *CRK* gene members associated with calcium signaling differs significantly across evolutionary stages (during the transition from lower plants to core angiosperms), and this phenomenon may be due to the abundant occurrence of WGD events and gene loss at these evolutionary stages. These polyploidy events then promoted the functional differentiation of corresponding proteins (Xiao et al., 2017; Zhang X. X. et al., 2020). Although only two *PEBP* genes, which are bind phospholipids and have roles in signal transduction, have been characterized in gymnosperms, they are particularly abundant in angiosperms, and their secondary expansion appears to be related to the formation of seed plants and angiosperms (Hedman et al., 2009; Karlgren et al., 2011). *GPAT* genes, which are associated with glycerol 3-phosphate biosynthesis, emerged earlier than those present in green algae, from which GPAT and GPAT9 developed into several *GPAT* genes in land plants (Waschburger et al., 2018; **Tables 1**, **2**; **Figure 3**).

Evolution of other gene families

During evolution, other plant gene families have generated a high number of members with functional differentiation.

In the salt or nutrient signaling pathways, the phosphorus transporter-encoding gene (*PHO*) contains obvious differences in copy number [from 0/1 when developed in green algae to two gradually more complex branches (C-1 and C-2) in land plants], protein structure, and number of introns (He et al., 2013). The ion transduction *VP* gene is divided into two branches, II and I, which originated from red algae and green algae, respectively. These branches were affected by polyploidy and were expanded in angiosperms (Zhang Y. M. et al., 2020). The plant ferritin *Fer* gene was already present in red algae and marginally increased in copy number in the later clades. Notably, the *Fer* gene of the monocotyledonous plant *Lycoris aurea* (Asparagales) appears more comparable to that of dicotyledonous plants (Strozycki et al., 2010). *VIT* genes encoding iron transporters consist of five ancient branches; however, two duplication events and six loss events led to substantial contraction of non-angiosperm *VIT* genes, and a subsequent expansion in copy number in angiosperms (Cao, 2019). Meanwhile, there is no significant difference in the number of methionine biosynthesis-related gene family (*CIMS*) members among green plants; however, multiple gene loss and gene duplication events occurred. In addition, WGT (wide-genome triploidy) led to the expansion of *CIMS* genes in soybean and alfalfa (Rody and de Oliveira, 2018; **Tables 1**, **2**; **Figure 3**).

There has been obvious expansion and gene loss of the β-glucohydrolase (*BAM*) gene in different groups of hydrolases, which were divided into eight branches (Bam1, Bam10, Bam3, Bam4, Bam9, Bam5/6, Bam2/7, and Bam8) that existed before the formation of land plants. However, significant gene losses have occurred in basal land plants (Thalmann et al., 2019). The *SUS* gene family, which is involved in glycolysis, can be divided into three groups containing members that may have developed from WGD and that have also undergone obvious expansion in certain higher plants (Xu et al., 2019). Among the genes related to epigenetic factors, the methylation-related *HMT* family has two branches (Class 1 and Class 2) in land plants, especially in seed plants, indicating that the *HMT* genes underwent two separate functional differentiation events (Zhao et al., 2018). The ubiquitin-related *FBP* family that originated in green algae has undergone significant expansion in lower plants, monocotyledons, and dicotyledons, such as Brassicaceae (Navarro-Quezada et al., 2013; **Tables 1**, **2**; **Figure 3**).

Concluding remarks and perspectives

Although it is desirable to develop better plant-based products and improve plant stress resistance for commercial reasons, it can be challenging to decipher the molecular profiles of plants and efficiently generate molecular resources (Nelson and Werck-Reichhart, 2011; Zhang et al., 2019). The development of plant molecular biology techniques has enabled the key events in plant evolution to be systematically characterized, including the molecular mechanisms underlying the adaptation of plants to life on land and plant hybrid formation (Cheng et al., 2019; Wang et al., 2021). To adequately assess the molecular evolution of plants, it is necessary to investigate a large variety of plant gene families. In particular, it is critical to analyze the unique features of the origin and evolutionary branches of different gene families.

The evidence described in this review suggests that gene duplication and gene loss occurred in nearly all gene families during plant evolution. Genes encoding TFs, proteins involved in disease and stress resistance, structural proteins, and signal transduction-related proteins have been extensively studied compared to genes in the hydrolase gene family (Shao et al., 2019; Lucero et al., 2020; Jin et al., 2021). Moreover, most research on molecular evolution has employed a small number of species and lacks systematics analysis. Therefore, it is necessary to conduct large-scale evolutionary studies on a broader selection of species groups, as well as the evolution of other functional genes, such as those encoding RNA-modifying proteins and autophagy-associated proteins.

Considering the content of these related studies, we believe that the following three aspects can be explored in the future to promote the understanding of plant molecular evolution-related processes. (A) the subfunctionalization of large families and the systematic evolutionary patterns of signaling pathways; (B) the comprehensiveness of the selection of representative plant taxa in molecular evolution studies and the statistical determination of related properties; (C) the origin of families, especially gene families associated with specific evolutionary events.

In summary, we have reviewed the molecular evolution of plants and discussed the potential contributions, challenges, and strategies associated with the gene families involved in the molecular evolution of plants as plants adapted to terrestrial environments and developed resistance to stress. The formation of different plant taxonomic units is closely associated with various plant gene families and their subsequent changes, most of which are characterized by traits that promote their environmental adaptability (Cheng et al., 2019; Shao et al., 2019; Man et al., 2020; Schilling et al., 2020). The transition of basal plants, such as Spiragloeophycidae and Streptophyte algae, often involved elaborate mechanisms to enhance plant resistance to environmental stress. For example, differences in the degree of water dependence and oxygen use occurred during the adaptation of plants for terrestrial environments. Investigation into relevant molecules, such as proteins encoded by key genes associated with the plant transition to terrestrial environments, can provide a pathway to enhancing the natural resistance of plants, thereby reducing their dependence on environmental

growth conditions, and improving crop yield (Cheng et al., 2019; **Figure 3**).

Author contributions

YF wrote the manuscript. XL, JJ, XH, JG, DZ, and XX completed the revision of the manuscript. All authors contributed to the article and approved the submitted version.

Funding

This research was funded by the National Natural Science Foundation of China (32060614), the Guizhou Provincial Science and Technology Project ([2022]091), the China Postdoctoral Science Foundation (2022MD713740), Department of Education of Guizhou Province (QianJiaoHe YJSKYJJ[2021]056), and Project of Serving the Country Industrial Revolution Strategic Action Plan of Regular Undergraduate Regular Higher Institutions in Guizhou Province (Qian Jiao He KY Zi [2018] 093).

Conflict of interest

The authors declare that the research was conducted in the absence of any commercial or financial relationships that could be construed as a potential conflict of interest.

Publisher's note

References

Airoldi, C. A., and Davies, B. (2012). Gene duplication and the evolution of plant MADS-box transcription factors. *J. Genet. Genom.* 39, 157–165. doi: 10.1016/j.jgg.2012.02.008

Bondino, H. G., Valle, E. M., and Ten Have, A. (2012). Evolution and functional diversification of the small heat shock protein/alpha-crystallin family in higher plants. *Planta* 235, 1299–1313. doi: 10.1007/s00425-011-1575-9

Borrelli, G. M., Mazzucotelli, E., Marone, D., Crosatti, C., Michelotti, V., Vale, G., et al. (2018). Regulation and evolution of NLR genes: A close interconnection for plant immunity. *Int. J. Mol. Sci.* 19:1662. doi: 10.3390/ijms19061662

Boscolo-Galazzo, F., Crichton, K. A., Ridgwell, A., Mawbey, E. M., Wade, B. S., and Pearson, P. N. (2021). Temperature controls carbon cycling and biological evolution in the ocean twilight zone. *Science* 371, 1148–1152. doi: 10.1126/science.abb6643

Cao, J. (2016). Analysis of the Prefoldin gene family in 14 plant species. *Front. Plant Sci.* 7:317. doi: 10.3389/fpls.2016.00317

Cao, J. (2019). Molecular evolution of the vacuolar iron transporter (VIT) family genes in 14 plant species. *Genes* 10:144. doi: 10.3390/genes10020144

Cao, J., and Shi, F. (2012). Evolution of the RALF gene family in plants: Gene duplication and selection patterns. *Evol. Bioinform.* 8, 271–292. doi: 10.4137/EBO.S9652

Cao, J., Li, X. Y., and Lv, Y. Q. (2017). Dynein light chain family genes in 15 plant species: Identification, evolution and expression profiles. *Plant Sci.* 254, 70–81. doi: 10.1016/j.plantsci.2016.10.011

Cao, J., Lv, Y. Q., Hou, Z. R., Li, X., and Ding, L. N. (2016). Expansion and evolution of thaumatin-like protein (TLP) gene family in six plants. *Plant Growth Regul.* 79, 299–307. doi: 10.1007/s10725-015-0134-y

Cheng, S., Xian, W., Fu, Y., Marin, B., Keller, J., Wu, T., et al. (2019). Genomes of subaerial Zygnematophyceae provide insights into land plant evolution. *Cell* 179, 1057–1067. doi: 10.1016/j.cell.2019.10.019

Clavel, M., Pelissier, T., Montavon, T., Tschopp, M. A., Pouch-Pelissier, M. N., Descombin, J., et al. (2016). Evolutionary history of double-stranded RNA binding proteins in plants: Identification of new cofactors involved in easiRNA biogenesis. *Plant Mol. Biol.* 91, 131–147. doi: 10.1007/s11103-016-0448-9

Dong, S. S., Liu, M., Liu, Y., Chen, F., Yang, T., Chen, L., et al. (2021). The genome of Magnolia biondii Pamp. Provides insights into the evolution of Magnoliales and biosynthesis of terpenoids. *Hortic. Res.* 8:38. doi: 10.1038/s41438-021-00471-9

Duplais, C., Papon, N., and Courdavault, V. (2020). Tracking the origin and evolution of plant metabolites. *Trends Plant Sci.* 25, 1182–1184. doi: 10.1016/j.tplants.2020.08.010

Feng, G. Q., Burleigh, J. G., Braun, E. L., Mei, W. B., and Barbazuk, W. B. (2017). Evolution of the 3R-MYB gene family in plants. *Genome Biol. Evol.* 9, 1013–1029. doi: 10.1093/gbe/evx056

Finet, C., Berne-Dedieu, A., Scutt, C. P., and Marletaz, F. (2013). Evolution of the ARF gene family in land plants: Old domains, new tricks. *Mol. Biol. Evol.* 30, 45–56. doi: 10.1093/molbev/mss220

Finet, C., Floyd, S. K., Conway, S. J., Zhong, B. J., Scutt, C. P., and Bowmanb, J. L. (2016). Evolution of the YABBY gene family in seed plants. *Evol. Dev.* 18, 116–126. doi: 10.1111/ede.12173

Forero, A. B., and Cvrckova, F. (2019). SH3Ps-evolution and diversity of a family of proteins engaged in plant cytokinesis. *Int. J. Mol. Sci.* 20:5623. doi: 10.3390/ijms20225623

Gallie, D. R., and Liu, R. Y. (2014). Phylogenetic analysis reveals dynamic evolution of the poly(A)-binding protein gene family in plants. *BMC Evol. Biol.* 14:238. doi: 10.1186/s12862-014-0238-4

Gao, B., Chen, M. X., Li, X. S., Liang, Y. Q., Zhang, D. Y., Wood, A. J., et al. (2020). Ancestral gene duplications in mosses characterized by integrated phylogenomic analyses. *J. Syst. Evol.* 60, 144–159. doi: 10.1111/jse.12683

Geng, Y., Guo, L., Han, H., Liu, X., Banks, J. A., Wisecaver, J. H., et al. (2021). Conservation and diversification of HAIRY MERISTEM gene family in land plants. *Plant J.* 106, 366–378. doi: 10.1111/tpj.15169

Gramzow, L., Ritz, M. S., and Theissen, G. (2010). On the origin of MADS-domain transcription factors. *Trends Genet.* 26, 149–153. doi: 10.1016/j.tig.2010.01.004

Guo, H. S., Zhang, Y. M., Sun, X. Q., Li, M. M., Hang, Y. Y., and Xue, J. Y. (2016). Evolution of the KCS gene family in plants: The history of gene duplication, sub/neofunctionalization and redundancy. *Mol. Genet. Genom.* 291, 739–752. doi: 10.1007/s00438-015-1142-3

He, L. L., Zhao, M., Wang, Y., Gai, J. Y., and He, C. Y. (2013). Phylogeny, structural evolution and functional diversification of the plant PHOSPHATE1 gene family: A focus on Glycine max. *BMC Evol. Biol.* 13:103. doi: 10.1186/1471-2148-13-103

Hedman, H., Kallman, T., and Lagercrantz, U. (2009). Early evolution of the MFT-like gene family in plants. *Plant Mol. Biol.* 70, 359–369.

Hsu, H. F., Chen, W. H., Shen, Y. H., Hsu, W. H., Mao, W. T., and Yang, C. H. (2021). Multifunctional evolution of B and AGL6 MADS box genes in orchids. *Nat. Commun.* 12:902. doi: 10.1038/s41467-021-21229-w

Hussain, A., Tanveer, R., Mustafa, G., Farooq, M., Amin, I., and Mansoor, S. (2020). Comparative phylogenetic analysis of aquaporins provides insight into the gene family expansion and evolution in plants and their role in drought tolerant and susceptible chickpea cultivars. *Genomics* 112, 263–275. doi: 10.1016/j.ygeno.2019.02.005

Ifuku, K., Ishihara, S., Shimamoto, R., Ido, K., and Sato, F. (2008). Structure, function, and evolution of the PsbP protein family in higher plants. *Photosynth. Res.* 98, 427–437. doi: 10.1007/s11120-008-9359-1

Jin, J., Tian, F., Yang, D. C., Meng, Y. Q., Kong, L., Luo, J., et al. (2017). PlantTFDB 4.0: Toward a central hub for transcription factors and regulatory interactions in plants. *Nucleic Acids Res.* 45, D1040–D1045. doi: 10.1093/nar/gkw982

Jin, S., Nasim, Z., Susila, H., and Ahn, J. H. (2021). Evolution and functional diversification of flowering locus T/terminal flower 1 family genes in plants. *Semin. Cell Dev. Biol.* 109, 20–30. doi: 10.1016/j.semcdb.2020.05.007

Karlgren, A., Gyllenstrand, N., Kallman, T., Sundstrom, J. F., Moore, D., Lascoux, M., et al. (2011). Evolution of the PEBP gene family in plants: Functional diversification in seed plant evolution. *Plant Physiol.* 156, 1967–1977. doi: 10.1104/pp.111.176206

Lafon-Placette, C., Vallejo-Marin, M., Parisod, C., Abbott, R. J., and Kohler, C. (2016). Current plant speciation research: Unravelling the processes and mechanisms behind the evolution of reproductive isolation barriers. *New Phytol.* 209, 29–33. doi: 10.1111/nph.13756

Li, J., Yang, S., Yang, X., Wu, H., Tang, H., and Yang, L. (2022). PlantGF: An analysis and annotation platform for plant gene families. *Database* 2022:baab088. doi: 10.1093/database/baab088

Li, L. Z., Wang, S. B., Wang, H. L., Sahu, S. K., Marin, B., Li, H. Y., et al. (2020). The genome of *Prasinoderma coloniale* unveils the existence of a third phylum within green plants. *Nat. Ecol. Evol.* 4:1220. doi: 10.1038/s41559-020-1221-7

Li, W. Y., Liu, B., Yu, L. J., Feng, D. R., Wang, H. B., and Wang, J. F. (2009). Phylogenetic analysis, structural evolution and functional divergence of the 12-oxo-phytodienoate acid reductase gene family in plants. *BMC Evol. Biol.* 9:90. doi: 10.1186/1471-2148-9-90

Li, W., Liu, W., Wei, H. L., He, Q. L., Chen, J. H., Zhang, B. H., et al. (2014). Species-specific expansion and molecular evolution of the 3-hydroxy-3-methylglutaryl coenzyme a reductase (HMGR) gene family in plants. *PLoS One* 9:e94172. doi: 10.1371/journal.pone.0094172

Lian, G. B., Ding, Z. W., Wang, Q., Zhang, D. B., and Xu, J. (2014). Origins and evolution of wuschel-related homeobox protein family in plant kingdom. *Sci. World J.* 2017:534140. doi: 10.1155/2014/534140

Liang, Z., Geng, Y. K., Ji, C. M., Du, H., Wong, C. E., Zhang, Q., et al. (2020). *Mesostigma viride* genome and transcriptome provide insights into the origin and evolution of Streptophyta. *Adv. Sci.* 7:1901850. doi: 10.1002/advs.201901850

Little, A., Schwerdt, J. G., Shirley, N. J., Khor, S. F., Neumann, K., O'Donovan, L. A., et al. (2018). Revised phylogeny of the cellulose synthase gene superfamily: Insights into cell wall evolution. *Plant Physiol.* 177, 1124–1141. doi: 10.1104/pp.17.01718

Liu, D., Sun, W., Yuan, Y. W., Zhang, N., Hayward, A., Liu, Y. L., et al. (2014). Phylogenetic analyses provide the first insights into the evolution of OVATE family proteins in land plants. *Ann. Bot.* 113, 1219–1233. doi: 10.1093/aob/mcu061

Liu, M., Wang, M., Yang, J., Wen, J., Guo, P., Wu, Y., et al. (2019). Evolutionary and comparative expression analyses of TCP transcription factor gene family in land plants. *Int. J. Mol. Sci.* 20:3591. doi: 10.3390/ijms20143591

Lucero, L., Bazin, J., Melo, J. R., Ibanez, F., Crespi, M. D., and Ariel, F. (2020). Evolution of the small family of alternative splicing modulators nuclear speckle rna-binding proteins in plants. *Genes* 11:207. doi: 10.3390/genes11020207

Man, J. R., Gallagher, J. P., and Bartlett, M. (2020). Structural evolution drives diversification of the large LRR-RLK gene family. *New Phytol.* 226, 1492–1505. doi: 10.1111/nph.16455

Mukherjee, K., Campos, H., and Kolaczkowski, B. (2013). Evolution of animal and plant dicers: Early parallel duplications and recurrent adaptation of antiviral RNA binding in plants. *Mol. Biol. Evol.* 30, 627–641. doi: 10.1093/molbev/mss263

Naramoto, S., Hata, Y., and Kyozuka, J. (2020). The origin and evolution of the ALOG proteins, members of a plant-specific transcription factor family, in land plants. *J. Plant Res.* 133, 323–329. doi: 10.1007/s10265-020-01171-6

Navarro-Quezada, A., Schumann, N., and Quint, M. (2013). Plant F-Box protein evolution is determined by lineage-specific timing of major gene family expansion waves. *PLoS One* 8:e68672. doi: 10.1371/journal.pone.0068672

Nelson, D., and Werck-Reichhart, D. (2011). A P450-centric view of plant evolution. *Plant J.* 66, 194–211. doi: 10.1111/j.1365-313X.2011.04529.x

Ng, M., and Yanofsky, M. F. (2001). Function and evolution of the plant MADS-box gene family. *Nat. Rev. Genet.* 2, 186–195. doi: 10.1038/35056041

Nikolov, L. A., Runions, A., Das Gupta, M., and Tsiantis, M. (2019). Leaf development and evolution. *Curr. Top. Dev. Biol.* 131:109. doi: 10.1016/bs.ctdb.2018.11.006

Ogilvie, H. A., Imin, N., and Djordjevic, M. A. (2014). Diversification of the C-Terminally Encoded Peptide (CEP) gene family in angiosperms, and evolution of plant-family specific CEP genes. *BMC Genom.* 15:870. doi: 10.1186/1471-2164-15-870

Peremyslov, V., Mockler, T. C., Filichkin, S. A., Fox, S. E., Jaiswal, P., Makarova, K. S., et al. (2011). Expression, splicing, and evolution of the myosin gene family in plants. *Plant Physiol.* 15, 1191–1204. doi: 10.1104/pp.110.170720

Preston, J. C., and Hileman, L. C. (2013). Functional evolution in the plant Squamosa-Promoter Binding Protein-Like (SPL) gene family. *Front. Plant Sci.* 4:80. doi: 10.3389/fpls.2013.00080

Pu, X. J., Lv, X., and Lin, H. H. (2015). Unraveling the evolution and regulation of the alternative oxidase gene family in plants. *Dev. Genes Evol.* 225, 331–339. doi: 10.1007/s00427-015-0515-2

Qiu, Y., and Claudia, K. (2021). Endosperm evolution by duplicated and neofunctionalized type I MADS-box transcription factors. *Mol. Biol. Evol.* 39:msab355. doi: 10.1093/molbev/msab355

Reeves, P. A., and Olmstead, R. G. (2003). Evolution of the TCP gene family in Asteridae: Csladistic and network approaches to understanding regulatory gene family diversification and its impact on morphological evolution. *Mol. Biol. Evol.* 20, 1997–2009. doi: 10.1093/molbev/msg211

Rody, H. V. S., and de Oliveira, L. O. (2018). Evolutionary history of the cobalamin-independent methionine synthase gene family across the land plants. *Mol. Phylogenet. Evol.* 120, 33–42. doi: 10.1016/j.ympev.2017.12.003

Saand, M. A., Xu, Y. P., Munyampundu, J. P., Li, W., Zhang, X. R., and Cai, X. Z. (2015). Phylogeny and evolution of plant cyclic nucleotide-gated ion channel (CNGC) gene family and functional analyses of tomato CNGCs. *DNA Res.* 22, 471–483. doi: 10.1093/dnares/dsv029

Schilling, S., Kennedy, A., Pan, S., Jermiin, L. S., and Melzer, R. (2020). Genome-wide analysis of MIKC-type MADS-box genes in wheat: Pervasive duplications, functional conservation and putative neofunctionalization. *New Phytol.* 225, 511–529. doi: 10.1111/nph.16122

Schneider, H., Liu, H. M., Chang, Y. F., Ohlsen, D., Perrie, L. R., Shepherd, L., et al. (2017). Neo- and Paleopolyploidy contribute to the species diversity of *Asplenium*-the most species-rich genus of ferns. *J. Syst. Evol.* 55, 353–364. doi: 10.1111/jse.12271

Shao, Z., Xue, J., Wang, Q., Wang, B., and Chen, J. (2019). Revisiting the origin of plant NBS-LRR genes. *Trends Plant Sci.* 24, 9–12. doi: 10.1016/j.tplants.2018.10.015

Singh, R. K., Gase, K., Baldwin, I. T., and Pandey, S. P. (2015). Molecular evolution and diversification of the Argonaute family of proteins in plants. *BMC Plant Biol.* 15:23. doi: 10.1186/s12870-014-0364-6

Song, B., Buckler, E., Wang, H., Wu, Y., Rees, E., Kellogg, E., et al. (2021). Conserved noncoding sequences provide insights into regulatory sequence and loss of gene expression in maize. *Genome Res.* 31, 1245–1257. doi: 10.1101/gr.266528.120

Song, X. M., Wang, J. P., Sun, P. C., Ma, X., Yang, Q. H., Hu, J. J., et al. (2020). Preferential gene retention increases the robustness of cold regulation in Brassicaceae and other plants after polyploidization. *Hortic. Res.* 7:20. doi: 10.1038/s41438-020-0253-0

Strozycki, P. M., Szymanski, M., Szczurek, A., Barciszewski, J., and Figlerowicz, M. (2010). A new family of Ferritin genes from lupinus luteus-comparative analysis of plant ferritins, their gene structure, and evolution. *Mol. Biol. Evol.* 27, 91–101. doi: 10.1093/molbev/msp196

Su, D., Yang, L., Shi, X., Ma, X., Zhou, X., Hedges, S. B., et al. (2021). Large-scale phylogenomic analyses reveal the monophyly of bryophytes and Neoproterozoic origin of land plants. *Mol. Biol. Evol.* 38, 3332–3344. doi: 10.1093/molbev/msab106

Sun, W., Ma, Z., and Liu, M. (2021). Plant cytochrome P450 plasticity and evolution. *Mol. Plant* 14, 1244–1265. doi: 10.1016/j.molp.2021.06.028

Thalmann, M., Coiro, M., Meier, T., Wicker, T., Zeeman, S. C., and Santelia, D. (2019). The evolution of functional complexity within the -amylase gene family in land plants. *BMC Evol. Biol.* 19:66. doi: 10.1186/s12862-019-1395-2

Theissen, G., Melzer, R., and Rumpler, F. (2016). MADS-domain transcription factors and the floral quartet model of flower development: Linking plant development and evolution. *Development* 143, 3259–3271. doi: 10.1242/dev.134080

Vasco, A., Smalls, T. L., Graham, S. W., Cooper, E. D., Wong, G. K. S., Stevenson, D. W., et al. (2016). Challenging the paradigms of leaf evolution: Class III HD-Zips in ferns and lycophytes. *New Phytol.* 212, 745–758. doi: 10.1111/nph.14075

Vilela, M. M., Del Bem, L. E., Van Sluys, M. A., de Setta, N., Kitajima, J. P., Cruz, G. M., et al. (2017). Analysis of three sugarcane homo/homeologous regions suggests independent polyploidization events of *Saccharum officinarum* and *Saccharum spontaneum*. *Genome Biol. Evol.* 9, 266–278. doi: 10.1093/gbe/evw293

Wang, J. P., Yu, J. G., Li, J., Sun, P. C., Wang, L., Yuan, J. Q., et al. (2018). Two likely auto-tetraploidization events shaped kiwifruit genome and contributed to establishment of the Actinidiaceae family. *iScience* 7:230. doi: 10.1016/j.isci.2018.08.003

Wang, J., Qin, J., Sun, P., Ma, X., Yu, J., Li, Y., et al. (2019). Polyploidy index and its implications for the evolution of polyploids. *Front. Genet.* 10:807. doi: 10.3389/fgene.2019.00807

Wang, X., Feng, H., Chang, Y., Ma, C., Wang, L., Hao, X., et al. (2020). Population sequencing enhances understanding of tea plant evolution. *Nat. Commun.* 11:4447. doi: 10.1038/s41467-020-18228-8

Wang, Y. M., Yang, Q., Liu, Y. J., and Yang, H. L. (2016). Molecular evolution and expression divergence of the Aconitase (ACO) gene family in land plants. *Front. Plant Sci.* 7:1879. doi: 10.3389/fpls.2016.01879

Wang, Z., Jiang, Y., Bi, H., Lu, Z., Ma, Y., Yang, X., et al. (2021). Hybrid speciation via inheritance of alternate alleles of parental isolating genes. *Mol. Plant* 14, 208–222. doi: 10.1016/j.molp.2020.11.008

Waschburger, E., Kulcheski, F. R., Veto, N. M., Margis, R., Margis-Pinheiro, M., and Turchetto-Zolet, A. C. (2018). Genome-wide analysis of the glycerol-3-phosphate acyltransferase (GPAT) gene family reveals the evolution and diversification of plant GPATs. *Genet. Mol. Biol.* 41, 355–370. doi: 10.1590/1678-4685-Gmb-2017-0076

Wu, W. T., Liu, Y. X., Wang, Y. Q., Li, H. M., Liu, J. X., Tan, J. X., et al. (2017). Evolution analysis of the Aux/IAA gene family in plants shows dual origins and variable nuclear localization signals. *Int. J. Mol. Sci.* 18:2107. doi: 10.3390/ijms18102107

Xiao, X. H., Yang, M., Sui, J. L., Qi, J. Y., Fang, Y. J., Hu, S. N., et al. (2017). The calcium-dependent protein kinase (CDPK) and CDPK-related kinase gene families in *Hevea brasiliensis*-comparison with five other plant species in structure, evolution, and expression. *FEBS Open Bio* 7, 4–24. doi: 10.1002/2211-5463.12163

Xu, X. Y., Yang, Y. H., Liu, C. X., Sun, Y. M., Zhang, T., Hou, M. L., et al. (2019). The evolutionary history of the sucrose synthase gene family in higher plants. *BMC Plant Biol.* 19:566. doi: 10.1186/s12870-019-2181-4

Yang, Z. F., Gu, S. L., Wang, X. F., Li, W. J., Tang, Z. X., and Xu, C. W. (2008). Molecular evolution of the CPP-like gene family in plants: Insights from comparative genomics of *Arabidopsis* and rice. *J. Mol. Evol.* 67, 266–277. doi: 10.1007/s00239-008-9143-z

Yu, X., Xiao, J., Chen, S., Yu, Y., Ma, J., Lin, Y., et al. (2020). Metabolite signatures of diverse *Camellia sinensis* tea populations. *Nat. Commun.* 11:5586. doi: 10.1038/s41467-020-19441-1

Zhang, K., Wang, X. W., and Cheng, F. (2019). Plant polyploidy: Origin, evolution, and its influence on crop domestication. *Hortic. Plant. J.* 5, 231–239. doi: 10.1016/j.hpj.2019.11.003

Zhang, L. S., Chen, F., Zhang, X. T., Li, Z., Zhao, Y. Y., Lohaus, R., et al. (2020). The water lily genome and the early evolution of flowering plants. *Nature* 577, 79–84. doi: 10.1038/s41586-019-1852-5

Zhang, X. X., Li, X. X., Zhao, R., Zhou, Y., and Jiao, Y. N. (2020). Evolutionary strategies drive a balance of the interacting gene products for the CBL and CIPK gene families. *New Phytol.* 226, 1506–1516. doi: 10.1111/nph.16445

Zhang, Y. M., Feng, X., Wang, L. H., Su, Y. P., Chu, Z. D., and Sun, Y. X. (2020). The structure, functional evolution, and evolutionary trajectories of the H+-PPase gene family in plants. *BMC Genom.* 21:195. doi: 10.1186/s12864-020-6604-2

Zhao, J. F., Favero, D. S., Qiu, J. W., Roalson, E. H., and Neff, M. M. (2014). Insights into the evolution and diversification of the AT-hook Motif Nuclear Localized gene family in land plants. *BMC Plant Biol.* 14:266. doi: 10.1186/s12870-014-0266-7

Zhao, M., Chen, P., Wang, W. Y., Yuan, F. J., Zhu, D. H., Wang, Z., et al. (2018). Molecular evolution and expression divergence of HMT gene family in plants. *Int. J. Mol. Sci.* 19:1248. doi: 10.3390/ijms19041248

Zong, J., Yao, X., Yin, J., Zhang, D., and Ma, H. (2009). Evolution of the RNA-dependent RNA polymerase (RdRP) genes: Duplications and possible losses before and after the divergence of major eukaryotic groups. *Gene* 447, 29–39. doi: 10.1016/j.gene.2009.07.004

frontiers | Frontiers in Plant Science

TYPE Opinion
PUBLISHED 15 September 2022
DOI 10.3389/fpls.2022.1025165

OPEN ACCESS

EDITED BY
Yi Han,
Anhui Agricultural University, China

REVIEWED BY
Xi Luo,
University of Maryland, College Park, United States
Xi Cheng,
Beijing Academy of Agricultural and Forestry Sciences, China

*CORRESPONDENCE
Zhao Zhang
zhangzhao@cau.edu.cn

SPECIALTY SECTION
This article was submitted to Plant Bioinformatics, a section of the journal Frontiers in Plant Science

RECEIVED 22 August 2022
ACCEPTED 02 September 2022
PUBLISHED 15 September 2022

CITATION
Liu X, Bai Y and Zhang Z (2022) Priming defense by transiently suppressing plant susceptibility genes in ornamental crops: A novel strategy for post-harvest diseases management.
Front. Plant Sci. 13:1025165.
doi: 10.3389/fpls.2022.1025165

Priming defense by transiently suppressing plant susceptibility genes in ornamental crops: A novel strategy for post-harvest diseases management

Xintong Liu[1], Yuling Bai[2] and Zhao Zhang[1,2]*

[1]Beijing Key Laboratory of Development and Quality Control of Ornamental Crops, Department of Ornamental Horticulture, China Agricultural University, Beijing, China, [2]Plant Breeding, Wageningen University & Research, Wageningen, Netherlands

KEYWORDS

ornamental crops, disease resistance, susceptibility genes, *S*-genes, postharvest diseases

Introduction: Manipulating host susceptibility genes for resistance

The susceptibility genes (*S*-genes) refer to the plant genes required by phytopathogens to facilitate their compatible interaction with hosts (Pavan et al., 2010; Koseoglou et al., 2021). The pathogens exploit host *S*-genes for their invasion, consequently, the loss of function of *S*-genes disturb the compatible interaction and therefore lead to resistance. The resistance mediated by mutant alleles of *S*-genes have been reported in various plant species, and has been successfully applied to breeding for many years.

The *S*-genes, based on their involvement in different stages of infection, were classified into several functional groups (van Schie and Takken, 2014; Koseoglou et al., 2021). The first group includes genes required for early pathogen infestation or to promote pathogen infestation. MLO is one of the best-known typical members of the first group, of which a recessive mutant with powdery mildew (PM) resistance in barley was developed decades ago and this mutant is still used in European spring barley and confers resistance to all PM races in the field (Freisleben and Lein, 1942; Jørgensen, 1992; Dreiseitl, 2020). The mutation of *MLO* with CRISPR-Cas9 mediated system have been applied to confer PM resistance in several plant species including wheat (Shan et al., 2013), tomato (Nekrasov et al., 2017) and grape (Malnoy et al., 2016). The second group of *S*-genes encodes negative regulators in plant immune signaling. These genes are involved in regulating the levels of the phytohormones, and their crosstalk, such as salicylic acid (SA) and jasmonic acid (JA). For example, the recessive

mutation of *CESA3*, one of the cellulose synthesis-related genes, showed an increased level of JA, abscisic acid (ABA) and ethylene (ET), resulting in enhanced resistance to several pathogens (Ellis et al., 2002; Kumar and Turner, 2015). CESA4, CESA7 and CESA8 are also associated with susceptibility to pathogens and their corresponding mutants show increased resistance to both pathogenic fungus and bacteria (Hernández-Blanco et al., 2007). The third group of *S*-genes is associated with the nutrition of pathogenic bacteria, such as metabolite biosynthesis and sugar transport, endogenous replication and cell expansion. In rice, the loss of function of *SWEET14* increased the resistance to bacterial blight (Li et al., 2012). Recently, the plant transporter genes that targeted by bacterial pathogens for their effector translocation were suggested as a new functional group of *S*-genes (Koseoglou et al., 2021).

Translating knowledge from the laboratory to the field: Current difficulties in using *S*-genes for disease control of ornamental crops

The business of ornamental horticulture makes tens of billions of dollars annually, and pathogenic microorganisms pose a huge hazard to this industry worldwide. The rose production, for example, requires over $5,000 worth of pesticide spraying per hectare per year to control the disease. Therefore, the manipulation of *S*-genes for disease control of ornamental crops would have great potential to create significant value.

To utilize *S*-gene for defense in ornamental plants, the first step is the identification of those functional *S*-genes from the ornamental plant (Figure 1). As *S*-genes are often universal among different plant species, we can therefore use information from model plants or other crops and identify homologs of *S*-genes from the available genomic data of the ornamental crops of interest. In addition, *S*-genes, especially those encoding defense suppressors are usually induced by pathogens during the infection process. Thus plant transcriptome data under infection of various pathogens are also important clues for our identification of functional *S*-genes.

Although the homologous genes are often thought to be functionally conserved across species, not all homologs in a certain *S*-gene family will function as susceptibility factors in all plant species. The involvement of each homolog of an *S*-gene family demands a case-by-case assessment of their usefulness for resistance in each plant species. Therefore, the identification of functional *S*-gene homologs in each species is a challenge. In addition to RNAi strategy using stable transformation, a virus-

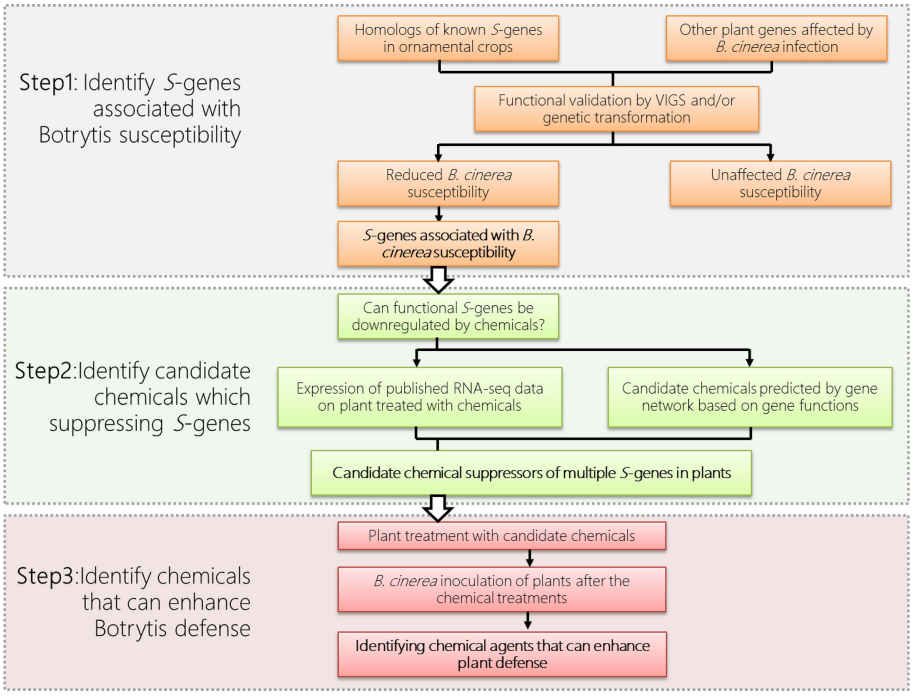

FIGURE 1
Priming defense by chemically suppressing plant *S*-genes in ornamental crops, using gray mold disease (caused by *Botrytis cinerea*) as an example.

induced gene silencing (VIGS) has also been demonstrated to be a rapid and effective method for transient knockdown of gene expression in various other plant species, including many ornamental plants, such as petunia (Spitzer et al., 2007), rose (Yan et al., 2018; Cao et al., 2019), gladiolus (Zhong et al., 2014), gerbera (Deng et al., 2012), and lily (Wu et al., 2018). With VIGS, we can quickly compare the differences in pathogen susceptibility, after partial loss of function of the *S*-gene in ornamentals. For instance, the report has identified 19 MLO genes in rose. Of these, VIGS of *RhMLO1* and *RhMLO2*, are required for infection by *Podosphaera pannosa* and suggest their potential as susceptibility targets for powdery mildew resistance breeding (Fang et al., 2021).

To manipulate the interesting *S*-genes for disease resistance in ornamentals, methods are needed to artificially downregulate/disable these genes. However, there are three major obstacles to achieving this goal: First, although loss-of-function mutations of *S*-genes could be generated *via* various approaches, such as using natural alleles from genetic resources, stable RNAi, and newly emerging gene editing techniques, these approaches are technically challenging in many other ornamental crops due to their polyploid genomes and the lack of efficient transformation techniques. Second, it is challenging to downregulate multiple *S*-genes simultaneously in these plants to improve the resistance effect. Third, there are severe limits to developing and propagating genetically modified crops in many countries, especially in Europe. All of these issues represent barriers to the successful use of *S*-gene in ornamental crops (Smulders et al., 2019; Gahlaut et al., 2021).

Suppressing (multiple) plant *S*-genes by using 'priming' agents: A novel strategy

Defense priming represents a "warm-up" strategy for plant resistance. During this process, the host plant enters a priming phase triggered by stimuli that act as an alarm from pathogens or beneficial microbes. In addition, the priming agents in the absence of pathogens, such as jasmonic acid (JA), salicylic acid (SA), β-aminobutyric acid (BABA), benzothiadiazole (BTH), hexanoic acid (Hx), chitosan, tricarboxylates, ergosterol and many other natural or synthetic agents can promote plant defense (Laquitaine et al., 2006; van Schie and Takken, 2014; Mauch-Mani et al., 2017; Balmer et al., 2018; Duanis-Assaf et al., 2022). Once the host plant enters the priming phase, only mild changes occur at the transcriptional and/or epigenetic level without the dramatic induction of many defense genes. Therefore, the priming stage is a low-cost strategy for the host plant. This stage can last for more than 10 days (almost spanning the entire transportation and shelf period of cut flowers) or throughout the plant lifecycle (Mauch-Mani et al., 2017).

Upon subsequent pathogen infection, the primed plant mounts a faster and/or stronger defense response than a non-primed plant, resulting in significantly increased resistance. Most studies of this process have focused on the increased expression of resistance (*R*) genes upon pre-exposure to a priming stimulus and subsequent pathogen infection; however, numerous genes are also substantially downregulated, this includes many known *S*-genes of plants (Verhagen et al., 2004; Finiti et al., 2014). Therefore, it is clear that priming agents could potentially be used to downregulate *S*-genes for enhanced resistance *via* the defense priming strategy.

Evidence has shown that *S*-genes can be silenced when plants are treated with chemicals. For example, in strawberry (Landi et al., 2017), 8 homologs of known *S*-genes (including *PLPs*,*WRKY57*,*PG1*,*MPK4*,*SWEET14*,*Cel1/2*) are differentially expressed upon treatment of BTH and chitosan at 6, 12, or 24 hours post treatment (hpt). In particular, four of them are significantly downregulated in BTH and seven of them are significantly downregulated in chitosan, suggesting that BTH and chitosan are candidate agents which can enhance *B. cinerea* resistance by suppressing the expression of multiple *S*-genes. Assumingly, agents identified by gene expression profiling that inhibit the expression of *S*-gene can subsequently be applied to plants to induce plant defense. In fact, the postharvest application of BTH effectively reduced latent infections and induced resistance to diseases in fruit and vegetables, such as strawberries (Feliziani et al., 2015), peaches (Liu et al., 2005) and melons (Feliziani et al., 2015).

The above examples illustrate that conventional priming agents (e.g. BTH) can function as suppressors to down-regulate expression of certain *S*-genes leading to resistance in plants. To apply this concept on priming defense to postharvest diseases in ornamental crops, we propose to transiently suppress the expression of certain plant *S*-genes, by using various suppressor agents (Figure 1). In addition to BTH, the analysis of the continuously generated 'Omics' data allows us to high-throughput screen for novel suppressor agents for the regulation of *S*-gene and modulation of plant resistance. These 'Omics' data include publicly available RNA-seq dataset of plants upon the treatment of chemicals, including Hx (Finiti et al., 2014), polyamines (Seifi et al., 2019), BTH (Cheng et al., 2018), chitosan (Landi et al., 2017), BABA (Bengtsson et al., 2014), phosphite (Burra et al., 2014) and various phytohormones (Ran et al., 2018).

As in the examples given in Figure 1, the functional *S*-genes and their suppressor agents can be identified through the bioinformatic, reverse genetic and phytopathological approaches. The identified functional *S*-genes (Figure 1 Step1) can be used as 'markers' to screen the candidate suppressor agents based on their expression (Figure 1 Step 2). The function of candidate suppressor agents can subsequently be verified by their application to plants and pathogen assays (Figure 1 Step 3). Multiple agents can also be used in combination to suppress the

expression of multiple *S*-genes to enhance disease resistance in ornamentals while taking into account the cost of application and environmental sustainability issues. Last but not the least, the molecular mechanisms of the newly identified suppressor agents should be further investigated.

Prospects

Recent research suggested various natural or synthetic agents could be used to downregulate multiple S-genes simultaneously. These findings prompted us to explore the feasibility of achieving induced defense priming in ornamental crops by downregulating their S-genes transiently by application of proper priming agents, which can be applied to pot-plants and cut-flowers during the period of transportation and on-shelf stage. Here we propose a strategy for controlling postharvest diseases in ornamental crops by transiently suppressing (multiple) plant *S*-genes to prime defense (Figure 1). To this end, based on the multi-omic dataset from a publicly available database or generated by experiments, the potential S-genes will be identified and evaluated for their expression pattern upon the treatment of certain agents, such as natural compounds or natural plant hormones. Agents that repress the expression of (multiple) S-genes will be applied to the plant to test their role in promoting plant defense. It is worth noting that S-genes identified from one plant species can be applied to another, with potentially different diseases. This approach means providing a strategy for broad-spectrum disease resistance in various ornamental plants, which will save the economic value of these crops from disease devastation. Another attractive feature of eliciting priming for plant protection is that it avoids the use of environmentally problematic fungicides; the use of these products can also lead to the appearance of fungal strains resistant to these fungicides. We expect that the knowledge about S-genes and defense priming obtained in our analysis will increasingly be put into practice in the field, thereby improving sustainable agriculture.

Author contributions

YB, ZZ, and XL conceived and wrote the paper. All authors contributed to the article and approved the submitted version.

Funding

This study was supported by the National Natural Science Foundation of China (grant number 31972444) to ZZ. The project is further supported by the Construction of Beijing Science and Technology Innovation and Service Capacity in Top Subjects (CEFF-PXM2019_014207_000032).

Conflict of interest

The authors declare that the research was conducted in the absence of any commercial or financial relationships that could be construed as a potential conflict of interest.

Publisher's note

References

Balmer, A., Pastor, V., Glauser, G., and Mauch-Mani, B. (2018). Tricarboxylates induce defense priming against bacteria in *Arabidopsis thaliana*. *Front. Plant Sci.* 9, 1221. doi: 10.3389/fpls.2018.01221

Bengtsson, T., Weighill, D., Proux-Wéra, E., Levander, F., Resjö, S., Burra, D. D., et al. (2014). Proteomics and transcriptomics of the BABA-induced resistance response in potato using a novel functional annotation approach. *BMC Genomics* 15 (1), 1–19. doi: 10.1186/1471-2164-15-315

Burra, D. D., Berkowitz, O., Hedley, P. E., Morris, J., Resjö, S., Levander, F., et al. (2014). Phosphite-induced changes of the transcriptome and secretome in *Solanum tuberosum* leading to resistance against *Phytophthora infestans*. *BMC Plant Biol.* 14 (1), 1–17. doi: 10.1186/s12870-014-0254-y

Cao, X., Yan, H., Liu, X., Li, D., Sui, M., Wu, J., et al. (2019). A detached petal disc assay and virus-induced gene silencing facilitate the study of botrytis cinerea resistance in rose flowers. *Hortic. Res.* 6, 136. doi: 10.1038/s41438-019-0219-2

Cheng, Z., Yu, X., Li, S., and Wu, Q. (2018). Genome-wide transcriptome analysis and identification of benzothiadiazole-induced genes and pathways potentially associated with defense response in banana. *BMC Genomics* 19 (1), 1–19. doi: 10.1186/s12864-018-4830-7

Deng, X., Elomaa, P., Nguyen, C. X., Hytönen, T., Valkonen, J. P., and Teeri, T. H. (2012). Virus-induced gene silencing for asteraceae–a reverse genetics approach for functional genomics in *Gerbera hybrida*. *Plant Biotechnol. J.* 10 (8), 970–978. doi: 10.1111/j.1467-7652.2012.00726.x

Dreiseitl, A. (2020). Specific resistance of barley to powdery mildew, its use and beyond. a concise critical review. *Genes* 11, 971. doi: 10.3390/genes11090971

Duanis-Assaf, D., Galsurker, O., Davydov, O., Maurer, D., Feygenberg, O., Sagi, M., et al. (2022). Double-stranded RNA targeting fungal ergosterol biosynthesis pathway controls *Botrytis cinerea* and postharvest grey mould. *Plant Biotechnol. J.* 20, 226–237. doi: 10.1111/pbi.13708

Ellis, C., Karafyllidis, I., Wasternack, C., and Turner, J. G. (2002). The arabidopsis mutant cev1 links cell wall signaling to jasmonate and ethylene responses. *Plant Cell* 14 (7), 1557–1566. doi: 10.1105/tpc.002022

Fang, P., Arens, P., Liu, X., Zhang, X., Lakwani, D., Foucher, F., et al. (2021). Analysis of allelic variants of RhMLO genes in rose and functional studies on susceptibility to powdery mildew related to clade V homologs. *Theor. Appl. Genet.* 134 (8), 2495–2515. doi: 10.1007/s00122-021-03838-7

Feliziani, E., Landi, L., and Romanazzi, G. (2015). Preharvest treatments with chitosan and other alternatives to conventional fungicides to control postharvest decay of strawberry. *Carbohydr. polym.* 132, 111–117. doi: 10.1016/j.carbpol.2015.05.078

Finiti, I., de la O. Leyva, M., Vicedo, B., Gómez-Pastor, R., López-Cruz, J., García-Agustín, P., et al. (2014). Hexanoic acid protects tomato plants against *Botrytis cinerea* by priming defence responses and reducing oxidative stress. *Mol. Plant Pathol.* 15 (6), 550–562. doi: 10.1111/mpp.12112

Freisleben, R., and Lein, A. (1942). Über die auffindung einer mehltauresistenten mutante nach röntgenbestrahlung einer anfälligen reinen linie von sommergerste. *Naturwissenschaften* 30 (40), 608–608. doi: 10.1007/BF01488231

Gahlaut, V., Kumari, P., Jaiswal, V., and Kumar, S. (2021). Genetics, genomics and breeding in Rosa species. *J. Hortic. Sci. Biotechnol.* 96, 545–559. doi: 10.1080/14620316.2021.1894078

Hernández-Blanco, C., Feng, D. X., Hu, J., Sánchez-Vallet, A., Deslandes, L., Llorente, F., et al. (2007). Impairment of cellulose synthases required for arabidopsis secondary cell wall formation enhances disease resistance. *Plant Cell* 19 (3), 890–903. doi: 10.1105/tpc.106.048058

Jørgensen, I. H. (1992). Discovery, characterization and exploitation of mlo powdery mildew resistance in barley. *Euphytica* 63 (1), 141–152. doi: 10.1007/BF00023919

Koseoglou, E., van der Wolf, J. M., Visser, R. G. F., and Bai, Y. (2021). Susceptibility reversed: modified plant susceptibility genes for resistance to bacteria. *Trends Plant Sci.* 27, 69–79. doi: 10.1016/j.tplants.2021.07.018

Kumar, M., and Turner, S. (2015). Plant cellulose synthesis: CESA proteins crossing kingdoms. *Phytochemistry* 112, 91–99. doi: 10.1016/j.phytochem.2014.07.009

Landi, L., De Miccolis Angelini, R. M., Pollastro, S., Feliziani, E., Faretra, F., and Romanazzi, G. (2017). Global transcriptome analysis and identification of differentially expressed genes in strawberry after preharvest application of benzothiadiazole and chitosan. *Front. Plant Sci.* 8, 235. doi: 10.3389/fpls.2017.00235

Laquitaine, L., Gomès, E., François, J., Marchive, C., Pascal, S., Hamdi, S., et al. (2006). Molecular basis of ergosterol-induced protection of grape against *Botrytis cinerea*: induction of type I LTP promoter activity, WRKY, and stilbene synthase gene expression. *Mol. Plant-Microbe Interact.* 19, 1103–1112. doi: 10.1094/MPMI-19-1103

Li, T., Liu, B., Spalding, M. H., Weeks, D. P., and Yang, B. (2012). High-efficiency TALEN-based gene editing produces disease-resistant rice. *Nat. Biotechnol.* 30 (5), 390–392. doi: 10.1038/nbt.2199

Liu, H., Jiang, W., Bi, Y., and Luo, Y. (2005). Postharvest BTH treatment induces resistance of peach (*Prunus persica* l. cv. jiubao) fruit to infection by penicillium expansum and enhances activity of fruit defense mechanisms. *Postharvest Biol. Technol.* 35 (3), 263–269. doi: 10.1016/j.postharvbio.2004.08.006

Malnoy, M., Viola, R., Jung, M.-H., Koo, O.-J., Kim, S., Kim, J.-S., et al. (2016). DNA-Free genetically edited grapevine and apple protoplast using CRISPR/Cas9 ribonucleoproteins. *Front. Plant Sci.* 7, 1904. doi: 10.3389/fpls.2016.01904

Mauch-Mani, B., Baccelli, I., Luna, E., and Flors, V. (2017). Defense priming: an adaptive part of induced resistance. *Annu. Rev. Plant Biol.* 68, 485–512. doi: 10.1146/annurev-arplant-042916-041132

Nekrasov, V., Wang, C., Win, J., Lanz, C., Weigel, D., and Kamoun, S. (2017). Rapid generation of a transgene-free powdery mildew resistant tomato by genome deletion. *Sci. Rep.* 7 (1), 1–6. doi: 10.1038/s41598-017-00578-x

Pavan, S., Jacobsen, E., Visser, R. G., and Bai, Y. (2010). Loss of susceptibility as a novel breeding strategy for durable and broad-spectrum resistance. *Mol. Breed.* 25 (1), 1–12. doi: 10.1007/s11032-009-9323-6

Ran, X., Liu, J., Qi, M., Wang, Y., Cheng, J., and Zhang, Y. (2018). GSHR, a web-based platform provides gene set-level analyses of hormone responses in arabidopsis. *Front. Plant Sci.* 9, 23. doi: 10.3389/fpls.2018.00023

Seifi, H. S., Zarei, A., Hsiang, T., and Shelp, B. J. (2019). Spermine is a potent plant defense activator against gray mold disease on *Solanum lycopersicum*, *Phaseolus vulgaris*, and *Arabidopsis thaliana*. *Phytopathology* 109 (8), 1367–1377. doi: 10.1094/PHYTO-12-18-0470-R

Shan, Q., Wang, Y., Li, J., Zhang, Y., Chen, K., Liang, Z., et al. (2013). Targeted genome modification of crop plants using a CRISPR-cas system. *Nat. Biotechnol.* 31 (8), 686–688. doi: 10.1038/nbt.2650

Smulders, M. J. M., Arens, P., Bourke, P. M., Debener, T., Linde, M., Riek, J. D., et al. (2019). In the name of the rose: a roadmap for rose research in the genome era. *Hortic. Res.* 6, 65. doi: 10.1038/s41438-019-0156-0

Spitzer, B., Zvi, M. M. B., Ovadis, M., Marhevka, E., Barkai, O., Edelbaum, O., et al. (2007). Reverse genetics of floral scent: application of tobacco rattle virus-based gene silencing in petunia. *Plant Physiol.* 145 (4), 1241–1250. doi: 10.1104/pp.107.105916

van Schie, C. C., and Takken, F. L. (2014). Susceptibility genes 101: how to be a good host. *Annu. Rev. Phytopathol.* 52, 551–581. doi: 10.1146/annurev-phyto-102313-045854

Verhagen, B. W., Glazebrook, J., Zhu, T., Chang, H.-S., Van Loon, L., and Pieterse, C. M. (2004). The transcriptome of rhizobacteria-induced systemic resistance in arabidopsis. *Mol. Plant-Microbe Interact.* 17 (8), 895–908. doi: 10.1094/MPMI.2004.17.8.895

Wu, Z., Liang, J., Wang, C., Zhao, X., Zhong, X., Cao, X., et al. (2018). Overexpression of lily HsfA3s in arabidopsis confers increased thermotolerance and salt sensitivity *via* alterations in proline catabolism. *J. Exp. Bot.* 69 (8), 2005–2021. doi: 10.1093/jxb/ery035

Yan, H., Shi, S., Ma, N., Cao, X., Zhang, H., Qiu, X., et al. (2018). Graft-accelerated virus-induced gene silencing facilitates functional genomics in rose flowers. *J. Integr. Plant Biol.* 60 (1), 34–44. doi: 10.1111/jipb.12599

Zhong, X., Yuan, X., Wu, Z., Khan, M. A., Chen, J., Li, X., et al. (2014). Virus-induced gene silencing for comparative functional studies in *Gladiolus hybridus*. *Plant Cell Rep.* 33 (2), 301–312. doi: 10.1007/s00299-013-1530-2

frontiers | Frontiers in Plant Science

TYPE Original Research
PUBLISHED 20 September 2022
DOI 10.3389/fpls.2022.988845

OPEN ACCESS

EDITED BY
Jian Chen,
Jiangsu University, China

REVIEWED BY
Sidra Tul Muntha,
Kohsar University Murree, Pakistan
Bo Wei,
Ghent University, Belgium

*CORRESPONDENCE
Xi Chen
chenxi_201402@163.com
Yuanda Lv
Lyd0527@126.com

†These authors have contributed equally to this work

SPECIALTY SECTION
This article was submitted to Plant Bioinformatics, a section of the journal Frontiers in Plant Science

RECEIVED 07 July 2022
ACCEPTED 24 August 2022
PUBLISHED 20 September 2022

CITATION
Luo C, He B, Shi P, Xi J, Gui H, Pang B, Cheng J, Hu F, Chen X and Lv Y (2022) Transcriptome dynamics uncovers long non-coding RNAs response to salinity stress in *Chenopodium quinoa*. *Front. Plant Sci.* 13:988845. doi: 10.3389/fpls.2022.988845

Transcriptome dynamics uncovers long non-coding RNAs response to salinity stress in *Chenopodium quinoa*

Chuping Luo[1†], Bing He[2†], Pibiao Shi[2†], Jinlong Xi[3], Hongbing Gui[4], Bingwen Pang[1,2], Junjie Cheng[1,2], Fengqin Hu[2], Xi Chen[5*] and Yuanda Lv[1,2*]

[1]School of Life Sciences and Food Engineering, Huaiyin Institute of Technology, Huaian, China, [2]Excellence and Innovation Center, Jiangsu Academy of Agricultural Sciences, Nanjing, China, [3]Zhejiang Institute of Standardization, Hangzhou, China, [4]College of Animal Husbandry and Veterinary Medicine, Jiangsu Vocational College of Agriculture and Forestry, Jurong, China, [5]School of Agronomy and Horticulture, Jiangsu Vocational College of Agriculture and Forestry, Jurong, China

Chenopodium quinoa is a crop with outstanding tolerance to saline soil, but long non-coding RNAs (LncRNAs) expression profile driven by salt stress in quinoa has rarely been observed yet. Based on the high-quality quinoa reference genome and high-throughput RNA sequencing (RNA-seq), genome-wide identification of LncRNAs was performed, and their dynamic response under salt stress was then investigated. In total, 153,751 high-confidence LncRNAs were discovered and dispersed intensively in chromosomes. Expression profile analysis demonstrated significant differences between LncRNAs and coding RNAs. Under salt stress conditions, 4,460 differentially expressed LncRNAs were discovered, of which only 54 were differentially expressed at all the stress time points. Besides, strongly significantly correlation was observed between salt-responsive LncRNAs and their closest neighboring genes (r = 0.346, p-value < 2.2e-16). Furthermore, a weighted co-expression network was then constructed to infer the potential biological functions of LncRNAs. Seven modules were significantly correlated with salt treatments, resulting in 210 hub genes, including 22 transcription factors and 70 LncRNAs. These results indicated that LncRNAs might interact with transcription factors to respond to salinity stress. Gene ontology enrichment of the coding genes of these modules showed that they were highly related to regulating metabolic processes, biological regulation and response to stress. This study is the genome-wide analysis of the LncRNAs responding to salt stress in quinoa. The findings will provide a solid framework for further functional research of salt responsive LncRNAs, contributing to quinoa genetic improvement.

KEYWORDS

quinoa, LncRNA, salt stress, RNA-seq, gene co-expression

Introduction

Quinoa (*Chenopodium quinoa* Willd.), an ancient annual dicotyledonous crop in the *Chenopodiaceae* family with approximately 7,000 years of cultivation, originated from the Andes mountains of South America (Jacobsen et al., 2003, 2005; Morales et al., 2017). Quinoa, like cereal crops such as rice, maize, and wheat, is most commonly consumed as seeds (Shi and Gu, 2020; Ma et al., 2021). Quinoa was a major food crop for the Indians, for instance, the Aztec and Inca civilizations. However, the cultivation process was interrupted after the arrival of Spanish immigrants because the conquerors prohibited local quinoa cultivation. Quinoa was rediscovered hundreds of years later, particularly as the twentieth century began, by developed countries due to its comprehensive nutrition. This orphan crop that belonged to poor Andes local farmers suddenly gained attention and became popular worldwide. Compared with cereal crops such as rice, quinoa offers an excellent balance between protein, oil and carbohydrate. The gluten-free starch of quinoa is suitable for celeriac patients (Jacobsen et al., 2003; Vega-Gálvez et al., 2010; Jarvis et al., 2017; Zou et al., 2017). The protein content of quinoa is as high as 15%, with an excellent balance in amino acids, and comparable to cheese and even better than beef (Kozioł, 1992). The lipid composition of quinoa is also superior due to its high concentration of polyunsaturated fatty acids like omega-3 fatty acid and docosahexaenoic acid (DHA), both of which are essential for human physiological demands and fit to a healthy diet. Finally, although the starch content in quinoa seed is relatively low compared to rice and wheat, it can simultaneously fulfil people's daily energy consumption with a lower glycemic index. Considering its excellent qualities, quinoa grain is a unique plant product covering all the nutrients for human survival and is recommended by the United Nations (FAO) and World Health Organization (WHO) for potential worldwide consumption. Furthermore, the year 2013 was announced as "The International Year of Quinoa" by the United Nations, which implied that the potential of this emerging crop was becoming more widely recognized (Jarvis et al., 2017; Schmöckel et al., 2017).

Quinoa is not only nutritious but also has many excellent agronomic characteristics. Quinoa is highly resistant to various abiotic stresses, including drought, salinity, cold, and soil nutrient defection, which makes it a robust candidate for agricultural development in marginal lands with poor soil conditions (Jacobsen et al., 2005; Razzaghi et al., 2011; Shi and Gu, 2020). Tidal flats and marshlands are potential resources of new farmland worldwide. In such areas, salinity is the primary limiting factor in local agriculture. High salinity can damage cells by causing ionic, osmotic, nutrient, and oxidative stresses, resulting in plants' growth inhibition and even death (Zhu, 2002; van Zelm et al., 2020; Zhao et al., 2021). As a salt-tolerant crop with high economic and nutrient values, quinoa is undoubtedly an attractive choice. Therefore, salt tolerance is a remarkable agronomy trait of quinoa, and many studies have been conducted, yielding promising results. For example, it has been found that quinoa has a unique tissue (epidermal bladder cell) for salt storage to prevent the somatic cell from salt stress (Zou et al., 2017). Jarvis et al. (2017) completed the first chromosome-level quinoa genome with a size as large as 1.4 Gb, which provides an excellent resource for quinoa molecular and genetic study.

Long non-coding RNAs (LncRNAs) are often recognized as transcripts larger than 200 nt in length but have no apparent protein-coding potential (Kung et al., 2013; Deng et al., 2018). LncRNAs have been discovered to be involved in a variety of biological regulatory processes, and their expression patterns are more tissue-specific than mRNA (Ponting et al., 2009; Rinn and Chang, 2012). According to their relative positions to nearby protein-coding genes in the genome, LncRNAs are generally classified into five types: sense, antisense, bidirectional, intergenic, and intronic (Liu et al., 2012; Lv et al., 2019; Chen et al., 2022). Previous studies have indicated that plant LncRNAs play functional roles in signal pathway transmission and molecular regulation under abiotic stresses such as salt stress. LncRNA973, for example, modulated the expression of a number of salt stress-related genes to positively regulate the response to salt stress in cotton (Zhang et al., 2019). In upland cotton, a competing endogenous RNA of miR160b regulated ARF genes in response to salt via a Long non-coding RNA-lncRNA354 (Zhang et al., 2021). A nucleus-localized drought-induced LncRNA (*DRIR*), which functioned in water transport and ABA signaling, could enhance the tolerance to drought and salt stress in *Arabidopsis* (Qin et al., 2017). Currently, stress-responsive LncRNAs have been identified in many species, such as maize (Lv et al., 2013, 2016; Chen et al., 2022), rice (Zhang et al., 2014), *Arabidopsis* (Liu et al., 2012), pistachio (Jannesar et al., 2020), chickpea (Kumar et al., 2021), and rapeseed (Tan et al., 2020). However, no systematic study on salt-responsive LncRNAs in quinoa has been reported. This study focused on quinoa LncRNAs and their dynamic responses to salt stress. The findings will provide a massive amount of salt-responsive LncRNAs in quinoa and enlighten the potential patterns of LncRNAs incorporation with the coding genes.

Results

Transcriptome assembly and long non-coding RNAs identification

To profile the LncRNA transcripts in response to salt stress, we performed the time-series dynamic analysis of RNA-sequencing on quinoa roots exposed to high salinity conditions (**Supplementary Table 1**). In total, 464 million raw reads were generated, and 430 million clean reads were obtained

after cleaning. Approximately 85.30% (367 million) of the clean reads were mapped to the quinoa reference genome and assembled into transcripts. Cleaned data (~30 Gb) was first mapped to the reference genome, and then alignments were assembled into transcripts in each sample (Supplementary Table 2). Transcripts from all samples were merged to form a unified set of transcripts, which consisted of 188,663 genes and 234,387 transcripts. There were 146,440 transcripts (62.5% of the predicted transcripts) with only one exon. There were 1.24 transcripts per gene and 3.15 exons in a transcript.

Coding potential ability was analyzed by CPC2, from which there were 153,751 non-coding LncRNAs identified (Supplementary Table 3). A genome location study showed these LncRNAs were intensely distributed in 18 chromosomes of *C. quinoa*, and the distribution intensity in the two ends of each chromosome was higher than in other parts (Figure 1A). According to the relationship between a transcript and the closest reference transcript, LncRNAs were grouped into different classes represented by characters and symbols by GffCompare software (Figure 1B). "u" was the most abundant type (72.8%), showing that most LncRNAs came from the intergenic region. The second most abundant class was the "x" type (12.1%), followed by "i" (6.7%) and "p"(3.3%). These results indicated that LncRNAs seldom overlapped with reference

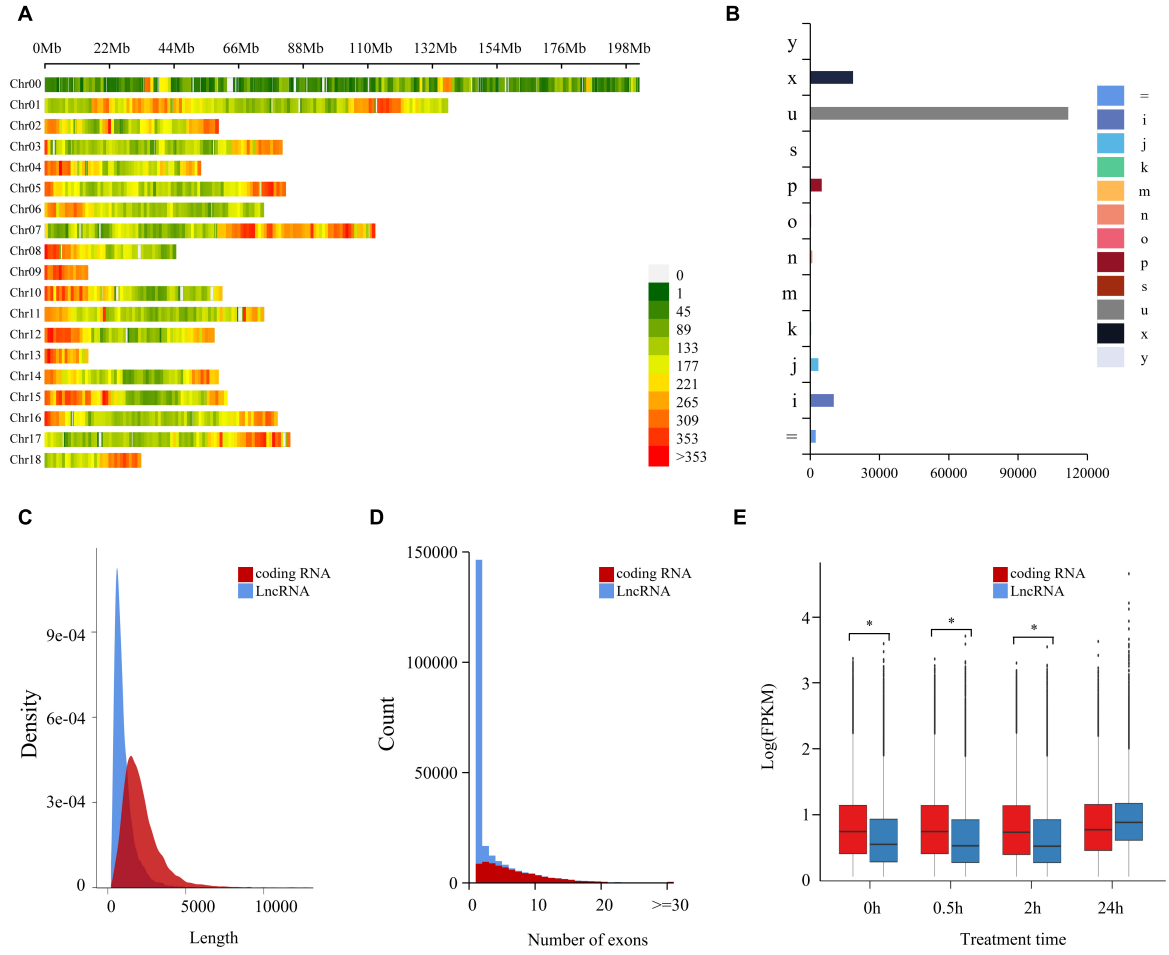

FIGURE 1
Genome-wide identification and characterization of LncRNA in quinoa root under salt stress. **(A)** Chromosome distribution of LncRNAs in quinoa reference genome. The LncRNAs density was demonstrated by the coloration. Numbers on the right hand of color bar indicated the amount of LncRNAs within 1 Mb window size. Chr: chromosome. **(B)** Annotation classification of LncRNAs based on reference gene set. Class codes were generated by Cuffcompare against quinoa reference gene set (*Chenopodium quinoa* v1.0). Different groups were represented in different colors and marked with characters and symbols. " = ": complete, exact match of intron chain; "i": fully contained within a reference intron; "j": multi-exon with at least one junction match; "k": containment of reference (reverse containment); "m": retained intron(s), all introns matched or retained; "n": retained intron(s), not all introns matched or retained; "o": other same strand overlap with reference exons; "p": possible polymerase run-on (no actual overlap); "s": intronic match on the opposite strand (likely a mapping error); "u": unkown, intergenic; "x": exonic overlap on the opposite strand; "y": contains a reference within its intron(s). **(C)** Length distribution of coding RNAs and LncRNAs. **(D)** Exons distribution of coding RNAs and LncRNAs. **(E)** The expression patterns of coding RNAs and LncRNAs at different time points of salt treatment. *$p < 0.05$ (Student's t-test).

transcripts. As shown in **Figures 1C,D**, the length of LncRNAs was generally much shorter than the coding RNAs, and LncRNA had less exon contained than the coding ones. The difference in expression pattern between coding RNAs and LncRNAs was measured statistically using a two-tailed Mann-Whitney *U*-Test (**Figure 1E**). The expression pattern of LncRNAs was significantly different from that of the coding genes. The overall expression level of LncRNA was significantly lower than that of coding RNAs at 0, 0.5, and 2 h of -salinity treatment ($p < 2.2e-16$). However, at 24 h of treatment, the overall expression level of LncRNAs increased sharply and was more significant than that of coding RNAs. The expression level of coding RNAs was relatively stable within 24 h of treatment. For further validating the reliability of LncRNAs, 50 randomly selected LncRNAs were aligned against Pacbio full-length cDNA datasets from Jarvis et al. (2017). A 47 of 50 LncRNAs were successfully aligned into full-length transcripts. Among them, 46 full-length cDNAs corresponding to LncRNAs were also no coding potential by CPC2 program prediction. These cross-validation results revealed that a set of high-confidence LncRNAs was obtained in the study (**Supplementary Table 8**).

Identification of differentially expressed long non-coding RNAs in response to salt stress

Differentially expressed transcripts, including coding RNAs and LncRNAs, were then identified by DESeq2 (**Supplementary Table 4**). We identified 4,460 DE-LncRNAs, of which 214, 1,731, and 3,102 were identified at 0.5, 2, and 24 h of treatment (**Figure 2A**). Only 54 LncRNAs were differentially expressed at all the three-time points, occupying 1.2% of total DE-LncRNAs (4,460) (**Figure 2B**). Totally 6,791 DE-coding RNAs were also identified, 104 (1.5%) differentially expressed at three-time points (**Figure 2B**). At 0.5 h of treatment 75% (161) DE-LncRNAs and 77% (237) DE-coding RNAs were upregulated, while at 2 h of treatment 48% (831) DE-LncRNAs and 56% (2,197) DE-coding RNAs were upregulated. At 24 h of treatment, as high as 81% (2,513) DE-LncRNAs were upregulated, whereas only 39% (1,462) DE-coding RNAs were upregulated (**Figure 2C** and **Supplementary Table 2**).

Previous studies have suggested lncRNAs may play *cis* regulation role against neighboring genes. To investigate this possibility, we further measured the expression correlation between salt-responsive LncRNAs and their closest neighboring gene in either the 5′ or 3′ direction, yielding a dataset of 1,740 LncRNA-Coding Genes pairs (differentially expressed LncRNAs and their neighboring genes). The correlation analysis showed lncRNAs were strongly and highly significantly correlated with the expression of their closest neighboring gene ($r = 0.346$, p-value $< 2.2e-16$) (**Figure 2D**). Suggesting that lncRNAs may either be involved in *cis*-acting regulation or are subject to some of the same *cis*-acting regulatory features as their neighboring genes.

Construction of gene co-expression network and analysis of salinity responsive modules

To infer the potential biological functions of the LncRNAs, a weighted gene co-expression network consisting of both LncRNAs and coding RNAs based on expression profiles was constructed by the WGCNA program (Langfelder and Horvath, 2008). The soft-thresholding power was predicted and defined as 7, as it was the lowest power for which the scale-free topology fit index reached 0.90 (**Figures 3A,B**). There were finally 36 modules (**Figure 3C**) generated, and they were named from M1 to M36. The relationship between modules and salinity treatment was calculated, of which seven modules were highly relevant to salinity treatment (**Figure 3D**). M30 ($r = 0.93$, $p = 1.57e-05$) and M12 ($r = 0.99$, $p = 9.12e-10$) were upregulated significantly at 0.5 and 2 h, respectively; M17 ($r = 0.90$, $p = 5.48e-05$) and M32 ($r = -0.99$, $p = 4.71e-09$) modules upregulated and downregulated at 24 h, respectively; M13 ($r = 0.90$, $p = 5.53e-05$) upregulated at 0.5 and 2 h both; M11 ($r = 0.90$, $p = 6.35e-05$) upregulated at both 2 and 24 h, while M33 ($r = 0.90$, $p = 6.35e-05$) downregulated at the same time. No module was significantly regulated at all the three-time points. The percentage of LncRNAs in salinity-responsive modules ranged from 20 to 40%. The genes with the highest connectivity in each module were selected as hub genes. Totally, 210 hub genes were identified from these seven salinity-responsive modules listed above, which constituted a subnetwork (**Figure 3E** and **Supplementary Table 6**). The hub genes of M30 included both TF genes and LncRNAs, and so did M13, M12, and M11 modules. This implied that LncRNAs within these modules might interact with transcript factors and their role in salinity response. However, TF genes were not included in the hub genes of M17 and M32 modules. Instead, more than half of the hub genes were LncRNAs in them. In M17 module as high as 23 LncRNAs were at the hub position (**Supplementary Table 6**).

Gene ontology enrichment analysis of salinity-responsive modules

Gene ontology analysis of coding RNAs was performed to predict the function of the LncRNAs within the same module (**Supplementary Table 5**). The most representative GO terms of high-salinity responsive modules are shown in **Figure 4A**. A large part of the GO terms was enriched in all the seven high-salinity responsive modules. They were related to various critical biological processes, including biological regulation (GO:0065007), regulation of gene

10.3389/fpls.2022.988845

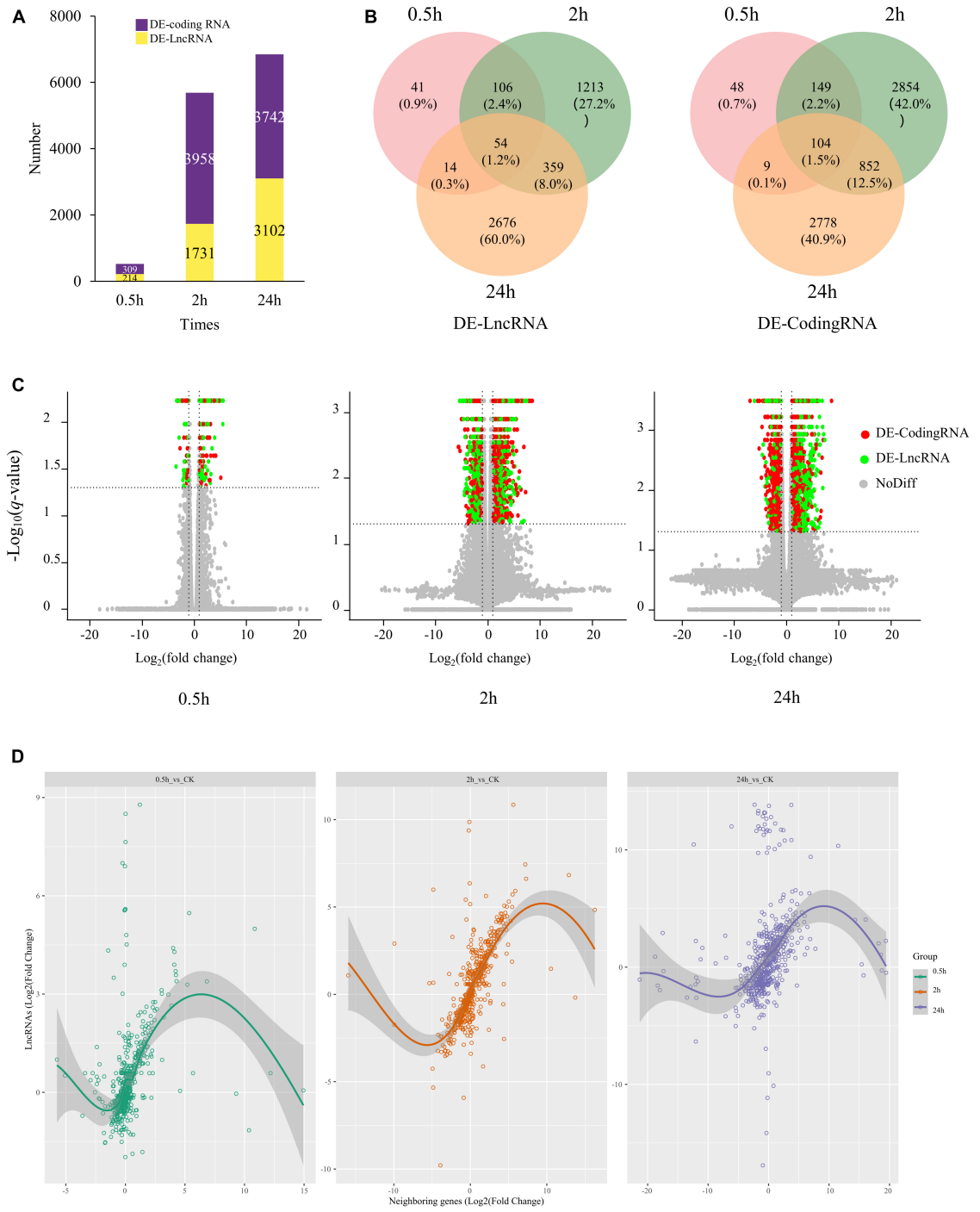

FIGURE 2
The expression profile of coding RNAs and LncRNAs under salt stress in quinoa roots. **(A)** Number of DE-coding RNAs and DE-LncRNAs identified at 0.5, 2, and 24 h of salt treatment. **(B)** Venn diagrams of DE-coding RNAs and DE-LncRNAs. **(C)** Volcano plots of DE transcripts at 0.5, 2, and 24 h of salt treatment. Red point represented DE-coding RNAs; green point represented DE-LncRNAs; gray point represented non-DE transcripts. **(D)** Correlation plot of salt-responsive LncRNAs and their closest neighboring genes at 0.5, 2, and 24 h under salt stress.

expression (GO:0010468), response to stress (GO:0006950), regulation of metabolic process (GO:0019222), transcription (GO:0006350) and developmental process (GO:0032502). Transport (GO:0006810) and metabolic process (GO:0008152) were enriched in six salinity-responsive modules. A small part of the GO terms was enriched in only two or three modules such

10.3389/fpls.2022.988845

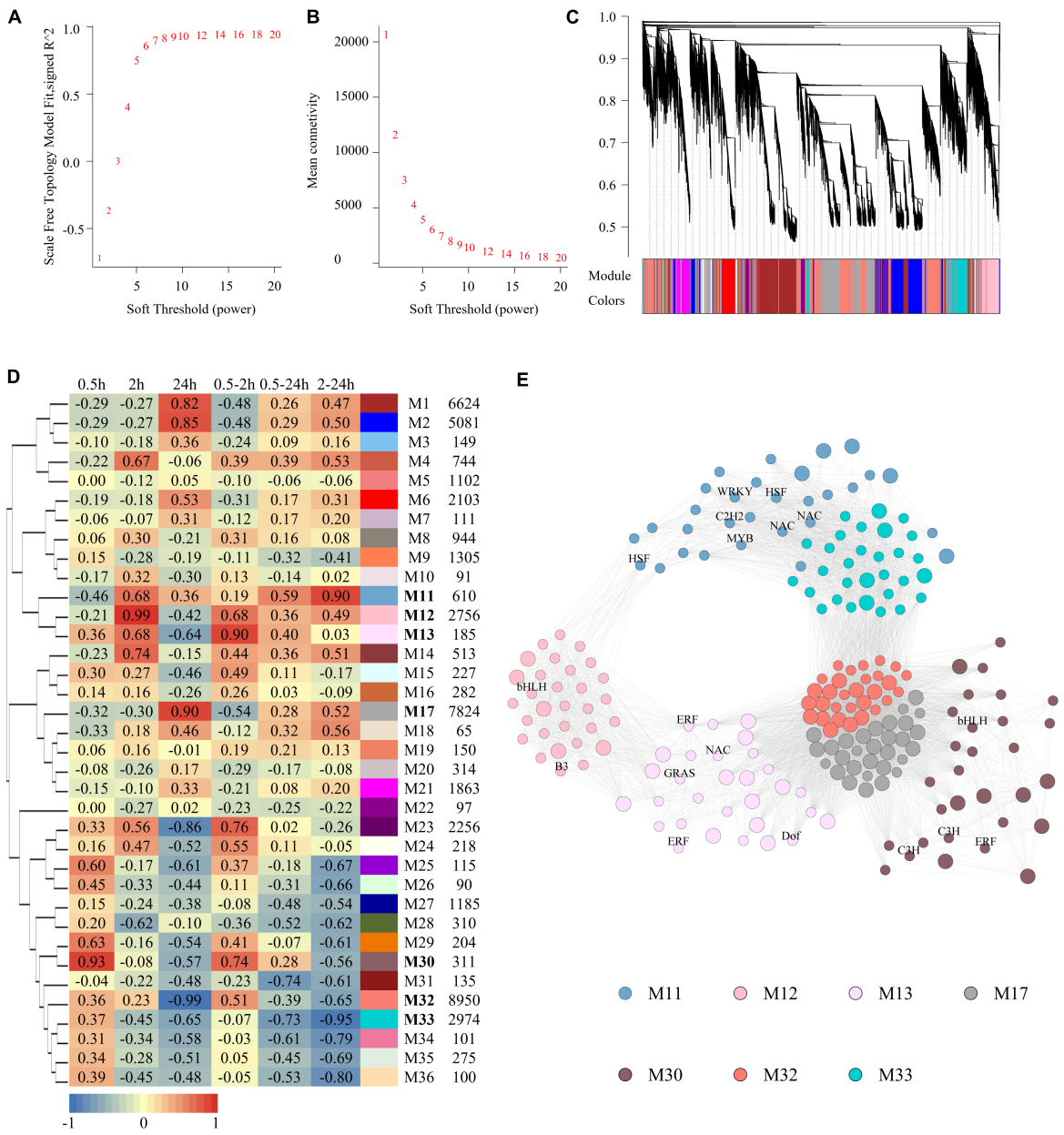

FIGURE 3

Construction of gene co-expression network and analysis of salt responsive modules. **(A)** The scale-free fit index as a function of the soft-thresholding power. **(B)** The mean connectivity as a function of the soft-thresholding power. **(C)** Clustering dendrogram of genes, with dissimilarity based on topological overlap. Modules were labeled by colors as indicated by the color band underneath the tree. **(D)** Heatmap showing the correlation between modules and salt treatment. Each cell contains the corresponding correlation. The table is color-coded by correlation according to the color legend. The columns on the right of heatmap showed module color, module name and module size in turn. **(E)** Subnetwork of hub genes of salt responsive modules. Modules were represented by different colors as described in **Figure 3D**. Small circle represented coding RNAs and big circle represent LncRNAs. TFs were labeled.

as cell cycle (GO:0007049). Within these modules, there were several genes directly responding to salt stress. For instance, in M11, a transcript encoding a salt tolerance zinc finger (C2H2 type) which is highly homologous to the *Arabidopsis* gene (AT1G27730.1); in M12, there is a transcript encoding calcineurin B-like protein 1, which is highly homologous to *Arabidopsis* gene (AT4G17615.1), it might function as a positive regulator of salt and drought responses and as a negative regulator of cold response, and mediates the activation of AKT1 by CIPK proteins (CIPK6, CIPK16, and CIPK23) in response to low potassium conditions; In M13, one transcript homologous to *Arabidopsis* gene AT5G12010 was included, which might

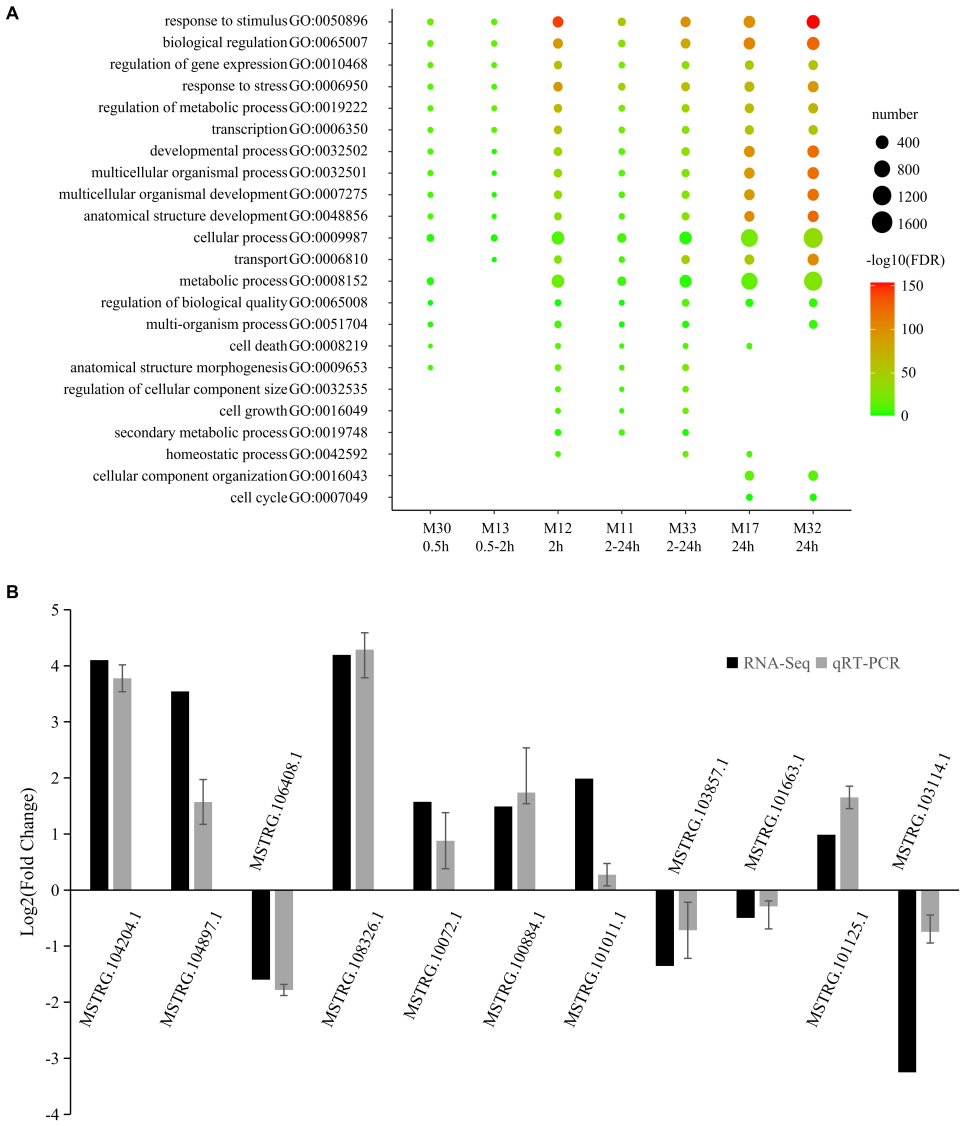

FIGURE 4
Most representative GO terms of salt responsive modules and qRT-PCR validation. **(A)** Color legend represented $-\log_{10}$ FDR. Point size represented number of genes enriched in the GO terms. The rows beneath the bubble chart showed module name, and the response time of each module. **(B)** The qRT-PCR histogram for each locus represents the mean ± standard error (SE) of three independent biological replicates, and the qRT-PCR are compared to fold-change data inferred from RNA-seq data.

respond to salt stress and function in ABA-activated signaling pathway.

Validation of salt-responsive long non-coding RNAs by quantitative real-time PCR analysis

To validate the reliability of salt-responsive LncRNAs, 15 salt-responsive LncRNAs were randomly selected and then subjected the 0 and 2 h salt-treated samples to quantitative real-time PCR (qRT-PCR) to compare expression changes between replicated control and salt-treated. As a result, 11 of 15 salt-responsive LncRNAs were successfully detected and showed a high degree of consistency (r = 0.877, p = 0.000392) between RNA-seq and qRT-PCR (**Figure 4B** and **Supplementary Table 7**).

Discussion

Because of its remarkable tolerance to soil salt, drought and infertility, high-quality and well-balanced nutrient, quinoa has become popular and well-studied for its unique nature

(Jacobsen et al., 2003; Jarvis et al., 2017; Zou et al., 2017). Quinoa is not only a species with high tolerance to salt stress, but also a plant preferring sodium (Wu et al., 2016). Hence, it is acknowledged as halophytic plant species by some studies. Up to date, there have been dozens of studies carried out to dissect the characteristic. It has been demonstrated that the quinoa plant has epidermal bladder cells on its leaves and that these could pump extra sodium chloride into it (Böhm et al., 2018). Sodium cation could be sequestrated in leaf-cell vacuole (Shabala and Mackay, 2011). The cellular potassium retention ability has been enhanced; on the other hand, cellular sodium exclusion and xylem loading in quinoa is also superior (Maughan et al., 2009). However, the salt tolerance trait of quinoa has a complicated underlying mechanism.

Plants have developed a series of physiological functions to alleviate stress or adapt to different environmental changes. The signal pathways and regulation systems lying behind are being dissected more and more. Non-coding RNAs have been illustrated to play important roles in the biological processes. These non-coding RNAs mainly include small non-coding RNA (sncRNA) and long non-coding (LncRNA). miRNA is one of the major parts of sncRNAs, as well as the siRNA; and they mediate gene silencing and hence regulate the expression levels of the genes (Negi et al., 2021). Mul-miR3954, for example, was discovered in *Arabidopsis* to improve the salt-tolerance level of transgenic plants (Gai et al., 2018); miR398b and miR298 could regulate Cu/Zn-*SOD* expression in response to ROS levels induced by salt stress (Feng et al., 2010). TCONS_00009717 is a miRNA found in soybean that may be induced by salt stress, its potential target is cytochrome P450 (Chen et al., 2019). Summarily, LncRNAs were also discovered and found to be involved in response to several abiotic stresses in plant species such as *Arabidopsis thaliana*, *Zea may*, and *Nicotiana tabacum* (Liu et al., 2012; Lv et al., 2013, 2019; Yu et al., 2019; Zhang et al., 2019, 2021; Chen et al., 2022). However, as a remarkable salt tolerant crop, the LncRNAs of quinoa responding to salt stress have not been reported yet.

In the study, we performed a time-course dynamic transcriptome analysis on quinoa under salinity treatment. Under salinity treatments, we extracted 234,387 transcripts from quinoa seedling roots. 153,751 LncRNAs and 51,667 genes were discovered among them. LncRNAs were generally shorter in length than coding RNA, which was likely due to the fact that nearly 90% of LncRNAs had only one exon (**Figures 1C,D**). In **Figure 2B**, time-course dynamic transcriptome analysis revealed a total of 4,460 identified DE-LncRNAs and 6,791 DE-coding RNAs and the DE-LncRNAs and DE-coding RNAs showed a time-dependent pattern, respectively. Meanwhile, as shown in **Figure 2A**, most of DE-LncRNAs were upregulated, which was probably why the overall expression level of LncRNAs increased enormously at 24 h of treatment (**Supplementary Table 2**).

Previous studies have suggested lncRNAs may play *cis* regulation role against neighboring genes. A dataset of 1,740 LncRNA-Coding Genes pairs (salt-responsive LncRNAs and their closest neighboring gene in either the 5′ or 3′ direction) was generated. Pearson correlation analysis showed highly significantly correlation level (r = 0.346, p-value < 2.2e-16) (**Figure 2D**), which illustrated that LncRNAs may play a *cis*-acting regulation role on their neighboring genes under salt stress.

The DE-LncRNAs and DE-coding RNAs were further examined, yielding 36 weighted gene co-expression network modules, seven of which showed responses to salinity stress. Highly connected hub genes in a module most likely played important roles in the same biological processes. The hub genes from each of the seven modules were shown as a subnetwork in **Figure 3E**. Some DE-coding RNAs are also classified as transcription factors (TF). For example, in module 11, one transcript encodes a homologous of *Arabidopsis* gene (ATG27730.1), which encodes a zinc finger TF involved in salt tolerance. It is also a hub gene in that module with high connectivity with others. In *Arabidopsis*, the homologous gene could respond to various kinds of stresses such as salt, cold, drought and oxidative. It is closely associated with the signal pathway of stress tolerance in plants. In modules 17 and 32, there were no TFs involved, which indicated that some LncRNAs might also work independently of TFs in response to salinity stress in quinoa. Another 48 TFs belonging to coding RNAs and 62 LncRNAs in this module implied that LncRNAs within these modules might interact with transcript factors and play a hub role in salinity response.

Conclusion

As a well-known salt-tolerant crop, few reports have identified long non-coding RNAs under salt stress in quinoa. Hence, we provided a bulk of LncRNAs in quinoa roots on a large scale and identified those induced or suppressed by salt treatment. Furthermore, we also predicted the potential gene-expression modules in which the LncRNAs might be included and function together with genes. Hopefully, these findings will serve as a dataset resource for further research on quinoa salt tolerance and provide a reference for quinoa breeding work.

Materials and methods

Plant material and salt treatment

Chenopodium quinoa cultivar QQ056 were acquired from the USDA-ARS National Plant Germplasm System (NPGS) with permission for scientific research. Detailed information on the variety could be found at npgsweb.ars-grin.gov (accession: PI

584524). The experiments were performed in a phytotron at 28°C under 16 h/8 h (day/night) photoperiod. Seeds of quinoa were surface sterilized, germinated for 7 days, and then moved into a half-strength Hoagland solution. Seedlings of 28-day-old were transferred to half-strength MS with 300 mM NaCl for salt treatment. Roots of quinoa were gathered at 0, 0.5, 2, and 24 h of treatment and stored at −80°C for further investigation. Three biological repeats were used at each time point.

Library preparation and RNA-seq sequencing

Total RNA was isolated, purified and concentrated with an RNAprep Pure Plant Kit (Tiangen, China). A Thermo 2000 Bioanalyzer evaluated the concentration and quality of RNA with an RNA NanoDrop (Thermo Scientific, United States). cDNA libraries were conducted using TruSeq mRNA Sample Prep Kit (Illumina, United States). RNA sequencing (RNA-seq) was performed on the Illumina NovaSeq 6000 platform (Illumina, United States) at Annoroad Gene Technology (Beijing) Co., Ltd., China.

RNA-seq data analysis

Raw data were trimmed with low-quality bases and short reads ($<$ 50 bp) using Fastp v0.23.2 (Chen et al., 2018). Cleaned reads were then mapped into the quinoa reference genome (Jarvis et al., 2017) by splice-aware alignment method using STAR v2.7.10a with two-pass mode (Dobin et al., 2013). The mapped reads of each sample were separately assembled by the reference annotation-based transcript (RABT) assembly algorithm and then combined with known transcript annotation (Jarvis et al., 2017) into an updated GTF file using StringTie v2.2.1 (Pertea et al., 2016). Finally, the abundance of transcripts was quantified and normalized with HTseq (Putri et al., 2022) and DESeq2 (Love et al., 2014). The transcripts with fragments per kilobase of transcript per million fragments mapped (FPKM) $<$ 1 in more than three samples were excepted for downstream analysis.

Coding potential prediction of long non-coding RNAs

Computational prediction of quinoa LncRNAs was followed as described by Lv et al. (2019) with some custom modification. Sequences of transcripts were firstly retrieved using Gffread v0.12.2 (Pertea and Pertea, 2020). Then transcripts were evaluated in their coding potential using CPC v2.0 (Kang et al., 2017). Default parameters were used. Finally, non-coding transcripts longer than 200 bp were considered as LncRNAs. The updated GTF file was also compared with the reference GTF file using gffCompare (Pertea et al., 2016) to generate class codes representing the position information between the updated transcript and the closest reference transcript.

Differential expression analysis

For differential expression analysis, we compared every time point (0.5, 2, and 24 h of treatment) with CK (0 h) using DESeq2 (Trapnell et al., 2010) based on the negative binomial distribution. Differentially expressed should be fulfilled the following criteria: (I) fold change $>$ = 1; (II) adjusted p value $<$ 0.05.

Gene co-expression network analysis

A weighted co-expression network was further constructed for linking coding RNAs and LncRNAs using the WGCNA program (Zhang and Horvath, 2005; Langfelder and Horvath, 2008). The correlation between module eigengenes and salt treatment was then calculated. Modules that showed a significant correlation ($|r| > 0.9, p < 0.001$) with a specific time of treatment were recognized as salt-responsive modules (Xue et al., 2013). The hub genes of each module were worked out based on the Topological overlap matrix (TOM).

Gene ontology enrichment analysis

Gene Ontology (GO) enrichment analysis was performed with agriGO v2.0 toolkit (Tian et al., 2017). Fisher's exact test was applied for the enrichment analysis, and the false discovery rate (FDR) was assessed using the Yekutieli method. GO terms with an FDR less than 0.05 were considered significant.

Quantitative real-time PCR validation

To validate the reliability and accuracy of the LncRNA analysis, ten salt-responsive LncRNAs were chosen and measured by quantitative real-time PCR (qRT-PCR). The first-strand cDNA of 0 and 2 h samples were synthesized using the PrimeScript TM RT-PCR Kit (Takara, Japan). We conducted the qRT-PCR on an ABI StepOnePlus Real-Time PCR System (Applied Biosystems, CA, United States) with FastStart Universal SYBR Green Master (Roche, Germany) according to the manufacturer's protocol. The primers were designed using Primer Premier v.5.0 software (Premier Biosoft International, CA, United States). CqEF1a (AUR62020767) was used as an internal standard to normalize the relative expression level and determine expression values based on the

$2^{-\Delta\Delta Ct}$ method. The primers for qRT-PCR were presented in **Supplementary Table 7**.

Data availability statement

The datasets presented in this study were deposited in National Center for Biotechnology Information (NCBI) BioProject database under accession number: PRJNA636120. All data can be found in the article/**Supplementary material**.

Author contributions

YL and XC conceived and designed the experiments. CL, BH, PS, JX, HG, BP, JC, and FH participated in experiments and data analyses. CL, BH, and PS wrote the manuscript with inputs and guidance from YL. All authors have read and approved the final manuscript.

Funding

This work was supported by the Jiangsu Agricultural Science and Technology Independent Innovation Fund (JASTIF) [CX(21)3127] and National Natural Science Foundation of China (31601818).

Conflict of interest

The authors declare that the research was conducted in the absence of any commercial or financial relationships that could be construed as a potential conflict of interest.

Publisher's note

All claims expressed in this article are solely those of the authors and do not necessarily represent those of their affiliated organizations, or those of the publisher, the editors and the reviewers. Any product that may be evaluated in this article, or claim that may be made by its manufacturer, is not guaranteed or endorsed by the publisher.

Supplementary material

The Supplementary Material for this article can be found online at: https://www.frontiersin.org/articles/10.3389/fpls.2022.988845/full#supplementary-material

References

Böhm, J., Messerer, M., Müller, H. M., Scholz-Starke, J., Gradogna, A., Scherzer, S., et al. (2018). Understanding the molecular basis of salt sequestration in epidermal bladder cells of *Chenopodium quinoa*. *Curr. Biol.* 28, 3075.e–3085.e. doi: 10.1016/j.cub.2018.08.004

Chen, R., Li, M., Zhang, H., Duan, L., Sun, X., Jiang, Q., et al. (2019). Continuous salt stress-induced long non-coding RNAs and DNA methylation patterns in soybean roots. *BMC Genomics* 20:730. doi: 10.1186/s12864-019-6101-7

Chen, S., Zhou, Y., Chen, Y., and Gu, J. (2018). fastp: An ultra-fast all-in-one FASTQ preprocessor. *Bioinformatics* 34, i884–i890. doi: 10.1093/bioinformatics/bty560

Chen, X., Meng, L., He, B., Qi, W., Jia, L., Xu, N., et al. (2022). Comprehensive transcriptome analysis uncovers hub long non-coding RNAs regulating potassium use efficiency in *Nicotiana tabacum*. *Front. Plant Sci.* 13:777308. doi: 10.3389/fpls.2022.777308

Deng, F., Zhang, X., Wang, W., Yuan, R., and Shen, F. (2018). Identification of *Gossypium hirsutum* long non-coding RNAs (lncRNAs) under salt stress. *BMC Plant Biol.* 18:23. doi: 10.1186/s12870-018-1238-0

Dobin, A., Davis, C. A., Schlesinger, F., Drenkow, J., Zaleski, C., Jha, S., et al. (2013). STAR: Ultrafast universal RNA-seq aligner. *Bioinformatics* 29, 15–21. doi: 10.1093/bioinformatics/bts635

Feng, X.-M., Qiao, Y., Mao, K., and Hao, Y.-J. (2010). Ectopic overexpression of AtmiR398b gene in tobacco influences seed germination and seedling growth. *Plant Cell Tissue Organ. Cult.* 102, 53–59. doi: 10.1007/s11240-010-9704-x

Gai, Y.-P., Yuan, S.-S., Zhao, Y.-N., Zhao, H.-N., Zhang, H.-L., and Ji, X.-L. (2018). A novel LncRNA, MuLnc1, associated with environmental stress in mulberry (*Morus multicaulis*). *Front. Plant Sci* 9:669. doi: 10.3389/fpls.2018.00669

Jacobsen, S. E., Mujica, A., and Jensen, C. R. (2003). The resistance of quinoa (*Chenopodium quinoa* Willd.) to adverse abiotic factors. *Food Rev. Int.* 19, 99–109. doi: 10.1081/FRI-120018872

Jacobsen, S.-E., Monteros, C., Christiansen, J. L., Bravo, L. A., Corcuera, L. J., and Mujica, A. (2005). Plant responses of quinoa (*Chenopodium quinoa* Willd.) to frost at various phenological stages. *Eur. J. Agron.* 22, 131–139. doi: 10.1016/j.eja.2004.01.003

Jannesar, M., Seyedi, S. M., Moazzam Jazi, M., Niknam, V., Ebrahimzadeh, H., and Botanga, C. (2020). A genome-wide identification, characterization and functional analysis of salt-related long non-coding RNAs in non-model plant *Pistacia vera* L. using transcriptome high throughput sequencing. *Sci. Rep.* 10:5585. doi: 10.1038/s41598-020-62108-6

Jarvis, D. E., Ho, Y. S., Lightfoot, D. J., Schmöckel, S. M., Li, B., Borm, T. J. A., et al. (2017). The genome of *Chenopodium quinoa*. *Nature* 542, 307–312. doi: 10.1038/nature21370

Kang, Y.-J., Yang, D.-C., Kong, L., Hou, M., Meng, Y.-Q., Wei, L., et al. (2017). CPC2: A fast and accurate coding potential calculator based on sequence intrinsic features. *Nucleic Acids Res.* 45, W12–W16. doi: 10.1093/nar/gkx428

Kozioł, M. J. (1992). Chemical composition and nutritional evaluation of quinoa (*Chenopodium quinoa* Willd.). *J. Food Compos. Anal.* 5, 35–68. doi: 10.1016/0889-1575(92)90006-6

Kumar, N., Bharadwaj, C., Sahu, S., Shiv, A., Shrivastava, A. K., Reddy, S. P. P., et al. (2021). Genome-wide identification and functional prediction of salt- stress related long non-coding RNAs (lncRNAs) in chickpea (*Cicer arietinum* L.). *Physiol. Mol. Biol. Plants* 27, 2605–2619. doi: 10.1007/s12298-021-01093-0

Kung, J. T. Y., Colognori, D., and Lee, J. T. (2013). Long noncoding RNAs: Past, present, and future. *Genetics* 193, 651–669. doi: 10.1534/genetics.112.146704

Langfelder, P., and Horvath, S. (2008). WGCNA: An R package for weighted correlation network analysis. *BMC Bioinform.* 9:559.

Liu, J., Jung, C., Xu, J., Wang, H., Deng, S., Bernad, L., et al. (2012). Genome-wide analysis uncovers regulation of long intergenic noncoding RNAs in *Arabidopsis*. *Plant Cell* 24, 4333–4345. doi: 10.1105/tpc.112.102855

Love, M. I., Huber, W., and Anders, S. (2014). Moderated estimation of fold change and dispersion for RNA-seq data with DESeq2. *Genome Biol.* 15:550. doi: 10.1186/s13059-014-0550-8

Lv, Y., Hu, F., Zhou, Y., Wu, F., and Gaut, B. S. (2019). Maize transposable elements contribute to long non-coding RNAs that are regulatory hubs for abiotic stress response. *BMC Genomics* 20:864. doi: 10.1186/s12864-019-6245-5

Lv, Y., Liang, Z., Ge, M., Qi, W., Zhang, T., Lin, F., et al. (2016). Genome-wide identification and functional prediction of nitrogen-responsive intergenic and intronic long non-coding RNAs in maize (*Zea mays* L.). *BMC Genomics* 17:350. doi: 10.1186/s12864-016-2650-1

Lv, Y., Zhao, L., Xu, X., Wang, L., Wang, C., Zhang, T., et al. (2013). Characterization of expressed sequence tags from developing fibers of *Gossypium barbadense* and evaluation of insertion-deletion variation in tetraploid cultivated cotton species. *BMC Genomics* 14:170. doi: 10.1186/1471-2164-14-170

Ma, Q., Su, C., and Dong, C.-H. (2021). Genome-wide transcriptomic and proteomic exploration of molecular regulations in quinoa responses to ethylene and salt stress. *Plants* 10:2281. doi: 10.3390/plants10112281

Maughan, P. J., Turner, T. B., Coleman, C. E., Elzinga, D. B., Jellen, E. N., Morales, J. A., et al. (2009). Characterization of salt overly sensitive 1 (SOS1) gene homoeologs in quinoa (*Chenopodium quinoa* Willd.). *Genome* 52, 647–657. doi: 10.1139/G09-041

Morales, A., Zurita-Silva, A., Maldonado, J., and Silva, H. (2017). Transcriptional responses of Chilean quinoa (*Chenopodium quinoa* Willd.) under water deficit conditions uncovers ABA-independent expression patterns. *Front. Plant Sci* 8:216. doi: 10.3389/fpls.2017.00216

Negi, P., Mishra, S., Ganapathi, T. R., and Srivastava, A. K. (2021). Regulatory short RNAs?: A decade's tale for manipulating salt tolerance in plants. *Physiol. Plant* 173, 1535–1555. doi: 10.1111/ppl.13492

Pertea, G., and Pertea, M. (2020). GFF utilities: GffRead and GffCompare. *F1000Res.* 9:304. doi: 10.12688/f1000research.23297.1

Pertea, M., Kim, D., Pertea, G. M., Leek, J. T., and Salzberg, S. L. (2016). Transcript-level expression analysis of RNA-seq experiments with HISAT, StringTie and Ballgown. *Nat. Protoc.* 11, 1650–1667. doi: 10.1038/nprot.2016.095

Ponting, C. P., Oliver, P. L., and Reik, W. (2009). Evolution and functions of long noncoding RNAs. *Cell* 136, 629–641. doi: 10.1016/j.cell.2009.02.006

Putri, G. H., Anders, S., Pyl, P. T., Pimanda, J. E., and Zanini, F. (2022). Analysing high-throughput sequencing data in Python with HTSeq 2.0. *Bioinformatics* 38, 2943–2945. doi: 10.1093/bioinformatics/btac166

Qin, T., Zhao, H., Cui, P., Albesher, N., and Xiong, L. (2017). A nucleus-localized long non-coding RNA enhances drought and salt stress tolerance. *Plant Physiol.* 175, 1321–1336. doi: 10.1104/pp.17.00574

Razzaghi, F., Ahmadi, S. H., Adolf, V. I., Jensen, C. R., Jacobsen, S.-E., and Andersen, M. N. (2011). Water relations and transpiration of quinoa (*Chenopodium quinoa* Willd.) Under Salinity and Soil Drying. *J. Agron. Crop Sci.* 197, 348–360. doi: 10.1111/j.1439-037X.2011.00473.x

Rinn, J. L., and Chang, H. Y. (2012). Genome regulation by long noncoding RNAs. *Annu. Rev. Biochem.* 81, 145–166. doi: 10.1146/annurev-biochem-051410-092902

Schmöckel, S. M., Lightfoot, D. J., Razali, R., Tester, M., and Jarvis, D. E. (2017). Identification of putative transmembrane proteins involved in salinity tolerance in *Chenopodium quinoa* by integrating physiological data, RNAseq, and SNP analyses. *Front. Plant Sci.* 8:1023. doi: 10.3389/fpls.2017.01023

Shabala, S., and Mackay, A. (2011). Ion transport in halophytes. *Adv. Bot. Res.* 57, 151–199. doi: 10.1016/B978-0-12-387692-8.00005-9

Shi, P., and Gu, M. (2020). Transcriptome analysis and differential gene expression profiling of two contrasting quinoa genotypes in response to salt stress. *BMC Plant Biol.* 20:568. doi: 10.1186/s12870-020-02753-1

Tan, X., Li, S., Hu, L., and Zhang, C. (2020). Genome-wide analysis of long non-coding RNAs (lncRNAs) in two contrasting rapeseed (*Brassica napus* L.) genotypes subjected to drought stress and re-watering. *BMC Plant Biol.* 20:81. doi: 10.1186/s12870-020-2286-9

Tian, T., Liu, Y., Yan, H., You, Q., Yi, X., Du, Z., et al. (2017). agriGO v2.0: A GO analysis toolkit for the agricultural community, 2017 update. *Nucleic Acids Res.* 45, W122–W129. doi: 10.1093/nar/gkx382

Trapnell, C., Williams, B. A., Pertea, G., Mortazavi, A., Kwan, G., van Baren, M. J., et al. (2010). Transcript assembly and quantification by RNA-Seq reveals unannotated transcripts and isoform switching during cell differentiation. *Nat. Biotechnol.* 28, 511–515. doi: 10.1038/nbt.1621

van Zelm, E., Zhang, Y., and Testerink, C. (2020). Salt tolerance mechanisms of plants. *Annu. Rev. Plant Biol.* 71, 403–433. doi: 10.1146/annurev-arplant-050718-100005

Vega-Gálvez, A., Miranda, M., Vergara, J., Uribe, E., Puente, L., and Martínez, E. A. (2010). Nutrition facts and functional potential of quinoa (*Chenopodium quinoa* willd.), an ancient Andean grain: A review. *J. Sci. Food Agric.* 90, 2541–2547. doi: 10.1002/jsfa.4158

Wu, G., Peterson, A. J., Morris, C. F., and Murphy, K. M. (2016). quinoa seed quality response to sodium chloride and sodium sulfate salinity. *Front. Plant Sci.* 7:790. doi: 10.3389/fpls.2016.00790

Xue, Z., Huang, K., Cai, C., Cai, L., Jiang, C. Y., Feng, Y., et al. (2013). Genetic programs in human and mouse early embryos revealed by single-cell RNA sequencing. *Nature* 500, 593–597. doi: 10.1038/nature12364

Yu, Y., Zhang, Y., Chen, X., and Chen, Y. (2019). Plant noncoding RNAs: Hidden players in development and stress responses. *Annu. Rev. Cell Dev. Biol.* 35, 407–431. doi: 10.1146/annurev-cellbio-100818-125218

Zhang, B., and Horvath, S. (2005). A general framework for weighted gene co-expression network analysis. *Stat. Appl. Genet. Mol. Biol* 4:17. doi: 10.2202/1544-6115.1128

Zhang, X., Dong, J., Deng, F., Wang, W., Cheng, Y., Song, L., et al. (2019). The long non-coding RNA lncRNA973 is involved in cotton response to salt stress. *BMC Plant Biol.* 19:459. doi: 10.1186/s12870-019-2088-0

Zhang, X., Shen, J., Xu, Q., Dong, J., Song, L., Wang, W., et al. (2021). Long noncoding RNA lncRNA354 functions as a competing endogenous RNA of miR160b to regulate ARF genes in response to salt stress in upland cotton. *Plant Cell Environ.* 44, 3302–3321. doi: 10.1111/pce.14133

Zhang, Y.-C., Liao, J.-Y., Li, Z.-Y., Yu, Y., Zhang, J.-P., Li, Q.-F., et al. (2014). Genome-wide screening and functional analysis identify a large number of long noncoding RNAs involved in the sexual reproduction of rice. *Genome Biol.* 15:512. doi: 10.1186/s13059-014-0512-1

Zhao, S., Zhang, Q., Liu, M., Zhou, H., Ma, C., and Wang, P. (2021). Regulation of plant responses to salt stress. *Int. J. Mol. Sci.* 22:4609. doi: 10.3390/ijms22094609

Zhu, J.-K. (2002). Salt and drought stress signal transduction in plants. *Annu. Rev. Plant Biol.* 53, 247–273. doi: 10.1146/annurev.arplant.53.091401.143329

Zou, C., Chen, A., Xiao, L., Muller, H. M., Ache, P., Haberer, G., et al. (2017). A high-quality genome assembly of quinoa provides insights into the molecular basis of salt bladder-based salinity tolerance and the exceptional nutritional value. *Cell Res.* 27, 1327–1340. doi: 10.1038/cr.2017.124

frontiers | Frontiers in Plant Science

TYPE Original Research
PUBLISHED 26 September 2022
DOI 10.3389/fpls.2022.1009723

OPEN ACCESS

EDITED BY
Yi Han,
Anhui Agricultural University, China

REVIEWED BY
Yongfeng Hu,
China Three Gorges University, China
Shengchun Li,
Hubei University, China
Yu Zhao,
Huazhong Agricultural University, China

*CORRESPONDENCE
Yuan Shen
yuan.shen@yahoo.com
Lei Shi
doudou246@163.com

SPECIALTY SECTION
This article was submitted to Plant Bioinformatics, a section of the journal Frontiers in Plant Science

RECEIVED 02 August 2022
ACCEPTED 29 August 2022
PUBLISHED 26 September 2022

CITATION
Shen Y, Chi Y, Lu S, Lu H and Shi L (2022) Involvement of JMJ15 in the dynamic change of genome-wide H3K4me3 in response to salt stress. *Front. Plant Sci.* 13:1009723. doi: 10.3389/fpls.2022.1009723

Involvement of JMJ15 in the dynamic change of genome-wide H3K4me3 in response to salt stress

Yuan Shen[1]*, Yuhao Chi[1], Shun Lu[1], Huijuan Lu[1] and Lei Shi[2]*

[1]School of Pharmacy, Xinxiang Medical University, Xinxiang, China, [2]School of Basic Medical Sciences, Xinxiang Medical University, Xinxiang, China

Post-translational histone modifications play important roles in regulating chromatin structure and transcriptional regulation. Histone 3 lysine 4 trimethylation (H3K4me3) is a prominent histone modification mainly associated with gene activation. Here we showed that a histone demethylase, JMJ15, belonging to KDM5/JARID group, is involved in salt stress response in *Arabidopsis thaliana*. *Jmj15* loss-of-function mutants displayed increased sensitivity to salt stress. Moreover, knockout of *JMJ15* impaired the salt responsive gene expression program and affected H3K4me3 levels of many stress-related genes under salt-stressed condition. Importantly, we demonstrated that *JMJ15* regulated the expression level of two WRKY transcription factors, *WRKY46* and *WRKY70*, which were negatively involved in abiotic stress tolerance. Furthermore, JMJ15 directly bound to and demethylated H3K4me3 mark in the promoter and coding regions of *WRKY46* and *WRKY70*, thereby repressing these two *WRKY* gene expression under salt stress. Overall, our study revealed a novel molecular function of the histone demethylase JMJ15 under salt stress in plants.

KEYWORDS

jumonji demethylase, H3K4me3, JMJ15, WRKY46, WRKY70, salt stress

Introduction

Higher plants can adapt to changing environmental conditions in different ways via adjustments in gene expression. Epigenetic regulation of gene expression involving chromatin modification such as histone 3 lysine 4 trimethylation (H3K4me3) plays essential roles in plant response to environmental conditions (van Dijk et al., 2010; Foroozani et al., 2021). H3K4me3 has long been known as an active mark for gene transcription (Santos-Rosa et al., 2002; Li et al., 2007). Genome-wide analysis revealed that a large number of genes were marked by H3K4me3 which predominantly found at the promoter and 5′ end of genes in plants (Zhang et al., 2009). H3K4me3 was often associated with stress-induced gene expression by plant internal and external

signals (Sokol et al., 2007; Kim et al., 2008; van Dijk et al., 2010), suggesting an active transcription role for H3K4me3. However, in some cases the increase of H3K4me3 was found to be lagged behind stressed gene activation (Kim et al., 2008; Hu et al., 2011), indicating that H3K4me3 might have a function to mark active gene status. In addition, H3K4me3 has also been found to play a role in transcriptional memory of stress-responsive genes in plants (Jaskiewicz et al., 2011; Ding et al., 2012; Kim et al., 2012, 2015). H3K4 methylation is mediated by the Trithorax group proteins (TRX), including five Trithorax-like (ATX) proteins and two ATX-related (ATXR) proteins in *Arabidopsis* (Ng et al., 2007). *Arabidopsis* ATX1, ATX4, and ATX5 were found to be necessary for abscisic acid (ABA) and dehydration stress responses (Ding et al., 2011; Liu et al., 2018).

Histone methylation could be reversed by histone demethylases. Lysine Specific Demethylase 1 (LSD1) was the first identified histone demethylase to remove mono- and di-methyl groups from H3K4 (Shi et al., 2004). Jumonji C (jmjC) domain-containing proteins were the second known class of histone demethylases. JmjC proteins, conserved in plants, animals and fungi, catalyze histone lysine demethylation through a ferrous ion [Fe(II)] and a-ketoglutaric acid (a-KG)-dependent oxidative reaction (Tsukada et al., 2006). JmjC domain containing demethylases are divided into distinct groups including KDM2A/JHDM1A, KDM5/JARID, KDM4/JMJD2, KDM6/JMJD3, and KDM3/JMJD1/JHDM2, depending on their binding and catalytic specificities. In humans, the KDM5/JARID group demethylases specially catalyze H3K4me2/3 demethylation (Mosammaparast and Shi, 2010). The *Arabidopsis* genome encodes ~20 jmjC domain-containing histone demethylases (JMJ11–JMJ31), among which six jmjC proteins (JMJ14, JMJ15, JMJ16, JMJ17, JMJ18, and JMJ19) belonging to KDM5/JARID group demethylate H3K4me1/2/3 (Lu et al., 2008; Sun and Zhou, 2008; Chen et al., 2011). JMJ14 demethylates H3K4me3 *in vitro* and represses floral integrator genes Flowering Locus T (*FT*) and Suppressor of overexpression of CO1 (*SOC1*) by removing H3K4me3 (Jeong et al., 2009; Lu et al., 2010; Yang et al., 2010, 2018). JMJ16 negatively regulates leaf senescence through repressing the positive regulators of *WRKY53* and *SAG201* by reducing H3K4me3 (Liu et al., 2019). JMJ15 and JMJ18 regulate flowering time by demethylating H3K4me3 at the locus of the floral repressor gene Flowering Locus C (*FLC*) (Yang et al., 2012a,b). In addition to the essential roles in plant development, JMJ15 and JMJ17 are also involved in stress response. The *jmj17* loss-of-function mutants display dehydration stress tolerance and ABA hypersensitivity (Huang et al., 2019; Wang et al., 2021). In detail, JMJ17 regulates the stomatal closure and ABA response through modulating *OPEN STOMATA1* (*OST1*) and *ABI5* genes by demethylating H3K4me3 (Huang et al., 2019; Wang et al., 2021). Our previous results showed that JMJ15 participated in salinity stress response (Shen et al., 2014). *Jmj15* gain-of-function mutants increased tolerance to salinity stress and down-regulated many genes encoding transcription regulators involved in stress responses (Shen et al., 2014). Although the overexpression of *JMJ15* confers tolerance to salt stress, the molecular mechanism of JMJ15 mediated salt tolerance remains elusive.

In the present study, we showed that two *jmj15* loss-of-function mutant alleles (*jmj15-3* and *jmj15-4*) revealed more sensitive phenotypes to salinity stress. Importantly, the *jmj15* loss-of-function mutations led to up-regulation of many stress-related genes under salt condition rather than under normal condition. In addition, chromatin immunoprecipitation sequencing (ChIP-seq) showed that knockout of *JMJ15* regulated H3K4me3 levels of many salt and water deprivation stress-related genes under salt-stressed condition. Furthermore, our results showed that JMJ15 directly bound to and repressed the genes of *WRKY46* and *WRKY70* that played negative roles in salt stress tolerance. Taken together, our data unravel a novel molecular function of JMJ15 in salt stress responsiveness, which is distinct from the function of other characterized jmjC genes in *Arabidopsis*.

Materials and methods

Plant materials and growth conditions

In this study, *Arabidopsis thaliana* wild type Col-0 and mutant lines *jmj15-1* (GABI_257F10), *jmj15-2* (GABI_876B01), *jmj15-3* (GABI-663C11), and *jmj15-4* (GABI-229F03) in the Col-0 background were used. The insertional knock-out lines *jmj15-3* (Shen et al., 2014) and *jmj15-4* (Yang et al., 2012b) have been previously characterized. The gain-of-function T-DNA mutant lines *jmj15-1*, *jmj15-2*, and the over-expressing tagged line *35s-JMJ15-HA* have been reported (Shen et al., 2014). The *Arabidopsis* seeds were surface-sterilized by 5% (w/v) sodium hypochlorite for 7 min, washed with 95% (v/v) ethanol twice, and then sown on 1/2 Murashige and Skoog (MS) medium. After stratification in darkness at 4°C for 2 days, seeds were transferred into a growth chamber (20°C) under white light (120 μmol m^{-2} s^{-1}) in 16 h light photoperiods. Wild-type and mutant plants were grown together and their mature seeds were harvested at the same time to avoid differences in post-maturation that can affect seed germination. Seeds of each genotype were harvested as a single bulk consisted of at least five plants. Seeds were stored in open tubes inside a closed box and maintained in darkness with silica gel at 4°C until the experiments were performed.

Seed germination assay

For measuring seed germination, more than 100 seeds of each genotype (Col-0, *jmj15-3,* and *jmj15-4*) were sown on NaCl-infused media (1/2 MS medium with 0, 100, 150, and 200 mM NaCl, respectively). After stratification in darkness

at 4°C for 2 days, the plates were transferred into a growth chamber under white light in 16 h light photoperiods. The germination (fully emerged radicle) rates were measured per day for a duration of 5 days. Each test was performed with more than three biological replicates.

Root elongation assay

Measure root elongation under salt stress mainly according to the previous protocol (Lee and Zhu, 2009). More than 50 seedlings of Col-0 and *jmj15* mutation lines were sown on 1/2 MS medium. After stratification in darkness at 4°C for 2 days, the plates were moved to a vertical position in the growth chamber (16 h white light photoperiod, 20°C) for germination. The 4-day-old germinated seedlings were transferred onto vertical 1/2 MS agar plates supplemented with 0 m M NaCl, 50 m M NaCl, 100 mM NaCl and 150 mM NaCl, respectively. After 5 days with the salt treatment, the primary root length was measured and statistical significance was determined by two-sided *t*-test. Three replicates were performed for each line and treatment.

RNA sequencing and data analysis

Ten-day-old wild type (Col-0) and *jmj15-4* mutants *Arabidopsis* plants treated with NaCl (0 mM or 150 mM NaCl solution in 1/2 MS liquid medium) for 5 h were pooled for RNA extraction and transcriptomic analysis. Plants harvested from three independent cultures were used as the biological replicates. Total RNA was extracted with Trizol (Invitrogen, Carlsbad, CA, United States), and treated with DNase I (Promega, Madison, WI, United States) to remove the genomic DNA. Then the mRNA was enriched by using oligo(dT) magnetic beads and broken into short fragments (200 bp) using the fragmentation buffer. The first strand cDNA was synthesized by using a random primer. RNase H, DNA polymerase I and dNTPs were used to synthesize the second strand. The double-strand cDNA was purified with magnetic beads. cDNA ends were repaired and a nucleotide A (adenine) was added at the 3′-end. Finally, PCR amplification was performed with fragments ligated by sequencing adaptors. The Agilent 2100 Bioanalyzer and the ABI Step One Plus real-time PCR system were used to qualify and quantify the QC library. The library products were sequenced with the Illumina HiSeqX-ten platform, and the library construction and sequencing were completed at Novogene Corporation (Tianjin, China). Gene expression was defined by RSEM (Li and Dewey, 2011) and estimated by FPKM. Differential expression analysis between two conditions/groups was performed using DESeq R package. The resulting *P*-values were adjusted using the Benjamini and Hochberg's approach for controlling the false discovery rate (Anders and Huber, 2010). The RNA-seq data were deposited to NCBI-SRA databases under the accession PEJNA822702.

Quantitative real-time RT-PCR

Total RNA was extracted from plant seedlings using Trizol (Invitrogen, Carlsbad, CA, United States) according to the manufacturer's instructions. RNA concentration was measured by using a Nanodrop. For RT-qPCR analysis, 2 μg of total RNA treated with DNaseI (RQ1, Promega, M6101, Madison, WI, United States) were used to synthesize first-strand cDNA with Oligo(dT)15 primers using ImPromII reverse transcriptase (M3104A, Promega, M3104A, Madison, WI, United States). RT-qPCR was performed with LightCycler 480 SYBR Green I Master mix on the LightCycler 480 (Roche, Mannheim, Germany). The reactions were performed in triplicate for each run and at least three biological replicates were carried out for each reaction. Transcript levels were calculated using the comparative Ct (threshold cycle) method and utilizing *ACTIN2* as an internal control for data normalization. Primer sequences used in this study were summarized in **Supplementary Table 1**.

Chromatin immunoprecipitation assay

Chromatin immunoprecipitation (ChIP) experiments were carried out as described previously with minor modifications (Shen et al., 2015). Ten-day-old plants were treated with NaCl (0 mM or 150 mM NaCl solution in 1/2 MS liquid medium) for 5 h before harvest. About 4 g of plant seedlings were harvested, which were then cross-linked with 1% formaldehyde for 10 min under vacuum and ground into fine powder in liquid nitrogen. The chromatin DNA was isolated and sonicated in the 200–1000 bp range with Diagenode Bioruptor UCD-300. The sonicated chromatin was pre-cleared and incubated with anti-H3K4me3 (Millipore, 07-473, Darmstadt, Germany), anti-RNAPII (Abcam, ab5408, Cambridge, United Kingdom) or anti-HA (Sigma, H6908, St. Louis, MO, United States) antibodies loaded Dynabeads^{TM} protein A (Invitrogen, #10002D, Carlsbad, CA, United States) at 4°C overnight. Subsequently, the immunoprecipitated DNA was decrosslinked and purified by using the MinElute PCR Purification Kit (Qiagen, #28004, Hilden, Germany) according to the manufacturer's instruction. ChIP DNA was used for sequencing or qPCR. ChIP-qPCR was performed with three biological replicates, and results were calculated as the percentage of input DNA. Sequences of the primers used for ChIP-qPCR were listed in **Supplementary Table 1**.

ChIP-seq and data analysis

At least 5 ng of each ChIP DNA was used to construct ChIP-seq library, and two biological replicates for each sample.

The Illumina libraries were constructed using the ChIP-seq DNA Sample Prep Kit (Illumina) according to manufacturer's protocol. The ChIP-seq library was sequenced by Novogene Corporation (Tianjin, China) on the Illumina HiSeq2500 sequencing system. Base calling and read quality control were performed following the standard Illumina protocol. Reads passing quality control were aligned to the *Arabidopsis* genome (TAIR10[1]) using BWA (Burrows Wheeler Aligner) with default parameters and only uniquely mapped reads were kept (Li and Durbin, 2009). MACS2 (version 2.1.0) peak calling software was used to identify regions of enriched intervals over the background. A *q*-value threshold of 0.05 was used for all data sets. Differential enrichments were assessed by MACS2 (bdgdiff), with an FDR cutoff < 0.001. The differential histone modification regions were intersected with annotated genes to obtain the target genes using BED tools[2]. The alignments were converted to wiggle (WIG) files. The data were then imported into the Integrated Genome Browser for visualization. The ChIP-seq data were deposited to NCBI-SRA databases under the accession PRJNA823378.

Results

H3K4me3 dynamical change is associated with plant response to salt stress

To explore the transcriptional level of genes involved in plant response to salt stress, we conducted RNA-seq analysis using wild type seedlings under normal or salt-stressed conditions (0 mM or 150 mM NaCl solution in 1/2 MS liquid medium for 5 h), each with three biological replicates. The RNA-seq results showed that the three biological replicates were all highly correlated (R = 0.91–0.99). Analysis of differentially expressed genes (DEGs) revealed that 5470 up-regulated genes (URGs) and 5393 down-regulated genes (DRGs) in wild type seedlings as a result of the salt stress ($P < 0.05$) (**Figure 1A** and **Supplementary Table 2**). Using the strict criteria (fold change > 4.0, $P < 0.001$), 619 URGs and 833 DRGs were found in salt treated *versus* normal growth seedlings (**Figure 1A** and **Supplementary Table 2**). Among the genes up-regulated by salt stress, inducible genes implicated in salt stress response in other studies were present, including *COR15A* (AT2G42540), *COR15B* (AT2G42530), *RD20* (AT2G33380), *RD29A* (AT5G52310), *RD29B* (AT5G52300) (**Figure 1B**; Chen et al., 2010; Zheng et al., 2016; Yang et al., 2019).

Increasing evidence has shown that transcriptional regulation directed by H3K4me3 is very important for environmental responses in plants (van Dijk et al., 2010; Huang et al., 2019; Foroozani et al., 2021). To reveal the possible regulatory role of H3K4me3 methylation in the plant response to salt stress, ChIP-seq was performed by using the wild type seedlings under normal and salt stress (the same conditions as the RNA-seq), each with two biological replicates. The results revealed that 21894 H3K4me3 methylation peaks in Col-0 samples under normal condition (**Supplementary Table 3**), while 24141 H3K4me3 peaks under salt stress treatment (**Supplementary Table 4**). The distribution of H3K4me3 was similar between normal and salt-treated seedlings, with the most enrichment occurring at the gene body (**Figure 1C**). In detail, most H3K4me3 amounts were found at exons (63–66%), followed by introns (16–19%) and 5′ untranslated regions (5′ UTR) (10%). Lower amounts of H3K4me3 were found at non-coding RNA (3.4%), intergenic region (3%) and 3′ UTR (1%) (**Figure 1D**), which was consistent with the previous data (Zhang et al., 2009; Huang et al., 2019). To determine whether/how salt stress-altered gene expression correlated with changes in H3K4me3, we examined the H3K4me3 changes for the 1452 genes with altered transcript abundance (|fold change| > 4.0, $P < 0.001$) (**Supplementary Table 5**). The plot analysis revealed a correlation between the H3K4me3 and transcript dynamic changes under salt stress (Pearson correlation coefficient R = 0.567, $P < 0.01$) (**Figure 1E**), indicating that H3K4me3 dynamics is associated with the transcript level of many genes involved in salt stress response. Totals of 2591 and 1905 genes were differentially hypermethylated and hypomethylated between salt and normal conditions ($P < 0.05$), respectively (**Figure 1F** and **Supplementary Table 6**). Gene ontology (GO) enrichment analysis revealed that the H3K4me3 changed genes under salt stress were categorized into 'response to water deprivation,' 'response to abiotic stimulus,' 'response to abscisic acid,' and 'response to chemical' (**Figure 2A**). In addition, the up-regulated salt-responsive genes (i.e., *COR15A*, *COR15B*, *RD20*, *RD29A*, *RD29B*) were found hypermethylated under salt stress condition by using the Integrated Genome Browser (**Figure 2B**). These results suggest that the H3K4me3 change is associated with the transcriptional change of the salt responsive genes during the stress process.

jmj15 loss-of-function display hypersensitivity to salinity stress

We have shown that gain-of-function mutants (*jmj15-1* and *jmj15-2*) exhibited increased tolerance to salinity stress, whereas one allele of loss-of-function mutant (*jmj15-3*) exhibited increased sensitivity to salinity stress (Shen et al., 2014). To further confirm the response of *jmj15* loss-of-function mutant to salt stress, we obtained another mutant allele *jmj15-4*. In *jmj15-4*, T-DNA was inserted in the 5th intron of *JMJ15* (**Figure 3A**).

1 www.arabidopsis.org

2 https://bedtools.readthedocs.io/en/latest/content/installation.html

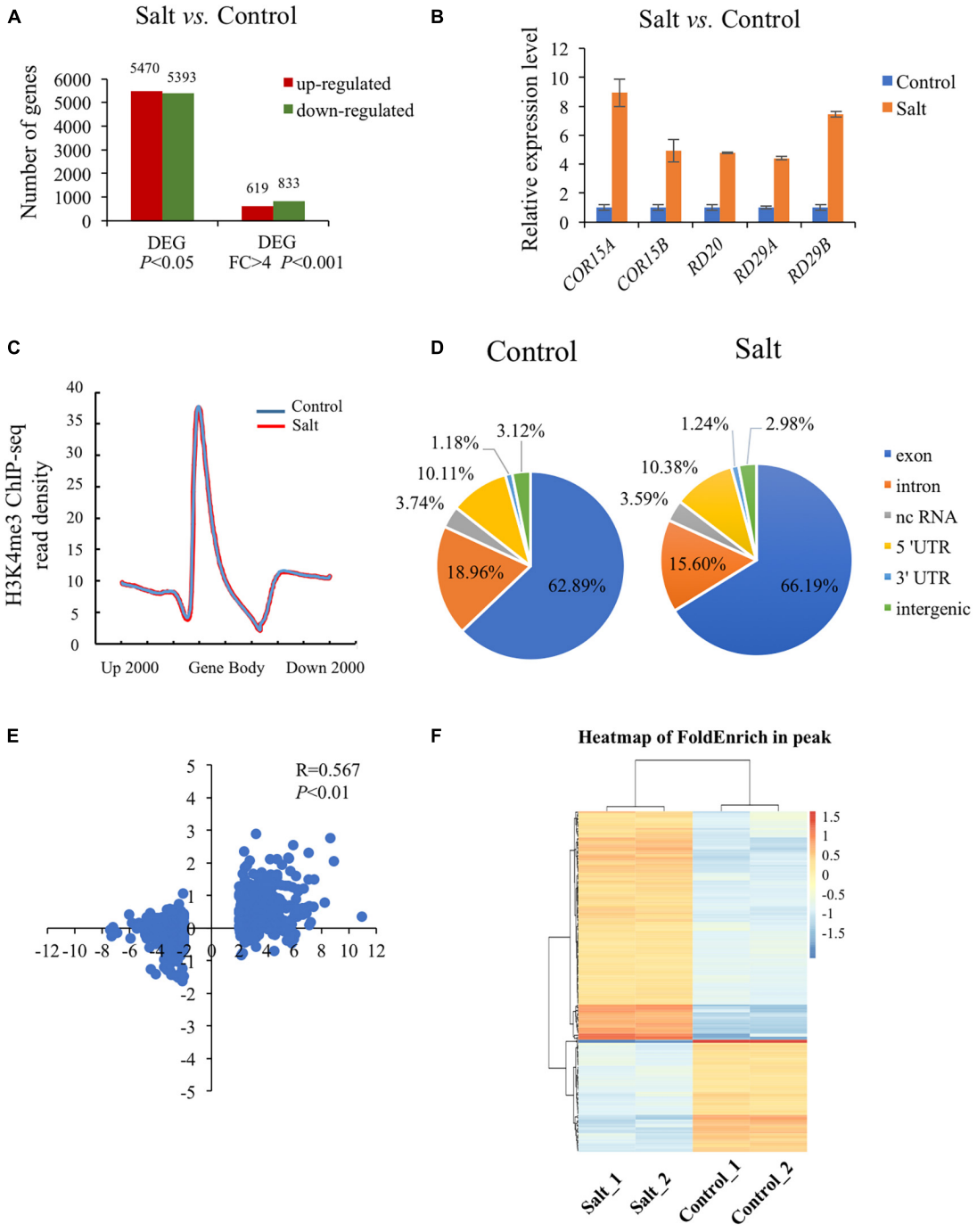

FIGURE 1
Global analysis of dynamic changes of H3K4me3 and mRNA levels during the plant response to salt stress. **(A)** Differently expressed genes in the wild type under salt condition compared with normal condition. The *Y*-axis represents the number of upregulated genes or downregulated genes by using the criteria $P < 0.05$ or fold change > 4, $P < 0.001$. **(B)** The mRNA level of 5 well known up-regulated genes which were strongly induced by salt stress. The data was calculated by $\log_2$(FPKM) and wild type under normal condition were set to 1. **(C)** Metaplot of the H3K4me3 distribution on genes in Col-0 under normal and salt stress conditions. Gene body in the *X*-axis represents all genes in the genome. Up 2000 represents 2000 bp upstream of Transcriptional Start Site (TSS) and down 2000 represents 2000 bp downstream of Transcriptional Terminal Site (TTS), respectively. The *Y*-axis represents read density of H3K4me3. **(D)** Genomic distribution of H3K4me3 peaks in Col-0 under normal and salt conditions. The definition of each region is described on the right. **(E)** Scatter plot of H3K4me3 and transcription changes of dysregulated genes in salt *vs.* normal (fold change > 4, $P < 0.001$). The horizontal axis represents the $\log_2$(fold change) of mRNA expression level. The vertical axis represents the $\log_2$(fold change) of H3K4me3 level. Pearson correlation indicates a correlation between the H3K4me3 and transcript dynamic changes under salt stress ($R = 0.567$, $P < 0.01$). **(F)** Heatmap shows the H3K4me3 enrichment of different peaks associated with genes under normal and salt condition ($P < 0.05$). The genes (rows) were subjected to hierarchical clustering. The color bar on the right indicates the Z-score.

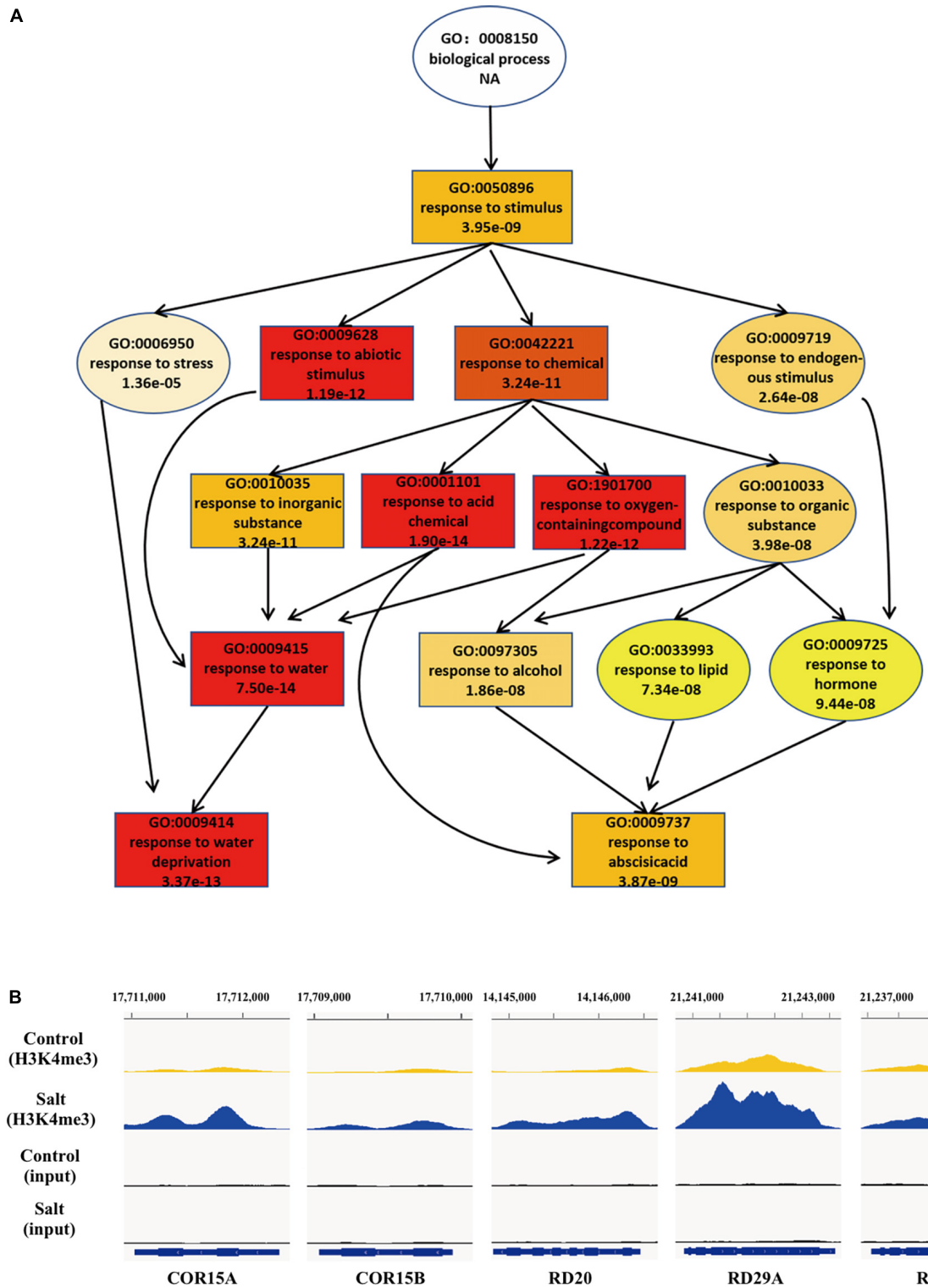

FIGURE 2
During the response to salt stress the H3K4me3 changes are associated with many of the genes involved in stress response. **(A)** A tree structure graph of the major significantly enriched GO terms of genes associated with different peaks ($P < 0.05$) of H3K4me3 between normal and salt conditions. GO terms are represented as boxes containing detailed description, including GO accession, description and *P*-value. **(B)** Integrative Genome Viewer (IGV) of H3K4me3 modifications at five representative salt-induced genes in **Figure 1B** under normal and salt-stressed conditions.

RT-qPCR analysis revealed that the *JMJ15* transcripts were abolished in both *jmj15-3* and *jmj15-4* alleles (**Figure 3B**). Both loss-of-function lines together with the wild type (Col-0) were tested for germination rates on normal MS media and MS supplemented with different salt concentrations. The germination rates were scored at different time points after 2 days. Seeds from three various harvests were tested. Under normal conditions, the germination rates of wild type and *jmj15* loss-of-function mutants were more than 95%. When treated with salt, the germination rate of *jmj15* loss-of-function mutants were lower than the wild type at different indicated salt concentration and time points (**Figures 3C,D**). Root elongation lengths were also measured to analyze the sensitivity of plants to the salt stress. The results revealed that after 5 days under normal condition, the root lengths of loss-of-function *jmj15* and wild type plants were similar. However, the root lengths of *jmj15* mutants were shorter than that of wild type after 5 days under various concentration of NaCl treatment (**Figures 3E,F**). Together, these results suggest that JMJ15 regulates the response to salt stress in *Arabidopsis*.

The loss-of-function *jmj15* mutants impaired the salt responsive gene expression program

The developmental phenotype between *jmj15-4* and wild type was highly significant different under salt stress (**Figure 3**). To explore the genome-wide transcriptional landscape directed by JMJ15, we conducted RNA-seq analysis of *jmj15* loss-of-mutation (*jmj15-4*) and Col-0 under normal and salt stress conditions, each with three replicates. The total of 897 and 1852 DEGs were identified in *jmj15-4* compared with Col-0 under normal and salt stress conditions, respectively ($P < 0.05$) (**Figure 4A**). Among 897 DEGs in *jmj15-4* under normal condition, 393 were upregulated (URGs) and 504 were downregulated (DRGs) in *jmj15-4* (**Figure 4A** and **Supplementary Table 7**), while among 1852 DEGs under salt stress, 1020 were URGs and 832 were DRGs in *jmj15-4* (**Figure 4A** and **Supplementary Table 8**), suggesting that JMJ15 may mainly play a role as a transcriptional repressor during the salt responsive process. GO enrichment revealed that the URGs in *jmj15*/Col-0 under salt stress were enriched in response to stress, peptide metabolic process, flavonoid metabolic process, pigment synthetic process, and the DRGs were enriched in response to stress, response to organic substance, response to chemical stimulus, systematic acquired resistance (**Figure 4B**). URGs in *jmj15*/Col-0 under normal condition were enriched in response to stress, but no GO enrichment for DRGs (**Figure 4B**). These results suggest that loss of *JMJ15* may mostly affect metabolism and the responsiveness to environmental stimuli of seedlings which is consistent with the previous result that overexpression of *JMJ15* preferentially represses the stress regulatory genes (Shen et al., 2014).

To investigate how the *jmj15* mutation affects the salt responsive gene expression program, we compared DEGs in *jmj15* mutation versus Col-0 under salt treatment (*jmj15*/Col-0 under salt) with that of Col-0 under salt versus normal condition (salt/normal in Col-0). Interestingly, we found that (507/1020, 49.7%) upregulated and (499/832, 55.6%) downregulated DEGs in *jmj15*/Col-0 under salt stress overlapped with the downregulated and upregulated DEGs in Col-0 under salt/normal respectively (**Figure 4C** red cycle and **Supplementary Table 9**). However, the overlap was much less between the upregulated (288/1020, 28.2%) and downregulated (142/832, 17.1%) DEGs in *jmj15*/Col-0 under salt stress with the upregulated and downregulated DEGs in Col-0 under salt/normal (**Figure 4C** green cycle). These data indicated that *jmj15* mutation impaired the salt responsive gene expression program, that may explain the salt-stress-sensitive phenotype in *jmj15* loss-of-function mutation. Further investigation of these 507 genes that were upregulated in *jmj15*/Col-0 under salt but downregulated in Col-0 under salt/normal found some key components of plant tolerance to stress, such as *PRXIIF* (AT3G06050), *ERF73* (AT1G72360), *PIP2B* (AT2G37170), *CAM1* (AT5G37780), *LTP5* (AT3G51600), *PDF1.2* (AT5G44420), *PDF1.2B* (AT2G26020), *PDF1.3* (AT2G26010), *LEA41*/*DI21* (AT4G15910), *SAP18* (AT2G45640), *ERD14* (AT1G76180), *SESA* (AT4G27170), *EARLI1* (AT4G12480), *GSTF9* (AT2G30860), *GSTU26* (AT1G17190), *GSTU20* (AT1G78370) (**Figure 4D** and **Supplementary Table 9**). The result suggested that loss of *JMJ15* derepressed the expression of some stress-responsive genes, which was inhibited during the salt treatment. Similarly, we found some stress related genes such as *CAT2* (AT1G58030), *XTH6* (AT5G65730), *XTH22*/*TCH4* (AT5G57560), *HSFA2* (AT2G26150), *NRT2.6* (AT3G45060), *HSP70-2* (AT5G02490), *COR15A* (AT2G42540), *COR15B* (AT2G42530), *NAC13* (AT1G32870), *VSP2* (AT5G24770) that were upregulated in Col-0 under salt/normal but downregulated in *jmj15*/Col-0 under salt stress (**Figure 4E** and **Supplementary Table 9**). Together, the analysis suggested that JMJ15 was required for both gene activation and repression of the salt-responsive gene expression program.

JMJ15 regulates H3K4me3 levels of many salt responsive genes

To investigate whether JMJ15 is involved in the salt stress response by demethylating H3K4me3, we examined H3K4me3 patterns in the *jmj15* loss-of-function mutants under normal and salt-stressed conditions by ChIP-seq. The result revealed that 21964 H3K4me3 methylation peaks in *jmj15* mutation under normal condition (**Supplementary Table 10**), while 24273 H3K4me3 methylation peaks under salt stress treatment (**Supplementary Table 11**). The distribution pattern is similar in *jmj15* to WT under both conditions (**Figures 1D**, **5A**).

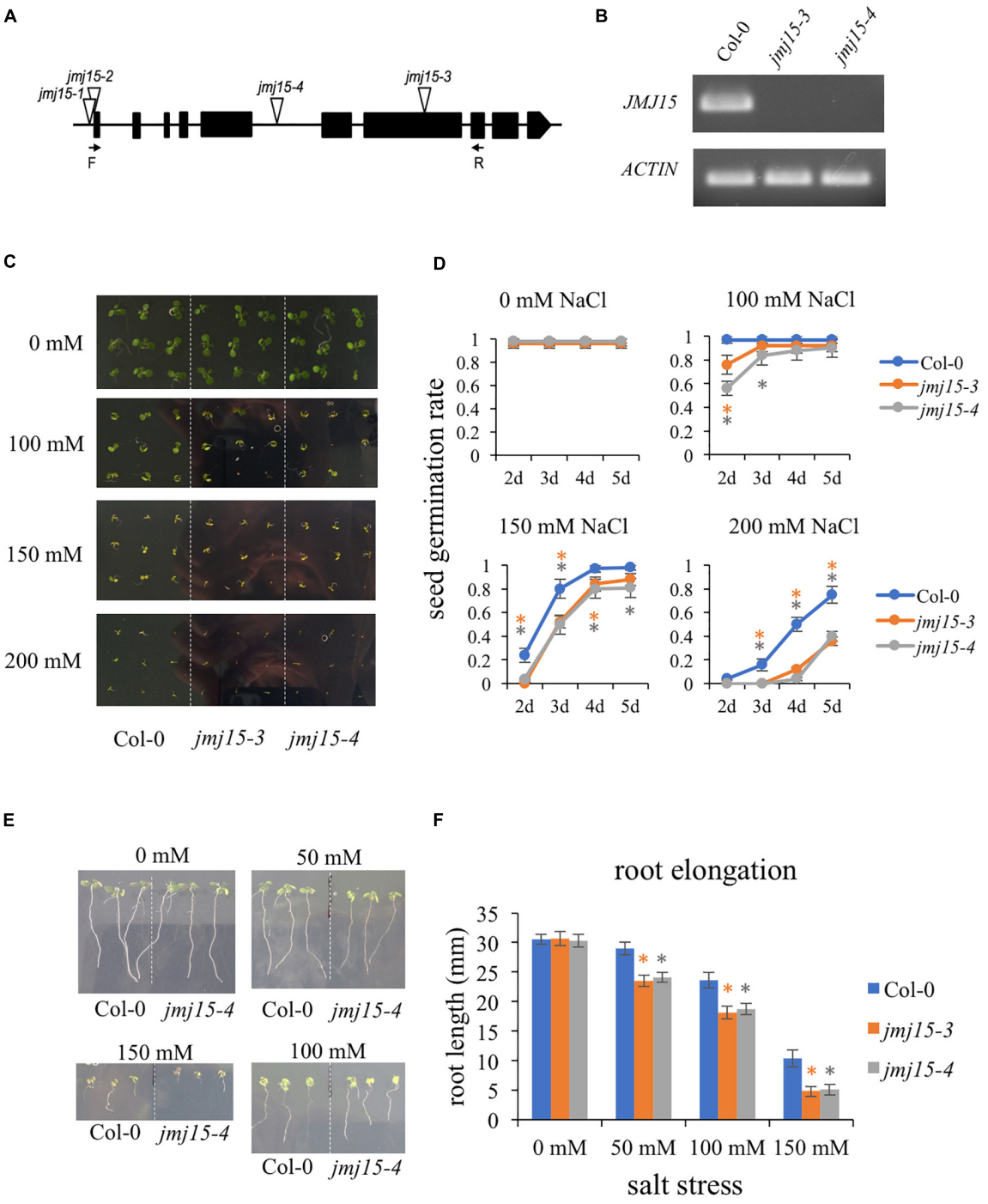

FIGURE 3
Loss-of-function of *JMJ15* in *Arabidopsis thaliana* are hypersensitive to salt stress. **(A)** Schematic diagram of the *JMJ15* gene. Exons are represented by black boxes. Triangles indicate T-DNA insertions. The primer positions of forward (F) and reverse (R) are indicated by arrows. **(B)** Reverse transcription polymerase chain reaction (RT-PCR) analysis of transcripts of Col-0, *jmj15-3* and *jmj15-4* by using the indicated primers. *ACTIN2* was used as an internal control. **(C,D)** Measurement of seed germination rates. **(C)** Images of the wild type, *jmj15-3* and *jmj15-4* seeds germinated on 1/2 MS medium supplemented with or without indicated concentrations of NaCl for 5 days. **(D)** Quantification of seed germination rates of genotypes shown in **(C)** at different time points. Data represent means of ± SD (n = 3, three biological replicates were performed with at least 100 seeds per genotype in each replicate). **(E,F)** Measurement of root elongation. **(E)** Wild-type and *jmj15* seedlings were grown on vertical 1/2 MS plate for 4 days and then transfered onto vertical 1/2 MS medium supplemented with or without different concentration of NaCl for 5 days. **(F)** The primary root length was measured after 5 days with different indicated concentrations of NaCl. Data represent means of ± SD (n = 3, three biological replicates were performed with at least 50 seedlings per genotype in each replicate). Asterisks indicate where the difference between Col-0 and mutant is statistically significant (Student's t-test, $^*P < 0.05$).

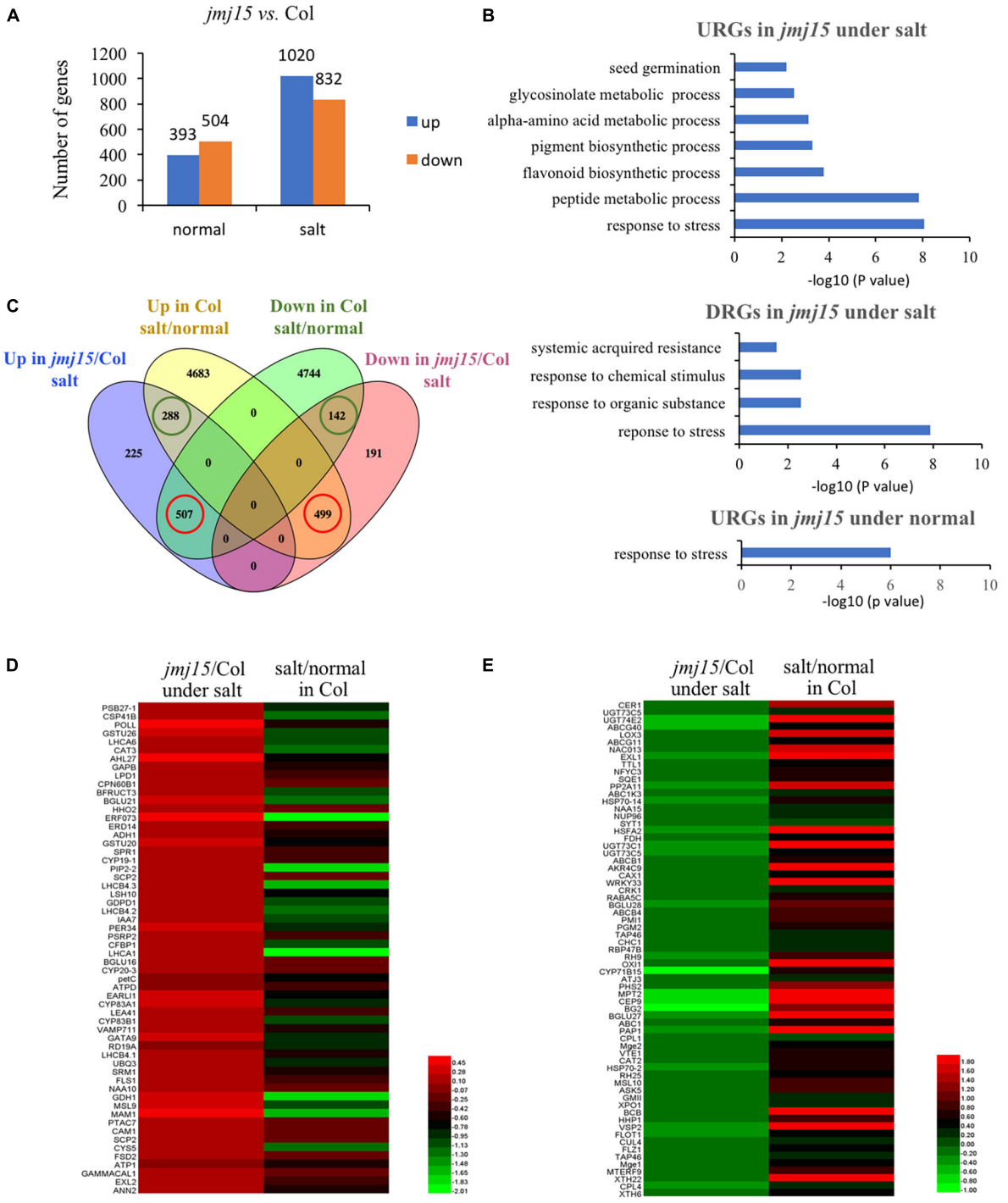

FIGURE 4
Transcriptomic analysis of *jmj15* loss-of-function mutants compared to Col-0 under normal and salt-stressed conditions. **(A)** Differently expressed genes in the wild type and *jmj15* mutations under normal and salt conditions. The *Y*-axis represents the number of upregulated genes or downregulated genes by using the criteria $P < 0.05$. **(B)** GO term enrichment of the upregulated genes (URGs) and downregulated genes (DRGs) in *jmj15* mutants at the salt and normal conditions. **(C)** Venn diagram of comparison of DEGs in *jmj15-4* (relative to Col-0 under salt condition) and DEGs in Col-0 (under salt relative to normal condition). The green cycles represent the number of genes that were up-regulated or down-regulated both in *jmj15*/Col-0 under salt condition and Col-0 under salt/normal. The red cycles represent the number of genes that were up-regulated in *jmj15*/Col-0 under salt condition but down-regulated in Col-0 under salt/normal, or down-regulated in *jmj15*/Col-0 under salt condition but up-regulated in Col-0 under salt/normal. **(D,E)** Heatmaps show the expression of the misregulated stress-related genes (GO: 0006950) in *jmj15*/Col-0 and salt/normal (red cycles in **C**). **(D)** Shows URGs in *jmj15*/Col-0 and DRGs under salt/normal; **(E)** shows DRGs in *jmj15*/Col-0 and URGs under salt/normal.

However, totals of 722 and 1763 genes were differentially hypermethylated and hypomethylated in the *jmj15* loss-of-function mutants under salt stress, respectively ($P < 0.05$) (**Supplementary Table 12**). Scatterplot analysis of increased expressed genes in *jmj15*/Col-0 under salt showed that most transcriptionally URGs were hypermethylated (**Figure 5B** and **Supplementary Table 13**). GO enrichment analysis of these hypermethylated and URGs in *jmj15* under salt was the most enriched in response to stimulus (**Figure 5C**). By using Integrated Genome Browser, the H3K4me3 level was increased for some stimulus responsive genes such as *EARLI* (AT4G12480), *DI21* (AT4G15910), *ERD14* (AT1G76180) and *LTP2* (AT2G38530) (**Figure 5D** and **Supplementary Table 13**), suggesting that the increased transcription of these stress related genes may be due to decreased demethylation activity of H3K4me3 in the *jmj15* mutants. Of note, we found some transcriptional factors that both the transcription and H3K4me3 levels increased in *jmj15* knockout mutations under salt condition such as some stress-responsive *WRKY* genes and ethylene-responsive-element binding factor genes (**Supplementary Table 14**), consisting with our previous data that overexpression of *JMJ15* preferentially represses the stress regulatory genes, especially some transcription factors.

JMJ15 controls the H3K4me3 levels of *WRKY46* and *WRKY70* in response to salt stress

Interestingly, among these hypermethylated and URGs in *jmj15* under salt stress, we found two known transcription factors, *WRKY46* and *WRKY70*, that function as negative regulators in abiotic stress signaling in plants (Li et al., 2013; Ding et al., 2015; Chen et al., 2017). WRKY46 modulates the lateral root development in salt stress condition via regulation of ABA signaling and auxin homeostasis (Ding et al., 2015). WRKY70·modulates osmotic stress response by regulating stomatal aperture in *Arabidopsis* (Li et al., 2013). Meanwhile, WRKY70 was shown to be a direct target of ATX1 and positively regulated by ATX1-generated H3K4me3 (Alvarez-Venegas et al., 2007). Therefore, we hypothesized that JMJ15 might be involved in salt stress responses by modulating the H3K4me3 level of *WRKY46* and *WRKY70* genes. First, we examined the transcript level of these two *WRKY* genes in the *jmj15* loss-of-function mutants (*jmj15-3* and *jmj15-4*), *jmj15* gain-of-function mutants (*jmj15-1* and *jmj15-2*) and wild type (Col-0) under normal and salt-stressed conditions. The result showed that the transcript level of *WRKY46* and *WRKY70* was induced in wild type by salt stress. In *jmj15* loss-of-function mutants, the transcript level of these two *WRKY* genes was enhanced compared to wild type under salt treatment, whereas the transcript level was obviously decreased in *jmj15* gain-of-function mutations compared to wild type under salt treatment (**Figure 6A**). However, no discernible alterations were detected in *jmj15* loss-of-function mutants under normal condition, but the transcript level of two *WRKY* genes were declined in *jmj15* gain-of-function mutants under normal condition (**Figure 6A**), which was consistent with our previous result that overexpression of JMJ15 inhibited the expression of some transcription factors including some *WRKY* genes under normal condition (Shen et al., 2014). To confirm the role of JMJ15 in regulating chromatin status at the loci of *WRKY46* and *WRKY70* during the salt responsive process, we performed ChIP-qPCR analysis of the *jmj15* loss-of-function mutants and *jmj15* gain-of-function mutants (**Figure 6B**). The results showed that H3K4me3 level of *WRKY46* and *WRKY70* were obviously increased in *jmj15-3* and *jmj15-4* compared with wild type under salt stress, but decreased in *jmj15-1* and *jmj15-2* compared to wild type under normal and salt stress conditions (**Figure 6C**), suggesting that JMJ15 regulates the transcript levels of *WRKY46* and *WRKY70* genes by modulating their H3K4me3 levels.

To investigate whether JMJ15 is directly associated with *WRKY46* and *WRKY70* genes, we analyzed the *35S-JMJ15-HA* plants by ChIP-qPCR using anti-HA antibody (Shen et al., 2014). The analysis revealed that JMJ15-HA was enriched in *WRKY46* and *WRKY70* relative to the negative control (IgG), and JMJ15-HA binding levels were higher at the promoter and gene body under the salt stress compared to normal condition (**Figure 6D**). The results suggest that JMJ15 is recruited to the *WRKY46* and *WRKY70* genes and regulates their expression during the salt stress process. It has been established that H3K4me3 levels have a positive correlation with transcription rates and occupancy of activated RNA polymerase II (RNAPII) (Ardehali et al., 2011). We then tested whether the RNAPII occupancy at *WRKY46* and *WRKY70* was affected by JMJ15 following salt treatment. The results revealed that binding of RNAPII to *WRKY46* and *WRKY70* were increased in *jmj15* loss-of-function mutants compared to wild type under salt stress (**Figure 6E**). Taken together, these results indicate that JMJ15 modulates H3K4me3 levels at the *WRKY46* and *WRKY70* loci and thus in turn affects RNAPII occupancy, which is essential for gene expression.

Discussion

H3K4me3 dynamics impact the abiotic stress response in plants

H3K4me3 has been implicated in the regulation of a number of environmental responses, such as drought stress, heat stress, submergence stress, and salt stress. For example, H3K4me3 abundance along with transcript levels of the inducible drought marker genes (*RD29A*, *RD29B*, *RD20,* and *RAP2.4*) were increased in response to drought (Kim et al., 2008). The

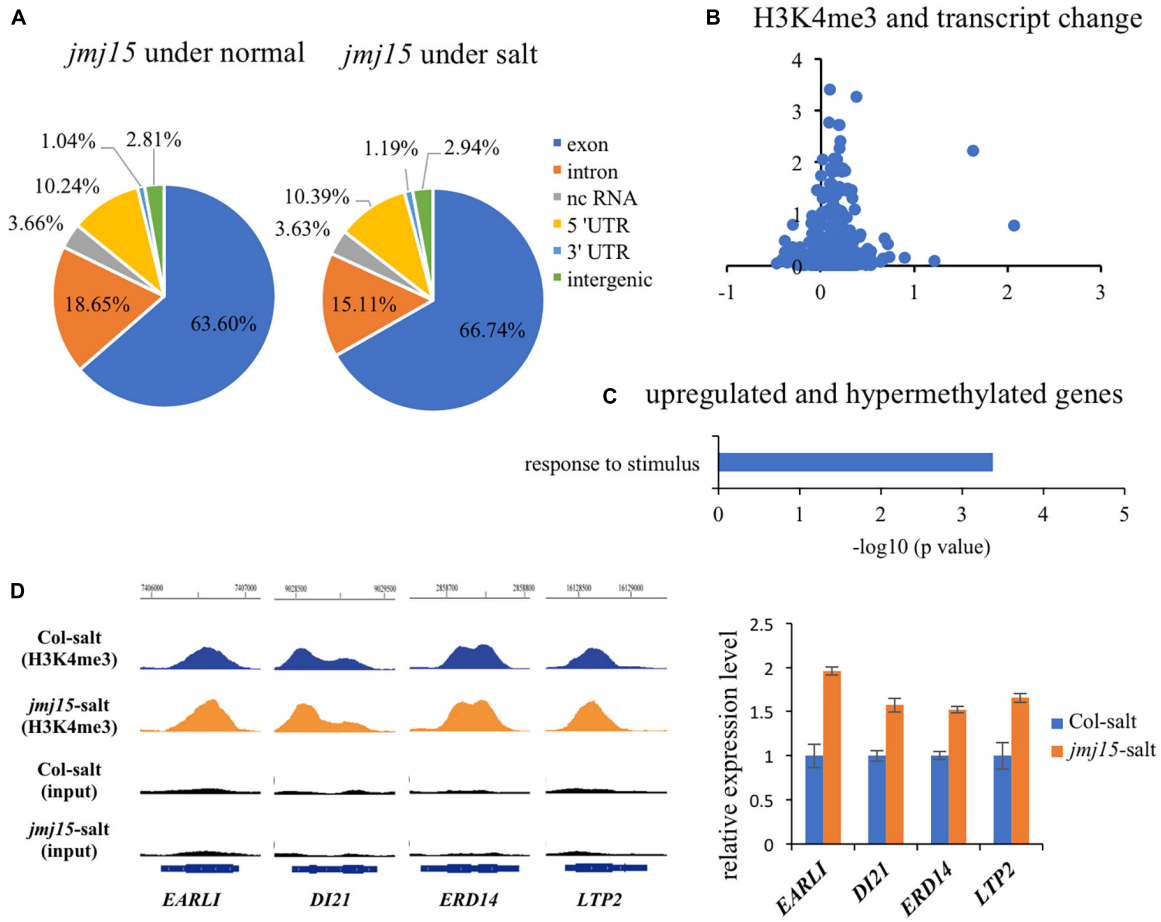

FIGURE 5
JMJ15 affects H3K4me3 levels at many stress-related genes under salt stress. **(A)** Genomic distribution of H3K4me3 peaks in *jmj15-4* under normal and salt conditions. **(B)** Scatterplot shows that most of up-regulated genes of *jmj15* mutation under salt stress were H3K4me3 hypermethylated. The *x*-axis represents the $\log_2$(fold change) of H3K4me3 level in *jmj15* compared to Col-0 under salt stress. The *y*-axis represents the $\log_2$(fold change) of mRNA level in *jmj15* compared to Col-0 under salt stress. **(C)** GO term enrichment of the genes upregulated and H3K4me3 hypermethylated in *jmj15* mutants compared to Col-0 under salt stress. **(D)** H3K4me3 and mRNA level of selective stress-related genes in *jmj15* mutants under salt stress. Left, IGV showing H3K4me3 levels of stress-related genes in *jmj15* mutants under salt stress. Right, the transcript level in *jmj15* mutants under salt stress. The data was calculated by $\log_2$(FPKM) and wild type were set to 1.

genome-wide studies also showed that many genes up- or down-regulated by dehydration exhibited the similar increased or decreased H3K4me3 abundance, respectively (van Dijk et al., 2010; Zong et al., 2013). ATX1, H3K4me3 methyltransferase, was reported to involve in drought stress by affecting biosynthesis of ABA resulting from regulating H3K4me3 and transcript of *NCED3* (Ding et al., 2011). Investigation of a number of stress-responsive genes in *Arabidopsis* has shown that several chromatin marks impact the responsiveness of salt-induced genes. For instance, salt stress led to enrichment of H3K4me3 and H3K9K14 acetylation, but decreased H3K9me2 at a subset of salt stress-responsive loci (Chen et al., 2010). Histone deacetylase 6 (HDA6) and HDA9 led to increased H3 acetylation at salt-inducible genes in *hda6* mutants compared to wild type (Chen et al., 2010; Zheng et al., 2016). Interestingly, mutation of HDA6 also abolished H3K4me3 enrichment of ABA-induced loci (Chen et al., 2010). A recent study showed that salt stress altered the distribution of H3K4me3 in a tissue specific manner. In response to salt, rice seedlings exhibited H3K4me3 decreases and increases in exons and introns respectively, whereas only exons decrease of H3K4me3 in roots (Zheng et al., 2019). In our study, the distribution pattern of H3K4me3 was similar between normal and salt-treated seedlings. However, when compared the H3K4me3 level and transcript dynamic abundance for some transcript changed genes ($|$ fold change$|$ > 4.0), there was a correlation between the H3K4me3 and transcript dynamic changes under salt stress (**Figure 1E**). In addition, the H3K4me3 peak difference associated genes under salt stress were enriched in response to stress (**Figure 2**). These results indicate that H3K4me3 dynamics is associated with the transcript level of many genes involved in salt stress response.

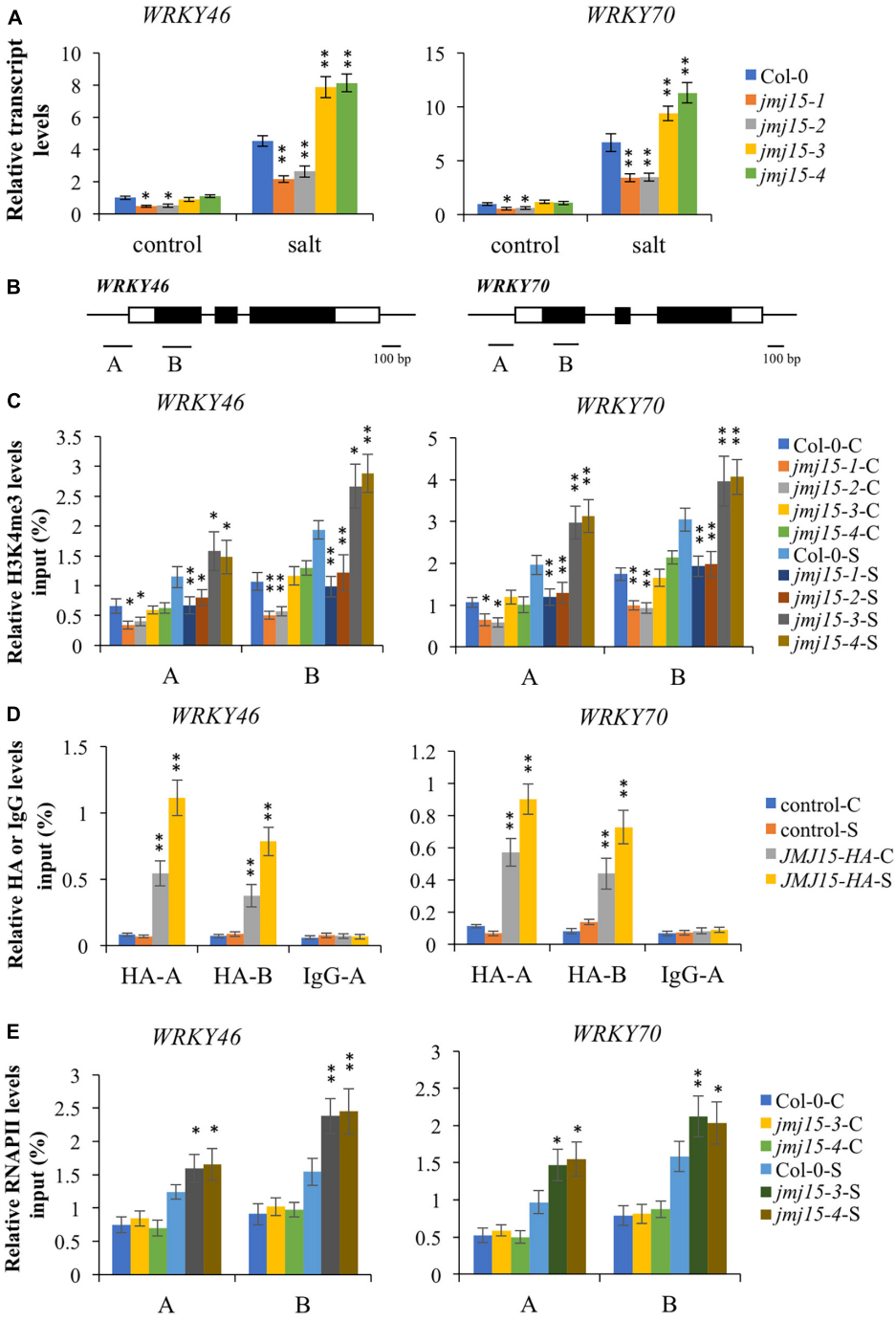

FIGURE 6
Transcript and chromatin changes at the *WRKY46* and *WRKY70* loci in *jmj15* mutations. **(A)** RT-qPCR analysis of the transcript level of *WRKY46* and *WRKY70* genes in *jmj15* mutants compared to Col-0 under normal and salt conditions. *ACTIN2* was used as an internal control to normalize the gene expression level. The wild type under normal condition were set to 1. Bars are means ± SD of data from three biological replicates. $^{*}P < 0.05$ and $^{**}P < 0.001$, Student's *t*-test. **(B)** Schematic diagram of *WRKY46* and *WRKY70*. Regions A and B of *WRKY* genes were used for ChIP-qPCR analysis. Black bar represents 100 bp. **(C)** ChIP-qPCR analysis of H3K4me3 of *WRKY46* and *WRKY70* genes in Col-0 and *jmj15* mutants under control condition (C) and salt condition (S). Results are presented as percentage of input. Bars are means ± SD of data from three biological replicates. $^{*}P < 0.05$ and $^{**}P < 0.001$, Student's *t*-test. **(D)** JMJ15-HA ChIP-qPCR was performed by using HA antibody to determine the occupancy of JMJ15-HA at the *WRKY46* and *WRKY70* loci under control condition (C) and salt condition (S). IgG was used as a negative control. Results are presented as percentage of input. Bars are means ± SD from three biological replicates. $^{*}P < 0.05$ and $^{**}P < 0.001$, Student's *t*-test. **(E)** ChIP-qPCR analysis of occupancy of RNA polymerase II (RNAPII) at the *WRKY46* and *WRKY70* loci in Col-0 and *jmj15* loss-of-function mutants under control condition (C) and salt stress condition (S). Results are presented as percentage of input. Bars are means ± SD from three biological replicates. $^{*}P < 0.05$ and $^{**}P < 0.001$, Student's *t*-test.

KDM5/JARID group proteins differently response to abiotic stress

In humans, KDM5/JARID group proteins are active histone H3K4me1/2/3 demethylases (Lu et al., 2008; Sun and Zhou, 2008). In *Arabidopsis*, six proteins (JMJ14-19) have been identified as members of this group based on phylogenetic analysis. Among these, JMJ14, JMJ15, JMJ16, JMJ18 harbor JmjN, JmjC, C5HC2, FY-rich N-terminus (FYRN), and FY-rich C-terminus (FYRC) domains. By contrast, JMJ19 harbors only JmjN, JmjC, and C5HC2 domains, whereas JMJ17 harbors JmjC, zf-C5HC2, PLU-1, and PHD domains (Lu et al., 2008). JMJ14, JMJ15, and JMJ18 play important roles in regulating flowering by reducing H3K4me3 abundance at various flowering regulatory genes. In addition to regulating the transition to flowering, *Arabidopsis* demethylases also play roles in RNA silencing (Searle et al., 2010); circadian clock (Song et al., 2019); defense (Li et al., 2020); senescence (Liu et al., 2019); de-etiolation process (Islam et al., 2021), and dehydration stress (Huang et al., 2019). JMJ17 played a role in dehydration stress by directly binding to *OST1* and demethylating H3K4me3 levels (Huang et al., 2019). JMJ17 also regulates ABA responsive genes by interacting with WRKY40 (Wang et al., 2021). Our data showed that JMJ15 involved in salt stress by directly binding to the chromatin and regulating the expression of *WRKY46* and *WRKY70* genes. It seems that JMJ17 did not function in salt stress response as *jmj17/jmj15* double mutations showed the similar salt stress response phenotype as *jmj15* single mutant while *jmj17* single mutant did not show discernible phenotype of salt stress response compared to wild type (Huang et al., 2019). These results indicate that these two KDM5/JARID histone demethylases function in different physiological processes without functional redundancy, which might be explained by their existing different domains and various target genes.

JMJ15 functions in salt stress tolerance by regulating *WRKY* genes

WRKY transcription factors, as a large family of plant transcription factors, participate in a variety of biological processes, including root growth, the quality of blossom clusters, senescence of leaf, fruit maturation, resistance to pathogens, abiotic stress response (Chen et al., 2017; Viana et al., 2018; Wang et al., 2020; de Bont et al., 2022; Goyal et al., 2022). *WRKY* gene family members were categorized into three groups (Rushton et al., 2010). WRKY46 and WRKY70 belonged to the group III with one WRKY domain and CCHC zinc finger motif, which played critical roles in the regulation of biotic stress response (Li et al., 2006; Hu et al., 2012). Furthermore, WRKY46 and WRKY70 acted as essential regulators in abiotic stress response which had also been demonstrated (Li et al., 2013; Ding et al., 2014; Chen et al., 2017). WRKY46 was found to negatively regulate plant responses to abiotic stress as the overexpression of *WRKY46* resulted in hypersensitivity to drought and salt stress with a higher rate of water loss (Ding et al., 2014). Similarly, WRKY70 functions as negative regulator in drought stress and osmotic stress response by affecting water retention and stomatal conductance (Li et al., 2013; Chen et al., 2017). In our study, we found that the expression of *WRKY46* and *WRKY70* were negatively regulated by JMJ15 under salt stress (**Figure 6A**), which was consistent with the hypersensitivity of *JMJ15* loss-of-function mutants to salt stress response. Furthermore, we found that JMJ15 bound to the chromatin of *WRKY46* and *WRKY70*, and the enrichment was slightly induced under salt stress treatment (**Figure 6D**). Notably, overexpression of *JMJ15* led to decrease the transcript levels of *WRKY* genes as well as H3K4me3 levels at these loci. According to publicly available microarray data[3] (Winter et al., 2007), the expression of *JMJ15* was low but rapidly induced by salt treatment (0.5–1 h), while *WRKY46* and *WRKY70* were induced at later time (3–6 h) (**Supplementary Figure 1**). These data suggest that JMJ15 may mainly repress the gene expression of *WRKY46* and *WRKY70* at the early stage of salt stress. Our results showed that H3K4me3 levels increased substantially at the *WRKY46* and *WRKY70* genes after 5 h salt treatment. This result suggests the existence of H3K4me3 methyltransferases and other chromatin remodelers that may also modulate the chromatin of *WRKY46* and *WRKY70* genes during the salt stress process. WRKY70 was previously reported as one target gene of H3K4me3 histone methyltransferase ATX1 (Ding et al., 2011, 2012). The SUMO E3 ligase, SIZ1 was found to modulate transcript and H3K4me3 level at the *WRKY70* gene (Miura et al., 2020). However, it is not excluded other chromatin remodelers regulate H3K4me3 abundance and the transcript levels of *WRKY46* and *WRKY70* genes. Further studies should be conducted to understand how JMJ15 cooperates with other chromatin remodelers to regulate target genes.

Data availability statement

The data presented in the study are deposited in the NCBI-SRA repository, accession number PRJNA822702 https://www.ncbi.nlm.nih.gov/bioproject/PRJNA822702 and PRJNA823378 https://www.ncbi.nlm.nih.gov/bioproject/PRJNA823378.

Author contributions

YS, YC, and LS designed the research and analyzed the data. YS, YC, SL, HL, and LS performed the experiments. YS and

3 http://bbc.botany.utoronto.ca/efp

LS wrote the manuscript. All authors have read and approved the final manuscript.

Funding

This work was supported by National Natural Science Foundation of China (No. 31500982) and the doctoral starting funds from Xinxiang Medical University (No. 505197).

Acknowledgments

The authors thank Dao-xiu Zhou (Institute of Plant Sciences Paris-Saclay, France) for constructive discussion.

Conflict of interest

The authors declare that the research was conducted in the absence of any commercial or financial relationships that could be construed as a potential conflict of interest.

Publisher's note

Supplementary material

The Supplementary Material for this article can be found online at: https://www.frontiersin.org/articles/10.3389/fpls.2022.1009723/full#supplementary-material

SUPPLEMENTARY FIGURE 1
Expression patterns of *JMJ15*, *WRKY46*, and *WRKY70* under 150 mM NaCl treatment for 24 h. The expression data were obtained from a public database, eFP browser (http://bar.utoronto.ca/efp_arabidopsis/cgi-bin/efpWeb.cgi). The color bar on the right indicates the absolute expression values.

References

Alvarez-Venegas, R., Abdallat, A. A., Guo, M., Alfano, J. R., and Avramova, Z. (2007). Epigenetic control of a transcription factor at the cross section of two antagonistic pathways. *Epigenetics* 2, 106–113. doi: 10.4161/epi.2.2.4404

Anders, S., and Huber, W. (2010). Differential expression analysis for sequence count data. *Genome. Biol.* 11:R106. doi: 10.1186/gb-2010-11-10-r106

Ardehali, M. B., Mei, A., Zobeck, K. L., Caron, M., Lis, J. T., and Kusch, T. (2011). Drosophila Set1 is the major histone H3 lysine 4 trimethyltransferase with role in transcription. *EMBO J.* 30, 2817–2828. doi: 10.1038/emboj.2011.194

Chen, J., Nolan, T. M., Ye, H., Zhang, M., Tong, H., Xin, P., et al. (2017). Arabidopsis WRKY46, WRKY54, and WRKY70 transcription factors are involved in brassinosteroid-regulated plant growth and drought responses. *Plant Cell* 29, 1425–1439. doi: 10.1105/tpc.17.00364

Chen, L. T., Luo, M., Wang, Y. Y., and Wu, K. (2010). Involvement of arabidopsis histone deacetylase HDA6 in ABA and salt stress response. *J. Exp. Bot.* 61, 3345–3353. doi: 10.1093/jxb/erq154

Chen, X., Hu, Y., and Zhou, D. X. (2011). Epigenetic gene regulation by plant Jumonji group of histone demethylase. *Biochim. Biophys. Acta* 1809, 421–426. doi: 10.1016/j.bbagrm.2011.03.004

de Bont, L., Mu, X., Wei, B., and Han, Y. (2022). Abiotic stress-triggered oxidative challenges: Where does H2S act? *J. Genet. Genom.* 49, 748–755. doi: 10.1016/j.jgg.2022.02.019

Ding, Y., Avramova, Z., and Fromm, M. (2011). The Arabidopsis trithorax-like factor ATX1 functions in dehydration stress responses via ABA-dependent and ABA-independent pathways. *Plant J.* 66, 735–744. doi: 10.1111/j.1365-313X.2011.04534.x

Ding, Y., Fromm, M., and Avramova, Z. (2012). Multiple exposures to drought 'train' transcriptional responses in Arabidopsis. *Nat. Commun.* 3:740. doi: 10.1038/ncomms1732

Ding, Z. J., Yan, J. Y., Li, C. X., Li, G. X., Wu, Y. R., and Zheng, S. J. (2015). Transcription factor WRKY46 modulates the development of Arabidopsis lateral roots in osmotic/salt stress conditions via regulation of ABA signaling and auxin homeostasis. *Plant J.* 84, 56–69. doi: 10.1111/tpj.12958

Ding, Z. J., Yan, J. Y., Xu, X. Y., Yu, D. Q., Li, G. X., Zhang, S. Q., et al. (2014). Transcription factor WRKY46 regulates osmotic stress responses and stomatal movement independently in Arabidopsis. *Plant J.* 79, 13–27. doi: 10.1111/tpj.12538

Foroozani, M., Vandal, M. P., and Smith, A. P. (2021). H3K4 trimethylation dynamics impact diverse developmental and environmental responses in plants. *Planta* 253:4. doi: 10.1007/s00425-020-03520-0

Goyal, P., Devi, R., Verma, B., Hussain, S., Arora, P., Tabassum, R., et al. (2022). WRKY transcription factors: Evolution, regulation, and functional diversity in plants. *Protoplasma* [Epub ahead of print]. doi: 10.1007/s00709-022-01794-7

Hu, Y., Dong, Q., and Yu, D. (2012). Arabidopsis WRKY46 coordinates with WRKY70 and WRKY53 in basal resistance against pathogen *Pseudomonas syringae*. *Plant Sci.* 185-186, 288–297. doi: 10.1016/j.plantsci.2011.12.003

Hu, Y., Shen, Y., Conde, E. S. N., and Zhou, D. X. (2011). The role of histone methylation and H2A.Z occupancy during rapid activation of ethylene responsive genes. *PLoS One* 6:e28224. doi: 10.1371/journal.pone.0028224

Huang, S., Zhang, A., Jin, J. B., Zhao, B., Wang, T. J., Wu, Y., et al. (2019). Arabidopsis histone H3K4 demethylase JMJ17 functions in dehydration stress response. *New Phytol.* 223, 1372–1387. doi: 10.1111/nph.15874

Islam, M. T., Wang, L. C., Chen, I. J., Lo, K. L., and Lo, W. S. (2021). Arabidopsis JMJ17 promotes cotyledon greening during de-etiolation by repressing genes involved in tetrapyrrole biosynthesis in etiolated seedlings. *New Phytol.* 231, 1023–1039. doi: 10.1111/nph.17327

Jaskiewicz, M., Conrath, U., and Peterhansel, C. (2011). Chromatin modification acts as a memory for systemic acquired resistance in the plant stress response. *EMBO Rep.* 12, 50–55. doi: 10.1038/embor.2010.186

Jeong, J. H., Song, H. R., Ko, J. H., Jeong, Y. M., Kwon, Y. E., Seol, J. H., et al. (2009). Repression of flowering locus T chromatin by functionally redundant histone H3 lysine 4 demethylases in Arabidopsis. *PLoS One* 4:e8033. doi: 10.1371/journal.pone.0008033

Kim, J. M., Sasaki, T., Ueda, M., Sako, K., and Seki, M. (2015). Chromatin changes in response to drought, salinity, heat, and cold stresses in plants. *Front. Plant Sci.* 6:114. doi: 10.3389/fpls.2015.00114

Kim, J. M., To, T. K., Ishida, J., Matsui, A., Kimura, H., and Seki, M. (2012). Transition of chromatin status during the process of recovery from drought stress in *Arabidopsis thaliana*. *Plant Cell Physiol.* 53, 847–856. doi: 10.1093/pcp/pcs053

Kim, J. M., To, T. K., Ishida, J., Morosawa, T., Kawashima, M., Matsui, A., et al. (2008). Alterations of lysine modifications on the histone H3 N-tail under drought stress conditions in *Arabidopsis thaliana*. *Plant Cell Physiol.* 49, 1580–1588. doi: 10.1093/pcp/pcn133

Lee, B. H., and Zhu, J. K. (2009). Phenotypic analysis of *Arabidopsis* mutants: Root elongation under salt/hormone-induced stress. *Cold Spring Harb. Protoc.* 2009:dbrot4968. doi: 10.1101/pdb.prot4968

Li, B., Carey, M., and Workman, J. L. (2007). The role of chromatin during transcription. *Cell* 128, 707–719. doi: 10.1016/j.cell.2007.01.015

Li, B., and Dewey, C. N. (2011). RSEM: Accurate transcript quantification from RNA-Seq data with or without a reference genome. *BMC Bioinform.* 12:323. doi: 10.1186/1471-2105-12-323

Li, D., Liu, R., Singh, D., Yuan, X., Kachroo, P., and Raina, R. (2020). JMJ14 encoded H3K4 demethylase modulates immune responses by regulating defence gene expression and pipecolic acid levels. *New Phytol.* 225, 2108–2121. doi: 10.1111/nph.16270

Li, H., and Durbin, R. (2009). Fast and accurate short read alignment with burrows-wheeler transform. *Bioinformatics* 25, 1754–1760. doi: 10.1093/bioinformatics/btp324

Li, J., Besseau, S., Toronen, P., Sipari, N., Kollist, H., Holm, L., et al. (2013). Defense-related transcription factors WRKY70 and WRKY54 modulate osmotic stress tolerance by regulating stomatal aperture in *Arabidopsis*. *New Phytol.* 200, 457–472. doi: 10.1111/nph.12378

Li, J., Brader, G., Kariola, T., and Palva, E. T. (2006). WRKY70 modulates the selection of signaling pathways in plant defense. *Plant J.* 46, 477–491. doi: 10.1111/j.1365-313X.2006.02712.x

Liu, P., Zhang, S., Zhou, B., Luo, X., Zhou, X. F., Cai, B., et al. (2019). The histone H3K4 demethylase JMJ16 represses leaf senescence in *Arabidopsis*. *Plant Cell* 31, 430–443. doi: 10.1105/tpc.18.00693

Liu, Y., Zhang, A., Yin, H., Meng, Q., Yu, X., Huang, S., et al. (2018). Trithorax-group proteins *Arabidopsis* Trithorax4 (ATX4) and ATX5 function in abscisic acid and dehydration stress responses. *New Phytol.* 217, 1582–1597. doi: 10.1111/nph.14933

Lu, F., Cui, X., Zhang, S., Liu, C., and Cao, X. (2010). JMJ14 is an H3K4 demethylase regulating flowering time in *Arabidopsis*. *Cell Res.* 20, 387–390. doi: 10.1038/cr.2010.27

Lu, F., Li, G., Cui, X., Liu, C., Wang, X. J., and Cao, X. (2008). Comparative analysis of JmjC domain-containing proteins reveals the potential histone demethylases in *Arabidopsis* and rice. *J Integr. Plant Biol.* 50, 886–896. doi: 10.1111/j.1744-7909.2008.00692.x

Miura, K., Renhu, N., and Suzaki, T. (2020). The PHD finger of Arabidopsis SIZ1 recognizes trimethylated histone H3K4 mediating SIZ1 function and abiotic stress response. *Commun. Biol.* 3:23. doi: 10.1038/s42003-019-0746-2

Mosammaparast, N., and Shi, Y. (2010). Reversal of histone methylation: Biochemical and molecular mechanisms of histone demethylases. *Annu. Rev. Biochem.* 79, 155–179. doi: 10.1146/annurev.biochem.78.070907.103946

Ng, D. W., Wang, T., Chandrasekharan, M. B., Aramayo, R., Kertbundit, S., and Hall, T. C. (2007). Plant SET domain-containing proteins: Structure, function and regulation. *Biochim. Biophys. Acta* 1769, 316–329. doi: 10.1016/j.bbaexp.2007.04.003

Rushton, P. J., Somssich, I. E., Ringler, P., and Shen, Q. J. (2010). WRKY transcription factors. *Trends Plant Sci.* 15, 247–258. doi: 10.1016/j.tplants.2010.02.006

Santos-Rosa, H., Schneider, R., Bannister, A. J., Sherriff, J., Bernstein, B. E., Emre, N. C., et al. (2002). Active genes are tri-methylated at K4 of histone H3. *Nature* 419, 407–411. doi: 10.1038/nature01080

Searle, I. R., Pontes, O., Melnyk, C. W., Smith, L. M., and Baulcombe, D. C. (2010). JMJ14, a JmjC domain protein, is required for RNA silencing and cell-to-cell movement of an RNA silencing signal in *Arabidopsis*. *Genes Dev.* 24, 986–991. doi: 10.1101/gad.579910

Shen, Y., Conde, E. S. N., Audonnet, L., Servet, C., Wei, W., and Zhou, D. X. (2014). Over-expression of histone H3K4 demethylase gene JMJ15 enhances salt tolerance in Arabidopsis. *Front. Plant Sci.* 5:290. doi: 10.3389/fpls.2014.00290

Shen, Y., Devic, M., Lepiniec, L., and Zhou, D. X. (2015). Chromodomain, Helicase and DNA-binding CHD1 protein, CHR5, are involved in establishing active chromatin state of seed maturation genes. *Plant Biotechnol. J.* 13, 811–820. doi: 10.1111/pbi.12315

Shi, Y., Lan, F., Matson, C., Mulligan, P., Whetstine, J. R., Cole, P. A., et al. (2004). Histone demethylation mediated by the nuclear amine oxidase homolog LSD1. *Cell* 119, 941–953. doi: 10.1016/j.cell.2004.12.012

Sokol, A., Kwiatkowska, A., Jerzmanowski, A., and Prymakowska-Bosak, M. (2007). Up-regulation of stress-inducible genes in tobacco and *Arabidopsis* cells in response to abiotic stresses and ABA treatment correlates with dynamic changes in histone H3 and H4 modifications. *Planta* 227, 245–254. doi: 10.1007/s00425-007-0612-1

Song, Q., Huang, T. Y., Yu, H. H., Ando, A., Mas, P., Ha, M., et al. (2019). Diurnal regulation of SDG2 and JMJ14 by circadian clock oscillators orchestrates histone modification rhythms in Arabidopsis. *Genome Biol.* 20:170. doi: 10.1186/s13059-019-1777-1

Sun, Q., and Zhou, D. X. (2008). Rice JmjC domain-containing gene JMJ706 encodes H3K9 demethylase required for floral organ development. *Proc. Natl. Acad. Sci. U. S. A.* 105, 13679–13684. doi: 10.1073/pnas.0805901105

Tsukada, Y., Fang, J., Erdjument-Bromage, H., Warren, M. E., Borchers, C. H., Tempst, P., et al. (2006). Histone demethylation by a family of JmjC domain-containing proteins. *Nature* 439, 811–816. doi: 10.1038/nature04433

van Dijk, K., Ding, Y., Malkaram, S., Riethoven, J. J., Liu, R., Yang, J., et al. (2010). Dynamic changes in genome-wide histone H3 lysine 4 methylation patterns in response to dehydration stress in *Arabidopsis thaliana*. *BMC Plant Biol.* 10:238. doi: 10.1186/1471-2229-10-238

Viana, V. E., Busanello, C., da Maia, L. C., Pegoraro, C., and Costa de Oliveira, A. (2018). Activation of rice WRKY transcription factors: An army of stress fighting soldiers? *Curr. Opin. Plant Biol.* 45, 268–275. doi: 10.1016/j.pbi.2018.07.007

Wang, T. J., Huang, S., Zhang, A., Guo, P., Liu, Y., Xu, C., et al. (2021). JMJ17-WRKY40 and HY5-ABI5 modules regulate the expression of ABA-responsive genes in *Arabidopsis*. *New Phytol.* 230, 567–584. doi: 10.1111/nph.17177

Wang, Y., Cui, X., Yang, B., Xu, S., Wei, X., Zhao, P., et al. (2020). WRKY55 transcription factor positively regulates leaf senescence and the defense response by modulating the transcription of genes implicated in the biosynthesis of reactive oxygen species and salicylic acid in *Arabidopsis*. *Development* 147:dev189647. doi: 10.1242/dev.189647

Winter, D., Vinegar, B., Nahal, H., Ammar, R., Wilson, G. V., and Provart, N. J. (2007). An "Electronic Fluorescent Pictograph" browser for exploring and analyzing large-scale biological data sets. *PLoS One* 2:e718. doi: 10.1371/journal.pone.0000718

Yang, H., Han, Z., Cao, Y., Fan, D., Li, H., Mo, H., et al. (2012a). A companion cell-dominant and developmentally regulated H3K4 demethylase controls flowering time in Arabidopsis via the repression of FLC expression. *PLoS Genet.* 8:e1002664. doi: 10.1371/journal.pgen.1002664

Yang, H., Mo, H., Fan, D., Cao, Y., Cui, S., and Ma, L. (2012b). Overexpression of a histone H3K4 demethylase, JMJ15, accelerates flowering time in *Arabidopsis*. *Plant Cell Rep.* 31, 1297–1308. doi: 10.1007/s00299-012-1249-5

Yang, R., Hong, Y., Ren, Z., Tang, K., Zhang, H., Zhu, J. K., et al. (2019). A role for pickle in the regulation of cold and salt stress tolerance in *Arabidopsis*. *Front. Plant Sci.* 10:900. doi: 10.3389/fpls.2019.00900

Yang, W., Jiang, D., Jiang, J., and He, Y. (2010). A plant-specific histone H3 lysine 4 demethylase represses the floral transition in *Arabidopsis*. *Plant J.* 62, 663–673. doi: 10.1111/j.1365-313X.2010.04182.x

Yang, Z., Qiu, Q., Chen, W., Jia, B., Chen, X., Hu, H., et al. (2018). Structure of the *Arabidopsis* JMJ14-H3K4me3 complex provides insight into the substrate specificity of KDM5 subfamily histone demethylases. *Plant Cell* 30, 167–177. doi: 10.1105/tpc.17.00666

Zhang, X., Bernatavichute, Y. V., Cokus, S., Pellegrini, M., and Jacobsen, S. E. (2009). Genome-wide analysis of mono-, di- and trimethylation of histone H3 lysine 4 in *Arabidopsis thaliana*. *Genome Biol.* 10:R62. doi: 10.1186/gb-2009-10-6-r62

Zheng, D., Wang, L., Chen, L., Pan, X., Lin, K., Fang, Y., et al. (2019). Salt-responsive genes are differentially regulated at the chromatin levels between seedlings and roots in rice. *Plant Cell Physiol.* 60, 1790–1803. doi: 10.1093/pcp/pcz095

Zheng, Y., Ding, Y., Sun, X., Xie, S., Wang, D., Liu, X., et al. (2016). Histone deacetylase HDA9 negatively regulates salt and drought stress responsiveness in Arabidopsis. *J. Exp. Bot.* 67, 1703–1713. doi: 10.1093/jxb/erv562

Zong, W., Zhong, X., You, J., and Xiong, L. (2013). Genome-wide profiling of histone H3K4-tri-methylation and gene expression in rice under drought stress. *Plant Mol. Biol.* 81, 175–188. doi: 10.1007/s11103-012-9990-2

frontiers | Frontiers in Plant Science

TYPE Original Research
PUBLISHED 27 September 2022
DOI 10.3389/fpls.2022.1018427

OPEN ACCESS

EDITED BY
Jian Chen,
Jiangsu University, China

REVIEWED BY
Lisong Ma,
Hebei Agricultural University, China
Huiming Guo,
Chinese Academy of Agricultural Sciences (CAAS), China
Xianqin Qiu,
Yunnan Academy of Agricultural Sciences, China

*CORRESPONDENCE
Xi Chen
chenxi_201402@163.com
Zhao Zhang
zhangzhao@cau.edu.cn

†These authors have contributed equally to this work

SPECIALTY SECTION
This article was submitted to Plant Bioinformatics, a section of the journal Frontiers in Plant Science

RECEIVED 13 August 2022
ACCEPTED 06 September 2022
PUBLISHED 27 September 2022

CITATION
Liu X, Fang P, Wang Z, Cao X, Yu Z, Chen X and Zhang Z (2022) ComparativeRNA-seq analysis reveals a critical role for ethylene in rose (*Rosa hybrida*) susceptible response to *Podosphera pannosa*. *Front. Plant Sci.* 13:1018427. doi: 10.3389/fpls.2022.1018427

Comparative RNA-seq analysis reveals a critical role for ethylene in rose (*Rosa hybrida*) susceptible response to *Podosphera pannosa*

Xintong Liu[1†], Peihong Fang[1†], Zicheng Wang[1], Xiaoqian Cao[1], Zhiyi Yu[1], Xi Chen[2,3*] and Zhao Zhang[1,4*]

[1]Beijing Key Laboratory of Development and Quality Control of Ornamental Crops, Department of Ornamental Horticulture, College of Horticulture, China Agricultural University, Beijing, China, [2]School of Agronomy and Horticulture, Jiangsu Vocational College of Agriculture and Forest, Jurong, China, [3]Engineering and Technical Center for Modern Horticulture, Jurong, China, [4]Horticulture College, Hainan University, Haikou, China

Rose is one of the most important ornamental flowers, accounting for approximately one-third of the world's cut flower market. Powdery mildew caused by *Podosphera pannosa* is a devastating fungal disease in rose, mainly infecting the young leaves and causing serious economic losses. Therefore, a study on the mechanism of the fungus infecting the rose leaves and the possibility to improve resistance hereby is interesting and meaningful. Accordingly, we conducted transcriptome sequencing of rose leaves infected by *P. pannosa* at different time points to reveal the molecular mechanism of resistance to powdery mildew. The high-quality reads were aligned to the reference genome of *Rosa chinensis*, yielding 51,230 transcripts. A total of 1,181 differentially expressed genes (DEGs) were identified in leaves during *P. pannosa* infection at 12, 24, and 48 hpi. The transcription factors of ERF, MYB, bHLH, WRKY, *etc.*, family were identified among DEGs, and most of them were downregulated during *P. pannosa* infection. The Kyoto Encyclopedia of Genes and Genomes analysis showed that the hormone signal transduction pathway, especially ethylene signal-related genes, was consistently showing a downregulated expression during powdery mildew infection. More importantly, exogenous 1-MCP (inhibitor of ethylene) treatment could improve the rose leaves' resistance to *P. pannosa*. In summary, our transcriptome of rose leaf infected by powdery mildew gives universal insights into the complex gene regulatory networks mediating the rose leaf response to *P. pannosa*, further demonstrating the positive role of 1-MCP in resistance to biotrophic pathogens.

KEYWORDS

powdery mildew, transcriptome, transcription factors, rose leaf, 1-MCP

Introduction

Rosa hybrida (modern rose) is independently domesticated in both Europe and China several thousands of years ago (Rusanov et al., 2009). Rose is one of the most important cut flowers and ornamental plants worldwide. Its planting area and market size rank as the first in global flower production, which means a remarkable commercial value. However, the rose is vulnerable to fungal diseases during cultivation and post-harvest transport, which cause huge economic losses. Among them, powdery mildew (PM) is one of the most common but devastating fungal diseases in the world (Debener and Byrne, 2014). In addition to the diseases of rose, it also affects other *Roseceae* plants, like apple, strawberry, pear, *etc*., and it is more serious in the greenhouse than in the open field. There are more than 650 species of *Erysiphales* in Ascomycota, including 15 sexual and four asexual species. This fungus has a wide range of hosts. More than 650 species of monocotyledonous plants and over 9,000 species of dicotyledonous plants have been reported (Schulzelefert and Vogel, 2000).

Rose powdery mildew was caused by *Podospheara pannosa* (*Pp*.). The fungus is a biotrophic ascomycete. In a warm, dry, or humid environment, PM infects the green vegetative organs such as young leaves and shoots of rose (Debener and Byrne, 2014). The rapid spread of PM causes the withered leaves of the plants to shrivel, shrink, or even fall off, and the surface is covered with white powder. PM is greatly damaging the ornamental and economic value of rose worldwide. An effective way to control the disease is to improve the resistance of plants (Vielba-Fernández et al., 2020). Comparative transcriptional analysis, using RNA-based sequencing (RNA-seq), is a common strategy of understanding the molecular mechanism of plant–pathogen interactions. This method has been widely applied in research about plant–pathogen interactions in horticultural crops, including rose (*Rosa hybrida*) (Liu et al., 2018), grape (*Vitis vinifera*) (Toffolatti et al., 2018), and apple (*Malus* × *domestica*) (Tian et al., 2019). However, to date, the lack of transcriptomic data on rose–PM interactions, coupled with the limitations of transgenesis and gene editing on rose, led to breeding in rose against PM with little progress achieved.

Normally, the onset of plant resistance to pathogens begins from the recognition of pathogens by plants, followed by the cascade of transmission of disease resistance signals depending on PAMP-triggered immunity and effector-triggered immunity. Signaling molecules and transcription factors (TFs) are the key components in both basal and race-specific immunity (Yuan et al., 2021). Plant hormones SA, JA, and ethylene (ET) are considered to be the main regulatory signals related to plant disease resistance. It is generally believed that SA is mainly the downstream signal of defense responding to the biotrophic fungi. JA and ET are involved in the downstream signal pathway of the defense response of necrotrophic fungi (Glazebrook, 2005). Studies have shown that, after a biotrophic infection, the plant cells in the infected area would accumulate SA in a short time (Duan et al., 2015). The function of plant defense-related TFs has also been reported in recent years. Overexpression of *VvZIP60* enhanced grape resistance to PM *via* the SA signaling pathway (Yu et al., 2019). Meanwhile, overexoression of *CmbHLH87* in pumpkin (Guo et al., 2020), HvNAC6 in barley (Chen et al., 2013), and FvWRKY42 (Wei et al., 2018) in strawberry enhanced the resistance to PM as a whole. However, a systematic study of the genes involved in rose early resistance to PM is still lacking.

Here we investigated the transcriptome dynamics of rose seedlings following *Pp*. primary, secondary, and tertiary infection, expecting to dig out more genes related to the resistance of rose to PM. Our aim is to provide a relevant rose gene pool with resistance to powdery mildew in order to improve the quality and the technology foundation, thereby achieving rose varieties resistant to powdery mildew and improving the commodity value of rose. Meanwhile, it is of great theoretical and practical significance to improve the plant disease resistance of powdery mildew by genetic engineering.

Materials and methods

Plant and fungal growth

Rosa hybrida 'Samantha' was propagated by tissue culture (Fang et al., 2021). Rose shoots with at least two leaves were cultured on half-strength Murashige and Skoog (MS) medium supplemented with 0.1 mg L^{-1} α-naphthaleneacetic (NAA) for 30 days at 22°C under a 16-h/8-h light/dark photoperiod for rooting. The rooted plants were transferred to pots containing peat moss/vermiculite (1:1) and grown at 25/16°C, 16-h/8-h light/dark photoperiod, and 60% humidity.

The powdery mildew *Podosphaera pannosa*, *Pp*, strain was cultivated with 'Samantha' seedlings at 25/16°C and 16-h/8-h light/dark photoperiod. Spore inoculums were prepared by harvesting spores from rose leaves in deionized water. The impurities were removed by centrifugation at 5,000 rmp for 10 min, and the culture was resuspended in distilled water to achieve experimental concentration.

Plant infection

For the RNA-seq samples, the healthy rose seedlings with young leaves (after having been transferred to pots for 4 weeks) are evenly inoculated with powdery mildew spore suspension with a concentration of 5×10^5/ml by spraying method to ensure that each leaf can be inoculated with powdery mildew. All the

seedlings were covered with white film to ensure nearly 100% humidity. The seedlings without roots were harvested at 12, 24, and 48 hours post-inoculation (hpi), immediately frozen in liquid nitrogen, and stored at -80°C for further use.

For the leaf discs, young stems with three to five pairs of dark red pinnate compound leaves were cut from 'Samantha' grown in glasshouses in Nankou, Changping District, Beijing, China, and their stems were immediately placed in water. Rose leaves, after the hormone treatments, were punched into 12.5-mm disks and placed in 0.4% water agar with back-up, at 16 disks per petri dish. Then, each leaf disc was sprayed with 1×10^7/ml powdery mildew spore suspension. The leaf discs were dried at room temperature before the petri dishes were closed. After 48 h of dark treatment, these were switched to a light culture grown at 25/16°C and 16-h/8-h light/dark photoperiod. The lesion sizes were measured at 6, 9, 12, and 15 dpi and analyzed statistically by Student's *t*-test.

Total RNA extraction and RNA-seq library preparation

Total RNA was extracted using the hot borate method as previously described (Wu et al., 2017), and the cultures were treated with RNase-free DNase I (Promega) to remove any contaminating genomic DNA. Two biological repeats were performed for each time point after the infection. Strand-specific RNA libraries were constructed using a protocol described previously (Jiang et al., 2011) and sequenced on the HiSeq2500 system according to the manufacturer's instructions. The raw reads were deposited in the NCBI SRA database under accession no. PRJNA661227.

RNA-seq data analysis

Firstly, the raw data was cleaned by removing the adaptor-containing sequences, the poly-N adaptor-containing sequences, and the low-quality reads (-L = 20, -*q* = 0.5). The clean reads were evaluated by FastQC (Brown et al., 2017). The reference genome of *Rosa chinensis* 'Old blash' (RchiOBHm-V2, GCF_002994745.1) was downloaded from the website (https://lipm-browsers.toulouse.inra.fr/pub/RchiOBHm-V2/) (Raymond et al., 2018). The reference genome index was constructed with Bowtie v2.2.3, and the reads were aligned to the reference genome with TopHat v2.0.12. All genes were annotated by non-redundant protein (NR), NCBI non-redundant transcript (NT), and Kyoto Encyclopedia of Genes and Genomes (KEGG) and Gene Ontology (GO) libraries with *e*-value $\leq 10^{-5}$.

The fragments per kilobase per million reads (FPKM) method was used for the gene expression calculation (Trapnell et al., 2010). Principal component analysis (PCA) was performed using the ggord package in R software. The differentially expressed genes (DEGs) were analyzed by DESeq (Anders et al., 2013) and defined as genes with $|\log_2$ fold change (FC)$| \geq 1$, an adjusted *P*-value <0.05, a false discovery rate of <0.001. The GO and KEGG enrichment analyses of the DEGs were conducted to identify the enriched biological functions using the GOseq R software package (Young et al., 2010) and KOBAS software (Xie et al., 2011).

Exogenous ACC treatment of rose leaves

Leaf stems were cut into 30 cm with three pairs of pinnate compound leaves and individually placed into 100 ml of 50 μM 1-aminocyclopropanecarboxylic acid (ACC) or deionized water as a control. After 24 h of treatment, the leaves were punched into discs.

Ethylene and 1-MCP treatment of rose leaves

Leaf stems placed in 100 ml deionized water were exposed to ethylene (10 μl/L), 1-methylcyclopropene (1-MCP, 2 μl/L), or regular air as a control for 24 h. 1M NaOH solution was added to the chambers to prevent CO_2 accumulation. The leaves were then punched into discs for inoculation.

Trypan blue staining assay

The rose leaves were harvested after inoculation for 0, 12, and 24 h and decolorized in the decolorizing solution (ethanol/glacial acetic acid = 1: 3) for 24–48 h until the leaves were bleached. The bleached leaves were stained with 0.05% trypan blue for 3 mins. The stained sections were visualized under an Olympus microscope. At least 4 leaves per time point were observed.

Results

RNA sequencing of rose seedling following *Podosphera pannosa* infection

In our previous study, after *P. pannosa* was infected for 12 h on rose leaves, the spores began to germinate and produce germinating tubes. Therefore, 12 hpi is the initiation of infection. At this time, the germination of spores produced a bud tube that extends into the epidermal cells of the rose leaves, and haustorium formed to obtain nutrients from plants, which is a key time point of initial infection. At 24 hpi, the conidia cluster formed, which means that the fungus was in the stage of asexual

propagation. At this point, the second-generation spore was about to mature, and the second infection will occur soon. Accordingly, the third-generation spore will be produced and mature in the next 24 hours (Supplementary Figure S1).

Therefore, we chose the points of 0, 12, 24, and 48 hpi samples for transcriptome sequencing. The expression profiles were obtained from rose seedlings infected with *P. pannosa*. About 195 million clean reads from eight libraries were generated by 150-bp paired-end RNA sequencing. The quality of clean data was evaluated by FastQC. The results showed that the effective rate of each sample was more than 99%, with ~99% Q20, ~95% Q30, and ~46% GC content. The mapping rate of all samples was between 83.78 and 85.23% (Supplementary Table S1). The high quality of the clean data meets the transcriptome analysis requirements. As a result, 51,230 transcripts were identified in each sample. The gene expression level was evaluated by FPKM. The transcripts were classified by FPKM values, as shown in Figure 1A. There were about 19.8% of genes expressed at low levels (0 < FPKM ≤1), ~37.6% at moderate levels (1 < FPKM ≤60), and ~3.4 at high levels (FPKM >60). The FPKM of eight samples representing different infection time points was subjected to PCA. Although the two samples collected in 24 hpi were shown to be more discrete than the others, every two samples collected in one time point were able to cluster together, and the clear separation between different infection time points was detected (Figure 1B).

The DEGs were determined by DEGseq in comparison with 0 hpi. A total of 1,181 significant DEGs were obtained (the value of FPKM fold change was more than two times, *P*-value <0.05; Figure 2), of which 518, 537, and 615 DEGs were identified at 12, 24, and 48 hpi, respectively. Among the DEGs, 371 genes were upregulated once at least, and 846 genes were downregulated once at least in three points. In total, 94 DEGs showed a differential expression at all three time points, of which 13 were upregulated and 59 were downregulated. The results indicated that, during *P. pannosa* infection, the rose seedlings downregulated more genes than upregulated them, and the DEGs greatly varied in primary infection, re-infection, and tertiary infection. The qRT-PCR was used to validate the DEGs (Figure 3).

The TFs involved in rose seedling defense response to *P. pannosa*

TFs are important components in plant defense, involving multiple cell physiological and molecular progress. Among 1,181 DEGs, we have identified 52 TFs involved in rose defense response once at least in three time points, including bHLH, bZIP, C2H2, ERF, HHO, GATA, MYB, NAC, NFY, OFP, PCL, WOX, WAKY, and Znf family members. The ERF family has the most of DEGs, followed by MYB, bHLH, and WRKY family, with 13, 11, 10, and seven DEGs, respectively (Figure 4A). There were 22, 15, and 40 TFs in 12, 24, and 48 hpi, respectively. Meanwhile, 80.2% of the TFs had a downregulated expression (Figure 4B). The downregulated TFs were sensitive to *P. pannosa*, and 10 of them were enriched in the KEGG analysis, which was related to the hormone signal transduction pathway and the MAPK signal pathway (Supplementary Table S3).

Identified DEGs related to plant hormone signal transduction response to *P. pannosa* infection

To investigate the important biological progresses and pathways in rose seedlings resistant to *P. pannosa*, we annotated all the DEGs based on GO and KEGG databases. A

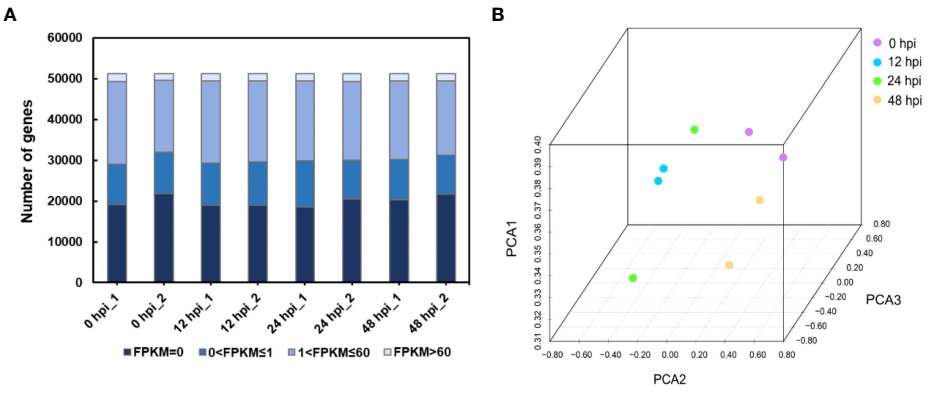

FIGURE 1
Overview of the RNA-seq data. **(A)** Distribution of the FPKM value in different samples. FPKM, fragments per kilobase per million reads. **(B)** Principal component analysis of rose RNA-seq data following *P. pannosa* infection.

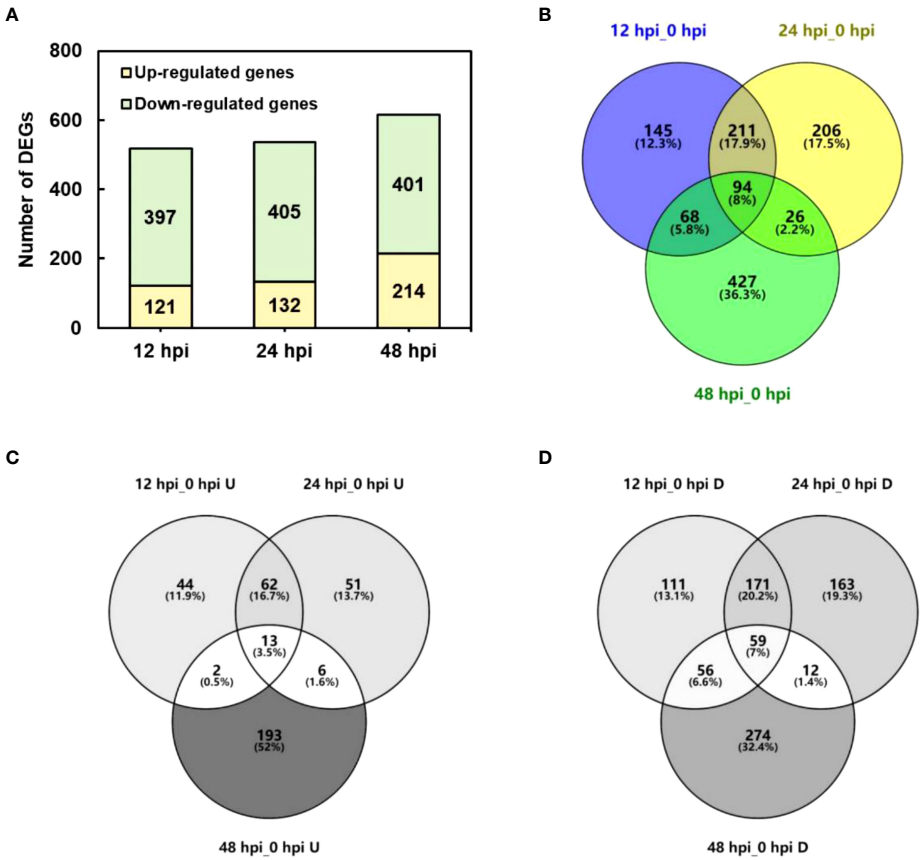

FIGURE 2
Number of DEGs in *P. pannosa*-infected rose seedlings at 12, 24, and 48 hpi. **(A)** Number of upregulated and downregulated DEGs at 12, 24, and 48 hpi. **(B–D)** Wayne figure of all upregulated and downregulated DEGs, respectively. DEGs, differentially expressed genes (cutoff ratio of >2, *p*-value <0.05, and *q*-value <0.05); U, upregulated DEGs; D, downregulated DEGs.

total of 518, 516, and 461 DEGs were enriched with GO terms in biological progress, cellular component, and molecular function, respectively (Supplementary Figure S2). Interestingly, in the KEGG analysis, we have identified plant hormone signal transduction, MAPK signal pathway, starch and sucrose metabolism, *etc*., to be involved in rose response to *P. pannosa* (Figure 5A). The DEGs were significantly enriched in abscisic acid (ABA), brassinosteroid (BR), ET, gibberellins (GA), auxin (IAA), JA, and SA in the plant hormone signal transduction pathway. More importantly, the expression of DEGs in ET, JA, and GA was opposite to that in SA; they showed a consistently downregulated expression (Figure 5B). However, although the ABA-, BR-, and IAA-related DEGs were also enriched, their expression patterns at different time points were not consistent.

With the deepening of research on plant hormones, it is generally believed that SA is mainly the downstream signal of defense responding to the biotrophic pathogens, and JA often play opposite roles to SA in plant defense responses (Caarls et al., 2015). In our results, the JA- and SA-related DEGs also play an opposite expression pattern, and the results further suggested that ET may play a particular role in the rose–*P. pannosa* interaction.

Exogenous ET inhibitor treatment improved rose resistance to *P. pannosa*

ACC is an ethylene precursor, which is chemically stable and is often used as a substitute for gaseous ET to evaluate plant susceptibility to ethylene. To investigate the role of ET in rose defense response to *P. pannosa*, a 50-μM-ACC vase treatment of fresh rose leaf stem was carried out for 24 h. The variations of susceptibility to *P. pannosa* under ACC-pretreated leaves and mock (H_2O-treated) leaves were observed at 6, 9, 12, and 15 dpi. The results showed that the ACC-treated rose leaves were more sensitive to *P. pannosa* than the mock leaves (Figures 6A, B). However, the gaseous-ET-pre-treated rose leaves showed no significant susceptibility to *P. pannosa*. On the contrary, the 1-

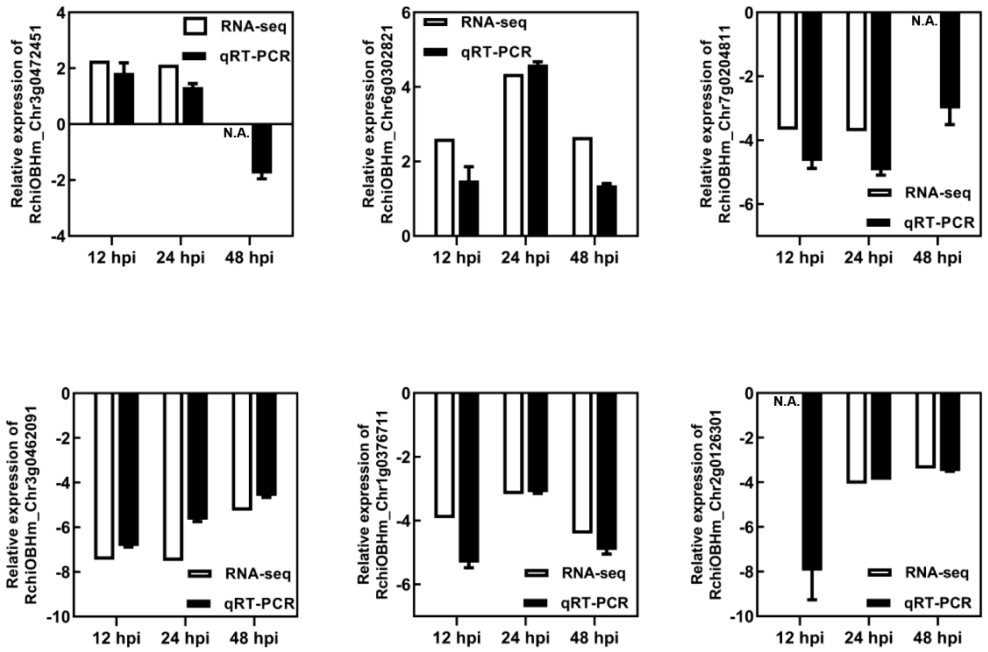

FIGURE 3
Validation of RNA-seq results using qRT-PCR. N.A. represented the RNA-seq data that was not available. RhUBI2 was used as the internal housekeeping gene control.

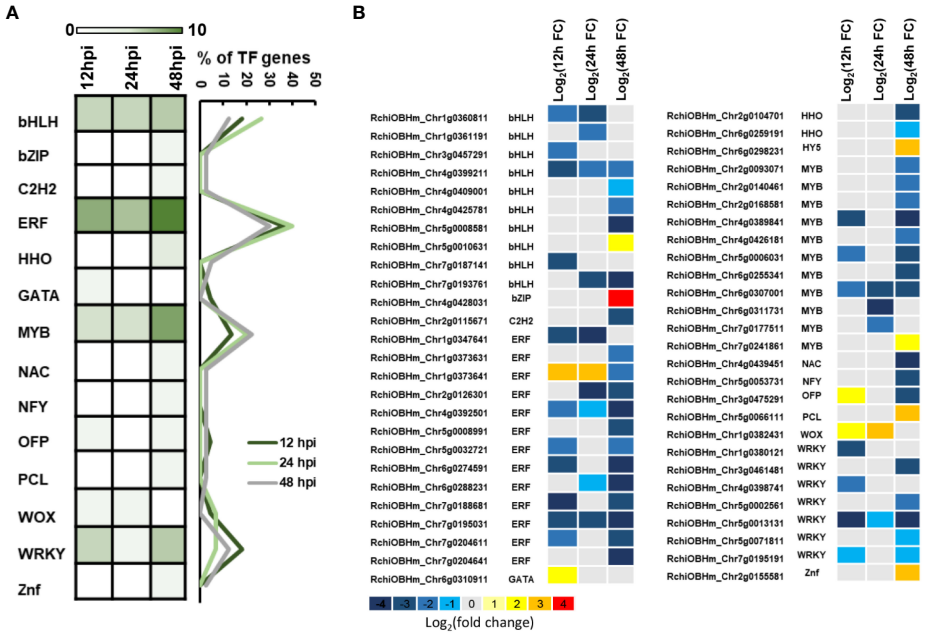

FIGURE 4
Kyoto Encyclopedia of Genes and Genomes (KEGG) pathways analysis for differentially expressed genes (DEGs). **(A)** KEGG pathway enrichment analysis of DEGs. **(B)** Relative expression changes of DEGs in plant hormone signal transduction pathway. ABA, abscisic acid; BR, brassinosteroid; ET, ethylene; GA, gibberellin; IAA, auxin; JA, jasmonic acid; SA, salicylic acid. The expression level was calculated using $\log_2$(FC). Log_2(FC) = $\log_2$ (fold change).

MCP (the ET inhibitor)-pre-treated leaves showed a strong resistance to *P. pannosa* (Figures 6C, D). The results imply that 1-MCP can be used in the prevention of rose powdery mildew.

Discussion

PM, caused by *P. pannosa*, is one of the most common and important fungal diseases of ornamental and horticultural plants around the world. *P. pannosa* is a biotrophic fungi which can be difficult to cultivate even though it is further studied compared with necrotrophic fungi. In agronomy cultivation, powdery mildew can infect the young leaves of roses, apples, strawberries, and other *Rosaceae* plants, which can lead to huge economic losses (Debener and Byrne, 2014; Vielba-Fernández et al., 2020). It is hence quite important and meaningful to study and explore the procedure and the mechanism behind *Pp.* infection on *Rosaceae* plants' leaves. Here the rose cultivar 'Samantha' and *P. pannosa* (Pp) strains were used as materials to conduct transcriptome sequencing, and this highlighted massive genes and several hormone signal transduction pathways relevant to the resistance to rose powdery mildew.

In recent years, RNA-seq has been applied on several studies of plant–PM interaction, revealing the core DEGs and the biological progress in plant defense response. In this study, we have identified 1,181 DEGs once at least following three *Pp.* infection time points. Among the 1,181 DEGs, there were 846 downregulated genes and 371 upregulated genes. Consistently, in apple, jointly belonging to *Rosaceae*, 1,177 DEGs were identified between apple leaves subjected to fungal infection and those grown without pathogens at 12, 24, and 48 hpi (Tian et al., 2019). In pumpkin leaves, they obtained more than 3,000 DEGs after PM was inoculated for 24 and 48 h (Guo et al., 2018).

Transcriptional regulation is a central step in plant defense responses. Therefore, for understanding the molecular basis of plant–pathogen interactions, it is critical to elucidate the complex regulatory mechanisms that control defense gene expression among plant species. Here we have found 52 TFs with significantly differential expression, including four major family members (ERF, MYB, bHLH, and WRKY) and other 10 family members (Figure 4). Previous studies have shown that WRKY family members are involved in the regulation of plant disease resistance as well as in the regulation of transcriptional reprograming associated with plant immune responses (Eulgem and Somssich, 2007; Buscaill and Rivas, 2014). However, we identified ERF members as the most common in the TF family, similar to our previous study of rose petal defense response to *Botrytis cinerea* (Liu et al., 2018). The results indicated that ERF family members played an important role in rose defense response to both biotrophic and necrotrophic fungus. In recent years, there are more and more studies that show that ERF family members acted as a positive regulator in plant resistance to PM (Xing et al., 2017; Li et al., 2021; Zhang et al., 2021) and to grey mold (Pré et al., 2008; Catinot et al., 2015; Li et al., 2020).

The KEGG analysis demonstrated that most of the DEGs were enriched in plant hormone signal transduction pathway, including ABA-, AUX-, BR-, ET-, GA-, JA-, and SA-related genes. Although only one DEG was identified in the SA signal pathway, the expression pattern of this gene (RchiOBHm_Chr6g0247671) was opposite to that of the DEGs (RchiOBHm_Chr7g0187141, RchiOBHm_Chr1g0360811, RchiOBHm_Chr2g0146371, and RchiOBHm_Chr4g0429271) related to the JA pathway (Figure 5). Various research have pointed out that SA and JA form the basic bone of plant immunity system (De Vleesschauwer et al., 2013). It is generally believed that SA is thought to mediate defense signaling in response to biotrophic and hemibiotrophic pathogens, while JA and ET are associated with defense responses to necrotrophs, and these two pathways work in an antagonistic manner (Caarls et al., 2015). In addition, SA can inhibit a series of JA response genes (such as PDH1.2) and JA biosynthesis-related genes (LOX2/AOS/AOC2/OPR3) (Leon-Reyes et al., 2010).

In this study, four DEGs were found in the ET signaling pathway. Interestingly, all of the four DEGs were downregulated during *Pp.* infection (Figure 5). These results indicated that ET may play a negative role in rose defense response to *Pp.* Ethylene is a gaseous plant hormone, which is involved in regulating the physiological and biochemical processes of many plants, including seed germination, plant growth, fruit ripening, organ abscission, and aging (Schulzelefert and Vogel, 2000). In addition, when plants are attacked by pathogens and herbivores, ethylene also plays an important role in plant defense system (Broekaert et al., 2006; Broekgaarden et al., 2015). ACC is the premise of ethylene synthesis to replace ethylene and added hormones to water agar to ensure the continuous supply of ethylene. The results showed that the treatment group had a later onset than the control group, had a significant difference at the time of inoculation for 6 days, then exceeded the control group (H_2O), and reached a significant difference at the time of inoculation for 15 days (Figures 6A, B). While we first found that 1-MCP, a gas ethylene inhibitor, can significantly improve the disease resistance of rose leaves after 9 dpi, gas ET treatment showed increased resistance at 9 dpi and gradually approached the control group at 15 dpi (Figures 6C, D). We speculated that the different phenotype between ACC and gas ET treatment may be due to the fact that the gas ethylene treatment in a short day cannot play a role in the detached leaves continuously. The continuous energy supply of ACC keeps producing gas ethylene, which makes the ethylene concentration

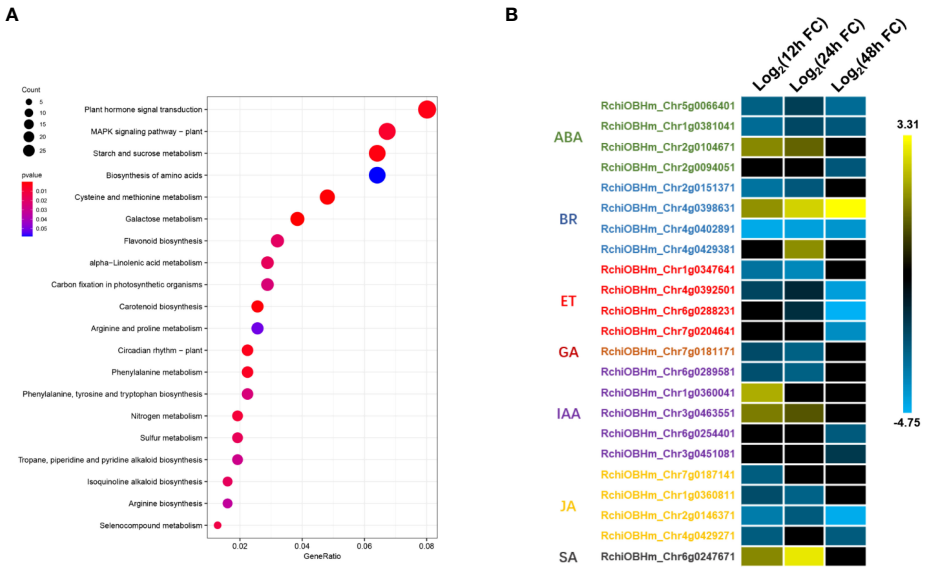

FIGURE 5
Differentially expressed transcription factors (TFs). **(A)** Number of TFs in *P. pannosa*-infected rose seedlings at 12, 24, and 48 hpi. **(B)** Relative expression changes of TFs at 12, 24, and 48 hpi. The expression level was calculated using log_2(FC). Log_2(FC) = log_2(fold change).

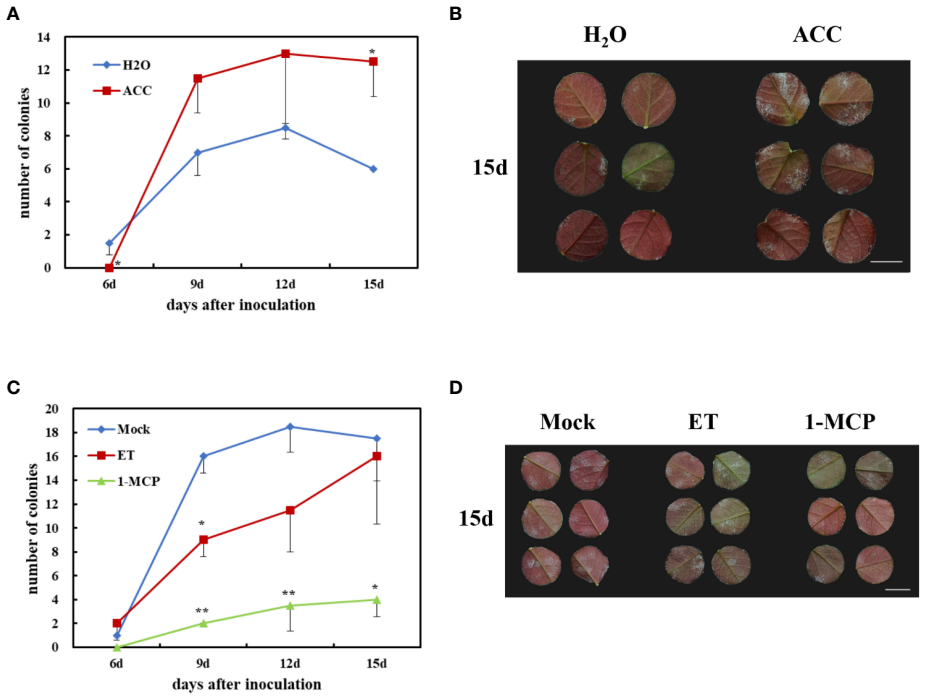

FIGURE 6
Effects of rose resistance to *P. pannosa* under exogenous 1-aminocyclopropanecarboxylic acid (ACC), ethylene (ET), and 1-methylcyclopropene (1-MCP) (ET inhibitor) treatments. **(A)** Quantification of *P. pannosa* colonies on rose leaves under ACC treatment. H_2O was set as mock. Data statistics were carried out at 6, 9, 12, and 15 days after *P. pannosa* inoculation. **(B)** Typical appearance of control (H_2O) and ACC-pre-treated rose seedlings at 15 days after *P. pannosa* inoculation. **(C)** Quantification of *P. pannosa* colonies on rose leaves under mock (air), ET, and 1-MCP. Data statistics were carried out at 6, 9, 12, and 15 days after *P. pannosa* inoculation. **(D)** Typical appearance of mock- (air), ET-, and 1-MCP-pre-treated rose seedlings at 15 days after *P. pannosa* inoculation. The asterisks indicate significant differences according to Student's *t*-test (*P < 0.05, **P < 0.01).

in the inoculated environment higher and higher. Therefore, based on the above-mentioned results, we clarified that 1-MCP could be a candidate for exogenous chemical agents for the economic and sustainable improvement of rose resistance to PM.

Conclusions

In conclusion, this study focused on rose early defense response to powdery mildew and identified 1,181 DEGs during infection. In total, 52 differentially expressed TFs, especially ERF, MYB, bHLH, and WRKY family members, consisted of the core regulatory factor network. Simultaneously, besides SA and JA, the KEGG enrichment highlighted the ET signaling pathway in the regulation of rose leaves' resistance. The application test of 1-MCP, an ethylene inhibitor, showed that 1-MCP played a positive role in rose resistance to PM.

Data availability statement

The datasets presented in this study can be found in online repositories. The names of the repository/repositories and accession number(s) can be found below: https://www.ncbi.nlm.nih.gov/, PRJNA661227.

Author contributions

XL and PF performed the experiments. XL, PF, XiaC, and ZW analyzed the data. XL, XQC, and ZZ complemented the writing of the manuscript. XiC and ZZ planned the project, designed and supervised the experiments, and coordinated the collaboration of the authors. All authors contributed to the article and approved the submitted version.

Funding

This work was supported by the National Natural Science Foundation of China (grant number 31501791), and the Construction of Beijing Science and Technology Innovation and Service Capacity in Top Subjects (CEFF-PXM2019_014207_000032) to ZZ. This study was further sponsored by the Natural Science Foundation of Jiangsu Province (BK20191224) and supported by the project of Jiangsu Vocational College of Agriculture and Forest (2019kj005) to XC, also the China Postdoctoral Science Foundation (2022M713391) to XL.

Conflict of interest

The authors declare that the research was conducted in the absence of any commercial or financial relationships that could be construed as a potential conflict of interest.

Publisher's note

All claims expressed in this article are solely those of the authors and do not necessarily represent those of their affiliated organizations, or those of the publisher, the editors and the reviewers. Any product that may be evaluated in this article, or claim that may be made by its manufacturer, is not guaranteed or endorsed by the publisher.

Supplementary material

The Supplementary Material for this article can be found online at: https://www.frontiersin.org/articles/10.3389/fpls.2022.1018427/full#supplementary-material

References

Anders, S., McCarthy, D. J., Chen, Y., Okoniewski, M., Smyth, G. K., Huber, W., et al. (2013). Count-based differential expression analysis of RNA sequencing data using r and bioconductor. *Nat. Protoc.* 8, 1765–1786. doi: 10.1038/nprot.2013.099

Broekaert, W. F., Delauré, S. L., De Bolle, M. F., and Cammue, B. P. (2006). The role of ethylene in host-pathogen interactions. *Annu. Rev. Phytopathol.* 44, 393–416. doi: 10.1146/annurev.phyto.44.070505.143440

Broekgaarden, C., Caarls, L., Vos, I. A., Pieterse, C. M., and Van Wees, S. C. (2015). Ethylene: traffic controller on hormonal crossroads to defense. *Plant Physiol.* 169, 2371–2379. doi: 10.1104/pp.15.01020

Brown, J., Pirrung, M., and McCue, L. A. (2017). FQC dashboard: integrates FastQC results into a web-based, interactive, and extensible FASTQ quality control tool. *Bioinformatics* 33, 3137–3139. doi: 10.1093/bioinformatics/btx373

Buscaill, P., and Rivas, S. (2014). Transcriptional control of plant defence responses. *Curr. Opin. Plant Biol.* 20, 35–46. doi: 10.1016/j.pbi.2014.04.004

Caarls, L., Pieterse, C. M., and Van Wees, S. C. (2015). How salicylic acid takes transcriptional control over jasmonic acid signaling. *Front. Plant Sci.* 6, 170. doi: 10.3389/fpls.2015.00170

Catinot, J., Huang, J. B., Huang, P. Y., Tseng, M. Y., Chen, Y. L., Gu, S. Y., et al. (2015). ETHYLENE RESPONSE FACTOR 96 positively regulates a rabidopsis resistance to necrotrophic pathogens by direct binding to GCC elements of jasmonate–and ethylene-responsive defence genes. *Plant Cell Environ.* 38, 2721–2734. doi: 10.1111/pce.12583

Chen, Y.-J., Perera, V., Christiansen, M. W., Holme, I. B., Gregersen, P. L., Grant, M. R., et al. (2013). The barley *HvNAC6* transcription factor affects ABA accumulation and promotes basal resistance against powdery mildew. *Plant Mol. Biol.* 83, 577–590. doi: 10.1007/s11103-013-0109-1

Debener, T., and Byrne, D. H. (2014). Disease resistance breeding in rose: current status and potential of biotechnological tools. *Plant Sci.* 228, 107–117. doi: 10.1016/j.plantsci.2014.04.005

De Vleesschauwer, D., Gheysen, G., and Höfte, M. (2013). Hormone defense networking in rice: tales from a different world. *Trends Plant Sci.* 18, 555–565. doi: 10.1016/j.tplants.2013.07.002

Duan, Y., Jiang, Y., Ye, S., Karim, A., Ling, Z., He, Y., et al. (2015). *PtrWRKY73*, a salicylic acid-inducible poplar WRKY transcription factor, is involved in disease

resistance in *Arabidopsis thaliana*. *Plant Cell Rep.* 34, 831–841. doi: 10.1007/s00299-015-1745-5

Eulgem, T., and Somssich, I. E. (2007). Networks of WRKY transcription factors in defense signaling. *Curr. Opin. Plant Biol.* 10, 366–371. doi: 10.1016/j.pbi.2007.04.020

Fang, P., Arens, P., Liu, X., Zhang, X., Lakwani, D., Foucher, F., et al. (2021). Analysis of allelic variants of RhMLO genes in rose and functional studies on susceptibility to powdery mildew related to clade V homologs. *Theor. Appl. Genet.* 134, 2495–2515. doi: 10.1007/s00122-021-03838-7

Glazebrook, J. (2005). Contrasting mechanisms of defense against biotrophic and necrotrophic pathogens. *Annu. Rev. Phytopathol.* 43, 205. doi: 10.1146/annurev.phyto.43.040204.135923

Guo, W.-L., Chen, B.-H., Chen, X.-J., Guo, Y.-Y., Yang, H.-L., Li, X.-Z., et al. (2018). Transcriptome profiling of pumpkin (*Cucurbita moschata* duch.) leaves infected with powdery mildew. *PloS One* 13, e0190175. doi: 10.1371/journal.pone.0190175

Guo, W.-L., Chen, B.-H., Guo, Y.-Y., Chen, X.-J., Li, Q.-F., Yang, H.-L., et al. (2020). Expression of pumpkin *CmbHLH87* gene improves powdery mildew resistance in tobacco. *Front. Plant Sci.* 11, 163. doi: 10.3389/fpls.2020.00163

Jiang, L., Schlesinger, F., Davis, C. A., Zhang, Y., Li, R., Salit, M., et al. (2011). Synthetic spike-in standards for RNA-seq experiments. *Genome Res.* 21, 1543–1551. doi: 10.1101/gr.121095.111

Leon-Reyes, A., Du, Y., Koornneef, A., Proietti, S., Körbes, A. P., Memelink, J., et al. (2010). Ethylene signaling renders the jasmonate response of arabidopsis insensitive to future suppression by salicylic acid. *Mol. Plant-Microbe Interact.* 23, 187–197. doi: 10.1094/MPMI-23-2-0187

Li, X., Han, R., Gong, W., Wang, X., and Zhang, X. (2021). Investigation of wheat ERF family revealed novel genes involved in powdery mildew responses. *Russian J. Genet.* 57, 1064–1072. doi: 10.1134/S1022795421090064

Li, D., Liu, X., Shu, L., Zhang, H., Zhang, S., Song, Y., et al. (2020). Global analysis of the AP2/ERF gene family in rose (*Rosa chinensis*) genome unveils the role of *RcERF099* in botrytis resistance. *BMC Plant Biol.* 20, 1–15. doi: 10.1186/s12870-020-02740-6

Liu, X., Cao, X., Shi, S., Zhao, N., Li, D., Fang, P., et al. (2018). Comparative RNA-seq analysis reveals a critical role for brassinosteroids in rose (*Rosa hybrida*) petal defense against botrytis cinerea infection. *BMC Genet.* 19, 1–10. doi: 10.1186/s12863-018-0668-x

Pré, M., Atallah, M., Champion, A., De Vos, M., Pieterse, C. M., and Memelink, J. (2008). The AP2/ERF domain transcription factor ORA59 integrates jasmonic acid and ethylene signals in plant defense. *Plant Physiol.* 147, 1347–1357. doi: 10.1104/pp.108.117523

Raymond, O., Gouzy, J., Just, J., Badouin, H., Verdenaud, M., Lemainque, A., et al. (2018). The Rosa genome provides new insights into the domestication of modern roses. *Nat. Genet.* 50, 772–777. doi: 10.1038/s41588-018-0110-3

Rusanov, K., Kovacheva, N., Stefanova, K., Atanassov, A., and Atanassov, I. (2009). Rosa Damascena–genetic resources and capacity building for molecular breeding. *Biotechnol. Biotechnol. Equip.* 23, 1436–1439. doi: 10.2478/V10133-009-0009-3

Schulzelefert, P., and Vogel, J. P. (2000). Closing the ranks to attack by powdery mildew. *Trends Plant Sci.* 5, 343–348. doi: 10.1016/S1360-1385(00)01683-6

Tian, X., Zhang, L., Feng, S., Zhao, Z., Wang, X., and Gao, H. (2019). Transcriptome analysis of apple leaves in response to powdery mildew (*Podosphaera leucotricha*) infection. *Int. J. Mol. Sci.* 20, 2326. doi: 10.3390/ijms20092326

Toffolatti, S. L., De Lorenzis, G., Costa, A., Maddalena, G., Passera, A., Bonza, M. C., et al. (2018). Unique resistance traits against downy mildew from the center of origin of grapevine (*Vitis vinifera*). *Sci. Rep.* 8, 1–11. doi: 10.1038/s41598-018-30413-w

Trapnell, C., Williams, B. A., Pertea, G., Mortazavi, A., Kwan, G., Van Baren, M. J., et al. (2010). Transcript assembly and quantification by RNA-seq reveals unannotated transcripts and isoform switching during cell differentiation. *Nat. Biotechnol.* 28, 511–515. doi: 10.1038/nbt.1621

Vielba-Fernández, A., Polonio, Á., Ruiz-Jiménez, L., de Vicente, A., Pérez-García, A., and Fernández-Ortuño, D. (2020). Fungicide resistance in powdery mildew fungi. *Microorganisms* 8, 1431. doi: 10.3390/microorganisms8091431

Wei, W., Cui, M.-Y., Hu, Y., Gao, K., Xie, Y.-G., Jiang, Y., et al. (2018). Ectopic expression of *FvWRKY42*, a WRKY transcription factor from the diploid woodland strawberry (Fragaria vesca), enhances resistance to powdery mildew, improves osmotic stress resistance, and increases abscisic acid sensitivity in *Arabidopsis*. *Plant Sci.* 275, 60–74. doi: 10.1016/j.plantsci.2018.07.010

Wu, L., Ma, N., Jia, Y., Zhang, Y., Feng, M., Jiang, C.-Z., et al. (2017). An ethylene-induced regulatory module delays flower senescence by regulating cytokinin content. *Plant Physiol.* 173, 853–862. doi: 10.1104/pp.16.01064

Xie, C., Mao, X., Huang, J., Ding, Y., Wu, J., Dong, S., et al. (2011). KOBAS 2.0: a web server for annotation and identification of enriched pathways and diseases. *Nucleic Acids Res.* 39, W316–W322. doi: 10.1093/nar/gkr483

Xing, L., Di, Z., Yang, W., Liu, J., Li, M., Wang, X., et al. (2017). Overexpression of ERF1-V from *Haynaldia villosa* can enhance the resistance of wheat to powdery mildew and increase the tolerance to salt and drought stresses. *Front. Plant Sci.* 8, 1948. doi: 10.3389/fpls.2017.01948

Young, M. D., Wakefield, M. J., Smyth, G. K., and Oshlack, A. (2010). Gene ontology analysis for RNA-seq: accounting for selection bias. *Genome Biol.* 11, 1–12. doi: 10.1186/gb-2010-11-2-r14

Yuan, M., Ngou, B. P. M., Ding, P., and Xin, X.-F. (2021). PTI-ETI crosstalk: an integrative view of plant immunity. *Curr. Opin. Plant Biol.* 62, 102030. doi: 10.1016/j.pbi.2021.102030

Yu, Y.-H., Jiao, Z.-L., Bian, L., Wan, Y.-T., Yu, K.-K., Zhang, G.-H., et al. (2019). Overexpression of *Vitis vinifera VvbZIP60* enhances arabidopsis resistance to powdery mildew *via* the salicylic acid signaling pathway. *Scientia Hortic.* 256, 108640. doi: 10.1016/j.scienta.2019.108640

Zhang, Y., Zhang, L., Ma, H., Zhang, Y., Zhang, X., Ji, M., et al. (2021). Overexpression of the apple (*Malus×domestica*) *MdERF100* in *Arabidopsis* increases resistance to powdery mildew. *Int. J. Mol. Sci.* 22, 5713. doi: 10.3390/ijms22115713

frontiers | Frontiers in Plant Science

TYPE Original Research
PUBLISHED 29 September 2022
DOI 10.3389/fpls.2022.1012231

OPEN ACCESS

EDITED BY
Weicong Qi,
Jiangsu Academy of Agricultural Sciences (JAAS), China

REVIEWED BY
Zhaojun Wei,
Hefei University of Technology, China
Xiangpeng Leng,
Qingdao Agricultural University, China

*CORRESPONDENCE
Ziping Chen
zpchen@ahau.edu.cn
Xianfeng Du
dxf@ahau.edu.cn

SPECIALTY SECTION
This article was submitted to Plant Bioinformatics, a section of the journal Frontiers in Plant Science

RECEIVED 05 August 2022
ACCEPTED 29 August 2022
PUBLISHED 29 September 2022

CITATION
Chen L, Xu S, Liu Y, Zu Y, Zhang F, Du L, Chen J, Li L, Wang K, Wang Y, Chen S, Chen Z and Du X (2022) Identification of key gene networks controlling polysaccharide accumulation in different tissues of *Polygonatum cyrtonema* Hua by integrating metabolic phenotypes and gene expression profiles. *Front. Plant Sci.* 13:1012231. doi: 10.3389/fpls.2022.1012231

Identification of key gene networks controlling polysaccharide accumulation in different tissues of *Polygonatum cyrtonema* Hua by integrating metabolic phenotypes and gene expression profiles

Longsheng Chen[1,2], Shuwen Xu[2], Yujun Liu[2], Yanhong Zu[2], Fuyuan Zhang[2], Liji Du[2], Jun Chen[2], Lei Li[3], Kai Wang[2], Yating Wang[2], Shijin Chen[2], Ziping Chen[2]* and Xianfeng Du[1]*

[1]Anhui Engineering Laboratory for Agro-Products Processing, School of Tea & Food Science and Technology, Anhui Agricultural University, Hefei, China, [2]Anhui Promotion Center for Technology Achievements Transfer, Anhui Academy of Science and Technology, Hefei, China, [3]Jinzhai Senfeng Agricultural Technology Development Co., Ltd., Lu'an, China

Plant polysaccharides, a type of important bioactive compound, are involved in multiple plant defense mechanisms, and in particular polysaccharide-alleviated abiotic stress has been well studied. *Polygonatum cyrtonema* Hua (*P. cyrtonema* Hua) is a medicinal and edible perennial plant that is used in traditional Chinese medicine and is rich in polysaccharides. Previous studies suggested that sucrose might act as a precursor for polysaccharide biosynthesis. However, the role of sucrose metabolism and transport in mediating polysaccharide biosynthesis remains largely unknown in *P. cyrtonema* Hua. In this study, we investigated the contents of polysaccharides, sucrose, glucose, and fructose in the rhizome, stem, leaf, and flower tissues of *P. cyrtonema* Hua, and systemically identified the genes associated with the sucrose metabolism and transport and polysaccharide biosynthesis pathways. Our results showed that polysaccharides were mainly accumulated in rhizomes, leaves, and flowers. Besides, there was a positive correlation between sucrose and polysaccharide content, and a negative correlation between glucose and polysaccharide content in rhizome, stem, leaf, and flower tissues. Then, the transcriptomic analyses of different tissues were performed, and differentially expressed genes related to sucrose metabolism and transport, polysaccharide biosynthesis, and transcription factors were identified. The analyses of the gene expression patterns provided novel regulatory networks for the molecular basis of high accumulation of polysaccharides, especially in the rhizome tissue. Furthermore, our findings explored that polysaccharide accumulation was highly correlated with the expression levels of *SUS*, *INV*, *SWEET*, and *PLST*, which are mediated by *bHLH*,

bZIP, *ERF*, *ARF*, *C2H2*, and other genes in different tissues of *P. cyrtonema* Hua. Herein, this study contributes to a comprehensive understanding of the transcriptional regulation of polysaccharide accumulation and provides information regarding valuable genes involved in the tolerance to abiotic stresses in *P. cyrtonema* Hua.

KEYWORDS

polysaccharides, sucrose metabolism and transport, transcription factors, gene expression, *Polygonatum cyrtonema* Hua

Introduction

Polygonati rhizoma, commonly known as Huangjing, is a vital traditional and classic Chinese herb and is widely distributed in the world (Luo et al., 2016). There are various species, including *Polygonatum cyrtonema* Hua, *Polygonatum kingianum* Collett and Hemsley, and *Polygonatum sibiricum* Red et al in China (Chinese Pharmacopoeia Commission, 2020). Among these, *Polygonatum cyrtonema* Hua (*P. cyrtonema* Hua) is a key constituent of herbal medicines in Anhui Province. Indeed, it usually grows on forested mountains, bushes, and shade hillsides at an altitude of 500–1,200 m above sea level (**Figures 1A,B**). *P. cyrtonema* Hua often blooms from late April to early June, and the perianth shows the yellow-green color (**Figures 1B,C**). Its fruit ripens around the middle of August. Moreover, the rhizomes are harvested in late October and are used to manufacture the Huangjing slice, nine cycles of steam-sun drying processing products, functional beverages, fruit wine, and well-received sweetmeats (**Figure 1C**; Chinese Pharmacopoeia Commission, 2020; Li et al., 2021; Wu et al., 2022). They have a high abundance of health benefit-promoting metabolites and are among the widely consumed medicines and functional foods (Cheng et al., 2021; Li et al., 2021; Hu et al., 2022; Zhu et al., 2022).

Polysaccharides of *P. cyrtonema* Hua are important bioactive compounds (Li et al., 2021). Numerous pharmaceutical results revealed that polysaccharides of rhizomes have a large set of functions, such as anti-oxidation, anti-herpes, antibacterial, anti-cancer, lowering of blood sugar levels, and lowering of blood lipids, as well as the lung-protective and anti-viral effects (Liu et al., 2004; Li et al., 2018a,b, 2020, 2021; Xie et al., 2020; Gan et al., 2022). For example, polysaccharides that are sequentially extracted from *P. cyrtonema* Hua exhibited anti-cancerous function against cervical cancer Hela cells *via* regulating the cell cycle and the genes related to different apoptosis pathways which are involved in Hela cell cycle arrest and apoptosis (Li et al., 2020). Previous studies also indicated that polysaccharides can act as compatible solutes and enhance abiotic stress tolerance, such as drought and salt stress in plants (Yu et al., 2017, 2021). In recent years, intermediate metabolites and genes related to polysaccharide biosynthesis have been explored in various plants, including *Arabidopsis*, wheat, rice, *Cyclocarya paliurus*, *Cynomorium songaricum*, *Dendrobium officinale*, and *Polygonatum odoratum* (Northcote and Pickett-Heaps, 1966; Meng et al., 2009; Oh et al., 2013; Zhang et al., 2016; He et al., 2017; Zhang et al., 2020; Lin et al., 2021; Wang et al., 2021a). Studies have discovered that polysaccharides are biosynthesized *via* continuous enzymatic reactions from sucrose, requiring invertase (INV), hexokinase (HK), fructokinase (scrK), mannose-6-phosphate isomerase (MPI), phosphomannomutase (PMM), mannose-1-phosphate guanylyltransferase (GMPP), GDP-mannose 4,6-dehydratase (GMDS), GDP-L-fucose synthase (TSTA3), UDP-glucose 4-epimerase (GALE), UDP-glucose 6-dehydrogenase (UGDH), UDP-apiose/xylose synthase (AXS), UDP-arabinose 4-epimerase (UXE), UDP-glucose 4,6-dehydratase (RHM), 3,5-epimerase/4-reductase (UER1), and glycosyltransferase (GT) (**Figure 2**; Zhang et al., 2020). First, sucrose is converted to glucose (Glc) and fructose (Fru) by INV. Then, HK and scrK convert Glc and Fru to glucose-6-phosphate (Glc-6P) and fructose-6-phosphate (Fru-6P), respectively. Later, they are used to synthesize UDP-glucose (UDP-Glc) and guanosine di phosphomannose (GDP-Man). A series of glycosyltransferase (GT) reactions result in the production of polysaccharides.

Recently, some molecular studies on the genes related to polysaccharide biosynthesis of *P. cyrtonema* Hua have been published (Wang et al., 2019; Li et al., 2022). For example, Wang et al. (2019) speculated the multiple genes encoding important enzymes, such as UDP glycosyltransferases (UGTs), and the transcription factors through comprehensive analyses of the transcriptome in leaf, root, and rhizome tissues. Besides, a positively correlated link between polysaccharide accumulation and the *MPI*, *TSTA3*, *AXS*, and *UGDH* transcript levels was also suggested *via* the transcriptome sequencing for rhizomes at different ages (Li et al., 2022).

Plant leaves capture light energy and convert this to carbohydrates, such as 3-phosphoglycerate (PGA) and glyceraldehyde-3-phosphate (GAP), during the process of photosynthesis (Osorio et al., 2014). Then, sucrose is synthesized by sucrose synthase (SUS), sucrose-phosphate

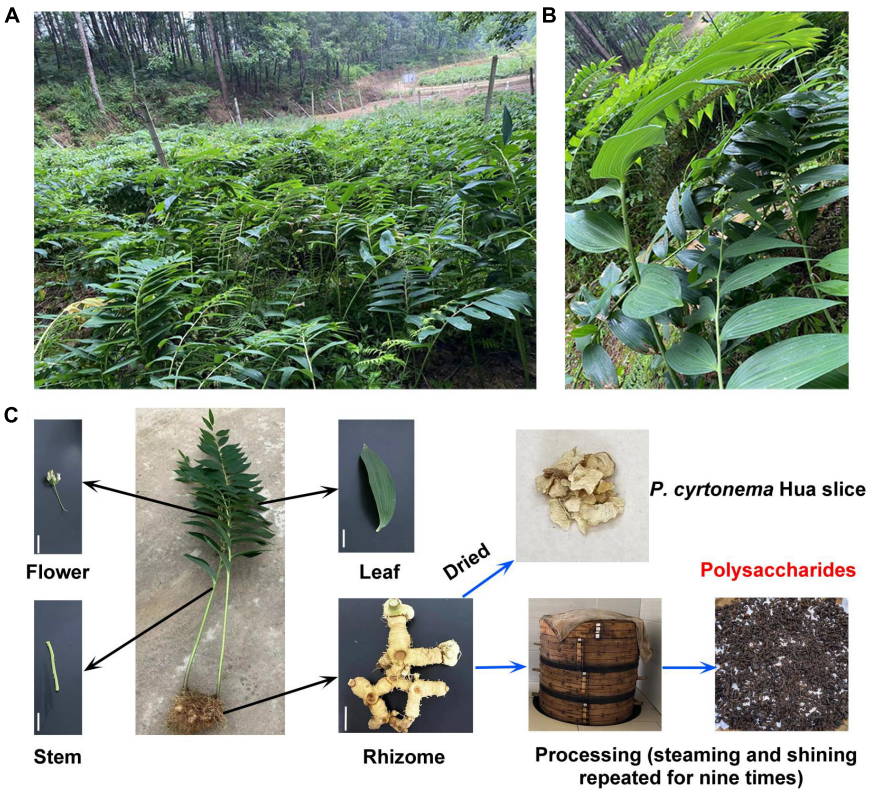

FIGURE 1
Growth environment, phenotype, and processing of *Polygonatum cyrtonema* (*P. cyrtonema*) Hua. **(A)** *P. cyrtonema* Hua is often grown on the mountainside by underwood planting. **(B,C)** The phenotype of the whole and different parts of *P. cyrtonema* Hua. Bar = 5 cm. To date, steaming and drying are the most used methods in the processing of rhizome of *P. cyrtonema* Hua. Polysaccharide (PCP) is one of the most crucial compounds of processed product and contributes to flavor and has health benefits.

synthase (SPS), and sucrose-6-phosphatase (SPP) in the chloroplast during the daytime (**Figure 2**; Osorio et al., 2014). Other enzymes, such as fructose-bisphosphate aldolase (ALDO), fructose-1,6-bisphosphatase (FBP), glucose-6-phosphate isomerase (GPI), phosphoglucomutase (PGM), and UTP-glucose-1-phosphate uridylyltransferase (UGP2), are also involved in the pathway of sucrose synthesis (**Figure 2**). Plants have evolved a complex system to balance the distribution and allocation of carbon (C) (Raines and Paul, 2006; Kircher and Schopfer, 2012). For example, sucrose metabolism is vital for both the allocation of crucial carbon resources and the initiation of hexose-based sugar signals (Koch, 2004). As a pivotal energy substance, sucrose is transported through the vasculature, type, and sink tissues by *SUTs/SUCs* (sucrose transporters or sucrose carriers) and/or *SWEETs* (Sugars Will Eventually be Exported Transporters) and serves as a metabolite for plant growth and development (Feng et al., 2019; Mathan et al., 2021a). These sugar metabolism and transport pathways are mainly controlled by transcription factors, such as *bZIP*, *WRKY*, *bHLH*, *AP2/ERF*, *NAC*, and *MYB* (Sun et al., 2003; Zhu et al., 2011; Phukan et al., 2018; Yang et al., 2021; Wang et al., 2021b; Zhang et al., 2022). Besides, this transporter-regulated sucrose accumulation played a specific role in plant abiotic stress tolerance and adaptation (Chandran, 2015; Eggert et al., 2016). Interestingly, in the rhizome of *P. cyrtonema* Hua, sucrose might act as a precursor for polysaccharide biosynthesis (Wang et al., 2019; Li et al., 2022). However, whether or not, or how polysaccharide accumulation in rhizomes is modulated by sucrose synthesis and transported in leaf and/or stem remains unknown in *P. cyrtonema* Hua.

In this study, we investigated the polysaccharides, sucrose, glucose, and fructose content in different parts (rhizome, stem, leaf, and flower) of *P. cyrtonema* Hua. By the whole-transcriptome analysis, we performed a systematic analysis of polysaccharide biosynthetic genes and estimated the transcript levels of these genes in rhizome, stem, leaf, and flower tissues. Furthermore, several sugar transporters, such as *SWEETs*, *ERDs*, and *SUTs*, were involved in sucrose transport from leaves to stem, rhizome, and flower tissues, thereby coordinately the regulation of the polysaccharide biosynthesis, especially in the rhizome. Finally, we filtrated some key transcription factors, such as *bZIP*, *bHLH*, and *ERF*, which might regulate the above genes related to sucrose metabolism and transport. Briefly, our findings would provide the potential

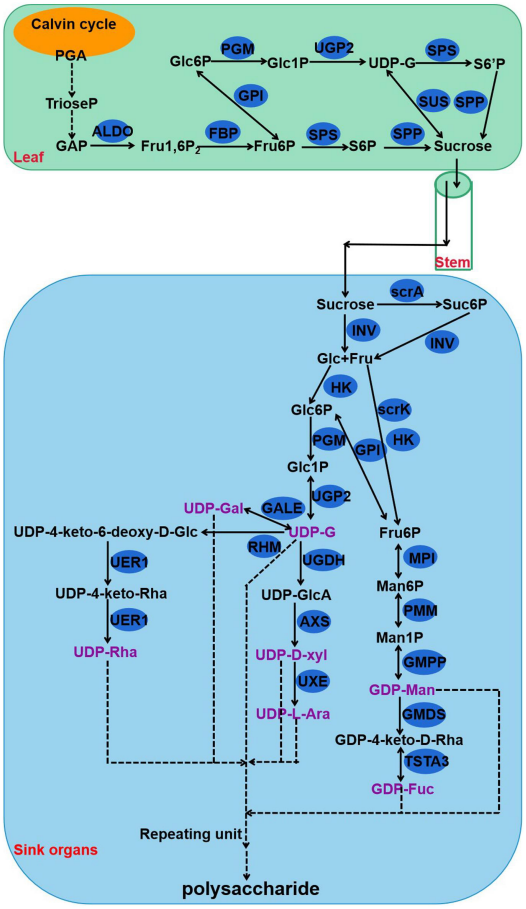

FIGURE 2
The proposed pathway for the biosynthesis of polysaccharides in *Polygonatum cyrtonema*. 3-phosphoglycerate, PGA; Triose phosphate, TrioseP; Glyceraldehyde-3-phosphate, GAP; fructose-1,6-diphosphatase, Fru1,6P; Fructose 6-phosophate, Fru-6P; Sucrose 6-phosophate, S6P; Glucose, Glc; Fructose, Fru; Glucose 6-phosophate, Glc-6P; Glucose 1-phosophate, Glc1P; Sucrose 6′-phosophate, S6′P; Uridine diphosphate glucose, UDP-G; Mannose-6-phosphate, Man6P; Mannose-1-phosphate, Man1P; Guanosine diphosphate mannose, GDP-Man; UDP-4keto-D-rhamnose, GDP-4keto-D-Rha; Guanosine diphosphate fucose, GDP-Fuc; UDP-glucuronic acid, UDP-GlcA; UDP-D-xylose, UDP-D-xyl; UDP-L-arabinose, UDP-L-Ara; UDP-galactose, UDP-Gal; UDP-4-keto-6-deoxy-D-Glucose, UDP-4-keto-6-deoxy-D-Glc; UDP-4-keto-rhamnose, UDP-4-keto-Rha; UDP-rhamnose, UDP-Rha; fructose-bisphosphate aldolase, ALDO; fructose-1,6-bisphosphatase, FBP; glucose-6-phosphate isomerase, GPI; phosphoglucomutase, PGM; UTP-glucose-1-phosphate uridylyltransferase, UGP2; sucrose synthase, SUS; sucrose PTS system EIIBCA or EIIBC component, scrA; sucrose-phosphate synthase, SPS; sucrose-6-phosphatase, SPP; invertase, INV; sucrose synthase, SUS; hexokinase, HK; fructokinase, scrK; mannose-6-phosphate isomerase, MPI; phosphomannomutase, PMM; mannose-1-phosphate guanylyltransferase, GMPP; GDPmannose 4,6-dehydratase, GMDS; GDP-L-fucose synthase, TSTA3; UDP-glucose 4-epimerase, GALE; UDP-glucose 6-dehydrogenase, UGDH; UDP-apiose/xylose synthase, AXS; UDP-arabinose 4-epimerase, UXE; UDP-glucose 4,6-dehydratase, RHM; 3,5-epimerase/4-reductase, UER1.

key regulatory points of polysaccharide accumulation in *P. cyrtonema* Hua.

Materials and methods

Plant materials and growth conditions

Plants of *P. cyrtonema* Hua were collected on May 20 from the *P. cyrtonema* Hua germplasm conservation and breeding base at Jinzhai County in Anhui Province, China. They were identified by Associate Professor Yujun Liu (Anhui Promotion Center for Technology Achievements Transfer, Anhui Academy of Science and Technology). Plants were cleaned and dried on filter paper, and then imaged using a Canon IXUS 130 camera. Meanwhile, rhizomes, leaves, stems, and flower parts were sampled, and immediately frozen in liquid nitrogen and stored at −80°C.

Measurement of the polysaccharide, glucose, fructose, and sucrose content

Rhizomes, leaves, stems, and flower parts of *P. cyrtonema* Hua were oven-dried at 70°C to constant weight. Then, the dried samples were ground into powder using the grinding mill and kept in a glassware dryer, and further used for the determination of polysaccharide, glucose, fructose, and sucrose content.

Total polysaccharides were extracted and detected from different dried tissues of *P. cyrtonema* Hua by the anthrone-sulfuric acid method in the Chinese Pharmacopoeia Commission (2020). Briefly, 0.2 g of samples was weighed into a round-bottom flask with 120 mL of 80% ethanol, and boiled for 1 h to remove the small organic compounds and pigments. Afterward, 120 mL of distilled water was added and extracted at 80°C for another 1 h. The supernatant was transferred and diluted in a 250 mL volumetric flask. Polysaccharide content was determined spectrophotometrically by measuring the absorbance at 582 nm with 1 mL of extract, 1 mL of distilled water, and 8 mL of 0.2% anthrone-sulfuric acid solution. The concentration was calculated according to the standard curve of glucose.

Sucrose in different tissues of *P. cyrtonema* Hua was extracted and determined as previously described (Feng et al., 2019). Samples were homogenized with 1 mL of extracting solution, heated to 80°C in a water bath for 10 min, and then centrifuged (10,000 × *g*; 25°C) for 15 min. About 5 mg of activated carbon was added to the supernatant for decoloring at 80°C for 30 min. After the solution was cooled to room temperature, 60 μL of 0.1 M NaOH solution was added to 100 μL of the supernatant in a 100°C water bath for 5 min. Then, 700 μL of 10 M HCl and 200 μL of 0.1% resorcinol were added to a 100°C water bath for 10 min. After cooling, the

sucrose content was determined and calculated by measuring the absorbance at 480 nm.

Glucose in different tissues of *P. cyrtonema* Hua was extracted and determined using the Glucose Assay Kit (Solarbio Life Sciences, Beijing, China) according to the manufacturer's instructions. Samples were homogenized with 1 mL of H_2O and heated to 80°C in a boiling water bath for 10 min, and then centrifuged (10,000 × *g*; 25°C) for another 10 min. Glucose concentration was determined by a glucose oxidase enzyme system and calculated by measuring the absorbance at 505 nm.

Fructose in different tissues of *P. cyrtonema* Hua was extracted and determined using the Fructose Assay Kit (Solarbio Life Sciences, Beijing, China) according to the manufacturer's instructions. Samples were homogenized with 1 mL of extracting solution, heated to 80°C in a water bath for 10 min, and then centrifuged (10,000 × *g*; 25°C) for 10 min. About 5 mg of activated carbon was added to the supernatant for decoloring at 80°C for 30 min. After the solution cooled to room temperature, 1.4 mL of 10 M HCl and 400 μL of 0.1% resorcinol were added to 200 μL of supernatant in a 100°C water bath for 10 min. After cooling, the fructose content was determined and calculated by measuring the absorbance at 480 nm.

Total RNA extraction, cDNA library construction, and sequencing

Total RNA of different tissues (rhizome, stem, leaf, and flower) of P. cyrtonema Hua was extracted using the Trizol reagent (Invitrogen, Carlsbad, CA, USA) according to the manufacturer's instructions. RNA concentration and quality were checked using the NanoDrop 2000 (Thermo Fisher Scientific, Inc., Waltham, MA, USA). Sequencing libraries were generated using the TruSeq RNA Sample Preparation Kit (Illumina Inc., San Diego, CA, USA) by using three biological replicates according to the manufacturer's instructions. Then, the libraries were sequenced using the next-generation sequencing (NGS) and Illumina HiSeq. Enrichment of mRNA, fragment interruption, addition of adapters, size selection, CR amplification, and RNA-Seq were performed by staff at Personal Biotechnology Co., Ltd., Shanghai, China.

Differential gene expression analysis

After the data filtration, the unigene set of sequences was constructed by the clean reads with high-quality samples using Trinity v2.10.0. The fragments per kilobase million (FPKM) of transcript sequence presented the expression level of each gene in each library. To determine the transcriptional changes among different parts of *P. cyrtonema* Hua, differentially expressed genes (DEGs) were identified by comparing the expression levels in rhizome vs. stem, rhizome vs. leaf, and rhizome vs. flower, respectively. Transcripts with $|\log_2\text{FoldChange}| > 1$ and P-value < 0.05 were considered as the thresholds for significant differences, which was performed by DEGseq 2.

Kyoto encyclopedia of genes and genome and gene ontology enrichment analysis

All unigenes were annotated against the Kyoto Encyclopedia of Genes and Genome (KEGG) and Gene ontology (GO). KEGG annotation[1] was performed to identify the metabolic pathways of genes. GO classifications[2] were obtained according to molecular function, biological process, and cellular component. Over-represented KEGG and GO terms were detected *via* Fisher's exact test, and multi-test adjustment was made using the Yekutieli (FDR under dependency) method with a cutoff of FDR < 0.05.

Statistical analysis

Statistical analysis was performed using SPSS 18.0 software. Values were mean values and SD of three independent experiments with three replicates for each. For statistical analysis, data were analyzed by one-way analysis of variance (ANOVA) followed by Duncan's multiple range test. P-values < 0.05 were considered statistically significant. The correlation coefficient between polysaccharide, sucrose, glucose, and fructose content and gene expression levels was analyzed *via* Pearson's correlation coefficient and Student's t-test ($^*P < 0.05$, $^{**}P < 0.01$, $^{***}P < 0.001$).

Results

Sugar composition in rhizome, stem, leaf, and flower tissues of *Polygonatum cyrtonema* Hua

Since sucrose is the major transportable form of photosynthate from source leaves to sink organs, we tested the polysaccharides, sucrose, glucose, and fructose contents in rhizome, stem, leaf, and flower tissues to unravel the mechanism underlying the polysaccharide biosynthesis in *P. cyrtonema* Hua (**Figures 1**, **3**). Among them, the polysaccharide content of rhizome was the highest (93.87 $mg{\cdot}g^{-1}DW$), followed by flower (59.03 $mg{\cdot}g^{-1}DW$), and lowest in stem (14.51 $mg{\cdot}g^{-1}DW$) (**Figure 3A**). We also found that sucrose and fructose levels

1 http://www.genome.jp/kegg

2 http://geneontology.org

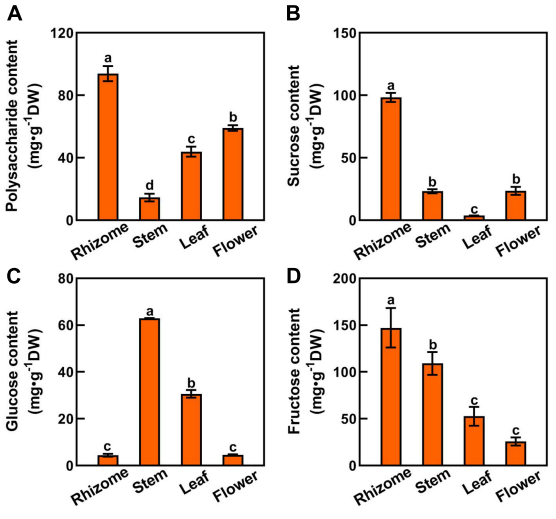

FIGURE 3
Sugar composition in different parts of *P. cyrtonema*. **(A–D)** Polysaccharide, sucrose, glucose, and fuctose content of rhizome, stem, leaf, and flower tissues of *P. cyrtonema*. Data represent mean ± SD (n = 3). Bars with different letters denote significant differences at $P < 0.05$ according to Duncan's multiple comparison test.

were higher in the rhizome than in the stem, leaf, and flower (Figures 3B,D). In contrast, the glucose content of the stem was the highest, followed by the leaf (Figure 3C). It was lowest in both rhizome and flower of *P. cyrtonema* Hua (Figure 3C). The above results clearly suggested that the polysaccharides are synthesized in rhizome, stem, leaf, and flower tissues. Meanwhile, the biosynthesis and transport of sucrose, glucose, and fructose in the leaf and stem significantly impacted the polysaccharide accumulation in the rhizome and flower of *P. cyrtonema* Hua.

Transcriptional analysis showed the overview of gene expression profiles among the different tissues

To elucidate the molecular mechanisms of polysaccharide biosynthesis, a genome-wide transcriptional analysis was performed in the rhizome, stem, leaf, and flower tissues of *P. cyrtonema* Hua. For transcriptomic analysis, total RNA was extracted and used to prepare cDNA libraries by using three biological replicates. After processing, the raw sequence reads (between 42,336,126 and 52,068,538 clean reads in total) were aligned, and the Q20% (the percentage of bases with a Phred value >20) value for the clean reads was >97% and the Q30% (the percentage of bases with a Phred value >30) value of the clean reads was >92% and were found to map (Supplementary Table 1). A total of 182,700 unigenes were assembled. With regard to the unigenes, the total length and mean length of the unigenes were 157,174,631 and 860.29 bp, respectively, and their GC% was 44.78% (Supplementary Table 2). These results implied that high-quality sequencing data were obtained for the following analyses.

In order to construct a detailed regulatory network for polysaccharide biosynthesis in different tissues, we compared differentially expressed genes (DEGs) between stem and rhizome, leaf and rhizome, and flower and rhizome, respectively. The DEGs were filtered by expression levels | log 2 (fold-change)| > 1 and FDR < 0.05 in each pairwise comparison, thus revealing 7,054 (3,963 up- and 3,091 downregulated) DEGs in stem/rhizome, 13,468 (7,440 up- and 6,028 downregulated) DEGs in leaf/rhizome, and 19,437 (18,010 up- and 1,427 downregulated) DEGs in flower/rhizome (Figure 4A). Then, we constructed a Venn diagram to investigate the numbers of co-expressed and uniquely expressed DEGs in each pairwise comparison. A total of 953 co-expressed DEGs were obtained among these (Figure 4B). Additionally, hierarchical clustering analysis showed that strong changes in DEG expression levels were observed in the different tissues (Figure 4C).

Functional annotation and expression overview of unigenes

The above-assembled unigenes were searched and annotated in NR, GO, KEGG, PFAM, eggNOG, and Swiss prot databases using the BLAST algorithm. Our results showed that 49.47, 21.77, 20.66, 30.53, 40.79, and 37.27% unigenes were annotated as significant hits in NR, GO, KEGG, PFAM, eggNOG, and Swiss prot databases, respectively (Supplementary Table 3).

To understand the biological processes and pathways involved in polysaccharide biosynthesis, Kyoto Encyclopedia of Genes and Genomes (KEGG) and Gene Ontology (GO) pathway-based enrichment analyses were performed (Figures 5, 6). The results showed that the top 20 pathway classifications with the smallest FDR value were selected by KEGG pathway-based enrichment analysis due to the DEGs between the rhizome and stem, leaf, or flower group (Figure 5A). Among these, genes related to photosynthesis, carbon fixation in photosynthetic organisms, galactose metabolism, and starch and sucrose metabolism processes were significantly enriched. Then, we screened 15 pathway classifications from the DEGs related to carbohydrate metabolism, which are most likely associated with polysaccharide biosynthesis, such as starch and sucrose metabolism, fructose and mannose metabolism, glycolysis/gluconeogenesis, and pentose and glucuronate interconversions (Figure 5B and Supplementary Table 4). For example, there were 52, 103, and 206 DEGs involved

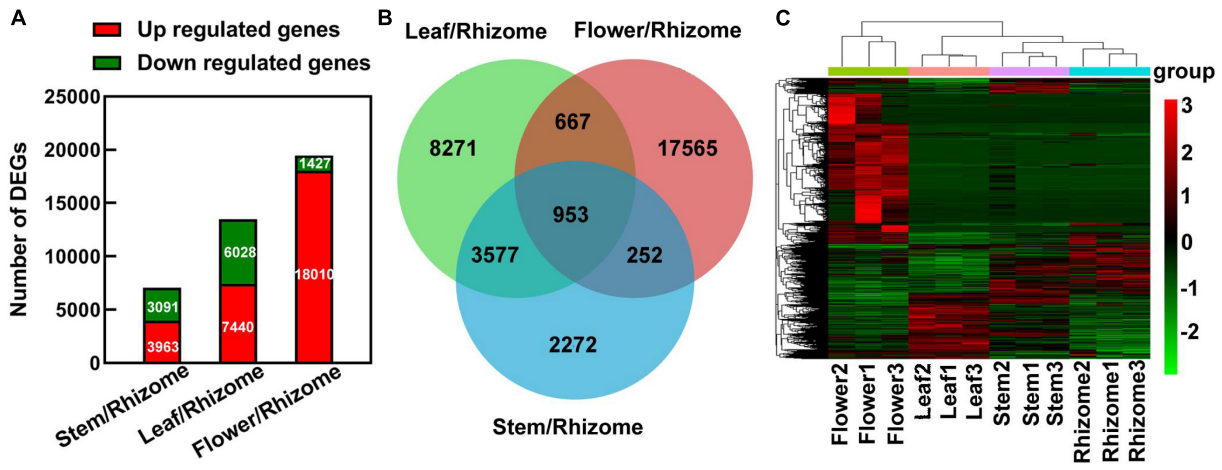

FIGURE 4
An overview of differentially expressed genes (DEGs) responsive to different parts of *Polygonatum cyrtonema*. **(A)** The number of DEGs was examined in the comparison between rhizome and stem, leaf, or flower. **(B)** Venn diagram showing the distribution of DEGs in the comparison between rhizome and stem, leaf, or flower. **(C)** Hierarchical clustering represents relative expression levels of DEGs in comparison between rhizome and stem, leaf, or flower. Multiple of differential expression [foldChange (Case/Control)]: foldChange (stem/rhizome), foldChange (leaf/rhizome), and foldChange (flower/rhizome). $\log_2$FoldChange > 1, *P*-value < 0.05. Red indicates upregulated genes, and green indicates downregulated genes.

in starch and sucrose metabolism among stem/rhizome, leaf/rhizome, and flower/rhizome, respectively. Moreover, GO pathway analysis revealed that there were numerous DEGs in the polysaccharide metabolic process, including cellular/cell wall polysaccharide biosynthetic and catabolic processes, directly related to polysaccharide biosynthesis in *P. cyrtonema* Hua (**Figure 6** and **Supplementary Table 5**).

Identification of genes involved in polysaccharide biosynthesis

To further comprehend the polysaccharide biosynthesis in different tissues, we compared DEGs between stem and rhizome, leaf and rhizome, and flower and rhizome, respectively (**Figure 7** and **Supplementary Table 6**). We found that 67 genes involved in polysaccharide biosynthesis showed significant differences in expression, such as *MPI*, *GMPP*, *GMDS*, *GALE*, and *RHM* (**Figure 7**). Interestingly, the transcript levels of *GMPP* (*DN3245_c1_g2*), *GMDS* (*DN608_c0_g1*), and *RHM* (*DN155122_c0_g1*) were lower in stem, leaf, and flower compared to these of rhizome, respectively. Moreover, multiple genes involved in sucrose metabolism, including sucrose synthesis and degradation, were also discovered, such as *SPS*, *SUS*, and *INV*. As expected, the transcript levels of *SPS* (*DN19938_c0_g1*) and *SUS* (*DN15329_c0_g1*) were higher in the leaf than in other tissues. Similarly, most of the genes involved in the glycolysis/gluconeogenesis pathway, such as *ALDO*, *FBP*, *GPI*, *PGM*, and *UGP2* transcript levels, showed a similar tendency. Besides, *PGM* (*DN27690_c0_g1* and *DN5147_c0_g1*), *GPI* (*DN12212_c0_g1*), *FBP* (*DN17750_c0_g1*), and *UGP2* (*DN2305_c0_g1* and *DN2305_c0_g2*) were mainly expressed in the flower tissues of *P. cyrtonema* Hua.

Identification of genes involved in sugar transport

Sugar transporters play key roles in source-sink dynamics, which is important for carbon distribution and plant growth (Hennion et al., 2019). Thus, we analyzed the expression levels of *SWEETs*, *SUTs*, *ERDs*, *MSTs*, *PLSTs*, and *STPs* in the different tissues of *P. cyrtonema* Hua (**Figure 8** and **Supplementary Table 7**). As shown in **Figure 8**, *SWEET* (*DN60284_c0_g1*) was mainly expressed in both leaf and stem, *SWEET* (*DN6616_c0_g1*) was mainly expressed in both stem and flower, and other *SWEETs* and *ERDs* were mainly expressed in stem and/or rhizome. *SUT* (*DN6616_c0_g1*) was mainly expressed in both rhizome and flower, and *SUT* (*DN2552_c0_g1*) was mainly expressed in both leaf and stem. Additionally, most of the monosaccharide transporters (*MSTs*), plastidic glucose transporters (*PLSTs*), and sugar transport proteins (*STPs*) were mainly expressed in the leaf. Combined with the content of sugar compositions, the above results indicated that these transporters might play important roles in the source-sink dynamics, especially in the accumulation of polysaccharides.

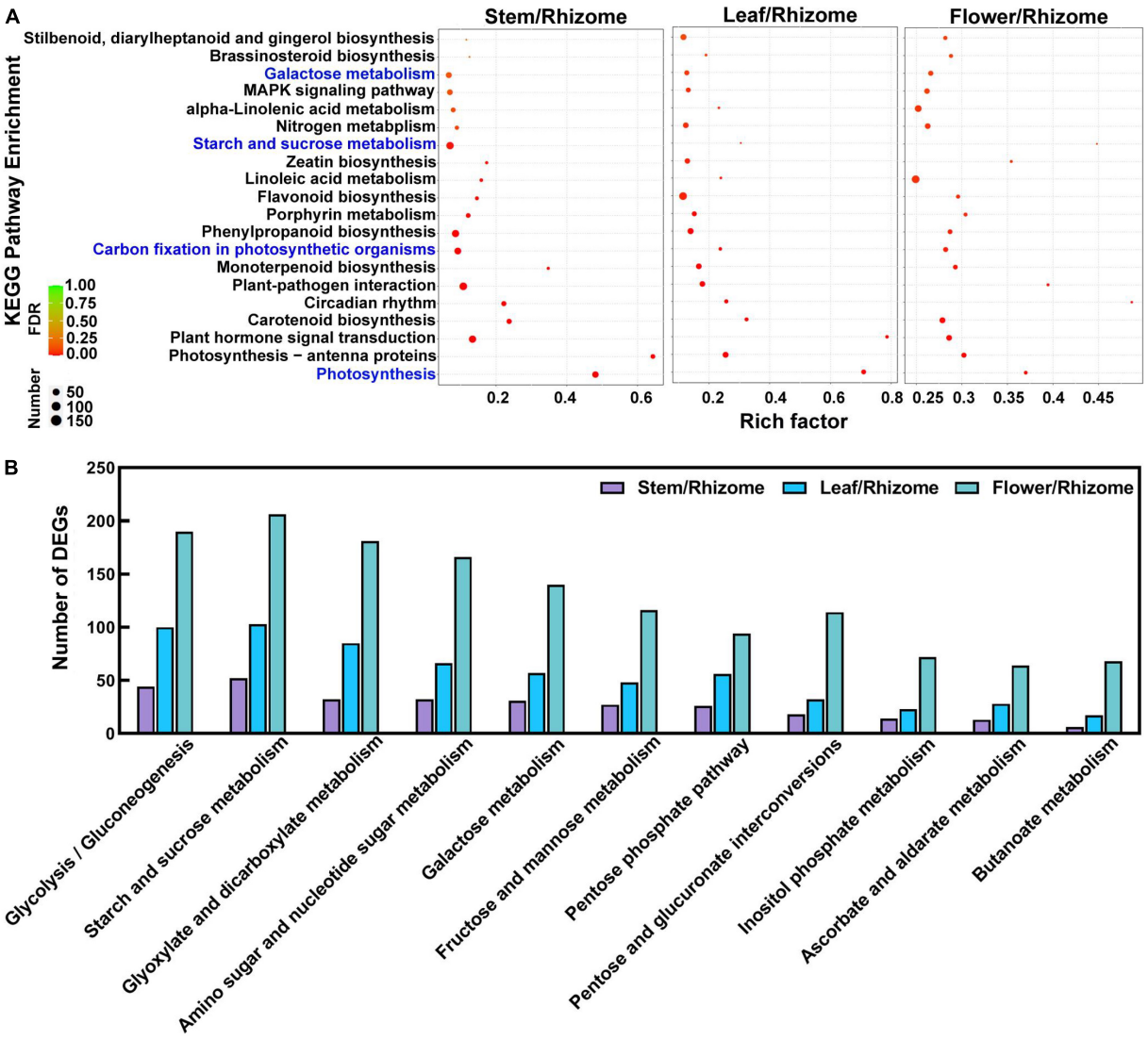

FIGURE 5
Functional enrichment analysis of differentially expressed genes (DEGs) by Kyoto Encyclopedia of Genes and Genomes (KEGG) pathway-based enrichment analysis. **(A)** The top 20 pathway classifications with the smallest FDR value were selected by KEGG pathway-based enrichment analysis due to the DEGs between rhizome and stem, leaf, or flower group. **(B)** The 11 pathway classifications for carbohydrate metabolism. Rich factor indicates the matched gene ratio, the circle size is proportional to the target gene number, and 0 < FDR (false discovery rate) <1.

Correlation between the polysaccharide accumulation and expression levels of genes related to polysaccharide biosynthesis and sugar transporters in different tissues

To get further insight into the regulation of polysaccharide accumulation, we next analyzed the correlation between polysaccharide, sucrose, glucose, and fructose contents and the expression levels of genes related to polysaccharide biosynthesis and sugar transporters in the rhizome, stem, leaf, and flower tissues (Figure 9). Here, we found sucrose content was generally and positively correlated with polysaccharide content ($r = 0.79$), while glucose content showed a significant negative correlation ($r = -0.90$). There was a highly significant correlation between the expression levels of *GPI* (*DN21137_c0_g1*), *SUS* (*DN7836_c0_g1*), *INV* (*DN56_c0_g1*, *DN1439_c0_g3*, *DN534_c0_g1*, *DN16555_c0_g3*, *DN534_c0_g2*, and *DN1915_c3_g2*), *HK* (*DN26120_c0_g1*), *scrK* (*DN7502_c0_g2*, *DN7502_c0_g1*, and *DN6713_c0_g1*), *MPI* (*DN8158_c0_g1*), *GMPP* (*DN3245_c1_g2*), *GMDS* (*DN608_c0_g1*), *GALE* (*DN159955_c0_g2* and *DN11833_c0_g1*), *ERD* (*DN8548_c0_g1*), and sucrose content. We also observed that the expression of *ALDO* (*DN89008_c1_g1*), *FBP*

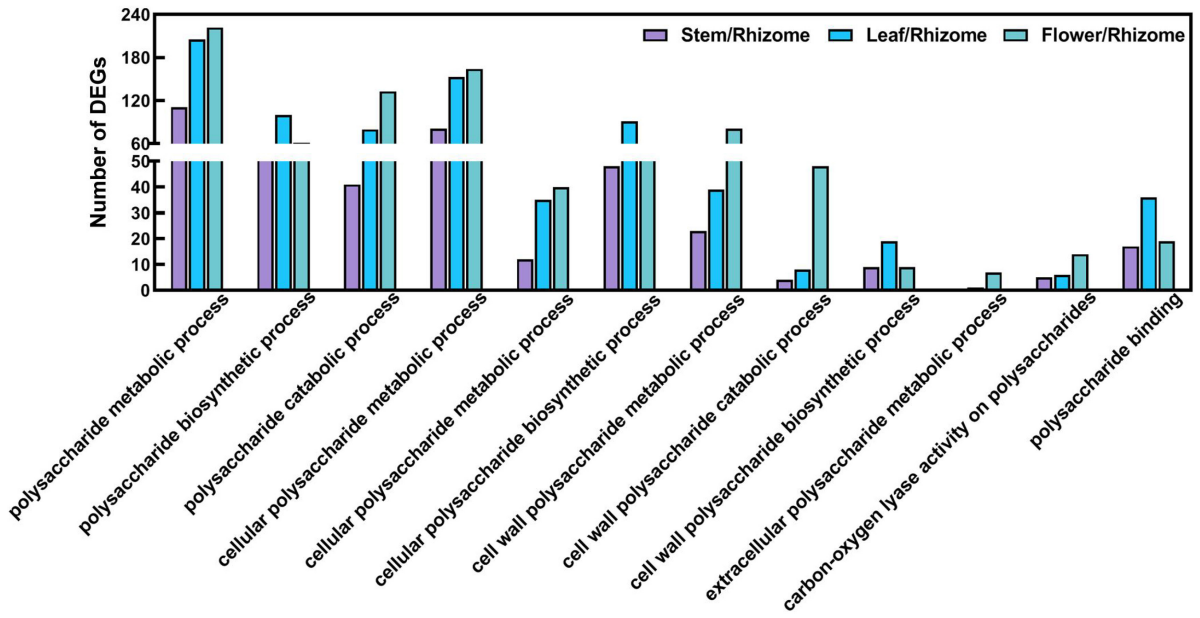

FIGURE 6
Functional enrichment analysis of differentially expressed genes (DEGs) by Gene Ontology (GO) pathway-based enrichment analysis. The 12 pathway classifications for the polysaccharide metabolism were selected by GO pathway-based enrichment analysis due to the DEGs between rhizome and stem, leaf, or flower group.

(*DN13010_c0_g1*), *UGP2* (*DN681_c1_g1*), and *SPS* (*DN48694_c1_g2*) showed high positive correlation with the glucose content. Besides, the expression of *scrK* (*DN7502_c0_g1*) and *GALE* (*DN159955_c0_g2*) was positively and negatively correlated with fructose content, respectively. Moreover, the expression levels of *SUS* (*DN2037_c0_g1* and *DN7836_c0_g1*), *INV* (*DN534_c0_g2*), *SWEET* (*DN32250_c0_g1*), and *PLST* (*DN32250_c0_g1*) genes significantly correlated with polysaccharide content. These results suggested that the above genes were involved in the polysaccharide biosynthesis in *P. cyrtonema* Hua.

Identification of transcription factors involved in polysaccharide accumulation

To explore the transcriptional regulation of genes related to polysaccharide accumulation, we next analyzed the transcription factors (TFs) in the rhizome, stem, leaf, and flower tissues of *P. cyrtonema* Hua. We found that 2,728 TFs were significantly up/downregulated (**Figure 10**). The major TF families were screened, including bHLH (296 unigenes), ERF (163 unigenes), MYB_related (158 unigenes), C2H2 (157 unigenes), NAC (147 unigenes), B3 (135 unigenes), FAR (131 unigenes), bZIP (119 unigenes), MYB (109 unigenes) groups (**Figure 10A** and **Supplementary Table 8**). Then, we constructed the co-expression network according to the differentially expressed transcription factors and sugar metabolism and transport genes (**Figure 10B**). There were 87 genes related to sugar metabolism and transport genes that presented very high correlations. For example, the *UGP2* (*DN681_c1_g1*) expression was highly and positively correlated with *bZIP* (*DN16926_c0_g1*), *bHLH* (*DN918_c1_g1*), and *ERF* (*DN25257_c0_g1*) expression (r = 0.96, 0.95, 0.98, $p < 0.001$). These results suggested that transcription factors might be involved in polysaccharide accumulation by regulating the expression of sugar metabolism and transport genes.

Discussion

Sugar accumulation pattern in different tissues of *Polygonatum cyrtonema* Hua

As bioactive ingredients, polysaccharides are of great value in the merits of medicinal plants (Li et al., 2021). Because rhizomes are the harvested targets, some studies have shown that rhizomes of *P. cyrtonema* Hua accumulated high content of polysaccharides, and unearthed several key genes involved in polysaccharide biosynthesis pathway from rhizomes at different ages by transcriptome sequencing (Li et al., 2022). Besides, polysaccharide accumulation is also highly cultivar- and tissue-dependent (Wang et al., 2019; Hu et al., 2022). For instance, Wang et al found that polysaccharide content was low in the leaf (1.62%) (Wang et al., 2019).

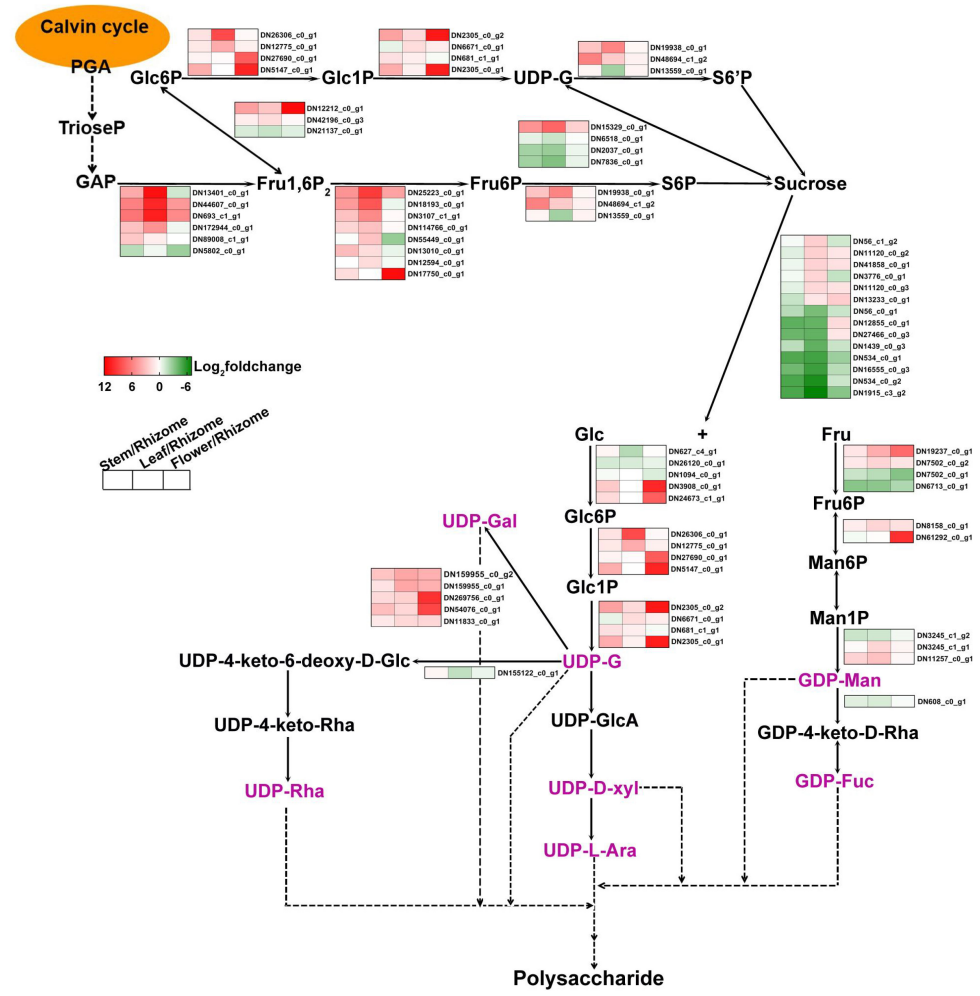

FIGURE 7
Heat map illustrating major expression profiles of differentially expressed genes (DEGs) involved in polysaccharide biosynthesis. Red indicates high expression, white indicates intermediate expression, and green indicates low expression.

Most of the studies on polysaccharide accumulation were performed by examining the gene expression involved in the proposed pathway from sucrose to polysaccharide (Wang et al., 2019; Li et al., 2022). Furthermore, sucrose is the main form that is transported from source leaves to different sinks *via SWEETs*, *SUTs*, and/or *ERDs* transporters (Julius et al., 2017). Previous developments indicated that the role of sucrose synthase involved in sucrose import may play a role in directing carbon toward polysaccharide biosynthesis (Koch, 2004). Therefore, polysaccharide accumulation is dynamic and highly regulated. However, whether or how sucrose metabolism is involved in polysaccharide accumulation of shoots and rhizomes remains to be investigated in *P. cyrtonema* Hua.

In this report, we clearly observed that polysaccharides highly accumulated in rhizome tissue, which is consistent with the previously published results (**Figure 3A**; Wang et al., 2019). In addition, our results also indicated that sucrose and fructose levels were higher in the rhizome than in stem, leaf, and flower tissues (**Figures 3B,D**). In contrast, glucose content was lower in both the rhizome and flower of *P. cyrtonema* Hua (**Figure 3C**). Then, we analyzed the correlation between polysaccharide content and sucrose, glucose, or fructose in different tissues, respectively (**Figure 9**). These results demonstrated that the contents of sucrose and glucose were generally correlated with polysaccharide content. This was consistent with the regulation of sugar metabolism in rhizomes of *P. cyrtonema* Hua and *P. sibiricum* Red (Hu et al., 2022). Sugars were involved in most of the metabolic and signaling pathways controlling plant growth and development, as well as the responses to abiotic stresses. For example, leaf-derived sucrose accumulated in large amounts in the hypocotyls of tomato plants under flooding stress conditions

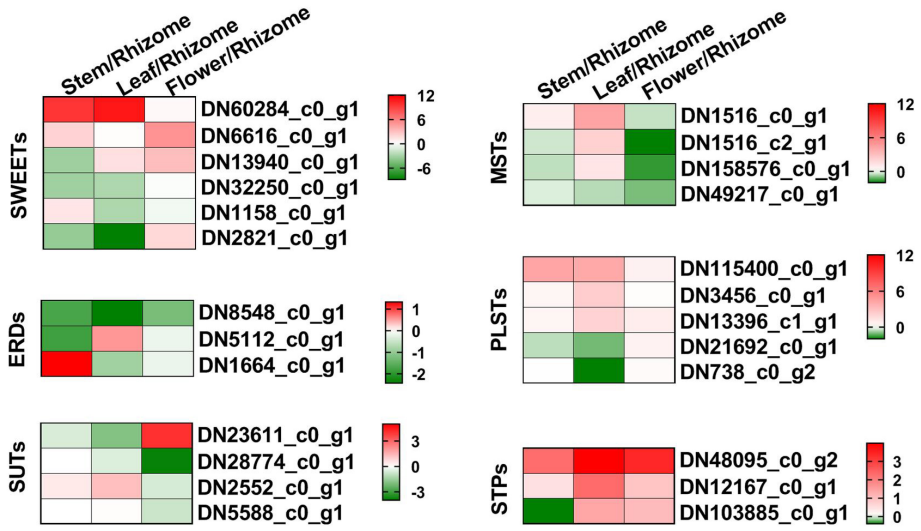

FIGURE 8
Heat map illustrating major expression profiles of differentially expressed genes (DEGs) related to the sugar transport. Sugar will eventually be exported transporters, SWEET; early response to dehydration, ERD; H + /sucrose transporters, SUT/SUC; monosaccharide transporters, MST; plastidic glucose transporter, PLST; sugar transport protein, STP. Red indicates high expression, white indicates intermediate expression, and green indicates low expression.

(Mignolli et al., 2021). The above results suggested that sucrose metabolism might be involved in regulating the polysaccharide accumulation, which might play a critical role in tolerance to abiotic stresses in *P. cyrtonema* Hua.

Response networks of the expression of polysaccharide biosynthesis and sugar transporter genes

The previous studies showed that a few hundred unigenes were involved in the sugar metabolism pathway. They found that the expression levels of unigenes encoding sacA, RHM, MPI, GMDS, TSTA3, UER1, and UGE enzymes were higher in rhizomes compared to leaves, while the expression levels of unigenes encoding *HK*, *scrK*, *UGP2*, *GPI*, *GMPP*, *GALE*, *UXE*, and *UGDH* were higher in leaves (Wang et al., 2019; Li et al., 2022). Combined with the sugar accumulation pattern in the above results, these findings led us to explore the regulation of the expression of polysaccharide biosynthesis genes in response to polysaccharide accumulation in rhizome, stem, leaf, and flower during the growth of *P. cyrtonema* Hua.

In this report, we analyzed the correlation between the expression of polysaccharide and sucrose biosynthesis pathway genes and polysaccharide, sucrose, or glucose content in rhizome, stem, leaf, and flower tissues, respectively. These results demonstrated that the expression of polysaccharide biosynthesis pathway genes is generally correlated with polysaccharide content in rhizomes (**Figures 3**, 7). Additionally, there were several unigenes, such as *HK* (*DN3908_c0_g1* and DN24673_*c1_g1*), *MPI* (*DN61292_c0_g1*), and *GALE* (*DN259756_c0_g1* and *DN54076_c0_g1*), specifically expressed in flowers, which are beneficial to polysaccharide biosynthesis in flowers (**Figure 7**). These results suggested that polysaccharide accumulation is generally regulated at the transcription level of polysaccharide biosynthesis genes.

In plants, sucrose, as an important form, is delivered to different tissues for metabolism and storage by the phloem (Hennion et al., 2019). This is apoplastically mediated through *SWEET*, *SUT/SUC*, and *EDR6* transporters (Stadler et al., 1995; Kiyosue et al., 1998; Milne et al., 2018; Chen et al., 2010, 2012). The molecular mechanisms of sugar transport, especially sucrose transport, are largely unknown in *P. cyrtonema* Hua. In this study, we found that there were several DEGs involved in sugar transport among rhizome, stem, leaf, and flower tissues (**Figure 8**). For example, *SWEET* (*DN60284_c0_g1*) was specifically expressed in both leaf and stem, while *SWEET* (*DN2821_c0_g1*) was specifically expressed in the rhizome. *SUT* (*DN23611_c0_g1*) was specifically expressed in the flower. These results suggested that the above genes showed different roles in sugar efflux and/or uptake, thereby participating in polysaccharide biosynthesis. Previous results showed that *OsSWEET13* and *OsSWEET15* genes modulated sucrose transport and distribution to maintain sugar homeostasis

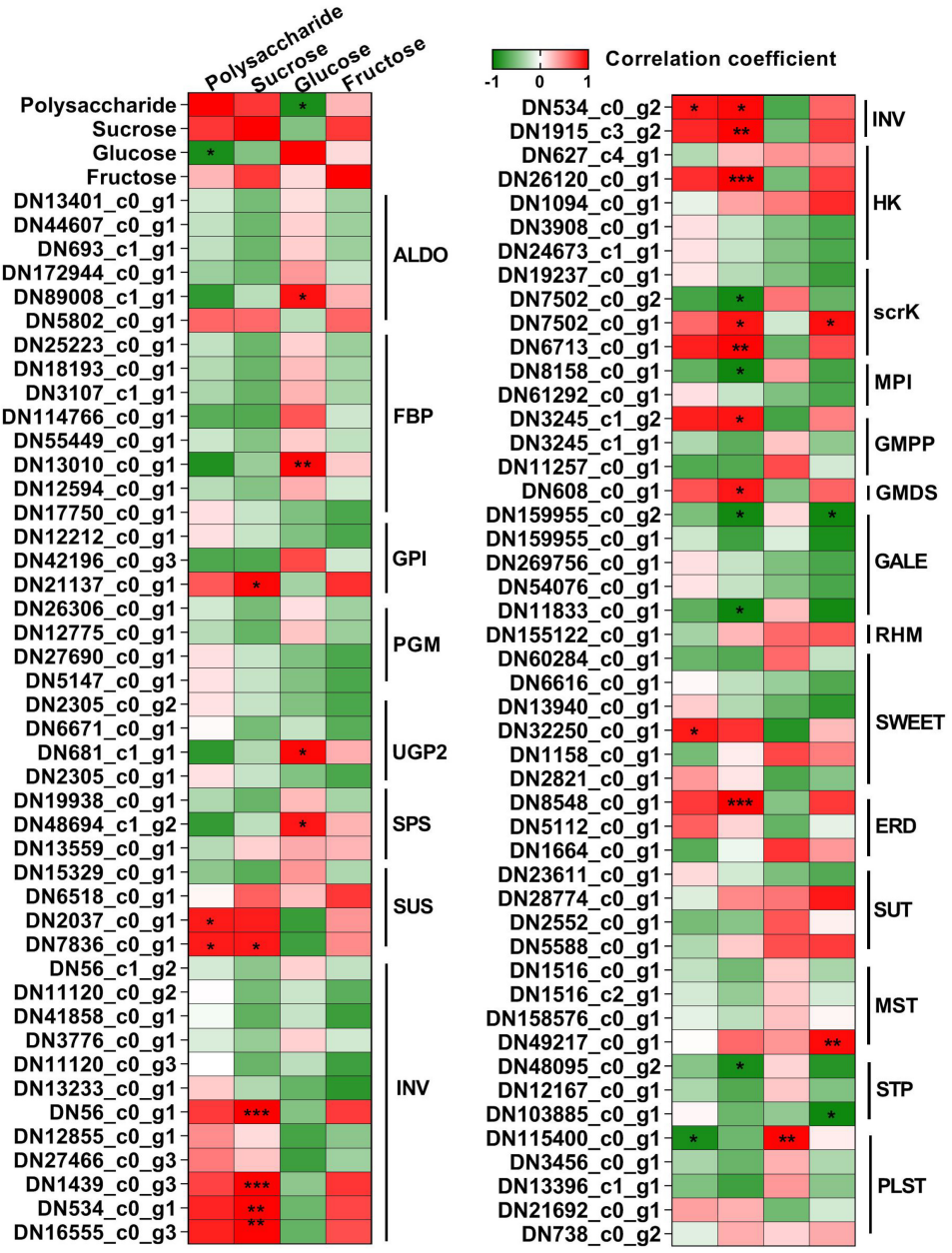

FIGURE 9
Heat map of the correlation coefficients between polysaccharide, sucrose, glucose, and fructose and the expression levels of genes related to sugar metabolism and transport in different tissues. Asterisks represent statistical significance determined by Student's *t*-test (*$P < 0.05$, **$P < 0.01$, and ***$P < 0.001$).

in response to drought and salinity stresses (Mathan et al., 2021b). It was also found that *AtSWEET17* was predicted to act as a vacuolar fructose importer, with a function in sequestering excess cytosolic fructose into vacuoles for storage in roots (Chardon et al., 2013). *AtSWEET16* overexpression increased the vacuolar sucrose and glucose accumulation to improve the freezing tolerance in *Arabidopsis* (Klemens et al., 2013). Furthermore, *AtSWEET15* was strongly induced by osmotic stresses, including cold, high salinity, and drought (Seo et al., 2011). It is also worth noting that both glucose content and plastidic glucose transporter (*PLST* and *DN115400_c0_g1*) expression showed a significantly negative correlation with polysaccharide content. Thus, the biological functions of these transporters should be further elucidated in *P. cyrtonema* Hua in the future.

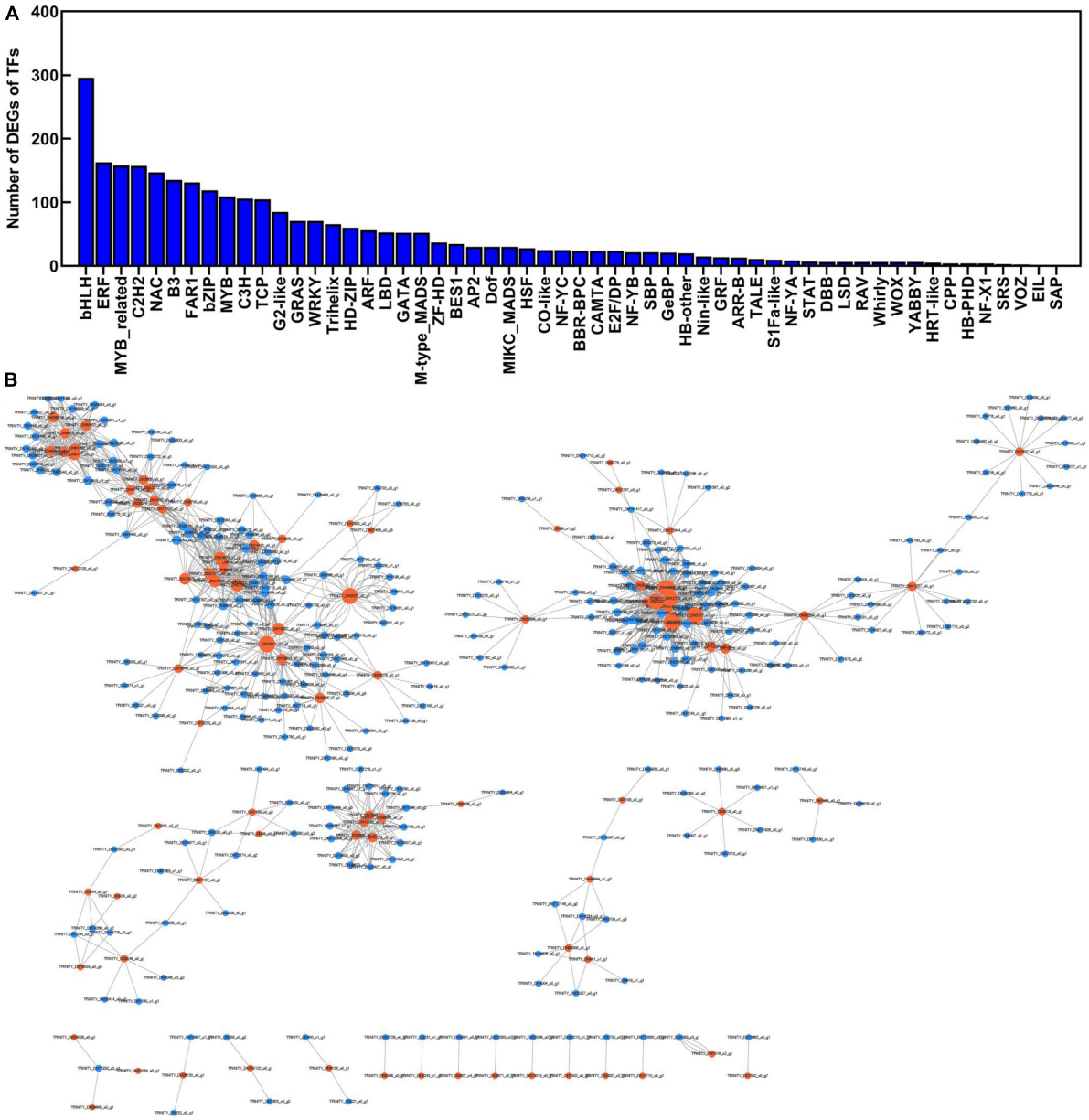

FIGURE 10
The co-expression network was constructed according to the differentially expressed transcription factors and sugar metabolism and transport genes in different tissues of *Polygonatum cyrtonema* Hua. **(A)** Type and number of transcription factors (TFs) of *P. cyrtonema* Hua. **(B)** The correlation coefficients of expression levels between transcription factors and sugar metabolism and transport in different tissues.

Putative key genes involved in the regulation of the sugar metabolism and homeostasis

In this study, we observed that the expression of sucrose synthesis and decomposition genes correlated differently with sucrose and polysaccharide contents among the different tissues (**Figure 9**). For example, *SUS* (*DN2037_c0_g1* and *DN7836_c0_g1*) and *INV* (*DN534_c0_g2*) transcripts positively correlated with the polysaccharide content. Emerging evidence had shed light on the potential role of *INVs* in the response to abiotic stress in various plant species (Dahro et al., 2016). Therefore, the vital role of *INV* in alleviating the abiotic stress in *P. cyrtonema* Hua needs to be explored in the future. Furthermore, the correlation between sucrose contents and the expression of polysaccharide biosynthesis genes was also discovered, such as *MPI* (*DN8158_c0_g1*), *GMPP* (*DN3245_c0_g2*), *GMDS* (*DN608_c0_g1*), and

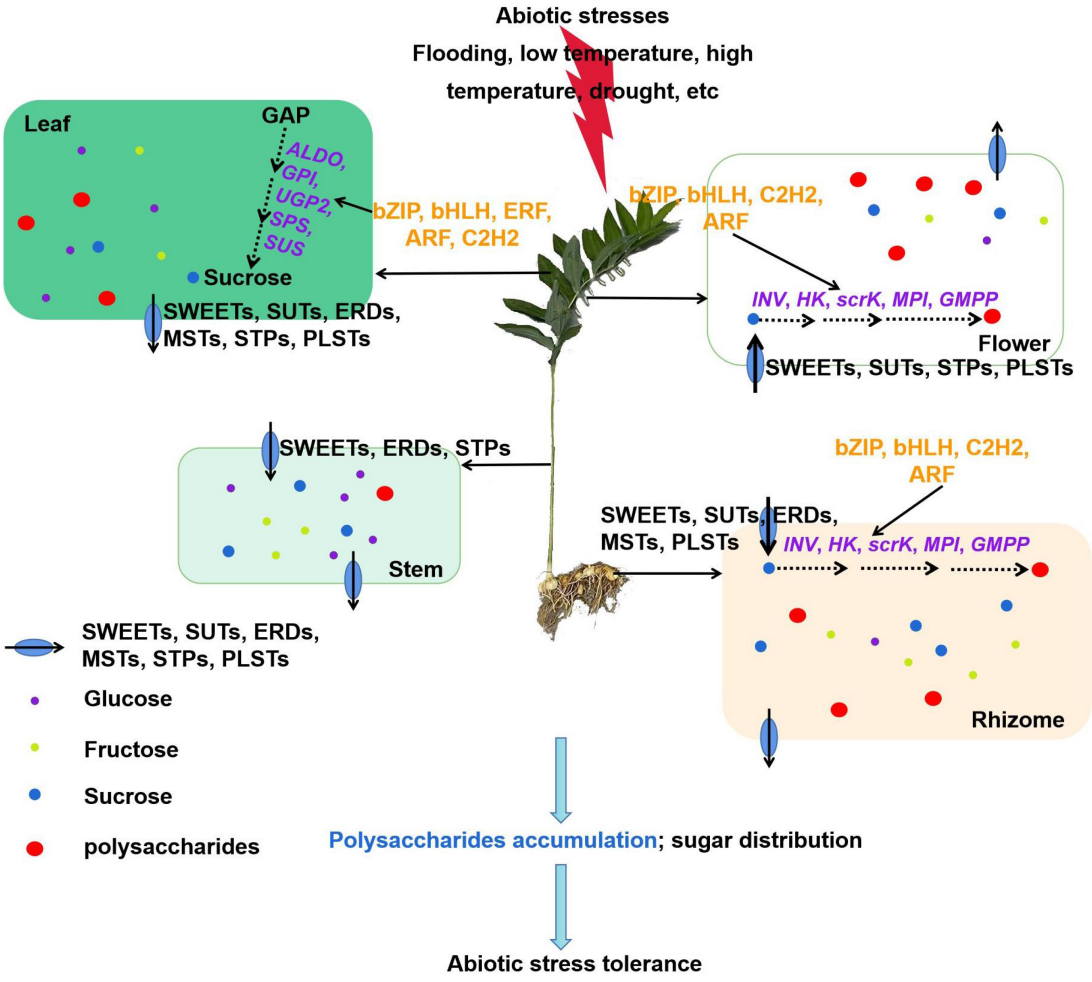

FIGURE 11
A model explaining the networks of transcriptional regulation of polysaccharide accumulation and their possible mechanisms in response to abiotic stress in *Polygonatum cyrtonema* Hua. Sucrose is mainly synthesized by the upregulation of *ALDO*, *GPI*, *UGP2*, *SPS*, and *SUS* genes in the leaf. Then, a high amount of sucrose and several monosaccharides is transported to the stem by *SWEETs*, *ERDs*, and/or *STPs* genes, and then get unloaded into the rhizome and flower tissues due to the functions of *SWEETs*, *SUTs*, *MSTs*, *ERDs*, *PLSTs*, and/or *STPs* genes. Afterward, sucrose is catalyzed by *INV*, and their products glucose and fructose are used to synthesize polysaccharides. Furthermore, these key genes are possibly regulated by transcription factors, such as *bZIP*, *bHLH*, *ERF*, *ARF*, and *C2H2*, which are involved in the regulatory processes of abiotic stresses. In general, our study contributes to a comprehensive understanding of the transcriptional regulation of polysaccharide accumulation.

GALE (*DN159955_c0_g2* and *DN11833_c0_g1*) (**Figure 9**). Correlations between polysaccharide content and the expression of *MPI*, *GMPP*, *GMDS*, and *GALE* genes were observed by other reports in *P. cyrtonema* Hua (Wang et al., 2019; Li et al., 2022). Therefore, these results suggested that sucrose might be transported by *SWEET* (*DN32250_c0_g1*) to rhizomes, and then decomposed by *INV* to promote polysaccharide biosynthesis. Furthermore, several studies revealed that various transcription factors are involved in the regulation of sugar metabolism pathways which overcome the negative effects of abiotic stress (Kumar et al., 2022). For example, *MaRAP2-4*, an ERF transcription factor, activated *SWEET10* that directly or indirectly assists in sugar accumulation, thus enhancing tolerance to waterlogging, drought, and salinity (Phukan et al., 2018). Future research will focus on the functional role of these key genes involved in polysaccharide accumulation and their roles in responses to abiotic stress in *P. cyrtonema* Hua. Other studies suggested that gas signaling molecules and hormones also enhanced plant tolerance to abiotic stress by regulating sugar metabolism (Wei et al., 2015; Yang et al., 2016; Chen et al., 2020; Rangani et al., 2020; Gu et al., 2021, 2022; de Bont et al., 2022). For example, exogenous melatonin application improved the tolerance to salinity and drought stresses *via* modulating the starch/sucrose metabolism in soybean (Wei et al., 2015). Therefore, the roles of gas signaling molecules and hormones involved in polysaccharide accumulation are also worth in-depth study in *P. cyrtonema* Hua.

Conclusion

In this study, we explored a detailed regulatory network for polysaccharide accumulation in *P. cyrtonema* Hua. Our results showed that polysaccharides generally accumulated in rhizome, stem, leaf, and flower tissues. Moreover, the polysaccharide biosynthesis in rhizome and flower is closely related to sucrose metabolism and transport in the leaf and stem (**Figure 11**). Sucrose is mainly synthesized by the upregulation of *ALDO*, *GPI*, *UGP2*, *SPS*, and *SUS* genes in the leaf. Then, a high amount of sucrose and several monosaccharides are transported to the stem, and then get unloaded into the rhizome and flower tissues due to the functions of *SWEET*s, SUTs, *MST*s, *ERD*s, *PLST*s, and/or *STP* genes. Afterward, sucrose is catalyzed by *INV*, and their products glucose and fructose are used to synthesize polysaccharides. Furthermore, these key genes are possibly regulated by transcription factors, such as *bZIP*, *bHLH*, *ERF*, *ARF*, and *C2H2*, which are involved in the regulatory processes of abiotic stresses. To our knowledge, this is the first report to link sucrose metabolism and transport with polysaccharide accumulation in *P. cyrtonema* Hua. This study provided new insights into the molecular mechanism of polysaccharide biosynthesis and valuable genes involved in abiotic stress tolerance in *P. cyrtonema* Hua. Our results also suggested that as polysaccharides have various health effects, not only rhizome, but leaves and flowers can also be used to process the foods to meet the market demand.

Data availability statement

Publicly available datasets were analyzed in this study. RNA-seq data of the tissues can be found in the publicly accessible NCBI under BioProject PRJNA878799.

Author contributions

XD, ZC, and LC conceived the study and designed the experiments. LC, SX, YL, YZ, FZ, LD, JC, KW, and SC performed the experiments. LL and YW participated in the preparation of plant materials. LC wrote the manuscript. XD and ZC revised and finalized the manuscript. All authors read and approved the final version of the manuscript.

Funding

This work was supported by the Anhui Province Key Research and Development Program (Grant No. 202204c06020010) and Postdoctoral Projects of Anhui Province (Grant No. 2020A396).

Conflict of interest

LL was employed by Jinzhai Senfeng Agricultural Technology Development Co., Ltd.

The remaining authors declare that the research was conducted in the absence of any commercial or financial relationships that could be construed as a potential conflict of interest.

Publisher's note

All claims expressed in this article are solely those of the authors and do not necessarily represent those of their affiliated organizations, or those of the publisher, the editors and the reviewers. Any product that may be evaluated in this article, or claim that may be made by its manufacturer, is not guaranteed or endorsed by the publisher.

Supplementary material

The Supplementary Material for this article can be found online at: https://www.frontiersin.org/articles/10.3389/fpls.2022.1012231/full#supplementary-material

References

Chandran, D. (2015). Co-option of developmentally regulated plant SWEET transporters for pathogen nutrition and abiotic stress tolerance. *IUBMB Life* 67, 461–471. doi: 10.1002/iub.1394

Chardon, F., Bedu, M., Calenge, F., Klemens, P. A., Spinner, L., Clement, G., et al. (2013). Leaf fructose content is controlled by the vacuolar transporter SWEET17 in Arabidopsis. *Curr. Biol.* 23, 697–702. doi: 10.1016/j.cub.2013.03.021

Chen, L. Q., Hou, B. H., Lalonde, S., Takanaga, H., Hartung, M. L., Qu, X. Q., et al. (2010). Sugar transporters for intercellular exchange and nutrition of pathogens. *Nature* 468, 527–532. doi: 10.1038/nature09606

Chen, L. Q., Qu, X. Q., Hou, B. H., Sosso, D., Osorio, S., Fernie, A. R., et al. (2012). Sucrose efflux mediated by SWEET proteins as a key step for phloem transport. *Science* 335, 207–211. doi: 10.1126/science.1213351

Chen, T., Tian, M., and Han, Y. (2020). Hydrogen sulfide: A multi-tasking signal molecule in the regulation of oxidative stress responses. *J. Exp. Bot.* 71, 2862–2869. doi: 10.1093/jxb/eraa093

Cheng, X., Ji, H., Cheng, X., Wang, D., Li, T., Ren, K., et al. (2021). Characterization, classification, and authentication of *Polygonatum sibiricum* samples by volatile profiles and flavor properties. *Molecules* 27:25. doi: 10.3390/molecules27010025

Chinese Pharmacopoeia Commission (2020). *Chinese Pharmacopoeia Commission*. Beijing: China Medical Science Press, 319–320.

Dahro, B., Wang, F., Peng, T., and Liu, J. H. (2016). PtrA/NINV, an alkaline/neutral invertase gene of Poncirus trifoliata, confers enhanced tolerance

to multiple abiotic stresses by modulating ROS levels and maintaining photosynthetic efficiency. *BMC Plant Biol.* 16:76. doi: 10.1186/s12870-016-0761-0

de Bont, L., Mu, X., Wei, B., and Han, Y. (2022). Abiotic stress-triggered oxidative challenges: Where does H_2S act? *J. Genet. Genom.* 49, 748–755. doi: 10.1016/j.jgg.2022.02.019

Eggert, E., Obata, T., Gerstenberger, A., Gier, K., Brandt, T., Fernie, A. R., et al. (2016). A sucrose transporter-interacting protein disulphide isomerase affects redox homeostasis and links sucrose partitioning with abiotic stress tolerance. *Plant Cell Environ.* 39, 1366–1380. doi: 10.1111/pce.12694

Feng, Y. X., Yu, X. Z., Mo, C. H., and Lu, C. J. (2019). Regulation network of sucrose metabolism in response to trivalent and hexavalent chromium in *Oryza sativa*. *J. Agric. Food Chem.* 67, 9738–9748. doi: 10.1021/acs.jafc.9b01720

Gan, Q., Wang, X., Cao, M., Zheng, S., Ma, Y., and Huang, Q. (2022). NF-κB and AMPK-Nrf2 pathways support the protective effect of polysaccharides from *Polygonatum cyrtonema* Hua in lipopolysaccharide-induced acute lung injury. *J. Ethnopharmacol.* 291:115153. doi: 10.1016/j.jep.2022.115153

Gu, Q., Wang, C., Xiao, Q., Chen, Z., and Han, Y. (2021). Melatonin confers plant cadmium tolerance: An update. *Int. J. Mol. Sci.* 22:11704. doi: 10.3390/ijms222111704

Gu, Q., Xiao, Q., Chen, Z., and Han, Y. (2022). Crosstalk between melatonin and reactive oxygen species in plant abiotic stress responses: An update. *Int. J. Mol. Sci.* 23:5666. doi: 10.3390/ijms23105666

He, C., Wu, K., Zhang, J., Liu, X., Zeng, S., Yu, Z., et al. (2017). Cytochemical localization of polysaccharides in *Dendrobium officinale* and the involvement of DoCSLA6 in the synthesis of mannan polysaccharides. *Front. Plant Sci.* 8:173. doi: 10.3389/fpls.2017.00173

Hennion, N., Durand, M., Vriet, C., Doidy, J., Maurousset, L., Lemoine, R., et al. (2019). Sugars en route to the roots. Transport, metabolism and storage within plant roots and towards microorganisms of the rhizosphere. *Physiol. Plant* 165, 44–57. doi: 10.1111/ppl.12751

Hu, Y., Yin, M., Bai, Y., Chu, S., Zhang, L., Yang, M., et al. (2022). An evaluation of traits, nutritional, and medicinal component quality of *Polygonatum cyrtonema* Hua and *P. sibiricum* Red. *Front. Plant Sci.* 13:891775. doi: 10.3389/fpls.2022.891775

Julius, B. T., Leach, K. A., Tran, T. M., Mertz, R. A., and Braun, D. M. (2017). Sugar transporters in plants: New insights and discoveries. *Plant Cell Physiol.* 58, 1442–1460. doi: 10.1093/pcp/pcx090

Kircher, S., and Schopfer, P. (2012). Photosynthetic sucrose acts as cotyledon-derived long-distance signal to control root growth during early seedling development in Arabidopsis. *Proc. Natl. Acad. Sci. U.S.A.* 109, 11217–11221. doi: 10.1073/pnas.1203746109

Kiyosue, T., Abe, H., Yamaguchi-Shinozaki, K., and Shinozaki, K. (1998). ERD6, a cDNA clone for an early dehydration-induced gene of Arabidopsis, encodes a putative sugar transporter. *Biochim. Biophys. Acta* 1370, 187–191. doi: 10.1016/s0005-2736(98)00007-8

Klemens, P. A., Patzke, K., Deitmer, J., Spinner, L., Le Hir, R., Bellini, C., et al. (2013). Overexpression of the vacuolar sugar carrier AtSWEET16 modifies germination, growth, and stress tolerance in Arabidopsis. *Plant Physiol.* 163, 1338–1352. doi: 10.1104/pp.113.224972

Koch, K. (2004). Sucrose metabolism: Regulatory mechanisms and pivotal roles in sugar sensing and plant development. *Curr. Opin. Plant Biol.* 7, 235–246. doi: 10.1016/j.pbi.2004.03.014

Kumar, S., Thakur, M., Mitra, R., Basu, S., and Anand, A. (2022). Sugar metabolism during pre- and post-fertilization events in plants under high temperature stress. *Plant Cell Rep.* 41, 655–673. doi: 10.1007/s00299-021-02795-1

Li, D., Wang, Q., Chen, S., Liu, H., Pan, K., Li, J., et al. (2022). De novo assembly and analysis of *Polygonatum cyrtonema* Hua and identification of genes involved in polysaccharide and saponin biosynthesis. *BMC Genom.* 23:195. doi: 10.1186/s12864-022-08421-y

Li, L., Liao, B. Y., Thakur, K., Zhang, J. G., and Wei, Z. J. (2018a). The rheological behavior of polysaccharides sequential extracted from *Polygonatum cyrtonema* Hua. *Int. J. Biol. Macromol.* 109, 761–771. doi: 10.1016/j.ijbiomac.2017.11.063

Li, L., Thakur, K., Cao, Y. Y., Liao, B. Y., Zhang, J. G., and Wei, Z. J. (2020). Anticancerous potential of polysaccharides sequentially extracted from *Polygonatum cyrtonema* hua in Human cervical cancer Hela cells. *Int. J. Biol. Macromol.* 148, 843–850. doi: 10.1016/j.ijbiomac.2020.01.223

Li, L., Thakur, K., Liao, B. Y., Zhang, J. G., and Wei, Z. J. (2018b). Antioxidant and antimicrobial potential of polysaccharides sequentially extracted from *Polygonatum cyrtonema* Hua. *Int. J. Biol. Macromol.* 114, 317–323. doi: 10.1016/j.ijbiomac.2018.03.121

Li, X. L., Ma, R. H., Zhang, F., Ni, Z. J., Thakur, K., Wang, S. Y., et al. (2021). Evolutionary research trend of *Polygonatum* species: A comprehensive account of their transformation from traditional medicines to functional foods. *Crit. Rev. Food Sci. Nutr.* of print]. [Epub ahead doi: 10.1080/10408398.2021.1993783

Lin, W., Chen, H., Wang, J., Zheng, Y., Lu, Q., Zhu, Z., et al. (2021). Transcriptome analysis associated with polysaccharide synthesis and their antioxidant activity in *Cyclocarya paliurus* leaves of different developmental stages. *PeerJ* 9:e11615. doi: 10.7717/peerj.11615

Liu, F., Liu, Y., Meng, Y., Yang, M., and He, K. (2004). Structure of polysaccharide from *Polygonatum cyrtonema* Hua and the antiherpetic activity of its hydrolyzed fragments. *Antivir. Res.* 63, 183–189. doi: 10.1016/j.antiviral.2004.04.006

Luo, M., Zhang, W. W., Deng, C. F., Tan, Q. S., Luo, C., and Luo, S. (2016). Advances in studies of medicinal crop *Polygonatum cyrtonema* Hua. *Lishizhen Med. Mater. Med. Res.* 27, 1467–1469.

Mathan, J., Singh, A., and Ranjan, A. (2021a). Sucrose transport and metabolism control carbon partitioning between stem and grain in rice. *J. Exp. Bot.* 72, 4355–4372. doi: 10.1093/jxb/erab066

Mathan, J., Singh, A., and Ranjan, A. (2021b). Sucrose transport in response to drought and salt stress involves ABA-mediated induction of OsSWEET13 and OsSWEET15 in rice. *Physiol. Plant* 171, 620–637. doi: 10.1111/ppl.13210

Meng, M., Geisler, M., Johansson, H., Harholt, J., Scheller, H. V., Mellerowicz, E. J., et al. (2009). UDP-glucose pyrophosphorylase is not rate limiting, but is essential in Arabidopsis. *Plant Cell Physiol.* 50, 998–1011. doi: 10.1093/pcp/pcp052

Mignolli, F., Barone, J. O., and Vidoz, M. L. (2021). Root submergence enhances respiration and sugar accumulation in the stem of flooded tomato plants. *Plant Cell Environ.* 44, 3643–3654. doi: 10.1111/pce.14152

Milne, R. J., Grof, C. P. L., and Patrick, J. W. (2018). Mechanisms of phloem unloading: Shaped by cellular pathways, their conductances and sink function. *Curr. Opin. Plant Biol.* 43, 8–15. doi: 10.1016/j.pbi.2017.11.003

Northcote, D. H., and Pickett-Heaps, J. D. (1966). A function of the Golgi apparatus in polysaccharide synthesis and transport in the root-cap cells of wheat. *Biochem. J.* 98, 159–167. doi: 10.1042/bj0980159

Oh, C. S., Kim, H., and Lee, C. (2013). Rice cell wall polysaccharides: Structure and biosynthesis. *J. Plant Biol.* 56, 274–282. doi: 10.1007/s12374-013-0236-x

Osorio, S., Ruan, Y. L., and Fernie, A. R. (2014). An update on source-to-sink carbon partitioning in tomato. *Front. Plant Sci.* 5:516. doi: 10.3389/fpls.2014.00516

Phukan, U. J., Jeena, G. S., Tripathi, V., and Shukla, R. K. (2018). MaRAP2-4, a waterlogging-responsive ERF from Mentha, regulates bidirectional sugar transporter AtSWEET10 to modulate stress response in Arabidopsis. *Plant Biotechnol. J.* 16, 221–233. doi: 10.1111/pbi.12762

Raines, C. A., and Paul, M. J. (2006). Products of leaf primary carbon metabolism modulate the developmental programme determining plant morphology. *J. Exp. Bot.* 57, 1857–1862. doi: 10.1093/jxb/erl011

Rangani, J., Panda, A., and Parida, A. K. (2020). Metabolomic study reveals key metabolic adjustments in the xerohalophyte Salvadora persica L. during adaptation to water deficit and subsequent recovery conditions. *Plant Physiol. Biochem.* 150, 180–195. doi: 10.1016/j.plaphy.2020.02.036

Seo, P. J., Park, J. M., Kang, S. K., Kim, S. G., and Park, C. M. (2011). An Arabidopsis senescence-associated protein SAG29 regulates cell viability under high salinity. *Planta* 233, 189–200. doi: 10.1007/s00425-010-1293-8

Stadler, R., Brandner, J., Schulz, A., Gahrtz, M., and Sauer, N. (1995). Phloem loading by the PmSUC2 sucrose carrier from Plantago major occurs into companion cells. *Plant Cell* 7, 1545–1554. doi: 10.1105/tpc.7.10.1545

Sun, C. X., Palmqvist, S., Olsson, H., Boren, M., Ahlandsberg, S., and Jansson, C. (2003). A novel WRKY transcription factor, SUSIBA2, participates in sugar signaling in barley by binding to the sugar-responsive elements of the iso1 promoter. *Plant Cell* 15, 2076–2092. doi: 10.1105/tpc.014597

Wang, C., Peng, D., Zhu, J., Zhao, D., Shi, Y., Zhang, S., et al. (2019). Transcriptome analysis of *Polygonatum cyrtonema* Hua: Identification of genes involved in polysaccharide biosynthesis. *Plant Methods* 15:65. doi: 10.1186/s13007-019-0441-9

Wang, J., Su, H., Han, H., Wang, W., Li, M., Zhou, Y., et al. (2021a). Transcriptomics reveals host-dependent differences of polysaccharides biosynthesis in *Cynomorium songaricum*. *Molecules* 27:44. doi: 10.3390/molecules27010044

Wang, J., Wang, Y., Zhang, J., Ren, Y., Li, M., Tian, S., et al. (2021b). The NAC transcription factor ClNAC68 positively regulates sugar content and seed development in watermelon by repressing ClINV and ClGH3.6. *Hortic. Res.* 8:214. doi: 10.1038/s41438-021-00649-1

Wei, W., Li, Q. T., Chu, Y. N., Reiter, R. J., Yu, X. M., Zhu, D. H., et al. (2015). Melatonin enhances plant growth and abiotic stress tolerance in soybean plants. *J. Exp. Bot.* 66, 695–707. doi: 10.1093/jxb/eru392

Wu, W., Huang, N., Huang, J., Wang, L., Wu, L., Wang, Q., et al. (2022). Effects of the steaming process on the structural properties and immunological activities of polysaccharides from *Polygonatum cyrtonema*. *J. Funct. Foods* 88:104866. doi: 10.1016/j.jff.2021.104866

Xie, S. Z., Yang, G., Jiang, X. M., Qin, D. Y., Li, Q. M., Zha, X. Q., et al. (2020). *Polygonatum cyrtonema* Hua polysaccharide promotes GLP-1 secretion from enteroendocrine L-Cells through sweet taste receptor-mediated cAMP signaling. *J. Agric. Food Chem.* 68, 6864–6872. doi: 10.1021/acs.jafc.0c02058

Yang, M., Qin, B. P., Ma, X. L., Wang, P., Li, M. L., Chen, L. L., et al. (2016). Foliar application of sodium hydrosulfide (NaHS), a hydrogen sulfide (H_2S) donor, can protect seedlings against heat stress in wheat (*Triticum aestivum* L.). *J. Integr. Agric.* 15, 2745–2758. doi: 10.1016/S2095-3119(16)61358-8

Yang, Y., Jiang, M., Feng, J., Wu, C., Shan, W., Kuang, J., et al. (2021). Transcriptome analysis of low-temperature-affected ripening revealed MYB transcription factors-mediated regulatory network in banana fruit. *Food Res. Int.* 148:110616. doi: 10.1016/j.foodres.2021.110616

Yu, Z., He, C., Teixeira da Silva, J. A., Zhang, G., Dong, W., Luo, J., et al. (2017). Molecular cloning and functional analysis of DoUGE related to water-soluble polysaccharides from *Dendrobium officinale* with enhanced abiotic stress tolerance. *Plant Cell Tiss. Organ.* 131, 579–599. doi: 10.1007/s11240-017-1308-2

Yu, Z., Zhang, G., Teixeira da Silva, J. A., Li, M., Zhao, C., He, C., et al. (2021). Genome-wide identification and analysis of DNA methyltransferase and demethylase gene families in *Dendrobium officinale* reveal their potential functions in polysaccharide accumulation. *BMC Plant Biol.* 21:21. doi: 10.1186/s12870-020-02811-8

Zhang, H., Tao, X., Fan, X., Zhang, S., and Qin, G. (2022). PpybZIP43 contributes to sucrose synthesis in pear fruits by activating PpySPS3 expression and interacts with PpySTOP1. *Physiol. Plant* 174:e13732. doi: 10.1111/ppl.13732

Zhang, J., He, C., Wu, K., Teixeira da Silva, J. A., Zeng, S., Zhang, X., et al. (2016). Transcriptome analysis of *Dendrobium officinale* and its application to the identification of genes associated with polysaccharide synthesis. *Front. Plant Sci.* 7:5. doi: 10.3389/fpls.2016.00005

Zhang, S., Shi, Y., Huang, L., Wang, C., Zhao, D., Ma, K., et al. (2020). Comparative transcriptomic analysis of rhizomes, stems, and leaves of *Polygonatum odoratum* (Mill.) Druce reveals candidate genes associated with polysaccharide synthesis. *Gene* 744:144626. doi: 10.1016/j.gene.2020.144626

Zhu, A., Li, W., Ye, J., Sun, X., Ding, Y., Cheng, Y., et al. (2011). Microarray expression profiling of postharvest Ponkan mandarin (*Citrus reticulata*) fruit under cold storage reveals regulatory gene candidates and implications on soluble sugars metabolism. *J. Integr. Plant Biol.* 53, 358–374. doi: 10.1111/j.1744-7909

Zhu, S., Liu, P., Wu, W., Li, D., Shang, E. X., Guo, S., et al. (2022). Multi-constituents variation in medicinal crops processing: Investigation of nine cycles of steam-sun drying as the processing method for the rhizome of *Polygonatum cyrtonema*. *J. Pharm. Biomed. Anal.* 209:114497. doi: 10.1016/j.jpba.2021.114497

frontiers | Frontiers in Plant Science

TYPE Original Research
PUBLISHED 19 October 2022
DOI 10.3389/fpls.2022.1007866

OPEN ACCESS

EDITED BY
Weicong Qi,
Jiangsu Academy of Agricultural Sciences (JAAS), China

REVIEWED BY
Chirag Gupta,
University of Wisconsin-Madison, United States
Moyang Liu,
Shanghai Jiao Tong University, China

*CORRESPONDENCE
Chao Sun
sunc@gsau.edu.cn
Jiangping Bai
baijp@gsau.edu.cn

SPECIALTY SECTION
This article was submitted to Plant Bioinformatics, a section of the journal Frontiers in Plant Science

RECEIVED 31 July 2022
ACCEPTED 28 September 2022
PUBLISHED 19 October 2022

CITATION
Qin T, Ali K, Wang Y, Dormatey R, Yao P, Bi Z, Liu Y, Sun C and Bai J (2022) Global transcriptome and coexpression network analyses reveal cultivar-specific molecular signatures associated with different rooting depth responses to drought stress in potato. *Front. Plant Sci.* 13:1007866. doi: 10.3389/fpls.2022.1007866

Global transcriptome and coexpression network analyses reveal cultivar-specific molecular signatures associated with different rooting depth responses to drought stress in potato

Tianyuan Qin[1], Kazim Ali[2], Yihao Wang[1], Richard Dormatey[1], Panfeng Yao[1], Zhenzhen Bi[1], Yuhui Liu[1], Chao Sun[1*] and Jiangping Bai[1*]

[1]State Key Laboratory of Aridland Crop Science, College of Agronomy, Gansu Agricultural University, Lanzhou, China, [2]National Institute for Genomics and Advanced Biotechnology, National Agricultural Research Centre, Islamabad, Pakistan

Potato is one of the most important vegetable crops worldwide. Its growth, development and ultimately yield is hindered by drought stress condition. Breeding and selection of deep-rooted and drought-tolerant potato varieties has become a prime approach for improving the yield and quality of potato (*Solanum tuberosum* L.) in arid and semiarid areas. A comprehensive understanding of root development-related genes has enabled scientists to formulate strategies to incorporate them into breeding to improve complex agronomic traits and provide opportunities for the development of stress tolerant germplasm. Root response to drought stress is an intricate process regulated through complex transcriptional regulatory network. To understand the rooting depth and molecular mechanism, regulating root response to drought stress in potato, transcriptome dynamics of roots at different stages of drought stress were analyzed in deep (C119) and shallow-rooted (C16) cultivars. Stage-specific expression was observed for a significant proportion of genes in each cultivar and it was inferred that as compared to C16 (shallow-rooted), approximately half of the genes were differentially expressed in deep-rooted cultivar (C119). In C16 and C119, 11 and 14 coexpressed gene modules, respectively, were significantly associated with physiological traits under drought stress. In a comparative analysis, some modules were different between the two cultivars and were associated with differential response to specific drought stress stage. Transcriptional regulatory networks were constructed, and key components determining rooting depth were identified. Through the results, we found that rooting depth (shallow vs deep) was largely determined by plant-type, cell wall organization or biogenesis, hemicellulose metabolic process, and polysaccharide metabolic process. In addition,

candidate genes responding to drought stress were identified in deep (C119) and shallow (C16) rooted potato varieties. The results of this study will be a valuable source for further investigations on the role of candidate gene(s) that affect rooting depth and drought tolerance mechanisms in potato.

KEYWORDS

potato, coexpression network, gene expression, root development, rooting depth, transcriptional modules

Introduction

Roots provide plants with water and nutrients. Root depth (deep or shallow) is an important agronomic trait related to yield potential and is particularly important in potato tubers (Xu et al., 2017; Wang et al., 2020b). In potato tubers, root development begins at tuber germination, and the first young buds appear with scaly or "embryo" leaves at the top, followed by young roots on several sections at the base of the buds (Nicolas et al., 2022). The early period is primarily for root formation and bud growth, which form the basis for tuber seedling rooting, tuber formation, and plant strengthening (Zhou et al., 2017; Omary et al., 2022). A comprehensive understanding of the molecular mechanisms regulating all aspects of root development is needed to facilitate the development of new cultivars.

Many biological processes and pathways control root development (Sheng et al., 2017; Zhao et al., 2020). Omics studies in model plants and crops provide molecular insights into gene pathways and regulatory networks and their interactions involved in various aspects of root development (Wang et al., 2020a; Chen et al., 2022). The molecular mechanisms controlling root depth (deep or shallow) have also been elucidated to some extent in some plants, such as *Arabidopsis* and rice (Jean-Baptiste et al., 2019; Maurel and Nacry, 2020; Reynoso et al., 2022). In the early stage of root development and carbohydrate partitioning, the supply of photoassimilates and the accumulation rate of storage substances are very important in determining rooting depth (Chai and Schachtman, 2022; Li et al., 2022). In addition, epigenetic mechanisms and hormone signalling have also been identified as important regulatory mechanisms that determine rooting depth (Gutierrez et al., 2009; Holzwart et al., 2018; Jia et al., 2019). Furthermore, the number of cells in Gramineae, including rice and maize, is positively correlated with rooting (Liu et al., 2021; Marand et al., 2021; Wang et al., 2021a).

Potato is a nutritionally and agriculturally important tuber crop that is commonly grown as a staple crop in arid and semiarid regions with an average annual rainfall less than 500 mm (Su et al., 2020). In these regions, potato tuber yield and quality s are constrained by numerous biotic and abiotic stresses, including prolonged or seasonal drought stress, which adversely affects canopy growth and tuber yield and market value (Fernie and Willmitzer, 2002; Barnaby et al., 2019). Access to potato transcriptomes and draft genome sequences (Zhou et al., 2020a; Sun et al., 2022) and next-generation NGS provide opportunities to uncover genetic diversity among different genotypes or cultivars, especially for important agronomic traits. Transcriptome studies have examined flower and leaf development and responses to abiotic stresses (Singh et al., 2013; Kudapa et al., 2014; Garg et al., 2016). However, similar WGCNA analysis method have not been conducted to determine the molecular mechanisms underlying root responses to drought stress or rooting depth in potato (Jain et al., 2017; Ma et al., 2021). Rooting depth (shallow or deep) is an important trait that influences plant response to abiotic stress (Vanhees et al., 2020). Although huge variations in rooting depth have been observed among potato genotypes, this phenotypic variability has not been used to improve rooting depth and to improve potato drought resistance of important potato cultivars. Deep-rooted genes in potato has not been exploited because the molecular mechanisms controlling rooting depth are poorly understood.

The availability of genotypes and cultivars with opposite phenotypes of specific traits provides an excellent opportunity to uncover the genetic factors controlling rooting depth. However, comparative transcriptome analysis of potato genotypes and cultivars with different rooting depths has not yet been performed. Therefore, in this study, RNA-seq technology was used to analyze the transcriptomes of roots of two potato cultivars that differed significantly in rooting depth (one deep-rooted and one shallow-rooted) at different stages of root response to drought stress. Data were analyzed to reveal transcriptome dynamics and transcriptional networks associated with root response to drought stress and to identify key genetic differences between deep-rooted and shallow-rooted potato cultivars in response to drought stress. Transcripts and modules of co-expressed genes that are predominantly or specifically expressed at different stages of root response to drought stress or in a particular cultivar were identified. The results of this study shed light on the molecular mechanisms that determine rooting depth and root response to drought stress in potato.

10.3389/fpls.2022.1007866

Results

Global transcriptome analysis of potato cultivar roots

To gain insights into the molecular mechanisms underlying root response to drought stress and controlling root length and volume. Root transcriptomes at different stages of root response to drought stress were analyzed in potato cultivars with differences in root length and volume (Figure 1, Figure S1). In this study, potato cultivar C16 was shallow-rooted and cultivar C119 was deep-rooted, and root length and volume of the two cultivars differed significantly. Nine stages of root responses to drought stress, representing important events within the root occurred (Figure 1). During the 15- to 25-day growth period, the average root length of C16 increased from 28 mm to 84 mm, while the average root length of C119 increased from 29 mm to 121 mm (Figure 1B). The average root volume of C16 increased from 22 mm3 to 107 mm3, while the average root volume of C119 increased from 23 mm3 to 122 mm3 (Figure 1C).

To investigate transcriptome dynamics during root response to drought stress, RNA-seq experiments were perform using total RNA from the three stages of root response to drought stress of potato cultivars C16 and C119. Three biological replicates of all samples were analyzed (54 samples in total). Each cultivar produced more than 0.6 billion high-quality reads (an average of about 23 million reads per sample) at different stages (Table S1). Reads were mapped to the potato genome (DM v4.04, http://spuddb.uga.edu/pgsc_download.shtml) using TopHat (Trapnell et al., 2012). The mapped files were processed using Cufflinks (Wang, 2018) and Cuffmerge (Li et al., 2016). which generated a consensus transcriptome assembly with a total of 40337 gene loci. Total mapped ratio of each sample (Table S1) were processed with Cufflinks to determine the standardized expression level of each transcript, i.e., transcripts read per million maps (TPM). Spearman correlation coefficient (SCC) (Liesecke et al., 2018) between the three biological replicates of different samples is from 0.93 to 0.99, indicating the high quality of the replicates of each treatment (Figure S2).

Overall, *a total of ~81% genes were identified as expressed in at least one of the 54 samples.* At different stages of drought stress, the number of genes expressed in the root samples ranged from 41.4% (C16-25d-150) to 43.2% (C16-20d-0) in C16 and from 59.3% (C119-25d-150) to 61.1% (C119-25d-0) in C119

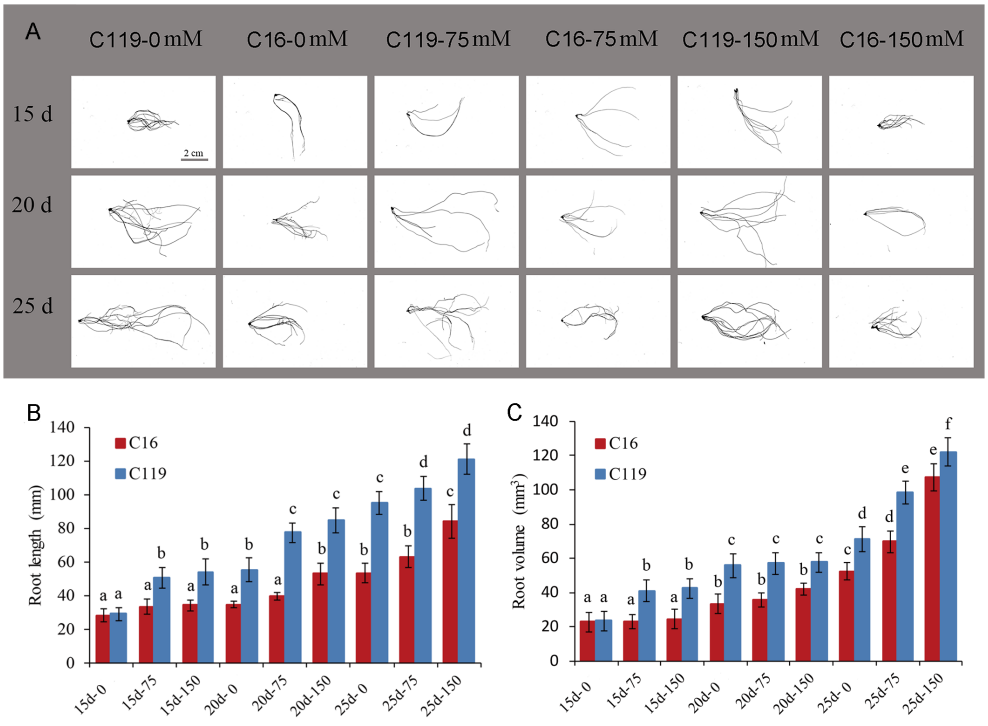

FIGURE 1
Root phenotypes at different stages of drought stress in potato cultivars C16 and C119. **(A)** Root phenotype at different stages of drought stress in C16 and C119. **(B, C)** Physical measurements showing variation in root length **(B)** and root volume **(C)** of C16 and C119 at different stages of drought stress. Root length (in mm) and root volume (in mm3) were plotted. The error bars indicate the standard error. The red bar represents C16, and the blue bar represents C119. The 15d, 20d and 25d represent the growth days; 0,75 and 150 represent the mannitol concentration.

(Figure S3A). The expression levels of about 14% to 23% of the genes were very high (TPM ≥ 50) in root samples at different stages of drought stress (Figure S3B). The number of genes that had high (10 ≤ TPM ≥ 50), moderate (2 ≤ TPM ≥ 10), and low (0.1 ≤ TPM ≥ 2) expression levels was similar in all root samples at different stages of drought stress. In general, the proportion of *highly* expressed genes was slightly higher in C16 than in C119 (Figure S3B). Overall, the analyses showed sufficient coverage of transcriptomes during root response to drought stress in the two potato cultivars.

Global comparison of transcriptomes revealed relations among root stages

To investigate global differences in transcriptome dynamics during root response to drought stress between C16 and C119 cultivars, hierarchical clustering and principal component analysis (PCA) were performed based on SCC analysis of the average TPM values of all genes expressed in at least one of the 54 root samples (Figure 2). Roots/stages with relatively high correlations were considered to have similar transcriptomes and associated functions. These analyses indicated that the root systems of the two cultivars were highly correlated at similar stages of drought stress. As expected, the root transcriptomes of each genotype were clustered together and showed significant differences in root responses drought stress stages (Figures 2A, B). Different stages of root drought stress response showed close correlations within the cultivars, indicating high similarity in transcriptional programs. Notably, the clustering of C119 and C16 under drought stress was significantly different, There is a large separation between the two varieties (Figure 2B). Overall, the results suggest there are large differences in the transcriptional programs of root responses to different stages of drought stress among cultivars. Furthermore, these large differences in transcriptional programs could determine cultivar-specific responses to drought stress and rooting depth.

Gene sets differentially expressed between potato cultivars

Gene sets were identified that showed significantly different expression between C16 and C119 at each stage of root response to drought stress. In C16, the expression of *9,564* genes were significantly increased, *and* of 11 590 genes was significantly decreased at different stages of root response to drought stress. *In C119, the expression of 8,325 genes was significantly increased, and of 11,721 genes was significantly decreased at different stages of root response to drought stress. In C16, the largest number of upregulated genes* (1,996) occurred at 15 days of drought stress, while in C119, the largest number of upregulated genes (1,644) occurred at 20 days of drought stress (Figure 3A). *Furthermore, in C16 and C119, we detected 2016 and 1766 differential genes, respectively, which were expressed under all drought stress treatments, suggesting that they had the ability to adapt to different drought stresses conditions (*Figure S4*).* Overall, *42 TF families* (transcription factors) in C119 showed differential expression than in C16, and these families had different functions during root response to different stages of drought stress (Figure 3B; Table S2). *For some TF families in C119, there are some genes with significantly high and low expression (*Figure 3B*).* For example, TF family members involved in cell proliferation and differentiation, such as ARF (auxin response

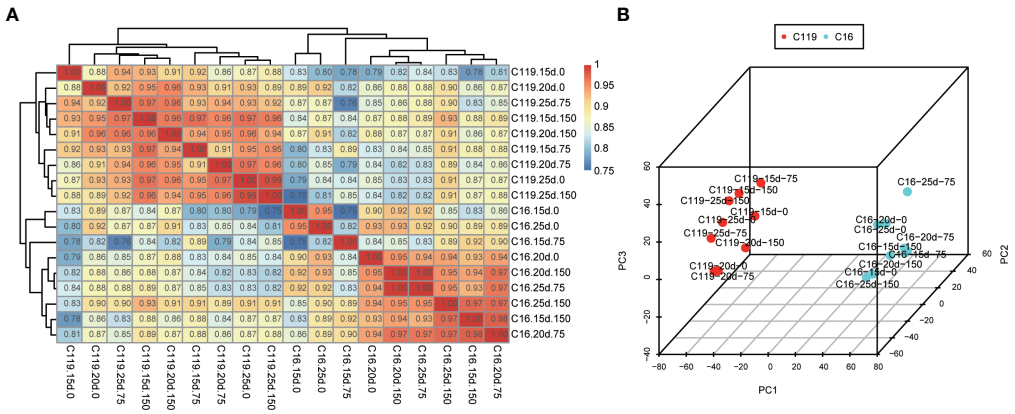

FIGURE 2
Correlations between transcriptomes of different stages of root response to drought stress in potato cultivars C16 and C119. **(A)** Spearman correlation coefficient analysis of RNA-seq data from root responses to drought stress. **(B)** Principal component (PC) analysis plot showing clustering of transcriptomes of root responses to drought stress. 15d, 20d and 25d represent the treatment days; 0, 75 and 150 represent the mannitol concentration.

factors) and GRF (growth regulatory factor), and those related to hormone signaling pathways, such as ARF and Aux/IAA (indole-3-acetic acid) and ARR-B (authentic typeB response regulator), and regulating polar development of lateral organs, such as HD-ZIP (homeodomain leucine zipper), showed significantly higher expression in C119 than in C16. Most TFs with lower expression in C119 than in C16 belonged to WRKY and Myb (myeloblastosis) -related families. Figure S5 shows expression profiles of selected TF families in both cultivars during root response to different stages of drought stress.

Gene ontology enrichment (GO) of differentially expressed genes in C119 identified several biological processes that were unique to or related to root response at different stages of drought stress. Terms related to cell division, such as cell wall tissue, cell wall tissue or biogenesis, and plant cell wall tissue or biogenesis, were significantly enriched in relatively highly expressed genes (Figure 3C). The GO terms regulation of hormone level and hormone biosynthesis process were also highly enriched at different stages of drought stress. In particular, the GO terms phloem or xylem histogenesis and lignin metabolic processes were significantly enriched and relatively strongly expressed in upregulated genes at different stages of drought stress. In addition, the GO terms auxin-activated signaling pathway and base excretion repair were significantly enriched in relatively highly expressed down-regulated genes (Figure 3C).

To investigate the metabolic pathways responsible for the differences in rooting depth between C119 and C16 in response to drought stress, the MapMan tool was used to superimpose the expression profiles of differentially expressed genes (DEGs) between cultivars on the available metabolic pathways (Bolger et al., 2021). Differences in the activity of some metabolic pathways were observed during the 20-day drought stress period. There were significant differences in the transcriptional activity of genes related to starch biosynthesis between different cultivars. Genes involved in starch metabolism and ester synthesis were more active in C119 than in C16, suggesting that active cell division in deep-rooted C119 requires an increase

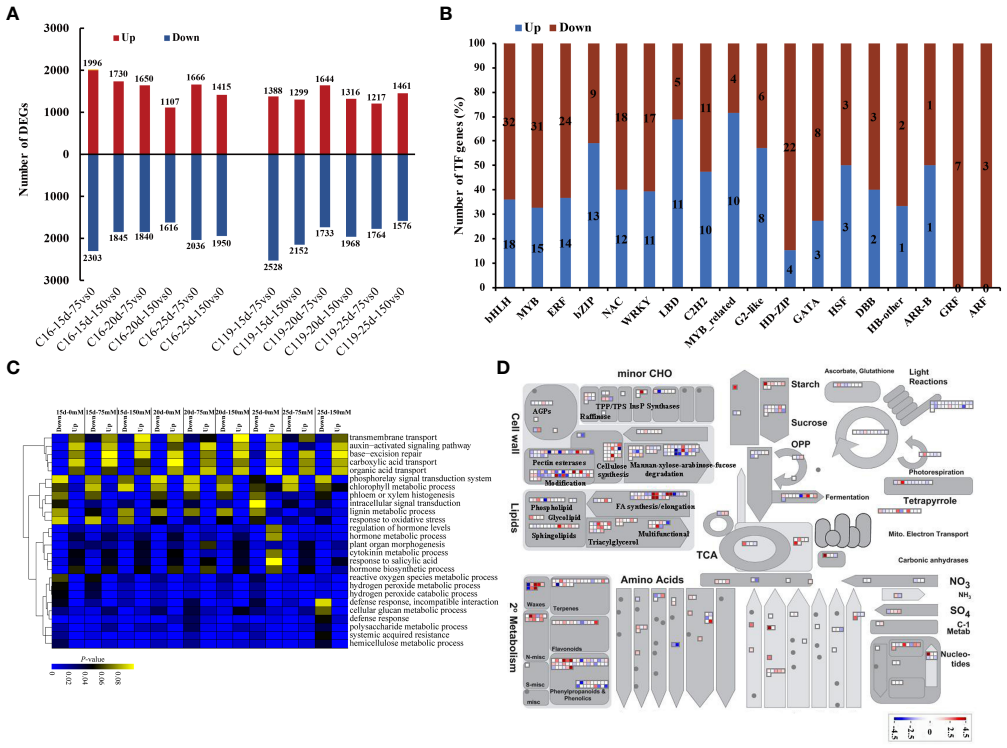

FIGURE 3
Differential gene expression in potato cultivars C119 and C16 at different stages of root development. **(A)** Number of up-regulated (red bars) and down-regulated (blue bars) differentially expressed genes (DEGs) at each stage of root development. **(B)** Number of genes from different transcription factor (TF) families up- or down-regulated in C119 during root responses at different stages of drought stress. **(C)** Enriched Gene Ontology terms (biological processes) for down- and up-regulated genes in C119 during root responses at different stages of drought stress. Lower color scale indicates significance (adjusted Pvalue). **(D)** Metabolic pathways with different expression profiles in C119 compared to those in C16 after 20 days of drought stress during root development. Differentially expressed genes (fold change ≥ 2, q-value ≤ 0.05) between C16 and C119 after 20 d of drought stress were loaded into MapMan to provide an overview. On the log2 scale, dark blue and dark red represent higher and lower expression, respectively, in C119 than in C16.

in energy (Figure 3D). Genes involved in cell wall synthesis and modification also showed consistently higher expression in C119 than in C16 (Figure 3D). In addition, genes involved in DNA repair, DNA synthesis, regulation of transcription, RNA synthesis, protein synthesis, protein modification, and protein degradation and transport showed higher transcriptional activity in C119 than in C16 from day 15 to 25 under drought stress (Figure S6), indicating that deep roots were more active under drought stress. Overall, the data showed that there were large transcriptional differences between C16 and C119 at different stages of drought stress.

Identification of gene coexpression modules of different potato cultivars

To investigate gene coexpression networks associated with responses of with shallow-rooted and deep-rooted cultivars to drought stress, the coexpression gene sets were determined by weighted gene coexpression network analysis (WGCNA). Genes with very low expression or low Spearman correlation coefficient (SCC) values were not included in the analysis to avoid inclusion of false edges in the network. Analysis of the differential gene regulatory networks of the two potato cultivars was performed separately. Several large subnetworks representing high coexpression between genes with similar expression profiles were identified as coexpression modules. Twenty modules (consisting of 89 to 1,198 genes) were identified in C16 (Figures 4A and S7A), whereas twenty-six modules (comprised of 101 to 1,873 genes) were identified in C119 (Figures 4B and S7B). Correlation analysis was used to determine the relationships between each coexpression module physiological indices [superoxide dismutase (SOD), peroxidase (POD), catalase (CAT), root vitality (RV), proline (Pro), soluble sugar (SS), root length (Len), root diameter (Diam), root volume (Vol), root tips (Tips), root forks (Forks)] of roots at different stages of drought stress were investigated (Figures S7A, B). In particular, 11 coexpression modules of C16 and 14 coexpression modules of C119 showed relatively high correlations ($r \geq 0.50$) with roots responding to different stages of drought stress (Figures S7A, B). Many modules were correlated with more than one physiological index at different stages of drought stress. For example, the turquoise module of C16 was correlated with all physiological indices, with 0.72 being the highest correlation. In addition, with the intensification of drought stress, correlations between the red module and all physiological indicators tended to change from positive to negative (Figure S7A). In C119, the purple module was correlated with all physiological indices, with 0.73 the highest correlation. In addition, with the intensification of drought stress, correlations between the purple module and all physiological indicators tended to change from negative to positive, whereas those with the light cyan module tended to change from positive to negative (Figure S7B). Next, we studied the preservation of coexpression modules between C16 and C119 at different stages of drought stress *via* cross-tabulation approach. The modules with the most

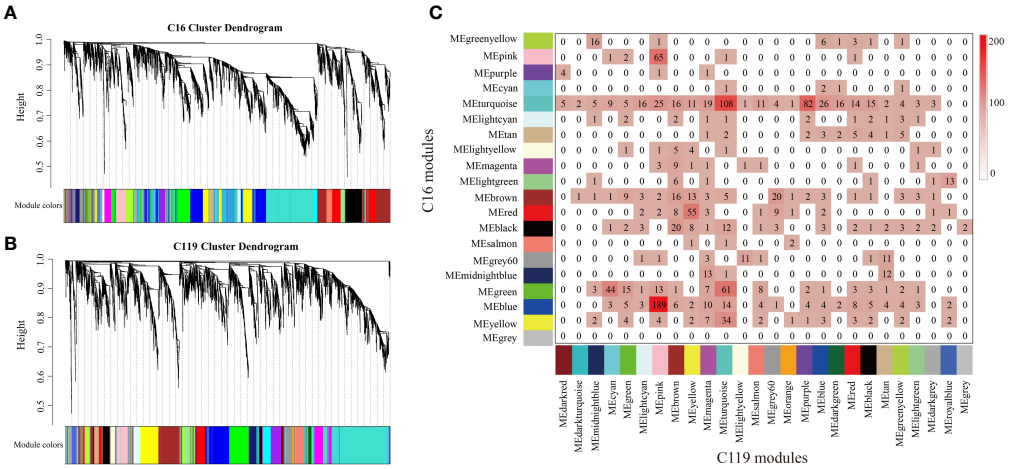

FIGURE 4
Coexpression networks in potato cultivars C16 and C119 during root development under drought stress. **(A, C)** hierarchical gene cluster tree (dendrogram) based on **(A)** C16 and **(B)** C119 coexpression network analysis. Each "leaf" (short vertical line) corresponds to a separate gene. Genes were clustered according to a diversity measure [1-TOM (topology model)]. The branches correspond to highly interconnected gene modules. The color bars under the dendrograms indicate module membership in **(A)** C16 and **(B)** C119. **(C)** Comparison of C16 and C119 modules based on cross-tabulation. Each C16 (row) and C119 (column) module is labeled by the corresponding module color. The numbers of genes for each intersection of the corresponding row and column modules are given. The color in the boxes represents numbers, according to the color legend on the right.

common genes are the turquoise and blue modules in C16, and the pink, turquoise and purple modules in C119, respectively (Figure 4C).

Because of the enormous number of genes in a module, dimensionality reduction can be used to study gene modules by selecting representative genes in a module as module eigengenes (ME) (Langfelder and Horvath, 2007). Using a ME, which represents thousands of genes in a module for correlation analysis, the method can further clarify the relationships between gene modules and phenotypic traits at different stages of drought stress and identify the target gene module (Panahi and Hejazi, 2021). In the cluster analysis of MEs of all modules, some MEs were highly correlated (Figure 5). In C16, the correlation between MEs in yellow and turquoise modules reached 0.75 and that between MEs in salmon and red modules reached 0.74. As drought stress intensified, the correlations between gene expression patterns and stress resistance-related physiological and biochemical indicators gradually changed from positive to negative (Figure 5A). At C119, the correlation between MEs in cyan and purple modules reached 0.77 and that between MEs in light cyan and pink modules reached 0.74. With the exacerbating of drought stress, the correlations between gene expression patterns and stress resistance-related physiological and biochemical indicators in the purple module gradually changed from negative to extremely significant positive. Moreover, the correlations between gene expression patterns and target traits in the cyan and light cyan modules gradually changed from positive to extremely significant negative with the intensification of drought stress (Figure 5B).

Transcriptional regulatory modules associated with rooting depth and root response to different stages of drought stress

To identify the hub genes in the eight modules, gene regulatory networks were visualized using Cytoscape software to identify the highly connected genes in the modules (Doncheva et al., 2019; Mousavian et al., 2021) (Figure 6). In a network, each node represents a gene, and lines connect the nodes, with genes at either end of a line usually involved in the same biological pathways (Mousavian et al., 2021). In C16, five nuclear genes were examined in the red module, six in the salmon module, seven in the turquoise module, and four in the yellow module. In C119, five nuclear genes were examined in the cyan module, nine in the light cyan module, ten in the pink module, and nine in the purple module. To obtain functional information on the nuclear genes, potato gene and NCBI databases (National Center for Biotechnology Information, https://www.ncbi.nlm.nih.gov/) were used to query relevant reports on the nuclear genes, and the TAIR database (https://www.arabidopsis.org/) was used to determine the functions of homologous genes of the nuclear genes in *Arabidopsis* (Table S3). The *PGSC0003DMG400032147* gene AT5G06720 homologous to C16 in *Arabidopsis* encodes a peroxidase with various functions in wound response, flower development, and syncytium formation (Shigeto et al., 2014). The homologous genes *AT5G40950* of *PGSC0003DMG400019631* and *AT5G56670* of *PGSC0003DMG401002397* in *Arabidopsis* may encode ribosomal proteins and participate in protein synthesis (Wang et al., 2008; Bach-Pages et al., 2020). The homologous gene of *PGSC0003DMG400009843* in *Arabidopsis AT5G67200* is involved in receptor protein kinase synthesis and regulates plant growth and development (ten Hove et al., 2011). In C119, the gene *AT3G61060* homologous to *PGSC0003DMG400010258* in *Arabidopsis* is involved in the formation of plant root phloem, and roots play a central role in plant growth, development, and stress response (Hanada et al., 2011). The homologous gene *AT3G01190* of *PGSC0003DMG400021801* in *Arabidopsis* has synergistic or antagonistic effects with plant hormones by regulating reactive oxygen species and redox signalling to elicit protective responses of plants to biological and abiotic stresses (Welinder et al., 2002). The gene *AT5G05340* homologous to *PGSC0003DMG400005062* in *Arabidopsis* regulates the formation of plant root xylem by encoding a protein involved in lignin biosynthesis (Fernández–Pérez et al., 2015). The gene *AT3G09790* homologous to *PGSC0003DMG400021791* in *Arabidopsis* is associated with the specificity of ubiquitination and may promote the transfer of ubiquitin to appropriate targets and regulate cell activities (Bachmair et al., 2001). Overall, the analysis identified transcriptional modules as the key regulatory network, and identified the hub genes of shallow-rooted and deep-rooted potato varieties in response to drought stress.

Hub gene binding sites (significantly enriched motifs) were identified in the roots of C16 and C119 in response to different stages of drought stress. This resulted in prediction of transcriptional modules linking the enriched regulatory motifs with the hub genes involved in different stages of drought stress and their association with specific GO terms represented significantly in the target genes. The transcriptional module in C16 (red, salmon, turquoise, and yellow modules) included significantly enriched GGTCA-motifs, GARE-motif, GC-motifs, ABRE, MBS, P-box, TATC-box, TCA-elements, TGA-elements, and TGACG-motifs. These motifs are mainly a gibberellin-responsive element, a MeJA-responsive element, an abscisic acid-responsive element, an auxin-responsive element, a salicylic acid-responsive element, and an MYB-binding site involved in dryness induction. The transcriptional modules included target genes involved in sequence-specific DNA binding, extracellular region, anatomical structure development, defense response and developmental process(red module); transferase activity, oxygen oxidoreductase activity, extracellular region, hydrolase activity and cell wall organization (salmon module); structural molecule activity, ribonucleoprotein complex, translation and structural

10.3389/fpls.2022.1007866

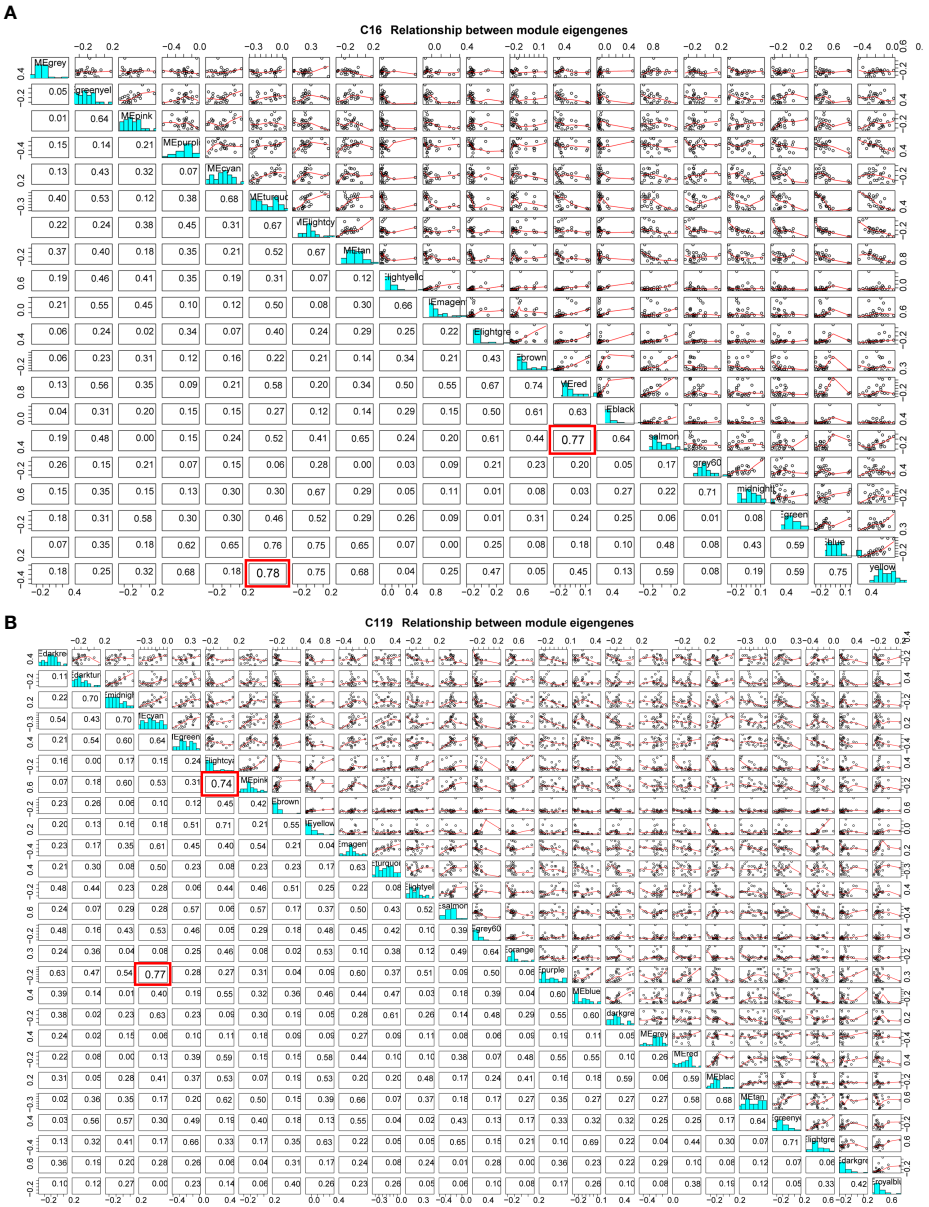

FIGURE 5
Module eigengene correlations between different modules in potato cultivars **(A)** C16 and **(B)** C119. Red box represents the two modules with the highest correlation.

constituent of ribosome (yellow module); structural constituent of ribosome, translation, response to abiotic stimulus, organelle subcompartment and structural molecule activity(turquoise module) (Figures 6A–D). Many of these components were similar to the transcriptional module in C119 (cyan, light cyan, pink, and purple modules), with some specific components including motifs, AuxRE, AuxRRcore, MSA-like, and TC-rich. Some of these regulatory motifs are known to be associated with elements involved in cell cycle regulation, elements involved in defense and stress response, and regulatory elements involved in auxin response. The transcriptional modules included target genes involved in extracellular region, external encapsulating structure, antioxidant activity, peroxidase activity, response to oxidative stress and cell wall organization (cyan module); peroxidase activity, antioxidant activity, extracellular region, signal transduction and response to endogenous stimulus (lightcyan module); active transmembrane transporter activity, tetrapyrrole binding, extracellular region, cell wall organization and response to oxygen–containing compound (pink module); zinc ion

10.3389/fpls.2022.1007866

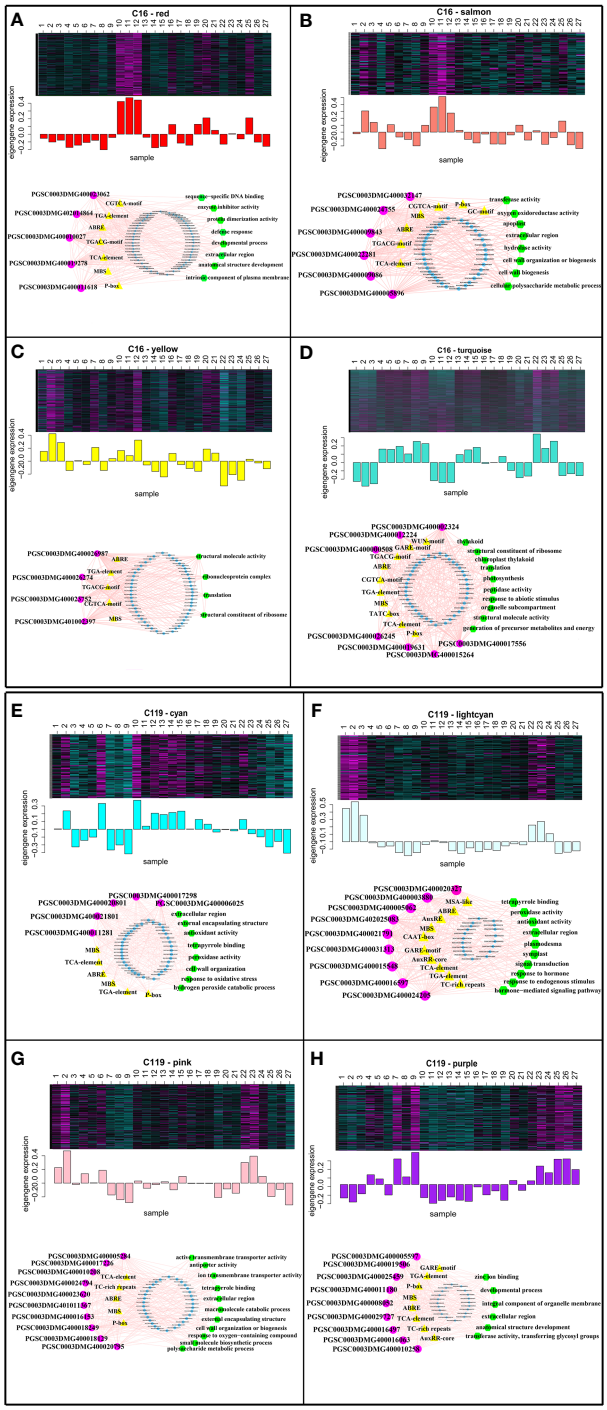

FIGURE 6
Expression profiles and transcriptional regulatory networks associated with modules in potato cultivars C16 and C119. Heatmaps show the expression profiles of all co-expressed genes in the modules (highlighted above). The bar graph (below the heatmap) shows the consistent expression pattern of the coexpressed genes in each module. The top-hub gene network is shown in circle below the bar graph. **(A–D)** Expression modules of C16, with networks of 5, 6, 4, and 7 hub genes, respectively. **(E-H)** Expression modules of C119, with networks of 5, 9, 10, and 9 hub genes, respectively. The names of the modules are indicated. The predicted transcriptional regulatory network [significantly enriched hub gene-binding sites along with the associated genes and enriched gene ontology (GO) terms] associated with the gene sets showing expression patterns at selected target gene modules are given. The significantly enriched cis-regulatory motifs (yellow triangles), GO terms (green hexagons) and other regulatory genes (blue circles) within the given set of genes. The hub genes are represented by magenta circles. Edges represent known interactions between the cis-regulatory motifs and hub genes.

binding, developmental process, integral component of organelle membrane, extracellular region and transferase activity (purple module) (Figures 6E–H). Overall, these analyses identified key regulators of root response to drought stress and suggested that root response to drought stress processes are regulated differentially in the two potato cultivars.

Reverse-transcription quantitative PCR verification of core genes

Fifty-five core genes potentially associated with drought stress were selected from the eight gene modules with the highest correlations (Table S3), and 18 candidate genes involved in different processes were randomly selected. These genes were selected as candidate genes to determine the mechanisms regulating potato rooting depth and root response to drought stress. Gene expression was verified by fluorescent quantitative reverse transcription PCR (RT-qPCR). The backup RNA used for transcriptome sequencing was reverse transcribed, and the responses of the 18 genes to drought stress in C16 and C119 were detected by RT-qPCR. The changes in expression were generally consistent with transcriptome results (Figure 7), further demonstrating the reliability of the transcriptome sequencing results and confirming the response of the major genes to drought stress.

Discussion

The molecular mechanisms underlying differences in rooting depth and root response to drought stress are poorly understood in potato. In this study, RNA-seq was used to determine transcriptome dynamics in two potato cultivars with different rooting depths (shallow vs. deep) at different stages of drought stress. The molecular mechanisms underlying root responses to drought stress and differences in rooting depth were then investigated. RNA-seq investigation allowed the discovery of new genes and their expression profiles. The expression data of the three root responses to drought stress phases showed high reproducibility in both potato cultivars and clear separation between cultivars in the PCA (principal component analysis) diagram, suggesting that potato cultivars may have different mechanisms for responding to drought stress. The dataset comprehensively describes the transcriptional activity of potato roots at different stages of drought stress. In coexpression networks and transcriptional modules, several coregulatory and specific transcriptional programs within and between cultivars have been linked to rooting depth and root response to drought stress.

The differential distribution of resources during root formation determines whether roots are deep or shallow in different plant species (Zhou et al., 2020b). In addition, greater root depth is associated with increases in other traits, including the number of lateral roots, stem thickness, and root strength (Gala et al., 2021). Common genetic components are thought to regulate root number and other organs *via* effects on cell cycle and developmental duration (Linkies et al., 2010). A prolonged phase of cell division that increases the number of cells in root hairs or lateral roots is thought to be responsible for root depth (Fernandez et al., 2020). Root length of the two potato cultivars increased after 20 days of drought stress, suggesting that this period represents a transition between cell division and maturation. The difference in the rate of increase in root length suggests that there were differences in the number of cell divisions between the two potato cultivars. Gene ontology enrichment analysis showed that C119 has a prolonged cell division cycle and relatively high expression of genes involved in cell division and cell cycle. In maize, a prolonged root growth

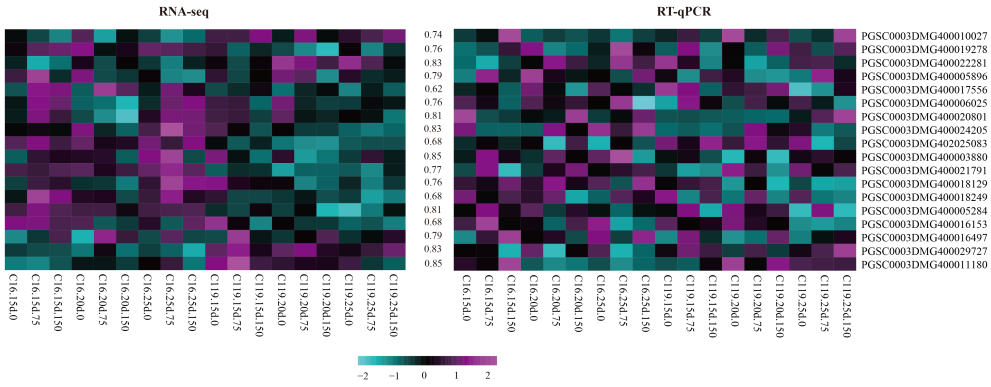

FIGURE 7
Heat maps of correlations between expression profiles of selected genes (highlighted on the right) obtained from RNA-sequencing (RNA-seq) and quantitative reverse-transcription PCR (RT-qPCR). The lower color scale represents *Z*-scores. The values between the two heatmaps represent the correlation coefficients between the expression profiles obtained from RNA-sequencing and RT-qPCR analysis of each gene.

period is associated with relatively high gluconeogenesis, which plays a key role in determining root length (Yu et al., 2021). The increased cell number in C119 could lead to increased accumulation of storage substances and proteins and stimulation of cell growth and proliferation. Meristem cell number and root length were also positively correlated (Di Mambro et al., 2019). In C119, the enriched GO terms mainly included peroxidase activity, cellular response to hormonal stimuli, and integral component of peroxisomal membrane, suggesting a relatively high cell division ability and an important role of peroxide signalling in determining potato root responses to drought stress. A crucial role of peroxidase in determining root responses to drought stress was also found in a previous study (Su et al., 2018). Moreover, relatively the high transcriptional activity of several genes related to the metabolic process of reactive oxygen species, signal transduction, response to oxygenated compounds, transferase activity, and glycosyl group transfer was associated with drought resistance in the deep-rooted potato cultivar. In previous studies, we found that C16 and C119 have significant differences in phytohormone signal transduction pathways, which is consistent with our previous findings (Qin et al., 2022). Thus, a prolonged cell division period that increases the number of cells could explain the deep rooting and strong drought resistance of C119.

Many TF families have been associated with root development (Yamada et al., 2020; Zhang et al., 2021) but few TFs have been associated with root length determination and drought resistance. In the data set of this study, about 60% of TFs were differentially expressed between C16 and C119, suggesting differences in transcriptional regulatory networks between potato cultivars. Among the differentially expressed TF-coding genes, TF families with known functions were represented; however, the exact functions of most of these genes remain unknown. The role of some members of TF families, such as ARF, bZIP, MYB-related, and WRKY, which exhibited differential regulation among potato cultivars, are well known in root responses to drought stress (Jiang et al., 2017; Joo et al., 2021; Wei et al., 2021; Yang et al., 2021). Differential regulation of the same gene family members in different potato cultivars may result in different regulatory networks that can determine cultivar-specific rooting depth and root response to drought stress. To better understand root responses to drought stress, coexpression networks were analyzed, and unique gene sets and modules were determined that contained a significant number of hub genes associated with responses to different stages of drought stress in both cultivars. Hub genes may serve as regulatory components to coordinate the activities of co-expressed genes within a module. The GO enrichment analysis of the modules highlighted the role of different biological processes and pathways in root response to drought stress and suggested that different regulatory pathways control root depth in response to drought stress.

In *Arabidopsis thaliana*, root regulatory gene circuits in response to drought stress have been elucidated based on comprehensive transcriptome mapping of roots (Rasheed et al., 2016; Bashir et al., 2018). Transcriptional module discovery can identify coexpression networks that control biological processes associated with root development (Du et al., 2020; Wang et al., 2021b). Therefore, we generated transcriptional modules of nuclear genes for potato root development and co-expressed target genes in C16 and C119 that could determine the differences in root development and rooting depth between the two potato cultivars. Analysis of potential binding motifs on the hub genes revealed that despite the extensive overlap of motifs on the hub genes of C16 and C119, several components exhibit cultivar specificity, which determines the unique transcriptional modules of the two potato cultivars.

This study has shown that transcriptional modules construction and coexpression network analysis are powerful tools for understanding the molecular mechanisms underlying agronomic traits, such as root development and root response to drought stress. However, further functional studies on individual members of the network are needed in order to fully understand the coexpression network.

Materials and methods

Plant Material

Two potato genotypes, C16 (CIP 397077.16, shallow rooted) and C119 (CIP 398098.119, deep-rooted), were provided by the International Potato Research Center (Peru). Both genotypes had the same growth cycle but different root structures and drought resistance. The Key Laboratory of Crop Genetic Improvement and Germplasm Innovation at Gansu Agricultural University provided tissue cultured seedlings of C16 and C119 (Table 1). Stem sections of potato test-tube plantlets were transferred to paper boats floating on liquid MS (Murashige and Skoog) medium containing 0 mM (control) or 75 mM or 150 mM mannitol (drought stress treatments) (Hamooh et al., 2021; Sattar et al., 2021). After 15, 20, and 25 days of growth, the paper boats containing the tube seedlings were carefully removed. There were three biological replicates for each treatment. After treatment, the roots of the seedlings were removed, immediately frozen in liquid nitrogen extraction, and then stored in the refrigerator at −80°C. Half of each stored sample was used for RNA for subsequent transcriptome sequencing. The other half was used to determine physiological and biochemical indicators of stress resistance.

Illumina sequencing, read mapping, and differential gene expression analyses

For RNA-seq, total RNA extraction and library preparation for each sample were performed as previously described (Garg et al., 2016). All 54 libraries (1 sample with three biological replicates) were sequenced on an Illumina platform (Zhang et al., 2014), Beijing Genomics Institute, Shenzhen, Guangdong, China) to

generate double-end sequence reads of 150 nucleotides. The NGS QC toolkit (Patel and Jain, 2012), as previously described (Garg et al., 2016), was used to evaluate the various quality parameters of the original sequence data and philtre high-quality reads. The filtered high-quality reads were mapped to the potato genome (Felcher et al., 2012) using TopHat (v2.0.0, Centre for Bioinformatics and Computational Biology at the University of Maryland, College Park, MD, USA) with default parameters. The mapped output was processed through Cufflinks (v2.0.2) to obtain TPM (transcripts per million) for all potato genes in each sample. Correlations between biological replicates were determined by calculating the SCC (Spearman correlation coefficient). The corrplot and scatterplot3d utilities of the R software package (version 4.1.1) were used for hierarchical clustering and PCA, respectively. Differential expression between different samples was measured using the DESeq2 of the R package. After correction for false discovery rate (Qvalue), genes with at least a *twofold* difference and a corrected P-value < 0.05 were considered significantly differentially expressed. For a given set of genes, the Z-score of a line was determined, and the heatmap2 of the R package was used to generate the heatmap.

Gene ontology and pathway enrichment analysis

Gene ontology enrichment analysis of DEG sets was performed using the AgriGo online tool (http://systemsbiology.cau.edu.cn/agriGOv2/index.php) (Tian et al., 2017; Liu et al., 2018). The enrichment P-value of each representative GO term was calculated and then corrected by the Benjamini–Hochberg error correction method. The significantly enriched GO terms had a corrected (after adjusting for false discovery rate) P-value ≤ 0.05. Pathway enrichment across different genomes was analyzed using MapMan (v3.5.1R2) classification for optimal Arabidopsis (TAIR10, https://www.arabidopsis.org/) homologues.

Reverse-transcription quantitative PCR analysis

Results of RNA-seq were verified by RT-qPCR experiment. Reverse-transcription PCR analysis was performed as previously described (Garg et al., 2016). First-strand cDNA was synthesized using a PrimeScript RT kit (Takara Bio Inc., Shiga, Japan). The gene-specific primers designed with Prime3Plus (http://primer3plus.com/cgi-bin/dev/primer3plus.cgi) are listed in Table S4. The internal reference gene was Actin I (Kühn and Mannherz, 2017). The qPCR was performed on a Quant Studio 5 (Life Technologies Holdings Pte Ltd., Singapore) using SYBR Premix Ex Taq II (Tli RNaseH Plus; Takara Bio Inc.). PCR analysis was performed using three biological replicates of each sample and at least three technical replicates of each biological replicate.

Determination of physiological and biochemical indicators

Physiological and biochemical indices (superoxide dismutase (SOD), peroxidase (POD), catalase (CAT), root vitality (RV), proline (pro), soluble sugar (SS)) were determined using a kit (elisa., Shanghai, China). Root length (Len), root diameter (Diam), root volume (Vol), root tips (Tips), and root forks (Forks) were measured using a root scanner (EPSON EXPRESSION 10000XL., Suwa, Japan). Each index was establishe with three biological replicates and three technical replicates.

Coexpression network analysis for construction of modules

The WGCNA package was used for coexpression network analysis (Massa et al., 2011; Childs et al., 2011; Jain et al., 2017; Ma et al., 2021). Based on log2 (1+TPM) values, the paired SCC matrix between all gene pairs was generated and converted to an adjacency matrix (connection strength matrix) using the following formula: Strength of connection (adjacency value) = |(1 + correlation)/2| β, where β represents the soft threshold of the correlation matrix that gives greater weight to the strongest correlation while maintaining gene–gene connectivity. A β-value of 10 was chosen according to the scale-free topological criteria described by Yang and Horvath (Langfelder and Horvath, 2008; Zhao et al., 2021). The adjacency matrix was converted to a topological overlap matrix (TO) by a TOM similarity algorithm, and genes were hierarchically clustered based on similarity. A dynamic tree pruning algorithm was used to prune the hierarchical cluster tree, and modules were defined after decomposing and combining branches to achieve a stable number of clusters (Langfelder and Horvath, 2008). For each module, the summary contour (characteristic module gene, ME) was calculated by PCA. In addition, modules with values

TABLE 1 Summary of the plant material used in this study.

Variety	CIP Number	Maternal Parent	Paternal Parent
C 16	CIP397077.16	392025.7 (=LR93.221)	392820.1 (=C93.154)
C 119	CIP398098.119	393371.58	392639.31

(the average TO of all genes in a given module) that were higher than the TO values of modules consisting of randomly selected genes were selected. *The Homer software was used for motif enrichment analysis (*Zhu et al., 2021*).* Cytoscape and Agrigo were used for GO enrichment analysis of each module.

Conclusions

In summary, RNA-seq data from two potato cultivars with different rooting depths (shallow and deep) provide a robust resource for studying potato root biology, including root development and root response to drought stress. Gene sets expressed at specific stages were identified, enriched biological processes and pathways were determined, and co-expressed gene sets were defined with high temporal resolution. In addition, genes coexpression networks that play a role in the response of deep and shallow roots to different stages of drought stress were identified, and nodal genes that regulate stage-specific root responses to drought stress were investigated. A prolonged period of cell division and an increase in peroxidase activity were primarily responsible for deep rooting and strong drought resistance in potato C119. Correlations between TFs with known functions and genes related to rooting depth and drought stress response identified 18 potential target genes that could determine rooting depth and root response to drought stress. Overall, this study demonstrates that transcriptional profiling and inferred coexpression networks, together with plant physiology approaches, can help identify the most promising candidate genes and determine the precise role in root response to drought stress. The comprehensive information presented in this study can be an important resource to improve our understanding of root responses to drought stress, especially the differences between deep-rooted and shallow-rooted potatoes. These new findings greatly improve our understanding of the genetic and molecular basis of drought resistance in two different potato genotypes and provide important clues for molecular breeding of drought-resistant cultivars.

Data availability statement

The datasets presented in this study can be found in online repositories: https://www.ncbi.nlm.nih.gov/bioproject/?term=PRJNA851475.

Author contributions

Conceptualization, TQ; methodology, TQ, AK; investigation, TQ, CS; data curation, TQ, CS, and JB; writing—original draft preparation, TQ; writing—review and editing, CS, YW. DR, AK, PY, ZB, YL, and JB; All authors have read and agreed to the published version of the manuscript.

Funding

This research was funded by the National Natural Science Foundation of China (Grant No. 32060502 and 31960442), Agriculture Potato Research System of MOF and MARA (CARS-09-P10), the Gansu Science and Technology fund (Grant No. 22JR5RA835, 22JR5RA833, 20YF8WA137, 21JR7RA804 and 19ZD2WA002-02).

Conflict of interest

The authors declare that the research was conducted in the absence of any commercial or financial relationships that could be construed as a potential conflict of interest.

Publisher's note

Supplementary material

The Supplementary Material for this article can be found online at: https://www.frontiersin.org/articles/10.3389/fpls.2022.1007866/full#supplementary-material

References

Bachmair, A., Novatchkova, M., Potuschak, T., and Eisenhaber, F. (2001). Ubiquitylation in plants: a post–genomic look at a post–translational modification. *Trends Plant Sci.* 6 (10), 463–470. doi: 10.1016/s1360–1385(01)02080–5

Bach-Pages, M., Homma, F., Kourelis, J., Kaschani, F., Mohammed, S., Kaiser, M., et al. (2020). Discovering the RNA–binding proteome of plant leaves with an improved RNA interactome capture method. *Biomolecules.* 10 (4), 661. doi: 10.3390/biom10040661

Barnaby, J. Y., Fleisher, D. H., Singh, S. K., Sicher, R. C., and Reddy, V. R. (2019). Combined effects of drought and CO 2 enrichment on foliar metabolites of potato (Solanum tuberosum l.) cultivars. *J. Plant Interactions.* 14 (1), 110–118. doi: 10.1080/17429145.2018.1562110

Bashir, K., Rasheed, S., Matsui, A., Iida, K., Tanaka, M., and Seki, M. (2018). Monitoring transcriptomic changes in soil-grown roots and shoots of *Arabidopsis thaliana* subjected to a progressive drought stress. *Methods Mol. Biol.* 1761, 223–230. doi: 10.1007/978-1-4939-7747-5_17

Bolger, M., Schwacke, R., and Usadel, B. (2021). MapMan visualization of RNA–seq data using Mercator4 functional annotations. *Methods Mol. Biol.* 2354, 195–212. doi: 10.1007/978–1–0716–1609–3_9

Chai, Y. N., and Schachtman, D. P. (2022). Root exudates impact plant performance under abiotic stress. trends. *Plant Sci.* 27 (1), 80–91. doi: 10.1016/j.tplants.2021.08.003

Chen, Q., Hu, T., Li, X., Song, C. P., Zhu, J. K., Chen, L., et al. (2022). Phosphorylation of SWEET sucrose transporters regulates plant root:shoot ratio under drought. *Nat. Plants.* 8 (1), 68–77. doi: 10.1038/s41477–021–01040–7

Childs, K. L., Davidson, R. M., and Buell, C. R. (2011). Gene coexpression network analysis as a source of functional annotation for rice genes. *PloS One* 6 (7), e22196. doi: 10.1371/journal.pone.0022196

Di Mambro, R., Svolacchia, N., Dello Ioio, R., Pierdonati, E., Salvi, E., Pedrazzini, E., et al. (2019). The lateral root cap acts as an auxin sink that controls meristem size. *Curr. Biol.* 29 (7), 1199–1205. doi: 10.1016/j.cub.2019.02.022

Doncheva, N. T., Morris, J. H., Gorodkin, J., and Jensen, L. J. (2019). Cytoscape StringApp: Network analysis and visualization of proteomics data. *J. Proteome Res.* 18 (2), 623–632. doi: 10.1021/acs.jproteome.8b00702

Du, H., Ning, L., He, B., Wang, Y., Ge, M., Xu, J., et al. (2020). Cross-species root transcriptional network analysis highlights conserved modules in response to nitrate between maize and sorghum. *Int. J. Mol. Sci.* 21 (4), 1445. doi: 10.3390/ijms21041445

Felcher, K. J., Coombs, J. J., Massa, A. N., Hansey, C. N., Hamilton, J. P., Veilleux, R. E., et al. (2012). Integration of two diploid potato linkage maps with the potato genome sequence. *PloS One* 7 (4), e36347. doi: 10.1371/journal.pone.0036347

Fernández–Pérez, F., Pomar, F., Pedreño, M. A., and Novo–Uzal, E. (2015). The suppression of AtPrx52 affects fibers but not xylem lignification in *Arabidopsis* by altering the proportion of syringyl units. *Physiol. Plant* 154 (3), 395–406. doi: 10.1111/ppl.12310

Fernandez, A. I., Vangheluwe, N., Xu, K., Jourquin, J., Claus, L. A. N., Morales–Herrera, S., et al. (2020). GOLVEN peptide signalling through RGI receptors and MPK6 restricts asymmetric cell division during lateral root initiation. *Nat. Plants.* 6 (5), 533–543. doi: 10.1038/s41477–020–0645–z

Fernie, A. R., and Willmitzer, L. (2002). Molecular and biochemical triggers of potato tuber development. *Plant Physiol.* 127 (4), 1459–1465. doi: 10.1104/pp.010764

Gala, H. P., Lanctot, A., Jean–Baptiste, K., Guiziou, S., Chu, J. C., Zemke, J. E., et al. (2021). A single–cell view of the transcriptome during lateral root initiation in *Arabidopsis thaliana*. *Plant Cell.* 33 (7), 2197–2220. doi: 10.1093/plcell/koab101

Garg, R., Shankar, R., Thakkar, B., Kudapa, H., Krishnamurthy, L., Mantri, N., et al. (2016). Transcriptome analyses reveal genotype– and developmental stage–specific molecular responses to drought and salinity stresses in chickpea. *Sci. Rep.* 6, 19228. doi: 10.1038/srep19228

Gutierrez, L., Bussell, J. D., Pacurar, D. I., Schwambach, J., Pacurar, M., and Bellini, C. (2009). Phenotypic plasticity of adventitious rooting in *Arabidopsis* is controlled by complex regulation of AUXIN RESPONSE FACTOR transcripts and microRNA abundance. *Plant Cell.* 21 (10), 3119–3132. doi: 10.1105/tpc.108.064758

Hamooh, B. T., Sattar, F. A., Wellman, G., and Mousa, M. A. A. (2021). Metabolomic and biochemical analysis of two potato (Solanum tuberosum l.) cultivars exposed to *In vitro* osmotic and salt stresses. *Plants (Basel).* 10 (1), 98. doi: 10.3390/plants10010098

Hanada, K., Sawada, Y., Kuromori, T., Klausnitzer, R., Saito, K., Toyoda, T., et al. (2011). Functional compensation of primary and secondary metabolites by duplicate genes in *Arabidopsis thaliana*. *Mol. Biol. Evol.* 28 (1), 377–382. doi: 10.1093/molbev/msq204

Holzwart, E., Huerta, A. I., Glöckner, N., Garnelo Gómez, B., Wanke, F., Augustin, S., et al. (2018). BRI1 controls vascular cell fate in the *Arabidopsis* root through RLP44 and phytosulfokine signaling. *Proc. Natl. Acad. Sci. U S A.* 115 (46), 11838–11843. doi: 10.1073/pnas.1814434115

Jain, P., Singh, P. K., Kapoor, R., Khanna, A., Solanke, A. U., Krishnan, S. G., et al. (2017). Understanding host–pathogen interactions with expression profiling of NILs carrying rice–blast resistance Pi9 gene. *Front. Plant Science.* 8, 93. doi: 10.3389/fpls.2017.00093

Jean-Baptiste, K., McFaline–Figueroa, J. L., Alexandre, C. M., Dorrity, M. W., Saunders, L., Bubb, K. L., et al. (2019). Dynamics of gene expression in single root cells of *Arabidopsis thaliana*. *Plant Cell.* 31 (5), 993–1011. doi: 10.1105/tpc.18.00785

Jia, K. P., Dickinson, A. J., Mi, J., Cui, G., Xiao, T. T., Kharbatia, N. M., et al. (2019). Anchorene is a carotenoid–derived regulatory metabolite required for anchor root formation in *Arabidopsis*. *Sci. Adv.* 5 (11), eaaw6787. doi: 10.1126/sciadv.aaw6787

Jiang, J., Ma, S., Ye, N., Jiang, M., Cao, J., and Zhang, J. (2017). WRKY transcription factors in plant responses to stresses. *J Integr Plant Biol.* 59 (2), 86–101. doi: 10.1111/jipb.12513

Joo, H., Baek, W., Lim, C. W., and Lee, S. C. (2021). Post–translational modifications of bZIP transcription factors in abscisic acid signaling and drought responses. *Curr. Genomics* 22 (1), 4–15. doi: 10.2174/1389202921999201130112116

Kudapa, H., Azam, S., Sharpe, A. G., Taran, B., Li, R., Deonovic, B., et al. (2014). Comprehensive transcriptome assembly of chickpea (Cicer arietinum l.) using sanger and next generation sequencing platforms: development and applications. *PloS One* 9 (1), e86039. doi: 10.1371/journal.pone.0086039

Kühn, S., and Mannherz, H. G. (2017). Actin: Structure, function, dynamics, and interactions with bacterial toxins. *Curr. Top. Microbiol. Immunol.* 399, 1–34. doi: 10.1007/82_2016_45

Langfelder, P., and Horvath, S. (2007). Eigengene networks for studying the relationships between co–expression modules. *BMC Syst. Biol.* 1, 54. doi: 10.1186/1752–0509–1–54

Langfelder, P., and Horvath, S. (2008). WGCNA: an r package for weighted correlation network analysis. *BMC Bioinf.* 9, 559. doi: 10.1186/1471-2105-9-559

Liesecke, F., Daudu, D., Dugé de Bernonville, R., Besseau, S., Clastre, M., Courdavault, V., et al. (2018). Ranking genome–wide correlation measurements improves microarray and RNA–seq based global and targeted co–expression networks. *Sci. Rep.* 8 (1), 10885. doi: 10.1038/s41598–018–29077–3

Linkies, A., Graeber, K., Knight, C., and Leubner–Metzger, G. (2010). The evolution of seeds. *New Phytol.* 186 (4), 817–831. doi: 10.1111/j.1469–8137.2010.03249.x

Li, W., Richter, R. A., Jung, Y., Zhu, Q., and Li, R. W. (2016). Web–based bioinformatics workflows for end–to–end RNA–seq data computation and analysis in agricultural animal species. *BMC Genomics* 17 (1), 761. doi: 10.1186/s12864–016–3118–z

Liu, Q., Liang, Z., Feng, D., Jiang, S., Wang, Y., Du, Z., et al. (2021). Transcriptional landscape of rice roots at the single–cell resolution. *Mol. Plant* 14 (3), 384–394. doi: 10.1016/j.molp.2020.12.014

Liu, W., Liu, J., and Rajapakse, J. C. (2018). Gene ontology enrichment improves performances of functional similarity of genes. *Sci. Rep.* 8 (1), 12100. doi: 10.1038/s41598-018-30455-0

Li, K., Zhang, S., Tang, S., Zhang, J., Dong, H., Yang, S., et al. (2022). The rice transcription factor Nhd1 regulates root growth and nitrogen uptake by activating nitrogen transporters. *Plant Physiol.* 20, 178. doi: 10.1093/plphys/kiac178

Marand, A. P., Chen, Z., Gallavotti, A., and Schmitz, R. J. (2021). A cis–regulatory atlas in maize at single–cell resolution. *Cell.* 184 (11), 3041–3055.e21. doi: 10.1016/j.cell.2021.04.014

Massa, A. N., Childs, K. L., Lin, H., Bryan, G. J., Giuliano, G., and Buell, C. R. (2011). The transcriptome of the reference potato genome solanum tuberosum group phureja clone DM1–3 516R44. *PloS One* 6 (10), e26801. doi: 10.1371/journal.pone.0026801

Maurel, C., and Nacry, P. (2020). Root architecture and hydraulics converge for acclimation to changing water availability. *Nat. Plants.* 6 (7), 744–749. doi: 10.1038/s41477–020–0684–5

Ma, L., Zhang, M., Chen, J., Qing, C., He, S., Zou, C., et al. (2021). GWAS and WGCNA uncover hub genes controlling salt tolerance in maize (Zea mays l.) seedlings. *Theor. Appl. Genet.* 134 (10), 3305–3318. doi: 10.1007/s00122–021–03897–w

Mousavian, Z., Khodabandeh, M., Sharifi-Zarchi, A., Nadafian, A., and Mahmoudi, A. (2021). StrongestPath: a cytoscape application for protein-protein interaction analysis. *BMC Bioinf.* 22 (1), 352. doi: 10.1186/s12859-021-04230-4

Nicolas, M., Torres–Pérez, R., Wahl, V., Cruz–Oró, E., Rodríguez–Buey, M. L., Zamarreño, A. M., et al. (2022). Spatial control of potato tuberization by the TCP transcription factor BRANCHED1b. *Nat. Plants.* 8 (3), 281–294. doi: 10.1038/s41477–022–01112–2

Omary, M., Gil–Yarom, N., Yahav, C., Steiner, E., Hendelman, A., and Efroni, I. (2022). A conserved superlocus regulates above– and belowground root initiation. *Science.* 37 (6584), eabf4368. doi: 10.1126/science.abf4368

Panahi, B., and Hejazi, M. A. (2021). Weighted gene co–expression network analysis of the salt–responsive transcriptomes reveals novel hub genes in green halophytic microalgae dunaliella salina. *Sci. Rep.* 11 (1), 1607. doi: 10.1038/s41598–020–80945–3

Patel, R. K., and Jain, M. (2012). NGS QC toolkit: a toolkit for quality control of next generation sequencing data. *PloS One* 7 (2), e30619. doi: 10.1371/journal.pone.0030619

Qin, T., Sun, C., Kazim, A., Cui, S., Wang, Y., Richard, D., et al. (2022). Comparative transcriptome analysis of deep-rooting and shallow-rooting potato

(*Solanum tuberosum* l.) genotypes under drought stress. *Plants (Basel).* 11 (15), 2024. doi: 10.3390/plants11152024

Rasheed, S., Bashir, K., Matsui, A., Tanaka, M., and Seki, M. (2016). Transcriptomic analysis of soil-grown *Arabidopsis thaliana* roots and shoots in response to a drought stress. *Front. Plant Sci.* 7. doi: 10.3389/fpls.2016.00180

Reynoso, M. A., Borowsky, A. T., Pauluzzi, G. C., Yeung, E., Zhang, J., and Formentin, E. (2022). Gene regulatory networks shape developmental plasticity of root cell types under water extremes in rice. *Dev. Cell.* 57 (9), 1177–1192. doi: 10.1016/j.devcel.2022.04.013

Sattar, F. A., Hamooh, B. T., Wellman, G., Ali, M. A., Shah, S. H., Anwar, Y., et al. (2021). Growth and biochemical responses of potato cultivars under *In vitro* lithium chloride and mannitol simulated salinity and drought stress. *Plants (Basel).* 10 (5), 924. doi: 10.3390/plants10050924

Sheng, L., Hu, X., Du, Y., Zhang, G., Huang, H., Scheres, B., et al. (2017). Non–canonical WOX11–mediated root branching contributes to plasticity in *Arabidopsis* root system architecture. *Development.* 144 (17), 3126–3133. doi: 10.1242/dev.152132

Shigeto, J., Nagano, M., Fujita, K., and Tsutsumi, Y. (2014). Catalytic profile of *Arabidopsis* peroxidases, AtPrx–2, 25 and 71, contributing to stem lignification. *PloS One* 9 (8), e105332. doi: 10.1371/journal.pone.0105332

Singh, V. K., Garg, R., and Jain, M. (2013). A global view of transcriptome dynamics during flower development in chickpea by deep sequencing. *Plant Biotechnol. J.* 11 (6), 691–701. doi: 10.1111/pbi.12059

Su, F., Li, Y., Liu, S., Liu, Z., and Xu, H. (2020). Application of xerophytophysiology and signal transduction in plant production: Partial root–zone drying in potato crops. *Potato Res.* 63, 41–56. doi: 10.1007/s11540-019-09427-y

Sun, H., Jiao, W. B., Krause, K., Campoy, J. A., Goel, M., Folz–Donahue, K., et al. (2022). Chromosome–scale and haplotype–resolved genome assembly of a tetraploid potato cultivar. *Nat. Genet.* 54 (3), 342–348. doi: 10.1038/s41588–022–01015–0

Su, T., Wang, P., Li, H., Zhao, Y., Lu, Y., Dai, P., et al. (2018). The *Arabidopsis* catalase triple mutant reveals important roles of catalases and peroxisome–derived signaling in plant development. *J. Integr. Plant Biol.* 60 (7), 591–607. doi: 10.1111/jipb.12649

ten Hove, C. A., Bochdanovits, Z., Jansweijer, V. M., Koning, F. G., Berke, L., Sanchez–Perez, G. F., et al. (2011). Probing the roles of LRR RLK genes in *Arabidopsis thaliana* roots using a custom T–DNA insertion set. *Plant Mol. Biol.* 76 (1–2), 69–83. doi: 10.1007/s11103–011–9769–x

Tian, T., Liu, Y., Yan, H., You, Q., Yi, X., Du, Z., et al. (2017). agriGO v2.0: a GO analysis toolkit for the agricultural community 2017 update. *Nucleic Acids Res.* 45 (W1), W122–W129. doi: 10.1093/nar/gkx382

Trapnell, C., Roberts, A., Goff, L., Pertea, G., Kim, D., Kelley, D. R., et al. (2012). Differential gene and transcript expression analysis of RNA–seq experiments with TopHat and cufflinks. *Nat. Protoc.* 7 (3), 562–578. doi: 10.1038/nprot.2012.016

Vanhees, D. J., Loades, K. W., Bengough, A. G., Mooney, S. J., and Lynch, J. P. (2020). Root anatomical traits contribute to deeper rooting of maize under compacted field conditions. *J. Exp. Bot.* 71 (14), 4243–4257. doi: 10.1093/jxb/eraa165

Wang, D. (2018). hppRNA–a snakemake–based handy parameter–free pipeline for RNA–seq analysis of numerous samples. *Brief Bioinform.* 19 (4), 622–626. doi: 10.1093/bib/bbw143

Wang, Y., Huan, Q., Li, K., and Qian, W. (2021a). Single–cell transcriptome atlas of the leaf and root of rice seedlings. *J. Genet. Genomics* 48 (10), 881–898. doi: 10.1016/j.jgg.2021.06.001

Wang, Y., Sun, H., Wang, H., Yang, X., Xu, Y., Yang, Z., et al. (2021b). Integrating transcriptome, co-expression and QTL-seq analysis reveals that primary root growth in maize is regulated *via* flavonoid biosynthesis and auxin signal transduction. *J. Exp. Bot.* 72 (13), 4773–4795. doi: 10.1093/jxb/erab177

Wang, C., Wang, H., Li, P., Li, H., Xu, C., Cohen, H., et al. (2020a). Developmental programs interact with abscisic acid to coordinate root suberization in *Arabidopsis*. *Plant J.* 104 (1), 241–251. doi: 10.1111/tpj.14920

Wang, X., Whalley, W. R., Miller, A. J., White, P. J., Zhang, F., and Shen, J. (2020b). Sustainable cropping requires adaptation to a heterogeneous rhizosphere. trends. *Plant Sci.* 25 (12), 1194–1202. doi: 10.1016/j.tplants.2020.07.006

Wang, Y., Zhang, W. Z., Song, L. F., Zou, J. J., Su, Z., and Wu, W. H. (2008). Transcriptome analyses show changes in gene expression to accompany pollen germination and tube growth in *Arabidopsis*. *Plant Physiol.* 148 (3), 1201–1211. doi: 10.1104/pp.108.126375

Wei, S., Chen, Y., Hou, J., Yang, Y., and Yin, T. (2021). Aux/iaa and arf gene families in salix suchowensis: identification, evolution, and dynamic transcriptome profiling during the plant growth process. *Front Plant Sci.* 12, 666310. doi: 10.3389/fpls.2021.666310

Welinder, K. G., Justesen, A. F., Kjaersgard, I. V., Jensen, R. B., Rasmussen, S. K., Jespersen, H. M., et al. (2002). Structural diversity and transcription of class III peroxidases from *Arabidopsis thaliana*. *Eur. J. Biochem.* 269(24), 6063–6081. doi: 10.1046/j.1432–1033.2002.03311.x

Xu, L., Zhao, H., Ruan, W., Deng, M., Wang, F., Peng, J., et al. (2017). ABNORMAL INFLORESCENCE MERISTEM1 functions in salicylic acid biosynthesis to maintain proper reactive oxygen species levels for root meristem activity in rice. *Plant Cell.* 29(3), 560–574. doi: 10.1105/tpc.16.00665

Yamada, M., Han, X., and Benfey, P. N. (2020). RGF1 controls root meristem size through ROS signalling. *Nat.* 577 (7788), 85–88. doi: 10.1038/s41586–019–1819–6

Yang, X., Guo, T., Li, J., Chen, Z., Guo, B., An, X., et al (2021). Genome-wide analysis of the MYB-related transcription factor family and associated responses to abiotic stressors in Populus. *Int J Biol Macromol.* 191, 359–376. doi: 10.1016/j.ijbiomac.2021.09.042

Yu, P., He, X., Baer, M., Beirinckx, S., Tian, T., Moya, Y. A. T., et al. (2021). Plant flavones enrich rhizosphere oxalobacteraceae to improve maize performance under nitrogen deprivation. *Nat. Plants.* 7 (4), 481–499. doi: 10.1038/s41477–021–00897–y

Zhang, Y., Mitsuda, N., Yoshizumi, T., Horii, Y., Oshima, Y., Ohme–Takagi, M., et al. (2021). Two types of bHLH transcription factor determine the competence of the pericycle for lateral root initiation. *Nat. Plants.* 7 (5), 633–643. doi: 10.1038/s41477–021–00919–9

Zhang, W., Song, W., Zhang, Z., Wang, H., Yang, M., Guo, R., et al. (2014). Transcriptome analysis of Dastarcus helophoroides (Coleoptera: Bothrideridae) using Illumina HiSeq sequencing. *PLoS One*. 9 (6), e100673. doi: 10.1371/journal.pone.0100673

Zhao, F., Maren, N. A., Kosentka, P. Z., Liao, Y. Y., Lu, H., Duduit, J. R., et al. (2021). An optimized protocol for stepwise optimization of real–time RT–PCR analysis. *Hortic. Res.* 8 (1), 179. doi: 10.1038/s41438-021-00616-w

Zhao, D., Wang, Y., Feng, C., Wei, Y., Peng, X., Guo, X., et al. (2020). Overexpression of MsGH3.5 inhibits shoot and root development through the auxin and cytokinin pathways in apple plants. *Plant J.* 103 (1), 166–183. doi: 10.1111/tpj.14717

Zhou, S., Jiang, W., Long, F., Cheng, S., Yang, W., Zhao, Y., et al. (2017). Rice homeodomain protein WOX11 recruits a histone acetyltransferase complex to establish programs of cell proliferation of crown root meristem. *Plant Cell.* 5, 1088–1104. doi: 10.1105/tpc.16.00908

Zhou, Q., Tang, D., Huang, W., Yang, Z., Zhang, Y., Hamilton, J. P., et al. (2020a). Haplotype–resolved genome analyses of a heterozygous diploid potato. *Nat. Genet.* 52 (10), 1018–1023. doi: 10.1038/s41588–020–0699–x

Zhou, Y., Wigley, B. J., Case, M. F., Coetsee, C., and Staver, A. C. (2020b). Rooting depth as a key woody functional trait in savannas. *New Phytol.* 227 (5), 1350–1361. doi: 10.1111/nph.16613

Zhu, H., Zhang, Y., Zhang, C., and Xie, Z. (2021). RNA-Binding profiles of CKAP4 as an RNA-binding protein in myocardial tissues. *Front. Cardiovasc. Med.* 8. doi: 10.3389/fcvm.2021.773573

frontiers | Frontiers in Plant Science

TYPE Original Research
PUBLISHED 02 November 2022
DOI 10.3389/fpls.2022.1041095

OPEN ACCESS

EDITED BY
Yi Han,
Anhui Agricultural University, China

REVIEWED BY
Fujun Qin,
Zhengzhou University, China
Xiaoyun Liu,
Jianghan University, China

*CORRESPONDENCE
Yongfeng Hu
huyongfeng@ctgu.edu.cn
Qiong Luo
qiongbf@aliyun.com
Feng Tan
tanfeng@niau.edu.cn

†These authors have contributed equally to this work

SPECIALTY SECTION
This article was submitted to Plant Bioinformatics, a section of the journal Frontiers in Plant Science

RECEIVED 10 September 2022
ACCEPTED 13 October 2022
PUBLISHED 02 November 2022

CITATION
Xu Y, Miao Y, Cai B, Yi Q, Tian X, Wang Q, Ma D, Luo Q, Tan F and Hu Y (2022) A histone deacetylase inhibitor enhances rice immunity by derepressing the expression of defense-related genes. *Front. Plant Sci.* 13:1041095. doi: 10.3389/fpls.2022.1041095

A histone deacetylase inhibitor enhances rice immunity by derepressing the expression of defense-related genes

Yan Xu[1†], Yuanxin Miao[1†], Botao Cai[2], Qingping Yi[1], Xuejun Tian[1], Qihai Wang[1], Dan Ma[1], Qiong Luo[3*], Feng Tan[4*] and Yongfeng Hu[5*]

[1]Hubei Engineering Research Center for Specialty Flowers Biological Breeding/College of Bioengineering, Jingchu University of Technology, Jingmen, China, [2]Center for Science Popularization Jingmen, Science and Technology Museum, Jingmen, China, [3]State Key Laboratory for Conservation and Utilization of Bio-Resources in Yunnan/Ministry of Education Key Laboratory of Agricultural Biodiversity for Plant Disease Management, Yunnan Agricultural University, Kunming, China, [4]Department of Biochemistry and Molecular Biology, College of Life Sciences, Nanjing Agricultural University, Nanjing, China, [5]Key Laboratory of Three Gorges Regional Plant Genetics and Germplasm Enhancement, Biotechnology Research Center, China Three Gorges University, Yichang, China

Histone deacetylase (HDAC) inhibitors (HDACis) have been widely used in plants to investigate the role of histone acetylation, particularly the function of HDACs, in the regulation of development and stress response. However, how histone acetylation is involved in rice (*Oryza sativa L.*) disease resistance has hardly been studied. In this paper, four HDACis including Sodium butyrate (NaBT), Suberoylanilide Hydroxamic Acid (SAHA), LBH-589 and Trichostatin A (TSA) were used to treat rice seedlings at different concentrations before inoculation of *Magnaporthe oryzae*. We found that only 10mM NaBT treatment can significantly enhanced rice blast resistance. However, treatment of the four HDACis all increased global histone acetylation but at different sites, suggesting that the inhibition selectivity of these HDACis is different. Notably, the global H3K9ac level was dramatically elevated after both NaBT and LBH589 treatment although LBH589 could not enhance rice blast resistance. This indicates that the HDACs they inhibit target different genes. In accordance with the phenotype, transcriptomic analysis showed that many defense-related genes were up-regulated by NaBT treatment. Up-regulation of the four genes *bsr-d1*, *PR10B*, *OsNAC4*, *OsKS4* were confirmed by RT-qPCR. ChIP-qPCR results revealed that H3K9ac level on these genes was increased after NaBT treatment, suggesting that these defense-related genes were repressed by HDACs. In addition, by promoter motif analysis of the genes that induced by both NaBT treatment and rice blast infection, we found that the motifs bound by ERF and AHL transcription factors (TFs) were the most abundant, which demonstrates that ERF and AHL proteins may act as the candidate TFs that recruit HDACs to defense-related genes to repress their expression when plants are not infected by rice blast.

KEYWORDS

HDAC inhibitors, rice blast, histone acetylation, defense-related genes, rice

Introduction

Rice (*Oryza sativa L.*) is one of the most important food crops and the main food source for more than 50% people in the world. Rice blast is the major diseases that affect the yield and quality of rice, and considered as the most serious threat to global rice production. The annual yield loss caused by rice blast can reach 10%~30% of the total rice yield (Skamnioti and Gurr, 2009; Zhou, 2016). At present, the commonly used methods to control rice blast mainly include cultivating resistant rice varieties, chemical agents and improved cultivation measures. Repeated and excessive use of fungicides to control plant diseases has lead to the serious global environment pollution. It is of great significance to reveal the molecular mechanism of rice blast resistance and cultivate resistant varieties for the safe production of rice. Large quantities of defense-related genes in rice have been identified. Those defense-related genes encode various recognition receptors, signal transduction proteins and transcription factors (Chujo et al., 2013; Lee et al., 2016; Li et al., 2017; Li et al., 2019b; Yin et al., 2021). In addition, epigenetic regulators also play important roles in disease resistance *via* regulating expression of defense-related genes (Zhu et al., 2016).

Histone acetylation, which is deposited by histone acetyltransferases (HATs) and removed by histone deacetylase (HDACs), is positively engaged in the regulation of gene expression. The HDACs can be classified into three families: Reduced Potassium Dependency 3 (RDP3)/Histone Deacetylase 1 (HDA1), Silent Information Regulator 2 (SIR2), and the plant-specific Histone Deacetylase 2 (HD2) (Pandey et al., 2002). The plant RPD3/HDA1 family is divided into three classes (I, II and IV) based on their homology to yeast HDACs (Ueda et al., 2017). In plants, the involvement of HDACs in the immune response has extensively studied. In Arabidopsis, HDA19 acts as a positive regulator of plant immunity, as overexpression of *HDA19* enhances plant resistance to the necrotrophic pathogen *Alternaria brassicicola* (Zhou et al., 2005). In *HDA19*-overexpression plants, expression of genes related to jasmonic acid and ethylene signaling is increased (Zhou et al., 2005). Besides, HDA19 inhibits transcription activation activity of WRKY38 and WRKY62 that function as negative regulators of plant immunity (Kim et al., 2008). However, later study revealed that *HDA19* negatively regulated plant resistance to *Pseudomonas syringae* by repressing *PR1* and *PR2* (Choi et al., 2012). So the role of *HDA19* in the regulation of plant immunity remains controversial. HDA9 and HOS15 form the complex HDA9-HOS15 to inhibit the expression of *NLR* genes by reducing H3K9ac and negatively regulate the immunity to *Pseudomonas syringae* pv *tomato* DC3000 (*Pst* DC3000) (Yang et al., 2020). The loss-of-function of *HOS15* or *HDA9* results in the increased expression of one third of 207 *NLR* genes and the consequent enhancement of resistance to pathogen infection. HDA6 inhibits pathogen-responsive genes by removing H3 acetylation at corresponding loci, thus negatively regulating plant immunity (Wang et al., 2017). In wheat, TaHOS15 serves as an adaptor protein to recruit TaHDA6 into the chromatin of defense-related genes (such as *TaPR1*, *TaPR2*, *TaPR5* and *TaWRKY45*, etc.), which together inhibit the acetylation of H3 and H4 at these genes (Liu et al., 2019). Down-regulation of *TaHOS15* or *TaHDA6* enhances defense-related genes expression under the infection of *blumeria graministhe*, which leads to the decreased susceptibility to *Blumeria graminis* f.sp. *tritici* (*Bgt*). TaHDT701 also can form HDAC complex with TaHDA6 and TaHOS15 to repress the expression of defense-related genes (Zhi et al., 2020). In rice, The function of rice HDT701, which is responsible for H4 deacetylation, in innate immunity has been characterized (Ding et al., 2012). Transgenic rice overexpressing *HDT701* is more sensitive to rice blast and bacterial leaf blight. On the contrary, *HDT701* RNAi plants exhibit enhanced resistance to rice blast and bacterial leaf blight. After treated with pathogen-related molecular pattern effectors, *HDT701* RNAi plants produce more reactive oxygen species and accumulate more transcripts of pattern recognition receptor genes *FLS2*, *CEBiP* and *SGT1*. In addition, HDT701 directly binds to defense-related genes *MAPK6* and *WRKY53* to inhibit their expression. These results demonstrate that HDT701 is a negative regulator of rice immune response.

HDAC inhibitors (HDACis) can specifically inhibit the activity of HDAC, and are widely used to clarify the function of these enzymes. A variety of HDACis with different selectivity to HDAC proteins have been developed (Waterborg, 2011; Patanun et al., 2016; Ueda et al., 2017; He et al., 2020). The research on application of HDACis in plants are also increasing. For example, Ky-2 and SAHA treatments enhance salt tolerance in Arabidopsis and cassava respectively (Patanun et al., 2016; Sako et al., 2016). Seven other HDACis screened by Ueda et al. can also induce salinity stress tolerance in Arabidopsis (Ueda et al., 2017). HDACis have been applied in rice to study the function of HDAC in root development and callus formation (Chung et al., 2009; Zhang et al., 2020). In this paper, we selected four HDACis to treat rice seedlings before inoculating *M. oryzae*. The plants treated with 10mM NaBT displayed enhanced resistance to rice blast, while those treated with the other HDACis did not. Global H3K9ac level was increased after NaBT treatment, suggesting the inhibitory effect of NaBT on HDAC activity. Furthermore, a number of defense-related genes were activated and H3K9ac levels on these genes were increase by NaBT treatment. These results indicate that NaBT enhances rice blast resistance by inhibiting the activity of HDACs, thereby increasing H3K9ac level and activating defense-related genes.

Materials and methods

Plant materials and growth conditions

Rice (*Oryza sativa ssp japonica* cv Hwayoung) plants were germinated and grown in a growth room kept at 26°C and 70%

relative humidity with a 12-h light/12-h dark cycle. The 7-day-old rice seedlings were treated with different concentrations of four HDACis, NaBT (1 mM, 5 mM, 10 mM, 20 mM, Wako Pure Chemical Industries, 193-01522), SAHA (100 uM, 300 uM, 500 uM, 1 mM, Selleck Chemicals LLC, S1047), LBH-589 (100 uM, 300 uM, 500 uM, 1 mM, Selleck Chemicals LLC, S1030) and Trichostatin A (500 uM, 1 mM, Sigma-Aldrich, T1952), respectively. HDACis with the same concentration were added when the rice hydroponic medium or nutrient solution was changed every week. DMSO-treated plants act as a control. After three weeks of 10 mM NaBT treatment of rice seedlings (28-day-old), the third leaves of NaBT-treated plants and the control were harvested at 12, 24 and 48h thereafter (Figure S1). Ten individual plants were harvested for each sample. The harvested samples were immediately put into liquid nitrogen for quickly freezing, and stored in a -70°C refrigerator for transcriptome sequencing, RT-qPCR, ChIP-qPCR and measurement of defense-related enzyme activity.

Pathogen infection assay and disease evaluation

The 28-day-old rice seedlings treated with HDACis were inoculated by spraying with *M. oryzae* JC2 spore suspension (2.0×10^5 spores/mL), and the DMSO-treated plants were used as the control (Figure S1). Five days after inoculation, the incidence of disease was counted (Figure S1). At least 80 leaves were used for counting for each treatment. The disease grade was identified according to the evaluation standard of rice blast resistance grade (Li et al., 2021).

Western blot analysis

Rice seedlings were treated with 10 mM NaBT, 1 mM SAHA, 1 mM LBH-589, 1 mM TSA as described above (Figure S1). Leaves were harvested and nuclear proteins were extracted by using extraction buffer I(0.4 M Sucrose, 10 mM pH 8.0Tris-HCl, 10 mM MgCl2, 5 mM β-ME, 0.1 mM PMSF, 1×complete protease inhibitors), extraction buffer II (0.25 M Sucrose, 10 mM pH 8.0 Tris-HCl, 10 mM $MgCl_2$, 10% Triton X-100, 5 mM β-ME, 0.1 mM PMSF, 1×complete protease inhibitors) and extraction buffer III (1.7 M Sucrose, 10 mM Tris-HCl(pH 8.0), 2 mM $MgCl_2$, 0.15% Triton X-100, 5 mM β-ME, 0.1 mM PMSF, 1×complete protease inhibitors) successively. Histone proteins were separated by 15% SDS-PAGE followed by immunoblotting using specific primary antibodies: H3 (Abcam, ab1791), H4 (Millipore, 06–598), H3K9ac (Millipore, 07-352), H3K27ac (Millipore, 07-360), H4K5ac (Millipore, 07-327), H4K16ac (Millipore, 07-329) and secondary antibody (Earthox, E03120-01). Chemiluminescent detection were performed with ECL reagent according to the manufacturer's protocol (Millipore, Cat.No.WBKLS0050). ImageJ software was used to quantify the band intensities.

RNA-seq and data analysis

Total RNA of Rice seedlings without roots was extracted using TRNzol Universal Reagent (TIANGEN). The RNA quality for RNA-seq and RT-qPCR was examined using a Bioanalyzer 2100 (Agilent). RNA-seq libraries were generated using the UltraTM RNA Library Preparation Kit (NEB, USA)for Illumina. A total of 18 libraries were sequenced on an Illumina platform and 150 bp paired-end read were generated. To obtain the RNA-seq data, Trimmomatic (version 0.33) was used to removing contaminations and low-quality reads (Xu et al., 2022). And clean reads were mapped to the reference genome of rice (MSU7.0) by Hisat2 v2.2.0 (Xu et al., 2022). To normalize counts and analyze the difference of RNA expression level, the R package of DESeq2 (v4.0.3) were used with adjusted P-value<0.05 and |log2 (Fold change)| ≥1 (Xu et al., 2022). KEGG analyses were conducted using the online site [DAVID Functional Annotation Bioinformatics Microarray Analysis (ncifcrf.gov)].

Chromatin immunoprecipitation

Chromatin Immunoprecipitation (ChIP) experiment was conducted as described in Hu et al. (2020). 2g of rice seedling without roots was cross-linked with 1% (v/v) formaldehyde before being used to isolate nuclei and chromatin. The chromatin was broken into 200 to 250bp fragments by sonication and immunoprecipitated with H3K9ac antibody. Dyna-beads Protein G (Invitrogen, 10003D) was used to harvest the immunocomplex. After extensive washing, immunoprecipitated chromatin was de-cross-linked to release the DNA for ChIP-qPCR.

RT-qPCR and ChIP-qPCR

According to the manufacturer's protocol, cDNAs were synthesized by reverse transcription with HiScript II QRT SuperMix for qPCR (+gDNA wiper) (Vazyme). RT-qPCR and ChIP-qPCR were performed using SuperReal PreMix Plus (SYBR Green) (TIANGEN) on an ABI System (Stepone). The PCR reactions were performed under the following conditions: preincubation at 95 °C for 15 min, then 40 cycles of 95 °C for 10 s, and 60 °C for 1min (Xu et al., 2022). In addition, the expression levels were calculated using the $2^{-\Delta\Delta Ct}$ method for each sample (Xu et al, 2022). For RT-qPCR the *Actin* gene was used as an internal control. The primers used in this study are listed in Table S1.

Measurement of SOD, POD, CAT and PAL activity

After sampling, according to the instructions of the detection kit (Total superoxide dismutase (T-SOD) test kit A001-1-2, Phenylalanine ammonia lyase (PAL) test kit A137-1-1, Peroxidase (POD) assay kit A084-3 -1, Catalase (CAT) assay kit A007-1-1, all from Nanjing Jiancheng Bioengineering Institute), first add the extraction solution and liquid nitrogen for grinding, and then perform the detection according to the operation steps.

Results

NaBT treatment enhances rice resistance to *M. oryzae*

In order to analyze the role of histone acetylation in the regulation of defense response in rice, four HDACis including NaBT, SAHA, LBH-589 and TSA were used to treat rice seedlings at different concentrations in the liquid culture medium one week after germination. The plants treated with DMSO were used as a control. The fresh liquid culture medium with HDACis was replaced every week. After three weeks treatment, we found that the shoot growth was not obviously affected and the plants were inoculated with *M. oryzae*. The results indicate that only treatment of NaBT at the concentration greater than 10mM could significantly enhance rice resistance to *M. oryzae* (Figure 1A; Figure S2A). The resistance grade was determined as grade 2 intermediate resistance (Figure 1B; Figure S2B). The plants treated with the other HDACis at various concentrations displayed similar resistance grade with the control (determined as grade 5 susceptible) (Figure 1B; Figure S2B). This suggests that only NaBT could activate rice defense response possibly by increasing histone acetylation at defense genes.

In response to pathogen infection, the activity of several defense-related enzymes are activated such as Superoxide dismutase (SOD), Peroxidase (POD), Catalase (CAT) responsible for scavenging reactive oxygen species (ROS) and Phenylalanine ammonia lyase (PAL) that is the key enzyme for phenylpropanoid biosynthesis (Appu et al., 2021; Song et al., 2022). To determine whether NabT-induced disease resistance involves these enzymes, we detected the activity of them after NaBT treatment. We found that the activity of different enzymes responded to NaBT in a different manner (Figure S3). In response to NaBT treatment, PAL activity was gradually increased after NaBT treatment, CAT activity was first increased and then decreased, whereas POD activity was deceased at early stage and then increased, SOD activity was however inhibited at three time points. These results indicate that the activity of the defense-related enzymes was affected by NaBT treatment, evidencing that defense response is activated after rice seedling is treated with NaBT.

Global H3K9ac is increased in rice after NaBT treatment

Several studies have shown that treatment of NaBT, TSA, SAHA can increase the acetylation level of histone H3 and H4 (Chua et al., 2003; Ueda et al., 2017; He et al., 2020), and treatment of LBH-589 can increase the acetylation level of histone H3 (Ueda et al., 2017). In order to investigate the effect of these four HDACis on the level of histone acetylation in rice, we treated rice seedlings with 10 mM NaBT, 1 mM SAHA, 1 mM LBH-589, and 1 mM TSA using the same method as described above. After three weeks treatment, the nucleoproteins of rice leaves were extracted. Western Blot was performed by using antibodies against H3K27ac, H3K9ac, H4K5ac, H4K16ac and internal reference H3 and H4. The results showed that TSA treatment slightly increased H4K5ac level and dramatically increase H3K27ac level (Figure 1C; Figure S4). SAHA treatment remarkably increased H4K5ac level. H3K9ac level significantly rose after LBH-589 and NaBT treatment (Figure 1C; Figure S4). These data demonstrate that different HDAC inhibitors may inhibit different HDACs leading to the increased histone acetylation at different sites, and NaBT mainly inhibits the HDACs responsible for H3K9 deacetylation in rice. Previously we reported that genome-wide H3K9ac was related to the activation of defense-related genes (Xu et al., 2022), supporting that inhibition of H3K9 deacetylation by NaBT treatment possibly causes derepression of defense-related genes.

RNA-seq analysis reveals up-regulation of defense-related genes by NaBT treatment

To understand the underlying mechanism of enhanced blast resistance in rice seedlings under NaBT treatment, samples were harvested at 12h, 24h and 48h after rice seedlings were treated with 10 mM NaBT. Total RNA was extracted and high-throughput sequencing was performed. More than 40M clean reads were obtained for each sample and were mapped to the rice reference genome (MSU7.0), and the mapping rate all exceeded 96% (Table S2). Differentially expressed genes (DEGs) between NaBT treatment and control were analyzed at the three time points respectively based on the transcriptome data. The results showed that 2889, 3369 and 434 genes were up-regulated (up-DEGs, log2 (Fold change)≥1, FDR<0.05) at 12, 24 and 48h, respectively, while 3726, 4161 and 413 genes were down-regulated (down-DEGs, log2 (Fold change) ≤-1, FDR<0.05) at 12, 24 and 48 hours, respectively (Figure 2A). These data demonstrated that NaBT dramatically affected transcriptional programme within 24h, and the effect was attenuated at 48h after treatment. We analyzed H3K9ac enrichment

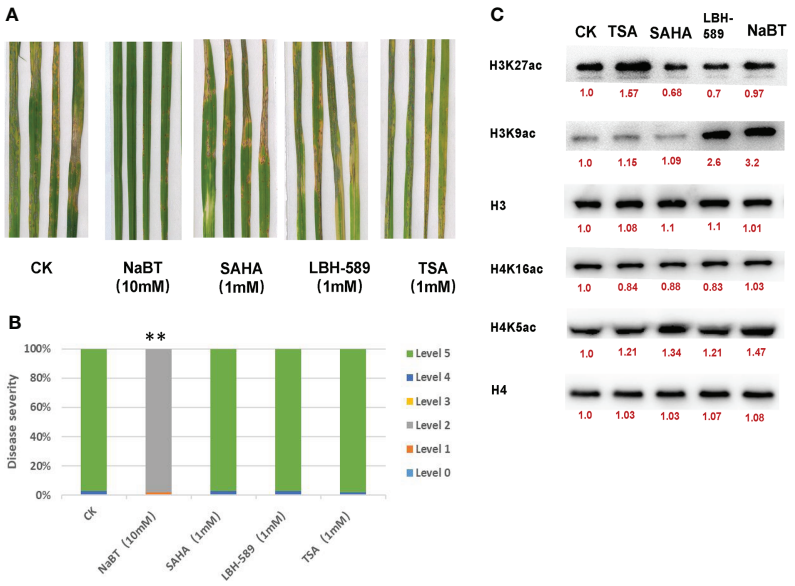

FIGURE 1
The effect of HDAC inhibitors treatment on rice blast resistance and histone acetylation in rice seedlings. **(A)** Leaf phenotypes after *M. oryzae* inoculation. Seven-day-old rice seedlings were treated with 10 mM NaBT, 1 mM SAHA, 1 mM LBH-589, 1 mM TSA. DMSO treatment serves as a control. After three weeks treatment the seedlings were inoculated with *M. oryzae*. Disease severity were investigated five days after inoculation. **(B)** Estimation of the disease grade after *M. oryzae* inoculation in **(A)** (**P< 0.01). **(C)** Immunoblot analysis of histone acetylation in rice seedlings treated with 10mM NaBT, 1 mM SAHA,1 mM LBH-589, 1 mM TSA. ImageJ software was used to quantify the band intensities (red number).

on the up-DEGs (a total of 4932 genes at the three time points) by using ChIP-seq data we had published previously (Xu et al., 2022). The samples used for RNA-seq and ChIP-seq experiment were 28-day-old seedlings inoculated with *M. oryzae* (Xu et al., 2022), which are consistent with the materials used in this study. We found that 3459 genes were marked with H3K9ac, which comprised about 70% of all the up-DEGs. These genes might be the potential targets regulated by histone deacetylases, whose activity is inhibited by NaBT. Unexpectedly, more down-DEGs than up-DEGs were observed (Figure 2A), which was not consistent with the predicted consequence after HDAC activity was inhibited by NaBT, since HDACs are mainly involved in gene repression. It is possible that many transcriptional repressors may be induced after NaBT treatment, thus resulting in the down-regulation of large amounts of genes. In addition, we found that most of up-DEGs were transiently up-regulated at different time points except that 77 genes were induced at all three time points (Figure 2B; Table S3). These genes continuously up-regulated by increased histone acetylation might serve as candidates for responding to developmental or environmental stimuli epigenetically. However, among these 77 genes no defense-related genes have been annotated. This indicates that defense-related genes can only be activated temporarily after the activity of histone deacetylases is inhibited.

To further identify the defense-related genes regulated by histone deacetylases, we combined the RNA-seq data in this study and in our previously published paper where transcriptomic change at 12h, 24h, 48h after inoculation of *M. oryzae* has been analyzed (Xu et al., 2022). Totally 1110 genes were induced by rice blast infection at the three time points. We found that about one third of these rice blast-induced genes (317 genes) were up-regulated by NaBT treatment (Figure 3A; Table S4). KEGG enrichment pathway analysis revealed that 317 genes were concentrated in metabolic pathways, amino sugar and nucleotide sugar metabolism, plant MAPK signaling pathway, and diterpenoid biosynthesis (Figure 3B). In addition, 27 of 317 up-DEGs were annotated as defense-related genes (Table 1), which means the up-regulated expression of these 27 defense-related genes is likely to be both induced by *M. oryzae* and regulated by histone acetylation. To verify the up-regulation of these 27 defense-related up-DEGs by NaBT treatment, we selected four genes *bsr-d1*, *PR10B*, *OsNAC4*, *OsKS4* for RT-qPCR. The results indicated that the expression levels of *OsKS4* at 24 h, *OsNAC4* at 12 h, *bsr-d1* at 12 h, *PR10B* at 24 h were significantly increased (Figure 4A), which is consistent with the RNA-seq results.

The global increment of histone acetylation induced by NaBT treatment was expected to result from either inhibition of HDAC activity or mis-regulation of HAT and HDAC genes. To verify the hypothesis, we obtained the expression value of these genes from our RNA-seq data and visualized the fold-change in response to NaBT treatment by heat maps. We found

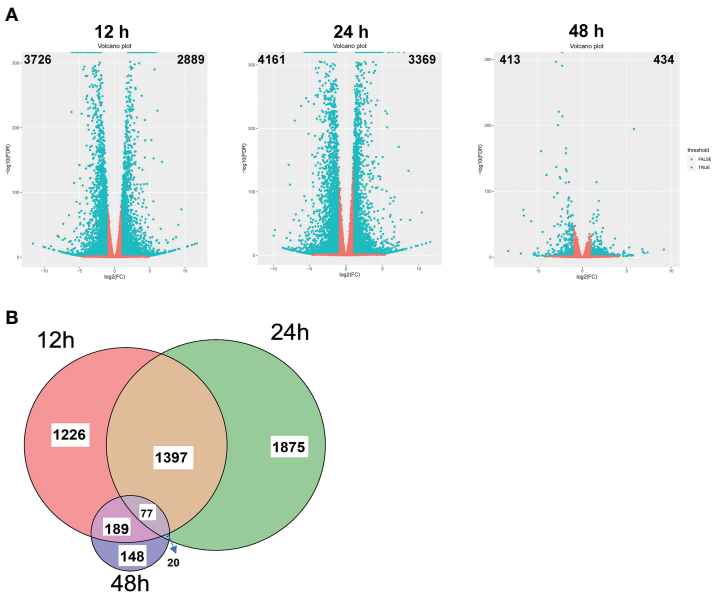

FIGURE 2
Transcriptomic changes induced by NaBT treatment. **(A)** Volcano plot of differential gene expression at 12, 24 and 48h induced by 10 mM NaBT. Red dots indicate genes with unchanged expression, and blue dots indicate differentially expressed genes (DEGs). Overlapping of up-DEGs **(B)** at 12, 24 and 48h treated with 10mM NaBT is presented by venn diagram.

that three HAT genes (*HAG703*, *HAC701* and *HAC704*) and four HDAC genes (*HDA704*, *HDA709*, *HDA710*, and *HDA716*) were activated, and one HAT gene (*HAG704*) and two HDAC genes (*HDA714* and *OsSRT2*) were repressed by NaBT treatment (Figure S5A and S5B). Thus, based on these results we proposed that transcriptional activation of HAT genes or repression of HDAC genes induced by NaBT could possibly contribute to the increase of histone acetylation.

H3K9ac on four NaBT-induced defense-related genes is increased after NaBT treatment

To confirm whether the four defense-related genes *OsKS4*, *bsr-d1*, *OsNAC4* and *PR10B* were regulated by histone acetylation, ChIP-qPCR were performed using the samples harvested at 12h, 24h and 48h after NaBT treatment. The

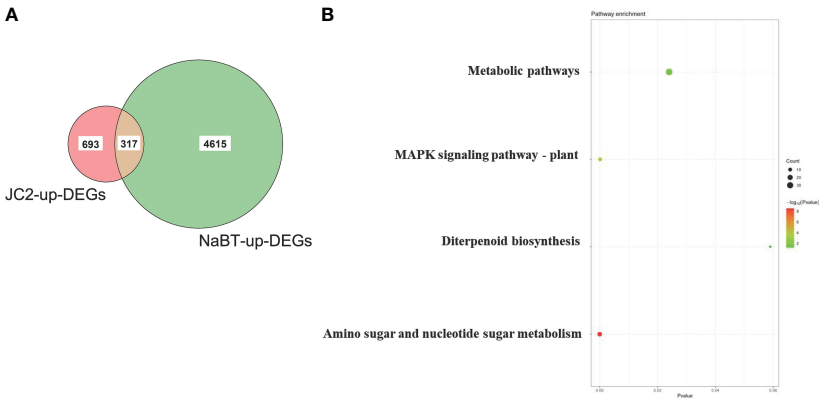

FIGURE 3
Identification of genes induced by both rice blast infection and NaBT treatment. **(A)** The number of genes induced by rice blast infection (JC2) and NaBT treatment is presented by venn diagram. **(B)** The Kyoto Encyclopedia of Genes and Genomes (KEGG) analysis of 317 up-DEGs identified in **(A)**.

10.3389/fpls.2022.1041095

TABLE 1 List of 27 defense-related genes up-regulated by inoculation of *M. oryzae* (JC2) and NaBT treatment.

Gene locus No.	Gene name	Log2(FC) induced by JC2			Log2(FC) induced by NaBT		
		12h	24h	48h	12h	24h	48h
LOC_Os01g21120	*OsERF68*	0.25	1.36	0.28	-1.4	2.13	-0.26
LOC_Os01g28500	*OsPR1#012*	-0.12	1.74	2.46	1.18	2.81	-0.07
LOC_Os01g43550	*OsWRKY12*	1.05	0.4	3.13	2.52	-0.65	0.24
LOC_Os01g60020	*OsNAC4*	0.59	0.84	1.12	1.57	0.75	0.23
LOC_Os01g71670	*OsPR2*	0.28	2.03	1.8	1.62	3.49	-0.19
LOC_Os02g32610	*OsCTR2*	0.55	1.2	0.74	2.88	0.21	0.23
LOC_Os02g36140	*OsKS7*	0.77	1.66	2.39	-0.29	1.68	-1.61
LOC_Os03g32230	*bsr-d1*	0.69	0.9	1.35	1.15	-1.44	-0.72
LOC_Os03g49260	*OsLOX3*	0.91	0.95	1.22	4.6	1.84	-0.92
LOC_Os03g52860	*LOX-L2*	1.92	1.68	0.55	2.46	3.22	-0.9
LOC_Os04g10060	*OsKS4*	2.08	3.15	3.34	-0.21	2.91	0.13
LOC_Os04g41620	*Cht4*	0.13	3.29	3.24	0.76	3.33	0.23
LOC_Os04g41680	*Cht5*	-0.14	2.45	1.99	-0.5	2.18	-0.22
LOC_Os05g33130	*Cht2*	1.4	3.33	5.35	3.5	4.43	-0.03
LOC_Os05g33140	*Cht9*	0.92	2.24	0.28	1.16	2.89	-0.81
LOC_Os06g44010	*OsWRKY28*	1.67	1.02	0.4	1.24	0.69	-0.72
LOC_Os06g51050	*Cht3*	2.72	4.25	3.7	0.56	2.33	0.3
LOC_Os06g51060	*Cht1*	0.88	1.01	1.24	0.23	1.19	-0.83
LOC_Os07g48730	*OsRLCK241*	0.62	0.53	1.07	0.87	1.76	-0.63
LOC_Os09g25070	*OsWRKY62*	1.41	2.36	1.06	0.01	2.72	-2.74
LOC_Os10g02070	*poxA*	0.32	0.06	1.65	1.46	0.38	0.31
LOC_Os10g11500	*OsPR1#101*	2.72	3.44	5.61	-0.35	4.47	0.04
LOC_Os11g37960	*OsPR4b*	1.11	1.12	1.54	1.46	0.65	-0.34
LOC_Os11g37970	*OsPR4*	0.58	2.76	1.75	0.31	1.96	-0.24
LOC_Os11g47580	*RIXI*	-0.27	3.85	2.79	2.79	5	-0.13
LOC_Os12g36850	*PR10B*	0.75	0.95	2.14	-0.45	1.3	-1.91
LOC_Os12g36860	*RPR10*	0.78	0.89	2.23	0.21	2.04	-2.32

H3K9ac level on *bsr-d1*, *OsNAC4* and *PR10B* was significantly increased at 12, 24 and 48h although the expression of these genes are increased only at 12h and decreased to the level comparable with the control (Figure 4B). We speculate that these genes may be activated by NaBT treatment at early stage, but their transcriptional repressors are also up-regulated giving rise to the repression of the three defense-related genes at later stage possibly independent of histone deacetylation. The H3K9ac level on *OsKS4* was also significantly increased at 24h (Figure 4B), which is in accordance with the induced expression of *OsKS4* at 24h after NaBT treatment (Figure 4A). The results indicate that up-regulation of the four defense-related genes *OsKS4*, *bsr-d1*, *OsNAC4* and *PR10B* by NaBT treatment all involves histone acetylation. As these genes are also induced by rice blast infection, we would like to learn whether induction of these genes by rice blast infection necessitate histone acetylation. We used IGV software to visualize the data of H3K9ac enrichment before and after inoculation of *M. oryzae* we obtained previously (Xu et al., 2022). It was shown that H3K9ac was enriched on *bsr-d1* and *OsNAC4* but not on *OsKS4* and *PR10B* (Figure S6A). Besides, quantitative analysis suggested that H3K9ac on all four genes were not significantly increased after inoculation of *M. oryzae* (Figure S6B), which indicates that induction of these defense-related genes in response to rice blast infection does not involve H3K9ac increase.

ERF and AHL TF-binding Cis-elements are enriched in the promoter of NaBT-induced defense genes

HDACs could be recruited to target genes by various TFs to exert histone deacetylation (Li et al., 2019a; Xu et al., 2022). To identify TFs that may be responsible for the recruitment of HDACs to *M. oryzae*-inducible genes, we performed TF-binding motif analysis in the promoters of 317 genes that both induced by *M. oryzae* and up-regulated by NaBT treatment. The results showed that most of identified motifs were GCC-box-containing cis-elements including DEAR3, DEAR4_2, ERF1, RAP2.6,

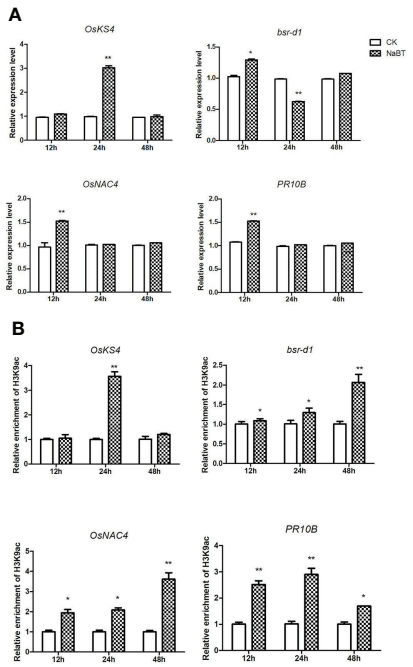

FIGURE 4
Validation of four defense-related gene expression **(A)** and H3K9ac enrichment **(B)** on these genes responding to NaBT treatment by RT-qPCR and ChIP-qPCR. The *actin* gene was used as internal control for RT-qPCR. The input was used as internal control for ChIP -qPCR. Three independent biological repeats were performed for each experiment. (*P< 0.05; **P< 0.01).

ORA47_2, RRTF1, RAP2.3, ATERF1, DREB2C, and RAP2.3_2 (Figures 5A, B). These motifs are recognized by ERF family TFs, suggesting that recruitment of HDAC to defense-related genes are mainly mediated by ERF TFs. Interestingly, we have previously reported that ERF TFs may also recruit HATs to defense-related genes for their induction (Xu et al., 2022). We also revealed that ERF genes could either activated or repressed by rice blast infection (Xu et al., 2022). This indicates that different ERF proteins are responsible for recruiting HATs and HDACs respectively. In addition, the "AWWWWWWT" motif, designated as AHL12_3ary and bound by the AHL family proteins, were also identified. Expression analysis showed that two AHL genes (*AHL4* and *AHL9*) were down-regulated and five AHL genes (*AHL11*, *AHL15*, *AHL17*, *AHL19*, *AHL20*) were up-regulated by inoculation of *M. oryzae* (Figure S7). This demonstrates that AHL genes are possibly involved in defense response in rice.

Discussion

HDACis can be divided into three classes based on their target selectivity, which has been studied in human (Ueda et al., 2017). Class I and Class II HDACis inhibit the activity of Class I and Class II HDACs of RPD3/HDA1 family, while Class III HDACis, also coined Pan-HDACi, inhibit the activity of the whole family HDACs. However, treatment of HDACis leads to increased histone acetylation at multiple sites in various plant species. For example, TSA treatment increases H4ac, H3K9ac, and H4K5ac levels in maize (Hu et al., 2011), H3ac and H4ac levels in tobacco (Chua et al., 2003), H3ac, H4ac, H3K14ac, H3K9ac, and H4K5ac levels in Arabidopsis (Mengel et al., 2017). SAHA treatment increases H3ac and H4ac levels in cassava (Patanun et al., 2016), H3K9ac and H4K5ac levels in cotton (He et al., 2020). LBH-589 and NaBT treatment increases H3ac levels in Arabidopsis (Ueda et al., 2017). NaBT treatment increases H3ac and H4ac levels in tobacco (Chua et al., 2003). In this study, we used TSA, SAHA, LBH-589 and NaBT to treat rice seedlings and detected changes of H3K9ac, H3K27ac, H4K5ac and H4K16ac levels by Western blot. We found that the treatment of different HDACis induced elevated histone acetylation level at different sites despite that TSA, LBH-589 and NaBT are classified as Pan-HDACi in human (Figure 1C). This suggests that the inhibition selectivity of HDACi in plants may differ from that in animals. In addition, H3K9ac levels can be enhanced by TSA treatment in maize and Arabidopsis but not significantly in rice reveled in this study. Instead, H3K27ac level was dramatically elevated after TSA treatment, which is consistent with the result reported by Zhang et al. (Zhang et al., 2020), suggesting that inhibitory effects of TSA on HDACs varies in different plant species. We speculate that the genome-wide increment of histone acetylation level induced by treatment of HDACi could be the consequence of inhibition of HDAC activity or mis-regulation of HAT or HDAC genes. Indeed, we found that several HAT and HDAC genes expression was affected by NaBT treatment (Figures S3A, B), indicating that these genes themselves are regulated by histone acetylation. However, it has been revealed that accumulation of HDAC1 transcripts was decreased by NaBT treatment even in HDAC1-overexpression rice plants (Chung et al., 2009). This demonstrates that NaBT may promote degradation of HDAC1 mRNA.

The distinct inhibitory effects of HDACis could also be reflected by their roles in development and stress tolerance. It has been reported that TSA can promote wheat embryo regeneration and inhibit spruce pollen tube elongation and rice callus formation (Cui et al., 2015; Bie et al., 2020; Zhang et al., 2020), enhance drought resistance of peanut cold tolerance of Arabidopsis (Song et al., 2017; Zhang et al., 2018). SAHA treatment improves salt tolerance in cassava and cotton (Patanun et al., 2016; He et al., 2020). LBH-589 treatment also improves salt tolerance in Arabidopsis (Ueda et al., 2017). NaBT was found to inhibit root growth in a dose-dependent manner in rice (Chung et al., 2009). However, the effect of HDACi treatment on plant biotic stress tolerance has never been reported before. In this study, NaBT, SAHA, TSA

and LBH-589 were used to treat rice seedlings at different concentrations. Only 10 mM NaBT could enhance the rice blast resistance of rice seedlings even though NaBT and LBH-589 can both induce notable elevation of H3K9ac level (Figures 1A-C). We suspect that NaBT and LBH-589 inhibit the activity of different HDACs target different sets of genes. RNA-seq analysis indicated that many defense-related genes induced by rice blast infection were up-regulated by NaBT treatment. Among them, several genes have been unveiled to be involved in blast resistance such as *bsr-d1*, *PR10B*, *OsNAC4*, *OsKS4*, which were confirmed to be regulated by NaBT by RT-qPCR (Figure 4A). We found that H3K9ac level on these genes was increased after HDAC activity was inhibited by NaBT treatment but was not increased after rice blast infection (Figures 4B and S4), suggesting that induction of these genes in response to biotic stress does not require the increase of H3K9ac on the genes. However, inhibition of HDAC activity is indeed related to disease resistance. In Arabidopsis, S-nitrosylation of HDAC promoted by NO inhibits HDAC activity, consequently leading to global increase of H3 and H4 acetylation and activation of stress genes (Mengel et al., 2017). It has been proved that NO production can be stimulated by both SA and TSA treatment, indicating that inhibition of HDAC by NO may serve as one of the pathway to activate immune response.

In plants, recruitment of HDAC by TFs is an important way for HDAC targeting downstream genes (Liu et al., 2014). To identify possible TFs responsible for recruiting HDAC to defense-related genes, we analyzed the common motifs in promoter of the genes that were up-regulated by NaBT treatment and inoculation of *M. oryzae*. The motifs bound by ERF and AHL proteins were determined to be the most abundant (Figures 5A, B). The direct interaction of HDAC with both ERF and AHL proteins have been unraveled before (Deng et al; Yun et al., 2012; Han et al., 2016; Hu et al., 2022). Besides, it has been revealed that overexpression of several *AHL* genes suppressed PAMP-induced *NHO1* and *FRK1* expression in Arabidopsis (Lu et al., 2010). The negative role of *ERF* genes in plant immunity has also been reported (Huang et al., 2016). Therefore, it is speculated that ERF and AHL proteins may recruit HDAC to defense-related genes to repress their expression under normal conditions. After pathogen infection, the expression of these TF genes is repressed and the recruitment of HDAC is blocked leading to increased histone acetylation and gene activation. Indeed, we found some *ERF* and *AHL* genes were down-regulated in response to rice blast infection (Xu et al.,

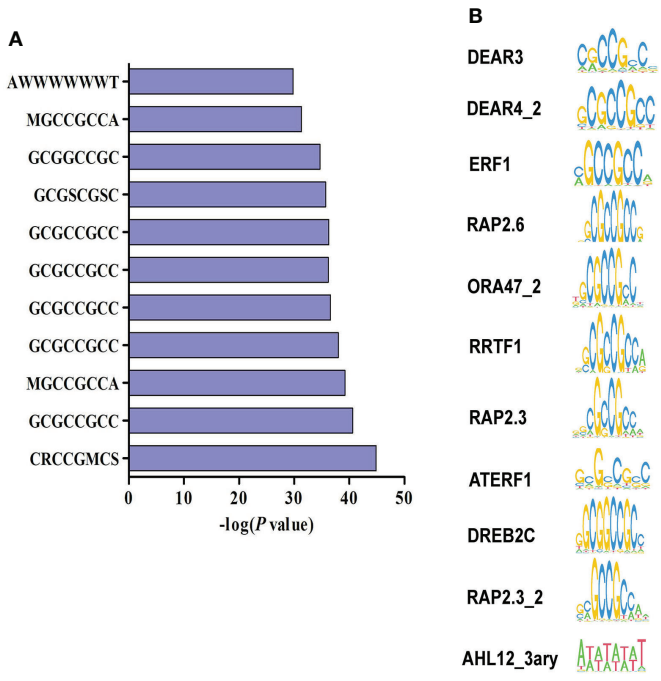

FIGURE 5
Identification of transcription factor binding motifs related to the repression of defense-related genes by HDAC. **(A)** Promoter motif enrichment analysis of 317 genes up-regulated by both rice blast infection and NaBT treatment. W represents for A or T, S represents for C or G, R represents for A or G, M represents for A or C. **(B)** The motifs enriched in the promoters of 317 up-DEGs.

2022, Figure S5). In consistent with this hypothesis, HDA19 directly represses *PR1* and *PR2* expression by deacetylate histones at the promoter (Choi et al., 2012). Loss-of-function of *HDA19* enhances resistance to *P. syringae* (Choi et al., 2012). HDA6 and HDA9 also negatively regulate the immunity in Arabidopsis (Wang et al., 2017; Yang et al., 2020). It is of great interest to identify HDAC-interacting TFs involved in regulating plant immunity.

Conclusion and perspectives

Collectively, in this study we found a HDAC inhibitor, NaBT, can significantly enhance rice blast resistance by activating defense-related genes with increased histone H3K9ac. The results not only prove the importance of RPD3/HDA1 family HDAC in immune response in rice, which has never been reported before, but also provide the evidence for the potential use of the HDAC inhibitors as agricultural chemicals to improve rice disease resistance. However, application of the other HDACis that also increased global histone acetylation could not enhance rice blast resistance, demonstrating that not all the HDACs are involved in rice disease resistance. Functional analysis of HDACs is required to find which HDACs are responsible for rice blast resistance.

Data availability statement

The data presented in the study are deposited in the NCBI repository, accession number PRJNA879115.

Author contributions

YX: Investigation; Methodology; Data curation. YM: Data curation; Formal analysis. BC: Data curation. QY: Formal analysis. XT: Data curation. QW: Formal analysis. DM: Formal analysis. QL: Writing - review and editing. Supervision; FT: Writing - review and editing. Supervision; YH: Conceptualization; Funding acquisition; Writing - original draft; Writing - review and editing. All authors contributed to the article and approved the submitted version.

Funding

This work was supported by the Opening Project of Hubei Engineering Research Center for Specialty Flowers Biological Breeding (2022ZD005) and Natural Science Foundation of Jiangsu Province (BK20190535)

Conflict of interest

The authors declare that the research was conducted in the absence of any commercial or financial relationships that could be construed as a potential conflict of interest.

Publisher's note

Supplementary material

The Supplementary Material for this article can be found online at: https://www.frontiersin.org/articles/10.3389/fpls.2022.1041095/full#supplementary-material

SUPPLEMENTARY FIGURE 1
The process of NaBT treatment and sample collection in this study.

SUPPLEMENTARY FIGURE 2
Test of rice blast resistance in rice seedlings treated with HDACi at other concentrations. **(A)** Leaf phenotypes after *M. oryzae* inoculation. Seven-day-old rice seedlings were treated with 1 mM NaBT, 5 mM NaBT, 20 mM NaBT, 100 uM SAHA, 300 uM SAHA, 500 uM SAHA, 100 uM LBH-589, 300 uM LBH-589, 500 uM LBH-589, 500 uM TSA. DMSO treatment serves as a control. After three weeks treatment the seedlings were inoculated with *M. oryzae*. Disease severity were investigated five days after inoculation. **(B)** Estimation of the disease grade after *M. oryzae* inoculation in **(A)** (**, P< 0.01).

SUPPLEMENTARY FIGURE 3
The activity of defense-related enzymes change in response to NaBT treatment.

SUPPLEMENTARY FIGURE 4
Immunoblot analysis of histone acetylation in rice seedlings treated with 10mM NaBT, 1 mM SAHA,1 mM LBH-589, 1 mM TSA (Repeat of). ImageJ software was used to quantify the band intensities (red number).

SUPPLEMENTARY FIGURE 5
Changes of HAT **(A)** and HDAC **(B)** gene expression in response to NaBT treatment.

SUPPLEMENTARY FIGURE 6
H3K9ac level on four defense-related genes responding to *M. oryzae* inoculation.

SUPPLEMENTARY FIGURE 7
Changes of AHL family gene expression in response to *M. oryzae* inoculation.

References

Appu, M., Ramalingam, P., Sathiyanarayanan, A., and Huang, J. (2021). An overview of plant defense-related enzymes responses to biotic stresses. *Plant Gene* 27, 100302. doi: 10.1016/j.plgene.2021.100302

Bie, X. M., Dong, L., Li, X. H., Wang, H., Gao, X. Q., and Li, X. G. (2020). Trichostatin a and sodium butyrate promotes plant regeneration in common wheat. *Plant Signal Behav.* 15 (12), 1820681. doi: 10.1080/15592324.2020.1820681

Choi, S. M., Song, H. R., Han, S. K., Han, M., Kim, C. Y., Park, J., et al. (2012). HDA19 is required for the repression of salicylic acid biosynthesis and salicylic acid-mediated defense responses in arabidopsis. *Plant J.* 71 (1), 135–146. doi: 10.1111/j.1365-313X.2012.04977.x

Chua, Y. L., Watson, L. A., and Gray, J. C. (2003). The transcriptional enhancer of the pea plastocyanin gene associates with the nuclear matrix and regulates gene expression through histone acetylation. *Plant Cell* 15 (6), 1468–1479. doi: 10.1105/tpc.011825

Chujo, T., Miyamoto, K., Shimogawa, T., Shimizu, T., Otake, Y., Yokotani, N., et al. (2013). OsWRKY28, a PAMP-responsive transrepressor, negatively regulates innate immune responses in rice against rice blast fungus. *Plant Mol. Biol.* 82 (1-2), 23–37. doi: 10.1007/s11103-013-0032-5

Chung, P. J., Kim, Y. S., Jeong, J. S., Park, S. H., Kim, J., and Biology, M. (2009). The histone deacetylase OsHDAC1 epigenetically regulates the OsNAC6 gene that controls seedling root growth in rice. *Plant J.* 59 (5), 764–776. doi: 10.1111/j.1365-313X.2009.03908.x

Cui, Y., Ling, Y., Zhou, J., and Li, X. (2015). Interference of the histone deacetylase inhibits pollen germination and pollen tube growth in picea wilsonii mast. *PloS One* 10 (12), e0145661. doi: 10.1371/journal.pone.0145661

Deng, H., Chen, Y., Liu, Z., Liu, Z., Shu, P., Wang, R., et al. (2022). SlERF.F12 modulates the transition to ripening in tomato fruit by recruiting the co-repressor TOPLESS and histone deacetylases to repress key ripening genes. *Plant Cell* 34 (4), 1250–1272. doi: 10.1093/plcell/koac025

Ding, B., Bellizzi Mdel, R., Ning, Y., Meyers, B. C., and Wang, G. L. (2012). HDT701, a histone H4 deacetylase, negatively regulates plant innate immunity by modulating histone H4 acetylation of defense-related genes in rice. *Plant Cell* 24 (9), 3783–3794. doi: 10.1105/tpc.112.101972

Han, Y. C., Kuang, J. F., Chen, J. Y., Liu, X. C., Xiao, Y. Y., Fu, C. C., et al. (2016). Banana transcription factor MaERF11 recruits histone deacetylase MaHDA1 and represses the expression of MaACO1 and expansins during fruit ripening. *Plant Physiol.* 171 (2), 1070–1084. doi: 10.1104/pp.16.00301

Hu, Y., Lai, Y., Chen, X., Zhou, D.X., and Zhao, Y. (2020). Distribution pattern of histone marks potentially determines their roles in transcription and RNA processing in rice. *J. Plant Physiol.* 249, 153167. doi: 10.1016/j.jplph.2020.153167

He, S., Hao, Y., Zhang, Q., Zhang, P., Ji, F., Cheng, H., et al. (2020). Histone deacetylase inhibitor SAHA improves high salinity tolerance associated with hyperacetylation-enhancing expression of ion homeostasis-related genes in cotton. *Int. J. Mol. Sci.* 21 (19), 7105. doi: 10.3390/ijms21197105

Huang, P. Y., Catinot, J., and Zimmerli, L. (2016). Ethylene response factors in arabidopsis immunity. *J. Exp. Bot.* 67 (5), 1231–1241. doi: 10.1093/jxb/erv518

Hu, Y., Han, Z., Wang, T., Li, H., Li, Q., Wang, S., et al. (2022). Ethylene response factor MdERF4 and histone deacetylase MdHDA19 suppress apple fruit ripening through histone deacetylation of ripening-related genes. *Plant Physiol.* 188 (4), 2166–2181. doi: 10.1093/plphys/kiac016

Hu, Y., Zhang, L., Zhao, L., Li, J., He, S., Zhou, K., et al. (2011). Trichostatin a selectively suppresses the cold-induced transcription of the ZmDREB1 gene in maize. *PloS One* 6 (7), e22132. doi: 10.1371/journal.pone.0022132

Kim, K.-C., Lai, Z., Fan, B., and Chen, Z. (2008). Arabidopsis WRKY38 and WRKY62 transcription factors interact with histone deacetylase 19 in basal defense. *Plant Cell* 20 (9), 2357–2371. doi: 10.1105/tpc.107.055566

Lee, M., Jeon, H. S., Kim, H. G., and Park, O. K. (2016). An arabidopsis NAC transcription factor NAC4 promotes pathogen-induced cell death under negative regulation by microRNA164. *New Phytol.* 214 (1), 343–360. doi: 10.1111/nph.14371

Li, W., Chern, M., Yin, J., Wang, J., and Chen, X. (2019b). Recent advances in broad-spectrum resistance to the rice blast disease. *Curr. Opin. Plant Biol.* 50 (50), 114–120. doi: 10.1016/j.pbi.2019.03.015

Li, S., Lin, Y. J., Wang, P., Zhang, B., Li, M., Chen, S., et al. (2019a). The AREB1 transcription factor influences histone acetylation to regulate drought responses and tolerance in populus trichocarpa. *Plant Cell* 31 (3), 663–686. doi: 10.1105/tpc.18.00437

Liu, X., Yang, S., Zhao, M., Luo, M., Yu, C. W., Chen, C. Y., et al. (2014). Transcriptional repression by histone deacetylases in plants. *Mol. Plant* 7 (5), 764–772. doi: 10.1093/mp/ssu033

Liu, J., Zhi, P., Wang, X., Fan, Q., and Chang, C. (2019). Wheat WD40-repeat protein TaHOS15 functions in a histone deacetylase complex to fine-tune defense responses to blumeria graminis f.sp. tritici. *J. Exp. Bot.* 70 (1), 255–268. doi: 10.1093/jxb/ery330

Li, J.L, Zhang, H., Yang, R., Zeng, Q.C, Han, G.Y, Du, Y.I, et al. (2021). Identification of miRNAs contributing to the broad-spectrum and durable blast resistance in the yunnan local rice germplasm. *Front. Plant Sci* 12,749919. doi: 10.3389/fpls.2021.749919

Li, W., Zhu, Z., Chern, M., Yin, J., Yang, C., Ran, L., et al. (2017). A natural allele of a transcription factor in rice confers broad-spectrum blast resistance. *Cell* 170 (1), 114–126 e115. doi: 10.1016/j.cell.2017.06.008

Lu, H., Zou, Y., and Feng, N. (2010). Overexpression of AHL20 negatively regulates defenses in arabidopsis. *J. Integr. Plant Biol.* 52 (9), 801–808. doi: 10.1111/j.1744-7909.2010.00969.x

Mengel, A., Ageeva, A., Georgii, E., Bernhardt, J., Wu, K., Durner, J., et al. (2017). Nitric oxide modulates histone acetylation at stress genes by inhibition of histone deacetylases. *Plant Physiol.* 173 (2), 1434–1452. doi: 10.1104/pp.16.01734

Pandey, R., Müller, A., Napoli, C. A., Selinger, D. A., Pikaard, C. S., Richards, E. J., et al. (2002). Analysis of histone acetyltransferase and histone deacetylase families of arabidopsis thaliana suggests functional diversification of chromatin modification among multicellular eukaryotes. *Nucleic Acids Res.* 30 (23), 5036–5055. doi: 10.1093/nar/gkf660

Patanun, O., Ueda, M., Itouga, M., Kato, Y., Utsumi, Y., Matsui, A., et al. (2016). The histone deacetylase inhibitor suberoylanilide hydroxamic acid alleviates salinity stress in cassava. *Front. Plant Sci.* 7. doi: 10.3389/fpls.2016.02039

Sako, K., Kim, J. M., Matsui, A., Nakamura, K., Tanaka, M., Kobayashi, M., et al. (2016). Ky-2, a histone deacetylase inhibitor, enhances high-salinity stress tolerance in arabidopsis thaliana. *Plant Cell Physiol.* 57 (4), 776–783. doi: 10.1093/pcp/pcv199

Skamnioti, P., and Gurr, S. J. (2009). Against the grain: safeguarding rice from rice blast disease. *Trends Biotechnol.* 27 (3), 141–150. doi: 10.1016/j.tibtech.2008.12.002

Song, Y., Liu, L., Li, G., An, L., and Tian, L. (2017). Trichostatin a and 5-Aza-2'-Deoxycytidine influence the expression of cold-induced genes in arabidopsis. *Plant Signal Behav.* 12 (11), e1389828. doi: 10.1080/15592324.2017.1389828

Song, X., Mo, F., Yan, M., Zhang, X., Zhang, B., Huang, X., et al. (2022). Effect of smut infection on the photosynthetic physiological characteristics and related defense enzymes of sugarcane. *Life (Basel).* 12 (8), 1201. doi: 10.3390/life12081201

Ueda, M., Matsui, A., Tanaka, M., Nakamura, T., Abe, T., Sako, K., et al. (2017). The distinct roles of class I and II RPD3-like histone deacetylases in salinity stress response. *Plant Physiol.* 175 (4), 1760–1773. doi: 10.1104/pp.17.01332

Wang, Y., Hu, Q., Wu, Z., Wang, H., Han, S., Jin, Y., et al. (2017). HISTONE DEACETYLASE 6 represses pathogen defence responses in arabidopsis thaliana. *Plant Cell Environ.* 40 (12), 2972–2986. doi: 10.1111/pce.13047

Waterborg, J. H. (2011). Plant histone acetylation: in the beginning. *Biochim. Et. Biophys. Acta* 1809 (8), 353–359. doi: 10.1016/j.bbagrm.2011.02.005

Xu, Y., Miao, Y., Tian, X., Wang, Q., Hu, Y., and Luo, Q. (2022). Transcriptomic and epigenomic assessment reveals epigenetic regulation of WRKY genes in response to magnaporthe oryzae infection in rice. *Curr. Genomics* 23 (3), 182–194. doi: 10.2174/1389202923666220510195910

Yang, L., Chen, X., Wang, Z., Sun, Q., Hong, A., Zhang, A., et al. (2020). HOS15 and HDA9 negatively regulate immunity through histone deacetylation of intracellular immune receptor NLR genes in arabidopsis. *New Phytol.* 226 (2), 507–522. doi: 10.1111/nph.16380

Yin, J., Zou, L., Zhu, X., Cao, Y., He, M., and Chen, X. (2021). Fighting the enemy: How rice survives the blast pathogen's attack. *Crop J.* 9 (3), 543–552. doi: 10.1016/j.cj.2021.03.009

Yun, J., Kim, Y. S., Jung, J. H., Seo, P. J., and Park, C. M. (2012). The AT-hook motif-containing protein AHL22 regulates flowering initiation by modifying FLOWERING LOCUS T chromatin in arabidopsis. *J. Biol. Chem.* 287 (19), 15307–15316. doi: 10.1074/jbc.M111.318477

Zhang, H., Guo, F., Qi, P., Huang, Y., Xie, Y., Xu, L., et al. (2020). OsHDA710-mediated histone deacetylation regulates callus formation of rice mature embryo. *Plant Cell Physiol.* 61 (9), 1646–1660. doi: 10.1093/pcp/pcaa086

Zhang, B., Su, L., Hu, B., and Li, L. (2018). Expression of AhDREB1, an AP2/ERF transcription factor gene from peanut, is affected by histone acetylation and increases abscisic acid sensitivity and tolerance to osmotic stress in arabidopsis. *Int. J. Mol. Sci.* 19 (5), 1441. doi: 10.3390/ijms19051441

Zhi, P., Kong, L., Liu, J., Zhang, X., Wang, X., Li, H., et al. (2020). Histone deacetylase TaHDT701 functions in TaHDA6-TaHOS15 complex to regulate wheat defense responses to blumeria graminis f.sp. tritici. *Int. J. Mol. Sci.* 21 (7), 2640. doi: 10.3390/ijms21072640

Zhou, J. M. (2016). Plant pathology: A life and death struggle in rice blast disease. *Curr. Biol.* 26 (18), R843–R845. doi: 10.1016/j.cub.2016.08.038

Zhou, C., Zhang, L., Duan, J., Miki, B., and Wu, K. (2005). HISTONE DEACETYLASE19 is involved in jasmonic acid and ethylene signaling of pathogen response in arabidopsis. *Plant Cell* 17 (4), 1196–1204. doi: 10.1105/tpc.104.028514

Zhu, Q. H., Shan, W. X., Ayliffe, M. A., and Wang, M. B. (2016). Epigenetic mechanisms: An emerging player in plant-microbe interactions. *Mol. Plant Microbe Interact.* 29 (3), 187–196. doi: 10.1094/MPMI-08-15-0194-FI

frontiers | Frontiers in Plant Science

TYPE Original Research
PUBLISHED 03 November 2022
DOI 10.3389/fpls.2022.1050216

OPEN ACCESS

EDITED BY
Jihong Hu,
Northwest A&F University, China

REVIEWED BY
Tao Zhang,
Institute of Microbiology, (CAS), China
Yin Song,
Northwest A&F University, China

*CORRESPONDENCE
Xiaofeng Su
suxiaofeng@caas.cn
Enliang Liu
liuenliang@cau.edu.cn

†These authors have contributed equally to this work

SPECIALTY SECTION
This article was submitted to Plant Pathogen Interactions, a section of the journal Frontiers in Plant Science

RECEIVED 21 September 2022
ACCEPTED 19 October 2022
PUBLISHED 03 November 2022

CITATION
Liu L, Wang D, Zhang C, Liu H, Guo H, Cheng H, Liu E and Su X (2022) The heat shock factor GhHSFA4a positively regulates cotton resistance to *Verticillium dahliae*. *Front. Plant Sci.* 13:1050216. doi: 10.3389/fpls.2022.1050216

The heat shock factor GhHSFA4a positively regulates cotton resistance to *Verticillium dahliae*

Lu Liu[1†], Di Wang[2†], Chao Zhang[3], Haiyang Liu[4], Huiming Guo[1,5], Hongmei Cheng[1,5], Enliang Liu[6*] and Xiaofeng Su[1,5*]

[1]Biotechnology Research Institute, Chinese Academy of Agricultural Sciences, Beijing, China, [2]Center for Advanced Measurement Science, National Institute of Metrology, Beijing, China, [3]State Key Laboratory of North China Crop Improvement and Regulation, College of Life Science, Hebei Agricultural University, Baoding, China, [4]Institute of Plant Protection, Xinjiang Academy of Agricultural Sciences, Urumqi, China, [5]Hainan Yazhou Bay Seed Lab, Sanya, China, [6]Institute of Grain Crops, Xinjiang Academy of Agricultural ScienceS, Urumqi, China

Heat shock factors (HSFs) play a crucial role in the environmental stress responses of numerous plant species, including defense responses to pathogens; however, their role in cotton resistance to *Verticillium dahliae* remains unclear. We have previously identified several differentially expressed genes (DEGs) in *Arabidopsis thaliana* after inoculation with *V. dahliae*. Here, we discovered that *GhHSFA4a* in *Gossypium hirsutum* (cotton) after inoculation with *V. dahliae* shares a high identity with a DEG in *A. thaliana* in response to *V. dahliae* infection. Quantitative real-time PCR (qRT-PCR) analysis indicated that *GhHSFA4a* expression was rapidly induced by *V. dahliae* and ubiquitous in cotton roots, stems, and leaves. In a localization analysis using transient expression, GhHSFA4a was shown to be localized to the nucleus. Virus-induced gene silencing (VIGS) revealed that downregulation of *GhHSFA4a* significantly increased cotton susceptibility to *V. dahliae*. To investigate *GhHSFA4a*-mediated defense, 814 DEGs were identified between *GhHSFA4a*-silenced plants and controls using comparative RNA-seq analysis. The Kyoto Encyclopedia of Genes and Genomes (KEGG) analysis showed that DEGs were enriched in "flavonoid biosynthesis", "sesquiterpenoid and triterpenoid biosynthesis", "linoleic acid metabolism" and "alpha-linolenic acid metabolism". The expression levels of marker genes for these four pathways were triggered after inoculation with *V. dahliae*. Moreover, *GhHSFA4a*-overexpressing lines of *A. thaliana* displayed enhanced resistance against *V. dahliae* compared to that of the wild type. These results indicate that *GhHSFA4a* is involved in the synthesis of secondary metabolites and signal transduction, which are indispensable for innate immunity against *V. dahliae* in cotton.

KEYWORDS

cotton, *Verticillium* wilt, *Verticillium dahliae*, heat shock factors, GhHSFA4a

Introduction

As a major source of fiber and oil, cotton forms the economic backbone of several developing countries (Wu et al., 2022). Cotton yields are reduced by numerous diseases, the most destructive being cotton *Verticillium* wilt (CVW), sometimes called the "cancer" of cotton (Shaban et al., 2018). Approximately 40% of the cotton-growing areas in China are affected by this disease, causing annual losses of 250 to 310 million US dollars (Wang et al., 2016; Gong et al., 2017). The fungus *Verticillium dahliae*, the cause of CVW, has numerous races and produces microsclerotia that are highly resistant to biotic as well as abiotic stresses and can survive in the soil for decades (Deketelaere et al., 2017; Harting et al., 2020). In addition, chemical and biotechnological methods are ineffective in controlling pathogens and reducing losses (Zhang et al., 2018). Therefore, identifying resistance genes and breeding resistant varieties of cotton with broad-spectrum resistance are primary control measures (Zhang et al., 2014).

During the activation of plant defense responses in resistant plants, transcription factors (TFs) play an essential role in modulating downstream gene expression to induce stress adaptation signaling or strategic regulators in pathways (Udvardi et al., 2007; Kilian et al., 2012). The R2R3-type MYB protein GhMYB36 is involved in *Verticillium* wilt resistance in *Arabidopsis* and cotton by positively regulating the expression of PR1 (Liu et al., 2022). Two TFs, vascular plant one-zinc finger 1 (OsVOZ1) and OsVOZ2, are involved in rice resistance to *Magnaporthe oryzae* by regulating the accumulation of nucleotide-binding leucine-rich repeat (NLR) protein Piz-t (Andrási et al., 2021).

TFs, including heat shock factors (HSFs), ERF/AP2, bZIP, MYB, MYC, NAC, and WRKY are classified into different families based on their functional regions (Alves et al., 2014; Guo et al., 2016): DNA-binding regions, transcriptional regulatory regions (including activation and repression regions), oligomerization sites, and localization signals (Franco-Zorrilla and Solano, 2017). HSFs have a DNA-binding domain (DBD) and oligomerization domain (OD). Usually, the DBD is a highly conserved segment and the OD consists of two hydrophobic heptapeptide repeat regions, HR-A/B. HSFs can be classified into three categories, A, B, and C, based on the difference between DBD and HR-A/B. HSFs specifically bind to heat shock elements (HSEs), which are highly conserved promoter regions in heat shock protein (*HSP*) genes, and bind to other TFs to form a transcriptional complex that regulates the expression of *HSP* genes (von Koskull-Döring et al., 2007; Scharf et al., 2012). Previous studies on HSF function have mainly focused on plant resistance to abiotic stresses, such as drought, cold, heat, salt, and oxidative stress. ZmHSF08 has been shown to negatively regulate several stress/ABA-responsive genes under salt and drought stress conditions in maize (Wang et al., 2021). The expression of *TaHSFA2e-5D* is highly upregulated in wheat seedlings by heat, cold, drought, high salinity, and multiple phytohormones (Bi et al., 2022).

Among the results of several studies investigating the HSF function in plant disease resistance, the transcription factor CIGR2 suppresses excessive cell death caused by rice blast fungus by activating the expression of *OsHSF23* in rice (Tanabe et al., 2016). MeHSF3 directly targets the HSEs of *enhanced disease susceptibility 1* (*EDS1*) and *pathogenesis-related gene 4* (*PR4*), which positively regulate the immune response of *Manihot esculenta* against *Xanthomonas axonopodis pv. manihotis* (*Xam*) (Wei et al., 2018). After infection of tomato roots with *Meloidogyne incognita*, HSFA1a increases the expression of the respiratory burst oxidase homolog (RBOH) family protein Wfi1, initiating the HSFA1a-Wif1 cascade reaction and triggering a reactive oxygen species (ROS) burst (Zhou et al., 2018). The resistance response of pepper against *Pseudomonas solanacearum* involves CaHSFB2a through a positive feedback loop involving CaWRKY6 and CaWRKY40 (Ashraf et al., 2018). Overexpression OsHSFB4d in rice exhibited enhanced resistance to *Xanthomonas oryzae* pv. *oryzicola* as well as *Xanthomonas oryzae* pv. *oryzae* and an increased expression of *OsHsp18.0-CI* as well as pathogenesis-related genes (Yang et al., 2020).

Although multiple lines of evidence support a critical regulatory function of HSFs in plant disease resistance pathways, the role of HSFs in cotton resistance to *V. dahliae* remains unknown. In our previous study, we identified a number of differentially expressed genes (DEGs) through in-depth transcriptomic and metabolic analyses of *A. thaliana* infected with *V. dahliae* (Su et al., 2018) and used BlastP to identify the homolog of a DEG in *Gossypium hirsutum*, the heat shock factor A-4a-like gene (*GhHSFA4a*, XM_016875437.1). In the present study, we investigated the function of *GhHSFA4a* and analyzed (1) the physicochemical properties as well as phylogeny of GhHSFA4a, (2) the expression pattern of *GhHSFA4a* after infection with *V. dahliae*, (3) the subcellular location of GhHSFA4a in tobacco cells, (4) the disease resistance phenotype in cotton seedlings after virus-induced silencing (VIGS) of *GhHSFA4a*, (5) determined the defense pathway mediated by GhHSFA4a based on transcriptome and quantitative real-time PCR (qRT-PCR) analyses, and (6) generated *GhHSFA4a*-overexpressing *A. thaliana* plants as well as evaluated their resistance to *V. dahliae*.

Materials and methods

Plant materials, fungal strains, and growth conditions

Seedlings of cotton cultivar Coker 312 were grown in an autoclaved mixture of nutrient soil and vermiculite (1:1) in a greenhouse at 25 ± 2°C, 75 ± 5% relative humidity, with a photoperiod 16 h light/8 h dark. Seedlings of *Arabidopsis*

(Columbia-0) were grown in nutrient-supplemented soil with 16 h light/8 h dark at 22 °C and 60% relative humidity. Strain V991 of *V. dahliae*, a highly virulent and defoliating pathogenic strain provided by Prof. Xiaofeng Dai of the Institute of Plant Protection, Chinese Academy of Agricultural Sciences (CAAS), was cultured on potato dextrose agar (PDA) at 25°C for 7 - 10 days or in liquid complete medium (CM) at 200 rpm and 25°C, for 2 - 3 days to be used as inoculum.

Bioinformatic analysis

The amino acid sequences of GhHSFA4a and homologous proteins from *A. thaliana*, *Solanum lycopersicum*, *Malus domestica*, *G. hirsutum*, *Fragaria vesca*, *Oryza sativa*, and *Zea mays* were downloaded from the NCBI database (https://www.ncbi.nlm.nih.gov/). A phylogenetic tree was constructed using the neighbor-joining method in the MEGA software (version 5.0, Auckland, New Zealand). Amino acid sequence alignment and mapping were performed using ClustalW and ESPript 3.0 (https://espript.ibcp.fr/ESPript/ESPript/). The PlantCARE database was used to analyze *cis*-acting elements in a 2000-bp region located upstream of *GhHSFA4a* (Lescot et al., 2002), and the motif was drawn using TBtools (https://github.com/CJ-Chen/TBtools-Manual). Protein structure was predicted and analyzed using the AlphaFold Protein Structure Database (https://alphafold.com/) and UCSF Chimera (Pettersen et al., 2004), while subcellular locations were predicted using Uniport (https://www.uniprot.org).

Subcellular localization and confocal microscopy

In combination with the predicted subcellular localization results from the online platform WoLFPROST (https://wolfpsort.hgc.jp/), the full-length coding sequence (CDS) of the *GhHSFA4a* gene was cloned using 1132-GhHSFA4a-F/R (Table S1) and inserted into the expression vector *pYBA1132* (BamHI and EcoRI) containing the green fluorescent protein gene (*GFP*). The construct was inserted into *Agrobacterium tumefaciens* EHA105, which was subsequently used for agrobacterial transformation of *Nicotiana benthamiana*. Cells were observed under an LSM980 confocal laser-scanning microscope (Zeiss, Jena, Germany). The nuclear marker *H2B-mCherry* was provided by Prof. Lei Wang from the Biotechnology Research Institute, CAAS (Lu et al., 2022).

Pathogenicity assay

When cotton seedlings had two true leaves, plants were carefully uprooted and the roots were submerged in a suspension of *V. dahliae* conidia (10^7 cfu/mL) for 5 min. Each group consisted of five plants. Plants were replanted and grown for 15 days in the greenhouse, and their disease severity was scored on a 0 to 4 scale: 0, no disease; 1, both cotyledons yellow and true leaves were disease-free; 2, both cotyledons had symptoms and 1-3 true leaves had symptoms; 3, more than 5 leaves, including cotyledons, had symptoms; level 4, all leaves had symptoms, leaves had fallen off, and the plant was dead. The disease index (DI) was calculated as [Σ (number of diseased plants at each severity × disease score)/(total checked plants × 4)] × 100 (Li et al., 2020).

VIGS in cotton and RNA-seq analysis

The pTRV2 vector was digested using restriction endonucleases EcoRI and BamHI. The VIGS interference fragment in *GhHSFA4a* was amplified using the primers pTRV2-GhHSFA4a-F/R (Table S1) and then ligated using the seamless cloning method. The pTRV2::*GhHSFA4a* plasmid was inserted into *A. tumefaciens* GV3101 for the VIGS assay (Gao et al., 2011). Following injection, when the second true leaf on the pTRV2::*CLA1* positive control plants developed photobleaching, silencing efficiency was assessed using qRT-PCR with primers qGhHSFA4a-F/R (Table S1). The pTRV2::*00* and pTRV2::*GhHSFA4a* cotton were sampled, subjected to RNA-seq, and analyzed (Sajjad et al., 2021). Cotton *polyubiquitin* (*UBQ*, LOC107925174) was used as the housekeeping gene (Table S1).

To assess the integrity and total amount of RNA, an Agilent 2100 Bioanalyzer (Santa Clara, CA, USA) and Qubit 2.0 (Life Technologies, Carlsbad, CA, USA) were used to assess the quality of total RNA. The mRNA was enriched using oligo (dT) magnetic beads and randomly interrupted using NEB Fragmentation Buffer, and each sample was pooled in three replicates to form a single RNA sequencing library and the NEBNext® Ultra™ RNA Library Prep Kit for Illumina® Kit (Illumina, San Diego, CA, USA). Transcriptome sequencing was performed using an Illumina NovaSeq 6000 system. Clean reads for subsequent analyses were obtained after raw data filtering, sequencing error rate examination, and GC content distribution determination. The position information of the gene alignment on *G. hirsutum* TM-1 was analyzed to obtain the original read counts. Using DESeq, we obtained normalized read counts, which were screened for DEGs using the $|\log2(\text{Fold change})| \geq 1$ and $\text{padj} \leq 0.05$ standard (Purayil et al., 2020). Gene Ontology (GO), Kyoto Encyclopedia of Genes and Genomes (KEGG), and Gene Set Enrichment Analysis (GSEA) were used for gene enrichment analyses and functional annotation.

Analysis of relative gene expression and fungal biomass

After inoculation with *V. dahliae*, roots were collected at 0, 0.5, 1, 2, 4, 12, 24, 48, and 72 hours post-inoculation (hpi). The cDNA was obtained from the total RNA by reverse transcription, and a

primer pair qGhHSFA4a-F/R was used to amplify *GhHSFA4a*. *UBQ* was used as the housekeeping gene (Table S1). Roots of *V. dahliae*-infected cotton were harvested at 0, 2, 12, and 72 hpi and the expression pattern of marker genes in four pathways was detected using qRT-PCR and primers for UBQ as well as the other marker genes (Table S1). Fungal biomass was quantified by extracting genomic DNA from *V. dahliae*-infected roots at 15 days post-inoculation (dpi) for qRT-PCR using Vd-ITS-F/R (Table S1) for ribosomal RNA genes ITS1 and ITS2 (MT899267.1). The internal reference gene was *UBQ*. An ABI7500 Fast (Applied Biosystems, Waltham, MA, USA) instrument was used and the data were analyzed using the $2^{-\Delta\Delta Ct}$ method (Su et al., 2020).

Genetic transformation of *A. thaliana*

The overexpression vector, pCAMBIA2300, was cleaved using BamHI and SalI restriction endonucleases. The CDS sequence of *GhHSFA4a*, amplified using 2300-GhHSFA4a-F/R (Table S1), was ligated to the cleaved pCAMBIA2300-35S-eGFP vector using In-Fusion Cloning and then inserted into *A. tumefaciens* GV3101. Transgenic *A. thaliana* was obtained using the floral dip method (Clough and Bent, 1998). Seeds were collected from the plants as well as sown, and the resultant seedlings were planted to screen for transgenic lines. DNA was extracted from the positive material and tested with eGFP-F/R, and the transcript levels were quantified using qGhHSFA4a-F/R and AtRubisco-F/R (Table S1). Relative gene expression was analyzed using the $2^{-\Delta\Delta Ct}$ method (Livak and Schmittgen, 2001).

Statistical analyses

SPSS version 20.0 (IBM, Armonk, NY, USA) was used for all the statistical analyses. One-way analysis of variance (ANOVA) and *post hoc* Duncan's multiple range test were used to analyze the data. Differences were considered statistically significant at $P < 0.05$.

Results

GhHSFA4a structure

Based on our previous study, we cloned the 1212-bp full-length CDS of *GhHSFA4a*, which was identified using BlastP search IF. *GhHSFA4a*, which contains two exons, was mapped to chromosome D10 at *NC_053446.1*, and was shown to encode a protein of 403 amino acids with an estimated molecular mass of 46 kDa and an isoelectric point of 5.12. GhHSFA4a was found to contain an HSF-type DBD (Figure S1). Phylogenetic analysis of the fourth subcategory of HSFs A-type proteins in cotton and its homologous proteins from other plants showed that it was evolutionarily close to *F. vesca* HSFA4a (Figure 1A).

Multiple sequence alignments of the amino acid sequences of GhHSFA4a and other fourth subcategory A-type proteins were performed (Figure 1B). Its secondary structure is mainly composed of 37% alpha helix, 3% beta strand, and 58% disordered. The three-dimensional model showed that GhHSFA4a contains a solution NMR structure of heat shock factor protein 1 DBD from *Homo sapiens*, the Northeast Structural Genomics Consortium target HR3023C (Figure 1C).

A *cis*-element analysis of the sequence 2000- bp upstream of *GhHSFA4a* was performed to better understand its regulatory relationship at the transcriptional level (Figure 1D), which indicated that the GhHSFA4a promoter region contains hormone-related elements, such as the ABA response element (ABRE) and the methyl jasmonate (MeJA) response element (TGACG-motif), as well as other promoter *cis*-elements, such as the response defense and stress responsiveness element (TC-rich repeats), the light response element (TCCC-motif, Box 4), and elements associated with endosperm expression (GCN4_motif). Thus, *GhHSFA4a* might respond to biological stress through hormone induction.

GhHSFA4a responds to *V. dahliae* stress

The presence of *cis*-elements associated with immunity or defense reactions, including the ERF-box (Nishizawa-Yokoi et al., 2009), ABRE-box (Guo et al., 2016), and TGACG motif (Zander et al., 2012) within the promoter region of *GhHSFA4a* implies that the gene product may be involved in responses to pathogen infection. To test this assumption and investigate the role of *GhHSFA4a* in resistance to *V. dahliae* in cotton, we analyzed the expression of *GhHSFA4a* using qRT-PCR and discovered that expression was slightly induced at 0.5 hpi and peaked at 12 hpi. In a tissue-specific analysis, *GhHSFA4a* was constitutively expressed in cotton roots, stems, and leaves (Figure 2). These results indicate that *GhHSFA4a* can be induced after *V. dahliae* infection in cotton and might participate in cotton resistance to *V. dahliae*.

GhHSFA4a is localized in the nucleus

To localize GhHSFA4a, we inserted a *pYBA1132*-controlled *GhHSFA4a-GFP* chimeric gene (*pYBA1132-GhHSFA4a-GFP*) or the control *pYBA1132-GFP* vector with H2B-mCherry as a nucleus marker into *N. benthamiana* leaves and then examined the cells for fluorescence using laser-scanning confocal microscopy at 48 hpi with *V. dahliae* (Figure 3). The GhHSFA4a-GFP fusion protein colocalized with H2B-mCherry exclusively within the nucleus. In contrast, in cells overexpressing pYBA1132-GFP, GFP signals were observed throughout the cell, including in the plasma membrane, cytoplasm, and nucleus. These results suggest that GhHSFA4a is localized to the nucleus and may be the TF responsible for activating the expression of downstream resistance genes.

10.3389/fpls.2022.1050216

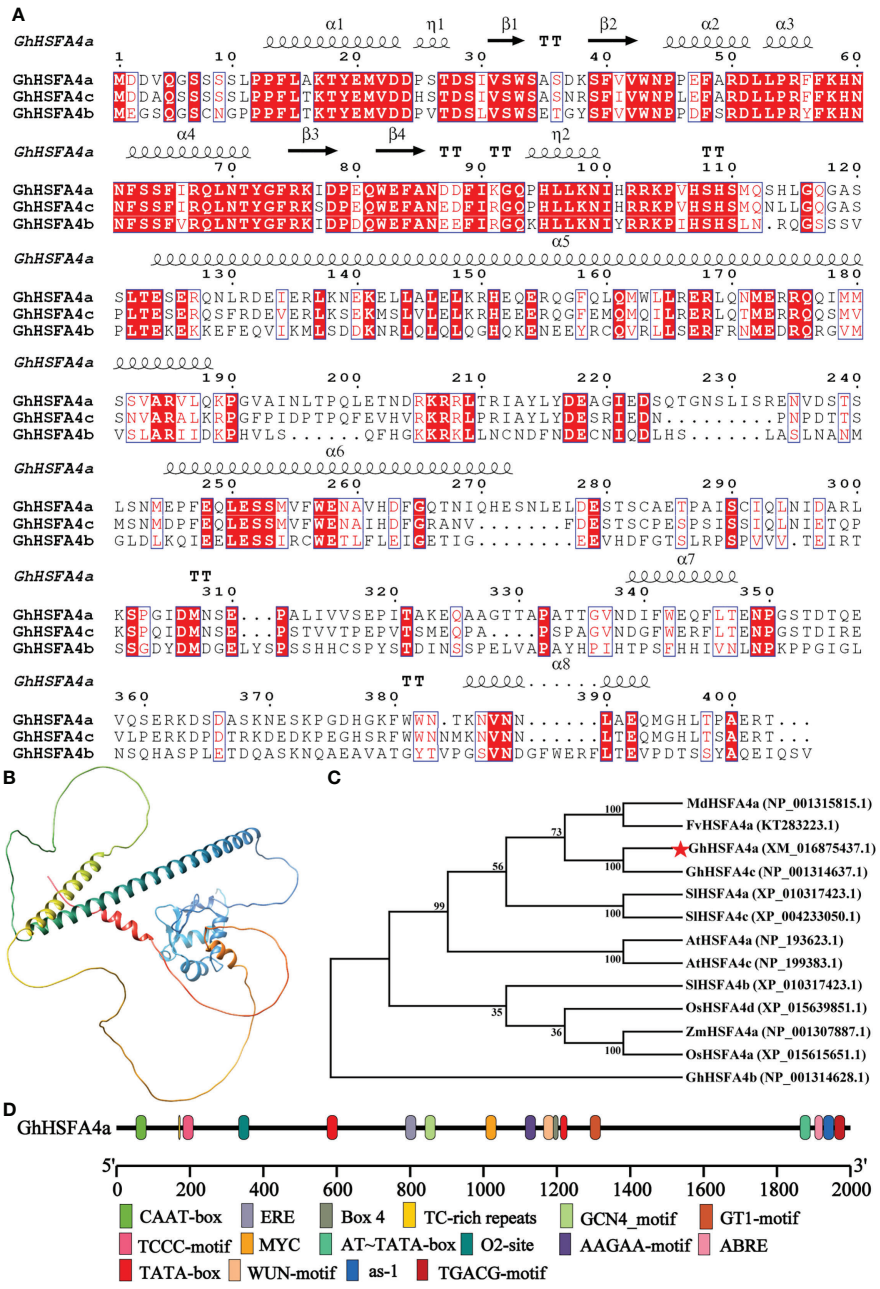

FIGURE 1
Structural characteristics of GhHSFA4a. **(A)** Alignment of GhHSFA4a, GhHSFA4b, GhHSFA4c proteins. **(B)** Three-dimensional GhHSFA4a model. **(C)** Phylogenetic tree of HSFA4 proteins from *G.hirsutum* (Gh), *Solanum lycopersicum* (Sl), *A. thaliana* (At), *Fragaria vesca* (Fv), *Malus domestica* (Md), *Oryza sativa* (Os), and *Zea mays* (Zm). **(D)** Analysis of *cis*-acting element of the *GhHSFA4a* promoter region.

Silencing of *GhHSFA4a* enhanced sensitivity to *V. dahliae* in cotton

To verify the function of *GhHSFA4a* in cotton resistance to *V. dahliae*, we used VIGS to reduce the expression of *GhHSFA4a* in Coker 312 cotton. One fully developed seedling cotyledon was infiltrated with pTRV2::*00* (negative control), and the other cotyledon was infiltrated with pTRV2::*GhHSFA4a*. After two weeks, strong photobleaching was present on newly emerged leaves on the seedlings transformed with pTRV2::*CLA1*, indicating that the VIGS system was successful under our experimental conditions (Figure 4A). *GhHSFA4a* expression levels were distinctly reduced in pTRV2::*GhHSFA4a* plants compared to those in pTRV2::*00* seedlings, and the qRT-PCR

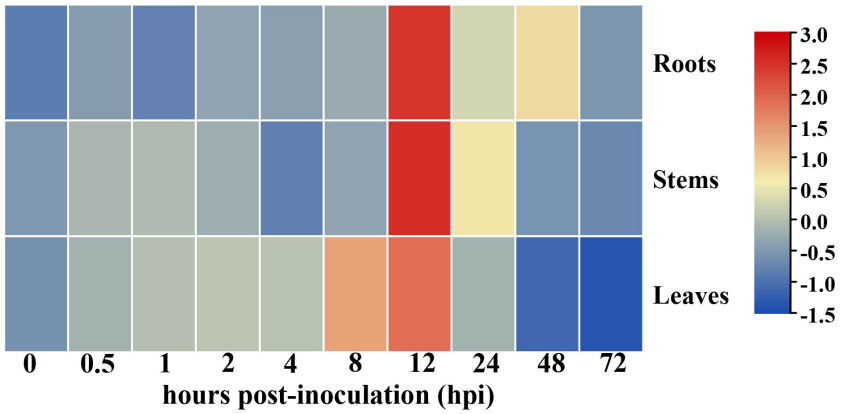

FIGURE 2
Expression of *GhHSFA4a* in cotton inoculated with *V. dahliae*. RNA was extracted from roots, stems, and leaves of 3-week-old seedings at 0, 0.5, 1, 2, 4, 8, 12, 24, 48, and 72 hours post-inoculation (hpi) with *V. dahliae*. Relative transcript levels were quantified using qRT-PCR with *UBQ* as the internal reference gene. The experiments were performed in duplicate using different RNA samples for the template.

analysis indicated a silencing efficiency of 61% (Figure 4B). Two weeks after treatment with *V. dahliae*, the pTRV2::*GhHSFA4a* plants displayed more severe symptoms, such as wilted leaves and browned vascular bundles, than those observed in control plants (Figure 4C). The DI of *GhHSFA4a*-slienced cotton was significantly higher than that of the control cotton, and *GhHSFA4a* silencing was associated with the highest number of cotton plants with level 4 disease severity (Figure 4D). Supporting these results, the fungal biomass in silenced seedlings was 5-fold higher than that in control seedlings (Figure 4E). These results suggest that knockdown of *GhHSFA4a* attenuates the resistance of cotton plants to *V. dahliae*.

RNA-seq revealed *GhHSFA4a* functions through GO, KEGG, and GSEA analysis

To investigate whether *GhHSFA4a* is involved in the disease resistance pathway, we used RNA-seq and analyzed the DEGs between pTRV2::*00* and pTRV2::*GhHSFA4a* seedlings (Figure 5). After filtering the original read quality, 38 Gb of clean sequence data were obtained for the two samples (5.81-6.72 Gb of clean reads for each sample). Using the *G. hirsutum* TM-1 transcriptome as the reference genome (ASM98774v1), 93.31-94.16% of the clean reads were mapped to the reference genome. Through standardization and screening of the read count, we identified 814 DEGs (424 upregulated and 390 down

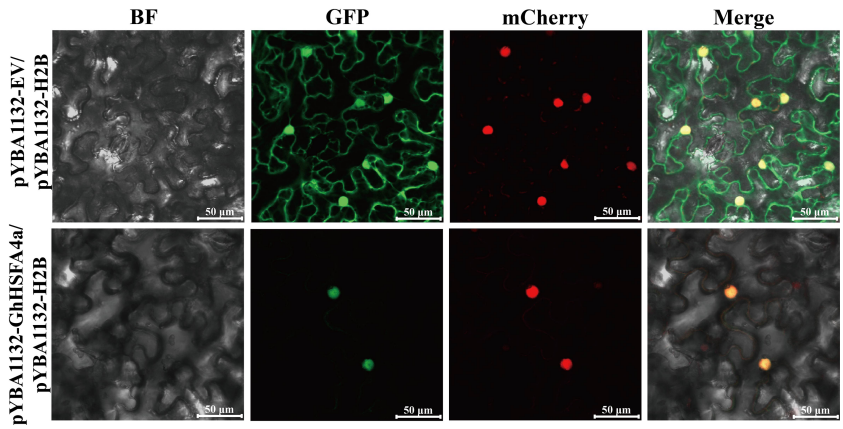

FIGURE 3
GhHSFA4a was localized in nucleus after transient overexpression of GhHSFA4a in leaves of *N. benthamiana*. *N. benthamiana* leaves were infiltrated with EHA105 cells containing pYBA1132::GhHSFA4a::GFP and using pYBA1132::GFP as a control. Shown are the confocal micrographs of *Agrobacterium*-infiltrated *N. benthamiana* leaves harvested at 48 hpi and counterstained with H2B-mCherry to localize GhHSFB4a-GFP. Bars = 50 μm.

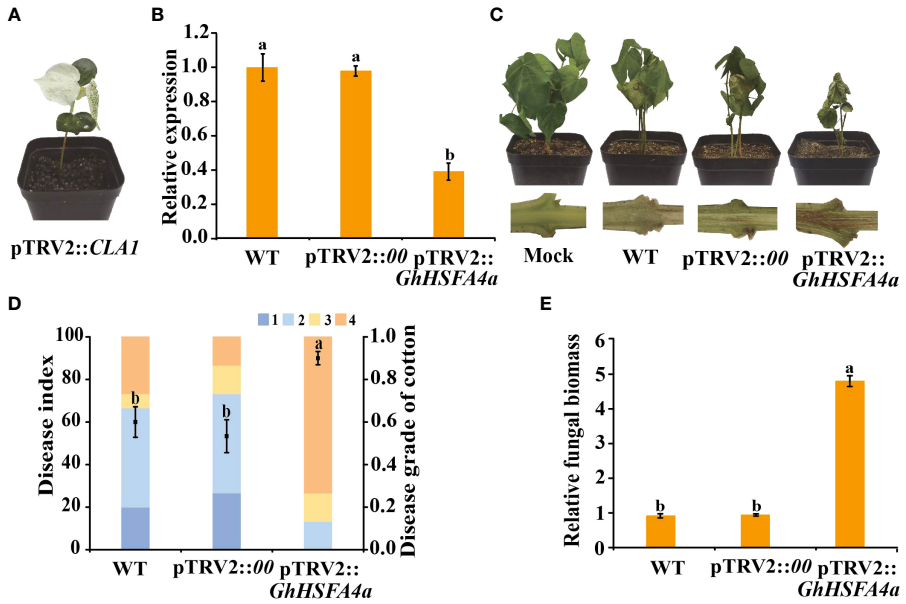

FIGURE 4
Silencing of *GhHSFA4a* attenuates plant resistance to *V. dahliae*. **(A)** Phenotype of pTRV2::*CLA1* at 14 days post *Agrobacterium* infiltration. **(B)** Expression of *GhHSFA4a* in pTRV2::*GhHSFA4a* and control plants. UBQ was the internal reference gene ($2^{-\Delta\Delta Ct}$). **(C)** Disease phenotypes of *GhHSFA4a*-silenced plants at 15 dpi with *V. dahliae* strain V991. **(D)** Disease index of pTRV2::*GhHSFA4a* and control plants at 15 dpi with *V. dahliae*. **(E)** Fungal biomass determined using qRT-PCR at 15 dpi with *V. dahliae*. Error bars represent the standard deviations and different letters indicate significant differences at $p<0.05$.

regulated). A heatmap was constructed for cluster analysis, which illustrates the global expression pattern of all DEGs and the repeatability between parallel groups (Figure 5A). DEGs were visualized using a volcano map, which showed the degree of difference among the 814 DEGs (Figure 5B). These DEGs reflect the response induced by *GhHSFA4a* knockdown.

All DEGs between pTRV2::*00* and pTRV2::*GhHSFA4a* cotton were annotated for GO terms and classified into three functional categories. For biological process, "response to oxidative stress" revealed that DEGs were highly enriched in metabolic pathways closely related to disease resistance. For molecular function, "oxidoreductase activity", "terpene synthase activity", and "peroxidase activity" indicated that DEG were highly enriched for plant disease resistance pathways. Analysis of cellular components revealed that DEGs were associated with the "cell wall", "external encapsulating structure", "cell periphery", and "apoplast" (Figure 6A). KEGG analysis showed that DEGs were enriched for 67 biological pathways in *G. hirsutum*. DEGs in pTRV2::*GhHSFA4a* cotton were enriched in pathways related to disease resistance, such as "flavonoid biosynthesis", "sesquiterpenoid and triterpenoid biosynthesis", "alpha-linolenic acid metabolism", and "linoleic acid metabolism". These functional annotations indicate that the disease resistance potential of cotton changed with *GhHSFA4a* silencing (Figure 6B). GSEA was performed using VIGS plants to further elucidate the function of *GhHSFA4a*. Compared to the gene sets in plants injected with the mock construct, 12 resistance-related gene sets were significantly activated in *GhHSFA4a*-silenced plants (e.g., "linoleic acid metabolism" and "flavonoid biosynthesis"; Figure 6C, Table S2). These results suggest that numerous genes in signaling and metabolic pathways involved in cotton disease resistance may be regulated by *GhHSFA4a* in a complex regulatory network for disease resistance. Downregulation of *GhHSFA4a* adversely affected related transcription and signaling pathways, seriously impairing disease resistance.

Validation of some key genes in important pathways

To analyze the relationship between metabolic pathways and resistance of cotton infected with *V. dahliae* using qRT-PCR, we selected marker genes dihydroflavonol 4-reductase (*GhDFR*, LOC107905441), anthocyanidin reductase (*GhANR*, LOC107905961), (+)-δ-cadinene synthase isozyme C2 (*GhTPS-C2*, LOC107920690), (+)-δ-cadinene synthase isozyme XC14 (*GhTPS-XC14*, LOC107920806), jasmonic acid carboxyl methyltransferase (*GhJMT*, LOC107905447), allene oxide cyclase (*GhAOC*, LOC107910216), lipoxygenase 6 (*GhLOX6*, LOC107961400), and linoleate 9S-lipoxygenase 4 (*Gh9S-LOX4*, LOC107954973), that responded to "flavonoid biosynthesis", "sesquiterpenoid and triterpenoid biosynthesis", "linoleic acid

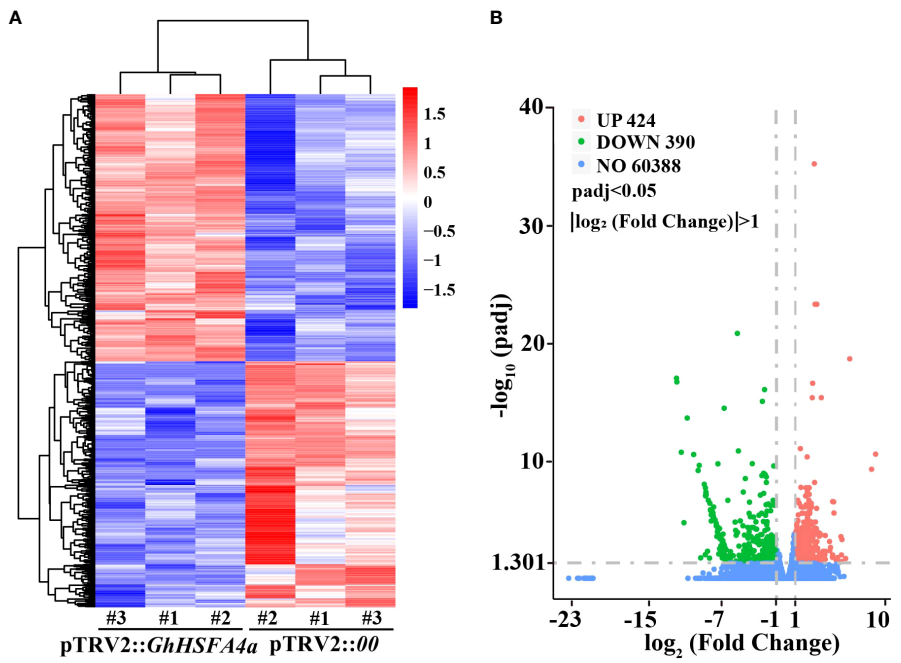

FIGURE 5
Analysis of DEGs between the transcriptomes of pTRV2::*00* and pTRV2::*GhHSFA4a* cottons. **(A)** Heat map of DEGs in each sample. **(B)** Volcano map of DEGs.

metabolism", and "alpha-linolenic acid metabolism" pathways. The expression of these eight genes was consistently upregulated in *V. dahliae*-infected plants; however, peak expression occurred at different times (Figure 7). These results indicate that *GhHSFA4a* contributed to cotton resistance to *V. dahliae* by modulating the four DEG-enriched pathways.

Overexpression of *GhHSFA4a* enhanced *V. dahliae* resistance in *Arabidopsis*

To further assess the function of *GhHSFA4a* in *V. dahliae* resistance, *Arabidopsis* seedlings were transformed with *GhHSFA4a* using *Agrobacterium* harvard recombinant plasmid with the CDS of *GhHSFA4a* and the 35S promoter. The expression levels of *GhHSFA4a* in five positive *GhHSFA4a*-transgenic lines were determined using PCR and qRT-PCR (Figures 8A, B). T3 homozygous generations of two independent *GhHSFA4a*-transgenic lines (OE-2 and OE-4) with high expression levels of *GhHSFA4a* were further analyzed. Wild-type and transgenic *Arabidopsis* plants were inoculated with the *V. dahliae* strain V991 and symptoms were monitored over time until 21 dpi. The transgenic plants had less wilting, chlorosis, and fungal biomass (Figures 8C, D); thus, supporting the view that GhHSFA4a positively contributes to plant resistance to *V. dahliae*.

Discussion

Plant HSFs are integral to the complex regulatory systems that coordinate plant development and molecular responses to biotic and abiotic stresses (Li et al., 2014). A few members of class A HSFs mainly play a positive regulatory role in plant abiotic stress such as heat (Liu et al., 2011; Shi et al., 2015; Meena et al., 2022; Zheng et al., 2022). HSFA4 can enhance plant tolerance to heat, high salinity, cadmium, light, and oxidative stress in *Arabidopsis*, rice, wheat, and other plants (Shim et al., 2009; Lang et al., 2017; Chen et al., 2018; Huang et al., 2018; Li et al., 2018; Andrási et al., 2019). We previously identified a set of DEGs in the transcriptome and metabolomic profiles of *Arabidopsis* plants inoculated with *V. dahliae* (Su et al., 2018). One of these DEGs is homologous to *G. hirsutum GhHSFA4a*, which encodes a TF belonging to the HSF family. Therefore, we hypothesized that *GhHSFA4a* might be involved in the resistance of cotton to *V. dahliae* and here, we characterized its biological functions.

Structural characteristics revealed that HSFA class proteins usually contain DBD, HR-A/B region, NLS as well as NES motifs, and AHA domains (Scharf et al., 1998; Scharf et al., 2012). GhHSFA4a contains a conserved DBD domain (Figure S1). We visualized the *GhHSFA4a*-GFP fusion protein in the nucleus, a feature consistent with the location of HSFs identified in previous studies (Figure 3) (Gai et al., 2020; Zhang et al.,

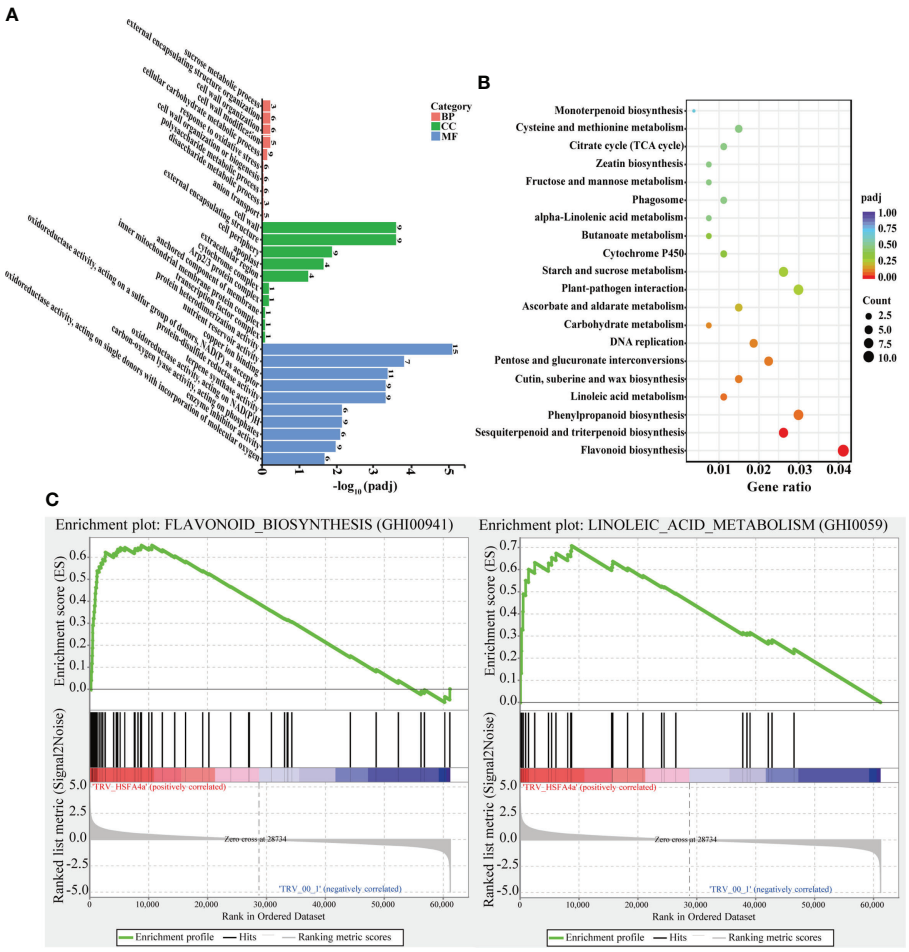

FIGURE 6
GO, KEGG, and GSEA metabolic pathway enrichment for DEGs in pTRV2::*00* and pTRV2::*GhHSFA4a* cotton. **(A)** GO terms. **(B)** KEGG terms. **(C)** GSEA analysis shows that two plant resistance-related gene sets are significantly activated in *GhHSFA4a*-silenced cotton compared with those in the control group. BP, biological process; CC, cellular component; MF, molecular function.

2020). Our phylogenetic analysis indicated that GhHSFA4a might have a function similar to that of *F. vesca* HSFA4a (Figure 1C). Additionally, the *cis*-element analysis showed that the *GhHSFA4a* promoter region consists of several elements that respond to defense, stress, and hormones (Figure 1D). Based on our bioinformatic analysis and previous research related to HSFA4a, we hypothesized that GhHSFA4 may confer resistance to *V. dahliae* in cotton by modulating a defense pathway.

Plants protect themselves against microbes through structural resistance and a sophisticated immune system that activates defense responses. Numerous lines of evidence support the hypothesis that HSFs are required for plant pathogen resistance (Kumar et al., 2009; Daurelio et al., 2013). However, few studies have been conductedon HSFs and their involvement in cotton resistance against *V. dahliae*. In our study, *GhHSFA4a* expression was significantly induced at 12 hpi, an early stage of *V. dahliae* infection (Figure 2). The HSF-like transcription factor *TB1* acts as a major molecular switch from plant growth to defense by binding to the *TL1* (GAAGAAGAA) *cis*-element required for the induction of endoplasmic-reticulum-resident genes (Pajerowska-Mukhtar et al., 2012). Previous studies have shown that microbes such as *Pseudomonas syringae* and various fungal pathogens activate a well-defined subset of HSF genes, including *HSFA2*, *HSFA4A*, *HSFA8*, *HSFB1*, and *HSFB2B* (Andrási et al., 2021). In addition, *HSFA4A/HSFA5* factors have been implicated in cell death triggered by pathogenic infection (Baniwal et al., 2007).

In rice, the *spl7* mutation disrupts the *HSFA4* gene, leading to enhanced heat- and UV- light-induced cell necrosis and susceptibility to several pathogens (Yamanouchi et al., 2002). Overexpression of the transcription factor MYB49 in tomatoes

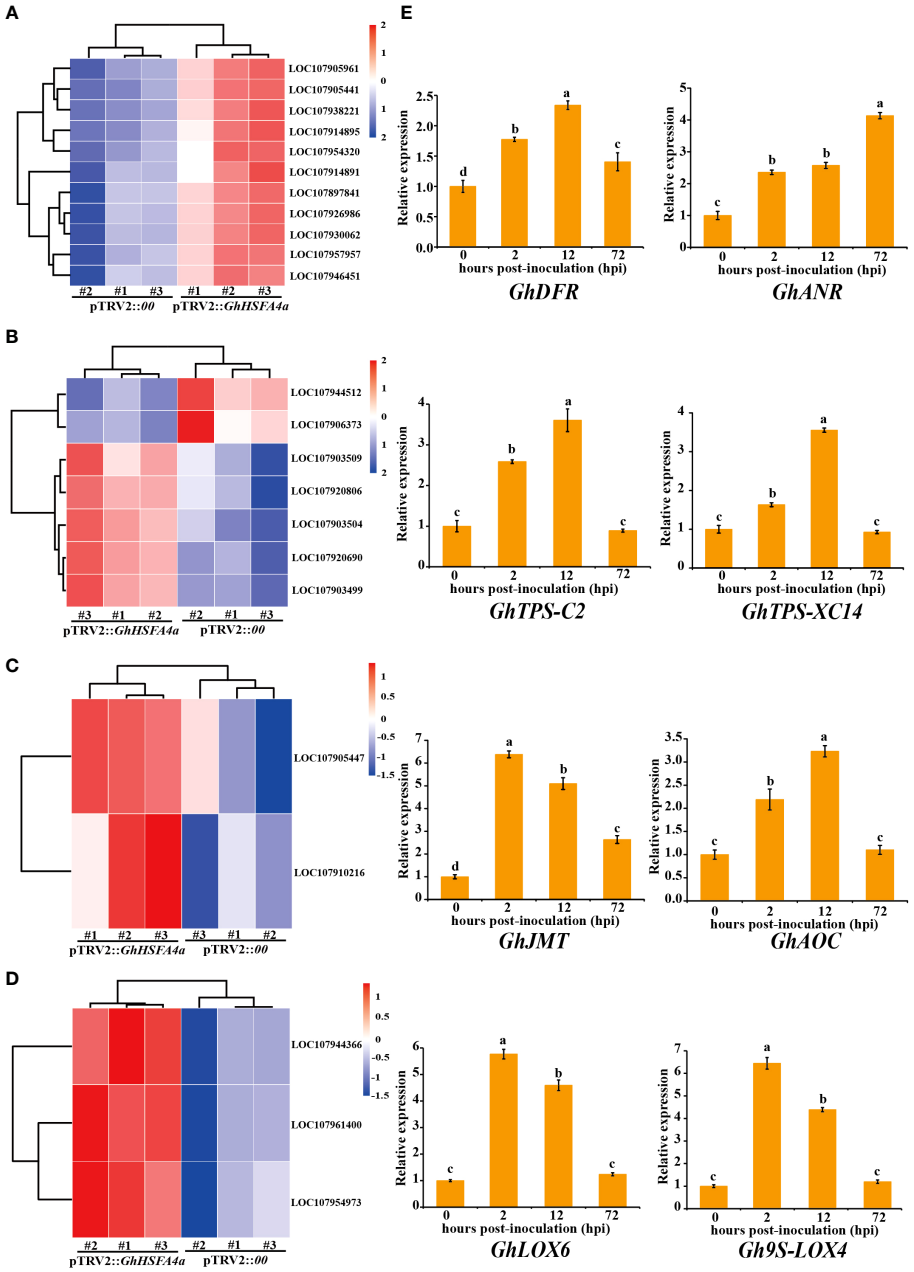

FIGURE 7
Validation of metabolic pathways significantly enriched for DEGs in pTRV2::*GhHSFA4a* cotton. Detailed expression profiles of genes related to **(A)** "flavonoid biosynthesis", **(B)** "sesquiterpenoid and triterpenoid biosynthesis", **(C)** "alpha-linolenic acid metabolism", and **(D)** "linoleic acid metabolism". **(E)** Relative expression levels over time of marker genes for the four pathways. Error bars represent the standard deviations and different letters indicate significant differences at $p<0.05$.

decreases the DI and enhances resistance to *Phytophthora infestans* (Cui et al., 2018). The VIGS-mediated silencing of cyclic nucleotide-gated ion channels (CNGCs) *MdCNGC2* in fruits improves resistance to *Botryosphaeria dothidea* (Zhou et al., 2020). These results are consistent with our findings from the VIGS of *GhHSFA4a* in cotton and the overexpression of *GhHSFA4a* in *Arabidopsis*. The increased DI and fungal biomass in cotton after silencing *GhHSFA4a* in seedlings was evidence that resistance was compromised (Figure 4). Alternatively, overexpression of *GhHSFA4a* in *Arabidopsis* enhanced its resistance to *V. dahliae* (Figure 8). Our preliminary results support the prediction that *GhHSFA4a*

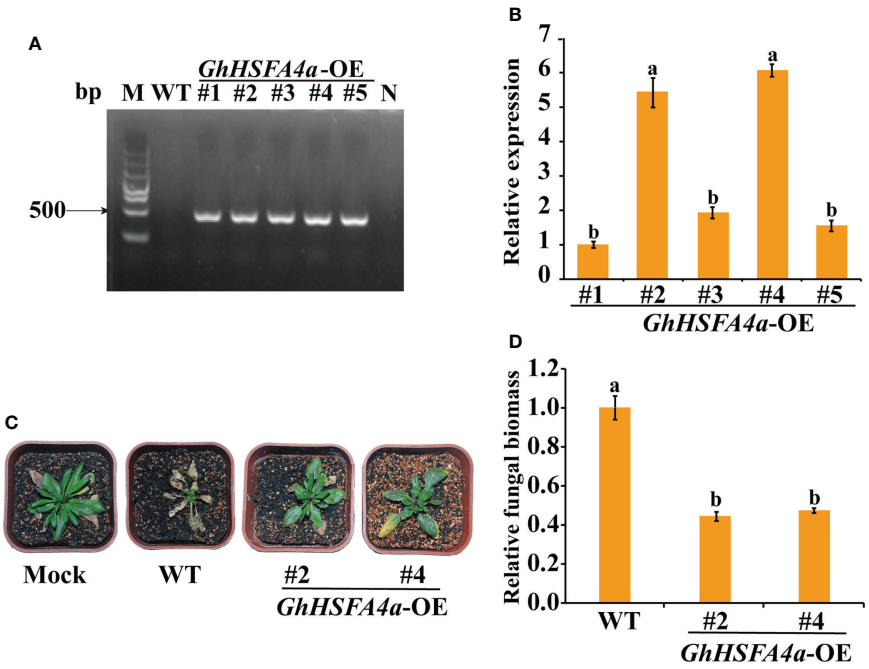

FIGURE 8
Enhanced *V. dahliae* resistance of *Arabidopsis* plants overexpressing *GhHSFA4a*. **(A)** PCR amplicons of *GhHSFA4a* in positive transgenic *Arabidopsis*. **(B)** Expression levels of *GhHSFA4a* in transgenic *Arabidopsis* lines (#1-#5). *AtRubisco* was used as an internal control. **(C)** Symptoms in wild-type and two *GhHSFA4a*-overexpressing (OE) lines of *Arabidopsis* plants at 21 dpi with *V. dahliae*. **(D)** Fungal biomass determined using qRT-PCR in wild-type (WT) and transgenic *Arabidopsis* plants. Error bars represent the standard deviations and different letters indicate significant differences at $p<0.05$.

participates in *V. dahliae* resistance. However, the regulatory network involved in *GhHSFA4a* in cotton disease resistance needs to be elucidated.

A complex regulatory network of flavor-related metabolites was revealed in *Actinidia chinensis* through the analysis of metabolome and transcriptome data, which helped identify key structural genes and TFs that regulate the metabolism of soluble sugars, organic acids, and important volatiles (Wang et al., 2022). In non-stressed *HSFA1b*-overexpressing (*HSFA1bOx*) *Arabidopsis*, the expression of 509 genes involved in responses to biotic stress were altered (Bechtold et al., 2013). Following our RNA-seq analysis of the transcriptome of *GhHSFA4a*-silenced plants meant to identify the molecular role of GhHSFA4a after inoculation with *V. dahliae*, we identified 814 DEGs between pTRV2::*00* and pTRV2::*GhHSFA4a* plants; 424 genes were upregulated and 390 genes were downregulated after *GhHSFA4a*-silencing (Figure 5).

The KEGG analysis revealed that DEGs were mainly enriched in pathways for the synthesis of secondary metabolites ("flavonoid biosynthesis", "sesquiterpenoid and triterpenoid biosynthesis"; Figure 6B). Flavonoids are involved in plant development as well as defense and help plants adapt to environmental conditions (Hichri et al., 2011). Triterpenoids are considered to be defensive compounds against pathogens (Vincken et al., 2007; Szakiel et al., 2011). *Nbnrp1* mediates PevD1-induced defense responses by regulating the sesquiterpenoid phytoalexin biosynthesis pathway (Liang et al., 2021). In our study, DEGs were involved in plant hormone-related pathways, such as "linoleic acid metabolism" and "alpha-linolenic acid metabolism" (Figure 6B). Linolenic acid and linoleic acid are key components in the synthesis of the hormones jasmonic acid (JA) and MeJA, which have numerous physiological functions in disease resistance such as direct inhibition of pathogens, transmission of resistance signals, and induction of defense compound synthesis (Creelman et al., 1992; Gundlach et al., 1992; Harms et al., 1995; Singh et al., 2011). *Arabidopsis* mutants *fad3*-2, *fad7*-2, and *fad8*, which lack linolenic acid, express low JA contents, and the expression of JA-related genes is not induced. These mutants are sensitive to *Pythium mastophorum*, and their antifungal ability is restored after MeJA application (Vijayan et al., 1998).

Based on our transcriptomic results, we hypothesize that GhHSFA4a is involved in cotton disease resistance by regulating the synthesis of secondary metabolites and plant hormones. This hypothesis is supported by the qRT-PCR results that showed that eight marker genes for "flavonoid biosynthesis", "sesquiterpenoid and triterpenoid biosynthesis", and "alpha-linolenic acid metabolism" pathways were induced by *V. dahliae* (Figure 7). In previous studies, these marker genes were identified as key genes in the above pathways and were

involved in stress resistance. For example, in tobacco, the overexpression of *DFR* or *ANR*, which encode crucial regulatory enzymes for flavonoid synthesis, improves the resistance of plants to biotic or abiotic stresses (Tan et al., 2018; Sun et al., 2021). The transcription levels of TPS family genes and jasmonate-responsive genes in cotton plants treated with plant-growth-promoting rhizobacteria were higher than those in the untreated control plants and exhibited improved resistance to *Spodoptera exigua* (Zebelo et al., 2016). In *Arabidopsis*, JMT catalyzes the conversion of JA into MeJA and participates in JA-responsive defense mechanisms (Seo et al., 2001). In *Arachis hypogaea*, *AhAOC* can be induced by JA to enhance plant resistance to stress (Liu et al., 2015). Tobacco *NaLOX3* expression is induced by the fungal initiator ergosterol (Dadakova et al., 2013), while *Pisum sativum* L enhances waterlogging tolerance by regulating linoleate *Ps9S-LOX5* gene expression (Zaman et al., 2019).

Conclusions

In this study, *GhHSFA4a*, encoding a heat shock factor located in the nucleus, was induced by *V. dahliae* and was constitutively expressed in the roots, stems, and leaves of cotton. When *GhHSFA4a* was silenced, cotton resistance to *V. dahliae* was compromised, whereas its overexpression in *Arabidopsis* significantly improved resistance. Furthermore, *GhHSFA4a* was shown to be involved in "flavonoid biosynthesis", "sesquiterpenoid and triterpenoid biosynthesis", "linoleic acid metabolism" and "alpha-linolenic acid metabolism" pathways. In summary, GhHSFA4a contributes positively to plant resistance against *V. dahliae* and mediates flavonoid and terpenoid secondary metabolic pathways and JA biosynthesis and signaling pathways, indicating that it is a potential candidate gene for molecular genetic breeding.

Data availability statement

The original contributions presented in the study are publicly available. This data can be found here: NCBI, PRJNA877353.

Author contributions

Conceptualization, XS and EL. Methodology, HL. Software, HL. Validation, HC. Formal analysis, LL and DW. Investigation, LL and DW. Resources, HG. Data curation, LL and DW. Writing—original draft preparation, LL and DW. Writing—review and editing, XS and LL. Visualization, EL. Supervision, EL. Funding acquisition, XS, HC, and HL All authors contributed to the article and approved the submitted version.

Funding

This research was supported by Hainan Yazhou Bay Seed Laboratory (project of B21HJ0215), the National Natural Science Foundation of China (32072376 and 32160624), and Central Public-interest Scientific Institution Basal Research Fund (No. Y2022CG05).

Conflict of interest

The authors declare that the research was conducted in the absence of any commercial or financial relationships that could be construed as a potential conflict of interest.

Publisher's note

Supplementary material

The Supplementary Material for this article can be found online at: https://www.frontiersin.org/articles/10.3389/fpls.2022.1050216/full#supplementary-material

References

Alves, M. S., Dadalto, S. P., Gonçalves, A. B., De Souza, G. B., Barros, V. A., and Fietto, L. G. (2014). Transcription factor functional protein-protein interactions in plant defense responses. *Proteomes* 2, 85–106. doi: 10.3390/proteomes2010085

Andrási, N., Pettkó-Szandtner, A., and Szabados, L. (2021). Diversity of plant heat shock factors: Regulation, interactions, and functions. *J. Exp. Bot.* 72, 1558–1575. doi: 10.1093/jxb/eraa576

Andrási, N., Rigó, G., Zsigmond, L., Pérez-Salamó, I., Papdi, C., Klement, E., et al. (2019). The mitogen-activated protein kinase 4-phosphorylated heat shock factor A4A regulates responses to combined salt and heat stresses. *J. Exp. Bot.* 70, 4903–4918. doi: 10.1093/jxb/erz217

Ashraf, M. F., Yang, S., Wu, R., Wang, Y., Hussain, A., Noman, A., et al. (2018). *Capsicum annuum HsfB2a* positively regulates the response to *Ralstonia solanacearum* infection or high temperature and high humidity forming

transcriptional cascade with *CaWRKY6* and *CaWRKY40*. *Plant Cell Physiol.* 59, 2608–2623. doi: 10.1093/pcp/pcy181

Baniwal, S. K., Chan, K. Y., Scharf, K. D., and Nover, L. (2007). Role of heat stress transcription factor HsfA5 as specific repressor of HsfA4. *J. Biol. Chem.* 282, 3605–3613. doi: 10.1074/jbc.M609545200

Bechtold, U., Albihlal, W. S., Lawson, T., Fryer, M. J., Sparrow, P. A., Richard, F., et al. (2013). *Arabidopsis HEAT SHOCK TRANSCRIPTION FACTORA1b* overexpression enhances water productivity, resistance to drought, and infection. *J. Exp. Bot.* 64, 3467–3481. doi: 10.1093/jxb/ert185

Bi, H., Miao, J., He, J., Chen, Q., Qian, J., Li, H., et al. (2022). Characterization of the wheat heat shock factor TaHsfA2e-5D conferring heat and drought tolerance in *Arabidopsis*. *Int. J. Mol. Sci.* 23, 2784–2797. doi: 10.3390/ijms23052784

Chen, S. S., Jiang, J., Han, X. J., Zhang, Y. X., and Zhuo, R. Y. (2018). Identification, expression analysis of the hsf family, and characterization of class A4 in *Sedum alfredii* hance under cadmium stress. *Int. J. Mol. Sci.* 19, 1216–1232. doi: 10.3390/ijms19041216

Clough, S. J., and Bent, A. F. (1998). Floral dip: a simplified method for *Agrobacterium*-mediated transformation of *Arabidopsis thaliana*. *Plant J.* 16, 735–743. doi: 10.1046/j.1365-313x.1998.00343.x

Creelman, R. A., Tierney, M. L., and Mullet, J. E. (1992). Jasmonic acid/methyl jasmonate accumulate in wounded soybean hypocotyls and modulate wound gene expression. *Proc. Natl. Acad. Sci. U. S. A.* 89, 4938–4941. doi: 10.1073/pnas.89.11.4938

Cui, J., Jiang, N., Zhou, X., Hou, X., Yang, G., Meng, J., et al. (2018). Tomato MYB49 enhances resistance to *Phytophthora infestans* and tolerance to water deficit and salt stress. *Planta* 248, 1487–1503. doi: 10.1007/s00425-018-2987-6

Dadakova, K., Klempova, J., Jendrisakova, T., Lochman, J., and Kasparovsky, T. (2013). Elucidation of signaling molecules involved in ergosterol perception in tobacco. *Plant Physiol. Biochem.* 73, 121–127. doi: 10.1016/j.plaphy.2013.09.009

Daurelio, L. D., Romero, M. S., Petrocelli, S., Merelo, P., Cortadi, A. A., Talón, M., et al. (2013). Characterization of *Citrus sinensis* transcription factors closely associated with the non-host response to *Xanthomonas campestris* pv. *vesicatoria*. *J. Plant Physiol.* 170, 934–942. doi: 10.1016/j.jplph.2013.01.011

Deketelaere, S., Tyvaert, L., França, S. C., and Höfte, M. (2017). Desirable traits of a good biocontrol agent against *Verticillium* wilt. *Front. Microbiol.* 8. doi: 10.3389/fmicb.2017.01186

Franco-Zorrilla, J. M., and Solano, R. (2017). Identification of plant transcription factor target sequences. *Biochim. Biophys. Acta Gene Regul. Mech.* 1860, 21–30. doi: 10.1016/j.bbagrm.2016.05.001

Gai, W. X., Ma, X., Li, Y., Xiao, J. J., Khan, A., Li, Q. H., et al. (2020). *CaHsfA1d* improves plant thermotolerance *via* regulating the expression of stress- and antioxidant-related genes. *Int. J. Mol. Sci.* 21, 8374–8397. doi: 10.3390/ijms21218374

Gao, X., Wheeler, T., Li, Z., Kenerley, C. M., He, P., and Shan, L. (2011). Silencing *GhNDR1* and *GhMKK2* compromises cotton resistance to *Verticillium* wilt. *Plant J.* 66, 293–305. doi: 10.1111/j.1365-313X.2011.04491.x

Gong, Q., Yang, Z., Wang, X., Butt, H. I., Chen, E., He, S., et al. (2017). Salicylic acid-related cotton (*Gossypium arboreum*) ribosomal protein GaRPL18 contributes to resistance to *Verticillium dahliae*. *BMC Plant Biol.* 17, 59–73. doi: 10.1186/s12870-017-1007-5

Gundlach, H., Müller, M. J., Kutchan, T. M., and Zenk, M. H. (1992). Jasmonic acid is a signal transducer in elicitor-induced plant cell cultures. *Proc. Natl. Acad. Sci. U. S. A.* 89, 2389–2393. doi: 10.1073/pnas.89.6.2389

Guo, M., Liu, J. H., Ma, X., Luo, D. X., Gong, Z. H., and Lu, M. H. (2016). The plant heat stress transcription factors (HSFs): structure, regulation, and function in response to abiotic stresses. *Front. Plant Sci.* 7, 114–126. doi: 10.3389/fpls.2016.00114

Harms, K., Atzorn, R., Brash, A., Kuhn, H., Wasternack, C., Willmitzer, L., et al. (1995). Expression of a flax allene oxide synthase cDNA leads to increased endogenous jasmonic acid (JA) levels in transgenic potato plants but not to a corresponding activation of JA-responding genes. *Plant Cell* 7, 1645–1654. doi: 10.1105/tpc.7.10.1645

Harting, R., Höfer, A., Tran, V. T., Weinhold, L. M., Barghahn, S., Schlüter, R., et al. (2020). The Vta1 transcriptional regulator is required for microsclerotia melanization in *Verticillium dahliae*. *Fungal Biol.* 124, 490–500. doi: 10.1016/j.funbio.2020.01.007

Hichri, I., Barrieu, F., Bogs, J., Kappel, C., Delrot, S., and Lauvergeat, V. (2011). Recent advances in the transcriptional regulation of the flavonoid biosynthetic pathway. *J. Exp. Bot.* 62, 2465–2483. doi: 10.1093/jxb/erq442

Huang, H. Y., Chang, K. Y., and Wu, S. J. (2018). High irradiance sensitive phenotype of *Arabidopsis hit2/xpo1a* mutant is caused in part by nuclear confinement of AtHsfA4a. *Biol. Plant* 62, 69–79. doi: 10.1007/s10535-017-0753-4

Kilian, J., Peschke, F., Berendzen, K. W., Harter, K., and Wanke, D. (2012). Prerequisites, performance and profits of transcriptional profiling the abiotic stress response. *Biochim. Biophys. Acta Gene Regul. Mech.* 1819, 166–175. doi: 10.1016/j.bbagrm.2011.09.005

Kumar, M., Busch, W., Birke, H., Kemmerling, B., Nürnberger, T., and Schöffl, F. (2009). Heat shock factors HsfB1 and HsfB2b are involved in the regulation of *Pdf1.2* expression and pathogen resistance in *Arabidopsis*. *Mol. Plant* 2, 152–165. doi: 10.1093/mp/ssn095

Lang, S., Liu, X., Xue, H., Li, X., and Wang, X. (2017). Functional characterization of BnHSFA4a as a heat shock transcription factor in controlling the re-establishment of desiccation tolerance in seeds. *J. Exp. Bot.* 68, 2361–2375. doi: 10.1093/jxb/erx097

Lescot, M., Déhais, P., Thijs, G., Marchal, K., Moreau, Y., Van De Peer, Y., et al. (2002). PlantCARE, a database of plant *cis*-acting regulatory elements and a portal to tools for *in silico* analysis of promoter sequences. *Nucleic Acids Res.* 30, 325–327. doi: 10.1093/nar/30.1.325

Li, X., Su, X., Lu, G., Sun, G., Zhang, Z., Guo, H., et al. (2020). *VdOGDH* is involved in energy metabolism and required for virulence of *Verticillium dahliae*. *Curr. Genet.* 66, 345–359. doi: 10.1007/s00294-019-01025-2

Liang, Y., Li, Z., Zhang, Y., Meng, F., Qiu, D., Zeng, H., et al. (2021). Nbnrp1 mediates *Verticillium dahliae* effector PevD1-triggered defense responses by regulating sesquiterpenoid phytoalexins biosynthesis pathway in *Nicotiana benthamiana*. *Gene* 768, 145280–145291. doi: 10.1016/j.gene.2020.145280

Liu, H. C., Liao, H. T., and Charng, Y. Y. (2011). The role of class A1 heat shock factors (HSFA1s) in response to heat and other stresses in *Arabidopsis*. *Plant Cell Environ.* 34, 738–751. doi: 10.1111/j.1365-3040.2011.02278.x

Liu, H. H., Wang, Y. G., Wang, S. P., and Li, H. J. (2015). Cloning and characterization of peanut allene oxide cyclase gene involved in salt-stressed responses. *Genet. Mol. Res.* 14, 2331–2340. doi: 10.4238/2015.March.27.18

Liu, T., Chen, T., Kan, J., Yao, Y., Guo, D., Yang, Y., et al. (2022). The GhMYB36 transcription factor confers resistance to biotic and abiotic stress by enhancing *PR1* gene expression in plants. *Plant Biotechnol. J.* 20, 722–735. doi: 10.1111/pbi.13751

Li, F., Zhang, H., Zhao, H., Gao, T., Song, A., Jiang, J., et al. (2018). Chrysanthemum *CmHSFA4* gene positively regulates salt stress tolerance in transgenic chrysanthemum. *Plant Biotechnol. J.* 16, 1311–1321. doi: 10.1111/pbi.12871

Li, P. S., Yu, T. F., He, G. H., Chen, M., Zhou, Y. B., Chai, S. C., et al. (2014). Genome-wide analysis of the hsf family in soybean and functional identification of *GmHsf-34* involvement in drought and heat stresses. *BMC Genomics* 15, 1–16. doi: 10.1186/1471-2164-15-1009

Livak, K.J., and Schmittgen, T. (2001). Analysis of relative gene expression data using real-time quantitative PCR and the 2−ΔΔCT method. *Methods* 25, 402–408. doi: 10.1006/meth.2001.1262

Lu, J., Wang, L., Zhang, Q., Ma, C., Su, X., Cheng, H., et al. (2022). AmCBF1 transcription factor regulates plant architecture by repressing *GhPP2C1* or *GhPP2C2* in *Gossypium hirsutum*. *Front. Plant Sci.* 13, 914206–914219. doi: 10.1006/meth.2001.1262

Meena, S., Samtani, H., and Khurana, P. (2022). Elucidating the functional role of heat stress transcription factor A6b (*TaHsfA6b*) in linking heat stress response and the unfolded protein response in wheat. *Plant Mol. Biol.* 108, 621–634. doi: 10.1007/s11103-022-01252-1

Nishizawa-Yokoi, A., Yoshida, E., Yabuta, Y., and Shigeoka, S. (2009). Analysis of the regulation of target genes by an *Arabidopsis* heat shock transcription factor, HsfA2. *Biosci. Biotechnol. Biochem.* 73, 890–895. doi: 10.1271/bbb.80809

Pajerowska-Mukhtar, K. M., Wang, W., Tada, Y., Oka, N., Tucker, C. L., Fonseca, J. P., et al. (2012). The HSF-like transcription factor TBF1 is a major molecular switch for plant growth-to-defense transition. *Curr. Biol.* 22, 103–112. doi: 10.1016/j.cub.2011.12.015

Pettersen, E. F., Goddard, T. D., Huang, C. C., Couch, G. S., Greenblatt, D. M., Meng, E. C., et al. (2004). UCSF chimera–a visualization system for exploratory research and analysis. *J. Comput. Chem.* 25, 1605–1612. doi: 10.1002/jcc.20084

Purayil, F. T., Rajashekar, B., Kurup, S. S., Cheruth, A. J., Subramaniam, S., Tawfik, N. H., et al. (2020). Transcriptome profiling of *Haloxylon persicum* (Bunge ex boiss and buhse) an endangered plant species under PEG-induced drought stress. *Genes* 11, 640–659. doi: 10.3390/genes11060640

Sajjad, M., Wei, X., Liu, L., Li, F., and Ge, X. (2021). Transcriptome analysis revealed GhWOX4 intercedes myriad regulatory pathways to modulate drought tolerance and vascular growth in cotton. *Int. J. Mol. Sci.* 22, 898–922. doi: 10.3390/ijms22020898

Scharf, K. D., Berberich, T., Ebersberger, I., and Nover, L. (2012). The plant heat stress transcription factor (Hsf) family: structure, function and evolution. *Biophys. Acta Gene Regul. Mech.* 1819, 104–119. doi: 10.1016/j.bbagrm.2011.10.002

Scharf, K. D., Heider, H., HoüHfeld, I., Lyck, R., Schmidt, E., and Nover, L. (1998). The tomato hsf system: HsfA2 needs interaction with HsfA1 for efficient nuclear import and may be localized in cytoplasmic heat stress granules. *Mol. Cell. Biol.* 18, 2240–2251. doi: 10.1128/MCB.18.4.2240

Seo, H. S., Song, J. T., Cheong, J. J., Lee, Y. H., Lee, Y. W., Hwang, I., et al. (2001). Jasmonic acid carboxyl methyltransferase: A key enzyme for jasmonate-regulated plant responses. *Proc. Natl. Acad. Sci. U. S. A.* 98, 4788–4793. doi: 10.1073/pnas.081557298

Shaban, M., Miao, Y., Ullah, A., Khan, A. Q., Menghwar, H., Khan, A. H., et al. (2018). Physiological and molecular mechanism of defense in cotton against *Verticillium dahliae*. *Plant Physiol. Biochem.* 125, 193–204. doi: 10.1016/j.plaphy.2018.02.011

Shim, D., Hwang, J. U., Lee, J., Lee, S., Choi, Y., An, G., et al. (2009). Orthologs of the class A4 heat shock transcription factor HsfA4a confer cadmium tolerance in wheat and rice. *Plant Cell* 21, 4031–4043. doi: 10.1105/tpc.109.066902

Shi, H., Tan, D. X., Reiter, R. J., Ye, T., Yang, F., and Chan, Z. (2015). Melatonin induces class A1 heat-shock factors (HSFA1s) and their possible involvement of thermotolerance in *Arabidopsis*. *J. Pineal Res.* 58, 335–342. doi: 10.1111/jpi.12219

Singh, A. K., Fu, D. Q., El-Habbak, M., Navarre, D., Ghabrial, S., and Kachroo, A. (2011). Silencing genes encoding omega-3 fatty acid desaturase alters seed size and accumulation of bean pod mottle virus in soybean. *Mol. Plant Microbe Interact.* 24, 506–515. doi: 10.1094/mpmi-09-10-0201

Su, X., Lu, G., Guo, H., Zhang, K., Li, X., and Cheng, H. (2018). The dynamic transcriptome and metabolomics profiling in *Verticillium dahliae* inoculated *Arabidopsis thaliana*. *Sci. Rep.* 8, 1–11. doi: 10.1038/s41598-018-33743-x

Su, X., Lu, G., Li, X., Rehman, L., Liu, W., Sun, G., et al. (2020). Host-induced gene silencing of an adenylate kinase gene involved in fungal energy metabolism improves plant resistance to *Verticillium dahliae*. *Biomolecules* 10, 127–142. doi: 10.3390/biom10010127

Sun, W., Zhou, N., Feng, C., Sun, S., Tang, M., Tang, X., et al. (2021). Functional analysis of a dihydroflavonol 4-reductase gene in *Ophiorrhiza japonica* (OjDFR1) reveals its role in the regulation of anthocyanin. *PeerJ* 9, e12323–e12340. doi: 10.7717/peerj.12323

Szakiel, A., Pączkowski, C., and Henry, M. (2011). Influence of environmental abiotic factors on the content of saponins in plants. *Phytochem. Rev.* 10, 471–491. doi: 10.3390/molecules24162907

Tanabe, S., Onodera, H., Hara, N., Ishii-Minami, N., Day, B., Fujisawa, Y., et al. (2016). The elicitor-responsive gene for a GRAS family protein, *CIGR2*, suppresses cell death in rice inoculated with rice blast fungus *via* activation of a heat shock transcription factor, *OsHsf23*. *Biosci. Biotechnol. Biochem.* 80, 145–151. doi: 10.1080/09168451.2015.1075866

Tan, L., Wang, M., Kang, Y., Azeem, F., Zhou, Z., Tuo, D., et al. (2018). Biochemical and functional characterization of anthocyanidin reductase (ANR) from *Mangifera indica* l. *Molecules* 23, 2876–2895. doi: 10.3390/molecules23112876

Udvardi, M. K., Kakar, K., Wandrey, M., Montanari, O., Murray, J., Andriankaja, A., et al. (2007). Legume transcription factors: global regulators of plant development and response to the environment. *Plant Physiol.* 144, 538–549. doi: 10.1104/pp.107.098061

Vijayan, P., Shockey, J., Lévesque, C. A., Cook, R. J., and Browse, J. (1998). A role for jasmonate in pathogen defense of *Arabidopsis*. *Proc. Natl. Acad. Sci. U. S. A.* 95, 7209–7214. doi: 10.1073/pnas.95.12.7209

Vincken, J. P., Heng, L., De Groot, A., and Gruppen, H. (2007). Saponins, classification and occurrence in the plant kingdom. *Phytochemistry* 68, 275–297. doi: 10.1016/j.phytochem.2006.10.008

Von Koskull-Döring, P., Scharf, K. D., and Nover, L. (2007). The diversity of plant heat stress transcription factors. *Trends Plant Sci.* 12, 452–457. doi: 10.1016/j.tplants.2007.08.014

Wang, J., Chen, L., Long, Y., Si, W., Cheng, B., and Jiang, H. (2021). A novel heat shock transcription factor (*ZmHsf08*) negatively regulates salt and drought stress responses in maize. *Int. J. Mol. Sci.* 22, 11922–11937. doi: 10.3390/ijms222111922

Wang, R., Shu, P., Zhang, C., Zhang, J., Chen, Y., Zhang, Y., et al. (2022). Integrative analyses of metabolome and genome-wide transcriptome reveal the regulatory network governing flavor formation in kiwifruit (Actinidia chinensis). *New Phytol* 233, 373–389. doi: 10.1111/nph.17618

Wang, Y., Liang, C., Wu, S., Zhang, X., Tang, J., Jian, G., et al. (2016). Significant improvement of cotton *Verticillium* wilt resistance by manipulating the expression of *Gastrodia* antifungal proteins. *Mol. Plant* 9, 1436–1439. doi: 10.1016/j.molp.2016.06.013

Wei, Y., Liu, G., Chang, Y., He, C., and Shi, H. (2018). Heat shock transcription factor 3 regulates plant immune response through modulation of salicylic acid accumulation and signalling in cassava. *Mol. Plant Pathol.* 19, 2209–2220. doi: 10.1111/mpp.12691

Wu, M., Pei, W., Wedegaertner, T., Zhang, J., and Yu, J. (2022). Genetics, breeding and genetic engineering to improve cottonseed oil and protein: A review. *Front. Plant Sci.* 13. doi: 10.3389/fpls.2022.864850

Yamanouchi, U., Yano, M., Lin, H., Ashikari, M., and Yamada, K. (2002). A rice spotted leaf gene, *Spl7*, encodes a heat stress transcription factor protein. *Proc. Natl. Acad. Sci. U. S. A.* 99, 7530–7535. doi: 10.1073/pnas.112209199

Yang, W., Ju, Y., Zuo, L., Shang, L., Li, X., Li, X., et al. (2020). OsHsfB4d binds the promoter and regulates the expression of *OsHsp18.0-CI* to resistant against *Xanthomonas oryzae*. *Rice* 13, 28–41. doi: 10.1186/s12284-020-00388-2

Zaman, M. S. U., Malik, A. I., Erskine, W., and Kaur, P. (2019). Changes in gene expression during germination reveal pea genotypes with either "quiescence" or "escape" mechanisms of waterlogging tolerance. *Plant Cell Environ.* 42, 245–258. doi: 10.1111/pce.13338

Zander, M., Chen, S., Imkampe, J., Thurow, C., and Gatz, C. (2012). Repression of the *Arabidopsis thaliana* jasmonic acid/ethylene-induced defense pathway by TGA-interacting glutaredoxins depends on their c-terminal ALWL motif. *Mol. Plant* 5, 831–840. doi: 10.1093/mp/ssr113

Zebelo, S., Song, Y., Kloepper, J. W., and Fadamiro, H. (2016). Rhizobacteria activates (+)-δ-cadinene synthase genes and induces systemic resistance in cotton against beet armyworm (*Spodoptera exigua*). *Plant Cell Environ.* 39, 935–943. doi: 10.1111/pce.12704

Zhang, J., Fang, H., Zhou, H., Sanogo, S., and Ma, Z. (2014). Genetics, breeding, and marker-assisted selection for *Verticillium* wilt resistance in cotton. *Crop Sci.* 54, 1289–1303. doi: 10.2135/cropsci2013.08.0550

Zhang, W. Q., Gui, Y. J., Short, D. P. G., Li, T. G., Zhang, D. D., Zhou, L., et al. (2018). *Verticillium dahliae* transcription factor VdFTF1 regulates the expression of multiple secreted virulence factors and is required for full virulence in cotton. *Mol. Plant Pathol.* 19, 841–857. doi: 10.1111/mpp.12569

Zhang, H., Li, G., Hu, D., Zhang, Y., Zhang, Y., Shao, H., et al. (2020). Functional characterization of maize heat shock transcription factor gene *ZmHsf01* in thermotolerance. *PeerJ* 8, e8926–e8947. doi: 10.7717/peerj.8926

Zheng, L., Wu, W., Chen, Q., Zhang, G., Gao, F., and Zhou, Y. (2022). Integrated transcriptomics, proteomics, and metabolomics identified biological processes and metabolic pathways involved in heat stress response in jojoba. *Ind. Crop Prod.* 183, 114946–114959. doi: 10.1016/j.indcrop.2022.114946

Zhou, H., Bai, S., Wang, N., Sun, X., Zhang, Y., Zhu, J., et al. (2020). CRISPR/Cas9-mediated mutagenesis of *MdCNGC2* in apple callus and VIGS-mediated silencing of *MdCNGC2* in fruits improve resistance to *Botryosphaeria dothidea*. *Front. Plant Sci.* 11. doi: 10.3389/fpls.2020.575477

Zhou, J., Xu, X. C., Cao, J. J., Yin, L. L., Xia, X. J., Shi, K., et al. (2018). Heat shock factor HsfA1a is essential for *R* gene-mediated nematode resistance and triggers H_2O_2 production. *Plant Physiol.* 176, 2456–2471. doi: 10.1104/pp.17.01281

frontiers | Frontiers in Plant Science

TYPE Original Research
PUBLISHED 21 November 2022
DOI 10.3389/fpls.2022.1077229

OPEN ACCESS

EDITED BY
Weicong Qi,
Jiangsu Academy of Agricultural Sciences (JAAS), China

REVIEWED BY
Fengqi Li,
Guizhou University, China
Qi Su,
Yangtze University, China

*CORRESPONDENCE
Wangpeng Shi
wpshi@cau.edu.cn
Yongjun Zhang
yjzhang@ippcaas.cn

†These authors have contributed equally to this work

SPECIALTY SECTION
This article was submitted to Plant Bioinformatics, a section of the journal Frontiers in Plant Science

RECEIVED 22 October 2022
ACCEPTED 07 November 2022
PUBLISHED 21 November 2022

CITATION
Huang X, Zhang H, Li H, Wang M, Guo X, Liu E, Han X, Zhen C, Li A, Shi W and Zhang Y (2022) Functional characterization of a terpene synthase responsible for (*E*)-β-ocimene biosynthesis identified in *Pyrus betuleafolia* transcriptome after herbivory. *Front. Plant Sci.* 13:1077229. doi: 10.3389/fpls.2022.1077229

Functional characterization of a terpene synthase responsible for (*E*)-β-ocimene biosynthesis identified in *Pyrus betuleafolia* transcriptome after herbivory

Xinzheng Huang[1†], Hang Zhang[2,3,4†], Huali Li[1], Mengting Wang[1], Xinyue Guo[1], Enliang Liu[5], Xiaoqiang Han[4], Congai Zhen[1], Aili Li[2], Wangpeng Shi[1*] and Yongjun Zhang[2*]

[1]Department of Entomology, MOA Key Lab of Pest Monitoring and Green Management, College of Plant Protection, China Agricultural University, Beijing, China, [2]State Key Laboratory for Biology of Plant Diseases and Insect Pests, Institute of Plant Protection, Chinese Academy of Agricultural Sciences, Beijing, China, [3]General Station of Agricultural Technology Extension, Xinjiang Production and Construction Corps, Urumqi, China, [4]Key Laboratory of Oasis Agricultural Pest Management and Plant Protection Resources Utilization, Xinjiang Uygur Autonomous Region, College of Agriculture, Shihezi University, Shihezi, China, [5]Institute of Grain Crops, XinJiang Academy of Agricultural Sciences, Urumqi, China

(*E*)-β-ocimene, a ubiquitous monoterpene volatile in plants, is emitted from flowers to attract pollinators and/or from vegetative tissues as part of inducible defenses mediated by complex signaling networks when plants are attacked by insect herbivores. Wild pear species *Pyrus betuleafolia* used worldwide as rootstock generally displays valuable pest-resistant traits and is a promising genetic resource for pear breeding. In the current study, transcriptional changes in this wild pear species infested with a polyphagous herbivore *Spodoptera litura* and the underlying molecular mechanisms were fully investigated. A total of 3,118 differentially expressed genes (DEGs) were identified in damaged pear leaf samples. *Spodoptera litura* larvae infestation activated complex phytohormonal signaling networks in which jasmonic acid, ethylene, brassinosteroids, cytokinin, gibberellic acid and auxin pathways were induced, whereas salicylic acid and abscisic acid pathways were suppressed. All DEGs associated with growth-related photosynthesis were significantly downregulated, whereas most DEGs involved in defense-related early signaling events, transcription factors, green leaf volatiles and volatile terpenes were significantly upregulated. The *PbeOCS* (GWHGAAYT028729), a putative (*E*)-β-ocimene synthase gene, was newly identified in *P. betuleafolia* transcriptome. The upregulation of *PbeOCS* in *S. litura*-infested pear leaves supports a potential role for *PbeOCS* in herbivore-induced plant defenses. In enzyme-catalyzed reaction, recombinant PbeOCS utilized only geranyl pyrophosphate but not neryl diphosphate, farnesyl pyrophosphate or geranylgeranyl diphosphate as a substrate, producing (*E*)-β-ocimene as the major product and a trace amount of (*Z*)-β-ocimene. Moreover, as a catalytic product of PbeOCS, (*E*)-β-ocimene showed repellent effects on larvae of *S.*

litura in dual-choice bioassays. What is more, (*E*)-β-ocimene increased mortalities of larvae in no-choice bioassays. These findings provide an overview of transcriptomic changes in wild pears in response to chewing herbivores and insights into (*E*)-β-ocimene biosynthesis in pear plants, which will help elucidate the molecular mechanisms underlying pear-insect interactions.

KEYWORDS

wild pear, *Spodoptera litura*, plant-insect interactions, (*E*)-β-ocimene biosynthesis, plant defense

Introduction

Plants, especially perennial fruit trees such as pear, are frequently subject to attack by a variety of insect pests. In response to insect herbivore attack, plants have evolved highly sophisticated strategies allowing them to perceive various herbivory-associated molecules from insects' oral secretions (or regurgitant), oviposition fluids or larval frass and trigger complex defense systems (Mao et al., 2022; Zhang et al., 2022). After the recognition of herbivores, plant initiate a series of early signaling events such as *V*m variation, Ca^{2+} elevation, production of reactive oxygen species and activation of MAP kinases, as well as phytohormone-centered regulatory networks to broad transcriptional reprogramming, ultimately leads to the synthesis and accumulation of defensive proteins and defense-associated secondary metabolites (Erb and Reymond, 2019). Cross-talk between different phytohormone signaling pathways help plants to fine-tune their responses to herbivore-specific cues. It is well known that the jasmonic acid (JA) pathway as a core route in plant defenses generally acts antagonistically toward the salicylic acid (SA) pathway (Erb and Reymond, 2019).

(*E*)-β-ocimene, a secondary metabolite commonly found in plants, plays important physiological and ecological roles in attracting pollinators and natural enemies of pests, as well as protecting plants directly against herbivores and pathogens (Shimoda et al., 2012; Su et al., 2022). This compound belongs to monoterpene which are derived from the methyl-erythritol-phosphate (MEP) pathway mainly in plastids and produced by terpene synthases (TPSs) using geranyl diphosphate (GPP) or neryl diphosphate (NPP) as the substrate. Several TPSs including (*E*)-β-ocimene synthase have been functionally characterized in many plants except for wild pear *Pyrus betuleafolia* (Chen et al., 2011; Jiang et al., 2019; Ding et al., 2020). According to phylogenetic relationships, plant TPS family fall into seven subfamilies including TPS-a, TPS-b, TPS-c, TPS-d, TPS-e/f, TPS-g and TPS-h, two of which, angiosperm TPS-b and TPS-g, consists mainly of monoterpenes (Karunanithi and Zerbe, 2019).

In modern pear production, cultivated species are generally used as scions, while wild species such as *P. betuleafolia* was commonly used as rootstocks (Dong et al., 2020). Native to China, *P. betuleafolia* is widely cultivated in pear orchards across the world due to its vigorous growth, high-affinity for different cultivars of Asian pears and European pears, and resistance or tolerance to several abiotic as well as biotic environmental stresses. It has thus been gaining more scientific attention, and its recently released genomic sequence (Dong et al., 2020) is an excellent resource for mining functional genes.

Pear trees emit more than 40 different volatile organic compounds, mostly composed of terpenes, esters, aldehydes and alcohols (Chen et al., 2020). Various terpenes are present in pear fruits, flowers and vegetative tissues. For instance, α-farnesene is a major terpenoid released from ripe fruits (Chen et al., 2006). Pear trees at the flowering and fruiting stages emit 14 terpenes including (*E*)-β-ocimene, caryophyllene, pinene, limonene and α-farnesene, which play crucial roles in the seasonal host shift of the lepidopteran pest *Grapholita molesta* from peach to pear trees (Najar-Rodriguez et al., 2013). (*E*)-β-ocimene and linalool emitted by flowers of *Pyrus bretschneideri* and *P. communis* were crucial for attracting honey bees (Su et al., 2022). Emissions of 17 terpenes including (*E*)-β-ocimene and α-farnesene are increased in leaves of pear trees after *pear psylla* infestation (Scutareanu et al., 2003), which is attractive to conspecifics of this insect (Horton and Landolt, 2007).

Transcriptional changes of *P. betuleafolia* in response to abiotic stresses such as drought and potassium deficiency have been well investigated (Li et al., 2016; Yang et al., 2020b). However, little is known about transcriptional changes in wild pears infested by herbivores. It was reported that PcAFS1, a sesquiterpene synthase in *Pyrus communis*, could catalyze the formation of α-farnesene attracting natural enemies of herbivores (Gapper et al., 2006). Yet, the biosynthesis of monoterpenoid including (*E*)-β-ocimene in pears, especially in *P. betuleafolia* has not been elucidated. Here, transcriptional

changes in *P. betuleafolia* infested by lepidopteran *Spodoptera litura*, a notorious agricultural and horticultural pest, were investigated to figure out the molecular mechanisms underlying defense responses of pear plants to chewing insects and identify candidate TPSs responsible for terpene biosynthesis. Based on RNA-seq, *PbeOCS*, the (*E*)-β-ocimene synthase gene, was newly identified. Recombinant PbeOCS was then heterologously expressed in *Escherichia coli*, and its catalytic products were characterized using *in vitro* enzymatic assays. The impacts of (*E*)-β-ocimene on choice behavior and growth of *S. litura* larvae were also assessed. Our findings provide valuable insights in understanding of the molecular mechanisms underlying defense responses of pear plants against chewing insects and shed new light on the (*E*)-β-ocimene biosynthesis in pear plants.

Materials and methods

Plants and insects

One-year-old seedlings of *P. betuleafolia* planted in plastic pots (height, 30 cm; diameter, 35 cm) were placed in a greenhouse compartment. A month later, pear seedlings were used for further experiments. Eggs of *S. litura* was kindly provided by the Xinxiang experimental station of the Institute of Plant Protection, Chinese Academy of Agricultural Sciences (Henan Province, 35.09°N, 113.48°E). Insects were reared in artificial incubators at (26 ± 1)°C and 60% ± 10% humidity with a photoperiod of L:D=16:8 h.

Plant treatment

Ten *S. litura* larvae were placed on one pear seedling in a nylon mesh cage at 18:00 PM. After 36 h infestation, larvae were removed from each plant, and the infested leaves were collected for subsequent RNA extraction. Non-infested seedlings were maintained under the same conditions and collected as controls. Three biological replicates were performed for each treatment.

RNA extraction and RNA sequencing

Total RNA was extracted from seedlings leaves using EASYspin Total RNA Extraction Kit (Aidlab Biotechnologies Co., Ltd, Beijing, China), and assessed for quality using an Agilent 2100 Bioanalyzer (Agilent Technologies, CA, USA). A total amount of 1 μg RNA per sample was used for cDNA library preparation, and then was sequenced using a PE150 strategy on the Illumina Hiseq 2500 platform as described previously (Duan et al., 2021; Zhang et al., 2022). The clean reads were mapped to the wild pear *P. betuleafolia* genome (Dong et al., 2020). Genes with false discovery rate < 0.05 and $\log_2$(Foldchange) > 1 were used as differentially expressed genes (DEGs), which were functionally enriched to the Gene Ontology (GO) database using Blast2GO and KEGG pathways.

qPCR measurement

The qPCR analysis was conducted using SuperReal PreMix Plus (SYBR Green) reagent kit (TianGen, Beijing, China) as described previously (Huang et al., 2018). The *tubulin* (accession number: AB239681) was used as an endogenous control. All primers are listed in Table S1. The qPCR analysis was carried out using the same RNA samples used for the RNA-seq.

Cloning of PbeOCS and heterologous expression

Total RNA was extracted from herbivory-treated pear leaves to synthesize cDNA as described above for qPCR measurement. From the transcriptomic data, 43 putative TPS genes were annotated (Table S2), and the *PbeOCS* (GWHGAAYT028729) was cloned using specific primers (Table S1). For *in vitro* expression of *PbeOCS*, the ORF sequence was inserted into the expression vector pET-30a (+), and transformed into the *E. coli* strain BL21 (DE3), which were cultured at 37°C to an OD_{600} of 0.6 in 500 mL LB containing 100 μg/mL kanamycin. Then, the cultures were induced by addition of 1 mM isopropyl 1-thio-β-D-galactopyranoside and incubated at 18°C and 150 rpm for 20 h. Subsequently, cells were harvested by centrifugation, resuspended in extraction buffer and disrupted by sonication (Zhang et al., 2022).

In vitro enzymatic assay

Enzymatic activity assays of the recombinant PbeOCS were performed using geranyl pyrophosphate (GPP), neryl diphosphate (NPP), farnesyl pyrophosphate (FPP) and geranylgeranyl diphosphate (GGPP) as substrates (Huang et al., 2018; Zhang et al., 2022). Reaction mixtures consisted of 500 μL of *E. coli* crude extract, 10 μM substrate, 10 mM MOPS (pH 7.0), 10 mM $MgCl_2$, 0.2 mM Na_2WO_4, 0.05 mM $MnCl_2$ and 0.1 mM NaF, 1 mM dithiothreitol and 10% (v/v) glycerol. Samples were incubated at 30°C for 1 h, and the volatile products were trapped by solid phase microextraction (SPME) with a 65 μm polydimethylsiloxane (PDMS) fiber for 30 min at 30°C, and then analyzed by a GC-MS system (GCMS-QP2010 SE, Shimadzu, Kyoto, Japan) fitted with an Rxi-5Sil column (30 m × 0.25 mm × 0.25 μm) (Qi et al., 2018; Zhang et al., 2022). The PbeOCS product was identified by comparing retention time and mass spectrum with that of the authentic (*E*)-β-

ocimene standard (CAS: 3779-61-1, J&K Chemical Company, Beijing, China) under the same conditions. Meanwhile, bacterial cells harboring empty vector pET-30a (+) were used as the negative control.

Effect of (E)-β-ocimene on larval behavior and survival rates of *S. litura*

The (*E*)-β-ocimene was dissolved in hexane at 0.1 μg/μL, 1 μg/μL and 10 μg/μL. The behavioral choices of 3rd instar *S. litura* larvae to (*E*)-β-ocimene were assessed in a 9 cm diameter plastic petri dishe as described by previous studies (Guo et al., 2021; Zhang et al., 2022). Each concentration was tested with 30 *S. litura* larvae, and five biological replicates were performed. After 2 hours, the choice of *S. litura* larvae was recorded.

Moreover, survival rate of larvae exposed to (*E*)-β-ocimene (0.1 μg/μL, 1 μg/μL and 10 μg/μL), dissolved in 20 μL hexane and added to the 500 mg of artificial diet, was also recorded. Artificial diet containing n-hexane was employed as the control. Newly hatched larvae were reared on the artificial diet in 24-well plates (one larva per well) and allowed to feed for 9 consecutive days. Each concentration was tested with 24 larvae, and three biological replicates were performed.

Statistical analysis

All data were analyzed using SPSS Statistics software (version 17.0) (SPSS Inc., Chicago, IL, USA). Data are presented as the mean ± SEM. Gene expression data and survival rate data were analyzed using Student's *t*-test. Larval choice data were subjected to a χ^2 test (50:50 distribution) to determine any differences between controls and treatments.

Results

Transcriptome analysis of *P. betuleafolia* induced by *S. litura*

After assembly, 60,965 genes were found in infested and non-infested leaves of *P. betuleafolia*. Based on transcriptomic data, a principal component analysis plot was constructed (Figure S1). A total of 3,118 DEGs were identified in *P. betuleafolia* leaves induced by *S. litura* infestation. Among these DEGs,1,545 were significantly upregulated and 1,573 were significantly downregulated (Figure S2; Table S3).

Using Gene Ontology (GO) analysis, these detected DEGs were classified into three GO categories: biological process, cellular component and molecular function (Figure 1). The top three terms within biological process category were metabolic process (GO 0008152; 383 up- and 449 downregulated genes), cellular process (GO 0009987; 332 up- and 413 downregulated genes), and single-organism process (GO 0044699; 291 up- and 339 downregulated genes). The most abundant terms in category of cellular component were cell (GO 0005623; 150 up- and 183 downregulated genes), and cell part (GO 0044464; 150 up- and 183 downregulated genes), followed by membrane (GO 0016020; 116 up- and 177 downregulated genes), organelle (GO 0043226; 116 up- and 133 downregulated genes) and membrane part (GO 0044425; 90 up- and 139 downregulated genes). Most DEGs in molecular function ontology were involved in catalytic activity (GO 0003824; 386 up- and 444 downregulated) and binding (GO 0005488; 276 up- and 291 downregulated). In the KEGG pathway analysis to identify pathways activated by *S. litura* infestation, the top three KEGG pathways were metabolic pathways (411 genes), biosynthesis of secondary metabolites (245) and plant hormone signal transduction (65) (Figure 2).

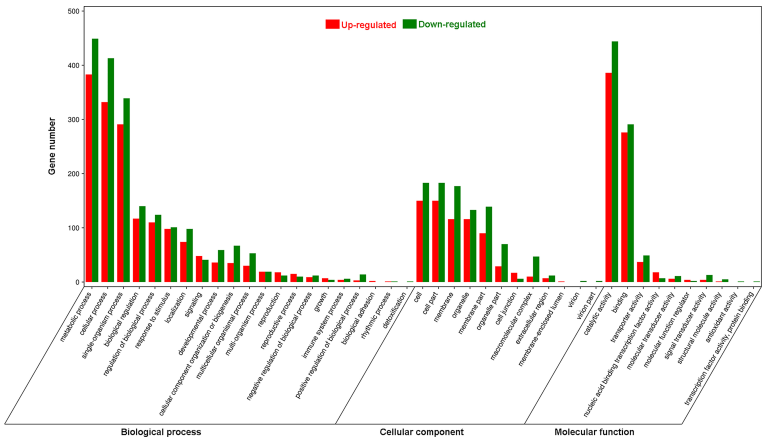

FIGURE 1
Gene Ontology (GO) analysis of differentially expressed genes (DEGs) in *Pyrus betuleafolia* leaves after *Spodoptera litura* infestation.

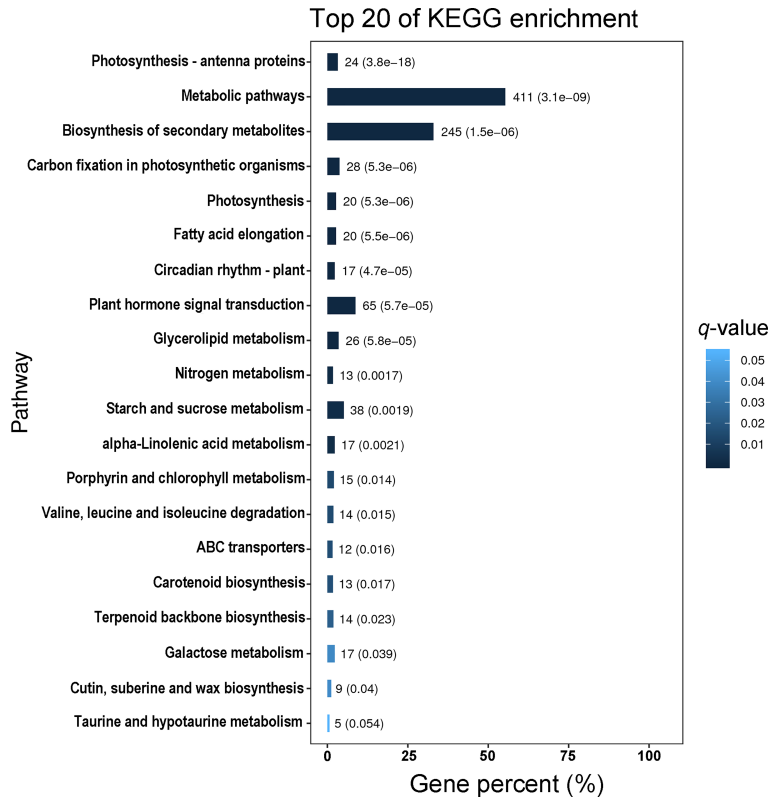

FIGURE 2
The top 20 KEGG pathways enriched with differentially expressed genes (DEGs) in *Pyrus betuleafolia* leaves after *Spodoptera litura* infestation.

Eight DEGs involved in JA pathway, SA pathway, ethylene pathway, abscisic acid pathway, photosynthesis, terpene volatiles biosynthesis and the green leaf volatiles biosynthesis were selected for qPCR validation. Based on these results, these DEGs were highly consistent with the data from the RNA-seq (Figure 3), indicating the reliability and repeatability of the RNA-seq data.

DEGs involved in phytohormone pathways

Nineteen genes associated with JA biosynthesis pathway and 13 genes related to the JA signaling pathway were differentially expressed in *S. litura*-infested *P. betuleafolia* leaves, and most (29 of 32) of these genes were significantly upregulated. In contrast, genes associated with SA (6 of 8) were mostly downregulated (Table S4). In addition, most of the DEGs related to ethylene (10 of 12), brassinosteroids (6 of 6), cytokinin (6 of 11), gibberellic acid (5 of 8) and auxin (23 of 41) were upregulated, whereas genes involved in abscisic acid (22 of 33) were mostly downregulated (Table S4).

DEGs involved in early signaling events and transcription factors (TFs)

Several DEGs related to Ca^{2+} signaling (3 up- and 4 downregulated), reactive oxygen species (28 up- and 19 downregulated) and MAP kinases (7 up- and 3 downregulated) were present in leaves of *P. betuleafolia* after *S. litura* infestation (Table S5). There were 135 genes annotated as TFs were differentially expressed after *S. litura* infestation, amongst of which 93 genes were upregulated and 42 genes were downregulated. Most DEGs belonged to the gene family bHLH (16 up- and 13 downregulated), followed by AP2-EREBP (19 up- and 9 downregulated genes) and WRKY (21 up- and 2 downregulated) (Table S6).

DEGs associated with primary and secondary metabolism

Many genes involved in amino acid metabolism (51 up- and 33 downregulated), carbohydrate metabolism (79 up- and 81 downregulated) and nucleotide metabolism (10 up- and 7

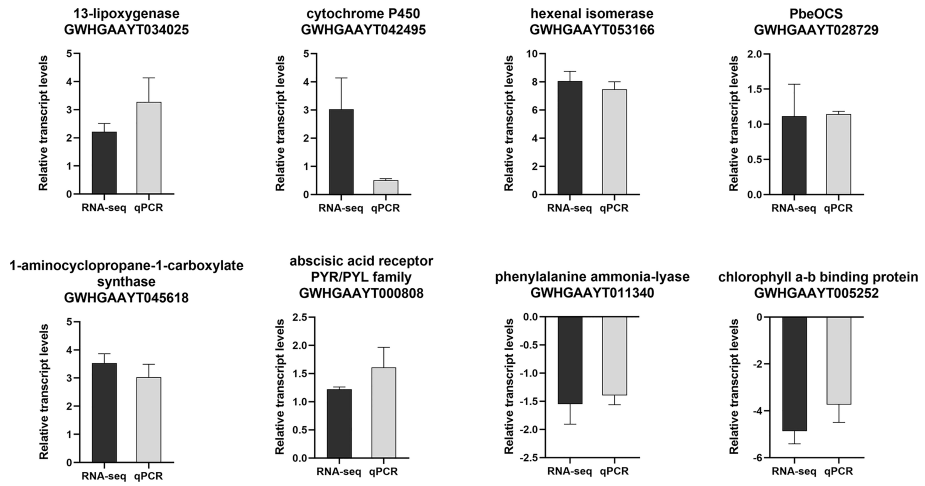

FIGURE 3
The relative expression levels of selected genes from the RNA-seq (black bar) and qPCR (gray bar) analysis.

downregulated) were differentially expressed after *S. litura* infestation. Additionally, all of the 44 DEGs related to photosynthesis were significantly downregulated (Table S7).

Numerous genes related to cytochrome P450 (CYP, 30 up- and 34 downregulated) and UDP-dependent glucosyltransferases (UGTs; 7 up- and 11 downregulated) that contribute to pest and disease resistances were differentially expressed (Table S8). Moreover, many DEGs associated with volatile secondary metabolite biosynthesis were present in *P. betuleafolia* leaves after infestation. Although all six DEGs for phenylpropanoid or benzenoid biosynthesis were downregulated, eight of 11 DEGs involved in green leaf volatiles production were upregulated (Table S8), including two hexenal isomerase genes involved in the conversion of (*Z*)-3-hexenal to (*E*)-2-hexenal (Spyropoulou et al., 2017). Most DEGs related to terpenoid volatiles biosynthesis (13 of 18 DEGs), including six TPSs, were significantly upregulated (Table S8).

Functional characterization of PbeOCS

A monoterpene synthase gene *PbeOCS* (GWHGAAYT028729) was identified in the transcriptome of *P. betuleafolia* after *S. litura* infestation. The *PbeOCS* had a 1647-bp ORF encoding 548 amino acids with a deduced molecular mass of ca. 62.65 kDa. Phylogenetic analysis showed that *PbeOCS* shared highest similarity (97.26% identity) with the (*E*)-β-ocimene synthase gene in *Malus domestica* (accession no: JX848733) (Nieuwenhuizen et al., 2013), followed by the (*E*)-β-ocimene synthase gene in *Camellia sinensis* (65.28%; accession no: QID05625) (Figure 4) (Chen et al., 2021). The PbeOCS protein has conserved structural features such as the DDxxD motif, the NSE/DTE motif, the $RS(X)_8W$ motif in the N-terminal region, and the arginine-rich RxR motif located at 35 amino acids upstream of the DDxxD motif, all of which are highly conserved in TPSs in plants (Karunanithi and Zerbe, 2019). ChloroP and TargetP showed that PbeOCS sequence does not have a signal peptide. The qPCR analysis revealed that *PbeOCS* was upregulated after *S. litura* infestation.

The recombinant PbeOCS *in vitro* only used GPP as the substrate to produce (*E*)-β-ocimene as the major product (Figure 5) and a trace amount of (*Z*)-β-ocimene detected in the m/z 93 spectrum (not shown in the Figure 5). When NPP, FPP and GGPP were provided as substrates, no product was detected. Meanwhile, cells harboring empty vector did not yield any detectable terpene product (Figure 5).

Larval preference for (E)-β-ocimene and herbivore performance test

In the dual-choice bioassay, *S. litura* larvae showed significantly preference for control diet than those containing (*E*)-β-ocimene at 10 μg/μL ($\chi^2 = 42.655$, $P < 0.001$) or 1 μg/μL ($\chi^2 = 8.877$, $P = 0.003$), although larvae did not display a significant response to 0.1 μg/μL (*E*)-β-ocimene ($\chi^2 = 3.000$, $P = 0.083$; Figure 6). In the no-choice bioassay, the *S. litura* larvae feeding on the diet treated with different concentration of (*E*)-β-ocimene (0.1 μg/μL, 1 μg/μL and 10 μg/μL) displayed significantly higher mortalities compared to those feeding on control diet (0.1 μg/μL: 3d, $P = 0.018$; 6d, $P = 0.011$; 9d, $P = 0.036$; 1.0 μg/μL: 3d, $P = 0.028$; 6d, $P < 0.001$; 9d, $P < 0.001$; 10 μg/μL: 3d, $P = 0.005$; 6d, $P < 0.001$; 9d, $P < 0.001$; Figure 7).

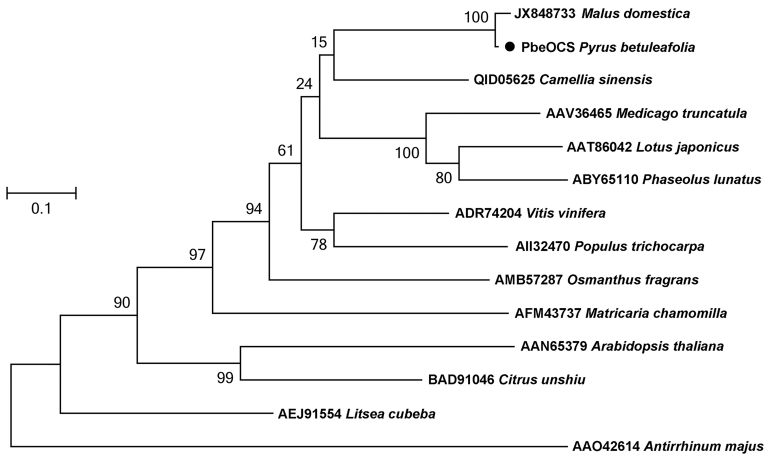

FIGURE 4
Phylogenetic tree of amino acid sequences of PbeOCS from *Pyrus betuleafolia* and *(E)*-β-ocimene synthase from other plants. The tree was generated using the maximum-likelihood method with 1,000 bootstrap replications

Discussion

In this study, transcriptional changes in *P. betuleafolia* in response to chewing *S. litura* were investigated. Phytohormone biosynthesis and signaling pathways have been reported to play a central role in mediating plant defense responses against herbivores attack through linking perception of herbivore-derived stimuli and early signaling networks to broad downstream transcriptional reprogramming and defense induction (Erb and Reymond, 2019). Different herbivores often trigger distinct transcriptional responses and signal-transduction pathways in plants. Generally, chewing herbivores such as caterpillars and cell-content feeders such as thrips and mites activate JA pathway, while phloem-feeding insects such as whiteflies and aphids trigger SA pathway (Stam et al., 2014). SA signaling and JA signaling pathways often act through negative crosstalk. So not surprisingly, our findings consistently showed that chewing *S. litura* larvae activated JA signaling pathway while SA-dependent defenses were suppressed (Table S4). Moreover, other phytohormone pathways such as ethylene, brassinosteroids, cytokinin, gibberellic acid, auxin and abscisic acid were also involved in pear defenses against *S. litura* (Table S4). These findings indicated that *S. litura* larvae infestation triggered complex phytohormone signaling networks in pear plants, and crosstalk between these phytohormones might allow the pear seedlings to fine-tune its induced defense response to specific herbivores.

TF families are known to play important roles in herbivore-induced direct and indirect defenses in plants, which regulate the transcript levels of the target genes and potentiate defense responses (Erb and Reymond, 2019). In the present study, 135 TFs, primarily bHLH (29 genes), AP2-EREBP (28 genes) and WRKY (23 genes), were differentially expressed in *S. litura*-infested *P. betuleafolia* leaves (Table S6). Several TFs involved in

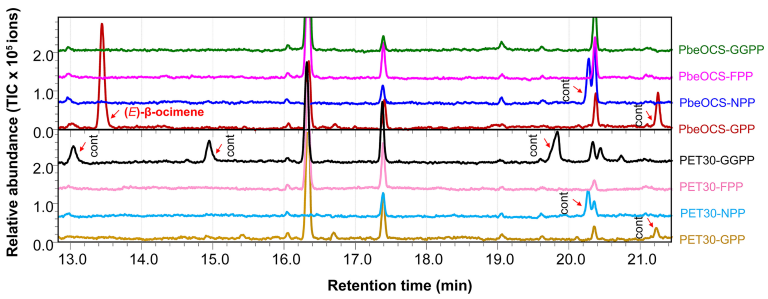

FIGURE 5
In vitro enzymatic assays of recombinant PbeOCS using different substrates. Cont, contamination.

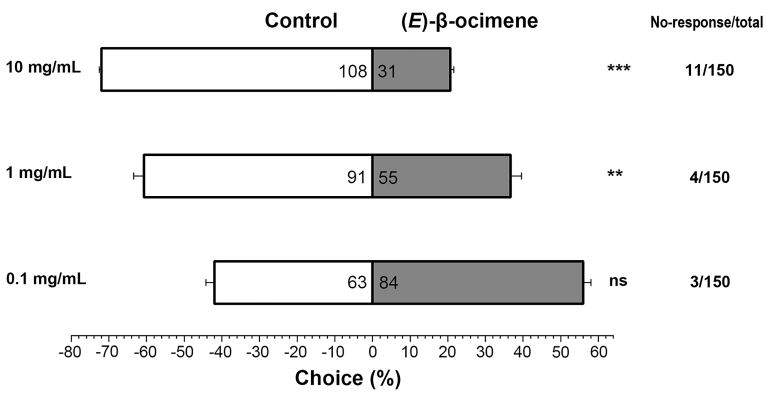

FIGURE 6
Behavioral preference of *Spodoptera litura* larvae for (*E*)-β-ocimene. Data were tested for significant differences using a χ^2 test **P < 0.01; ***P < 0.001; ns, no significance.

the transcriptional regulation of insect-induced volatile terpenes, including (*E*)-β-caryophyllene in *Arabidopsis thaliana* (Hong et al., 2012), (*E*)-β-farneseneas and (*E*)-α-bergamotene in *Zea mays* (Li et al., 2015) linalool in *Freesia hybrida* (Yang et al., 2020a), and *Dendrobium officinale* (Yu et al., 2021), valencene and (*E*)-geraniol in *Citrus sinensis* (Shen et al., 2016; Li et al., 2017) and α-farnesene in *M. domestica* (Wang et al., 2020), have been identified and functionally characterized. However, the role of TFs in terpene biosynthesis in pear is still not clear and need further investigation.

Many genes involved in biosynthesis of defensive metabolites, such as CYP (64 genes) and UGTs (18 genes), were differentially expressed (Table S8). In addition, 24 genes associated with the biosynthetic pathways of volatile terpenoids and HPL-derived green leaf volatiles were upregulated after *S. litura* infestation, highlighting their potential roles in *S. litura*-induced pear defenses. Unlike defense-related nonvolatile and volatile secondary metabolites, growth-related photosynthesis was suppressed in *S. litura*-infested *P. betuleafolia* (Table S7), which is similar to the findings reported in the defense response of potato (Mao et al., 2022), cotton (Zhang et al., 2022), rice (Wang et al., 2020; Satturu et al., 2021), wheat (Zhang et al., 2020) and tomato (Ke et al., 2021) plants induced by herbivores. In herbivore-damaged plants, suppression of photosynthesis might be a

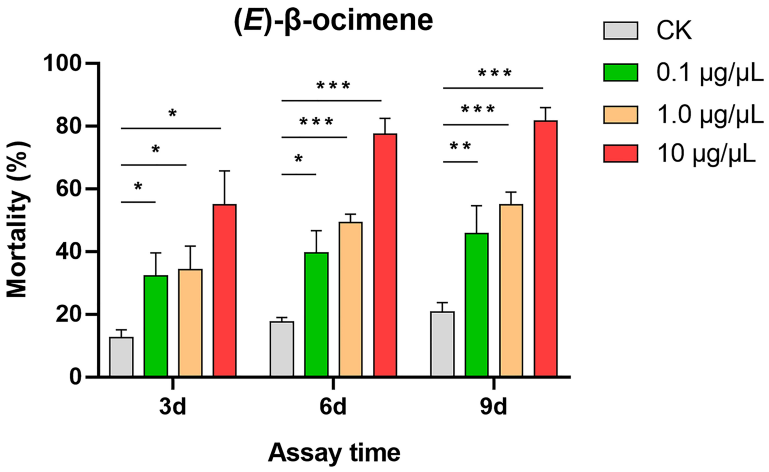

FIGURE 7
Larval mortality of *Spodoptera litura* caused by (*E*)-β-ocimene. Data were tested for differences using Student's *t*-test (*P < 0.05; **P < 0.01; ***P < 0.001).

general phenomenon as a result of a trade-off between growth and defense, which allow plants to reallocate its limited resources toward activation of anti-herbivore defense responses and production of inducible secondary metabolites (Zhou et al., 2015).

In plants, (*E*)-β-ocimene is one of the most common volatiles that act as an attractant in flower-pollinator interactions, a defensive compound in leaf-pest interactions and/or a priming signal in plant-plant communication (Fernández-Milmanda, 2022; Onosato et al., 2022). (*E*)-β-ocimene in flower and leaves of pear has multiple ecological roles in attracting pollinators and plant-pest interactions (Scutareanu et al., 2003; Su et al., 2022). The TPS in catalyzing (*E*)-β-ocimene biosynthesis, namely (*E*)-β-ocimene synthase, has been functionally characterized in several plant species such as *Antirrhinum majus* (Dudareva et al., 2003), *Arabidopsis thaliana* (Fäldt et al., 2003), *Camellia sinensis* (Chen et al., 2021; Jian et al., 2021), *Citrus unshiu* (Shimada et al., 2005), *Lotus japonicus* (Arimura et al., 2004), *Malus domestica* (Nieuwenhuizen et al., 2013), *Matricaria recutita* (Irmisch et al., 2012), *Medicago truncatula* (Navia-Giné et al., 2009), *Morus notabilis* (Ding et al., 2020), *Nicotiana attenuata* (Xu et al., 2020), *Osmanthus fragrans* (Zeng et al., 2015), *Phaseolus lunatus* (Arimura et al., 2008), *Populus trichocarpa* (Irmisch et al., 2014) and *Vitis vinifera* (Martin et al., 2010). In the current study, the (*E*)-β-ocimene synthase gene *PbeOCS* was present in the RNA-seq data and functionally characterized *in vitro* (Figure 5). The upregulation of *PbeOCS* after *S. litura* infestation suggested that *PbeOCS* and its enzymatic product (*E*)-β-ocimene are likely to be involved in insect-induced pear defenses. Interestingly, subsequent insect bioassay revealed that (*E*)-β-ocimene had a repellent effect on *S. litura* larvae (Figure 6) and significantly increased larval mortality (Figure 7). Additionally, candidate *TPSs* involved in the biosynthesis of α-pinene, limonene, linalool, germacrene D, β-caryophyllene (3*E*)-4,8-dimethyl-1,3,7-nonatriene (DMNT) and (*E*,*E*)-4,8,12-trimethyl-1,3,7,11-tridecatetraene (TMTT) were identified in our transcriptomic data, which still need to be further functionally characterized.

In this study, transcriptomic analyses of wild pear *P. betuleafolia* after *S. litura* infestation were performed to elucidate the molecular mechanisms underlying pear-herbivore interactions and to mine new TPSs. Our results revealed that *S. litura* infestation triggered a drastic and extensive transcriptomic reprogramming in pear leaves, including activation of a series of early signaling events and induction of complex phytohormone signaling networks. Significantly, almost all DEGs in the JA pathway were significantly upregulated, indicating that the chewing *S. litura* mainly activated JA-dependent defense responses. Moreover, defense-related transcription factors and genes involved in biosynthetic pathway of green leaf volatiles and volatile terpenes were also activated, whereas growth-related photosynthesis and SA-dependent defenses were suppressed. In addition, a terpene synthase gene *PbeOCS* was present in the RNA-seq data and functionally characterized *in vitro*. Recombinant PbeOCS catalyzed GPP as substrate to produce (*E*)-β-ocimene and the compound had significant impacts on choice behavior and growth of *S. litura* larvae in insect bioassays. These findings should contribute to generating valuable markers for further breeding insect-resistant pear varieties and developing an environmentally friendly strategy for pest control.

Data availability statement

The original contributions presented in the study are publicly available. This data can be found here: NCBI, PRJNA783361 and GenBank, OK635579.

Author contributions

WS and YZ conceived and designed the study. XZH, HZ, HL, MW, XG, and EL performed the experiments and analyzed the data. XQH, CZ, and LL contributed the resources. XZH, HZ, WS, and YZ wrote the manuscript. All authors read and approved the submitted manuscript.

Funding

This work was supported by the National Natural Science Foundation of China (32272638, 31972338, 31772176, 31701800), and the Open Fund Project of State Key Laboratory for Biology of Plant Diseases and Insect Pests (SKLOF201901).

Conflict of interest

The authors declare that the research was conducted in the absence of any commercial or financial relationships that could be construed as a potential conflict of interest.

Publisher's note

Supplementary material

The Supplementary Material for this article can be found online at: https://www.frontiersin.org/articles/10.3389/fpls.2022.1077229/full#supplementary-material

SUPPLEMENTARY FIGURE 1
Principal component analysis of transcriptomic data.

SUPPLEMENTARY FIGURE 2
Number of up- and downregulated genes in *Pyrus betuleafolia* leaves after *Spodoptera litura* infestation.

References

Arimura, G., Köpke, S., Kunert, M., Volpe, V., David, A., Brand, P., et al. (2008). Effects of feeding *Spodoptera littoralis* on lima bean leaves: IV. diurnal and nocturnal damage differentially initiate plant volatile emission. *Plant Physiol.* 146, 965–973. doi: 10.1104/pp.107.111088

Arimura, G., Ozawa, R., Kugimiya, S., Takabayashi, J., and Bohlmann, J. (2004). Herbivore-induced defense response in a model legume. two-spotted spider mites induce emission of (*E*)-beta-ocimene and transcript accumulation of (*E*)-beta-ocimene synthase in lotus japonicus. *Plant Physiol.* 135, 1976–1983. doi: 10.1104/pp.104.042929

Chen, J., Lü, J., He, Z., Zhang, F., Zhang, S., and Zhang, H. (2020). Investigations into the production of volatile compounds in korla fragrant pears (*Pyrus sinkiangensis* yu). *Food Chem.* 302, 125337. doi: 10.1016/j.foodchem.2019.125337

Chen, F., Tholl, D., Bohlmann, J., and Pichersky, E. (2011). The family of terpene synthases in plants: A mid-size family of genes for specialized metabolism that is highly diversified throughout the kingdom. *Plant J.* 66, 212–229. doi: 10.1111/j.1365-313X.2011.04520.x

Chen, J. L., Wu, J. H., Wang, Q., Deng, H., and Hu, X. S. (2006). Changes in the volatile compounds and chemical and physical properties of kuerle fragrant pear (*Pyrus serotina* reld) during storage. *J. Agric. Food Chem.* 54, 8842–8847. doi: 10.1021/jf061089g

Chen, S., Xie, P., Li, Y., Wang, X., Liu, H., Wang, S., et al. (2021). New insights into stress-induced β-ocimene biosynthesis in tea (*Camellia sinensis*) leaves during oolong tea processing. *J. Agric. Food Chem.* 69, 11656–11664. doi: 10.1021/acs.jafc.1c04378

Ding, G., Zhang, S., Ma, B., Liang, J., Li, H., Luo, Y., et al. (2020). Origin and functional differentiation of (*E*)-β-ocimene synthases reflect the expansion of monoterpenes in angiosperms. *J. Exp. Bot.* 71, 6571–6586. doi: 10.1093/jxb/eraa353

Dong, X., Wang, Z., Tian, L., Zhang, Y., Qi, D., Huo, H., et al. (2020). *De novo* assembly of a wild pear (*Pyrus betuleafolia*) genome. *Plant Biotechnol. J.* 18, 581–595. doi: 10.1111/pbi.13226

Duan, X., Xu, S., Xie, Y., Li, L., Qi, W., Parizot, B., et al. (2021). Periodic root branching is influenced by light through an HY1-HY5-auxin pathway. *Curr. Biol.* 31, 3834–3847. doi: 10.1016/j.cub.2021.06.055

Dudareva, N., Martin, D., Kish, C. M., Kolosova, N., Gorenstein, N., Fäldt, J., et al. (2003). (*E*)-beta-ocimene and myrcene synthase genes of floral scent biosynthesis in snapdragon: Function and expression of three terpene synthase genes of a new terpene synthase subfamily. *Plant Cell* 15, 1227–1241. doi: 10.1105/tpc.011015

Erb, M., and Reymond, P. (2019). Molecular interactions between plants and insect herbivores. *Annu. Rev. Plant Biol.* 70, 527–557. doi: 10.1146/annurev-arplant-050718-095910

Fäldt, J., Arimura, G., Gershenzon, J., Takabayashi, J., and Bohlmann, J. (2003). Functional identification of attps03 as (*E*)-beta-ocimene synthase: A monoterpene synthase catalyzing jasmonate- and wound-induced volatile formation in *Arabidopsis thaliana*. *Planta* 216, 745–751. doi: 10.1007/s00425-002-0924-0

Fernández-Milmanda, G. L. (2022). Smells like trouble: β-ocimene primes plant defenses through chromatin remodeling. *Plant Physiol.* 189, 452–453. doi: 10.1093/plphys/kiac109

Gapper, N. E., Bai, J., and Whitaker, B. D. (2006). Inhibition of ethylene-induced α-farnesene synthase gene PcAFS1 expression in 'd'anjou'pears with 1-MCP reduces synthesis and oxidation of α-farnesene and delays development of superficial scald. *Postharvest Biol. Tec.* 41, 225–233. doi: 10.1016/j.postharvbio.2006.04.014

Guo, M., Du, L., Chen, Q., Feng, Y., Zhang, J., Zhang, X., et al. (2021). Odorant receptors for detecting flowering plant cues are functionally conserved across moths and butterflies. *Mol. Biol. Evol.* 38, 1413–1427. doi: 10.1093/molbev/msaa300

Hong, G. J., Xue, X. Y., Mao, Y. B., Wang, L. J., and Chen, X. Y. (2012). Arabidopsis MYC2 interacts with DELLA proteins in regulating sesquiterpene synthase gene expression. *Plant Cell* 24, 2635–2648. doi: 10.1105/tpc.112.098749

Horton, D. R., and Landolt, P. J. (2007). Attraction of male pear psylla, *Cacopsylla pyricola*, to female-infested pear shoots. *Entomol. Exp. Appl.* 123, 177–183. doi: 10.1111/j.1570-7458.2007.00537.x

Huang, X. Z., Xiao, Y. T., Köllner, T. G., Jing, W. X., Kou, J. F., Chen, J. Y., et al. (2018). The terpene synthase gene family in *Gossypium hirsutum* harbors a linalool synthase GhTPS12 implicated in direct defence responses against herbivores. *Plant Cell Environ.* 41, 261–274. doi: 10.1111/pce.13088

Irmisch, S., Jiang, Y., Chen, F., Gershenzon, J., and Köllner, T. G. (2014). Terpene synthases and their contribution to herbivore-induced volatile emission in western balsam poplar (*Populus trichocarpa*). *BMC Plant Biol.* 14, 270. doi: 10.1186/s12870-014-0270-y

Irmisch, S., Krause, S. T., Kunert, G., Gershenzon, J., Degenhardt, J., and Köllner, T. G. (2012). The organ-specific expression of terpene synthase genes contributes to the terpene hydrocarbon composition of chamomile essential oils. *BMC Plant Biol.* 12, 84. doi: 10.1186/1471-2229-12-84

Jiang, S. Y., Jin, J., Sarojam, R., and Ramachandran, S. (2019). A comprehensive survey on the terpene synthase gene family provides new insight into its evolutionary patterns. *Genome Biol. Evol.* 11, 2078–2098. doi: 10.1093/gbe/evz142

Jian, G., Jia, Y., Li, J., Zhou, X., Liao, Y., Dai, G., et al. (2021). Elucidation of the regular emission mechanism of volatile β-ocimene with anti-insect function from tea plants (*Camellia sinensis*) exposed to herbivore attack. *J. Agric. Food Chem.* 69, 11204–11215. doi: 10.1021/acs.jafc.1c03534

Karunanithi, P. S., and Zerbe, P. (2019). Terpene synthases as metabolic gatekeepers in the evolution of plant terpenoid chemical diversity. *Front. Plant Sci.* 10. doi: 10.3389/fpls.2019.01166

Ke, L., Wang, Y., Schäfer, M., Städler, T., Zeng, R., Fabian, J., et al. (2021). Transcriptomic profiling reveals shared signalling networks between flower development and herbivory-induced responses in tomato. *Front. Plant Sci.* 12. doi: 10.3389/fpls.2021.722810

Li, S., Wang, H., Li, F., Chen, Z., Li, X., Zhu, L., et al. (2015). The maize transcription factor ereb58 mediates the jasmonate-induced production of sesquiterpene volatiles. *Plant J.* 84, 296–308. doi: 10.1111/tpj.12994

Li, K. Q., Xu, X. Y., and Huang, X. S. (2016). Identification of differentially expressed genes related to dehydration resistance in a highly drought-tolerant pear, *Pyrus betulaefolia*, as through RNA-seq. *PloS One* 11, e0149352. doi: 10.1371/journal.pone.0149352

Li, X., Xu, Y., Shen, S., Yin, X., Klee, H., Zhang, B., et al. (2017). Transcription factor CitERF71 activates the terpene synthase gene CitTPS16 involved in the synthesis of *E*-geraniol in sweet orange fruit. *J. Exp. Bot.* 68, 4929–4938. doi: 10.1093/jxb/erx316

Mao, Z., Ge, Y., Zhang, Y., Zhong, J., Munawar, A., Zhu, Z., et al. (2022). Disentangling the potato tuber moth-induced early-defense response by simulated herbivory in potato plants. *Front. Plant Sci.* 13. doi: 10.3389/fpls.2022.902342

Martin, D. M., Aubourg, S., Schouwey, M. B., Daviet, L., Schalk, M., Toub, O., et al. (2010). Functional annotation, genome organization and phylogeny of the grapevine (*Vitis vinifera*) terpene synthase gene family based on genome assembly, flcdna cloning, and enzyme assays. *BMC Plant Biol.* 10, 226. doi: 10.1186/1471-2229-10-226

Najar-Rodriguez, A., Orschel, B., and Dorn, S. (2013). Season-long volatile emissions from peach and pear trees in situ, overlapping profiles, and olfactory attraction of an oligophagous fruit moth in the laboratory. *J. Chem. Ecol.* 39, 418–429. doi: 10.1007/s10886-013-0262-7

Navia-Giné, W. G., Yuan, J. S., Mauromoustakos, A., Murphy, J. B., Chen, F., and Korth, K. L. (2009). *Medicago truncatula* (*E*)-beta-ocimene synthase is induced by insect herbivory with corresponding increases in emission of volatile ocimene. *Plant Physiol. Biochem.* 47, 416–425. doi: 10.1016/j.plaphy.2009.01.008

Nieuwenhuizen, N. J., Green, S. A., Chen, X., Bailleul, E. J., Matich, A. J., Wang, M. Y., et al. (2013). Functional genomics reveals that a compact terpene synthase gene family can account for terpene volatile production in apple. *Plant Physiol.* 161, 787–804. doi: 10.1104/pp.112.208249

Onosato, H., Fujimoto, G., Higami, T., Sakamoto, T., Yamada, A., Suzuki, T., et al. (2022). Sustained defense response *via* volatile signaling and its epigenetic transcriptional regulation. *Plant Physiol.* 189, 922–933. doi: 10.1093/plphys/kiac077

Qi, W., Tinnenbroek-Capel, I. E., Salentijn, E. M., Zhang, Z., Huang, B., Cheng, J., et al. (2018). Genetically engineering *Crambe abyssinica*-a potentially high-value oil crop for salt land improvement. *Land. Degrad. Dev.* 29, 1096–1106. doi: 10.1002/ldr.2847

Satturu, V., Kudapa, H. B., Muthuramalingam, P., Nadimpalli, R. G. V., Vattikuti, J. L., Anjali, C., et al. (2021). RNA-Seq based global transcriptome analysis of rice unravels the key players associated with brown planthopper resistance. *Int. J. Biol. Macromol.* 191, 118–128. doi: 10.1016/j.ijbiomac.2021.09.058

Scutareanu, P., Bruin, J., Posthumus, M. A., and Drukker, B. (2003). Constitutive and herbivore-induced volatiles in pear, alder and hawthorn trees. *Chemoecology* 13, 63–74. doi: 10.1007/s00049-002-0228-7

Shen, S. L., Yin, X. R., Zhang, B., Xie, X. L., Jiang, Q., Grierson, D., et al. (2016). CitAP2. 10 activation of the terpene synthase cstps1 is associated with the synthesis of (+)-valencene in 'newhall' orange. *J. Exp. Bot.* 67, 4105–4115. doi: 10.1093/jxb/erw189

Shimada, T., Endo, T., Fujii, H., Hara, M., and Omura, M. (2005). Isolation and characterization of (*E*)-beta-ocimene and 1, 8 cineole synthases in *Citrus unshiu* marc. *Plant Sci.* 168, 987–995. doi: 10.1016/j.plantsci.2004.11.012

Shimoda, T., Nishihara, M., Ozawa, R., Takabayashi, J., and Arimura, G. I. (2012). The effect of genetically enriched (*E*)-β-ocimene and the role of floral scent in the attraction of the predatory mite *Phytoseiulus persimilis* to spider mite-induced volatile blends of torenia. *New Phytol.* 193, 1009–1021. doi: 10.1111/j.1469-8137.2011.04018.x

Spyropoulou, E. A., Dekker, H. L., Steemers, L., van Maarseveen, J. H., de Koster, C. G., Haring, M. A., et al. (2017). Identification and characterization of (3*Z*):(2*E*)-hexenal isomerases from cucumber. *Front. Plant Sci.* 8. doi: 10.3389/fpls.2017.01342

Stam, J. M., Kroes, A., Li, Y., Gols, R., van Loon, J. J., Poelman, E. H., et al. (2014). Plant interactions with multiple insect herbivores: From community to genes. *Annu. Rev. Plant Biol.* 65, 689–713. doi: 10.1146/annurev-arplant-050213-035937

Su, W., Ma, W., Zhang, Q., Hu, X., Ding, G., Jiang, Y., et al. (2022). Honey bee foraging decisions influenced by pear volatiles. *Agriculture* 12, 1074. doi: 10.3390/agriculture12081074

Wang, Q., Liu, H., Zhang, M., Liu, S., Hao, Y., and Zhang, Y. (2020). MdMYC2 and MdERF3 positively co-regulate α-farnesene biosynthesis in apple. *Front. Plant Sci.* 11. doi: 10.3389/fpls.2020.512844

Xu, S., Kreitzer, C., McGale, E., Lackus, N. D., Guo, H., Köllner, T. G, et al. (2020). Allelic differences of clustered terpene synthases contribute to correlated intraspecific variation of floral and herbivory-induced volatiles in a wild tobacco. *New Phytol.* 228, 1083–1096. doi: 10.1111/nph.16739

Yang, Z., Li, Y., Gao, F., Jin, W., Li, S., Kimani, S., et al. (2020a). Myb21 interacts with MYC2 to control the expression of terpene synthase genes in flowers of *Freesia hybrida* and *Arabidopsis thaliana*. *J. Exp. Bot.* 71, 4140–4158. doi: 10.1093/jxb/eraa184

Yang, H., Li, Y., Jin, Y., Kan, L., Shen, C., Malladi, A., et al. (2020b). Transcriptome analysis of *Pyrus betulaefolia* seedling root responses to short-term potassium deficiency. *Int. J. Mol. Sci.* 21, 8857. doi: 10.3390/ijms21228857

Yu, Z., Zhang, G., Teixeira da Silva, J. A., Zhao, C., and Duan, J. (2021). The methyl jasmonate-responsive transcription factor DobHLH4 promotes DoTPS10, which is involved in linalool biosynthesis in *Dendrobium officinale* during floral development. *Plant Sci.* 309, 110952. doi: 10.1016/j.plantsci.2021.110952

Zeng, X., Liu, C., Zheng, R., Cai, X., Luo, J., Zou, J., et al. (2015). Emission and accumulation of monoterpene and the key terpene synthase (TPS) associated with monoterpene biosynthesis in *Osmanthus fragrans* lour. *Front. Plant Sci.* 6. doi: 10.3389/fpls.2015.01232

Zhang, Y., Fu, Y., Wang, Q., Liu, X., Li, Q., and Chen, J. (2020). Transcriptome analysis reveals rapid defence responses in wheat induced by phytotoxic aphid schizaphis graminum feeding. *BMC Genomics* 21, 339. doi: 10.1186/s12864-020-6743-5

Zhang, H., Liu, E., Huang, X., Kou, J., Teng, D., Lv, B., et al. (2022). Characterization of a novel insect-induced sesquiterpene synthase GbTPS1 based on the transcriptome of *Gossypium barbadense* feeding by cotton bollworm. *Front. Plant Sci.* 13. doi: 10.3389/fpls.2022.898541

Zhou, S., Lou, Y. R., Tzin, V., and Jander, G. (2015). Alteration of plant primary metabolism in response to insect herbivory. *Plant Physiol.* 169, 1488–1498. doi: 10.1104/pp.15.01405

frontiers | Frontiers in Plant Science

TYPE Opinion
PUBLISHED 24 November 2022
DOI 10.3389/fpls.2022.1076193

OPEN ACCESS

EDITED BY
Yi Han,
Anhui Agricultural University, China

REVIEWED BY
Maofeng Jing,
Nanjing Agricultural University, China
Zhiqiang Li,
Institute of Plant Protection, Chinese Academy of Agricultural Sciences, China

*CORRESPONDENCE
Yuanda Lv
Lyd0527@126.com
Xi Chen
chenxi_201402@163.com

SPECIALTY SECTION
This article was submitted to Plant Bioinformatics, a section of the journal Frontiers in Plant Science

RECEIVED 21 October 2022
ACCEPTED 11 November 2022
PUBLISHED 24 November 2022

CITATION
He B, Hu F, Du H, Cheng J, Pang B, Chen X and Lv Y (2022) Omics-driven crop potassium use efficiency breeding.
Front. Plant Sci. 13:1076193.
doi: 10.3389/fpls.2022.1076193

Omics-driven crop potassium use efficiency breeding

Bing He[1], Fengqin Hu[2], Hongyang Du[3], Junjie Cheng[2], Bingwen Pang[2], Xi Chen[4]* and Yuanda Lv[2]*

[1]Institute of Germplasm Resources and Biotechnology, Jiangsu Academy of Agricultural Sciences, Nanjing, China, [2]Excellence and Innovation Center, Jiangsu Academy of Agricultural Sciences, Nanjing, China, [3]Key Laboratory of Rice Genetic Breeding of Anhui Province, Rice Research Institute, Anhui Academy of Agricultural Science, Hefei, China, [4]School of Agronomy and Horticulture, Jiangsu Vocational College of Agriculture and Forestry, Jurong, China

KEYWORDS

omics, KUE, crop, integration analysis, breeding

Introduction

Potassium (K) is one of the essential mineral nutrients for plant growth and development, which plays a vital role in a wide range of physiological and biochemical processes in plants (Ragel et al., 2019). Plants must absorb plenty of potassium ions (K^+) to maintain normal development and growth. However, many agricultural lands in the world lack K because of leakage loss and large-scale agricultural production (Zörb et al., 2014). K deficiency seriously limits plant growth and decreases crop yield and quality (Jordan-Meille and Pellerin, 2004; Gerardeaux et al., 2010; Wang et al., 2015; Hu et al., 2019).

Recent studies on K nutrition in plants mainly focus on K transport and signaling (Wang Y. et al., 2021). Many K^+ channels, transporters, and signaling pathways have been well studied, such as Shaker K^+ channel AKT1, KUP/HAK/KT K^+ transporter HAK5 and CBL-CIPK pathways (Xu et al., 2006; Véry et al., 2014). However, only a few of these genes have been used to improve crop KUE (Potassium use efficiency) through the transgenic approach. For example, the ectopic expression of the *WOX11* gene driven by the promoter of a low-K-enhanced K transporter improved rice tolerance to K deficiency (Chen et al., 2015). Applying K fertilizer is a common strategy for enhancing crop yield. However, the high input of K fertilizer and the low KUE increase production costs and have led to environmental problems. It is necessary to breed crop varieties tolerant to low K (Yang et al., 2003; Cao et al., 2007; Damon et al., 2007; Zhao et al., 2014; Song et al., 2018) to reduce K fertilizer and increase agricultural income and maintain the sustainable development of agriculture.

Characteristics of crop varieties tolerant to low K

Usually, soil potassium deficiency inhibits crop growth and reduces crop quantity and quality. However, some crop varieties grow well and show a slight decrease in yields in the low-K field (Yang et al., 2004; Damon et al., 2007; Hu et al., 2016; Song et al., 2018). Varieties of this kind are recognized as low-K-tolerant varieties. Compared with low-K-sensitive varieties, low-K-tolerant varieties have a common characteristic: more robust K uptake capacity and higher K concentration. In soybeans, the total K accumulation per plant (mg/plant) of the low-K-tolerant variety is 2.36 times that of the low-K-sensitive variety under the K deficiency condition (Wang et al., 2012). In barley, the low-K-tolerant variety has a significantly higher shoot and root K concentration (mg/g dry weight) and K accumulation than the low-K-sensitive variety under the K deficiency condition (Ye et al., 2021). The same phenomena have been observed in other species like rice (Yang et al., 2004), maize (Cao et al., 2007), wheat (Zhao et al., 2020) and cotton (Tian et al., 2008). Furthermore, it has been observed that some low-K-tolerant varieties have more extraordinary K translocation ability than the low-K-sensitive varieties in the K deficiency condition. Low-K tolerant rice varieties preferentially distribute K to leaves at the booting and grain-filling stages to maintain stomatal conductance and ribulose diphosphate carboxylase (RuBPCase) activity in functioning leaves under low K, whereas low-K-sensitive varieties do not have this capacity (Yang et al., 2004). The efficient distribution of K to functioning leaves contributes to the relatively high grain yield in low-K-tolerant varieties at low K. Cotton has a high requirement for K, and lint yield and fiber quality could be damaged by K deficiency (Zhang et al., 2007). Jiang et al. (2008) found that low-K-sensitive varieties mainly transported K nutrition to vegetal organs (stems, branches and petioles), but low-K-tolerant varieties transported more K to the reproductive organs (bolls) that provide products. The efficient distribution of K to bolls probably help to maintain lint yield and fiber quality under K deficiency condition.

Therefore, plant K use efficiency is affected by the capability of K uptake and transportation and distribution of K. The low-K-tolerant crops should have better K uptake, transportation and distribution capability in low K soil, and all factors played important roles in crop yield and quality.

High-throughput screening of crop varieties tolerant to low K

Tolerance to low K is a complex phenotype determined by genotype and environmental factors. To ensure the screening efficiency and accuracy, low-K-tolerant varieties should be screened through indoor and field experiments. Indoor experiments are usually performed in a growth chamber or greenhouse under hydroponic culture. It has the advantage of precise environmental control. Indoor experiments are usually carried out for screening at the seedling stage and thus could screen many varieties simultaneously. However, plant K nutrition is dynamic. Even a genotype probably shows different tolerance to low K at different growth stages. Tian et al. once screened five varieties that tolerant to low K at the seeding stage but sensitive to low K at the mature stage from 50 cotton varieties (Tian et al., 2008). Low-K-tolerance indicators in the seeding stage are commonly related to biomass and K uptakes, such as dry weight, leaf area, root length, number and volume, K accumulation amount per plant, and K content per unit dry weight. These indicators are not directly related to the economic productivity of crops like cotton, rice and canola (Woodend and Glass, 1993). Therefore indoor experiments are usually adopted for preliminary screening. Low-K-tolerant varieties selected through indoor experiments should be further confirmed in the field based on yield and quality indicators.

The K requirements are different for different crops. Some crops like soybean, potato, maize and cotton have relatively high requirements for K nutrition, whereas other crops like wheat and millet have a relatively low requirement for K nutrition. The K requirement of crops significantly differed at different growth stages. In rice, for instance, the K requirement maximizes from tillering period to the jointing stage. Therefore the treating concentration and treating time of K should be determined from crop physiological characteristics.

Omics data-driven KUE breeding

Low-K-tolerant varieties can be directly used in agricultural production or applied in crop breeding as germplasm resources. The core of modern crop breeding is the introgression of genes responsible for good agronomic characteristics into the desirable genetic background. K-deficiency tolerance is a complex quantitative trait with strong interactions between genotype and the environment (Atienza et al., 2003; Prinzenberg et al., 2010). Many quantitative trait loci (QTLs) for low K tolerance have been identified *via* map-based cloning, and various molecular markers closely linked to these QTLs have been obtained (Wu et al., 1998; Prinzenberg et al., 2010; Zhao et al., 2014). With the help of marker-assisted selection (MAS) breeding, the crop breeding process has been accelerated. Nowadays, with a significant boom in omics technologies, omics-based interdisciplinarity further accelerates crop breeding (Li and Yan, 2020; Shen et al., 2022). Omics data such as genomics, proteomics, transcriptomics, metabolomics, phenomics, epigenomics allowed the understanding of physiological, biochemical, and molecular mechanisms underlining target traits and complex interactions between genes, proteins, and metabolites (Figure 1).

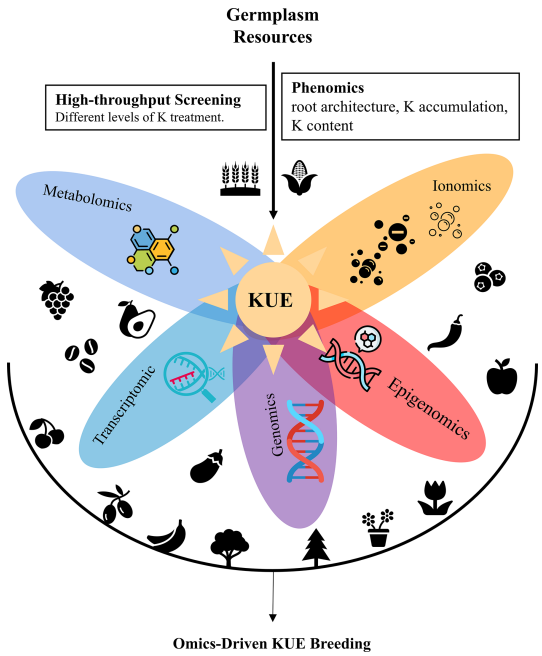

FIGURE 1
Integration of multi-omics technologies for accelerating crop KUE breeding.

Genomics technology is widely exploited in genome diversification, evolutionary analysis, QTL mapping, and gene identification. High-quality reference genomes and vast genome-wide re-sequencing data greatly facilitate the identification of genes responsible for low-K tolerance *via* QTL mapping and genome-wide association study (GWAS). Wang W. et al. (2021) identified the candidate genes for QTLs that impact shoot dry weight at low K by whole-genome re-sequencing. Next-generation sequencing has helped construct high-resolution physical/genetic maps. Based on the high-resolution physical/genetic map, novel genomic loci controlling potassium use efficiency in bread wheat have been identified *via* GWAS (Safdar et al., 2020).

Transcriptomic data provides an insight into how genes are expressed under different K treatments, thus, have been extensively used to study genes, biological pathways and metabolic pathways that influence low K tolerance. Combining QTL mapping and transcriptome profiling helps to identify candidate genes for controlling low-K tolerance. Wang W. et al. (2021) investigated the variation in mRNA abundance of candidate genes between the two parental lines to assess whether any of these genes might contribute to K use efficiency. Transcriptome analyses of low K responsiveness have been performed in various crops, like rice, tomato, banana and maize (Fan et al., 2014; Shen et al., 2017; Zhang et al., 2017; Zhao et al., 2018; He et al., 2020; Ma et al., 2020). Genes coding transcription factors, transporters, kinases, oxidative stress proteins, and hormone signaling and glycometabolism-related genes are confirmed to be responsive to low-K signaling (Zhao et al., 2018). Gene regulation network roots under different potassium stress are constructed (He et al., 2020). Pathways related to jasmonic acid and reactive oxygen species production, Ca^{2+} and receptor-like kinase signaling, lignin biosynthesis and carbohydrate metabolism are significantly affected by K starvation (Fan et al., 2014; Shen et al., 2017).

Proteomics, metabolomics and ionomics studies about K use efficiency have been carried out in crops but are much less than transcriptomic studies. K deficiency could elicit complex proteomic alterations that refer to oxidative phosphorylation, plant-pathogen interactions, glycolysis/gluconeogenesis, sugar metabolism, and transport in stems (Li et al., 2019). Proteome-wide mapping of protein kinases indicates the potential role of CIPK23 and its substrates in regulating root architecture upon K starvation (Wang et al., 2020). Nkrumah et al. (2021) measure the variation in the ionome of tropical "metal crops" in response to soil K availability to study their K uptake ability at low K. The combined analysis of ionome and metabolome reveals the association between low K tolerance and drought tolerance in rapeseed (Zhu B. et al., 2020). A comprehensive transcriptome and ionome analysis showed the interaction among nitrogen (N), phosphorus (P) and K during the combined NPK starvation in sorghum (Zhu Z. et al., 2020). Metabolomic and transcriptomic changes induced by K Deficiency provided new insight into the role of K in alleviating *Sarocladium oryzae* infection (Zhang et al., 2021). Leaf metabolome and proteome appear to be good predictors of carbon balance (Cui et al., 2019).

Phenomics and epigenomics studies about low K tolerance lag relatively behind. Epigenomics studies are mainly about non-coding RNAs and alternative mRNA splicing (AS). Long Non-coding RNAs sense environmental K concentrations and play regulatory roles in the K response network (Chen et al., 2022). AS modulation is independent of transcription regulation and plays a unique regulatory role in response to low potassium (He et al., 2021). Phenomics is the study of high-throughput phenotyping through crop development. However, phenomics data about KUE is relatively rare. Only Weksler et al. (2020) constructed a hyperspectral-physiological phenomics system to monitor and evaluate pepper response to varying levels of K fertilization.

Prospects

K deficiency in farmland is a global problem. Improving KUE is a strategy to ensure higher crop productivity within sustainable environments. Low-K-tolerant varieties should have good K uptake and distribution capacities in low K soil to absorb sufficient K and prioritize the requirement for K of functioning organs. Generally, low-K-tolerant varieties are applied in crop breeding as germplasm resources. It is necessary to introgress low-K-tolerant traits into desirable genetic backgrounds or

pyramid tolerance-related QTLs from different genetic resources. However, high-throughput screening technology of low-K tolerant varieties with efficiency and accuracy will still be a challenge. Omics data could reveal physiological, biochemical, and molecular mechanisms underlining low K tolerance and help identify QTLs determining KUE. With multi-omics development, we believe integrating these technologies will greatly boost the strategies of KUE breeding.

Author contributions

YL and XC conceived and designed the study and revised the manuscript. BH wrote the manuscript. FH, HD, JC, and BP participated in data collection and analysis. All authors have read and approved the final manuscript.

Funding

This work was supported by grants from Natural Science Foundation of Anhui Province (2108085QC108), National Natural Science Foundation of China (31601818), Natural Science Foundation of Jiangsu Province (BK20191224) and Project of Jiangsu Vocational College of Agriculture and Forest (2019kj005).

Conflict of interest

The authors declare that the research was conducted in the absence of any commercial or financial relationships that could be construed as a potential conflict of interest.

Publisher's note

All claims expressed in this article are solely those of the authors and do not necessarily represent those of their affiliated organizations, or those of the publisher, the editors and the reviewers. Any product that may be evaluated in this article, or claim that may be made by its manufacturer, is not guaranteed or endorsed by the publisher.

References

Atienza, S. G., Satovic, Z., Petersen, K. K., Dolstra, O., and Martín, A. (2003). Identification of QTLs influencing combustion quality in *Miscanthus sinensis* anderss. II. chlorine and potassium content. *Theor. Appl. Genet.* 107, 857–863. doi: 10.1007/s00122-003-1218-z

Cao, M., Yu, H., Yan, H., and Jiang, C. (2007). Difference in tolerance to potassium deficiency between two maize inbred lines. *Plant Prod. Sci.* 10, 42–46. doi: 10.1626/pps.10.42

Chen, G., Feng, H., Hu, Q., Qu, H., Chen, A., Yu, L., et al. (2015). Improving rice tolerance to potassium deficiency by enhancing *OsHAK16p:WOX11*-controlled root development. *Plant Biotechnol. J.* 13, 833–848. doi: 10.1111/pbi.12320

Chen, X., Meng, L., He, B., Qi, W., Jia, L., Xu, N., et al. (2022). Comprehensive transcriptome analysis uncovers hub long non-coding RNAs regulating potassium use efficiency in *Nicotiana tabacum*. *Front. Plant Sci.* 13. doi: 10.3389/fpls.2022.777308

Cui, J., Davanture, M., Zivy, M., Lamade, E., and Tcherkez, G. (2019). Metabolic responses to potassium availability and waterlogging reshape respiration and carbon use efficiency in oil palm. *New Phytol.* 223, 310–322. doi: 10.1111/nph.15751

Damon, P. M., Osborne, L. D., and Rengel, Z. (2007). Canola genotypes differ in potassium efficiency during vegetative growth. *Euphytica* 156, 387–397. doi: 10.1007/s10681-007-9388-4

Fan, M., Huang, Y., Zhong, Y., Kong, Q., Xie, J., Niu, M., et al. (2014). Comparative transcriptome profiling of potassium starvation responsiveness in two contrasting watermelon genotypes. *Planta* 239, 397–410. doi: 10.1007/s00425-013-1976-z

Gerardeaux, E., Jordan-Meille, L., Constantin, J., Pellerin, S., and Dingkuhn, M. (2010). Changes in plant morphology and dry matter partitioning caused by potassium deficiency in *Gossypium hirsutum* (L.). *Environ. Exp. Bot.* 67, 451–459. doi: 10.1016/j.envexpbot.2009.09.008

He, Y., Li, R., Lin, F., Xiong, Y., Wang, L., Wang, B., et al. (2020). Transcriptome changes induced by different potassium levels in banana roots. *Plants* 9, 11. doi: 10.3390/plants9010011

He, B., Meng, L., Tang, L., Qi, W., Hu, F., Lv, Y., et al. (2021). The landscape of alternative splicing regulating potassium use efficiency in *Nicotiana tabacum*. *Front. Plant Sci.* 12. doi: 10.3389/fpls.2021.774829

Hu, W., Di, Q., Wang, Z., Zhang, Y., Zhang, J., Liu, J., et al. (2019). Grafting alleviates potassium stress and improves growth in tobacco. *BMC Plant Biol.* 19, 130. doi: 10.1186/s12870-019-1706-1701

Hu, W., Zhao, W., Yang, J., Oosterhuis, D. M., Loka, D. A., and Zhou, Z. (2016). Relationship between potassium fertilization and nitrogen metabolism in the leaf subtending the cotton (*Gossypium hirsutum* l.) boll during the boll development stage. *Plant Physiol. Bioch.* 101, 113–123. doi: 10.1016/j.plaphy.2016.01.019

Jiang, C., Chen, F., Gao, X., Lu, J., Wan, K., Nian, F., et al. (2008). Study on the nutrition characteristics of different K use efficiency cotton genotypes to K deficiency stress. *Agr. Sci. China* 7, 740–745. doi: 10.1016/S1671-2927(08)60109-1

Jordan-Meille, L., and Pellerin, S. (2004). Leaf area establishment of a maize (*Zea mays* l.) field crop under potassium deficiency. *Plant Soil* 265, 75–92. doi: 10.1007/s11104-005-0695-z

Li, L. Q., Lyu, C. C., Li, J. H., Tong, Z., Lu, Y. F., Wang, X. Y., et al. (2019). Physiological analysis and proteome quantification of alligator weed stems in response to potassium deficiency stress. *Int. J. Mol. Sci.* 20, 221. doi: 10.3390/ijms20010221

Li, Q., and Yan, J. (2020). Sustainable agriculture in the era of omics: knowledge-driven crop breeding. *Genome Biol.* 21, 154. doi: 10.1186/s13059-020-02073-5

Ma, N., Dong, L., Lü, W., Lü, J., Meng, Q., and Liu, P. (2020). Transcriptome analysis of maize seedling roots in response to nitrogen-, phosphorus-, and potassium deficiency. *Plant Soil* 447, 637–658. doi: 10.1007/s11104-019-04385-3

Nkrumah, P. N., Echevarria, G., Erskine, P. D., Chaney, R. L., Sumail, S., and van der Ent, A. (2021). Variation in the ionome of tropical 'metal crops' in response to soil potassium availability. *Plant Soil* 465, 185–195. doi: 10.1007/s11104-021-04995-w

Prinzenberg, A. E., Barbier, H., Salt, D. E., Stich, B., and Matthieu, R. (2010). Relationships between growth, growth response to nutrient supply, and ion content using a recombinant inbred line population in arabidopsis. *Plant Physiol.* 154, 1361–1371. doi: 10.1104/pp.110.161398

Ragel, P., Raddatz, N., Leidi, E. O., Quintero, F. J., and Pardo, J. M. (2019). Regulation of k^+ nutrition in plants. *Front. Plant Sci.* 10. doi: 10.3389/fpls.2019.00281

Safdar, L. B., Andleeb, T., Latif, S., Umer, M. J., Tang, M., Li, X., et al. (2020). Genome-wide association study and QTL meta-analysis identified novel genomic

loci controlling potassium use efficiency and agronomic traits in bread wheat. *Front. Plant Sci.* 11. doi: 10.3389/fpls.2020.00070

Shen, C., Wang, J., Shi, X., Kang, Y., Xie, C., Peng, L., et al. (2017). Transcriptome analysis of differentially expressed genes induced by low and high potassium levels provides insight into fruit sugar metabolism of pear. *Front. Plant Sci.* 8. doi: 10.3389/fpls.2017.00938

Shen, Y., Zhou, G., Liang, C., and Tian, Z. (2022). Omics-based interdisciplinarity is accelerating plant breeding. *Curr. Opin. Plant Biol.* 66, 102167. doi: 10.1016/j.pbi.2021.102167

Song, W., Xue, R., Song, Y., Bi, Y., Liang, Z., Meng, L., et al. (2018). Differential response of first-order lateral root elongation to low potassium involves nitric oxide in two tobacco cultivars. *J. Plant Growth Regul.* 37, 114–127. doi: 10.1007/s00344-017-9711-9

Tian, X. L., Wang, G. W., Zhu, R., Yang, P. Z., Duan, L. S., and Li, Z. H. (2008). Conditions and indicators for screening cotton (*Gossypium hirsutum* l.) varieties tolerant to low potassium. *Acta Agronomica. Sin.* 34, 1435–1443. doi: 10.1016/S1875-2780(08)60050-4

Véry, A. A., Nieves-Cordones, M., Daly, M., Khan, I., Fizames, C., and Sentenac, H. (2014). Molecular biology of k^+ transport across the plant cell membrane:what do we learn from comparison between plant species? *J. Plant Physiol.* 171, 748–769. doi: 10.1016/j.jplph.2014.01.011

Wang, C., Chen, H., Hao, Q., Sha, A., Shan, Z., Chen, L., et al. (2012). Transcript profile of the response of two soybean genotypes to potassium deficiency. *PloS One* 7, e39856. doi: 10.1371/journal.pone.0039856

Wang, Y., Chen, Y. F., and Wu, W. H. (2021). Potassium and phosphorus transport and signaling in plants. *J. Integr. Plant Biol.* 63, 34–52. doi: 10.1111/jipb.13053

Wang, P., Hsu, C. C., Du, Y., Zhu, P., Zhao, C., Fu, X., et al. (2020). Mapping proteome-wide targets of protein kinases in plant stress responses. *Proc. Natl. Acad. Sci. U. S. A.* 117, 3270–3280. doi: 10.1073/pnas.1919901117

Wang, X. G., Zhao, X. H., Jiang, C. J., Chun-Hong, L. I., Cong, S., Di, W. U., et al. (2015). Effects of potassium deficiency on photosynthesis and photoprotection mechanisms in soybean (*Glycine max* (L.) merr.). *J. Integr. Agr.* 14, 856–863. doi: 10.1016/S2095-3119(14)60848-0

Wang, W., Zou, J., White, P. J., Ding, G., Li, Y., Xu, F., et al. (2021). Identification of QTLs associated with potassium use efficiency and underlying candidate genes by whole-genome resequencing of two parental lines in *Brassica napus*. *Genomics* 113, 755–768. doi: 10.1016/j.ygeno.2021.01.020

Weksler, S., Rozenstein, O., Haish, N., Moshelion, M., Walach, R., and Ben-Dor, E. (2020). A hyperspectral-physiological phenomics system: measuring diurnal transpiration rates and diurnal reflectance. *Remote Sens.* 12, 1493. doi: 10.3390/rs12091493

Woodend, J. J., and Glass, A. D. M. (1993). Genotype-environment interaction and correlation between vegetative and grain production measures of potassium use-efficiency in wheat (*T. aestivum* l.) grown under potassium stress. *Plant Soil* 151, 39–44. doi: 10.1007/BF00010784

Wu, P., Ni, J. J., and Luo, A. C. (1998). QTLs underlying rice tolerance to low-potassium stress in rice seedlings. *Crop Sci.* 38, 1458–1462. doi: 10.2135/cropsci1998.0011183X003800060009x

Xu, J., Li, H. D., Chen, L. Q., Wang, Y., Liu, L. L., He, L., et al. (2006). A protein kinase, interacting with two calcineurin b-like proteins, regulates k^+ transporter AKT1 in *Arabidopsis*. *Cell* 125, 1347–1360. doi: 10.1016/j.cell.2006.06.011

Yang, X. E., Liu, J. X., Wang, W. M., Li, H., Luo, A. C., Ye, Z. Q., et al. (2003). Genotypic differences and some associated plant traits in potassium internal use efficiency of lowland rice (*Oryza sativa* l.). *Nutr. Cycl. Agroecosys.* 67, 273–282. doi: 10.1023/B:FRES.0000003665.90952.0c

Yang, X. E., Liu, J. X., Wang, W. M., Ye, Z. Q., and Luo, A. C. (2004). Potassium internal use efficiency relative to growth vigor, potassium distribution, and carbohydrate allocation in rice genotypes. *J. @ Plant Nutr.* 27, 837–852. doi: 10.1081/PLN-120030674

Ye, Z., Zeng, J., Ma, X., Long, L., and Zhang, G. (2021). Transcriptome profiling analysis reveals involvement of SAM cycle and methionine pathway in low potassium tolerance in barley. *Curr. Plant Biol.* 25, 100190. doi: 10.1016/j.cpb.2020.100190

Zhang, X., Jiang, H., Wang, H., Cui, J., Wang, J., Hu, J., et al. (2017). Transcriptome analysis of rice seedling roots in response to potassium deficiency. *Sci. Rep.* 7, 5523. doi: 10.1038/s41598-017-05887-9

Zhang, J., Lu, Z., Ren, T., Cong, R., Lu, J., and Li, X. (2021). Metabolomic and transcriptomic changes induced by potassium deficiency during *Sarocladium oryzae* infection reveal insights into rice sheath rot disease resistance. *Rice* 14, 81. doi: 10.1186/s12284-021-00524-6

Zhang, Z. Y., Tian, X. L., Duan, L. S., Wang, B. M., He, Z. P., and Li, Z. H. (2007). Differential responses of conventional and bt-transgenic cotton to potassium deficiency. *J. Plant Nutr.* 30, 659–670. doi: 10.1080/01904160701289206

Zhao, X., Liu, Y., Liu, X., and Jiang, J. (2018). Comparative transcriptome profiling of two tomato genotypes in response to potassium-deficiency stress. *Int. J. Mol. Sci.* 19, 2402. doi: 10.3390/ijms19082402

Zhao, Y., Li, X., Zhang, S., Wang, J., Yang, X., Tian, J., et al. (2014). Mapping QTLs for potassium-deficiency tolerance at the seedling stage in wheat (*Triticum aestivum* l.). *Euphytica* 198, 185–198. doi: 10.1007/s10681-014-1091-7

Zhao, Y., Sun, R., Liu, H., Liu, X., Xu, K., Xiao, K., et al. (2020). Multi-omics analyses reveal the molecular mechanisms underlying the adaptation of wheat (*Triticum aestivum* l.) to potassium deprivation. *Front. Plant Sci.* 11. doi: 10.3389/fpls.2020.588994

Zhu, Z., Li, D., Wang, P., Li, J., and Lu, X. (2020). Transcriptome and ionome analysis of nitrogen, phosphorus and potassium interactions in sorghum seedlings. *Theor. Exp. Plant Physiol.* 32, 271–285. doi: 10.1007/s40626-020-00183-w

Zhu, B., Xu, Q., Zou, Y., Ma, S., Zhang, X., Xie, X., et al. (2020). Effect of potassium deficiency on growth, antioxidants, ionome and metabolism in rapeseed under drought stress. *Plant Growth Regul.* 90, 455–466. doi: 10.1007/s10725-019-00545-8

Zörb, C., Senbayram, M., and Peiter, E. (2014). Potassium in agriculture-status and perspectives. *J. Plant Physiol.* 171, 656–669. doi: 10.1016/j.jplph.2013.08.008

frontiers | Frontiers in Plant Science

TYPE Original Research
PUBLISHED 29 November 2022
DOI 10.3389/fpls.2022.1074029

OPEN ACCESS

EDITED BY
Yi Han,
Anhui Agricultural University, China

REVIEWED BY
Kailou Liu,
Jiangxi Institute of Red Soil, China
Gaofei Jiang,
Nanjing Agricultural University, China

*CORRESPONDENCE
Bing He
hebing1980@aliyun.com
Fushan Sun
sunfushan@caas.cn

†These authors have contributed equally to this work

SPECIALTY SECTION
This article was submitted to Plant Bioinformatics, a section of the journal Frontiers in Plant Science

RECEIVED 19 October 2022
ACCEPTED 10 November 2022
PUBLISHED 29 November 2022

CITATION
Meng L, Song W, Chen S, Hu F, Pang B, Cheng J, He B and Sun F (2022) Widely targeted metabolomics analysis reveals the mechanism of quality improvement of flue-cured tobacco.
Front. Plant Sci. 13:1074029.
doi: 10.3389/fpls.2022.1074029

Widely targeted metabolomics analysis reveals the mechanism of quality improvement of flue-cured tobacco

Lin Meng[1†], Wenjing Song[1†], Shuaiwei Chen[2], Fengqin Hu[3], Bingwen Pang[3], Junjie Cheng[3], Bing He[3*] and Fushan Sun[1*]

[1]Key Laboratory of Tobacco Biology and Processing, Ministry of Agriculture, Tobacco Research Institute, Chinese Academy of Agricultural Sciences (CAAS), Qingdao, China, [2]Technology Center, China Tobacco Shandong Industrial Co., Ltd, Jinan, China, [3]Excellence and Innovation Center, Jiangsu Academy of Agricultural Sciences (JAAS), Nanjing, China

Flue-curing of top leaves with stems is a widely applied curing technology. Owing to the presence of stems, the quality of flue-cured leaves was significantly improved. However, the contribution of stems to flue-cured leaves is still unknown. In this study, the differences in physicochemical properties and metabolomics data between separated leaves (stem(-)) and leaves with stems (stem(+)) were investigated. The metabolic profiling of stem (+) was significantly different from that of stem(-), with phytohormone indole-3-acetic acid (IAA) being one of the most differential metabolites. The presence of stems reduced the rate of water loss in leaves, which led to less ROS accumulation, higher antioxidant enzyme activities and a lower level of membrane lipid peroxidation in stem(+) than in stem(-). The presence of stems also helped maintain the cellular membrane integrity of leaf cells by preventing the accumulation of IAA in leaf cells. Better cellular membrane integrity during flue-curing means a lower risk of leaf browning. In addition, stem(+) had a lower starch content than stem(-) because of a higher level of amylase activity. In summary, these results indicated that the presence of stems caused metabolism changes in leaves, prevented flue-cured leaves from browning and enhanced starch degradation in leaves during flue-curing.

KEYWORDS

metabolomics, flue-curing, quality improvement, stem, tobacco

Introduction

Flue-cured tobacco is an important economic crop. After being harvested from the field, tobacco leaves are subjected to specific flue-curing processing, during which some complex physiological and biochemical reactions occur in flue-cured leaves. Therefore physicochemical properties of tobacco leaves and the curing method are vital factors in

determining flue-cured leaf quality (Chen et al., 2019; Zong et al., 2020; Li et al., 2021). Based on the position of leaves on plants, tobacco leaves were divided into top leaves, medium leaves and bottom leaves. Compared with medium and bottom leaves, top leaves have low moisture and high dry matter content and are accessible to browning during flue-curing. Besides the flue-cured top leaves are of poor sensory quality and appearance quality. Top leaves were once considered to be of low economic value. Recently, it was found that if top leaves were flue-cured with stems, browning reaction seldom occurred during flue-curing and flue-cured leaves quality was significantly improved. In this situation, flue-cured leaves were lustrous, elastic, rich in oil and of good aroma quantity, full aroma quality, weak offensive odor and comfortable lingering smell. Flue-curing of top leaves with stems has been widely applied in production. However, the underlining mechanism of the contribution of stems to top leaves is still unknown.

The chemical composition of flue-cured tobacco leaves is very complex, in which thousands of chemical compounds have been identified (Kaiser et al., 2018). Flue-cured tobacco leaf quality is highly related to chemical compositions (Talhout et al., 2006). Therefore, it is necessary to study the influence of different curing methods on flue-cured tobacco leaf quality by quantifying important compounds related to quality. Generally, it is unrealistic to quantify and determine each compound in separate measurements. That is time and cost-consuming. Metabolomics is a technique for large-scale detection of all metabolites in a biological system, like whole organisms, tissues, or individual cells. Metabolomics study includes targeted metabolomics, untargeted metabolomics, and widely targeted metabolomics. Widely targeted metabolomic analysis is a novel approach combining non-targeted and targeted metabolomics advantages (Chen et al., 2013). It has the characteristics of high throughput, ultra sensitivity, wide coverage, and accurate qualitative and quantitative analysis. Metabolomics has been used to characterize the quality and composition of flue-cured tobacco leaves under different conditions (Zhao et al., 2014; Zhao et al., 2018; Hu et al., 2021). However, the influence of stem on metabolic profiling of flue-cured tobacco leaves has not yet been reported.

The flue-curing process is divided into three stages: yellowing stage, leaf drying stage and stem drying stage. In the yellowing stage, macromolecular substances are decomposed into small molecule substances to form aroma precursors. The yellowing stage is crucial for improving flue-curd leaves characteristics and the critical stage of flue-cured leaves appearance quality formation. During the yellowing stage, separated top leaves changed easily from yellow to brown, severely reducing the flue-cured leaves' quality. In this study, we investigated the contribution of stems to the quality of flue-cured top leaves by analyzing the differences in physicochemical properties and metabolomics data between separated leaves and leaves with stems. Leaf samples were collected at the end of the yellowing stage. Metabolomics analysis was performed with the widely targeted method. Based on the MWDB database, more than 3000 metabolites could be determined in a measurement. Our results will provide a theoretical basis for further optimizing the flue-curing technology of top leaves.

Materials and methods

Materials

Tobacco genotype "Yunyan87" was seeded in seedling trays in a greenhouse. The 50-day-old seedlings were then transplanted into fields located in Yunnan, China (98°68′E, 24°56′N) on 20 April 2021. Pure nitrogen at 105 kg/ha was applied in the field period and fertilizer at N: P_2O_5: K_2O (1:1:2.5) was applied. 50% of the total amount was used as base fertiliser, 15% was used as seedling promoting fertilizer, and the other 35% was additional fertilizer. At the time of top pruning (9 July 2021), tobacco plants' apical buds were removed, and 15 to 16 leaves per plant were left. At the maturing stage (5 September 2021), the top five leaves with stems were harvested. Two groups of flue-cured samples (leaf with stem, stem(+), and leaf without stem, stem(-)) were prepared. Stem(+): Leaves with stems were flue-curd. After curing, stems were separated from leaves, with leaves being used for further metabonomics and physicochemical analysis. Stem(-): Stems were separated from leaves before flue-curing. Only leaves were flue-cured and used for further metabonomics and physicochemical analysis. Additionally, the fresh leaves (stems were removed) were also used as the control sample (CK). Three biological replicates were generated for each group of samples (9 samples in total). The flue-curing procedure is shown in Figure 1.

The samples of tobacco leaves were collected at the end of the yellowing stage. After removing the main vein, leaves were put in liquid nitrogen immediately and then transferred to the -80°C fridge for further analysis.

Physicochemical analysis

Moisture content of tobacco leaves

To determine moisture content of leaves, 10 leaves from each group were weighed immediately after harvest (fresh weight, FW). Then the leaves were dried in the oven at 70°C for 24 h to obtain dry weight (DW). Moisture content was calculated using the following formula.

$$Moisture \quad content = (FW - DW)/FW \times 100$$

H_2O_2, O_2-, MDA and starch contents

H_2O_2, O_2-, MDA and starch contents were determined with commercially available assay kit (Suzhou Comin Biotechnology Co., Ltd., China).

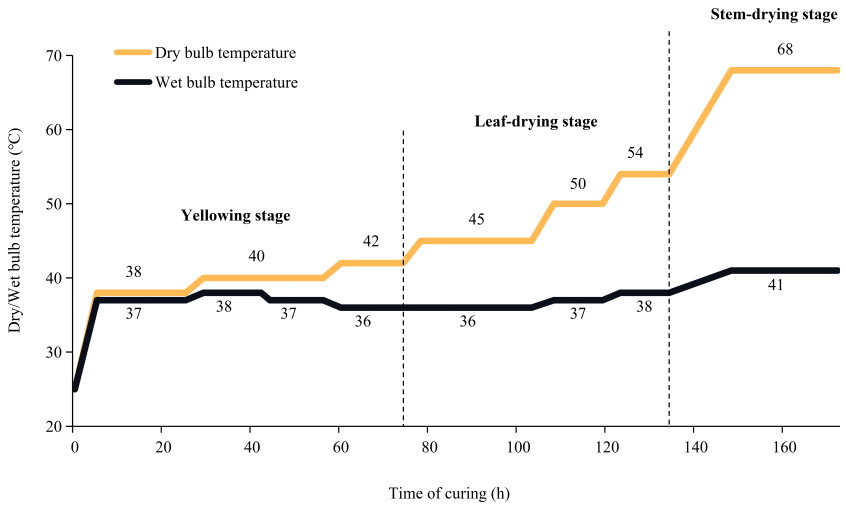

FIGURE 1
Flue-curing method.

Enzyme activities

Activities of superoxide dismutases (SOD), catalase (CAT), glutathione reductase (GR), polyphenol oxidase (PPO) and total amylase were determined with commercially available assay kit (Suzhou Comin Biotechnology Co., Ltd., China).

Widely targeted metabolomics analysis

Leaf samples (stem(+), stem(-) and CK) were vacuum freeze-dried and milled. Then, 100 mg lyophilized powder was extracted with 1.2 mL 70% methanol, vortexed for 30 s every 30 min for 6 times in total, and stored at 4°C overnight. Following centrifugation at 10,000 rpm for 10 min, the supernatants were filtrated through a 0.22 μm membrane. Finally, sample extracts were analyzed using a UPLC-ESI-MS/MS system (UPLC, SHIMADZU Nexera X2; MS, Applied Biosystems 6500 Q TRAP).

Column (1.8 μm, 2.1 mm × 100 mm, Agilent SB-C18); solvent system, water (0.1% formic acid) and acetonitrile (0.1% formic acid); gradient program, 95:5 v/v at 0 min, 5:95 V/V at 9 min, hold for 1 min, 95:5 v/v at 11.1 min, hold for 2.9 min; flow rate, 0.35 mL/min; column temperature, 40°C; injection volume, 2 μL. The effluent was alternatively connected to an ESI-triple quadrupole-linear ion trap (Q TRAP)-MS.

Linear ion trap (LIT) and triple quadrupole (QQQ) scans were acquired form the Applied Biosystems 6500 Q TRAP UPLC/MS/MS System, which was equipped with an ESI Turbo Ion-Spray interface. Positive and negative ion modes are operated by Analyst 1.6.3 software (AB Sciex). The ESI source operation parameters were as follows: ion source, turbo spray; source temperature, 550°C; ion spray voltage (IS), 5500 V (positive ion mode)/-4500 V (negative ion mode); ion source gas I (GSI), gas II (GSII), curtain gas (CUR) were set at 50, 60, and 25.0 psi, respectively; the collision-activated dissociation (CAD) was set to high. Instrument tuning and mass calibration were performed with 10 and 100 μM polypropylene glycol solutions in QQQ and LIT modes, respectively. QQQ scans were performed through multiple reaction monitoring (MRM) model, with collision gas (nitrogen) set to medium. Declustering potential (DP) and collision energy (CE) for each MRM transition were determined through optimization. A specific set of MRM transitions were monitored for each period, according to the metabolites eluted within this period.

Qualitative and quantitative analysis

Metabolites were identified based on the Metware database (MWDB) created by MetWare Biotechnology Co., Ltd. (Wuhan, China) using secondary mass-spectrometry data. The interference from isotope signals, duplicate signals of K^+, Na^+, and NH_4^+ ions, as well as duplicate signals of fragment ions derived from other larger molecules, were excluded.

Metabolites were quantified using the MRM model of QQQ mass spectrometry. In MRM mode, the quadrupole firstly searched for precursor ions (parent ions) of target substances to eliminate the interference from the ions derived from substances of different molecular weights. The precursor ions were then fragmented *via* induced ionization in the collision chamber into many fragment ions, from which a characteristic ion was selected. Using characteristic ions eliminated the interference from non-target ions and made more precise and repeatable quantification results. When metabolite mass spectrometry data were obtained for different samples, mass spectrum peaks of all metabolites were

subjected to area integration. The mass spectrum peaks of the same metabolite in different samples were subjected to integration correction. The relative quantity of a metabolite was represented by the area of its corresponding mass spectrum peak.

Multivariate statistical analysis

Principal component analysis (PCA) analysis was performed using the Clustvis tool (Metsalu and Vilo, 2015). Orthogonal partial least square-discriminant analysis (OPLS-DA) was generated using the R package MetaboAnalystR. To avoid overfitting, a permutation test (200 permutations) was performed. Boxplot, heatmap and clustered dendrogram were drawn using the R package.

Differential metabolite analysis

Two screening criteria for differential metabolites were established: p-value< 0.05; variable importance in projection (VIP) was ≥ 1. VIP values were extracted from the OPLS-DA result.

Results and discussion

Effect of stem on tobacco leaves metabolome

Metabolome analysis of flue-cured tobacco leaves was carried out based on widely targeted metabolomics analysis using the self-built database MWDB. Totally, 1236 metabolites were identified in flue-cured tobacco leaves, with 1213 and 1234 metabolites being identified in stem(+) and stem(-), respectively. The quantities of metabolites were subjected to hierarchical clustering (Figure 2A) and PCA analysis (Figure 2B). They both showed two distinct groups corresponding to stem(+) and stem(-) samples, respectively. Stem(+) and stem(-) were clearly separated by the first component (PC1: 40.86% variance explained). There was obviously distinct grouping of the samples based on whether to reserve stems. To evaluate the metabolic alteration caused by the presence of stems, OPLS-DA was performed. As shown in the OPLS-DA score plot, stem(+) and stem(-) were well separated. The model parameters were $R^2X = 0.567$, $R^2Y = 0.999$, and $Q^2 = 0.8$ (Figure 2C). 160 metabolites significantly differed (VIP ≥ 1, p< 0.05) between stem(+) and stem(-). Compared with stem(+), 126 metabolites were up-regulated and 34 were down-regulated (Figure 2D). Sinapic acid was the most up-regulated metabolite between stem(+) and stem(-) (Figure 2E). Indole-3-acetic acid (IAA) was the second most differential metabolites, which was abundant in stem(-) but did not exist in stem(+). 3-deoxysappanchalcone was the most down-regulated metabolite, followed by p-coumaric acid ethyl ester.

Effect of stem on the moisture content of tobacco leaves

During flue-curing, tobacco leaves were dehydrated. At the end of the yellowing stage, the leaf moisture content decreased significantly from 75.17% in CK to 62.82% and 50.37% in stem (+) and stem(-), respectively (Figure 3). This result agreed with a previous study that the presence of stem could reduce leaves' water loss during the withing process (Zeng et al., 2017; Wei et al., 2018). In our study, stem(+) and stem(-) were processed by the same curing method with the only difference being whether leaves were processed with stems. The moisture content decreased more slowly (p< 0.05) in stem(+) than in stem(-), because water migrated from the stem to the leaf *via* the midrib during flue-curing (Wei et al., 2018), which reduced the dehydration rate of tobacco leaves.

Effect of stem on H_2O_2 content, O_2- content in tobacco leaves

During flue-curing, tobacco leaves were subjected to various stresses such as heat and drought stresses. Such stresses could lead to reactive oxygen species (ROS) accumulation at the cellular level (Bouchard and Purdie, 2011; Petrov et al., 2015; Medina et al., 2021). H_2O_2 and O_2^- are essential components of ROS (Gill and Tuteja, 2010). Both of them significantly accumulated in flue-cured leaves (Figure 4). Both H_2O_2 and O_2^- contents were significantly higher in stem(-) than in stem(+). The H_2O_2 content in stem(-) was 48% higher than that in stem(+) (Figure 4A), while the O_2^- content was 45% higher in stem(-) than in stem(+) (Figure 4B). The difference in ROS contents between stem(+) and stem(-) was attributed to the difference in leaf moisture content. Our results showed a decrease in tobacco leaf moisture content was accompanied by increases in H_2O_2 and O_2^- concentrations. Such association between ROS contents and leaf water deficit has been observed in other species, such as maize and wheat (Khanna-Chopra and Selote, 2007; Yao et al., 2013). The presence of stem attenuated ROS accumulation in flue-cured tobacco leaves.

Effect of stem on SOD, CAT and GR activity in tobacco leaves

The overproduction of ROS can cause oxidative cell damage, directly attack membrane lipids, inactivate metabolic enzymes and damage the nucleic acids (Mittler, 2002). Plants have developed antioxidant defense systems to cope with the ROS generation to maintain intracellular homeostasis, consisting of antioxidant enzymes like SOD, CAT and GR and non-enzymatic antioxidants like GSH.

SOD is the most effective intracellular enzymatic antioxidant, which catalyzes the dismutation of O_2^- to H_2O and O_2 (Gill and Tuteja, 2010). The SOD activity could increase under mild water deficiency and decrease under severe water deficiency (Jiang and Huang, 2001; Yao et al., 2013). The activity of SOD in stem(+) and stem(-) was 81% and 93% below that in CK (Figure 4C), showing that the combined stresses (heat stress and drought stress) during the flue-curing process greatly limited SOD activity and impaired O_2^- scavenging in the cell (Jiang and Huang, 2001). The SOD activity in stem(+) was considerably higher than in stem(-), indicating that SOD activity is proportional to leaf tissue

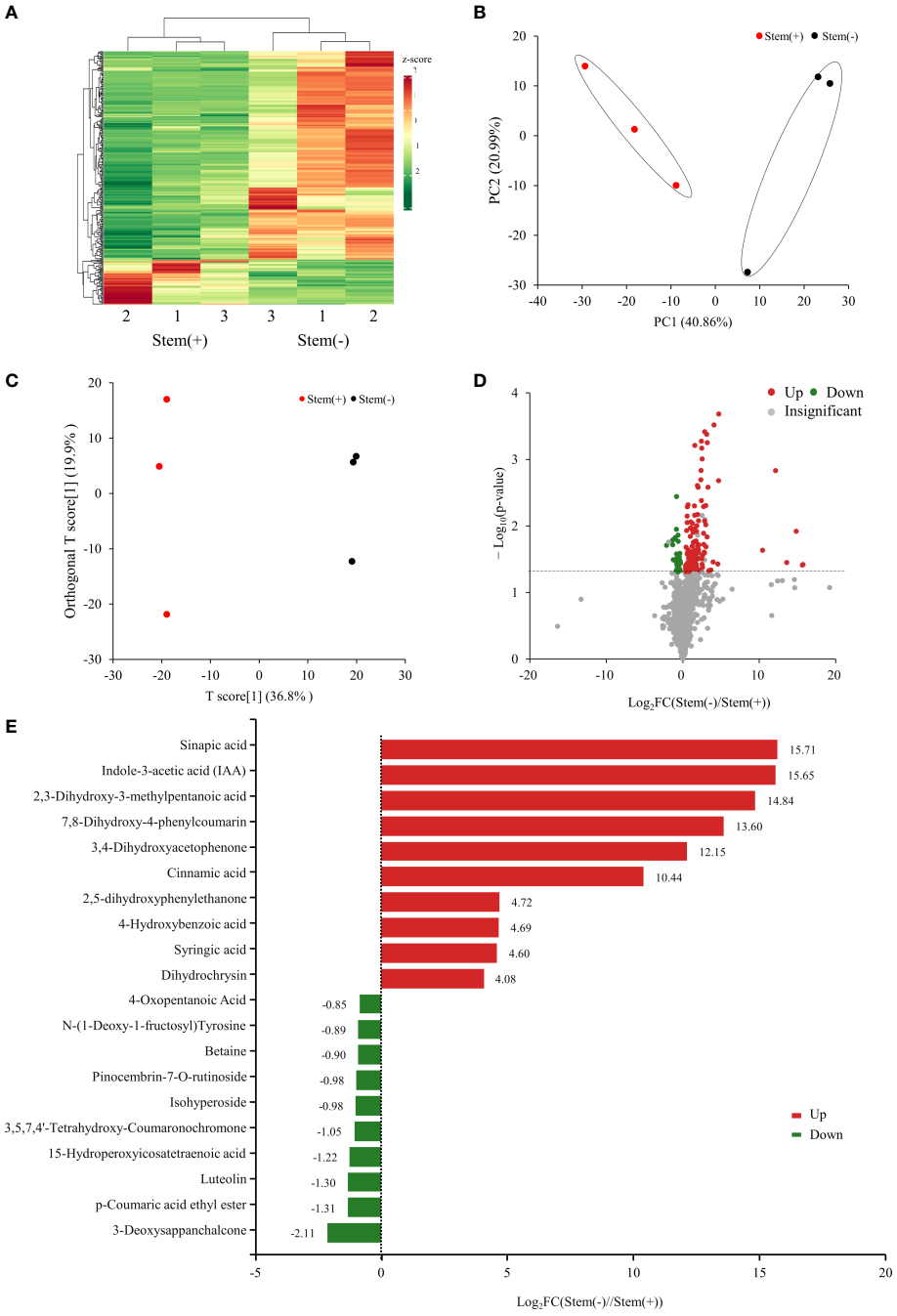

FIGURE 2
Metabolome analysis of tobacco leaves. **(A)** Heatmap of relative metabolites concentrations. The clustered dendrogram of samples was on the top. **(B)** PCA score plot of metabolite profiles. **(C)** Score scatter plots of the OPLS-DA model for stem(+) versus stem(-). **(D)** Volcano plot of differential metabolites between stem(+) and stem(-). **(E)** Top 20 differential metabolites between stem(+) and stem(-). FC, fold change.

moisture content under severe water deficit conditions in tobacco leaves.

CAT dismutases H_2O_2 into H_2O and O_2 and are indispensable for ROS scavenging during stress conditions (Garg and Manchanda, 2009). CAT activity could be up-regulated, unaffected or down-regulated by water deficit (Jiang and Huang, 2001; Pan et al., 2006; Yao et al., 2013). Like SOD, CAT activity declined significantly in flue-cured tobacco leaves

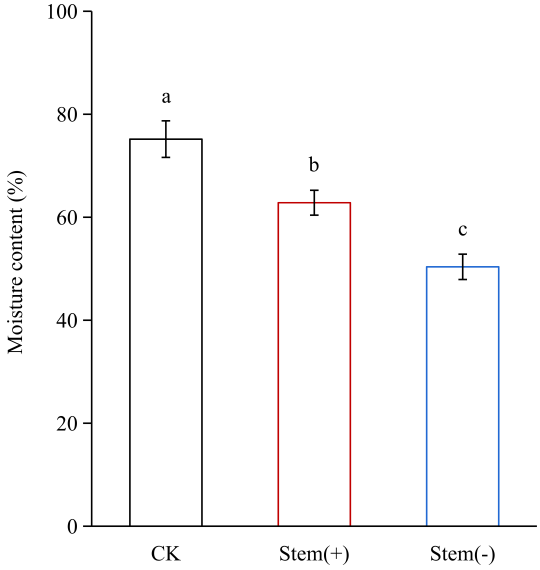

FIGURE 3
Effect of stem on leaf moisture content in flue-cured tobacco leaves. Different letters indicate statistically significant difference at $p < 0.05$, as determined by t-test.

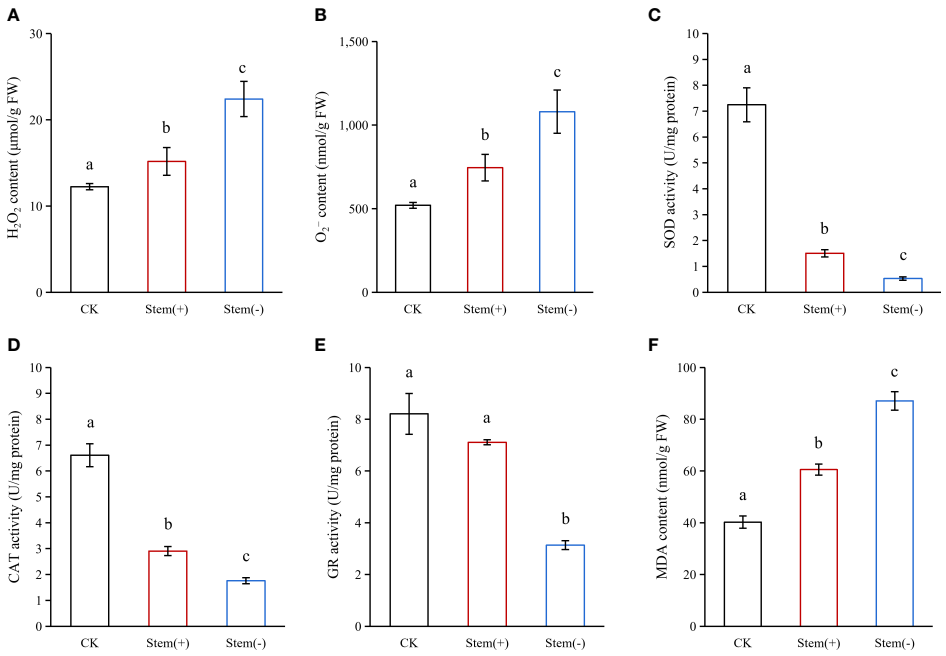

FIGURE 4
Effect of stem on ROS, antioxidant enzymes and cell integrity in flue-cured tobacco leaves. FW, fresh weight. Different letters indicate statistically significant difference at $p < 0.05$, as determined by t-test.

(Figure 4D). Compared to CK, the activity of CAT decreased by 56% and 73% in stem(+) and stem(-), respectively, which favored the accumulation of H_2O_2. The CAT activity in stem (-) was about 60% as much as that in stem(+), showing that the decline of CAT activity increases with the degree of water deficit in flue-cured tobacco leaves.

GR converts oxidized glutathione (GSSG) to reduced GSH, thus helping maintain the GSH pool and reducing the environment in the cell, which is crucial for the active functioning of proteins (Trivedi et al., 2013). The response of GR to stresses varied due to species variation. In *Sedum album* L., GR activity increased even under severe water deficit, whereas in turfgrasses, GR activity decreased under severe water deficit (Castillo, 1996; Jiang and Huang, 2001). Flue-curing tended to reduce the activity of GR in stem(+), but this effect was not statistically significant (Figure 4E). However, flue-curing significantly reduced the activity of GR in stem(-). Our results showed that flue-curing inhibited the GR activity in tobacco leaves, and the effect increased with decreasing leaf moisture content.

Due to flue-curing, the activities of SOD, CAT and GR decreased, which contributed to the accumulation of ROS in tobacco cells. However, the ROS scavenging system was relatively less damaged in stem(+), because of the higher leaf moisture content. The presence of stems alleviated ROS scavenging system damage in leaves, which probably led to less ROS accumulation in stem(+).

Effect of stem on MDA content in tobacco leaves

Accumulation of ROS can induce membrane lipid peroxidation. MDA is the end product of membrane lipid peroxidation and the indicator of biomembrane integrity (Wongsheree et al., 2009). The higher the MDA content, the more severe the biomembrane is injured. The MDA content increased by 50% and 116% in stem(+) and stem(-), respectively, compared to CK. The MDA content was enormously higher in stem(-) than in Stem(+) (Figure 4F). This is because the dehydration rate was more rapid in stem(-), leading to lower antioxidant enzyme activities and higher ROS accumulation (Jiang and Huang, 2001; Su et al., 2017; Zhao et al., 2022). Our observation showed that separated leaves (stem(-)) underwent a higher level of membrane lipid peroxidation than leaves with stems (stem(+)) during flue-curing.

Effect of stem on polyphenol contents in tobacco leaves

Polyphenols are secondary metabolites produced by plants such as tobacco. They play an essential role in determining the flue-cured tobacco quality, principally the color and aroma of flue-cured leaves and the odor and taste of smoke (Gong et al., 2006; Dagnon et al., 2006). During flue-curing of separated top tobacco leaves, however, polyphenols were easily oxidized into quinone by PPO to form brown-colored substances, which cause cured leaf browning and reduce flue-cured tobacco quality (Chen et al., 2021; Zhao et al., 2022). In tobacco, polyphenols exist in the form of glucoside and ester (Romero et al., 2004). The polyphenol contents dramatically change during flue-curing, because of the pyrolysis and the enzymatic degradation of the phenolic glycoside. Chlorogenic acid, rutin, and scopoletin are major polyphenols in tobacco leaves. Metabolome data showed that the chlorogenic acid content and rutin content did not differ significantly among CK, stem(+) and stem(-), whereas the scopoletin content showed an increasing trend due to flue-curing (Table 1). The scopoletin content was significantly higher in stem(-) than in stem(+), suggesting that its accumulation was probably related to the dehydration rate in tobacco leaves.

Effect of stem on PPO activity in tobacco leaves

PPO catalyzes the oxidation of polyphenols to quinones. In tobacco, PPO mainly exists in chloroplasts (Lax and Vaughn, 1991; Mayer, 2006). Previous studies showed that PPO activity positively correlates with the environmental moisture content during tobacco leaf processing (Song et al., 2010; Zhao et al., 2022). In our study, the moisture content of tobacco leaves decreased in the following order: CK > stem(+) > stem(-). The PPO activity was the lowest in the stem(-), about 30% and 50% that of CK and stem(+), respectively, and the differences among the three groups of samples were statistically significant (Figure 5A). That is, PPO activity in stem(-) was lower than that in stem(+), because of the lower moisture content in stem(-).

At the end of the yellowing stage, tobacco leaf moisture content is high. Thus, cells in leaves still had high PPO activity. Typically, tobacco leaves undergo a low degree of polyphenols oxidation at this moment, because the intracellular membrane system provides a barrier between the PPO and polyphenols. In stem(-), rapid dehydration sharply increased membrane lipid peroxidation levels and consequently reduced the integrity of the cell membrane. If the

TABLE 1 Polyphenols contents in flue-cured tobacco leaves.

Sample	Chlorogenic acid	Scopoletin	Rutin
CK	7.03E+06 ± 1.11E+06 a	1.03E+07 ± 2.60E+06 b	6.48E+07 ± 1.62E+07 a
Stem(+)	8.82E+06 ± 1.24E+06 a	1.59E+07 ± 3.68E+06 b	7.60E+07 ± 1.23E+07 a
Stem(-)	8.11E+06 ± 2.56E+05 a	6.42E+07 ± 7.64E+06 a	5.98E+07 ± 1.72E+07 a

The relative quantity of a metabolite was represented by the area of its corresponding mass spectrum peak.

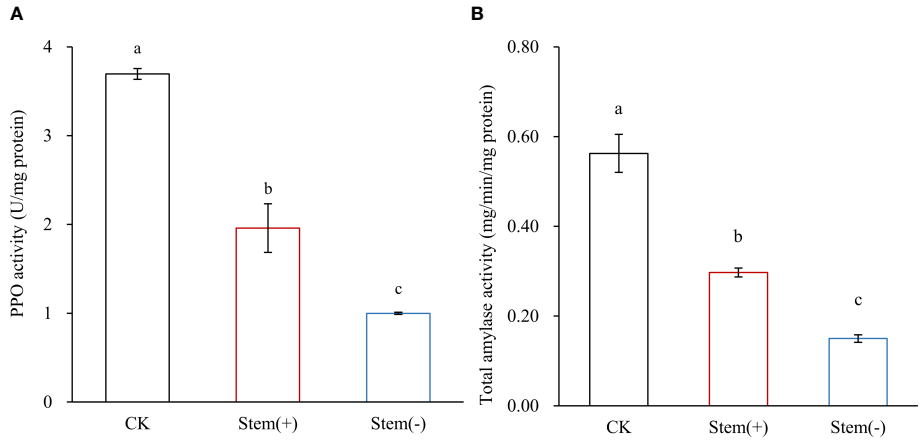

FIGURE 5
Effect of stem on PPO activity and total amylase activity in flue-cured tobacco leaves. Different letters indicate statistically significant difference at $p < 0.05$, as determined by t-test.

membrane system destructed due to a high level of membrane lipid peroxidation, polyphenols would come into contact with PPO and much oxygen would enter cells, which increases the oxidation rate of polyphenols to form brown substances (Chen et al., 2019; Zhao et al., 2022). Such browning reactions were to cause the appearance of dark-colored spots and stripes on the leaf surface and seriously reduce flue-cured tobacco leaf quality. Unlike stem(-), stem(+) had a low risk of browning reaction because of a suitable dehydration rate and relatively intact cellular membrane system. Due to the unique physicochemical properties of tobacco top leaves, the browning reaction can quickly occur during flue-curing of separated top leaves, making them have low economic value. Nevertheless, browning reaction seldom occurred during flue-curing of top leaves with stems. Our observation suggested that the presence of stem helped maintain suitable leaf moisture content and cell membrane integrity during the yellowing stage, reducing the risk of browning reaction.

Effect of stem on phytohormone contents of tobacco leaves

Based on our metabolome data, four plant hormones, salicylic acid (SA), indole-3-acetic acid (IAA), jasmonic acid (JA) and abscisic acid (ABA), were identified in tobacco leaves (Table 2). IAA and SA were significantly different between stem (+) and stem(-), probably due to the different moisture content.

IAA was one of the most differential metabolites between stem(+) and stem(-). Stem(+), as well as CK, did not contain IAA, but stem(-) accumulated a high level of IAA, which is probably due to the leaf moisture content of stem(-) being significantly lower than that in stem(+) and CK. It is reasonable to speculate that IAA was synthesized in separated tobacco leaves during flue-curing. This is the first time the synthesis and accumulation of auxin are observed during tobacco leaf flue-curing. IAA is the main naturally occurring auxin, which controls plant growth and development *via* promoting cell division (proliferation), growth (expansion, elongation) and differentiation (Mor et al., 2002). Various studies have shown that during cell expansion and elongation, IAA causes cell wall loss by promoting xyloglucan degradation (Mor et al., 2002; dos Santos et al., 2004; Mateusz and Robert, 2018). The degradation of cell wall substances made plastids and membrane systems vulnerable. The cell membrane integrity was poor in stem(-) due to a high level of membrane lipid peroxidation. IAA accumulation further increased the risk of

TABLE 2 Phytohormone contents in flue-cured tobacco leaves.

Sample	IAA	JA	SA	ABA
CK	9 ± 0 b	7.39E+03 ± 1.28E+04 c	3.66E+05 ± 2.19E+05 c	1.31E+05 ± 2.44E+04 b
Stem(+)	9 ± 0 b	8.32E+03 ± 1.44E+04 bc	6.23E+05 ± 1.91E+05 bc	4.76E+05 ± 2.57E+04 a
Stem(-)	4.61E+05 ± 1.62E+05 a	5.51E+04 ± 9.91E+03 a	1.28E+06 ± 4.49E+05 ab	5.98E+05 ± 8.56E+04 a

The relative quantity of a metabolite was represented by the area of its corresponding mass spectrum peak.

TABLE 3 Carbohydrates contents in flue-cured tobacco leaves.

Sample	Starch(mg/g FW)	Glucose*	Fructose*	Sucrose*	Maltose*
CK	212.34 ± 15.79 a	7.41E+06 ± 8.86E+05 b	9.54E+06 ± 1.48E+06 b	3.12E+07 ± 9.29E+06 b	2.90E+06 ± 7.92E+05 a
Stem(+)	112.58 ± 5.21 c	1.86E+07 ± 1.52E+06 a	2.20E+07 ± 4.95E+06 a	5.66E+07 ± 5.12E+06 a	4.66E+06 ± 1.26E+06 a
Stem(-)	158.24 ± 11.81 b	2.08E+07 ± 1.34E+06 a	2.19E+07 ± 6.67E+06 a	7.26E+07 ± 2.14E+07 a	6.58E+06 ± 2.20E+06 a

FW, fried weight. *, The relative quantity of a metabolite was represented by the area of its corresponding mass spectrum peak.

cell membrane destruction. At the end of the yellowing stage, PPO activity in leaves was still high. If the cell membrane were disrupted, polyphenols would be oxidized by PPO, causing a browning reaction (Chen et al., 2019; Zhao et al., 2022). Therefore the accumulation of IAA was probably another reason for the frequent occurrence of browning reaction during flue-curing of separated top leaves. The presence of stem probably inhibited or postponed IAA accumulation in flue-cured leaves, which awaits further study.

Effect of stem on carbohydrates contents of tobacco leaves

The starch content is an important indicator of the quality of flue-cured tobacco leaves. Starch adversely affects the combustion rate and complete combustibility of cigarettes and produces a bitter and irritating taste when it burns. Starch degradation in tobacco leaves during the curing process is predominantly catalyzed by amylolytic enzymes, which are sensitive to leaf moisture content (Song et al., 2009; Yamaguchi et al., 2013). Low humidity can significantly reduce their activity in tobacco leaves (Song et al., 2009). Therefore, it is essential to maintain the appropriate leaf moisture content during flue-curing processing to degrade starch fully. Compared to CK, both starch content and total amylase activity significantly decreased in flue-cured leaves (Figure 5B, Table 3). The starch content was significantly higher in stem(-) than in stem(+), while the total amylase activity was significantly lower in stem(-) than in stem(+). These results coincided with the prediction, because leaf moisture content was lower in stem (-) than in stem(+). Compared to stem(+), the moisture content decreased rapidly in stem(-), resulting in lower total amylase activity and less starch degradation. In conclusion, stems could slow the decrease of amylase activity and strengthen starch degradation by maintaining appropriate leaf moisture content, which is advantageous to flue-cured tobacco qualities.

Water-soluble sugars also contribute to the quality of cured tobacco leaves. Cured tobacco leaves with high water-soluble sugars are lustrous, elastic, rich in oil, elegant flavor, and mellow taste. It is usually considered that the main ingredient of soluble sugar in flue-cured leaves are glucose, fructose, sucrose and maltose (Banožić et al., 2020). Our metabolome analysis showed that glucose, fructose and sucrose contents significantly increased during processing, while maltose content remained almost the same (Table 3). However, there was no significant difference in glucose, fructose, sucrose and maltose contents between stem(+) and stem (-). These results indicated that the presence of stem did not significantly improve the water-soluble sugar content of leaves.

Conclusion

To reveal the underlining mechanism of the contribution of stems to leaves, this paper investigated the effects of stem on the metabolic profiling and physicochemical properties of flue-cured tobacco leaf at the end yellowing stage. Stems reduced the dehydration rate of leaves, which led to less ROS accumulation, higher antioxidant enzyme activities and a lower level of membrane lipid peroxidation in stem(+). Stem also prohibited IAA accumulation in leaves, which probably be related to the difference in leaf moisture content between stem(+) and stem(-). IAA accumulation could make the cellular membrane system vulnerable to external damage. That is stems helped maintain cellular membrane integrity of leaf cells through alleviating oxidative membrane damage and inhibiting IAA accumulation, which reduced the risks of browning reaction in flue-cured leaves. Stems enhanced starch degradation in leaves, which was favorable to sensory quality of flue-cured leaves. The activity of amylase in stem(+) was higher than that in stem(-), because leaf moisture content was higher in stem(+). Stems caused various metabolic and physicochemical differences between stem(+) and stem(-) during flue-curing, all of which could be attributed to that, stems slowed down the rate of leaf dehydration.

Data availability statement

The original contributions presented in the study are included in the article/Supplementary Material. Further inquiries can be directed to the corresponding authors.

Author contributions

FS and BH conceived and designed the experiments; LM, WS, SC, FH, JC, BP participated in experiments and data analyses; LM and WS wrote the manuscript with inputs and guidance from BH and FS. All authors contributed to the article and approved the submitted version.

Funding

This work was financially supported by the Agricultural Science and Technology Innovation Program (ASTIP-TRIC03).

Conflict of interest

SC is employed by China Tobacco Shandong Industrial Co., Ltd.

The remaining authors declare that the research was conducted in the absence of any commercial or financial relationships that could be construed as a potential conflict of interest.

Publisher's note

References

Banožić, M., Jokić, S., Ačkar, Đ., Blažić, M., and Šubarić, D. (2020). Carbohydrates–key players in tobacco aroma formation and quality determination. *Molecules* 25, 1734. doi: 10.3390/molecules25071734

Bouchard, J. N., and Purdie, D. A. (2011). Effect of elevated temperature, darkness and hydrogen peroxide treatment on oxidative stress and cell death in the bloom - forming toxic cyanobacterium microcystis aeruginosa. *J. Phycol.* 47, 1316–1325. doi: 10.1111/j.1529-8817.2011.01074

Castillo, F. J. (1996). Antioxidant protection in the inducible CAM plant sedum album l. following the imposition of severe water stress and recovery. *Oecologia* 107, 469–477. doi: 10.1007/BF00333937

Chen, W., Gong, L., Guo, Z., Wang, W., Zhang, H., Liu, X., et al. (2013). A novel integrated method for large-scale detection, identification, and quantification of widely targeted metabolites: application in the study of rice metabolomics. *Mol. Plant* 6, 1769–1780. doi: 10.1093/mp/sst080

Chen, J., Li, Y., He, X., Jiao, F., Xu, M., Hu, B., et al. (2021). Influences of different curing methods on chemical compositions in different types of tobaccos. *Ind. Crop Prod.* 167, 113534. doi: 10.1016/j.indcrop.2021.113534

Chen, Y., Ren, K., He, X., Gong, J., Hu, X., Su, J., et al. (2019). Dynamic changes in physiological and biochemical properties of flue-cured tobacco of different leaf ages during flue-curing and their effects on yield and quality. *BMC Plant Biol.* 19, 555. doi: 10.1186/s12870-019-2143-x

Dagnon, S., Zaprianova, P., and Edreva, A. (2006). Colour and aroma in virginia tobaccos as influenced by the polyphenol and essential oil cultivar characteristics: a chemometric approach. *Biotechnol. Biotec. Eq.* 20, 23–29. doi: 10.1080/13102818.2006.10817299

dos Santos, H. P., Purgatto, E., Mercier, H., and Buckeridge, M. S. (2004). The control of storage xyloglucan mobilization in cotyledons of hymenaea courbaril. *Plant Physiol.* 135, 287–299. doi: 10.1104/pp.104.040220

Garg, N., and Manchanda, G. (2009). ROS generation in plants: boon or bane? *Plant Biosys.* 143, 81–96. doi: 10.1080/11263500802633626

Gill, S. S., and Tuteja, N. (2010). Reactive oxygen species and antioxidant machinery in abiotic stress tolerance in crop plants. *Plant Physiol. Bioch.* 48, 909–930. doi: 10.1016/j.plaphy.2010.08.016

Gong, C. R., Wang, A. H., and Wang, S. F. (2006). Changes of polyphenols in tobacco leaves during the flue-curing process and correlation analysis on some chemical components. *Agr. Sci. China* 5, 928–932. doi: 10.1016/S1671-2927(07)60006-6

Hu, Z., Pan, Z., Yang, L., Wang, K., Yang, P., Xu, Z., et al. (2021). Metabolomics analysis provides new insights into the medicinal value of flavonoids in tobacco leaves. *Mol. Omics* 17, 620–629. doi: 10.1039/d1mo00092f

Jiang, Y., and Huang, B. (2001). Drought and heat stress injury to two cool-season turfgrasses in relation to antioxidant metabolism and lipid peroxidation. *Crop Sci.* 41, 436–442. doi: 10.2135/cropsci2001.412436x

Kaiser, S., Dias, J. C., Ardila, J. A., Soares, F. L. F., Marcelo, M. C. A., Porte, L. M. F., et al. (2018). High-throughput simultaneous quantitation of multi-analytes in tobacco by flow injection coupled to high-resolution mass spectrometry. *Talanta* 190, 363–374. doi: 10.1016/j.talanta.2018.08.007

Khanna-Chopra, R., and Selote, D. (2007). Acclimation to drought stress generates oxidative stress tolerance in drought-resistant than -susceptible wheat cultivar under field conditions. *Environ. Exp. Bot.* 60, 276–283. doi: 10.1016/j.envexpbot.2006.11.004

Lax, A. R., and Vaughn, K. C. (1991). Colocalization of polyphenol oxidase and photosystem II proteins. *Plant Physiol.* 96, 26–31. doi: 10.1104/pp.96.1.26

Li, Y., Ren, K., Hu, M., He, X., Gu, K., Hu, B., et al. (2021). Cold stress in the harvest period: effects on tobacco leaf quality and curing characteristics. *BMC Plant Biol.* 21, 131. doi: 10.1186/s12870-021-02895-w

Mateusz, M., and Robert, S. (2018). The role of auxin in cell wall expansion. *Int. J. Mol. Sci.* 19, 951. doi: 10.3390/ijms19040951

Mayer, A. M. (2006). Polyphenol oxidases in plants and fungi: Going places? a review. *Phytochemistry* 67, 2318–2331. doi: 10.1016/j.phytochem.2006.08.006

Medina, E., Kim, S. H., Yun, M., and Choi, W. G. (2021). Recapitulation of the function and role of ROS generatedin response to heat stress in plants. *Plants* 10, 371. doi: 10.3390/plants10020371

Metsalu, T., and Vilo, J. (2015). Clustvis: a web tool for visualizing clustering of multivariate data using principal component analysis and heatmap. *Nucleic Acids Res.* 43, W566–W570. doi: 10.1093/nar/gkv468

Mittler, R. (2002). Oxidative stress, antioxidants and stress tolerance. *Trends Plant Sci.* 7, 405–410. doi: 10.1016/S1360-1385(02)02312-9

Mor, I. R., Gokani, S. J., and Chanda, S. V. (2002). Effect of mercury toxicity on hypocotyl elongation and cell wall loosening in phaseolus seedlings. *J. Plant Nutr.* 25, 843–860. doi: 10.1081/PLN-120002964

Pan, Y., Wu, L. J., and Yu, Z. L. (2006). Effect of salt and drought stress on antioxidant enzymes activities and SOD isoenzymes of liquorice (Glycyrrhiza uralensis fisch). *Plant Growth Regul.* 49, 157–165. doi: 10.1007/s10725-006-9101-y

Petrov, V., Hille, J., Mueller-Roeber, B., and Gechev, T. S. (2015). ROS-mediated abiotic stress-induced programmed cell death in plants. *Front. Plant Sci.* 6. doi: 10.3389/fpls.2015.00069

Romero, C., Brenes, M., García, P., García, A., and Garrido, A. (2004). Polyphenol changes during fermentation of naturally black olives. *J. Agric. Food Chem.* 52, 1973–1979. doi: 10.1021/jf030726p

Song, Z., Li, T., and Gong, C. (2009). A review on starch changes in tobacco leaves during flue-curing. *Front. Agric. China* 3, 435–439. doi: 10.1007/s11703-009-0076-0

Song, Z. P., Li, T. S., Zhang, Y. G., Cao, H. J., Gong, C. R., and Zhang, W. J. (2010). The mechanism of carotenoid degradation in flue-cured tobacco and changes in the related enzyme activities at the leaf-drying stage during the bulk curing process. *Agr. Sci. China* 9, 1381–1388. doi: 10.1016/S1671-2927(09)60229-7

Su, X., Wei, F., Huo, Y., and Xia, Z. (2017). Comparative physiological and molecular analyses of two contrasting flue-cured tobacco genotypes under progressive drought stress. *Front. Plant Sci.* 8. doi: 10.3389/fpls.2017.00827

Talhout, R., Opperhuizen, A., and van Amsterdam, J. G. C. (2006). Sugars as tobacco ingredient: effects on mainstream smoke composition. *Food Chem. Toxicol.* 44, 1789–1798. doi: 10.1016/j.fct.2006.06.016

Trivedi, D. K., Gill, S. S., Yadav, S., and Tuteja, N. (2013). Genome-wide analysis of glutathione reductase (GR) genes from rice and arabidopsis. *Plant Signal. Behav.* 8, e23021. doi: 10.4161/psb.23021

Wei, S., Tian, B. Q., Jia, H. F., Zhang, H. Y., He, F., and Song, Z. P. (2018). Investigation on water distribution and state in tobacco leaves with stalks during

curing by LF-NMR and MRI. *Dry. Technol.* 36, 1515–1522. doi: 10.1080/07373937.2017.1415349

Wongsheree, T., Ketsa, S., and Doorn, W. G. V. (2009). The relationship between chilling injury and membrane damage in lemon basil (Ocimum × citriodourum) leaves. *Postharvest. Biol. Technol.* 51, 91–96. doi: 10.1016/j.postharvbio.2008.05.015

Yamaguchi, N., Suzuki, S., and Makino, A. (2013). Starch degradation by alpha-amylase in tobacco leaves during the curing process. *Soil Sci. Plant Nutr.* 59, 904–911. doi: 10.1080/00380768.2013.842884

Yao, Y., Liu, X., Li, Z., Ma, X., Rennenberg, H., Wang, X., et al. (2013). Drought-induced H2O2 accumulation in subsidiary cells is involved in regulatory signaling of stomatal closure in maize leaves. *Planta* 238, 217–227. doi: 10.1007/s00425-013-1886-0

Zeng, L., Zhou, Y., Fu, X., Mei, X., Cheng, S., Gui, J., et al. (2017). Does oolong tea (Camellia sinensis) made from a combination of leaf and stem smell more aromatic than leaf only tea? contribution of the stem to oolong tea aroma. *Food Chem.* 237, 488–498. doi: 10.1016/j.foodchem.2017.05.137

Zhao, J., Li, L., Zhao, Y., Zhao, C., Chen, X., Liu, P., et al. (2018). Metabolic changes in primary, secondary, and lipid metabolism in tobacco leaf in response to topping. *Anal. Bioanal. Chem.* 410, 839–851. doi: 10.1007/s00216-017-0596-z

Zhao, S., Wu, Z., Lai, M., Zhao, M., and Lin, B. (2022). Determination of optimum humidity for air-curing of cigar tobacco leaves during the browning period. *Ind. Crop Prod.* 183, 114939. doi: 10.1016/j.indcrop.2022.114939

Zhao, Y., Zhao, C., Li, Y., Chang, Y., Zhang, J., Zeng, Z., et al. (2014). Study of metabolite differences of flue-cured tobacco from different regions using a pseudotargeted gas chromatography with mass spectrometry selected-ion monitoring method. *J. Sep. Sci.* 37, 2177–2184. doi: 10.1002/jssc.201400097

Zong, J., He, X., Lin, Z., Hu, M., Xu, A., Chen, Y., et al. (2020). Effect of two drying methods on chemical transformations in flue-cured tobacco. *Dry. Technol.* 40, 188–196. doi: 10.1080/07373937.2020.177928

frontiers | Frontiers in Plant Science

TYPE Original Research
PUBLISHED 06 December 2022
DOI 10.3389/fpls.2022.1092774

OPEN ACCESS

EDITED BY
Weicong Qi,
Jiangsu Academy of Agricultural Sciences (JAAS), China

REVIEWED BY
Zhou Hongjun,
Zhongkai University of Agriculture and Engineering, China
Lidong Cao,
Chinese Academy of Agricultural Sciences, China

*CORRESPONDENCE
Xiangge Du
duxge@cau.edu.cn
Jie Shen
shenjie@cau.edu.cn

†These authors have contributed equally to this work

SPECIALTY SECTION
This article was submitted to Plant Bioinformatics, a section of the journal Frontiers in Plant Science

RECEIVED 08 November 2022
ACCEPTED 24 November 2022
PUBLISHED 06 December 2022

CITATION
Yan S, Hu Q, Wei Y, Jiang Q, Yin M, Dong M, Shen J and Du X (2022) Calcium nutrition nanoagent rescues tomatoes from mosaic virus disease by accelerating calcium transport and activating antiviral immunity. *Front. Plant Sci.* 13:1092774. doi: 10.3389/fpls.2022.1092774

Calcium nutrition nanoagent rescues tomatoes from mosaic virus disease by accelerating calcium transport and activating antiviral immunity

Shuo Yan[1†], Qian Hu[2†], Ying Wei[1], Qinhong Jiang[1], Meizhen Yin[3], Min Dong[1], Jie Shen[1*] and Xiangge Du[1*]

[1]Department of Plant Biosecurity and MARA Key Laboratory of Surveillance and Management for Plant Quarantine Pests, College of Plant Protection, China Agricultural University, Beijing, China, [2]Development Center for Science and Technology, Ministry of Agriculture and Rural Affairs, Beijing, China, [3]State Key Laboratory of Chemical Resource Engineering, Beijing Lab of Biomedical Materials, Beijing University of Chemical Technology, Beijing, China

As an essential structural, metabolic and signaling element, calcium shows low remobilization from old to young tissues in plants, restricting the nutrient-use efficiency and control efficacy against mosaic virus disease. Nanotechnology has been applied to prevent/minimize nutrient losses and improve the accessibility of poorly-available nutrients. Herein, the current study applied a star polycation (SPc) to prepare a calcium nutrition nanoagent. The SPc could assemble with calcium glycinate through hydrogen bond and Van der Waals force, forming stable spherical particles with nanoscale size (17.72 nm). Transcriptomic results revealed that the calcium glycinate/SPc complex could activate the expression of many transport-related genes and disease resistance genes in tomatoes, suggesting the enhanced transport and antiviral immunity of SPc-loaded calcium glycinate. Reasonably, the calcium transport was accelerated by 3.17 times into tomato leaves with the help of SPc, and the protective effect of calcium glycinate was remarkably improved to 77.40% and 67.31% toward tomato mosaic virus with the help of SPc after the third and fifth applications. Furthermore, SPc-loaded calcium glycinate could be applied to increase the leaf photosynthetic rate and control the unusual fast growth of tomatoes. The current study is the first success to apply nano-delivery system for enhanced calcium transport and antiviral immunity, which is beneficial for increasing nutrient-use efficiency and shows good prospects for field application.

KEYWORDS

calcium nutrition, calcium transport, nano-fertilizer, nutrient-use efficiency, polymer

Introduction

Calcium is an essential structural, metabolic and signaling element, which is required either for nutritional or signaling purpose (Demidchik et al., 2018; Thor, 2019). It thereby shows a dual function, both as a structural component of cell walls and membranes and as a second messenger, which is involved in plant growth and responses to abiotic as well as biotic stress (Knight et al., 1997; Cheong et al., 2002; Monshausen et al., 2011; Xu et al., 2015; Zhang et al., 2017). Calcium is mainly present in soil solution, and low soil availability of calcium is usually not the reason for calcium deficiency (White and Broadley, 2003). Deficiency symptoms are usually observed in developing tissues such as young leaves and fruits, due to the low remobilization of calcium from old to young tissues. Symplastic pathway is mainly used for short-distance calcium delivery, and the long-distance translocation is dependent on apoplastic pathway *via* xylem (Jovanović et al., 2021). Transpiring organs tend to accumulate high calcium levels, and calcium is usually deposited inside the vacuoles or sequestrated into leaf-trichomes to impose calcium phloem immobility, which leads to low calcium levels in young leaves and fruits (White, 2001; Gilliham et al., 2011; Kumar et al., 2015). This property leads to low nutrient-use efficiency of calcium and further restricts its antiviral immunity toward devastating mosaic virus disease. Thus, efficient delivery of calcium into plant young tissues is crucial for calcium bioavailability, especially for alleviating mosaic virus disease that is regarded as "tomato cancer".

Achieving sustainable agricultural productivity and global food security requires innovative technologies during the Green Revolution. One of concerns is the inefficient overuse of agrochemicals, and nanotechnology has the potential to boost agricultural industry through their nanospecific properties (Wang et al., 2022a). Nanocarriers have been applied to prevent/minimize nutrient losses, allow the controlled-release of nutrients, and improve the accessibility of poorly-available nutrients (Chhipa, 2016; Zuverza-Mena et al., 2017; Jakhar et al., 2022). Nano-sized nutrients can increase the surface mass ratio of fertilizers, which allows a remarkable enhancement of root absorption. With the help of nanocarriers, slow, targeted and efficient nutrient release becomes possible, which can reduce application dosage/cost to minimize nutrient losses and increase nutrient-use efficiency (Fellet et al., 2021). During the last decade, great attention has been paid to calcium nanoparticles as potential nano-fertilizers with superior nutrient-use efficiency compared to their conventional counterparts (Carmona et al., 2022). Previous study reports a nano calcium phosphate that can significantly increase the shoot and root dry weights, nutrient content, yield components, and nutrient concentration and protein percentage in the pods of snap bean plants (El-Ghany et al., 2021).

Our studying group has designed and constructed a star polycation (SPc)-based nano-delivery system that can be applied to deliver various exogenous substances such as double-stranded RNA (dsRNA) and synthetic/botanical pesticides (Li et al., 2019a; Yan et al., 2021a; Yan et al., 2021b; Ma et al., 2022a; Zhang et al., 2022a). The SPc-based nano-delivery system can reduce the particle size of synthetic/botanical pesticides and increase their water solubility and dispersity (Yan et al., 2021b; Yan et al., 2022; Wang et al., 2022b). At the cellular level, the SPc can activate the clathrin-mediated endocytosis for enhanced cellular uptake and promote the endosomal escape for intracellular spreading of exogenous substances (Wang et al., 2021; Ma et al., 2022b; Yang et al., 2022; Zhang et al., 2022b). *In vivo*, the SPc can increase plant uptake to improve the bioactivity of various exogenous substances (Wang et al., 2022b; Jiang et al., 2022a; Jiang et al., 2022b). A recent publication has demonstrated that the SPc can co-deliver dsRNA and matrine to overcome the short life disadvantage of dsRNA and slow-acting property of matrine simultaneously (Li et al., 2022). Applying SPc-based nano-delivery system for efficient plant uptake of nutrients is a new topic.

Calcium glycinate ($C_4H_8CaN_2O_4$) is formed by glycine and calcium compounds through chemical reactions, which is a new-type and ideal nutrient supplement (Yin et al., 2017). To this context, the current study aimed to construct a SPc-based nano-delivery system for calcium glycinate to control tomato mosaic virus (ToMV) disease by accelerating calcium transport and activating antiviral immunity. We tested the drug loading content (DLC) using freeze drying method, measured the complex particle size using dynamic light scattering (DLS), observed the complex morphology using transmission electron microscope (TEM), and determined the interaction force between calcium glycinate and SPc using isothermal titration calorimetry (ITC) to illustrate the self-assembly mechanism. Then, we determined the differentially expressed genes (DEGs) between calcium glycinate/SPc complex and calcium glycinate alone to explore the potential function of SPc. Finally, we tested the calcium transport in plant with the aid of SPc using flame atomic absorption spectrometry (FAAS) system, and determined the bioactivity of SPc-loaded calcium glycinate, including the control efficacy against ToMV, and effects on leaf photosynthetic rate and internodes length of seedlings.

Materials and methods

Chemicals and SPc synthesis

Pure calcium glycinate (≥98%) was purchased from Jiangsubaiye Biotechnology Co., Ltd (Nanjing, China). N,N,N′,N′,N″-Pentamethyl diethylenetriamine (PMDETA, 98%) and CuBr (99.999%) purchased from Sigma-Aldrich (Saint Louis, MO, USA), 2-bromo-2-methylpropionyl bromide and triethylamine purchased from Heowns BioChem Technologies (Tianjin, China), and 2-(Dimethyl amino) ethyl methacrylate

(DMAEMA, 99%) purchased from Energy Chemical (Shanghai, China) were used for SPc synthesis. Other chemical reagents such as ethanol, methanol, etc. were purchased from Beijing Chemical Works (Beijing, China).

SPc was synthesized through two reaction steps following a previously described method (Li et al., 2019a). Briefly, the star initiator Pt-Br was constructed by adding 2-bromo-2-methylpropionyl bromide (253 mg, 1.11 mmol) dropwise into pentaerythritol solution (25 mg, 0.18 mmol) in dry tetrahydrofuran (20 mL) and triethylamine (111.3 mg, 1.11 mmol) at 0°C, and stirring for 24 h at room temperature. The reaction was quenched by adding methanol, and obtained Pt-Br was polymerized with DMAEMA (2.2g, 7.7 mmol) in an oil bath at 60°C for 7 h with the help of tetrahydrofuran (8 mL), PMDETA (110 mg, 0.44 mmol) and CuBr (46 mg, 0.22 mmol). The reaction was quenched by cooling and air exposure, and dialysis was then carried out to purify the crude product of SPc. The SPc was dissolved in double distilled water (ddH_2O) to prepare the 60 mg/mL stock.

Loading capacity measurement

DLC was tested according to previous described methods (Yan et al., 2022; Wang et al., 2022b). Briefly, excess calcium glycinate (603.5 mg) was mixed with SPc (229.26 mg) in ddH_2O (23 mL). The mixture was dialyzed using the regenerated cellulose with a molecular weight cut off of 1 000 Da (Shanghai Yuanye Bio-Technology Co., Shanghai, China) for 12 h, freeze-dried and weighed. DLC was calculated as DLC (%) = weight of calcium glycinate loaded in complex/ weight of calcium glycinate – loaded complex × 100%.

Isothermal titration calorimetry (ITC) assay

The SPc and calcium glycinate were dissolved in ddH_2O, respectively. The 300 μL calcium glycinate (monomer content: 200 μmol/L) was titrated with 40 μL SPc aqueous solution (250 μmol/L) in MicroCal iTC200 (GE Healthcare Life Sciences, MA, USA). During each injection, the heating temperature of interaction was calculated by integrating each titration peak *via* Origin7 software (OriginLab Co., Ltd., MA, USA). The test temperature was set at 25°C, and the ΔG value was calculated using the formula of $\Delta G = \Delta H - T\Delta S$.

Particle size measurement and morphology observation

Calcium glycinate was dissolved in ddH_2O, and mixed with SPc at the mass ratio of 1:8.8 to prepare calcium glycinate/SPc complex (1 mg/mL) according to the DLC. The calcium glycinate was too big for particle size measurement, thus only calcium glycinate/SPc complex was measured using Particle Sizer and Zeta Potential Analyzer (Brookhaven NanoBrook Omni, New York City, NY, USA) at 25°C. The particle size of calcium glycinate/SPc complex was also measured after 14 d storage to test the complex stability. Each assay was repeated 3 times. Furthermore, morphological characteristics of calcium glycinate and calcium glycinate/SPc complex were observed using TEM (JEOL-1200, Japan). A few microliters of each sample were dropped on microgrid, treated with 2% phosphotungstic acid, and air-dried before the observation.

RNA-seq analysis and quantitative real time PCR (qRT-PCR) for gene expression changes

Tomato (*Solanum lycopersicum*) seedlings were cultured in growth chamber at 26°C under a 12-h light: 12-h dark photoperiod. The roots of 15 cm height seedlings were immersed in ddH_2O for 48 h, and then transferred to the solutions of calcium glycinate (0.4 mg/mL) and calcium glycinate/SPc complex (0.4 mg/mL at the mass ratio of 1:1) respectively. The whole seedlings were homogenized in liquid nitrogen at 3 d post immersion, and total RNAs were isolated using RNA simple Total RNA Kit (Tiangen, Beijing, China). Each treatment included 3 biological replicates.

RNA sequencing libraries were constructed and then sequenced on Illumina Hiseq platform (Biomics, Beijing, China). Raw data were purified by trimming the adapters and removing low quality reads ($Q \leq 10$), and the clean reads were assembled into contigs using Trinity software (Grabherr et al., 2011). Assembled transcripts were aligned to the reference genome (http://plants.ensembl.org/Solanum_lycopersicum/Info/Index) using TopHat2 (Kim et al., 2013). The expression level of each transcript was presented by FPKM values. The DEGs were analyzed using DESeq2 R package, and the genes with fold change ≥2 and with false discovery rate <0.01 were considered to be differentially expressed (Love et al., 2014).

QRT-PCR was further carried out to verify the DEGs using the primers in Table S1. Total RNAs were extracted from calcium glycinate or calcium glycinate/SPc complex-exposed seedlings, and the cDNAs were synthesized using Hifair First Strand cDNA Synthesis Kit (Yeasen Biotech, Shanghai, China). The qRT-PCR was conducted on ABI QuantStudio 6 Flex System (Thermo Fisher, MA, USA) using Perfect Start Green qPCR Super Mix (TransGen Biotech, Beijing, China). Reactions were carried out in triplicate following the amplification protocols: one cycle at 95°C for 10 min, 40 cycles of 95°C for 15 s, 57°C for 30 s, and 72°C for 35 s, and a melting curve ramp to confirm that each reaction did not produce nonspecific amplification. The *actin* gene was used as the internal control

for qRT-PCR, and the gene expression level was calculated using $2^{-\Delta\Delta Ct}$ method (Livak and Schmittgen, 2001).

Calcium transport assay

Fifty cm height tomato seedlings were cultured in ddH_2O for 48 h, and then transferred in the solutions of calcium glycinate and calcium glycinate/SPc complex similarly as above. The ddH_2O and SPc were also employed as controls. Each treatment included 3 independent samples. At 24 h after the treatment, all leaves were collected, dried and homogenized. The 0.2 g leaf tissues were added with 8 mL nitric acid, incubated for 3 h, and treated using microwave digestion system (MARS-6, CEM, Matthews, USA) that comprised a power system with selectable output of 0-1200 W. The heating program was (i) 1200 W for 60 min and (ii) 0 W for 25 min (cooling). The above samples were diluted with ddH_2O to the volume of 50 mL, and 10 mL sample was used to determine calcium content using the flame atomic absorption spectrometry (FAAS) system (TRACE AI1200, AURORA Instruments, Vancouver, Canada) equipped with deuterium lamp for background correction system. The lamp operated at 10 mA (wavelength 422.7 nm) for calcium content measurement. The calcium transport was calculated using the formula of calcium transport = calcium content in each treatment – calcium content in ddH_2O treatment. The standard calibration curve was constructed using $CaCO_3$. The 2.597 g $CaCO_3$ was dissolved in 100 mL H_2O, and added with 10 mL nitric acid to prepare the stock. The stock was further diluted with 5% nitric acid to prepare a series of $CaCO_3$ dilutions (Ca concentration: 10, 20, 40, 60, 80 and 100 mg/L), and the calcium content was examined similarly as above.

Bioactivity assay of SPc-loaded calcium glycinate

The bioactivity of SPc-loaded calcium glycinate was evaluated in a tomato greenhouse (Haotianyuan farm, Beijing, China) with a day/night temperature of 25/18°C. According to the field layout (Figure S1), the area of each plot was approximately 12 m^2, and each plot contained 30-40 seedlings. Each treatment included 3 independent plots. The formulations of calcium glycinate/SPc complex (0.8 and 0.4 mg/mL at the mass ratio of 1:1, 80% and 40% recommended field concentration), calcium glycinate (0.8 and 0.4 mg/mL), SPc (0.8 and 0.4 mg/mL) and H_2O were sprayed against tomato seedlings every 10 days for 5 times with the application amount of 140 mL/m^2.

The disease indexes (DIs) of seedlings treated with calcium glycinate/SPc complex (40% recommended concentration) and calcium glycinate were evaluated toward ToMV at 10 d after the third, fourth and fifth applications, respectively. All seedlings from each plot were observed to record disease grades that were classified as follows. Grade 0: no symptoms; Grade 1: mild malformation and mosaic of spear leaf; Grade 2: lesion area of all leaves was less than 1/3; Grade 3: leaf malformation and mosaic in all leaves; Grade 4: all leaves showing severe mosaic, dwarfing and malformation. DI and protective effect (PE) were calculated using the following formulas.

$$DI = \frac{\sum (\text{number of diseased plants} \times \text{grade})}{(\text{number of investigated plants} \times 4)} \times 100$$

$$PE = \left(1 - \frac{\text{DI in treatment plot}}{\text{DI in control plot}}\right) \times 100\,\%$$

Leaf photosynthetic rate and internodes length of seedlings were also measured at 10 d post the first and second application. According to the previous method (Zhang et al., 2021), leaf photosynthetic measurements were performed on fully expanded leaves (the second leaf from the top) at 9:00-10:00 a.m. using portable photosynthesis system (Shijiazhuang Shiya Technology, Co., Ltd, Shijiazhuang, China). Each leaf was allowed sufficient time for equilibration in chamber, and 5 leaves were tested in each plot. Internodes length was measured from the third to fourth leaf, and each plot contained 5 independent seedlings.

Data analysis

Statistical analysis was carried out using SPSS 26.0 software (SPSS Inc., New York, USA). Descriptive statistics are shown as the mean value and standard errors of the mean. Data was analyzed using the one-way ANOVA with Tukey HSD test or independent t test at the $P = 0.05$ level of significance.

Results

Loading capacity and self-assembly of calcium glycinate/SPc complex

The SPc could spontaneously combine with calcium glycinate into calcium glycinate/SPc complex in aqueous solution. The added calcium glycinate was excess for assembling with SPc, and the dialysis could separate free calcium glycinate from the mixture. The weight of freeze-dried sample was 255.3 mg (calcium glycinate/SPc complex), revealing that the weight of loaded calcium glycinate was 26.04 mg. The DLC was calculated to be 10.2%. Furthermore, the interaction forces between SPc and calcium glycinate was analyzed by ITC (Figure 1). The high affinity constant (K_a) of 2.68×10^5 suggested that there was a strong interaction between SPc and calcium glycinate, and the negative ΔG value of -11.35 kcal/mol revealed that this interaction was automatic. The negative values of ΔH

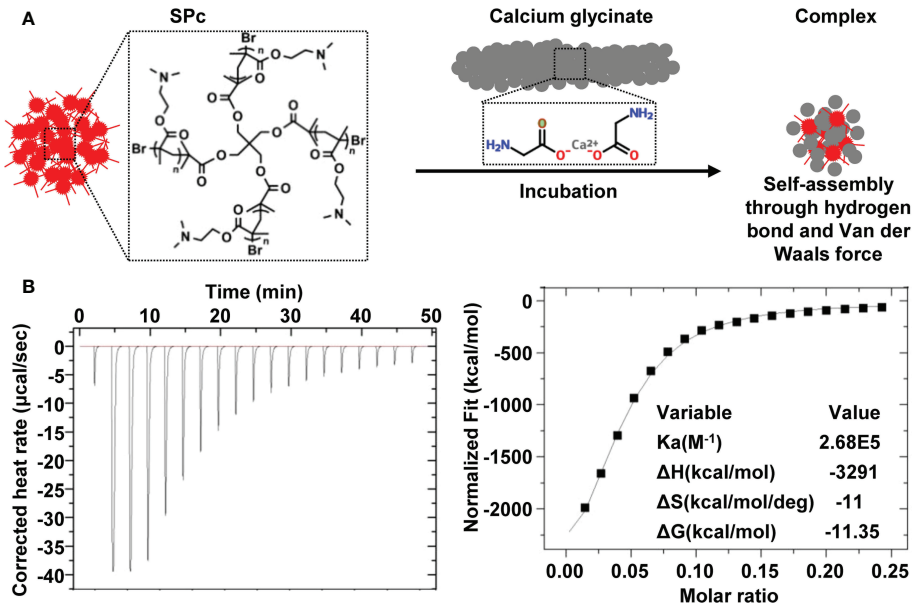

FIGURE 1
Schematic illustration of calcium glycinate/SPc complex **(A)** and ITC titration of SPc (250 μmol/L) into calcium glycinate solution (200 μmol/L) **(B)**.

and ΔS suggested that the self-assembly of calcium glycinate/SPc complex was through hydrogen bond and Van der Waals force.

Characterization of calcium glycinate/SPc complex

As shown in Figure 2 and Table 1, the self-assembly of calcium glycinate/SPc complex disturbed the self-aggregated structure of calcium glycinate, decreasing its particle size down to 17.7 nm. Meanwhile, small polydispersity value revealed good dispersity and stability of calcium glycinate/SPc complex in aqueous solution. Representative TEM images showed that the most of self-aggregated calcium glycinate was composed of stable rod-shaped particles, whereas the morphological characteristics of SPc-loaded calcium glycinate was remarkably changed, which was the spherical particle with much smaller size. Furthermore, the particle size of calcium glycinate/SPc complex was relatively stable after 14 d storage at room temperature.

Gene expression changes induced by calcium glycinate/SPc complex

Transcriptomic analysis was performed to illustrate the plant responses upon calcium glycinate/SPc complex exposure. The RNA samples had high sequencing quality (Table S2) and good parallelism (Figure S2). Compared to calcium glycinate/SPc complex, a total of 1842 DEGs were identified in tomatoes upon calcium glycinate exposure, among which 870 genes were up-regulated and 972 genes were down-regulated (Figure 3A). The DEGs could be divided into three categories including biological process, cellular component and molecular function, and GO enrichment analysis revealed that several signaling pathways related with defense response, transport, membrane, cell wall and calcium were strongly influenced (Figure 3B).

Typical DEGs with calcium glycinate/SPc complex exposure are shown in Figure 3C. Compared to calcium glycinate alone, calcium glycinate/SPc complex up-regulated many transport-related genes of tomatoes, such as *cyclic nucleotide-gated ion channel 1* (*CNGC1*), *putative calcium-transporting ATPase 11, plasma membrane-type* (*ACA11*), *ABC transporter C family member 3* (*ABCC3*), *ABCC4*, *oligopeptide transporter 4* (*OPT4*), etc. The up-regulation of these genes suggested the enhanced delivery of calcium glycinate with the help of SPc. Meanwhile, the SPc-loaded calcium glycinate also activated the expression of multiple disease resistance genes, such as *TMV resistance protein N*, *defensing-like protein 6*, *disease resistance protein RPP13* (*RPP13*), *putative late blight resistance protein homology R1B-14* (*R1B-14*), etc. The up-regulation of these genes suggested that the SPc-loaded calcium glycinate could further activate plant systemic immunity to resist adverse stresses. Furthermore, the expression of some other calcium-related genes was significantly altered by SPc-based nano-delivery system. More specifically, *sodium/calcium exchanger NCL* (*NCL*), *calcium-dependent protein kinase 18* (*CPK18*), *Probable calcium-binding protein CML10* (*CML10*), *Guard cell S-type anion channel SLAC1* (*SLAC1*), etc. were remarkably up-

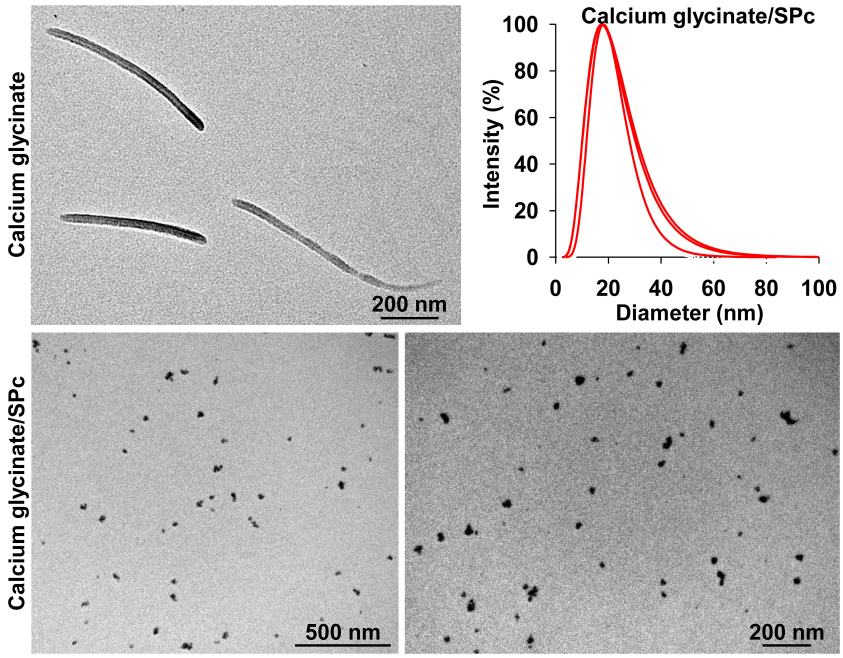

FIGURE 2
Transmission electron microscope image and particle size distribution of calcium glycinate/SPc complex at the mass ratio of 1:8.8.

TABLE 1 Particle size and polydispersity of SPc-loaded calcium glycinate before and after the storage.

Condition	Sample number	Polydispersity	Average polydispersity	Size (nm)	Average size (nm)
Before storage	1	0.147		18.10	
	2	0.244	0.215 ± 0.034	17.39	17.72 ± 0.21
	3	0.255		17.68	
After 14 d storage	1	0.241		17.70	
	2	0.245	0.239 ± 0.004	17.90	17.83 ± 0.07
	3	0.232		17.89	
			t = 0.695, df = 2.050, P = 0.557		t = 0.494, df = 4, P = 0.648

The independent t test was used to analyze the data at P = 0.05 level of significance.

regulated in tomato seedlings treated with SPc-loaded calcium glycinate. The quantitative real time PCR (qRT-PCR) analysis revealed that the expression levels of above genes were in accordance with transcriptome results (Figure S3). More specifically, expressions of *CNGC1*, *ACA11* and *TMV resistance protein N* genes were up-regulated by 5.13, 2.70 and 2.88-fold, respectively.

Enhanced transport of SPc-loaded calcium glycinate

Whether the nano-sized calcium glycinate exhibits stronger transport property is an interesting topic. The current study demonstrated that the SPc could promote the transport of calcium glycinate to increase the calcium content in tomato leaves (Figure 4). More specifically, the calcium content was increased from 17.58 to 22.38 g/mg with the help of SPc, and the calcium transport was accelerated by 3.17 times. Plant uptake and bioaccumulation are directly related with the bioactivity of calcium glycinate.

Enhanced bioactivity of SPc-loaded calcium glycinate

The DIs of tomato seedlings sprayed with calcium glycinate/SPc complex and calcium glycinate were firstly evaluated and

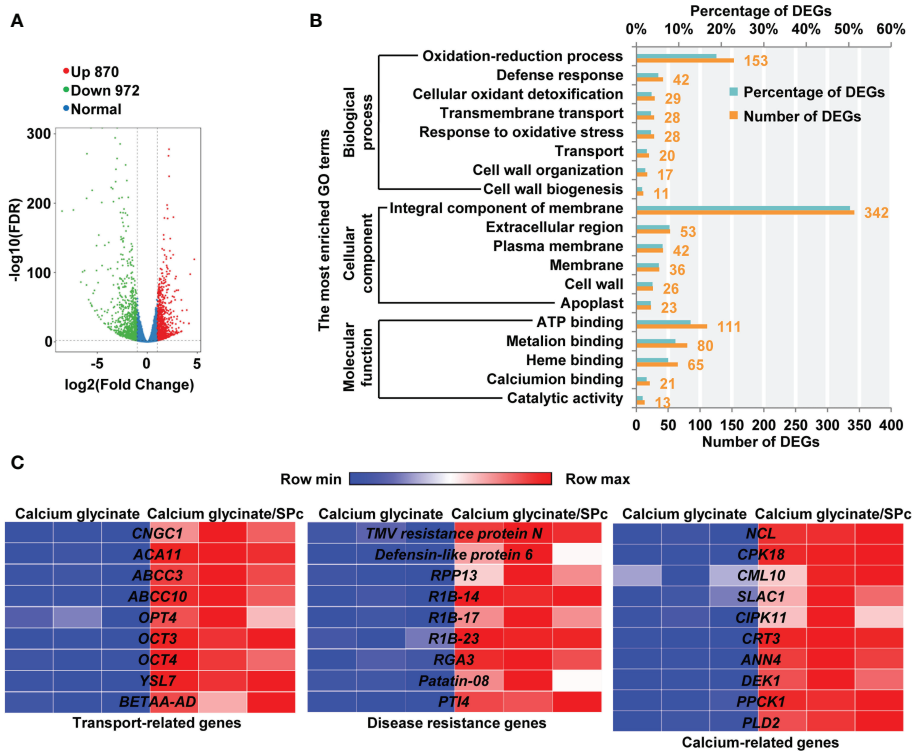

FIGURE 3
RNA-seq analysis of tomatoes treated with calcium glycinate and calcium glycinate/SPc complex. **(A)** Analysis of differentially expressed genes (DEGs) in tomatoes with a volcano plot. Up-regulated and down-regulated DEGs are represented by red and green dots, respectively. **(B)** GO enrichment analysis of DEGs in biological process, cellular component and molecular function. **(C)** Heatmaps of differentially expressed genes. Highly and lowly expressed genes are labeled as red and blue, respectively. Gene names are listed in the middle.

compared toward ToMV (Figure 5). Due to the SPc application, the control effect of calcium glycinate was significantly improved with DI reduction from 28.21 to 17.46 and 24.69 to 11.47 after the fourth and fifth applications, respectively. Meanwhile, the protective effect of calcium glycinate was significantly increased to 77.40% and 67.31% with the help of SPc after the third and fifth applications, revealing the good application prospect of calcium glycinate/SPc complex in field.

Leaf photosynthetic rate was also measured and compared to illustrate the enhanced bioactivity of SPc-loaded calcium glycinate. As shown in Figure 6A, the photosynthetic rate of tomato leaves was increased with the help of SPc, ranging from 6.90 to 8.42 μmol/m^2•s (80% concentration) and from 6.78 to 7.92 μmol/m^2•s (40% concentration) after the first application, revealing the stronger photosynthesis of tomato leaves. Furthermore, the internodes length of tomato seedlings tended to decrease by applying calcium glycinate/SPc complex compared to calcium glycinate alone, suggesting that the SPc-loaded calcium glycinate could be applied to control the unusual fast growth of tomato plants (Figure 6B).

Discussion

The SPc could spontaneously combine with calcium glycinate into calcium glycinate/SPc complex in aqueous solution. However, its DLC was lower than those toward pesticides such as imidaclothiz (16.31%), dinotefuran (17.41%) and osthole (17.09%) (Yan et al., 2021b; Jiang et al., 2022a; Jiang et al., 2022b). According to the previous interpretation of ITC data (Ross and Subramanian, 1981), the self-assembly of calcium glycinate/SPc complex was through hydrogen bond and Van der Waals force, and this interaction was automatic. The complexation of SPc with exogenous substance can be achieved *via* different interaction forces, such as electrostatic interaction with thiamethoxam (Yan et al., 2021a) and lufenuron (Zhang et al., 2022b), hydrogen bond and Van der Waals force with chitosan (Wang et al., 2021) and dinotefuran (Jiang et al., 2022a), and hydrophobic association with thiocyclam (Wang et al., 2022b). Thus, the application area of SPc is broad for delivering various types of exogenous substances.

The self-assembly of calcium glycinate/SPc complex disturbed the self-aggregated structure of calcium glycinate,

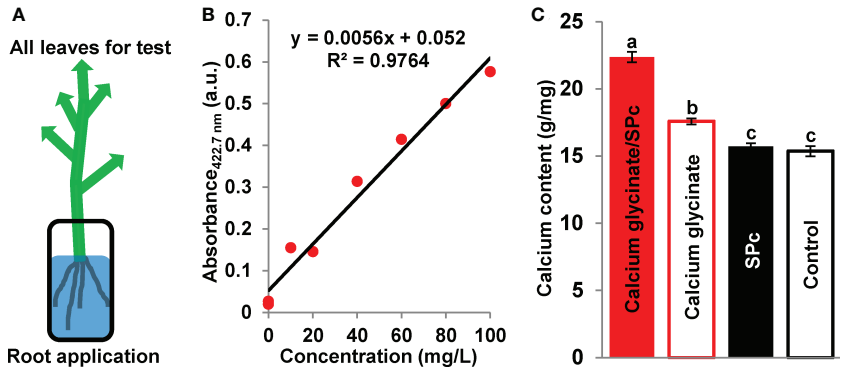

FIGURE 4
Enhanced transport of SPc-loaded calcium glycinate. **(A)** Schematic diagram. Tomato seedlings were cultured in the solutions of calcium glycinate and calcium glycinate/SPc complex for 24 h. All leaves were collected, dried and homogenized for calcium content measurement. **(B)** Standard calibration curve of calcium. **(C)** Calcium content in leaves. Each treatment included 3 independent samples. Different letters indicate significant differences according to Tukey HSD test ($P < 0.05$).

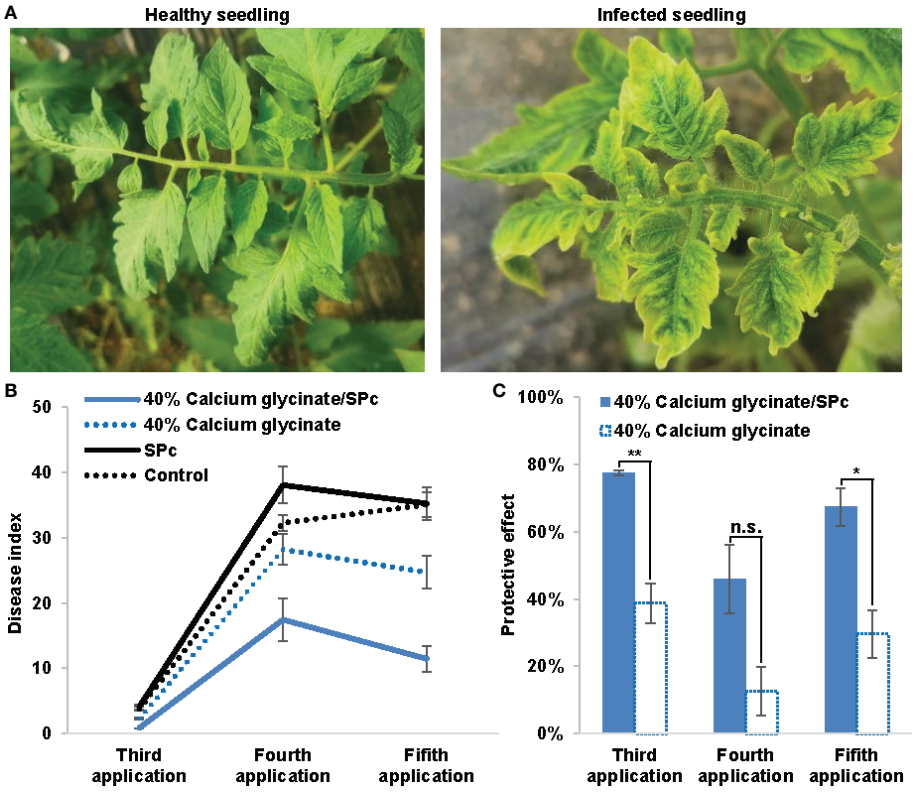

FIGURE 5
Enhanced bioactivity of SPc-loaded calcium glycinate toward tomato mosaic virus. **(A)** Photos of healthy and infected seedlings. **(B)** Disease indexes of seedlings were evaluated at 10 d post the third, fourth and fifth applications, respectively. All seedlings from each plot were observed to record the disease grades. **(C)** Protective effect was assessed by disease index. The "*" and "**" indicate significant differences (Independent *t* test, $P < 0.05$ and $P < 0.01$), and "n.s." indicates no significant difference.

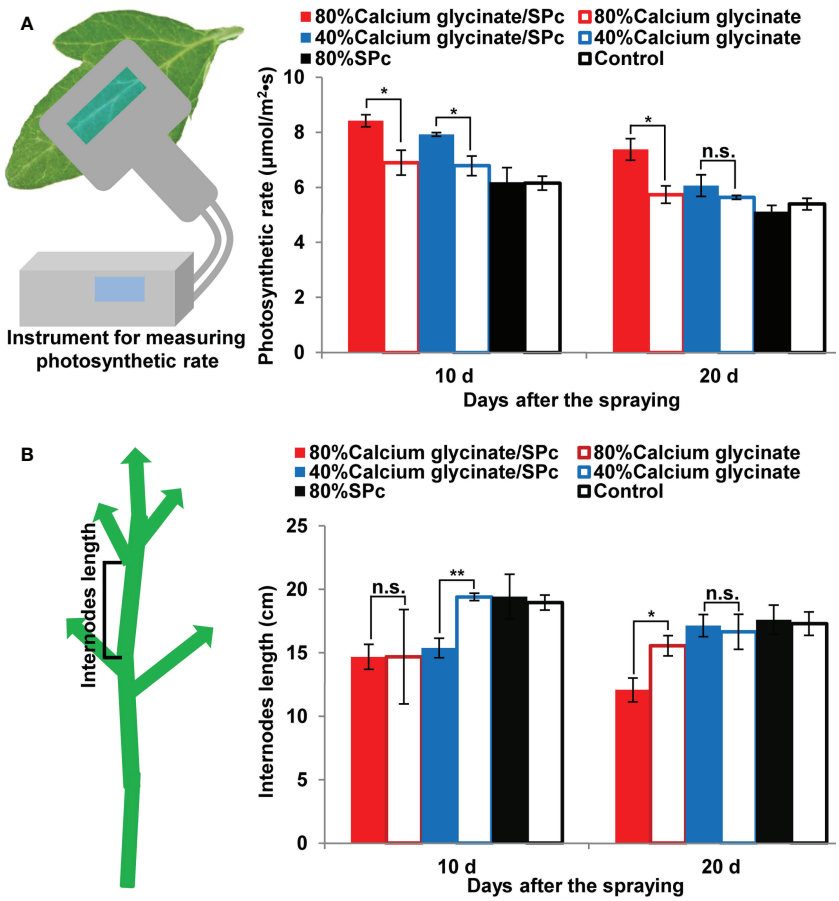

FIGURE 6
Effects of SPc-loaded calcium glycinate on the photosynthetic rate **(A)** and internodes length **(B)** of tomato leaves/seedlings. The seedlings were sprayed with various formulations at 80% and 40% recommended field concentration. The photosynthetic rate and internodes length were measured at 9:00-10:00 a.m. at 10 d post the first and second applications. Five leaves/seedlings were tested in each plot. The "*" and "**" indicate significant differences (Independent *t* test, $P < 0.05$ and $P < 0.01$), and "n.s." indicates no significant difference.

decreasing its particle size down to nanoscale. The SPc has been widely applied as a universal adjuvant for various pesticides, which can decrease the particle sizes of thiamethoxam, dinotefuran and osthole in aqueous solution (Yan et al., 2021a; Yan et al., 2021b; Jiang et al., 2022a). The smaller particle size of SPc-loaded calcium glycinate may be beneficial for not only improving plant uptake and systematic transmission, but also increasing nutrient-use efficiency to minimize nutrient losses.

Calcium is involved in mediating plant responses to various adverse environmental conditions, and some transcriptome studies have confirmed the great function of calcium in multiple responses to pathogens, wounding, heat stresses, salt stresses, etc. (Cheong et al., 2002; Navarro et al., 2004; Xu et al., 2015; Wang et al., 2019a). Compared to calcium glycinate alone, calcium glycinate/SPc complex up-regulated many transport-related genes of tomatoes. For instance, CNGC1 protein is responsible for cAMP-induced calcium entry in cells, thus is involved in calcium signal transduction (Sunkar et al., 2000). CAC11 is a magnesium-dependent enzyme that can catalyze the hydrolysis of ATP coupled with the translocation of calcium from the cytosol out of the cell or into organelles (Boursiac et al., 2010). The up-regulation of these two important genes suggested the enhanced delivery of calcium glycinate with the aid of SPc. Our previous studies have demonstrated that the endocytosis-related genes of plants/insects can be activated by SPc application to increase the cellular uptake (Wang et al., 2021; Ma et al., 2022b; Yang et al., 2022). The SPc can also promote the translocation of insect growth regulator/dsRNA across insect cuticle (Yan et al., 2020; Ma et al., 2022a; Zhang et al., 2022a; Zhang et al., 2022b).

The SPc-loaded calcium glycinate also activated the expression of multiple disease resistance genes. TMV resistance protein N can trigger the defense system to restrict the mosaic virus, and it's up-regulation leads to stronger

antiviral immunity (Whitham et al., 1994; Dinesh-Kumar and Baker, 2000; Marathe et al., 2002). Defensing-like protein is a major component of plant immune system, which plays an important role in host defenses against biotic and abiotic stresses (Spelbrink et al., 2004; Wang et al., 2019b). RPP13 guards the plants against pathogens containing an appropriate avirulence protein (Bittner-Eddy et al., 2000). Furthermore, the expression of some other calcium-related genes was also altered. NCL protein has the ability to bind calcium *in vitro*, which is involved in the maintenance of calcium homeostasis and response to auxin and salt stress (Wang et al., 2012; Li et al., 2016). As key messengers in signal transduction, CPKs are involved in responses to cold stress, salt stress, wounding and drought (Liu et al., 2018; Shu et al., 2020). The up-regulation of these important genes suggested that the SPc-loaded calcium glycinate could further activate plant systemic immunity to resist adverse stresses.

Vacuole deposition of calcium imposes the low mobility in phloem, which causes deleterious nutritional disorders (Gilliham et al., 2011; Kumar et al., 2015; Jovanović et al., 2021). The first step for the plant uptake of calcium is facilitated by cation exchange in soil, then calcium is transported apoplastically to endodermis, and finally calcium reaches the xylem sap and is translocated *via* the transpiration stream to aerial plant parts (Bauer et al., 2011; Ghosh et al., 2022). The current study demonstrated that the SPc could promote the transport of calcium glycinate to increase the calcium content in tomato leaves. The enhanced plant uptake of SPc-loaded agrochemicals has been previously observed in tobacco, oilseed rape and strawberry (Yan et al., 2021b; Jiang et al., 2022a; Jiang et al., 2022b). For instance, the SPc can increase the plant uptake of a synthetic pesticide dinotefuran for 1.45-1.53 times due to the smaller particle size and reduced contact angle (Jiang et al., 2022a). Meanwhile, a plant elicitor chitosan can be efficiently delivered into potato plants to amplify the plant defense responses with the help of SPc (Wang et al., 2021). Plant uptake and bioaccumulation are directly related with the bioactivity of calcium glycinate.

Calcium is an essential element in diverse biological processes, such as disease resistance and plant development (Springer et al., 2007; Wang et al., 2015; Tian et al., 2020; Guo et al., 2021). Extensive studies have demonstrated that the calcium changes can mediate plant defense against pathogen infections, and many exogenous agents are able to increase TMV tolerance through calcium signaling pathway (Lu et al., 2010; Li et al., 2019b). Meanwhile, our transcriptome and qRT-PCR results confirmed the up-regulation of many disease resistance genes especially *TMV resistance protein N*. Thus, the DIs of tomato seedlings sprayed with calcium glycinate/SPc complex and calcium glycinate were evaluated and compared toward ToMV. Due to the SPc application, the control effect of calcium glycinate was improved, indicating the good application prospect of calcium glycinate/SPc complex in field.

Previous studies have revealed that the exogenous calcium application can improve plant photosynthesis. For instance, the tobacco photosynthesis can be improved by $CaCl_2$ application under high temperature stress (Tian et al., 2011). Seed priming with $CaCl_2$ before germination can improve the photosynthesis of faba bean plants under cadmium stress (Nouairi et al., 2019). In the current study, the SPc application could further increase the photosynthesis of tomato plants induced by calcium glycinate. The potential mechanism of SPc-mediated bioactivity enhancement could be explained as follows. The SPc-based nano-delivery system decreased the particle size of calcium glycinate in aqueous solution, thus increasing the delivery/plant uptake of calcium glycinate for enhanced bioactivity. The SPc can act as a universal nanocarrier to deliver various agrochemicals for high utilization efficiency.

Conclusion

In summary, the current study constructed a SPc-based nano-delivery system to load calcium glycinate through hydrogen bond and Van der Waals force. The self-assembly of calcium glycinate/SPc complex formed stable spherical particles with nanoscale size (17.7 nm). Compared to calcium glycinate, calcium glycinate/SPc complex activated the expression of many transport-related genes and disease resistance genes in tomatoes, suggesting the enhanced transport and bioactivity of SPc-loaded calcium glycinate. As expected, the calcium content in tomato leaves was increased from 17.58 to 22.38 g/mg with the help of SPc, and the control effect of calcium glycinate was significantly improved toward ToMV with DI reduction from 24.69 to 11.47 after the fifth application. Furthermore, SPc-loaded calcium glycinate could be applied to increase the leaf photosynthetic rate and control the unusual fast growth of tomatoes. The current calcium nutrition nanoagent can be sprayed directly to plant leaves for increasing nutrient-use efficiency and antiviral immunity in actual production.

Data availability statement

The original contributions presented in the study are publicly available. This data can be found here: NCBI, PRJNA907413.

Author contributions

SY and QH contributed equally to this study. SY, JS, and XD designed the research. SY, QH, YW, QJ, and MD performed the research. All authors analyzed the date. SY wrote the paper.

Funding

This work was supported by the Modern Agricultural Industrial Technology System Beijing Innovation Team (BAIC08-2022-YJ03) and National Natural Science Foundation of China (32072497).

Conflict of interest

The authors declare that the research was conducted in the absence of any commercial or financial relationships that could be construed as a potential conflict of interest.

Publisher's note

All claims expressed in this article are solely those of the authors and do not necessarily represent those of their affiliated organizations, or those of the publisher, the editors and the reviewers. Any product that may be evaluated in this article, or claim that may be made by its manufacturer, is not guaranteed or endorsed by the publisher.

Supplementary material

The Supplementary Material for this article can be found online at: https://www.frontiersin.org/articles/10.3389/fpls.2022.1092774/full#supplementary-material

References

Bauer, P., Elbaum, R., and Weiss, I. M. (2011). Calcium and silicon mineralization in land plants: transport, structure and function. *Plant Sci.* 180, 746–756. doi: 10.1016/j.plantsci.2011.01.019

Bittner-Eddy, P. D., Crute, I. R., Holub, E. B., and Beynon, J. L. (2000). *RPP13* is a simple locus in *Arabidopsis thaliana* for alleles that specify downy mildew resistance to different avirulence determinants in *Peronospora parasitica*. *Plant J.* 21, 177–188. doi: 10.1046/j.1365-313x.2000.00664.x

Boursiac, Y., Lee, S. M., Romanowsky, S., Blank, R., Sladek, C., Chung, W. S., et al. (2010). Disruption of the vacuolar calcium-ATPases in arabidopsis results in the activation of a salicylic acid-dependent programmed cell death pathway. *Plant Physiol.* 154, 1158–1171. doi: 10.1104/pp.110.159038

Carmona, F. J., Guagliardi, A. , and Masciocchi, N. (2022). Nanosized calcium phosphates as novel macronutrient nano-fertilizers. *Nanomaterials* 12, 2709. doi: 10.3390/nano12152709

Cheong, Y. H., Chang, H. S., Gupta, R., Wang, X., Zhu, T., and Luan, S. (2002). Transcriptional profiling reveals novel interactions between wounding, pathogen, abiotic stress, and hormonal responses in arabidopsis. *Plant Physiol.* 129, 661–677. doi: 10.1104/pp.002857

Chhipa, H. (2016). Nanofertilizers and nanopesticides for agriculture. *Environ. Chem. Lett.* 15, 15–22. doi: 10.1007/s10311-016-0600-4

Demidchik, V., Shabala, S., Isayenkov, S., Cuin, T. A., and Pottosin, I. (2018). Calcium transport across plant membranes: mechanisms and functions. *New Phytol.* 220, 49–69. doi: 10.1111/nph.15266

Dinesh-Kumar, S. P., and Baker, B. J. (2000). Alternatively spliced *N* resistance gene transcripts: their possible role in tobacco mosaic virus resistance. *P. Natl. Acad. Sci. U.S.A.* 97, 1908–1913. doi: 10.1073/pnas.020367497

El-Ghany, M. F. A., El-Kherbawy, M. I., Abdel-Aal, Y. A., El-Dek, S. I., and Abd El-Baky, T. (2021). Comparative study between traditional and nano calcium phosphate fertilizers on growth and production of snap bean (*Phaseolus vulgaris* l.) plants. *Nanomaterials* 11, 2913. doi: 10.3390/nano11112913

Fellet, G., Pilotto, L., Marchiol, L., and Braidot, E. (2021). Tools for nano-enabled agriculture: fertilizers based on calcium phosphate, silicon, and chitosan nanostructures. *Agronomy* 11, 1239. doi: 10.3390/agronomy11061239

Ghosh, S., Bheri, M., Bisht, D., and Pandey, G. K. (2022). Calcium signaling and transport machinery: potential for development of stress tolerance in plants. *Curr. Plant Biol.* 29, 100235. doi: 10.1016/j.cpb.2022.100235

Gilliham, M., Dayod, M., Hocking, B. J., Xu, B., Conn, S. J., Kaiser, B. N., et al. (2011). Calcium delivery and storage in plant leaves: exploring the link with water flow. *J. Exp. Bot.* 62, 2233–2250. doi: 10.1093/jxb/err111

Grabherr, M. G., Haas, B. J., Yassour, M., Levin, J. Z., Thompson, D. A., Amit, I., et al. (2011). Full-length transcriptome assembly from RNA-seq data without a reference genome. *Nat. Biotechnol.* 29, 644–652. doi: 10.1038/nbt.1883

Guo, Y., Liu, Y., Zhang, Y., Liu, J., Gul, Z., Guo, X. R., et al. (2021). Effects of exogenous calcium on adaptive growth, photosynthesis, ion homeostasis and phenolics of *Gleditsia sinensis* lam. plants under salt stress. *Agriculture* 11, 978. doi: 10.3390/agriculture11100978

Jakhar, A. M., Aziz, I., Kaleri, A. R., Hasnain, M., Haider, G., Ma, J., et al. (2022). Nano-fertilizers: a sustainable technology for improving crop nutrition and food security. *NanoImpact* 27, 100411. doi: 10.1016/j.impact.2022.100411

Jiang, Q., Peng, M., Yin, M., Shen, J., and Yan, S. (2022b). Nanocarrier-loaded imidaclothiz promotes plant uptake and decreases pesticide residue. *Int. J. Mol. Sci.* 23, 6651. doi: 10.3390/ijms23126651

Jiang, Q., Xie, Y., Peng, M., Wang, Z., Li, T., Yin, M., et al. (2022a). A nanocarrier pesticide delivery system with promising benefits in the case of dinotefuran: strikingly enhanced bioactivity and reduced pesticide residue. *Environ. Sci. Nano* 9, 988–999. doi: 10.1039/D1EN00752A

Jovanović, P., Rachmilevitch, S., Roitman, N., and Erel, R. (2021). Strontium as a tracer for calcium: uptake, transport and partitioning within tomato plants. *Plant Soil* 466, 303–316. doi: 10.1007/s11104-021-05024-6

Kim, D., Pertea, G., Trapnell, C., Pimentel, H., Kelley, R., and Salzberg, S. L. (2013). TopHat2: accurate alignment of transcriptomes in the presence of insertions, deletions and gene fusions. *Genome Biol.* 14, R36. doi: 10.1186/gb-2013-14-4-r36

Knight, H., Trewavas, A. J., and Knight, M. R. (1997). Calcium signalling in *Arabidopsis thaliana* responding to drought and salinity. *Plant J.* 12, 1067–1078. doi: 10.1046/j.1365-313X.1997.12051067.x

Kumar, A., Singh, U. M., Manohar, M., and Gaur, V. S. (2015). Calcium transport from source to sink: understanding the mechanism(s) of acquisition, translocation, and accumulation for crop biofortification. *Acta Physiol. Plant* 37, 1722. doi: 10.1007/s11738-014-1722-6

Li, M., Ma, Z., Peng, M., Li, L., Yin, M., Yan, S., et al. (2022). A gene and drug co-delivery application helps to solve the short life disadvantage of RNA drug. *Nano Today* 43, 101452. doi: 10.1016/j.nantod.2022.101452

Li, J., Qian, J., Xu, Y., Yan, S., Shen, J., and Yin, M. (2019a). A facile-synthesized star polycation constructed as a highly efficient gene vector in pest management. *ACS Sustain. Chem. Eng.* 7, 6316–6322. doi: 10.1021/acssuschemeng.9b00004

Li, Z., Shi, J., Hu, D., and Song, B. (2019b). A polysaccharide found in *Dendrobium nobile* lindl stimulates calcium signaling pathway and enhances tobacco defense against TMV. *Int. J. Biol. Macromol.* 137, 1286–1297. doi: 10.1016/j.ijbiomac.2019.06.179

Liu, Y., Xu, C., Zhu, Y., Zhang, L., Chen, T., Zhou, F., et al. (2018). The calcium-dependent kinase OsCPK24 functions in cold stress responses in rice. *J. Integr. Plant Biol.* 60, 173–188. doi: 10.1111/jipb.12614

Livak, K. J., and Schmittgen, T. D. (2001). Analysis of relative gene expression data using real-time quantitative PCR and the $2^{-\Delta\Delta CT}$ method. *Methods* 25, 402–408. doi: 10.1006/meth.2001.1262

Li, P., Zhang, G., Gonzales, N., Guo, Y., Hu, H., Park, S., et al. (2016). Ca^{2+}-regulated and diurnal rhythm-regulated Na^{+}/Ca^{2+} exchanger AtNCL affects flowering time and auxin signaling in *Arabidopsis*. *Plant Cell Environ.* 39, 377–392. doi: 10.1111/pce.12620

Love, M. I., Huber, W., and Anders, S. (2014). Moderated estimation of fold change and dispersion for RNA-seq data with DESeq2. *Genome Biol.* 15, 550. doi: 10.1186/s13059-014-0550-8

Lu, H., Zhao, X., Wang, W., Yin, H., Xu, J., Bai, X., et al. (2010). Inhibition effect on *tobacco mosaic virus* and regulation effect on calreticulin of oligochitosan in tobacco by induced Ca^{2+} influx. *Carbohyd. Polym.* 82, 136–142. doi: 10.1016/j.carbpol.2010.04.049

Marathe, R., Anandalakshmi, R., Liu, Y., and Dinesh-Kumar, S. P. (2002). The tobacco mosaic virus resistance gene, n. *Mol. Plant Pathol.* 3, 167–172. doi: 10.1046/j.1364-3703.2002.00110.x

Ma, Z., Zhang, Y., Li, M., Chao, Z., Du, X., Yan, S., et al. (2022a). A first greenhouse application of bacteria-expressed and nanocarrier-delivered RNA pesticide for *Myzus persicae* control. *J. Pest Sci*. doi: 10.1007/s10340-022-01485-5

Ma, Z., Zheng, Y., Chao, Z., Chen, H., Zhang, Y., Yin, M., et al. (2022b). Visualization of the process of a nanocarrier-mediated gene delivery: stabilization, endocytosis and endosomal escape of genes for intracellular spreading. *J. Nanobiotechnol.* 20, 124. doi: 10.1186/s12951-022-01336-6

Monshausen, G. B., Miller, N. D., Murphy, A. S., and Gilroy, S. (2011). Dynamics of auxin-dependent Ca^{2+} and pH signaling in root growth revealed by integrating high-resolution imaging with automated computer vision-based analysis. *Plant J.* 65, 309–318. doi: 10.1111/j.1365-313X.2010.04423.x

Navarro, L., Zipfel, C., Rowland, O., Keller, I., Robatzek, S., Boller, T., et al. (2004). The transcriptional innate immune response to flg22. interplay and overlap with avr gene-dependent defense responses and bacterial pathogenesis. *Plant Physiol.* 135, 1113–1128. doi: 10.1104/pp.103.036749

Nouairi, I., Jalali, K., Zribi, F., Barhoumi, F., Zribi, K., and Mhadhbi, H. (2019). Seed priming with calcium chloride improves the photosynthesis performance of faba bean plants subjected to cadmium stress. *Photosynthetica* 57, 438–445. doi: 10.32615/ps.2019.055

Ross, P. D., and Subramanian, S. (1981). Thermodynamics of protein association reactions: forces contributing to stability. *Biochemistry* 20, 3096–3102. doi: 10.1021/bi00514a017

Shu, B., Jue, D., Zhang, F., Zhang, D., Liu, C., Wu, Q., et al. (2020). Genome-wide identification and expression analysis of the citrus calcium-dependent protein kinase (CDPK) genes in response to arbuscular mycorrhizal fungi colonization and drought. *Biotechnol. Biotec. Eq.* 34, 1304–1314. doi: 10.1080/13102818.2020.1837011

Spelbrink, R. G., Dilmac, N., Allen, A., Smith, T. J., Shah, D. M., and Hockerman, G. H. (2004). Differential antifungal and calcium channel-blocking activity among structurally related plant defensins. *Plant Physiol.* 135, 2055–2067. doi: 10.1104/pp.104.040873

Springer, Y. P., Hardcastle, B. A., and Gilbert, G. S. (2007). Soil calcium and plant disease in serpentine ecosystems: a test of the pathogen refuge hypothesis. *Oecologia* 151, 10–21. doi: 10.1007/s00442-006-0566-1

Sunkar, R., Kaplan, B., Bouché, N., Arazi, T., Dolev, D., Talke, I. N., et al. (2000). Expression of a truncated tobacco *NtCBP4* channel in transgenic plants and disruption of the homologous *Arabidopsis CNGC1* gene confer Pb^{2+} tolerance. *Plant J.* 24, 533–542. doi: 10.1046/j.1365-313x.2000.00901.x

Thor, K. (2019). Calcium-nutrient and messenger. *Front. Plant Sci.* 10, 440. doi: 10.3389/fpls.2019.00440

Tian, W., Meng, Q. W., Brestic, M., Olsovska, K., and Yang, X. (2011). Photosynthesis is improved by exogenous calcium in heat-stressed tobacco plants. *J. Plant Physiol.* 168, 2063–2071. doi: 10.1016/j.jplph.2011.06.009

Tian, W., Wang, C., Gao, Q., Li, L., and Luan, S. (2020). Calcium spikes, waves and oscillations in plant development and biotic interactions. *Nat. Plants* 6, 750–759. doi: 10.1038/s41477-020-0667-6

Wang, P., Li, Z., Wei, J., Zhao, Z., Sun, D., and Cui, S. (2012). A Na^+/Ca^{2+} exchanger-like protein (AtNCL) involved in salt stress in *Arabidopsis*. *J. Biol. Chem.* 287, 44062–44070. doi: 10.1074/jbc.M112.351643

Wang, J. P., Munyampundu, J. P., Xu, Y. P., and Cai, X. Z. (2015). Phylogeny of plant calcium and calmodulin-dependent protein kinases (CCaMKs) and functional analyses of tomato CCaMK in disease resistance. *Front. Plant Sci.* 6, 1075. doi: 10.3389/fpls.2015.01075

Wang, Q., Qiu, B. L., Li, S., Zhang, Y. P., Cui, X. M., Ge, F., et al. (2019b). A methyl jasmonate induced defensing like protein from panax notoginseng confers resistance against *Fusarium solani* in transgenic tobacco. *Biol. Plantarum* 63, 797–807. doi: 10.32615/bp.2019.123

Wang, D., Saleh, N. B., Byro, A., Zepp, R., Sahle-Demessie, E., Luxton, T. P., et al. (2022a). Nano-enabled pesticides for sustainable agriculture and global food security. *Nat. Biotechnol.* 17, 347–360. doi: 10.1038/s41565-022-01082-8

Wang, Y., Xie, Y. H., Jiang, Q. H., Chen, H. T., Ma, R. H., Wang, Z. J., et al. (2022b). Efficient polymer-mediated delivery system for thiocyclam: nanometerization remarkably improves the bioactivity toward green peach aphids. *Insect Sci.* doi: 10.1111/1744–7917.13033

Wang, M., Zhang, X., Li, Q., Chen, X., and Li, X. (2019a). Comparative transcriptome analysis to elucidate the enhanced thermotolerance of tea plants (*Camellia sinensis*) treated with exogenous calcium. *Planta* 249, 775–786. doi: 10.1007/s00425-018-3039-y

Wang, X., Zheng, K., Cheng, W., Li, J., Liang, X., Shen, J., et al. (2021). Field application of star polymer-delivered chitosan to amplify plant defense against potato late blight. *Chem. Eng. J.* 417, 129327. doi: 10.1016/j.cej.2021.129327

White, P. J. (2001). The pathways of calcium movement to the xylem. *J. Exp. Bot.* 52, 891–899. doi: 10.1093/jexbot/52.358.891

White, P. J., and Broadley, M. R. (2003). Calcium in plants. *Ann. Bot.* 92, 487–511. doi: 10.1093/aob/mcg164

Whitham, S., Dinesh-Kumar, S. P., Choi, D., Hehi, R., Corr, C., and Baker, B. (1994). The product of the tobacco mosaic virus resistance gene *N*: similarity to toll and the interleukin-1 receptor. *Cell* 78, 1101–1115. doi: 10.1016/0092-8674(94)90283-6

Xu, Y., Li, X., Lin, J., Wang, Z., Yang, Q., and Chang, Y. (2015). Transcriptome sequencing and analysis of major genes involved in calcium signaling pathways in pear plants (*Pyrus calleryana* decne.). *BMC Genomics* 16, 738. doi: 10.1186/s12864-015-1887-4

Yan, S., Cheng, W. Y., Han, Z. H., Wang, D., Yin, M. Z., Du, X. G., et al. (2021a). Nanometerization of thiamethoxam by a cationic star polymer nanocarrier efficiently enhances the contact and plant-uptake dependent stomach toxicity against green peach aphids. *Pest Manage. Sci.* 77, 1954–1962. doi: 10.1002/ps.6223

Yan, S., Gu, N., Peng, M., Jiang, Q., Liu, E., Li, Z., et al. (2022). A preparation method of nano-pesticide improves the selective toxicity toward natural enemies. *Nanomaterials* 12, 2419. doi: 10.3390/nano12142419

Yang, J., Yan, S., Xie, S., Yin, M., Shen, J., Li, Z., et al. (2022). Construction and application of star polycation nanocarrier-based microRNA delivery system in *Arabidopsis* and maize. *J. Nanobiotechnol.* 20, 219. doi: 10.1186/s12951-022-01443-4

Yan, S., Hu, Q., Jiang, Q., Chen, H., Wei, J., Yin, M., et al. (2021b). Simple osthole/nanocarrier pesticide efficiently controls both pests and diseases fulfilling the need of green production of strawberry. *ACS Appl. Mater. Inter.* 13, 36350–36360. doi: 10.1021/acsami.1c09887

Yan, S., Qian, J., Cai, C., Ma, Z., Li, J., Yin, M., et al. (2020). Spray method application of transdermal dsRNA delivery system for efficient gene silencing and pest control on soybean aphid *Aphis glycines*. *J. Pest Sci.* 93, 449–459. doi: 10.1007/s10340-019-01157-x

Yin, L. H., Liu, X. P., Yi, L. Y., Wang, J., Zhang, Y. J., and Feng, Y. F. (2017). Structural characterization of calcium glycinate, magnesium glycinate and zinc glycinate. *J. Innov. Opt. Heal. Sci.* 10, 1650052. doi: 10.1142/S1793545816500528

Zhang, Y., Chen, H., Li, S., Li, Y., Kanwar, M. K., Li, B., et al. (2021). Comparative physiological and proteomic analyses reveal the mechanisms of brassinolide-mediated tolerance to calcium nitrate stress in tomato. *Front. Plant Sci.* 12, 724288. doi: 10.3389/fpls.2021.724288

Zhang, Y. H., Ma, Z. Z., Zhou, H., Chao, Z. J., Yan, S., and Shen, J. (2022a). Nanocarrier-delivered dsRNA suppresses wing development of green peach aphids. *Insect Sci.* 29, 669–682. doi: 10.1111/1744-7917.12953

Zhang, S., Pan, Y., Tian, W., Dong, M., Zhu, H., Luan, S., et al. (2017). *Arabidopsis* CNGC14 mediates calcium influx required for tip growth in root hairs. *Mol. Plant* 10, 1004–1006. doi: 10.1016/j.molp.2017.02.007

Zhang, L., Yan, S., Li, M., Wang, Y., Shi, X., Liang, P., et al. (2022b). Nanodelivery system alters an insect growth regulator's action mode: From oral feeding to topical application. *ACS Appl. Mater. Inter.* 14, 35105–35113. doi: 10.1021/acsami.2c08239

Zuverza-Mena, N., Martínez-Fernández, D., Du, W., Hernandez-Viezcas, J. A., Bonilla-Bird, N., López-Moreno, M. L., et al. (2017). Exposure of engineered nanomaterials to plants: insights into the physiological and biochemical responses-a review. *Plant Physiol. Biochem.* 110, 236–264. doi: 10.1016/j.plaphy.2016.05.037

frontiers | Frontiers in Plant Science

TYPE Opinion
PUBLISHED 15 December 2022
DOI 10.3389/fpls.2022.1081740

OPEN ACCESS

EDITED BY
Weicong Qi,
Jiangsu Academy of Agricultural Sciences (JAAS), China

REVIEWED BY
Hongchun Xiong,
Institute of Crop Sciences (CAAS), China
Hongwei Cai,
China Agricultural University, China

*CORRESPONDENCE
Le Luo
luole@njau.edu.cn

SPECIALTY SECTION
This article was submitted to Plant Bioinformatics, a section of the journal Frontiers in Plant Science

RECEIVED 27 October 2022
ACCEPTED 16 November 2022
PUBLISHED 15 December 2022

CITATION
Luo L (2022) Is strigolactone signaling a key player in regulating tiller formation in response to nitrogen? *Front. Plant Sci.* 13:1081740. doi: 10.3389/fpls.2022.1081740

Is strigolactone signaling a key player in regulating tiller formation in response to nitrogen?

Le Luo*

MOA Key Laboratory of Plant Nutrition and Fertilization in Lower-Middle Reaches of the Yangtze River and State Key Laboratory of Crop Genetics and Germplasm Enhancement, Nanjing Agricultural University, Nanjing, China

KEYWORDS

nitrogen, tiller, strigolactones, rice, signal, plant hormone

Introduction

Rice (*Oryza sativa* L.) is one of the most important food crops, feeding half of the world's population. Its yield relies on its agronomy traits, such as the number of panicles (also known as effective tiller), the number of grains per panicle, and the grain weight. Uncovering and elucidating the mechanism which could influence or regulate rice tiller developments is thus interesting, because it would provide a theoretical foundation for yield promotion.

Rice tillers are developed from the tiller buds located in the axils of leaves. The tiller bud is composed of the axillary meristem and the leaf primordia generating from the lateral meristem. Some of the tiller buds (including effective tillers and ineffective tillers) are activated to grow and form new leaf primordia and finally develop as tillers bearing panicles, whereas other tiller buds are found to stop growing after formation, without elongation, but in dormancy (Oikawa and Kyozuka, 2009). Recently, many genes regulating the growth and development of tiller buds in rice have been identified, so the regulatory mechanism and factors underlying tiller bud growth has gradually elucidated. Among these factors, plant hormone strigolactone (SL) and its biosynthesis and signaling pathway genes play the most prominent role in dominating rice tiller formation (Umehara et al., 2008; Gomez-Roldan et al., 2008). On the other hand, the growth of tiller bud is affected not only by the endogenous hormone signal but also by the environmental factors largely, such as water and nutrition.

Nitrogen (N) is one of the essential macronutrients needed by all plant species, and N deficiency hinders plant growth, thus decreasing yield (Stitt and Krapp, 1999; Good et al., 2004). A study on rice tiller formation has shown that the number of tillers in rice plant was decreased significantly under low-N conditions, whereas it could be significantly

increased with sufficient N supply. To date, several genes coding such as nitrate transporters and transcription factors (TFs) have been identified as they are relevant in tiller formation in response to N supplies in the form of nitrate (NO_3^-) and ammonium (NH_4^+) mostly (Liu et al., 2021).

Although SL plays the key role in regulating tiller formation, little is known whether its biosynthesis and signaling genes are involved in N-dependent tiller formation. Therefore, in this opinion paper, we highlighted the emerging evidence to support a potential role of SL in mediating tiller formation in response to N availability. It further allows expanding the knowledge of the molecular mechanisms underlying tiller formation in response to environmental signals.

Nitrogen regulation of tiller number

Application of N fertilizer can accelerate the growth and increase the number of rice tillers, when excessive N application decreases the number of effective tillers (Haque and Haque, 2016). Nitrate/peptide transporter family (NPF/NRT) genes have been reported to regulate tiller number and panicle structure *via* modulating nitrogen absorption and transport (Huang et al., 2018; Wang et al., 2018; Huang W.T. et al., 2019). Overexpression of *NRT2.3b*, which encodes a nitrate transporter, increased the panicle length, number of branches, number of seeds per panicle, and seed setting rate (Fan et al., 2016). *NPF7.7* can increase the inflow of both NO_3^- and NH_4^+, thereby promoting the number of effective tillers and effective panicles of rice and grain yield (Huang et al., 2018). *NPF7.1* overexpression or *NPF7.4* knockout could promote rice axillary buds' outgrowth, thereby increasing the number of tillers in rice (Huang W.T. et al., 2019). Additionally, the low-affinity nitrate transporter *NPF7.2* can activate the cell division of tiller buds, thereby increasing the number of tillers and grain yield (Wang et al., 2018).

Studies on amino acid transporters (AATs/AAPs) have also suggested that they are involved in the regulation of tiller development. Knocking out *AAP3* can promote the growth of buds and the number of effective tillers, thereby increasing rice grain yield; *AAP3* overexpression leads to the accumulation of amino acids *in vivo* but inhibits the growth of tiller buds (Lu et al., 2018). *OsAAP5* can affect rice tiller number and yield by regulating cytokinin (CK) biosynthesis (Wang et al., 2019). The amino acid biosynthesis genes are also involved in the regulation of tiller growth. The mutant of *asparagine synthetase 1* (*ASN1*) in rice reduces the concentration of asparagine and inhibits tiller bud outgrowth, hence restraining the number of tillers. It indicates that *ASN1* is involved in the bioprocess regulating rice tiller development (Luo et al., 2019b). Glutamine synthetase GS1;2 functions in the primary assimilation of NH_4^+ and promotes the growth of tiller buds by regulating N-dependent biosynthesis of phytohormone cytokinin (Ohashi et al., 2017).

In addition to cytokinin, other phytohormones and several TFs are also involved into the process of which N regulates tiller outgrowth deeply. For instance, the gibberellin (GA) signaling pathway was identified to be essential for N regulation on tiller number (Wu et al., 2020). GA can reduce the epigenetic modification and induce the expression of target genes by promoting the degradation of APETALA2-domain transcription factor NGR5, resulting in the inhibition of N-induced growth and development of tiller buds; the excellent allele *GRF4 ngr2* can largely increase tiller number and thus result in high NUE in the current high-yielding rice (Li et al., 2018). Meanwhile, a MADS box transcription factor OsMADS57, which is induced by nitrate, interacts with TEOSINTE BRANCHED1 (TB1) and Dwarf14 (D14) to control the growth of axillary buds (Guo et al., 2013; Huang S. J. et al., 2019). Most recently, through a genome-wide association study on nitrogen use efficiency and N regulation of tiller number, TCP19, encoding a TCP transcription factor family member, was identified to inhibit N-regulated tillering by promoting *DLT* expression (Liu et al., 2021). The nitrogen-induced LATERAL ORGAN BOUNDARIES DOMAIN (LBD) proteins OsLBD37 and OsLBD39 can directly bind to the promoter of *OsTCP19* and inhibit its activity, and *OsTCP19*, in turn, regulates tiller number and N use efficiency (NUE).

Strigolactone plays a central role in the gene regulatory network of rice tiller development

In rice, SLs are biosynthesized from β-carotene, which is converted to carlactone (CL) by β-carotene isomerases CAROTINOID CLEAVAGE DEOXYGENASE 7 (CCD7) and CCD8, encoded by *DWARF17* (*D17*) and *D10*, respectively (Zou et al., 2006; Arite et al., 2007; Lin et al., 2009; Lopez-Obando et al., 2015; Waters et al., 2017). CL is further catalyzed to several types of SLs (Zhang et al., 2014). Finally, the SLs are percepted by DWARF14 (D14), which triggers the formation of a complex of D14, D3, and D53, leading to ubiquitination of D53 by the action of D3 and downstream genes (Arite et al., 2009; Gao et al., 2009; Liu et al., 2009; Jiang et al., 2013; Zhou et al., 2013; Lopez-Obando et al., 2015; Waters et al., 2017). Importantly, the mutants of SL biosynthesis genes *D10* and *D17* and SL signaling genes *D14*, *D3*, and *D53* all have increased the tiller number, suggesting a negative regulation role of SL on tiller number.

So far, several important factors dominating rice tiller development have been found to interact with the SL pathway. For instance, the well-known tiller-number suppressor, TB1, interacts with MADS57 to regulate tiller number by downregulating the expression of SL receptor gene *D14* (Guo et al., 2013). *Ideal Plant Architecture 1* (*IPA1*), which encodes a SQUAMOSA PROMOTER BINDING PROTEIN-LIKE (SPL) family TF *SPL14*, plays a significant role regulating rice plant

architecture (Jiao et al., 2010; Miura et al., 2010). Later, it was identified as a downstream gene of the SL signal pathway and relevant to tiller number (Song et al., 2017). IPA1 can directly interact with D53, the key repressor of the SL signaling, and *IPA1* expression is suppressed by D53. On the other hand, IPA1 can bind to the promoter of *D53* and activate its expression, suggesting a feedback regulation between IPA1 and SL (Song et al., 2017).

Previous studies also suggest crosstalk between SL and other plant hormones during rice tiller development. For example, auxin has similar negative regulation on tiller number as SL, which suggests auxin may act in the upstream of the SL pathway. This is supported by evidence that auxin can induce the expressions of SL biosynthesis genes *MAX3*/*D17* and *MAX4*/*D10* (Zha et al., 2019). GA has been found to regulate tiller bud elongation *via* suppressing SL biosynthesis, which depends on GA receptor GID1 and F-box protein GID2 (Ito et al., 2017). Meanwhile, DELLA protein SLENDER RICE 1 (SLR1), one suppressor of GA signaling, promotes tiller number by interacting with D14 in an SL-dependent manner (Nakamura et al., 2013). Genetic evidence also suggests that SL and brassinosteroids (BRs) coordinately regulate rice tillering *via* activating the D53–BZR1 signal complex which bind the promoter of TB1 and repress its transcription (Fang et al., 2020). On the other hand, there is also crosstalk between SLs and abscisic acid (ABA) during rice tillering and plant adaptability to the environment (Ruyter-Spira et al., 2013; Luo et al.,2019a).

Under phosphorus (P) deficiency conditions, endogenous SL content is elevated in wild-type seedlings, leading to attenuated tiller bud outgrowth. However, this inhibition does not occur in the SL signaling mutant (*d3*) and biosynthesis mutant (*d10*). It indicates that SL signaling is involved in the coordination of tiller development and P metabolism (Umehara et al., 2010). A recent study also revealed that the SL signal pathway is involved in circadian-clock-regulated tiller bud and panicle development in rice (Wang et al., 2020). The *D14* gene encoding SL receptor is transcriptionally induced by CIRCADIAN CLOCK ASSOCIATED1 (CCA1), a core regulator of the circadian clock, to repress the tiller number, whereas PSEUDORESPONSE REGULATOR1 (PPR1), the suppressor of the circadian clock, causes the opposite effects on *D14* expression and tiller development.

The potential role of strigolactones on nitrogen regulation of tiller development

The biosynthesis of SL is influenced largely by environmental factors, such as nutrients in soil. The increased level of SLs was also reported in response to P and N deficiency in many different species. Yoneyama et al. (2007a) found that the nature SL orobanchol exudate from red clover (*Trifolium pretense* L.) was elevated in response to various nutrients (P, N, K, Ca, and Mg) and, in sorghum, the major SL 5-deoxystrigol was much higher under low P and also N (Yoneyama et al., 2007b). A further study mainly focused on P which is involved in the SL regulation of tiller development. Under P-deficient conditions, the expression levels of SL biosynthesis genes were upregulated, resulting in the increase in 2′-epi-5-DS levels in rice seedlings. However, this effect was not observed in the SL mutants *d3* and *d10* (Umehara et al., 2010). Further studies suggested that the P levels are the real trigger of SL induction, whereas the N effect on SL levels depends on the type of plant, type of nutrient, degree of nutrient stress, and macronutrient uptake strategy (Yoneyama et al., 2012; Yoneyama et al., 2013).

Furthermore, the SL signal has been recently found to mediate the regulation of N in rice root development. N deficiency led to an increased SL content in rice root tissues, and N deficiency-induced root responses (i.e., increased seminal root length and reduced lateral root density) were significantly suppressed in SL biosynthetic and signaling mutants *d10*, *d27*, and *d3* (Umehara et al., 2010; Sun et al., 2014).

Because N is also an important restriction factor for the tiller outgrowth, its regulation on SL was also investigated. Under nitrogen-deficient conditions, the tiller number reduced in both WT and *d3* and *d10* mutants. However, the reduction was much severe in WT, which indicated that the responses to the N level was insensitive in the SL mutant compared with WT (Luo et al., 2018). To some extent, this phenomenon is like what occurred under P-deficient conditions. However, in N-deficient conditions, even at an early stage, the restriction of tiller outgrowth appeared. This is possible due to the different observation systems or the regulation pathways. SLs could also influence the translocation of N which was proven with the altered N metabolic genes between WT and *d* mutants (Luo et al., 2018). The restriction of tiller bud outgrowth under N-deficient conditions was possibly caused by the SL biosynthesis which was enhanced by the N deficiency; it could also be caused by the influenced N translocation which is regulated by SL as a signal.

Prospects

Tiller number is one of the important parameters and agronomy traits determining rice NUE and yield. Understanding the mechanism of its response to N availability is thus necessary and indispensable for high-efficiency agriculture in future. As the core regulator of tiller development, the SL signal is essential in mediating tiller development responses to various endogenous and environmental signals. This is based on promising evidence that several regulators, such as GA signal and TCP

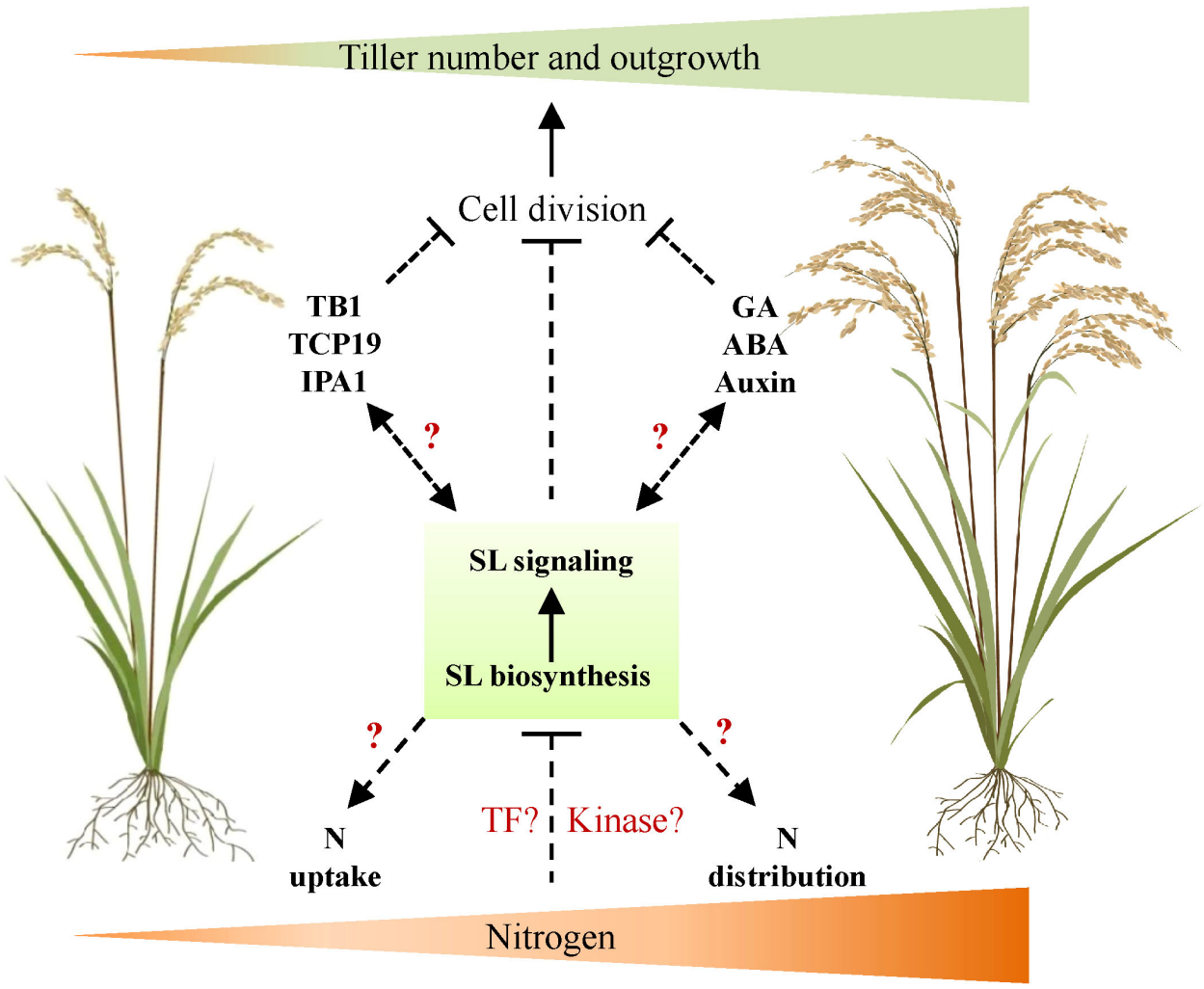

FIGURE 1
A proposed working model of SL signal on regulating rice tiller development in response to nitrogen. In this model, nitrogen supply increases rice tiller number and outgrowth through the negative regulation of SL biosynthesis and signaling transduction. However, it is uncharacterized whether specific transcription factors or kinases are activated by N to regulate SL signaling. Meanwhile, SL may also interact with well-known regulators of tiller number (e.g., TB1, TCP19, and IPA1) or plant hormones (e.g., GA, ABA, and auxin) to regulate the tiller number in response to external N supply. Furthermore, SL may also affect N uptake by root and N distribution in plant to regulate tiller number. TB1, TEOSINTE BRANCHED1; TCP19, TCP transcription factor 19; IPA1, Ideal Plant Architecture 1; N, nitrogen; TF, transcription factor; SL, strigolactone; GA, gibberellin; ABA, abscisic acid.

transcription factors, which mediate N-dependent tiller development, also interact with SL signaling components. Thus, we proposed a potential role of SL signals in regulating tiller development in response to the available N concentration underground, probably through the activation of the complex signaling cascades (Figure 1). Further investigation could be applied as, for instance, genetic approaches to explore SL signaling components that specifically regulate N-dependent tiller development and NUE; the possible molecular link between well-known tiller regulators and SL signals may be clarified.

Author contributions

The author contributed to the writing of the manuscript, to designing the figure, and to its approval for publication.

Funding

This work was supported by grants from the Jiangsu Key Research and Development Program (BE2020339) and

Jiangsu Seed Industry Revitalization Project (JBGS [2021]011).

Conflict of interest

The author declares that the research was conducted in the absence of any commercial or financial relationships that could be construed as a potential conflict of interest.

Publisher's note

References

Arite, T., Iwata, H., Ohshima, K., Maekawa, M., Nakajima, M., Kojima, M., et al. (2007). *DWARF10*, an RMS1/MAX4/DAD1 ortholog, controls lateral bud outgrowth in rice. *Plant J.* 51, 1019–1029. doi: 10.1111/j.1365-313X.2007.03210.x

Arite, T., Umehara, M., Ishikawa, S., Hanada, A., Maekawa, M., Yamaguchi, S., et al. (2009). *d14*, a strigolactone-insensitive mutant of rice, shows an accelerated outgrowth of tillers. *Plant Cell Physiol.* 50, 1416–1424. doi: 10.1093/pcp/pcp091

Fang, Z., Ji, Y., Hu, J., Guo, R., Sun, S., and Wang, X. (2020). Strigolactones and brassinosteroids antagonistically regulate the stability of the D53-OsBZR1 complex to determine *FC1* expression in rice tillering. *Mol. Plant* 13, 586–597. doi: 10.1016/j.molp.2019.12.005

Fan, X. R., Tang, Z., Tan, Y. W., Zhang, Y., Luo, B. B., Yang, M., et al. (2016). Overexpression of a pH-sensitive nitrate transporter in rice increases crop yields. *P Natl. Acad. Sci. U.S.A.* 113, 7118–7123. doi: 10.1073/pnas.1525184113

Gao, Z., Qian, Q., Liu, X., Yan, M., Feng, Q., Dong, G., et al. (2009). *Dwarf 88*, a novel putative esterase gene affecting architecture of rice plant. *Plant Mol. Biol.* 71, 265–276. doi: 10.1007/s11103-009-9522-x

Gomez-Roldan, V., Fermas, S., Brewer, P. B., Puech-Pages, V., Dun, E. A., Pillot, J. P., et al. (2008). Strigolactone inhibition of shoot branching. *Nature* 455 (7210), 189–194. doi: 10.1038/nature07271

Good, A. G., Shrawat, A. K., and Muench, D. G. (2004). Can less yield more? is reducing nutrient input into the environment compatible with maintaining crop production? *Trends Plant Sci.* 9, 597–605.

Guo, S. Y., Xu, Y. Y., Liu, H. H., Mao, Z. W., Zhang, C., Ma, Y., et al. (2013). The interaction between OsMADS57 and OsTB1 modulates rice tillering *via* DWARF14. *Nat. Commun.* 4, 1566. doi: 10.1038/ncomms2542

Haque, M. A., and Haque, M. M. (2016). Growth, yield and nitrogen use efficiency of new rice variety under variable nitrogen rates. *Am. J. Plant Sci.* 7, 612–622. doi: 10.4236/ajps.2016.73054

Huang, W. T., Bai, G. X., Wang, J., Zhu, W., Zeng, Q. S., Lu, K., et al. (2018). Two splicing variants of OsNPF7.7 regulate shoot branching and nitrogen utilization efficiency in rice. *Front. Plant Sci.* 9, 300. doi: 10.3389/fpls.2018.00300

Huang, S. J., Liang, Z. H., Chen, S., Sun, H. W., Fan, X. R., Wang, C. L., et al. (2019). A transcription factor, OsMADS57, regulates long-distance nitrate transport and root elongation. *Plant Physiol.* 180, 882–895. doi: 10.1104/pp.19.00142

Huang, W. T., Nie, H. P., Feng, F., Wang, J., Lu, K., and Fang, Z. M. (2019). Altered expression of *OsNPF7.1* and *OsNPF7.4* differentially regulates tillering and grain yield in rice. *Plant Sci.* 283, 23–31. doi: 10.1016/j.plantsci.2019.01.019

Ito, S., Yamagami, D., Umehara, M., Hanada, A., Yoshida, S., Sasaki, Y., et al. (2017). Regulation of strigolactone biosynthesis by gibberellin signaling. *Plant Physiol.* 174, 1250–1259. doi: 10.1104/pp.17.00301

Jiang, L., Liu, X., Xiong, G., Liu, H., Chen, F., Wang, L., et al. (2013). DWARF 53 acts as a repressor of strigolactone signalling in rice. *Nature* 504, 401–405. doi: 10.1038/nature12870

Jiao, Y. Q., Wang, Y. H., Xue, D. W., Wang, J., Yan, M. X., Liu, G. F., et al. (2010). Regulation of *OsSPL14* by OsmiR156 defines ideal plant architecture in rice. *Nat. Genet.* 42 (6), 541–544. doi: 10.1038/ng.591

Lin, H., Wang, R., Qian, Q., Yan, M., Meng, X., Fu, Z., et al. (2009). *DWARF27*, an iron-containing protein required for the biosynthesis of strigolactones, regulates rice tiller bud outgrowth. *Plant Cell* 21, 1512–1525. doi: 10.1105/tpc.109.065987

Li, S., Tian, Y. H., Wu, K., Ye, Y. F., Yu, J. P., Zhang, J. Q., et al. (2018). Modulating plant growth-metabolism coordination for sustainable agriculture. *Nature* 560 (7720), 595–600. doi: 10.1038/s41586-018-0415-5

Liu, Y. Q., Wang, H. R., Jiang, Z. M., Wang, W., Xu, R. N., Wang, Q. H., et al. (2021). Genomic basis of geographical adaptation to soil nitrogen in rice. *Nature* 590 (7847), 600–605. doi: 10.1038/s41586-020-03091-w

Liu, W., Wu, C., Fu, Y., Hu, G., Si, H., Zhu, L., et al. (2009). Identification and characterization of *HTD2*: A novel gene negatively regulating tiller bud outgrowth in rice. *Planta* 230, 649–658. doi: 10.1007/s00425-009-0975-6

Lopez-Obando, M., Ligerot, Y., Bonhomme, S., Boyer, F. D., and Rameau, C. (2015). Strigolactone biosynthesis and signaling in plant development. *Development* 142, 3615–3619. doi: 10.1242/dev.120006

Luo, L., Qin, R. Y., Liu, T., Yu, M., Yang, T. W., and Xu, G. H. (2019b). OsASN1 plays a critical role in asparagine-dependent rice development. *Int. J. Mol. Sci.* 20 (1), 130. doi: 10.3390/ijms20010130

Luo, L., Takahashi, M., Hiromu, K., Qin, R. Y., Shiga, T., Kanno, Y., et al. (2019a). Developmental analysis of the early steps in strigolactone-mediated axillary bud dormancy in rice. *Plant J.* 97, 1006–1021. doi: 10.1111/tpj.14266

Luo, L., Wang, H. X., Liu, X. H., Hu, J. Q., Zhu, X. L., Pan, S., et al. (2018). Strigolactones affect the translocation of nitrogen in rice. *Plant Scie* 270, 190–197. doi: 10.1016/j.plantsci.2018.02.020

Lu, K., Wu, B. W., Wang, J., Zhu, W., Nie, H. P., Qian, J. J., et al. (2018). Blocking amino acid transporter *OsAAP3* improves grain yield by promoting outgrowth buds and increasing tiller number in rice. *Plant Biotechnol. J.* 16, 1710–1722. doi: 10.1111/pbi.12907

Miura, K., Ikeda, M., Matsubara, A., Song, X. J., Ito, M., Asano, K., et al. (2010). *OsSPL14* promotes panicle branching and higher grain productivity in rice. *Nat. Genet.* 42 (6), 545–549. doi: 10.1038/ng.592

Nakamura, H., Xue, Y. L., Miyakawa, T., Hou, F., Qin, H. M., Fukui, K., et al. (2013). Molecular mechanism of strigolactone perception by DWARF14. *Nat. Commun.* 4, 2613. doi: 10.1038/ncomms3613

Ohashi, M., Ishiyama, K., Kojima, S., Kojima, M., Sakakibara, H., Yamaya, T., et al. (2017). Lack of cytosolic glutamine synthetase1;2 activity reduces nitrogen-dependent biosynthesis of cytokinin required for axillary bud outgrowth in rice seedlings. *Plant Cell Physiol.* 58, 679–690. doi: 10.1093/pcp/pcx022

Oikawa, T., and Kyozuka, J. (2009). Two-step regulation of LAX PANICLE1 protein accumulation in axillary meristem formation in rice. *Plant Cell* 21, 1095–1108. doi: 10.1105/tpc.108.065425

Ruyter-Spira, C., Al-Babili, S., van der Krol, S., and Bouwmeester, H. (2013). The biology of strigolactones. *Trends Plant Sci.* 18, 72–83. doi: 10.1016/j.tplants.2012.10.003

Song, X. G., Lu, Z. F., Yu, H., Shao, G. N., Xiong, J. S., Meng, X. B., et al. (2017). IPA1 functions as a downstream transcription factor repressed by D53 in strigolactone signaling in rice. *Cell Res.* 27, 1128–1141. doi: 10.1038/cr.2017.102

Stitt, M., and Krapp, A. (1999). The interaction between elevated carbon dioxide and nitrogen nutrition: The physiological and molecular background. *Plant Cell Environ.* 22, 583–621. doi: 10.1046/j.1365-3040.1999.00386.x

Sun, H., Tao, J., Liu, S., Huang, S., Chen, S., Xie, X., et al (2014). Strigolactones are involved in phosphate- and nitrate-deficiency-induced root development and auxin transport in rice. *J. Exp. Bot.* 65 (22), 6735–6746. doi: 10.1046/j.1365-3040.1999.00386.x

Umehara, M., Hanada, A., Yoshida, S., Akiyama, K., Arite, T., Takeda-Kamiya, N., et al. (2008). Inhibition of shoot branching by new terpenoid plant hormones. *Nature* 455 (7210), 195–200. doi: 10.1038/nature07272

Umehara, M., Hanada, A., Magome, H., Takeda-Kamiya, N., and Yamaguchi, S. (2010). Contribution of strigolactones to the inhibition of tiller bud outgrowth

under phosphate deficiency in rice. *Plant Cell Physiol.* 51 (7), 1118–1126. doi: 10.1093/pcp/pcq084

Wang, F., Han, T. W., Song, Q. X., Ye, W. X., Song, X. G., Chu, J. F., et al. (2020). The rice circadian clock regulates tiller growth and panicle development through strigolactone signaling and sugar sensing. *Plant Cell* 32, 3124–3138. doi: 10.1105/tpc.20.00289

Wang, J., Lu, K., Nie, H. P., Zeng, Q. S., Wu, B. W., Qian, J. J., et al. (2018). Rice nitrate transporter *OsNPF7.2* positively regulates tiller number and grain yield. *Rice* 11 (1), 12. doi: 10.1186/s12284-018-0205-6

Wang, J., Wu, B. W., Lu, K., Wei, Q., Qian, J. J., Chen, Y. P., et al. (2019). *The amino acid permease 5* (*OsAAP5*) regulates tiller number and grain yield in rice. *Plant Physiol.* 180, 1031–1045. doi: 10.1104/pp.19.00034

Waters, M. T., Gutjahr, C., Bennett, T., and Nelson, D. C. (2017). Strigolactone signaling and evolution. *Annu. Rev. Plant Biol.* 68, 291–322. doi: 10.1146/annurev-arplant-042916-040925

Wu, K., Wang, S. S., Song, W. Z., Zhang, J. Q., Wang, Y., Liu, Q., et al. (2020). Enhanced sustainable green revolution yield *via* nitrogen-responsive chromatin modulation in rice. *Science* 367 (6478), eaaz2046. doi: 10.1126/science.aaz2046

Yoneyama, K., Xie, X. N., Kim, H. I., Kisugi, T., Nomura, T., Sekimoto, H., et al. (2012). How do nitrogen and phosphorus deficiencies affect strigolactone production and exudation? *Planta* 235, 1197–1207. doi: 10.1007/s00425-011-1568-8

Yoneyama, K., Xie, X. N., Kisugi, T., Nomura, T., and Yoneyama, K. (2013). Nitrogen and phosphorus fertilization negatively affects strigolactone production and exudation in sorghum. *Planta* 238, 885–894. doi: 10.1007/s00425-013-1943-8

Yoneyama, K., Xie, X. N., Kusumoto, D., Sekimoto, H., Sugimoto, Y., Takeuchi, Y., et al. (2007b). Nitrogen deficiency as well as phosphorus deficiency in sorghum promotes the production and exudation of 5-deoxystrigol, the host recognition signal for arbuscular mycorrhizal fungi and root parasites. *Planta* 227, 125–132.

Yoneyama, K., Yoneyama, K., Takeuchi, Y., and Sekimoto, H. (2007a). Phosphorus deficiency in red clover promotes exudation of orobanchol, the signal for mycorrhizal symbionts and germination stimulant for root parasites. *Planta* 225, 1031–1038. doi: 10.1007/s00425-006-0410-1

Zha, M., Imran, M., Wang, Y., Xu, J., Ding, Y., and Wang, S. H. (2019). Transcriptome analysis revealed the interaction among strigolactones, auxin, and cytokinin in controlling the shoot branching of rice. *Plant Cell Rep.* 38, 279–293. doi: 10.1007/s00299-018-2361-y

Zhang, Y., Van Dijk, A., Scaffidi, A., Flematti, G. R., Hofmann, M., Charnikhova, T., et al. (2014). Rice cytochrome P450 MAX1 homologs catalyze distinct steps in strigolactone biosynthesis. *Nat. Chem. Biol.* 10 (12), 1028–1033. doi: 10.1038/nchembio.1660

Zhou, F., Lin, Q., Zhu, L., Ren, Y., Zhou, K., Shabek, N., et al. (2013). D14-SCF (D3)-dependent degradation of D53 regulates strigolactone signalling. *Nature* 504, 406–410. doi: 10.1038/nature12878

Zou, J., Zhang, S., Zhang, W., Li, G., Chen, Z., Zhai, W., et al. (2006). The rice HIGH-TILLERING DWARF1 encoding an ortholog of arabidopsis MAX3 is required for negative regulation of the outgrowth of axillary buds. *Plant J.* 48, 687–698. doi: 10.1111/j.1365-313X.2006.02916.x

frontiers | Frontiers in Plant Science

TYPE Original Research
PUBLISHED 23 December 2022
DOI 10.3389/fpls.2022.1076600

OPEN ACCESS

EDITED BY
Jian Chen,
Jiangsu University, China

REVIEWED BY
Liang Li,
Institute of Quality Standards and Testing Technology for Agro Products, Chinese Academy of Agricultural Sciences, China
Zhao Zhang,
China Agricultural University, China

*CORRESPONDENCE
Yuanda Lv
Lyd0527@126.com
Yadong Zhang
zhangyd@jaas.ac.cn

†These authors have contributed equally to this work

SPECIALTY SECTION
This article was submitted to Plant Bioinformatics, a section of the journal Frontiers in Plant Science

RECEIVED 21 October 2022
ACCEPTED 05 December 2022
PUBLISHED 23 December 2022

CITATION
Liang W, Du H, Pang B, Cheng J, He B, Hu F, Lv Y and Zhang Y (2022) High-density genetic mapping identified QTLs for anaerobic germination tolerance in rice.
Front. Plant Sci. 13:1076600.
doi: 10.3389/fpls.2022.1076600

High-density genetic mapping identified QTLs for anaerobic germination tolerance in rice

Wenhua Liang[1†], Hongyang Du[2,3†], Bingwen Pang[2], Junjie Cheng[2], Bing He[2], Fengqin Hu[2], Yuanda Lv[2*] and Yadong Zhang[1*]

[1]Institute of Food Crops, Jiangsu Academy of Agricultural Sciences, Nanjing, China, [2]Excellence and Innovation Center, Jiangsu Academy of Agricultural, Sciences, Nanjing, China, [3]Key Laboratory of Rice Genetic Breeding of Anhui Province, Rice Research Institute, Anhui Academy of Agricultural Science, Hefei, China

The tolerance of rice anaerobic germination (AG) is the main limiting factor for direct seeding application, yet the genetics mechanism is still in its infancy. In the study, recombinant inbred lines population of TD70 *Japonica* cultivar and Kasalath Indica cultivar, was employed to construct a high-density genetic map by whole genome re-sequencing. As a result, a genetic map containing 12,328 bin-markers was constructed and a total of 50 QTLs were then detected for CL (coleoptile length), CD (coleoptile diameter), CSA (coleoptile surface area) and CV (coleoptile volume) related traits in the two stages of anaerobic treatment using complete interval mapping method (inclusive composite interval mapping, ICIM). Among the four traits associated with coleoptile, coleoptile volume had the largest number of QTLs (17), followed by coleoptile diameter (16), and coleoptile length had 5 QTLs. These QTLs could explain phenotypic contribution rates ranging from 0.34% to 11.17% and LOD values ranging from 2.52 to 11.57. Combined with transcriptome analysis, 31 candidate genes were identified. Furthermore, 12 stable QTLs were used to detect the aggregation effect analysis. Besides, It was found that individuals with more aggregation synergistic alleles had higher phenotypic values in different environments. Totally, high-density genetic map, QTL mapping and aggregation effect analysis of different loci related to the anaerobic germination of rice seeds were conducted to lay a foundation for the fine mapping of related genes in subsequent assisted breeding.

KEYWORDS

Rice, High-density Genetic Map, Anaerobic Germination, QTL, RNA-seq

Introduction

Rice is an essential food crop for billions of people. However, rice transplanting is costly for labor and water resources. Along with the development of the economy and restrained water and labor supply, rice planting and production systems are gradually transforming. Direct seeding in rice cultivation (DSR) is increasingly adopted to save labor and production cost (Mahender et al., 2015). However, direct seeding in actual production conditions also has disadvantages, such as direct seeding in water. In cold conditions, hypoxia, competition with weeds, and other adverse factors make seeds have poor germination, and seedlings wilt or die (Farooq et al., 2011). Hypoxia stress, accompanied by the germination and seedling stage, is the primary environmental stress for direct water seeding, which limits the germination rate and seedling growth of rice, thus affecting the yield. Therefore, the tolerance of rice anaerobic germination (AG) is the main limiting factor for the large-scale development of direct seeding. Revealing the genetic and molecular mechanisms of AG tolerance under flooding conditions and cultivating rice varieties with excellent AG resistance are important ways to effectively solve the limitations of direct seeding in rice production.

The tolerance of rice seedlings to hypoxia stress during germination is a complex quantitative trait controlled by multiple gene loci. In previous studies, various genetic populations have been used for linkage and association mapping to identify many QTLs related to seed germination and early seedling tolerance to hypoxia stress (Angaji, 2008; Angaji et al., 2010; Septiningsih et al., 2013; Baltazar et al., 2014; Hsu and Tung, 2015; Baltazar et al., 2019; Yang et al., 2019; Ignacio et al., 2021; Liu et al., 2021). Using the Kinmaze/DV85 recombinant inbred line population, Jiang et al. identified five QTLs on chromosomes 1, 2, 5 and 7, respectively, which could explain 10.5% - 19.6% of the phenotypic variation. In another study, Jiang et al. (2006) identified two QTLs possibly related to AG potential by using an F_2 segregation population constructed by *Japonica* cultivar USSR5 and *Indica* cultivar N22, located on chromosomes 5 and 11, respectively, with the phenotypic variation of 11% - 15.5% (Jiang et al., 2006). Six QTLs related to AG were detected in the $F_{2:3}$ mapping population constructed by IR42 and MR; Among them, *qAG7.1* (AG2) is the most effective QTL on chromosome 7, with a LOD value of 14.5 and a phenotypic variation of 31.7% (Septiningsih et al., 2013). Baltazar et al. identified four QTLs related to anaerobic germination using the $F_{2:3}$ population of IR64/Kharsu, including three on chromosome 7 and one on chromosome 3, with a LOD value of 5.7-7.7, which could explain 8.1% - 12.6% of the phenotypic variation (Baltazar et al., 2019). In another study, a new site *qACE3.1* was identified in the chromosome segment substitution lines (CSSLs) population constructed by IR64 and Koshihikari under anaerobic conditions, which can promote the elongation of coleoptiles under anaerobic conditions (Nishimura et al., 2020).

Recently, the BC_2F_2 population was constructed with IR64 (*Japonica* cultivar) as the recurrent parent and Kho Hlan on (KHO, *Japonica* cultivar) as the receptor, and five possible QTLs related to flooding tolerance were detected. Among them, *qAG-9-2* (AG1 for short) is a major QTL located on the long arm of chromosome 9, with a LOD value of 20.3, which could explain 33.5% of the phenotypic variation (Angaji et al., 2010). Subsequently, the QTL was cloned as *OsTPP7* gene, encoding a trehalose-6-phosphate phosphatase. It is functional in the metabolism of trehalose-6-phosphate, and the expression of the gene could increase the pool capacity in heterotrophic tissues, and thus the utilization of starch, which resulted in promoting seed germination and coleoptile growth and enhancing hypoxia tolerance during germination (Kretzschmar et al., 2015). This QTL has been used for crop improvement and has been successfully verified (Chamara et al., 2018; Mondal et al., 2020; Mondal et al., 2020). These results provided important genetic information for improving the potential of AG and making it serve molecular breeding.

SNP genotyping by next-generation sequencing technology (NGS) improves the accuracy of genetic mapping and dramatically promotes the mining and identification of key genes. Through GWAS analysis and QTL mapping, a hexokinase gene (HXK6, LOC_Os01g53930) was identified in 144 RILs of Nipponbare/IR64. Studies showed that this gene was related to the elongation of rice coleoptiles under anaerobic conditions (Hsu and Tung, 2015). A total of 25 QTLs related to anaerobic germination were identified in YZX (Indica rice) and 02428 (*Japonica* cultivar) RIL populations using a high-density genetic map containing 2711 bin markers. 13 stable QTLs were further identified from them, and 88 differentially expressed bases were screened by combining transcriptome (Yang et al., 2019). A high-density map containing 1070 bin markers was constructed using 131 introgression lines with 93-11 as receptors and W2014 as donors. One QTL, *qAGP1* and *qAGP3* were detected on chromosomes 1 and 3, which could explain 15% of the phenotypic variation. These two QTLs improved hypoxia tolerance by increasing coleoptile length during rice germination (Liu et al., 2021). Although many QTLs related to hypoxia tolerance in germination have been identified, only a few use substitution lines or near-isogenic lines to evaluate their effects on rice seedling growth, and the molecular mechanism of anaerobic tolerance needs further study.

Traditional QTL mapping and molecular marker genotyping are time-consuming and laborious (Chen et al., 2014). Simple sequence repeats (SSRs) and other low throughput molecular markers are often used to construct rice QTL linkage maps and QTL analysis. Most of them have low density and cannot provide the precise location of QTLs controlling interesting traits (Matsunami et al., 2011). SNP occurs in almost all

population individuals with high density. The new generation of sequencing technology can facilitate directly obtaining population single nucleotide polymorphism (SNP) markers for genotyping (Kumar et al., 2012). Previous studies in rice have proved that the improvement of the quality and resolution of high-density genetic maps based on SNP markers has greatly improved the efficiency and accuracy of QTL mapping (Huang et al., 2009; Gao et al., 2013; Wang et al., 2018; Yang et al., 2021).

In this study, we demonstrated the difference in coleoptile phenotype in RILs populations during AG of two distinct genotypes. A high-density genetic map was constructed by whole genome resequencing. QTLs linked with coleoptile phenotype were identified at two stages of anaerobic germination. Furthermore, we performed transcriptome analysis to identify differentially expressed genes (DEG) in the localization regions related to AG tolerance, which could provide valuable information for verifying candidate genes and analyzing genetic and molecular mechanisms affecting seed AG tolerance. At the same time, it provides a reference for molecular marker-assisted selection of rice varieties suitable for direct seeding.

Materials and methods

F_1 was generated by crossing between *Japonica* cultivar TD70 and *Indica* cultivar Kasalath, and a population F_{10} containing 186 recombinant inbred lines (RIL) was constructed by the single seed descent method. *Japonica* cultivar TD70 is the offspring of Tianegu///9520//(72-496/Suyunuo), which is a stable line independently created by the research team. Kasalath is a conventional *Indica* rice variety in India, which is provided by the germplasm resources protection and utilization platform of Jiangsu Province. The experimental materials were planted in the experimental field of Jiangsu Academy of Agricultural Sciences, China. Each RIL or parent was planted in 4 rows, with ten plants in each row, 13.5cm plant spacing, 26.5cm row spacing, and conventional cultivation and management. Considering the influence of seed maturity on AG, the plants in the middle of each plot are harvested after the seeds are fully mature (50 days after heading). The harvested seeds were dried in a 40 °C hot-air dryer for 6 days and then stored at -20 °C.

A total of 30 plump and uniform seeds were selected from three independent individual plants harvested in each experimental plot and placed in an oven at 50 °C for seven days to relieve seed dormancy. Then, the seeds were disinfected with 6% sodium hypochlorite for 30 min, and rinsed with sterile water 6-7 times. Take five sterile seeds and place them in a glass tube with a height of 8 cm. Add sterile water with a depth of 5 cm to create a hypoxic environment (Hsu and Tung, 2015). Then put it into a 28 °C incubator for dark cultivation. On the 4-6th day of treatment, the coleoptile length (CL), coleoptile diameter (CD), coleoptile surface area (CSA) and coleoptile volume (CV) were measured using cloud platform (www.irootanalysis.cn/index/indexHome). Three replicates were analyzed for each strain. SPSS (version 22) and Excel software were used for statistical data analysis.

DNA extraction, sequencing, typing and SNP identification

DNA was isolated from the leaves of two parents and 186 F_{10} RILs at the tillering stage by the CTAB method. DNA quality was detected by agarose gel electrophoresis and nanodrop nd1000 spectrophotometer. In this study, the genome re-sequencing depth of parents TD70 and Kasalath is ~20×. The average sequencing depth of RILs is 10×. Sequencing was carried out with Illumina sequencing platform NovaSeq 6000, and the sequencing mode is paid end 150 bp. After low-quality base filtration of sequenced reads, they were compared to the reference genome using BWA software (Li and Durbin, 2009) (http://rapdb.dna.affrc.go.jp/ , IRGSP-1.0 version). Then, SAMtools (Li et al., 2009) and PICARD (http://picard.sourceforge.net) were used to remove redundancy. GATK (McKenna et al, 2010) was performed for calling SNP and genotype identification.

High-density genetic map construction and QTL analysis

The resequencing of 186 RIL lines from TD70/Kasalath was performed for SNP identification, and high-quality, biallelic homozygous loci were obtained. To avoid false positive SNP genotyping in the population, Huang et al. (2009) used the sliding window method and made appropriate modifications to evaluate a group of continuous SNPs and perform genotyping. The genotype of RILs is split into a series of recombinant bins according to recombination breakpoints. The sliding-window SNP number of these bins is 15 and adjacent Bins within 200 kb are merged. The bin genotype of the transition region between two different genotype blocks is set as the missing data. The abnormal separation mark showed that the partial separation ($P<0.01$) was discarded.

QTL IciMapping v4.1 software (Meng et al., 2015) was used to construct the genetic map using the Kosambi map method and analyze the four traits related to coleoptiles on the 4-6th days after anaerobic stress treatment of the recombinant inbred lines. The inclusive composite interval mapping (ICIM-ADD) method was used for QTL identification. The logarithm of odds (LOD) score threshold was set to 2.5. Loci with LOD ≥ 2.5 are deemed candidate QTLs associated with the trait. QTL naming refers to McCuch's method (McCouch, 2008).

RNA isolation, sequencing and expression profile analysis

In order to obtain expression profiles and differentially expressed genes related to anaerobic germination, the seeds of parents TD70 and Kasalath were taken for RNA Seq experiments with/without anaerobic treatment, respectively. The seeds were rinsed with double-distilled water, and then 5-6 seeds were taken from each sample, and three biological replicates were set, and thus a total of 12 samples were taken. These samples were immediately put into liquid nitrogen for quick freezing and stored at - 80 °C for RNA isolation. The purity, concentration and integrity of the total RNA isolated were evaluated, and RNA seq library construction and sequencing were referred to the previous process (Liang et al., 2022).

The Fastp program (Chen et al., 2018) was engaged to remove the adapter, low-quality sequencing tail, and then the Hiast2 program (Pertea et al., 2016) was used for mapping reads to the reference genome (http://rapdb.dna.affrc.go.jp/ , IRGSP-1.0 version). SAMtools (Li et al., 2009) were used for converting format. The expression abundance of transcripts was calculated based on fragments per kilobase of transcript per million fragments mapped (FPKM). The transcripts with a maximum FPKM value of less than 1 in multiple samples were eliminated as no expression or false positive transcripts (Trapnell et al., 2012). Differential expression genes were screened by the DESeq2 software package (Anders and Huber, 2010), with screening criteria of Log2 (fold change) ≥ 1 and q-value<0.05.

Results

Responses of parents and RIL opulations to AG at the germination stage

The faster the rice coleoptiles elongate, the sooner the seedlings escape from an anoxic environment and increase the survival chances of rice. Therefore, rice coleoptile is a classic tissue for studying AG tolerance (Narsai et al., 2015). In this study, we investigated the dynamic changes of coleoptiles of two parents under anaerobic conditions; Significant variation in coleoptile traits was observed between TD70 and Kasalath, which were the parents of both (Figure 1).

After one day of treatment, Kasalath seeds began to germinate, and obvious coleoptiles bulged, while TD70 showed no significant change. On the second day, Kasalath showed obviously elongated coleoptiles, while TD70 seeds had just begun to germinate, and prominent coleoptiles emerged, which showed that Kasalath seeds germinated faster than those of TD70. The development of Kasalath coleoptile was occurred mainly from the second to the fifth day of treatment, while the growth of TD70 coleoptile mainly occurred on the third day. On the second day of treatment, the growth rate of coleoptile length (CL) of Kasalath was significantly higher than that of TD70, and the difference was very significant; However, the CL of TD70 increased rapidly from the third day to the fourth day of the treatment, and there was no significant difference between them on the fourth day. Then, on the fifth and sixth days, the CL length of kasalath was significantly longer than that of TD70, and the difference was significant. It could be seen that, on average, the CL elongation speed of Kasalath was faster (Figures 1A, B). From the third day of treatment, the CSA and CV of Kasalath were significantly higher than those of TD70. However, from the third day, the CD of TD70 was significantly larger than that of Kasalath, and the difference was significant or extremely significant until the sixth day.

Thus, the phenomenon stated above indicated that the coleoptile development of Kasalath mainly occurred on the first and second days of treatment. In contrast, TD70 mainly occurred on the third day (Figure 1). Thus, the four agronomy traits with significant or extremely significant differences in AG anaerobic treatment between the parents TD70 and Kasalath indicate that there were great genetic differences between them, on which QTLs mapping was conductive based.

The four traits of the coleoptile phenotype showed different segregation in the RIL population (Figure 2). The coefficient of variation (CV) on the fourth day of treatment ranged from 18.92% to 66.19%; The coefficient of variation at six days was 17.09% - 52.21%. Moreover, these traits show transgressive segregation in variated degrees. All characters are continuous unimodal distribution, and the absolute skewness value is close to 0 in each character, indicating that all these characters conform to the normal distribution and are controlled by multiple micro genes (Table 1).

Population genotyping and binmap construction

This study obtained 1,304 Gb high-quality sequencing data from illumina paired-end sequencing. The average sequencing depth is 18.8×. Among them, ~97.25% of the reads could be uniquely mapped to the reference genome. These SNP sites of RIL individuals were identified, and SNPs with depth >5 were retained. After filtering exceptions, 1,344,770 high-quality SNPs were finally used for subsequent analysis of recombination events and construct binmap, and the map contains 12,328 bin markers. All bin markers are evenly distributed on 12 chromosomes. The number of markers on chromosome 1 was the largest, 148,582; chromosome 9 has the least markers, 87,301(Table S2).

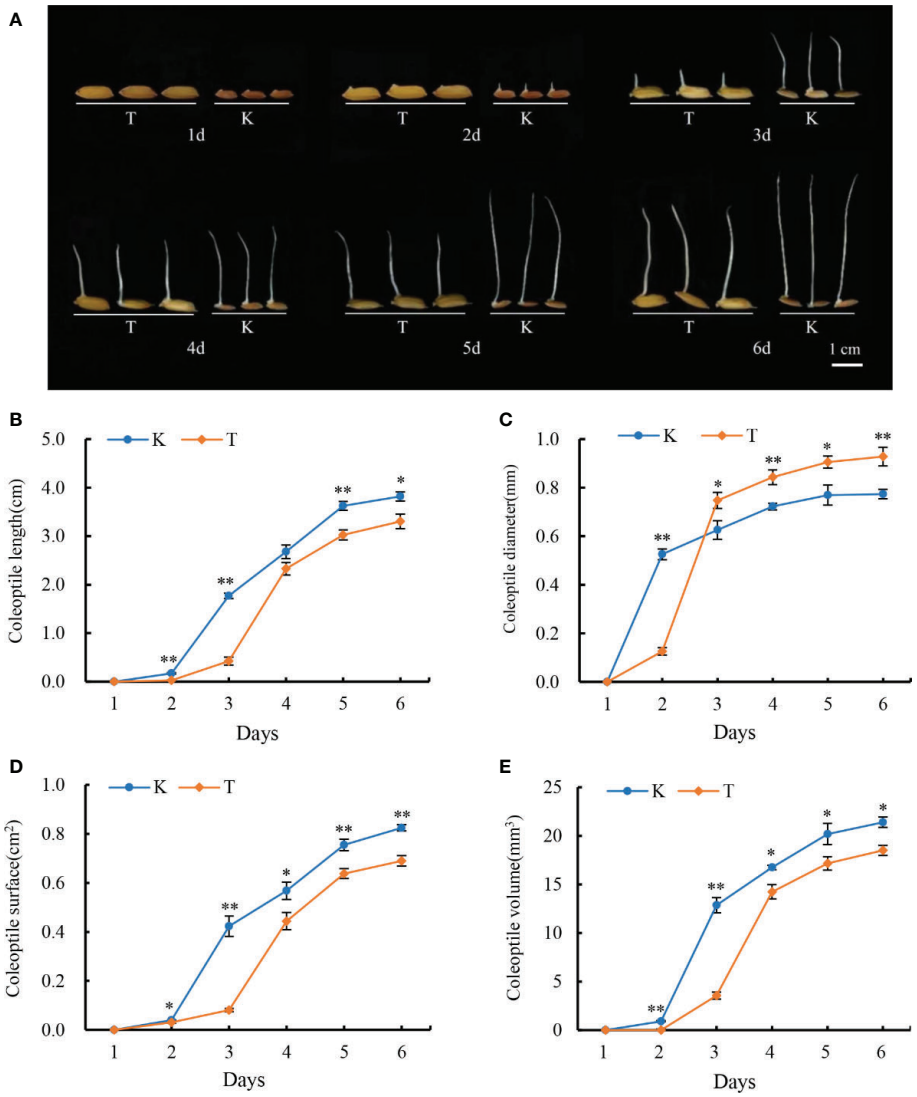

FIGURE 1
Dynamic of TD70 and Kasalath coleoptile developments under anaerobic conditions **(A)**. The phenotypes of two parents 1-6 days under anaerobic conditions; **(B–E)** represent the change of coleoptile length, diameter, surface area, and volume 1-6d under anaerobic conditions, respectively. K, Kasalath; T, TD70; * and ** represent the significant $p<0.05$ and $p< 0.01$, respectively.

Identification of AG-associated QTLs

Using the inclusive composite interval mapping (ICIM) method, 50 QTL loci associated with CL, CD, CSA and CV were identified in two stages of anaerobic treatment. These QTLs are distributed on all chromosomes except chromosome 9. There were as many as 10 loci distributed on chromosome 4, followed by 7 loci detected on chromosome 8 and 12, respectively; only one epistasis was detected on chromosome 2. Among the four traits related to coleoptile, the number of QTLs detected by coleoptile volume was the largest (17), followed by coleoptile diameter (16), and there were 5 QTLs associated with coleoptile length. These QTLs can explain phenotypic contribution rates ranging from 0.34% to 11.17% and LOD values ranging from 2.52 to 11.57. Some QTL loci in this study showed a positive additive effect and some negative additive effect, suggesting that both parents contributed favorable alleles.

There are 5 QTLs associated with CL. The contribution rate of a single QTL ranged from 4.85% - 10.99%. There were 12 loci associated with CSA, and the phenotypic contribution rate was between 1.40% to 9.39%. Sixteen QTLs were associated with CD, which could explain the phenotypic variation of 2.05% - 11.17%. Seventeen QTLs were associated with CVs, with phenotypic contribution rates ranging from 0.34% to 9.37%. QTLs showing

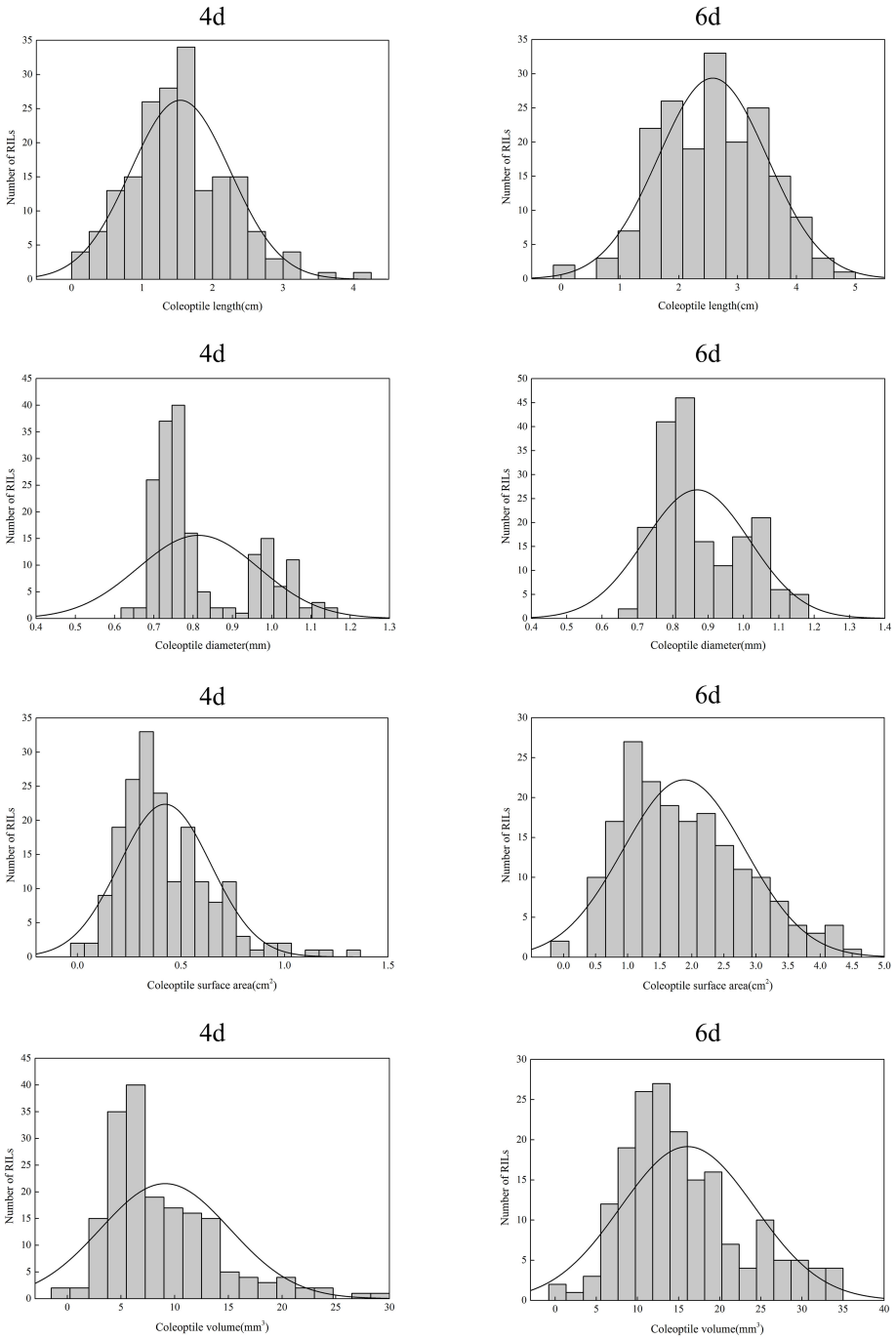

FIGURE 2
The distribution of four coleoptile phenotype traits in the RIL population.

physical-position overlap were considered as mere one QTL site. Finally, 42 QTLs were obtained in two stages of anaerobic germination. It was remarkable that five QTLs were detected in two germination stages: *qCD5*, *qCD8*, *qCV1-1*, *qCD10-2* and *qCV8-1*. Three loci were detected simultaneously by two different traits, of which *qCSA6* and *qCV6-5* overlapped as just one locus, and as well as *qCV4-2* and *qCL4-2*, *qCSA8* and *qCV8-1*, respectively; and they affected CL, CSA and CV (Table 2; Figure 3).

We found 6 out of the 42 loci have been previously reported (Table 2). The location of *qCV1-2* overlaps with the physical

TABLE 1 Phenotypes of TD70, Kasalath and RIL population of offspring at two germination stages under anaerobic conditions.

Trait	Days	Parents		RIL population				
		TD70	Kasalath	Mean	Range	Skewness	Kurtosis	CV[a] (%)
CL(cm)	4	2.32 ± 0.12	2.68 ± 0.14	1.54	0.13-4.23	0.54	0.75	45.84
	6	2.88 ± 0.08	3.81 ± 0.11	2.57	0.76-5.19	0.01	-0.15	35.91
CD(mm)	4	0.84 ± 0.03	0.72 ± 0.01	0.81	0.64-1.15	-0.95	6.92	18.92
	6	0.93 ± 0.04	0.77 ± 0.04	0.87	0.68-1.18	-1.73	10.91	17.09
CSA(cm^2)	4	0.44 ± 0.04	0.57 ± 0.04	0.42	0.09-1.34	1.13	1.97	52.21
	6	0.69 ± 0.02	0.82 ± 0.01	1.88	0.42-4.56	0.54	-0.37	50.55
CV(mm^3)	4	14.23 ± 0.73	16.75 ± 0.73	9.13	1.70-34.67	1.76	3.84	66.19
	6	19.33 ± 0.57	21.41 ± 0.53	16.12	3.13-45.78	0.95	0.72	50.47

CL, coleoptile length; CD, coleoptile diameter; CSA, coleoptile surface area; CV, coleoptile volume. Parent refers to the mean ± standard deviation (SD) of the parents; CV[a], coefficient of variation.

TABLE 2 QTLs associated with coleoptile traits during two periods of hypoxic germination.

QTL	Days	Chr.	Marker interval	Physical interval	LOD	PVE(%)	Add	Known locus
qCV1-1	4	1	Bin117-Bin118	2890073-2949395	10.45	0.55	-6.77	
qCV1-1	6	1			3.39	7.66	-6.30	
qCV1-2	6	1	Bin329-Bin330	9616532-9707372	3.19	1.62	-2.20	Liu et al., 2021
qCV1-3	4	1	Bin1250-Bin1251	39821205-39855940	8.20	0.55	-7.10	
qCSA1	6	1	Bin1193-Bin1194	37290282-37308515	4.48	4.34	-0.33	
qCL2	6	2	Bin2038-Bin2039	23247409-23313064	2.64	9.13	0.42	
qCSA3	6	3	Bin2655-Bin2656	13334166-13418232	4.24	9.39	-0.85	
qCD3	4	3	Bin2856-Bin2857	19769142-19898047	2.52	5.59	-0.05	
qCD4-1	4	4	Bin3370-Bin3371	1543556-1562998	2.65	3.64	-0.07	
qCSA4-1	6	4	Bin3374-Bin3375	1600851-1645142	3.04	2.90	0.32	
qCV4-1	4	4	Bin3454-Bin3455	3154153-3191419	5.10	0.54	-6.76	
qCL4-1	4	4	Bin3589-Bin3590	6944055-6998203	3.30	6.88	0.35	
qCD4-2	6	4	Bin3725-Bin3726	12757286-12823893	3.02	2.05	-0.04	
qCL4-2	6	4	Bin3788-Bin3789	14780687-14808655	3.15	5.59	0.25	Yang et al., 2021
qCV4-2					3.24	1.75	2.18	
qCSA4-2	6	4	Bin4035-Bin4036	22473081-22499182	3.42	3.31	0.25	Yang et al., 2019
qCSA4-3	6	4	Bin4274-Bin4275	29885854-29920615	8.28	9.21	0.45	
qCL4-3	6	4	Bin4275-Bin4276	29893048-29933483	2.80	4.85	0.28	
qCV5-1	4	5	Bin4778-Bin4779	8798783-8858855	8.14	0.55	-6.64	
qCV5-2	4	5	Bin5336-Bin5337	26369420-26471049	7.20	0.55	-6.96	
qCV5-3	4	5	Bin5337-Bin5338	26385407-26518791	4.34	0.51	-6.93	
qCD5	4	5	Bin5167-Bin5168	20629588-20770108	5.54	11.17	0.16	
qCD5	6	5			8.14	7.02	0.17	

(Continued)

TABLE 2 Continued

QTL	Days	Chr.	Marker interval	Physical interval	LOD	PVE(%)	Add	Known locus
qCSA6	4	6	Bin6167-Bin6168	20022371-20096670	2.57	2.24	-0.17	
qCV6-5	4	6			7.54	0.54	-6.65	
qCV6-1	4	6	Bin5442-Bin5443	80687-133609	7.51	0.55	-7.13	
qCV6-2	4	6	Bin5787-Bin5788	9858384-9898904	4.90	0.34	-11.06	
qCV6-3	4	6	Bin6097-Bin6098	17995332-18029267	7.98	0.55	-6.97	
qCV6-4	4	6	Bin6106-Bin6107	18133500-18186833	4.01	0.55	-6.24	
qCD7	6	7	Bin6768-Bin6769	6187353-6232165	2.98	2.15	-0.04	
qCSA7	6	7	Bin7527-Bin7528	28442520-28483618	2.76	3.62	0.24	Hsu and Tung, 2015
qCL8	4	8	Bin7664-Bin7665	2229665-2259731	5.82	10.99	0.26	
qCD8	4	8	Bin7843-Bin7844	7055955-7089043	6.82	8.89	0.37	
qCD8	6	8			8.71	5.25	0.38	
qCSA8	4	8	Bin7941-Bin7942	9196326-9222900	3.89	2.02	-0.21	
qCV8-1	4	8			11.57	0.55	-7.47	
qCV8-1	6	8			2.79	9.37	-6.48	
qCV8-2	4	8	Bin8412-Bin8413	21238647-21272554	6.14	0.53	-7.69	Yang et al., 2021
qCD10-1	6	10	Bin9581-Bin9582	5035933-5086795	5.48	6.86	0.32	
qCD10-2	4	10	Bin10082-Bin10083	19629777-19696813	3.09	4.61	-0.04	
qCD10-2	6	10			3.80	2.68	-0.04	
qCSA10	4	10	Bin9611-Bin9612	5704076-5752096	3.54	1.40	-0.37	
qCD11	4	11	Bin10524-Bin10525	9342548-9405943	2.59	3.48	-0.05	
qCSA12-1	6	12	Bin11505-Bin11506	6519288-6539105	3.62	4.40	-0.28	
qCSA12-2	4	12	Bin11694-Bin11695	10902983-10925501	2.71	2.09	-0.16	
qCSA12-3	4	12	Bin11695-Bin11696	10910092-10952995	2.62	2.02	-0.16	
qCD12-1	6	12	Bin11736-Bin11737	11680541-11708141	3.36	3.47	0.09	
qCD12-2	6	12	Bin11913-Bin11914	14891363-14927725	3.51	4.38	0.14	
qCD12-3	6	12	Bin12307-Bin12308	26918303-26957012	4.79	3.53	-0.05	Hsu and Tung, 2015; Yang et al., 2019
qCD12-4	4	12	Bin12318-Bin12319	27174700-27205921	3.90	5.82	-0.04	

ADD, Additive effect, a positive value indicates the superiority of japonica TD70.

interval of which *qAGP1* (Liu et al., 2021). *QCL4-2/qCV4-2* and *qCV8-2* are in the same physical regions as *qSFW-4* and *qRD-8*, respectively (Yang et al., 2021). The physical area of *qCSA4-2* is consistent with that of *qCL-4-1*; The physical location of *qCD12-3* coincides with that of *qAG12/qCSA-12-2* (Hsu and Tung, 2015; Yang et al., 2019). *qCSA7* locates on chromosome 7, and its physical location in a region from where many QTLs related to anaerobic germination were found (Ling et al., 2004; Angaji et al., 2010; Septiningsih et al., 2013; Hsu and Tung, 2015). The results of the above report indicate the accuracy of our mapping result.

Pyramiding effects of stable QTLs

In the present study, three kinds of QTLs were defined as stable QTLs, including overlapping QTLs associated with multiple traits; the loci detected in both periods and the loci colocalized with reported QTL loci. There were thus 12 stable loci discovered in this study, and they were associated with 20 QTLs (Table 3). To further clarify the effects of these QTLs, we summarized the phenotypic differences between two alleles at each locus in the RIL population.

Firstly, the RIL population was divided into TD70 type and Kasalath type according to the genotype of each marker site, and

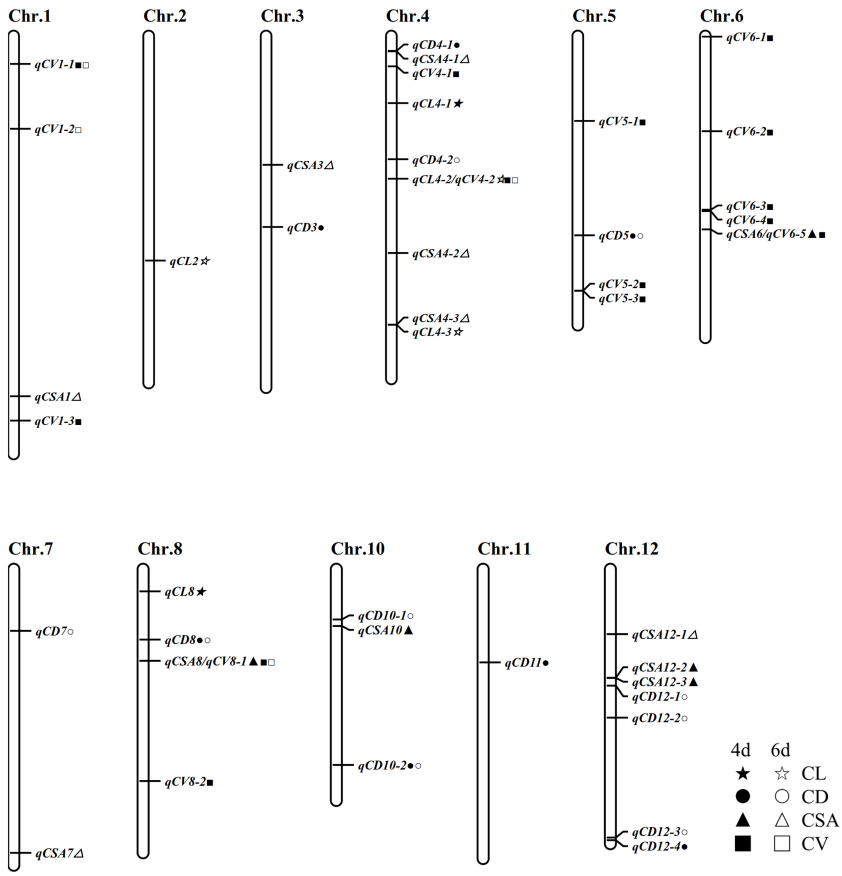

FIGURE 3
Chromosome distribution of these stable QTLs.

TABLE 3 Identified 12 stable QTL loci.

Loc	QTL	Chr.	Marker interval	Physical interval
Loc1	qCV1-1(4d/6d)	1	Bin117-Bin118	2890073-2949395
Loc2	qCV1-2(6d)	1	Bin329-Bin330	9616532-9707372
Loc3	qCL4-2(6d);qCV4-2(6d)	4	Bin3788-Bin3789	14780687-14808655
Loc4	qCSA4-2(6d)	4	Bin4035-Bin4036	22473081-22499182
Loc5	qCD5(4d/6d)	5	Bin5167-Bin5168	20629588-20770108
Loc6	qCSA6(4d);qCV6-5(4d)	6	Bin6167-Bin6168	20022371-20096670
Loc7	qCSA7(6d)	7	Bin7527-Bin7528	28442520-28483618
Loc8	qCD8(4d/6d)	8	Bin7843-Bin7844	7055955-7089043
Loc9	qCSA8(4d);qCV8-1(4d/6d)	8	Bin7941-Bin7942	9196326-9222900
Loc10	qCV8-2(4d)	8	Bin8412-Bin8413	21238647-21272554
Loc11	qCD10-2(4d/6d)	10	Bin10082-Bin10083	19629777-19696813
Loc12	qCD12-3(6d)	12	Bin12307-Bin12308	26918303-26957012

then the corresponding traits were compared between the individuals of the two types. The result showed that these 8 of 12 loci significantly affected coleoptile traits. The average value of the traits in the individuals with excellent alleles was higher than in those without excellent alleles. For instance, *qCL4-2*/*qCV4-2*, the maximum absolute difference in coleoptile length between the two alleles was 0.36 cm, and the volume difference was 2.44 mm^3 which was highly significant. The maximum difference in coleoptile volume of *qCV1-2* between the two alleles was 1.91 mm^3, and the maximum absolute difference of coleoptile length was 0.31 cm, which was significant. This shows that these 8 loci were reliable and responsible for phenotypic variation. The other four loci were associated with CV and CSA. The average phenotypes of individuals with excellent alleles were higher than those of individuals without (Supplementary Table S3).

In order to further confirm the result shown above, the effects of these excellent alleles were evaluated by polymerization of different loci. If the interaction between these 12 stable loci were not considered, the more excellent alleles aggregated in one individual would result in a better phenotypic value of these traits. In this study, most of the lines in the RIL population contain 3-7 favorable alleles, and their corresponding phenotypic value increased along with the aggregation of favorable alleles (Figure 4). In this study, 12 lines containing 7 favorable alleles were obtained. Under hypoxia conditions, the length of coleoptiles grew rapidly, and their surface area and volume were also larger. Hence their AG tolerance was strong (Figure 4; Supplementary Table S4). These results indicate that aggregation of favorable alleles could improve AG tolerance.

Candidate genes associated with AG

For identifying candidate genes associated with AG traits, we further investigated transcriptome response during the process of tolerance to anaerobic germination. As a result, 2,405 DEGs from kasalath under AG treatment were identified and consider as Kas-specific DEGs response to AG. Similarly, 2,620 TD70-specific AG-responsive genes were also identified (Figure 5D). GO and KEGG enrichment were further employed for dissecting the potential molecular mechanism under AG treatment. From GO/KEGG enrichment results, amount of DEGs were found to be invovled in many biological processes such as "response to oxidative stress, GO:0006979", "hormone-medidated signaling pathway, GO:0009755", "detoxification, GO:0098754", "Amino sugar and nucleotide sugar metabolism" (Figure 5). Combined with 12 stable QTLs, 103 expressed genes were located in QTL regions, of which 31 genes such as *OsUsp1*, *OsMADS4*, *PR5*, *OsSPARK4*, *OsSUAR56*, *TOND1* show significant among different groups (Supplementary Table S6).

Discussion

Phenotype identification of rice seed AG tolerance

Rice varieties with strong tolerance to anaerobic germination (AG) are suitable for direct sowing. So far, there are two methods to identify rice AG tolerance. One is according to the survival rate of 10-20 cm under submerged treatment for 21 days, which has been used to identify several QTLs (Angaji et al., 2010). However, this method is time-consuming and laborious. Another is to measure the coleoptile length. The QTL associated with coleoptile length coincided with that detected by using survival rate (Hsu and Tung, 2015). In order to study rice AG tolerance more comprehensively, four traits (CL, CD, CSA, CV) relevant to coleoptile were analyzed in this study.

Firstly, we identified the coleoptile phenotype of two parental materials under anaerobic treatment. The result showed that Kasalath germinated earlier than TD70, and the coleoptile grew rapidly. On the sixth day of treatment, the length, surface area and volume of Kasalath coleoptile were significantly higher than TD70 (but coleoptile diameter), which indicated that Kasalath had stronger AG tolerance than TD70 (Figure 1). Further analysis of the four traits of coleoptile in RIL populations under AG conditions showed that they segregated into various degrees, which showed the characteristics of normal distribution. Therefore, the result indicated it was possible to use Kasalath and TD70 construction population to locate QTL of AG tolerance.

Joint analysis using the high-density genetic map and RNA-Seq

Recently, the next-generation sequencing technology (NGS) has been used for population genotyping, which is improving the accuracy of QTL mapping (Huang et al., 2009; Wang et al., 2011). In this study, we sequenced 186 RILs and detected 1,344,770 high-quality population SNPs with uniform distribution in the whole genome. The recombination breakpoint was determined by checking the position of genotype change. This method transformed the original SNP markers into effective recombination bins, which could be considered an effective genetic marker (Wang et al., 2011). With this method, a high-density genetic map containing 12,328 bin markers was constructed in this study, and the mapping of QTLs was conducted using this map.

In this study, we measured four coleoptile traits, CL, CD, CSA and CV, on the fourth and sixth days of anaerobic treatment. The results showed that the phenotypic variations of CL, CD, CSA and CV were normal distribution in RILs, indicating that they were consistent with the characteristics of quantitative genetics controlled by multiple genes (Figure 2). In this population, 50 QTLs associated with coleoptile traits under the anaerobic were identified, and 12 stable loci, including 20 QTLs, were obtained through further analysis.

Hypoxia under anaerobic conditions changes plant metabolism, thus affecting plant growth. The change in the glycolysis pathway is one of the typical metabolomic responses

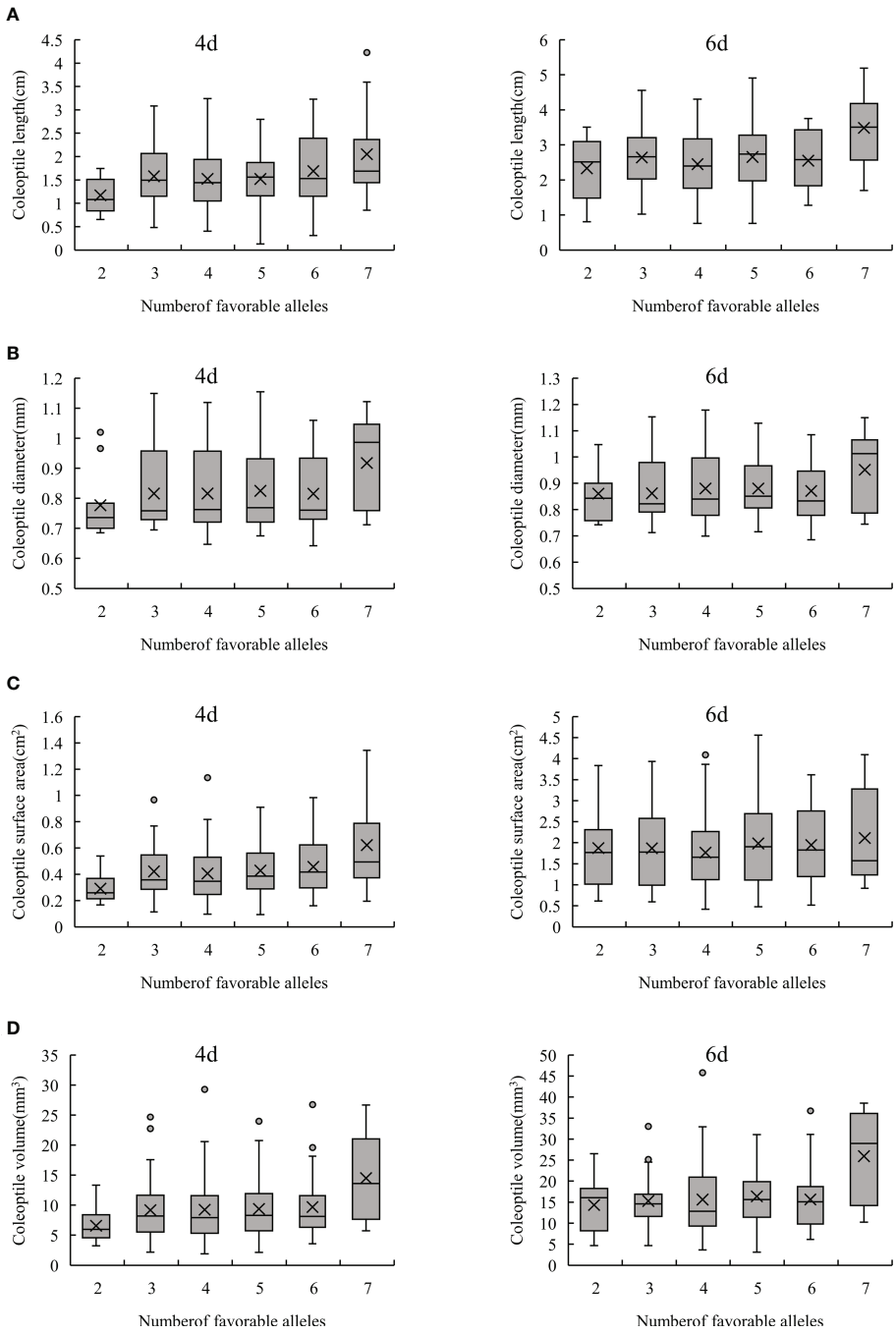

FIGURE 4
Phenotypic analysis of favorable alleles aggregation. **(A–D)** represents CL, CD, CSA and CV, respectively.

to hypoxia. Upregulation of amylase, trehalose-6-phosphate phosphatase, hexokinase and other enzyme activities under hypoxia conditions provided sufficient evidence (Magneschi and Perata, 2009; Kretzschmar et al., 2015; Loreti et al., 2018). When the oxygen concentration is low, carbohydrate metabolism is subsequently inhibited, especially the step of starch decomposition into monosaccharides for glycolysis (Miro and Ismail, 2013). These studies identified complex mechanisms related to coleoptile growth, including carbohydrate metabolism, fermentation, hormone induction,

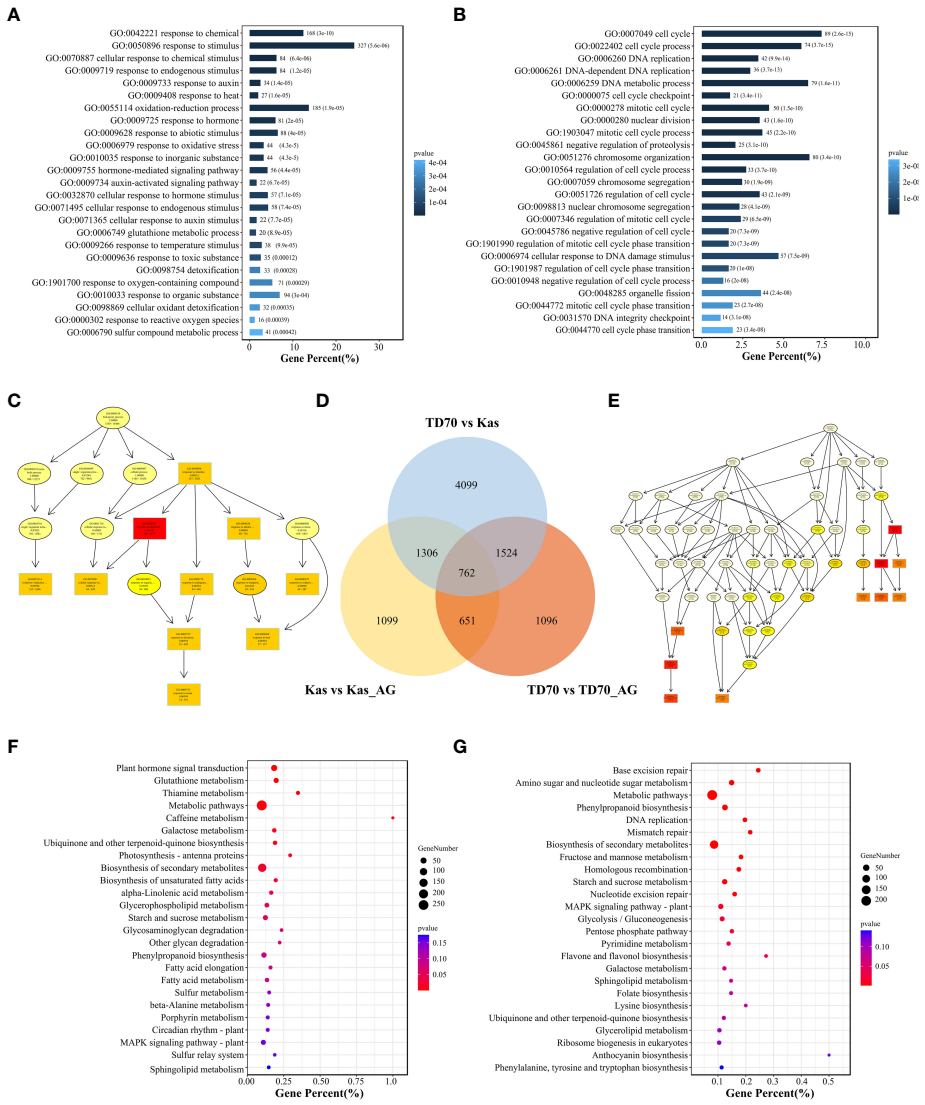

FIGURE 5
Transcriptome analysis of TD70 and Kasalath with/without AG treatment. **(A)** GO enrichment plot of TD70-specific DEGs response to AG treatment. **(B)** GO enrichment plot of Kasalath-specific DEGs response to AG treatment. **(C)** Biological process graphic result of TD70-specific DEGs. **(D)** Venn plot of DEGs among three groups: TD70 vs Kas, Kas vs Kas_AG and TD70 vs TD70_AG. **(C, E)** Biological process graphic result of Kasalath-specific DEGs. **(F)** KEGG enrichment plot of TD70-specific DEGs response to AG treatment. **(G)** KEGG enrichment plot of Kasalath-specific DEGs response to AG treatment.

cell division and expansion. Many transcriptome analyses are conducted to explore the molecular mechanism in regulating rice coleoptile growth under hypoxia and anaerobic conditions. The results showed that starch degradation and fermentation-related genes were up-regulated in anoxic rice seedlings (Narsai et al., 2015; Hsu and Tung, 2017).

Research shows that the elongation of rice coleoptiles is relevant to the hexokinase gene (*HXK6*, LOC_Os01g53930) under anaerobic conditions (Hsu and Tung, 2015). LOC_Os06g03520, a candidate gene encoding DUF domain protein, is highly expressed in the coleoptile under flooded conditions (Zhang et al., 2017). *OsTPP7* gene, encodes a trehalose-6-phosphate phosphatase. It indicates a low sugar utilization rate by increasing the turnover of trehalose-6-phosphate, which can also improve the pool capacity in heterotrophic tissue. Furthermore, it can enhance starch utilization, drive germinating embryo growth, prolong coleoptiles, and enhance anaerobic germination tolerance (Kretzschmar et al., 2015). AG tolerance can be achieved by combining the number of favorable alleles in different varieties.

Improving AG tolerance by pyramiding breeding

Recently, OsGF14h, a key gene determining its strong germination and emergence under hypoxia, was cloned from japonica weedy rice *via* genome-wide associating study and QTL mapping. This gene encodes a "14-3-3 protein", which is the upstream switch of abscisic acid (ABA) signal transduction. By interacting with two transcription factors, *OsHOX3* and *OsVP1*, the gene inhibits the activity of the ABA receptor *OsPYL5* in a hypoxic environment, reduces the sensitivity of ABA, and also activates the biosynthesis of gibberellin (GA), ultimately causing strong germination and emergence of weedy rice seeds. However, in modern genetic improvement, the lost of 4 bases of *OsGF14h* in cultivated *japonica* rice caused the the weakening of its function, so germination and emergence were limited under hypoxia conditions (Sun et al., 2022).

Conclusion

In this study, a high-density genetic map was constructed by whole genome resequencing to identify QTL for CL, CD, CSA and CV of the anaerobically treated coleoptile. A total of 42 loci were identified on 4 and 6 days of treatment. A total of 12 stable loci were identified, of which 6 coincided with previously reported loci. The localization results were further validated by verifying that the pyramiding of 12 QTLs could improve AG tolerance in rice in a population. We performed transcriptome sequencing analysis of three critical stages of germination in parental AG, and combined the mapping results of 12 QTLs to obtain 275 possible candidate genes. These results further elucidated the genetic mechanism of AG tolerance in rice seeds.

Data availability statement

The data presented in the study are deposited in the SRA repository, accession number PRJNA896343.

Author contributions

YZ and YL conceived and designed the study. WL, HD, BP, JC, BH, FH, and YL performed the QTL mapping and RNAseq analysis. WL constructed the NILs, performed phenotypic analysis. WL and YL wrote the manuscript. All authors contributed to the article and approved the submitted version.

Funding

This work was supported by the National Natural Science Foundation of China(31901485), Jiangsu Seed Industry Revitalization Program (JBGS [2021] 001), Jiangsu Science and technology Development Program (BE2022336) and Natural Science Foundation of Anhui Province (2108085QC108).

Conflict of interest

The authors declare that the research was conducted in the absence of any commercial or financial relationships that could be construed as a potential conflict of interest.

Publisher's note

Supplementary material

The Supplementary Material for this article can be found online at: https://www.frontiersin.org/articles/10.3389/fpls.2022.1076600/full#supplementary-material

References

Anders, S., and Huber, W. (2010). Differential expression analysis for sequence count data. *Genome Biol.* 11 (10), R106. doi: 10.1186/gb-2010-11-10-r106

Angaji, S. A. (2008). Mapping QTLs for submergence tolerance during germination in rice. *Afr. J. Biotechnol.* 7 (15), 2551–2558. doi: 10.5897/AJB08.511

Angaji, S. A., Septiningsih, E. M., Mackill, D. J., and Ismail, A. M. (2010). QTLs associated with tolerance of flooding during germination in rice (Oryza sativa l.). *Euphytica* 172 (2), 159–168. doi: 10.1007/s10681-009-0014-5

Baltazar, M. D., Ignacio, J. C. I., Thomson, M. J., Ismail, A. M., Mendioro, M. S., and Septiningsih, E. M. (2014). QTL mapping for tolerance of anaerobic germination from IR64 and the aus landrace nanhi using SNP genotyping. *Euphytica* 197 (2), 251–260. doi: 10.1007/s10681-014-1064-x

Baltazar, M. D., Ignacio, J. C. I., Thomson, M. J., Ismail, A. M., Mendioro, M. S., and Septiningsih, E. M. (2019). QTL mapping for tolerance to anaerobic germination in rice from IR64 and the aus landrace kharsu 80A. *Breed. Sci.* 69 (2), 227–233. doi: 10.1270/jsbbs.18159

Chamara, B. S., Marambe, B., Kumar, V., Ismail, A. M., Septiningsih, E. M., and Chauhan, B. S. (2018). Optimizing sowing and flooding depth for anaerobic germination-tolerant genotypes to enhance crop establishment, early growth, and weed management in dry-seeded rice *(Oryza sativa l.). Front. Plant Sci.* 9. doi: 10.3389/fpls.2018.01654

Chen, W., Chen, H., Zheng, T., Yu, R., Terzaghi, W. B., Li, Z., et al. (2014). Highly efficient genotyping of rice biparental populations by GoldenGate assays

based on parental resequencing. *Theor. Appl. Genet.* 127 (2), 297–307. doi: 10.1007/s00122-013-2218-2

Chen, S., Zhou, Y., Chen, Y., and Gu, J. (2018). Fastp: an ultra-fast all-in-one FASTQ preprocessor. *Bioinformatics* 34 (17), i884–i890. doi: 10.1093/bioinformatics/bty560

Farooq, M., Siddique, K., Rehman, H., Aziz, T., Lee, D. J., and Wahid, A. (2011). Rice direct seeding: Experiences, challenges and opportunities. *Soil Tillage Res.* 111 (2), 87–98. doi: 10.1016/j.still.2010.10.008

Gao, Z. Y., Zhao, S. C., He, W. M., Guo, L. B., Peng, Y. L., Wang, J. J., et al. (2013). Dissecting yield-associated loci in super hybrid rice by resequencing recombinant inbred lines and improving parental genome sequences. *Proc. Natl. Acad. Sci.* 35) 110 (35), 14492–14497. doi: 10.1073/pnas.1306579110

Hsu, S.-K., and Tung, C.-W. (2015). Genetic mapping of anaerobic germination-associated QTLs controlling coleoptile elongation in rice. *Rice* 8 (1), 38. doi: 10.1186/s12284-015-0072-3

Hsu, S.-K., and Tung, C.-W. (2017). RNA-Seq analysis of diverse rice genotypes to identify the genes controlling coleoptile growth during submerged germination. *Front. Plant Sci.* 8. doi: 10.3389/fpls.2017.00762

Huang, X., Feng, Q., Qian, Q., Zhao, Q., Wang, L., Wang, A., et al. (2009). High-throughput genotyping by whole-genome resequencing. *Genome Res.* 19 (6), 1068–1076. doi: 10.1101/gr.089516.108

Ignacio, J. C. I., Zaidem, M., Casal, C., Dixit, S., Kretzschmar, T., Samaniego, J. M., et al. (2021). Genetic mapping by sequencing more precisely detects loci responsible for anaerobic germination tolerance in rice. *Plants* 10 (4), 705. doi: 10.3390/plants10040705

Jiang, L., Liu, S., Hou, M., Tang, J., Chen, L., Zhai, H., et al. (2006). Analysis of QTLs for seed low temperature germinability and anoxia germinability in rice *(Oryza sativa l.)*. *Field Crops Res.* 98 (1), 68–75. doi: 10.1016/j.fcr.2005.12.015

Kretzschmar, T., Pelayo, M. A. F., Trijatmiko, K. R., Gabunada, L. F. M., Alam, R., Jimenez, R., et al. (2015). A trehalose-6-phosphate phosphatase enhances anaerobic germination tolerance in rice. *Nat. Plants* 1 (9), 15124. doi: 10.1038/nplants.2015.124

Kumar, S., Banks, T. W., and Cloutier, S. (2012). SNP discovery through next-generation sequencing and its applications. *Int. J. Plant Genomics* 2012. doi: 10.1155/2012/831460

Liang, W., Hu, F., Qi, W., Zhao, C., Chen, T., Wang, C., et al. (2022). Comprehensive transcriptome analysis of GS3 near-isogenic lines during panicle development in rice (Oryza sativa l.). *Front. Genet.* 13. doi: 10.3389/fgene.2022.857143

Li, H., and Durbin, R. (2009). Fast and accurate short read alignment with burrows-wheeler transform. *Bioinformatics* 25 (14), 1754–1760. doi: 10.1093/bioinformatics/btp324

Li, H., Handsaker, B., Wysoker, A., Fennell, T., Ruan, J., Homer, N., et al. (2009). The sequence Alignment/Map format and SAMtools. *Bioinformatics* 25 (16), 2078–2079. doi: 10.1093/bioinformatics/btp352

Liu, L., Li, X., Liu, S., Min, J., Liu, W., Pan, X., et al. (2021). Identification of QTLs associated with the anaerobic germination potential using a set of oryza nivara introgression lines. *Genes Genomics* 43 (4), 399–406. doi: 10.1007/s13258-021-01063-6

Loreti, E., Valeri, M. C., Novi, G., and Perata, P. (2018). Gene regulation and survival under hypoxia requires starch availability and metabolism. *Plant Physiol.* 176 (2), 1286–1298. doi: 10.1104/pp.17.01002

Magneschi, L., and Perata, P. (2009). Rice germination and seedling growth in the absence of oxygen. *Ann. Bot.* 103 (2), 181–196. doi: 10.1093/aob/mcn121

Mahender, A., Anandan, A., and Pradhan, S. K. (2015). Early seedling vigour, an imperative trait for direct-seeded rice: an overview on physio-morphological parameters and molecular markers. *Planta* 241 (5), 1027–1050. doi: 10.1007/s00425-015-2273-9

McCouch, S. R. (2008). Gene nomenclature system for rice. *Rice* 1 (1), 72–84. doi: 10.1007/s12284-008-9004-9

McKenna, A., Hanna, M., Banks, E., Sivachenko, A., Cibulskis, K., Kernytsky, A., et al. (2010). The genome analysis toolkit: a MapReduce framework for analyzing next-generation DNA sequencing data. *Genome Res.* 20, 1297–1303. doi: 10.1101/gr.107524.110

Meng, L., Li, H., Zhang, L., and Wang, J. (2015). QTL IciMapping: Integrated software for genetic linkage map construction and quantitative trait locus mapping in biparental populations. *Crop J.* 3 (3), 269–283. doi: 10.1016/j.cj.2015.01.001

Miro, B., and Ismail, A. M. (2013). Tolerance of anaerobic conditions caused by flooding during germination and early growth in rice *(Oryza sativa l.)*. *Front. Plant Sci.* 4. doi: 10.3389/fpls.2013.00269

Mondal, S., Khan, M. I. R., Dixit, S., Cruz, P. C. S., Septiningsih, E. M., and Ismail, A. M. (2020). Growth, productivity and grain quality of AG1 and AG2 QTLs introgression lines under flooding in direct-seeded rice system. *Field Crops Res.* 248 (107713). doi: 10.1016/j.fcr.2019.107713

Mondal, S., Khan, M. I. R., Entila, F., Dixit, S., Sta Cruz, P. C., Panna Ali, M., et al. (2020). Responses of AG1 and AG2 QTL introgression lines and seed pre-treatment on growth and physiological processes during anaerobic germination of rice under flooding. *Sci. Rep.* 10 (1), 10214. doi: 10.1038/s41598-020-67240-x

Narsai, R., Edwards, J. M., Roberts, T. H., Whelan, J., Joss, G. H., and Atwell, B. J. (2015). Mechanisms of growth and patterns of gene expression in oxygen-deprived rice coleoptiles. *Plant J.* 82 (1), 25–40. doi: 10.1111/tpj.12786

Nishimura, T., Sasaki, K., Yamaguchi, T., Takahashi, H., Yamagishi, J., and Kato, Y. (2020). Detection and characterization of quantitative trait loci for coleoptile elongation under anaerobic conditions in rice. *Plant Production Sci.* 23 (3), 374–383. doi: 10.1080/1343943X.2020.1740600

Pertea, M., Kim, D., Pertea, G. M., Leek, J. T., and Salzberg, S. L. (2016). Transcript-level expression analysis of RNA-seq experiments with HISAT, StringTie and ballgown. *Nat. Protoc.* 11 (9), 1650–1667. doi: 10.1038/nprot.2016.095

Septiningsih, E. M., Ignacio, J. C. I., Sendon, P. M. D., Sanchez, D. L., Ismail, A. M., and Mackill, D. J. (2013). QTL mapping and confirmation for tolerance of anaerobic conditions during germination derived from the rice landrace ma-zhan red. *Theor. Appl. Genet.* 126 (5), 1357–1366. doi: 10.1007/s00122-013-2057-1

Sun, J., Zhang, G., Cui, Z., Kong, X., Yu, X., Gui, R., et al. (2022). Regain flood adaptation in rice through a 14-3-3 protein OsGF14h. *Nat. Commun.* 13 (1), 5664. doi: 10.1038/s41467-022-33320-x

Trapnell, C., Roberts, A., Goff, L., Pertea, G., Kim, D., Kelley, D. R., et al. (2012). Differential gene and transcript expression analysis of RNA-seq experiments with TopHat and cufflinks. *Nat. Protoc.* 7 (3), 562–578. doi: 10.1038/nprot.2012.016

Wang, L., Wang, A., Huang, X., Zhao, Q., Dong, G., Qian, Q., et al. (2011). Mapping 49 quantitative trait loci at high resolution through sequencing-based genotyping of rice recombinant inbred lines. *Theor. Appl. Genet.* 122 (2), 327–340. doi: 10.1007/s00122-010-1449-8

Wang, X., Zou, B., Shao, Q., Cui, Y., Lu, S., Zhang, Y., et al. (2018). Natural variation reveals that OsSAP16 controls low-temperature germination in rice. *J. Exp. Bot.* 69 (3), 413–421. doi: 10.1093/jxb/erx413

Yang, J., Guo, Z., Luo, L., Gao, Q., Xiao, W., Wang, J., et al. (2021). Identification of QTL and candidate genes involved in early seedling growth in rice *via* high-density genetic mapping and RNA-seq. *Crop J.* 9 (2), 360–371. doi: 10.1016/j.cj.2020.08.010

Yang, J., Sun, K., Li, D., Luo, L., Liu, Y., Huang, M., et al. (2019). Identification of stable QTLs and candidate genes involved in anaerobic germination tolerance in rice *via* high-density genetic mapping and RNA-seq. *BMC Genomics* 20 (1), 355. doi: 10.1186/s12864-019-5741-y

Yu, H., Xie, W., Wang, J., Xing, Y., Xu, C., Li, X., et al. (2011). Gains in QTL detection using an ultra-high density SNP map based on population sequencing relative to traditional RFLP/SSR markers. *PloS One* 6 (3), e17595. doi: 10.1371/journal.pone.0017595

Zhang, M., Lu, Q., Wu, W., Niu, X., Wang, C., Feng, Y., et al. (2017). Association mapping reveals novel genetic loci contributing to flooding tolerance during germination in indica rice. *Front. Plant Sci.* 8 (678). doi: 10.3389/fpls.2017.00678

frontiers | Frontiers in Plant Science

TYPE Original Research
PUBLISHED 24 February 2023
DOI 10.3389/fpls.2023.1080427

OPEN ACCESS

EDITED BY
Weicong Qi,
Jiangsu Academy of Agricultural Sciences (JAAS), China

REVIEWED BY
Kang Wei,
Tea Research Institute, Chinese Academy of Agricultural Sciences, China
Lin Meng,
Tobacco Research Institute, Chinese Academy of Agricultural Sciences, China

*CORRESPONDENCE
Xinghui Li
lxh@njau.edu.cn

†These authors share first authorship

SPECIALTY SECTION
This article was submitted to Plant Bioinformatics, a section of the journal Frontiers in Plant Science

RECEIVED 26 October 2022
ACCEPTED 23 January 2023
PUBLISHED 24 February 2023

CITATION
Hu S, Hu Y, Mei H, Li J, Xuan W, Jeyaraj A, Zhao Z, Zhao Y, Han R, Chen X and Li X (2023) Genome-wide analysis of long non-coding RNAs (lncRNAs) in tea plants (*Camellia sinensis*) lateral roots in response to nitrogen application. *Front. Plant Sci.* 14:1080427. doi: 10.3389/fpls.2023.1080427

Genome-wide analysis of long non-coding RNAs (lncRNAs) in tea plants (*Camellia sinensis*) lateral roots in response to nitrogen application

Shunkai Hu[1†], Yimeng Hu[1†], Huiling Mei[2†], Jianjie Li[2], Wei Xuan[2], Anburaj Jeyaraj[1], Zhen Zhao[1], Yuxin Zhao[1], Rui Han[1], Xuan Chen[1] and Xinghui Li[1*]

[1]International Institute of Tea Industry Innovation for "One Belt, One Road", Nanjing Agricultural University, Nanjing, Jiangsu, China, [2]College of Resources and Environmental Sciences, Nanjing Agricultural University, Nanjing, Jiangsu, China

Tea (*Camellia sinensis*) is one of the significant cash crops in China. As a leaf crop, nitrogen supply can not only increase the number of new shoots and leaves but also improve the tenderness of the former. However, a conundrum remains in science, which is the molecular mechanism of nitrogen use efficiency, especially long non-coding RNA (lncRNA). In this study, a total of 16,452 lncRNAs were identified through high-throughput sequencing analysis of lateral roots under nitrogen stress and control conditions, of which 9,451 were differentially expressed lncRNAs (DE-lncRNAs). To figure out the potential function of nitrogen-responsive lncRNAs, co-expression clustering was employed between lncRNAs and coding genes. KEGG enrichment analysis revealed nitrogen-responsive lncRNAs may involve in many biological processes such as plant hormone signal transduction, nitrogen metabolism and protein processing in endoplasmic reticulum. The expression abundance of 12 DE-lncRNAs were further verified by RT-PCR, and their expression trends were consistent with the results of RNA-seq. This study expands the research on lncRNAs in tea plants, provides a novel perspective for the potential regulation of lncRNAs on nitrogen stress, and valuable resources for further improving the nitrogen use efficiency of tea plants.

KEYWORDS

long non-coding RNAs, nitrogen stress, RNA-seq, *Camellia sinensis*, lateral roots

Introduction

As a crucial element in plant growth, nitrogen is an essential component of biological compounds such as nucleic acid, protein, chlorophyll, and plant hormones. Nitrogen also regulates plants' absorption and utilization of other elements, such as phosphorus and potassium (Novoa and Loomis, 1981; Xu et al., 2012). In agricultural production, a large

amount of synthetic nitrogen fertilizer has been used in crop fields to promote the yield of crops (Good and Beatty, 2011; Zhang et al., 2012). Nitrogen fertilizer abuse increases agricultural costs and becomes one of the chief culprits of environmental pollution. (Han et al., 2015). Therefore, reducing the application of nitrogen fertilizer and improving the nitrogen use efficiency of crops are momentous to agriculture development. To this end, more and more researchers have carried out studies on crops with low nitrogen tolerance, providing new solutions for the underlying molecular mechanisms of nitrogen regulation and the improvement of nitrogen use efficiency (Kant et al., 2011; Krapp, 2015; Hu et al., 2020). Plant lateral roots (LRs) can absorb nitrogen in the form of organic (amino acids and peptides) and inorganic (nitrate and ammonium nitrogen), and different nitrogen sources can regulate the growth of LRs (Gruffman et al., 2014). The number and location of lateral roots determine the spatial configuration of roots, which means that their formation and development will directly affect plant growth (Duan et al., 2013). Nitrate use was reported to be positively associated with the development of LRs (Lynch, 2013). In other words, reducing the application of nitrate fertilizer can promote the growth of LRs, thereby improving the plant's nutrient uptake capacity and nitrogen use efficiency (Duan et al., 2013).

Long non-coding RNA (lncRNA) is an RNA transcript longer than 200 nucleotides with no or limited protein-coding capacity (Kung et al., 2013; Kopp and Mendell, 2018). According to their genomic location, they are usually divided into *i* (intron lncRNAs), *o* (overlapping lncRNAs), *u* (intergenic lncRNAs), and *x* (antisense lncRNA) types (Roberts et al., 2011). Much evidence, including epigenetics, transcriptional and post-transcriptional regulation in the form of RNA, can prove that lncRNAs have regulatory functions in gene expression (Sunkar et al., 2007; Caley et al., 2010). Through next-generation sequencing technology and bioinformatics methods, many lncRNAs have been found in *Arabidopsis*, wheat, maize, rice, and other model plants. It is significant in flowering regulation, photomorphogenesis, stress response, and other growth pathways. (Wang et al., 2014; Chekanova, 2015; Wang and Chekanova, 2017; Zhao et al., 2018; Liang et al., 2022). For example, through genome-wide analysis of *Arabidopsis* thaliana full-length cDNA database, 76 ncRNAs were identified, including 5 small interfering RNAs (siRNA) precursors and 14 natural antisense transcripts of protein-coding genes. A set of 127 RNA sequencing samples including total RNAseq datasets and PacBio fl-cDNA datasets in maize was used for identifying 1,077 differentially multiple abiotic stress-responsive TE-lncRNAs, and 39 are hubs in co-expression networks, including a small number that are evolutionary conserved (Lv et al., 2019). In the study of low nitrogen stress in barley, 498 lncRNAs were identified, of which 487 were newly discovered, and 56 lncRNAs responsive to low nitrogen stress were identified (Chen et al., 2020). 637 lncRNAs responsive to nitrogen and 664 lncRNAs responsive to drought were identified in maize seedlings (Zhang et al., 2014; Lv et al., 2016). However, studies of lncRNAs in many non-model plants are relatively limited, and correspondingly, studies on the genome-wide identification and analysis of tea plants lncRNAs are relatively few. Besides, there have been no published studies on the molecular mechanism of lncRNA response to nitrogen in tea plants.

In China, tea (*Camellia sinensis*) is one of the vital cash crops and stands out among traditional industries. As a leaf crop, tea plants consume a lot of nitrogen nutrition and have high requirements for soil nitrogen (Venkatesan et al., 2004; Zhu et al., 2014). The results showed that nitrogen nutrition could promote the germination and elongation of tea shoots, increase the number, weight and area of new shoots and leaves, and advance the tenderness of new shoots (Ruan et al., 2019). Nitrogen can benefit tea plants' vegetative growth and thwart their reproductive growth, thus increasing yield (Ruan et al., 2019). Within a reasonable dosage range, applying nitrogen in tea gardens can enrich the types of tea aroma substances, improve the freshness of tea leaves, and increase the content of amino acids, tea polyphenols, catechins and chlorophyll, especially free amino acids. (Ruan et al., 2010; Lin et al., 2021).Therefore, improving nitrogen absorption and utilization efficiency has been a focal point of tea nutrition research in recent years. Screening and breeding tea varieties with high nitrogen utilization is paramount to the tea industry (Hu et al., 2020). Most previous studies focused on revealing the coding genes regulated by nitrogen (Xia et al., 2017; Wei et al., 2018). Thanks to the release of the tea genome, we used High-Throughput Sequencing technology to analyze the lncRNAs expression profile of tea roots under high and low nitrogen conditions, analyzed these lncRNAs regulatory coding genes, and identified the function of lncRNAs involved in nitrogen metabolism. In conclusion, our research results provide many valuable references for clarifying the response mechanism of lncRNAs to nitrogen in LRs of tea plants and expand a new path for improving the nitrogen use efficiency of tea plants.

Materials and methods

Plant materials and nitrogen treatments

Purebred tea seeds (*Camellia sinensis* cv. Fuding dabai) were germinated in perlite and then cultured in nutrient solution (0.75mM $(NH_4)_2SO_4$, 0.25 mM $Ca(NO3)_2•4(H_2O)_3$, 0.05 mM KH_2PO_4, 0.35 mM K_2SO_4, 0.395 mM $CaCl_2$, 0.21 mM $MgSO_4$, 35.0 μM NaFeEDTA, 46.1 μM H_3BO_3, 2.0 μM $MnSO_4$, 0.3 μM $CuSO_4$, 2.0 μM $ZnSO_4$ and 0.5 μM Na_2MoSO_4). Nitrogen was divided into three concentrations: 0.25 mM (labeled as low nitrogen, LN), 1 mM (labelled as control, CK), and 2.5 mM (labelled as high nitrogen, HN). The control experiment (1 mM) was supplemented with 0.75 mM ammonium and 0.25 mM nitrate using $(NH4)_2SO_4$ and $Ca\ (NO3)_2•4(H_2O)$, respectively, which was the best combination of N concentration for seedlings growth. The growth conditions of seedlings in the light culture box were as follows: 28/25°C (day/night), 75% relative humidity, 16/8 h (light/darkness) photoperiod, and 300 $\mu mol^{-2}\ s^{-1}$ light intensity. The liquid culture medium was changed every 5 days. The lateral roots of the seedlings were sampled after 10 weeks of seedling growth. The control and nitrogen treatments were repeated three times (CK-1, CK-2, CK-3; LN-1, LN-2, LN-3, HN-1, HN-2, HN-3). The samples were immediately soaked in liquid nitrogen and stored in a refrigerator of -80°C for RNA-seq analysis and qRT-PCR verification.

RNA isolation, library construction and RNA sequencing

The total RNA of LH, CK, HN was isolated with the plant RNA extraction kit with DNase (TIANDZ, Inc., Beijing, China) according to the manufacturer's protocol. RNA was purified and concentrated using NanoDrop2000 Spectrophotometer (Thermo Fisher Scientific, USA), 1.2% agarose gel electrophoresis, and Agilent 2100 Bioanalyzer (Agilent Technologies, Inc., Santa Clara, CA, USA). High-quality RNA samples are used for library construction, and then the total RNA-seq library is constructed and sequenced using the IlluminaHiSeq platform. All sequencing data were deposited in the National Center for Biotechnology Information (NCBI) Sequence Read Archive (accession number PRJNA595712).

Transcriptome assembly

The SolexaQA++ v3.1 program was applied to execute quality trimming using the Q30 value (Cox et al., 2010). After removing rRNA, low-quality reads, aptamer sequences, and contaminating reads, the remaining clean reads were aligned with the reference genome of *C. sinensis* var. *sinensis* by Hierarchical Indexing of Spliced Transcript Alignment (HISat) software (Pertea et al., 2016; Xia et al., 2017). Use the gffCompare program to annotate the assembled transcript and the unknown transcript and then filter out possible lncRNAs by pfam databases (Kong et al., 2007; Han et al., 2016a; El-Gebali et al., 2018).

Identification of LncRNAs

In this study, a strict calculation method was used to determine the lncRNA of tea plants (Iyer et al., 2015; Xiao et al., 2015). The primary screening of transcripts should meet the following conditions: with a class code of "i", "x", "u", "o", and "e", a length ≥ 200 bp, and fragments per kilobase of transcript per million mapped reads (FPKM) value ≥ 0.1(Kelley and Rinn, 2012; Luo et al., 2022). Subsequently, transcripts were compared with uniref90 and Pfam protein databases using the CPC2 program to evaluate their protein-coding potential (Kang et al., 2017). Transcripts that meet these conditions are eventually considered as candidates for lncRNAs for further analysis: Non-coding transcripts larger than 200 bp; FPKM > 1; a CPC score < -1.

Differential expression analysis

The expression level of lncRNAs was quantitatively detected by FPKM value by StringTie software. DESeq2 software package (1.10.1) was used to analyze the differential expression between nitrogen concentration and control treatments. The P value of the result is adjusted by the methods of Benjamini and Hochberg to control the false discovery rate. The lncRNA with the adjustment value $P < 0.01$ and the absolute value $|\log2(\text{FPKM ratio})| \geq 1$ by DESeq is considered to be differentially expressed (Wan et al., 2020).

KEGG pathway enrichment analysis

To elucidate the potential functions of differentially expressed lncRNAs (DE-lncRNAs), co-expression analysis between Nitrogen-responsive lncRNAs and coding genes was employed for generating clusters with different expression patterns. Coding genes of clusters were used for the KEGG pathway enrichment by clusterProfiler (Yu et al., 2012). In the KEGG enrichment analysis, a false discovery rate ≤ 0.05 was used as a criterion to identify significantly enriched pathways (Altschul et al., 1990).

Validation and quantification of LncRNAs

Total RNA was extracted from the nine samples (CK-1, CK-2, CK-3; LN-1, LN-2, LN-3, HN-1, HN-2, HN-3) using Trizol reagent (Invitrogen). To validate the lncRNAs, Real-time PCR was performed Bio-Rad Real-time thermal cycler CFX96 with SYBR Premix ExTaq™ Kit (Takara Co. Ltd., Japan). The *glyceraldehyde-3-phosphate dehydrogenase* (GAPDH) and *β-actin* were used as controls. The $2^{-\Delta\Delta Ct}$ method was used to determine the relative expression levels (Livak and Schmittgen, 2001). Three biological replicates per sample. All qRT-PCR primers were designed with NCBI primer-BLAST (https://www.ncbi.nlm.nih.gov/tools/primer-blast/). Differences between groups were analyzed by one-way analysis of variance and Duncan's test, and $P < 0.05$ was considered to be significantly different between treatment groups.

Result

Phenotypic response of *C.sinensis* lateral roots to nitrogen treatments

In different nitrogen treatments, the growth of the underground part of the seedlings changed significantly in the tenth week (Figure 1A). The main results were as follows: with the increase in nitrogen concentration, the number and the length of lateral roots decreased significantly (Figure 1B, C). This showed that low nitrogen conditions could promote the growth of lateral roots of seedlings. On the contrary, it was inhibited under high nitrogen conditions.

Genome–wide prediction of LncRNAs candidates in *C. sinensis*

To investigate the lncRNAs in tea plants under nitrogen treatments, transcriptome sequencing analysis of three biological repeats of HN, CK and HN was carried out using the Illumina HiSeq2500 platform. Each sample had an average base of 9GB, and the lowest value of Q30 was 92.83% (Table S1). All clean reads were compared with the tea plants reference genome. A total of 86814 transcripts were identified, and the results showed that 38% (33515) of transcripts matched exactly and entirely with the intron chain and 30% (26279) were annotated as multi-exon with at least one junction match, while 7% (6049) transcripts were annotated as

10.3389/fpls.2023.1080427

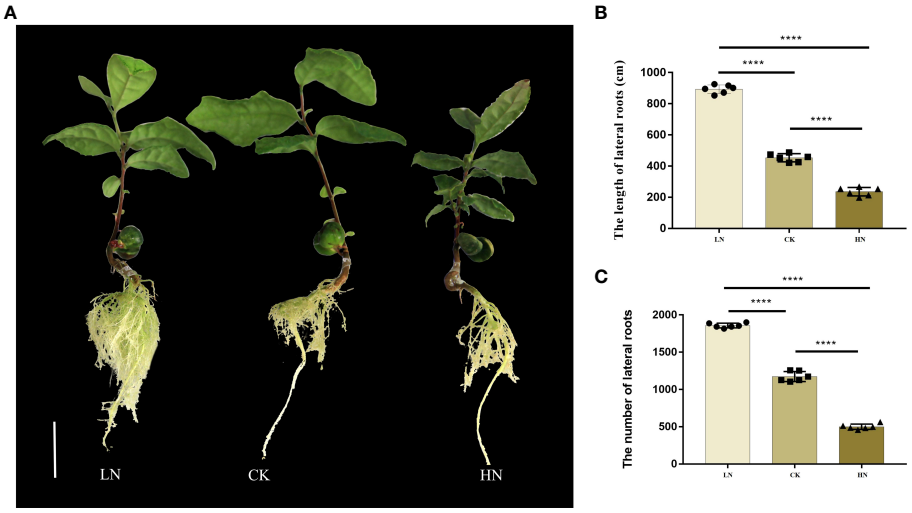

FIGURE 1
(A) Lateral roots (LRS) phenotype of low-nitrogen (LN), normal-nitrogen (CK) and high-nitrogen (HN). **(B)** The length of LRs in hydroponics culture. **(C)** The number of LRs in hydroponics culture. Scale bars = 2 cm. Values are mean ± S.D. *P ≤ 0.5, **P ≤ 0.01, ***P ≤ 0.001, ****P ≤ 0.0001, (Student's t-test).

containment of reference (reverse containment) (Figure 2A). Total RNA-seq technology could recover transcripts located in gene intergenic or intronic regions. After filtering the data through CPC2 and Pfam, a total of 16,452 candidate transcripts were obtained.

DE-lncRNAs under nitrogen treatments

To identify nitrogen-responsive lncRNAs in LRs of tea plants, the expression of lncRNAs was compared between the LN, CK and HN treatments. Based on the standardized FPKM value, 9,451 DE-

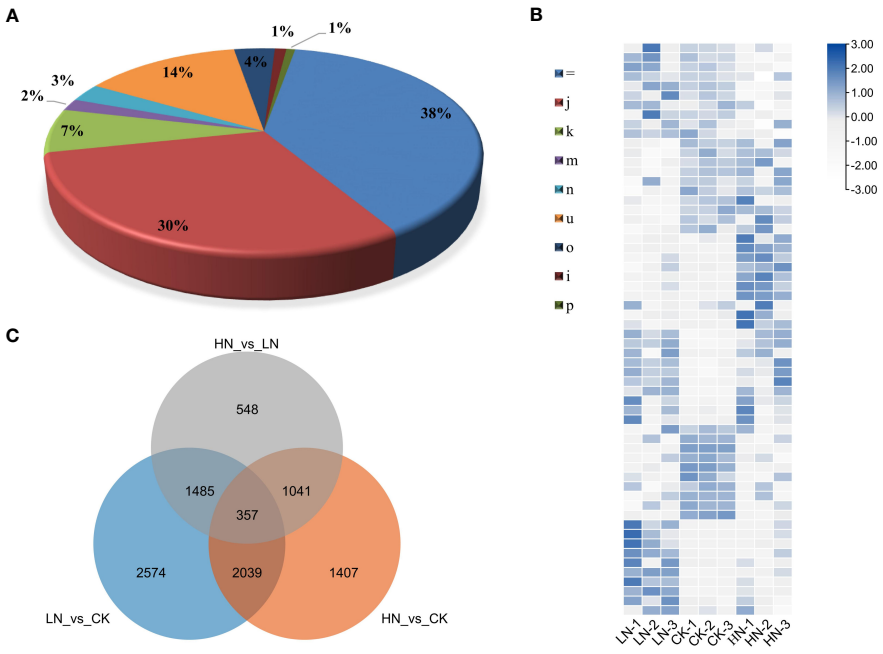

FIGURE 2
(A) Compare the category code generated by CuffCompare with the tea plants genome, and then calculate the percentage. "=": complete, exact match of intron chain; "j": multi-exon with at least one junction match; "k": containment of reference (reverse containment); "m": retained intron (s), all introns matched or retained; "n": retained introns (s), not all introns matched/covered.; "u": none of the above (unknown, intergene); "o": other same strand overlap with reference exons; "i": fully contained within a reference intron; "p": possible polymerase run-on (no actual overlap). (b~c) Analysis of transcripts in LRs (lateral roots) of tea plant under three nitrogen treatments, LN, CK and HN, with three replicates for each. **(B)** Cluster heat map of DE-lncRNAs (differentially expressed lncRNAs) in three treatments. **(C)** Venn diagram of common DE-lncRNAs.

lncRNAs were revealed in LN, CK, and HN treatments (Figure 2B). Moreover, 357 DE-lncRNAs overlapped in those treatments (Figure 2C). Furthermore, in the comparison of LN and CK treatments, there were 6,455 DE-lncRNAs, of which 3,805 were up-regulated and 2,650 were down-regulated (Figure 3A); in the comparison of HN and CK treatments, there were 4,844 DE-lncRNAs, of which 2,879 were up-regulated and 1,965 were down-regulated (Figure 3B); and 3,431 DE-lncRNAs were identified in the comparison of HN and LN, of which 1,780 were up-regulated and 1,651 were down-regulated (Figure 3C).

Enrichment analysis of nitrogen-responsive coding genes

The nitrogen-responsive coding genes were submitted into KEGG pathway enrichment, and the top 20 enriched pathways were shown in (Figure 3D-F). In the LN vs. CK comparisons, 2,161 coding genes were annotated in 128 KEGG pathways. Among them, the most enriched pathway was metabolic pathways (447), followed by biosynthesis of secondary metabolites (248), photosynthesis-antenna proteins (61) and starch and sucrose metabolism (35) (Figure 3D, Table S2). In addition, 1,514 coding genes were enriched in 116 KEGG pathways between HN vs. CK comparisons. Coding genes identified in metabolic pathways (327) were the most abundant, followed by biosynthesis of secondary metabolites (197), protein processing in endoplasmic reticulum (42) and amino sugar and nucleotide sugar metabolism (28) (Figure 3E, Table S3). Among the LN vs. HN comparisons, 1,140 coding genes were verified in 113 KEGG pathways. Moreover, the most significant pathway was metabolic pathways (242), followed by Biosynthesis of secondary metabolites (151), plant-pathogen interaction (36) and glutathione metabolism (20) (Figure 3F, Table S4).

Co-expression clustering analysis of nitrogen-responsive LncRNAs and coding genes in lateral roots development

In different nitrogen treatments, the lncRNAs with the same trend of coding genes expression were selected and annotated by KEGG (Figure 4). In LN treatment, compared with CK and HN treatments, the up-regulated and down-regulated DE-lncRNAs were clustered into cluster1 and cluster2, respectively, and then these up-regulated and down-regulated DE-lncRNAs were annotated to cluster 1 and cluster 2 KEGG pathways, severally. The down-regulated DE-lncRNAs compared with CK and HN was shown in cluster1. The cluster 1 KEGG pathway identified that 720 DE-lncRNAs were annotated in 104 KEGG pathways. The pathway with the most aggregation was ribosome (65), followed by protein processing in endoplasmic reticulum (26) and RNA transport (20) (Table S5); the up-regulated DE-lncRNAs were shown in cluster 2, and KEGG pathway (cluster 2) identified that 1311 DE-lncRNAs were annotated in 122 KEGG pathways, such as metabolic pathways (275), biosynthesis of secondary metabolites (145) and plant-pathogen interaction (32) (Table S6). In CK treatment, compared with LN and HN treatments, the up-regulated and down-regulated DE-lncRNAs were clustered into cluster 3 and 4, respectively, and then these up and down-regulated DE-lncRNAs were annotated to cluster 3 and cluster 4 KEGG pathways, severally. The down-regulated DE-lncRNAs were shown in cluster 3. The KEGG pathway (cluster 3) identified that 971 DE-lncRNAs were annotated in 121 KEGG pathways, such as metabolic pathways (202), biosynthesis of secondary metabolites (114) and carbon metabolism (38) (Table S7); the up-regulated DE-lncRNAs were shown in cluster 4, and KEGG pathway (cluster 4) identified that 815 DE-lncRNAs were annotated in 116 KEGG pathways, such as biosynthesis of secondary metabolites (99), biosynthesis of amino acids (25), plant hormone signal transduction (24) (Table S8). In HN

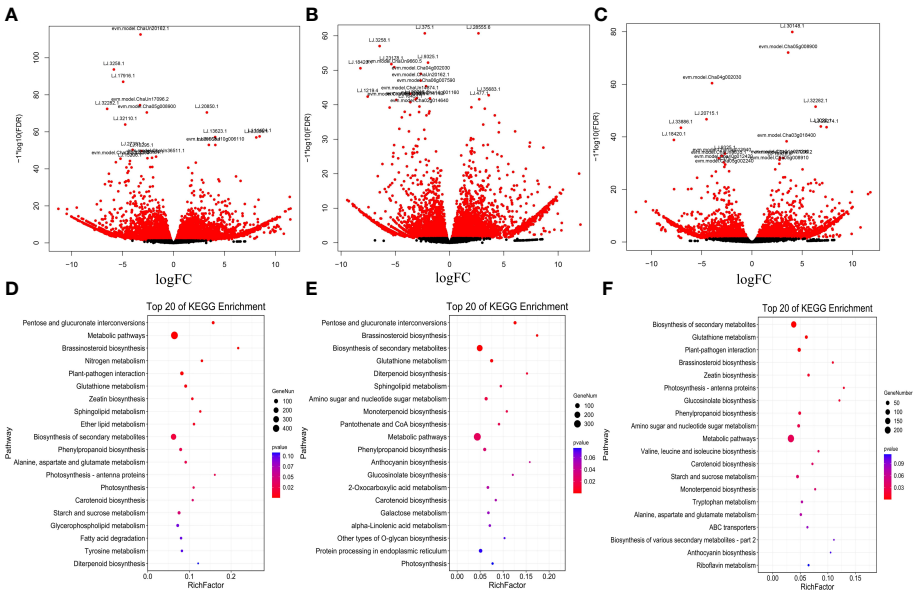

FIGURE 3
(A-C) Volcano map of DE-coding genes in LRs of tea plants under different nitrogen conditions. **(A)** LN vs CK. **(B)** HN vs CK. **(C)** HN vs LN. (d~f) KEGG pathways analysis. Top 20 pathways for the predicted coding genes of DE-coding genes. **(D)** LN vs CK. **(E)** HN vs CK. **(F)** HN vs LN.

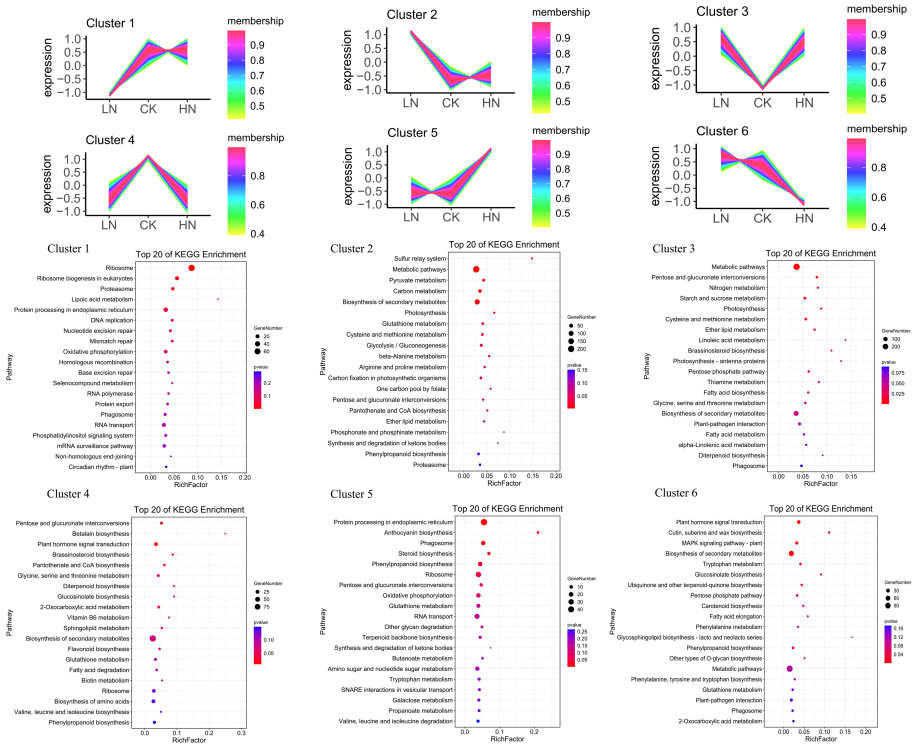

FIGURE 4
Nitrogen-responsive lncRNAs enrichment plot from KEGG pathway analysis for different coexpressed clusters.

treatment, compared with LN and CK treatments, the up-regulated and down-regulated DE-lncRNAs were clustered into cluster 5 and cluster 6, respectively, and then these up and down-regulated DE-lncRNAs were annotated to cluster 5 and cluster 6 KEGG pathways, severally. The up-regulated DE-lncRNAs were shown in cluster 5, and KEGG pathway (cluster 5) identified that 993 DE-lncRNAs were annotated in 114 KEGG pathways, such as protein processing in endoplasmic reticulum (45), ribosome (30) and RNA transport (25) (Table S9); the down-regulated DE-lncRNAs were shown in cluster 6, and KEGG pathway (cluster 6) identified that 556 DE-lncRNAs were annotated in 102 KEGG pathways, such as metabolic pathways (114), biosynthesis of secondary metabolites (74), and plant hormone signal transduction (25) (Table S10). The clustering results showed that nitrogen treatment could affect the expression of lncRNAs, associated with the nitrate transporter and controlling the growth of tea plants LRs. In addition, nitrogen treatment regulated the hormone signals of tea plants LRs, associated with auxin synthesis and auxin signals genes.

Validation of lncRNAs expression using qRT-PCR

To determine the reliability of RNA-seq transcriptome results, 12 DE-lncRNAs were selected for qRT-PCR verification. The result showed that the expression level of these DE-lncRNAs was in line with that of transcripts estimated from sequence data, suggesting the repeatability and accuracy of RNA-seq data (Figure 5). The identified DE-lncRNAs sequences were recorded in Table S11.

Discussion

Improving nitrogen use efficiency is of great significance in agricultural production and environmental protection.To promote nitrogen use efficiency and adapt to barren land, improving the resistance mechanism to low nitrogen or nitrogen deficiency is advisable. (Han et al., 2015). Previous studies have shown that the early nodulin gene was found in rice, which was identified by transcriptional analysis under low nitrogen stress and was related to increased nitrogen use efficiency (Bi et al., 2009). At the same time, barley is becoming a model crop for similar research because of its adaptability to barren land (Chen et al., 2018). Due to the particularity system of tea plants, nitrogen use efficiency is critical in recent research (Zhang et al., 2020). It includes nitrogen absorption efficiency, utilization efficiency and transport efficiency.

During past years, research on improving the nitrogen use efficiency of tea plants has been the top priority. In addition, nitrogen can also regulate the synthesis and transport of auxin, gibberellin, and other plant hormones through nitrogen signals, thus affecting the growth and development of plant LRs (Sun et al., 2017). In previous studies, nitrogen deficiency induced the expression of high-affinity nitrate transporters NRT1, NRT2.4 and NRT2.5 in *Arabidopsis thaliana* roots (Lezhneva et al., 2014). Moreover, NRT1 and NRT2 can transport not only NO_3^- but also auxin. So, under a low nitrogen environment, NRT1 and NRT2 are highly expressed and regulate the formation of LRs by inducing auxin accumulation and transport (Krouk et al., 2010). In this study, low nitrogen could also promote the growth of tea plants' LRs. However, accumulating evidence shows that lncRNAs are momentous in various plants'

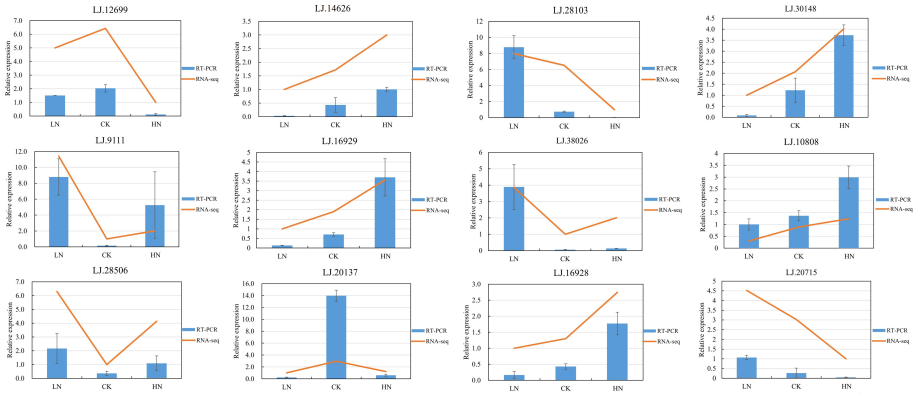

FIGURE 5
Comparison of expression profiles of selected lncRNAs as determined by Real Time-PCR.

biological processes, but their characteristics, expression patterns and potential functions in response to nitrogen in tea plants have not been reported. In this study, we identified the lncRNAs of tea plants according to the latest genome of tea plants, and confirmed the lncRNAs related to nitrogen response and LRs development. This study has gained discoveries of the regulatory function of lncRNAs on nitrogen in tea plants and provides a resource for further study of the molecular mechanism of nitrogen response.

In previous studies, 7,245 lncRNA were identified in RNA-seq analysis under nitrogen-deficiency treatment in maize, of which 673 were corresponding to low nitrogen deficiency (Lv et al., 2016). 918 differentially expressed lncRNAs was found in the study of nitrogen deficiency in rice (Shin et al., 2018). In the research on nitrogen deficiency in *Populus*, 126 differentially expressed lncRNAs were identified in N-starved (Chen et al., 2016). In this study, 16452 candidates lncRNAs revealed in LN and CK and HN treatments were selected from 9 LRs samples of tea plants. The results showed that 9451 lncRNAs with different functions were differentially expressed under nitrogen treatments. Therefore, these lncRNAs are involved in the response of tea plants to nitrogen stress, and the results can provide candidate genes for the study of nitrogen utilization in tea plants.

In this study, the results of KEGG pathway analysis showed that the DE-lncRNAs of the three treatments existed in multiple KEGG pathways, and the top three were "metabolic pathways", "biosynthesis of secondary metabolites", and "glutathione metabolism" (Figure 4). The results not only revealed that these pathways were related to nitrogen stress response, but also indicated that some components were involved in nitrogen stress response processes simultaneously. In addition, each group has specific DEGS and enrichment pathways, which means that there are different response mechanisms under different N stress. In addition, the up-regulated and down-regulated DE-lncRNAs of each group compared with the other groups were analyzed by KEGG pathway. The results demonstrated response mechanism varied with different N stresses.

In LN treatment, compared to the other two groups (CK, HN), up-regulated DE-lncRNAs were mainly annotated in "metabolic pathways" and "biosynthesis of secondary metabolites". This indicated that nitrogen deficiency could promote the expression of coding genes in these two pathways. Considering the involvement of stress response: It has been reported that for many plant species, an increase in plant secondary metabolism caused by biotic or abiotic stress is part of the stress response (Sathiyabama et al., 2016). In line with this, previous studies manifested that the production of terpenoids and cannabinoids in plants is stimulated under the stress of nitrogen and phosphorus nutrient deficiency. The results showed a negative correlation between secondary metabolism and plant stress. That is, the concentration of secondary metabolites decreased with the increase of nitrogen supply, and the optimal nitrogen condition and high nitrogen condition in plants have nothing to do with secondary metabolism (Shiponi and Bernstein, 2021a; Shiponi and Bernstein, 2021b). The result is supported by many other plant studies. Furthermore, the carbon nutrient balance hypothesis points out that the production of nitrogen-rich primary metabolites is limited under low nitrogen conditions. Plant metabolism and energy consumption changed from the production of nitrogen-containing metabolites to the production of nitrogen-free metabolites, promoting the accumulation of secondary metabolites (Massad et al., 2012; Albornoz, 2016). This result is also consistent with the results of DE-lncRNAs analysis in our study.

Low-affinity transport system (LATS) and high-affinity transport system (HATS) are two NO3 uptake systems in plants They are mediated by nitrate transporter 1 (NRT1) and nitrate transporter 2 (NRT2), respectively (Tong et al., 2005; Wang et al., 2012). The results showed that with the decrease in nitrogen use efficiency, high-affinity nitrate transporters (NRT2) activity replaced low-affinity nitrate transporters (NRT1) activity, so NRT2 may be the key target to improve nitrogen use efficiency, especially under the condition of low nitrogen condition (Huang et al., 1999). Moreover, studies have shown that under low nitrogen conditions, NRT2 not only transports NO_3, but also participates in the transport of auxin, thus promoting plant root growth (Krouk et al., 2010). In this study, the up-regulated DE-lncRNA in low nitrogen treatment were clustered in the "nitrogen metabolism" pathway, including LJ.29731 and LJ.29732 corresponding to coding genes NRT2.3 and NRT2.4. This indicates that lncRNAs cis-regulate the expression of corresponding NRT2 coding genes under low nitrogen treatment and participate in the growth of lateral roots of tea plants (Figure 1, Figure 4, cluster2).

Plant hormones can regulate plant growth through different signal pathways and contribute to cell elongation, seed germination, flower formation, leaf morphogenesis, fruit development and so on. The same is true for resistance to biotic and abiotic stress (Qaadt, 2020). In this

study, the normal nitrogen (CK), compared with the other two groups (LN and HN), up-regulated DE-lncRNAs were clustered in the "plant hormone signal transduction pathway". Auxin is a crucial signal of plant growth and the higher the concentration, the more inhibited it is. At the same time, the precise distribution of auxin in plants determines the top-down organ morphology of plants (De Smet et al., 2010). AUX/IAA family transcription factors and auxin response factor (ARF) are two main transcription factors in the signal transduction pathway. In the auxin signal transduction pathway, ARF binds to the auxin response element in the auxin response gene promoter to activate the expression of the auxin response genes (Figueiredo and Strader, 2022). At low auxin concentration, AUX/IAA binds to ARF to form a heterodimer, which inhibits the transcription of ARFs, and then the expression of ARF-regulated auxin-responsive genes was inhibited. When auxin rises to a certain concentration, auxin binds to its receptor SCF-TIRl (Han et al., 2020). By interacting with AUX/IAA, AUX/IAA proteins were ubiquitinated and ARFs were released. Thus, auxin response genes are expressed and plants undergo a series of growth responses (Figueiredo and Strader, 2022). In this study, compared with CK and HN treatments, 14 DE-lncRNAs coding to ARF genes were up-regulated in LN treatment, which indicated that lncRNAs regulated the expression of ARF genes in low nitrogen treatment, thus increasing the transcriptional activity of ARFs (Table S12). Jasmonic acid (JA) and their derivatives methyl jasmonate (MeJA) play an essential role in plant morphological, physiological and biochemical processes in response to drought, cold and salt stress (Ali and Baek, 2020; Zhang et al., 2021). Different nitrogen concentrations are also involved in the metabolism and synthesis of jasmonic acid. In previous studies, JAR1 (jasmonate resistant 1)-activated JA and ethylene signaling pathways could inhibit roots growth in Boron deficiency, and low nitrogen could inhibit the content of jasmonic acid (Li et al., 2020; Huang et al., 2021). In this study, three DE-lncRNAs (LJ.13289, LJ.13289, LJ.33982) corresponding to jasmonate resistant 4 were up-regulated in LN treatment. SAURs were discovered and named because of their response to the rapid induction of auxin. The expression of SAURs was also regulated by many internal and external factors (Wiesel et al., 2015). In addition to being induced by auxin, a small part of the expression of SAURs showed auxin inhibition or non-response (Ren and Gray, 2015). Many studies have shown that SAURs can also be induced by other plant hormones, such as brassinolide, gibberellin and cytokinin, while abscisic acid and jasmonic acid inhibit it (Bai et al., 2012). In addition, light, temperature, moisture and other environmental factors also affect the expression of SAURs (Ouyang et al., 2015). In this study, 7 DE-lncRNAs coding to SAUR genes were down-regulated in HN treatment compared with LN and HN treatments (LJ.1615, LJ.12746, LJ.11860, LJ.5020, LJ.12505, LJ.23544, LJ.36187). To sum up, DE-lncRNAs are involved in the synthesis and metabolism of hormones in tea plants under different nitrogen conditions.

Glutathione is a reductant that regulates signal molecules and scavenges free radicals and ROS in the redox system of plant cells. Glutathione participates in the metabolic process of all eukaryotes to improve plants' tolerance to abiotic stresses such as salt, temperature, drought, heavy metals and autotoxicity (Hodges et al., 1996; Koprivova et al., 2010; Niu et al., 2017). Glutathione adjusts continuously in plants, giving play to different metabolic processes and extremely significant antioxidant advantages, which can effectively scavenge free radicals in organisms, which cannot be reflected by glutamine, lycopene and other oxidants (Nakamura et al., 2019). Glutathione can oxidize GSH by reactive oxygen species and regulate the reduction of GSSG by glutathione reductase, thus regulating the balance between GSH (reduced) and GSSG (oxidized) (Bashandy et al., 2010). Exogenous GSSG could not induce root growth under normal conditions but could promote root development under auxin treatment (Tyburski and Tretyn, 2010). Therefore, the interaction between auxin and GSSG can regulate plant root development. It is reported that plants can inhibit the growth of lateral roots by regulating the reduction ratio of GSH/GSSG in the presence of auxin (Wei et al., 2013). Glutathione S-transferase (GSTs) converts GSH to GSSG, while glutathione reductase (GR) induces the reduction of GSSG to GSH, so glutathione S-transferase plays an essential role in plant growth and development (Jiang et al., 2010). In this study, cluster analysis of different treatments showed that a total of 82 De-lncRNAs coding glutathione S-transferase genes were distributed in six clusters, indicating that in nitrogen treatment, lncRNAs could regulate the coding glutathione S-transferase genes and participated in the growth and development of tea plants (Figure 4, Table S13).

Conclusion

Through RNA-seq and bioinformatics, this study identified 16,452 LncRNAs in the whole genome of tea plants, among which 9,451 DE-lncRNAs were differentially expressed under nitrogen stress. The KEGG pathway further analyzed the biological and regulation function of these lncRNAs. To sum up, this study expands the cognition of lncRNAs in tea plants and explores a path for further study of tea plants response to nitrogen and improvement of nitrogen use efficiency of woody plants.

Data availability statement

The data presented in the study are deposited in the National Center for Biotechnology Information (NCBI) Sequence Read Archive repository, accession number PRJNA595712.

Author contributions

SH: Project administration. Methodology, Formal analysis, Investigation, Data curation, Writing-original draft. XL: Methodology, Formal analysis, Investigation, Data curation, Writing-original draft. XC: Formal analysis, Investigation. WX: Formal analysis, Data curation, Writing-original draft. YH: Investigation, Visualization. JL: Investigation. HM: Conceptualization. ZZ: Formal analysis. YZ: Investigation. AJ: Visualization. RH: Formal analysis. All authors contributed to the article and approved the submitted version.

Acknowledgments

This study was financially supported by the Science and technology projects of Nanjing (202210013), Expert Workstation of

Yunnan Province (202105AF150045), National Natural Science Foundation of China (32172628), Top-notch Academic Programs Project of Jiangsu Higher Education Institutions (2022) and China Agriculture Research System of MOF and MARA (CARS-19). We thank Dr. Yuehua Ma (Central laboratory of College of Horticulture, Nanjing Agricultural University) for using Bio-Rad Real-time thermal cycler CFX96.

Conflict of interest

The authors declare that the research was conducted in the absence of any commercial or financial relationships that could be construed as a potential conflict of interest.

Publisher's note

Supplementary material

The Supplementary Material for this article can be found online at: https://www.frontiersin.org/articles/10.3389/fpls.2023.1080427/full#supplementary-material

References

Albornoz, F. (2016). Crop responses to nitrogen overfertilization: a review. *Sci. Hortic.* 205, 79–83. doi: 10.1016/j.scienta.2016.04.026

Ali, M., and Baek, K.-H. (2020). Jasmonic acid signaling pathway in response to abiotic stresses in plants. *Int. J. Mol. Sci.* 21, 621. doi: 10.3390/ijms21020621

Altschul, S. F., Gish, W., Miller, W., Myers, E. W., and Lipman, D. J. (1990). Basic local alignment search tool. *J. Mol. Biol.* 215, 403–410. doi: 10.1016/S0022-2836(05)80360-2

Bai, M. Y., Shang, J. X., Oh, E., Fan, M., Bai, Y., Zentella, R., et al. (2012). Brassinosteroid, gibberellin and phytochrome impinge on a common transcription module in arabidopsis. *Nat. Cell Biol.* 14 (8), 810–817. doi: 10.1038/ncb2546

Bashandy, T., Guilleminot, J., Vernoux, T., Caparros-Ruiz, D., Ljung, K., Meyer, Y., et al. (2010). Interplay between the NADP-linked thioredoxin and glutathione systems in arabidopsis auxin signaling. *Plant Cell.* 22 (2), 376–391. doi: 10.1105/tpc.109.071225

Bi, Y. M., Kant, S., Clark, J., Gidda, S., Ming, F., Xu, J., et al. (2009). Increased nitrogen-use efficiency in transgenic rice plants over-expressing a nitrogen-responsive early nodulin gene identified from rice expression profiling. *Plant Cell Environ.* 32, 1749–1760. doi: 10.1111/j.1365-3040.2009.02032.x

Caley, D., Pink, R., Trujillano, D., and Carter, D. (2010). Long noncoding RNAs, chromatin, and development. *ScientificWorldJournal* 10, 90–102. doi: 10.1100/tsw.2010.7

Chekanova, J. A. (2015). Long non-coding RNAs and their functions in plants. *Curr. Opin. Plant Biol.* 27, 207–216. doi: 10.1016/j.pbi.2015.08.003

Chen, Z., Jiang, Q., Jiang, P., Zhang, W., Huang, J., Liu, C., et al. (2020). Novel low-nitrogen stress-responsive long non-coding RNAs (lncRNA) in barley landrace B968 (Liuzhutouzidamai) at seedling stage. *BMC Plant Biol.* 20 (1), 142. doi: 10.1186/s12870-020-02350-2

Chen, Z., Li, Y., Liu, C., Wang, Y., He, T., Guo, G., et al. (2018). Reference gene selection for quantitative RT-PCR normalisation in barley under low-nitrogen stress, based on RNAseq data. *J. Cereal Sci.* 82, 213–215. doi: 10.1016/j.jcs.2018.06.014

Chen, M., Wang, C., Bao, H., Chen, H., and Wang, Y. (2016). Genome-wide identification and characterization of novel lncRNAs in populus under nitrogen deficiency. *Mol. Genet. Genom.* 291, 1663–1680. doi: 10.1007/s00438-016-1210-3

Cox, M. P., Peterson, D. A., and Biggs, P. J. (2010). SolexaQA: At-a-glance quality assessment of illumina second-generation sequencing data. *BMC Bioinf.* 11 (1), 485. doi: 10.1186/1471-2105-11-485

De Smet, I., Lau, S., Mayer, U., and Jürgens, G. (2010). Embryogenesis-the humble beginnings of plant life. *Plant J.* 61 (6), 959–970. doi: 10.1111/j.1365-313X.2010.04143.x

Duan, L. N., Dietrich, D., Ng, C. H., Chan, P. M. Y., Bhalerao, R., Bennett, M. J., et al. (2013). Endodermal ABA signaling promotes lateral root quiescence during salt stress in arabidopsis seedlings. *Plant Cell.* 25 (1), 324–341. doi: 10.1105/tpc.112.107227

El-Gebali, S., Mistry, J., Bateman, A., Eddy, S. R., Luciani, A., Potter, S. C., et al. (2018). The pfam protein families database in 2019. *Nucleic Acids Res.* 47, D427–D432. doi: 10.1093/nar/gky995

Figueiredo, M. R. A., and Strader, L. C. (2022). Intrinsic and extrinsic regulators of Aux/IAA protein degradation dynamics. *Trends Biochem. Sci.* 47 (10), 865–874. doi: 10.1016/j.tibs.2022.06.004

Good, A. G., and Beatty, P. H. (2011). Fertilizing nature: a tragedy of excess in the commons. *PloS Bio l.* 9, e1001124. doi: 10.1371/journal.pbio.1001124

Gruffman, L., Jamtgard, S., and Nasholm, T. (2014). Plant nitrogen status and cooccurrence of organic and inorganic nitrogen sources influence root uptake by scots pine seedlings. *Tree Physiol.* 34 (2), 205–213. doi: 10.1093/treephys/tpt121

Han, M., Okamoto, M., Beatty, P. H., Rothstein, S. J., and Good, A. G. (2015). The genetics of nitrogen use efficiency in crop plants. *Annu. Rev. Genet.* 49, 1–9. doi: 10.1146/annurev-genet-112414-055037

Han, H., Rakusová, H., Verstraeten, I., Zhang, Y., and Friml, J. (2020). SCF$^{TIR1/AFB}$ auxin signaling for bending termination during shoot gravitropism. *Plant Physiol.* 183 (1), 37–40. doi: 10.1104/pp.20.00212

Han, Z. X., Rana, M. M., Liu, G. F., Gao, M. J., Li, D. X., Wu, F. G., et al. (2016a). Green tea flavour determinants and their changes over manufacturing processes. *Food Chem.* 212, 739–748. doi: 10.1016/j.foodchem.2016.06.049

Hodges, D. M., Andrews, C. J., Johnson, D. A., and Hamilton, R. I. (1996). Antioxidant compound responses to chilling stress in differentially sensitive inbred maize lines. *Physiol. Plant* 98, 685–692. doi: 10.1111/j.1399-3054.1996.tb06672.x

Huang, N. C., Liu, K. H., Lo, H. J., and Tsay, Y. F. (1999). Cloning and functional characterization of an arabidopsis nitrate transporter gene that encodes a constitutive component of low-affinity uptake. *Plant Cell.* 11 (8), 1381–1392. doi: 10.1105/tpc.11.8.1381

Huang, Y., Wang, S., Shi, L., and Xu, F. (2021). JASMONATE RESISTANT 1 negatively regulates root growth under boron deficiency in arabidopsis. *J. Exp. Bot.* 72 (8), 3108–3121. doi: 10.1093/jxb/erab041

Huang, N. C., Liu, K. H., Lo, H. J., and Tsay, Y. F. (1999). Cloning and functional characterization of an Arabidopsis nitrate transporter gene that encodes a constitutive component of low-affinity uptake. *Plant Cell* 11 (8), 1381–1392.

Hu, S., Zhang, M., Yang, Y., Xuan, W., Zou, Z., Arkorful, E., et al. (2020). A novel insight into nitrogen and auxin signaling in lateral root formation in tea plant [Camellia sinensis (L.) o. kuntze]. *BMC Plant Biol.* 20 (1), 232. doi: 10.1186/s12870-020-02448-7

Iyer, M. K., Niknafs, Y. S., Malik, R., Singhal, U., Sahu, A., Hosono, Y., et al. (2015). The landscape of long noncoding RNAs in the human transcriptome. *Nat. Genet.* 47 (3), 199–208. doi: 10.1038/ng.3192

Jiang, H. W., Liu, M. J., Chen, I. C., Huang, C. H., Chao, L. Y., and Hsieh, H. L. (2010). A glutathione s-transferase regulated by light and hormones participates in the modulation of arabidopsis seedling development. *Plant Physiol.* 154 (4), 1646–1658. doi: 10.1104/pp.110.159152

Kang, Y., Yang, D., Kong, L., Hou, M., Meng, Y., Wei, L., et al. (2017). CPC2: a fast and accurate coding potential calculator based on sequence intrinsic features. *Nucleic Acids Res.* 45, W12–W16. doi: 10.1093/nar/gkx428

Kant, S., Bi, Y., and Rothstein, S. J. (2011). Understanding plant response to nitrogen limitation for the improvement of crop nitrogen use efficiency. *J. Exp. Bot.* 62 (4), 1499–1509. doi: 10.1093/jxb/erq297

Kelley, D., and Rinn, J. (2012). Transposable elements reveal a stem cell-specific class of long noncoding RNAs. *Genom. Biol.* 13, R107. doi: 10.1186/gb-2012-13-11-r107

Kong, L., Zhang, Y., Ye, Z., Liu, X., Zhao, S., Wei, L., et al. (2007). CPC: Assess the protein-coding potential of transcripts using sequence features and support vector machine. *Nucleic Acids Res.* 35 (suppl2), W345–9.

Kopp, F., and Mendell, J. T. (2018). Functional classification and experimental dissection of long noncoding RNAs. *Cell* 172, 393–407. doi: 10.1016/j.cell.2018.01.011

Koprivova, A., Mugford, S. T., and Kopriva, S. (2010). Arabidopsis root growth dependence on glutathione is linked to auxin transport. *Plant Cell* 29, 1157–1167. doi: 10.1007/s00299-010-0902-0

Krapp, A. (2015). Plant nitrogen assimilation and its regulation: a complex puzzle with missing pieces. *Curr. Opin. Plant Biol.* 25, 115–122. doi: 10.1016/j.pbi.2015.05.010

Krouk, G., Lacombe, B., Bielach, A., Perrine-Walker, F., Malinska, K., Mounier, E., et al. (2010). Nitrate-regulated auxin transport by NRT1.1 defines a mechanism for nutrient sensing in plants. *Dev. Cell* 18 (6), 927–937. doi: 10.1016/j.devcel

Kung, J. T. Y., Colognori, D., and Lee, J. T. (2013). Long noncoding RNAs: past, present, and future. *Genetics* 193 (3), 651–669. doi: 10.1534/genetics.112.146704

Lezhneva, L., Kiba, T., Feria-Bourrellier, A. B., Lafouge, F., Boutet-Mercey, S., Zoufan, P., et al. (2014). The arabidopsis nitrate transporter NRT2.5 plays a role in nitrate acquisition and remobilization in nitrogen-starved plants. *Plant J.* 80 (2), 230–241. doi: 10.1111/tpj.12626

Liang, W., Hu, F., Qi, W., Zhao, C., Chen, T., Wang, C., et al. (2022). Comprehensive transcriptome analysis of GS3 near-isogenic lines during panicle development in rice (Oryza sativa l.). *Front. Genet.* 13. doi: 10.3389/fgene.2022.857143

Li, S., Hamani, A. K. M., Si, Z., Liang, Y., Gao, Y., and Duan, A. (2020). Leaf gas exchange of tomato depends on abscisic acid and jasmonic acid in response to neighboring plants under different soil nitrogen regimes. *Plants (Basel).* 9 (12), 1674. doi: 10.3390/plants9121674

Lin, Z. H., Chen, C. S., Zhong, Q. S., Ruan, Q. C., Chen, Z. H., You, X. M., et al. (2021). The GC-TOF/MS-based metabolomic analysis reveals altered metabolic profiles in nitrogen-deficient leaves and roots of tea plants (Camellia sinensis). *BMC Plant Biol.* 21 (1), 506. doi: 10.1186/s12870-021-03285-y

Livak, K. J., and Schmittgen, T. D. (2001). Analysis of relative gene expression data using real-time quantitative PCR and the 2(T)(–delta delta c) method. *Methods* 25 (4), 402–408. doi: 10.1006/meth.2001.1262

Luo, C., He, B., Shi, P., Xi, J., Gui, H., Pang, B., et al. (2022). Transcriptome dynamics uncovers long non-coding RNAs response to salinity stress in chenopodium quinoa. *Front. Plant Sci.* 13. doi: 10.3389/fpls.2022.988845

Lv, Y., Hu, F., Zhou, Y., Wu, F., and Gaut, B. S. (2019). Maize transposable elements contribute to long non-coding RNAs that are regulatory hubs for abiotic stress response. *BMC Genomics* 20(1), 864. doi: 10.1186/s12864-019-6245-5

Lv, Y., Liang, Z., Ge, M., Qi, W., Zhang, T., Lin, F., et al. (2016). Genome-wide identification and functional prediction of nitrogen-responsive intergenic and intronic long non-coding RNAs in maize (Zea mays l.). *BMC Genomics* 17, 350. doi: 10.1186/s12864-016-2650-1

Lynch, J. P. (2013). Steep, cheap and deep: an ideotype to optimize water and n acquisition by maize root systems. *Ann. Bot-London.* 112 (2), 347–357. doi: 10.1093/aob/mcs293

Massad, T. J., Dyer, L. A., and Vega, C. G. (2012). Costs of defense and a test of the carbon-nutrient balance and growth-differentiation balance hypotheses for two co-occurring classes of plant defense. *PloS One* 7, e47554. doi: 10.1371/journal.pone.0047554

Nakamura, S. I., Wongkaew, A., Nakai, Y., Rai, H., and Ohkama-Ohtsu, N. (2019). Foliar-applied glutathione activates zinc transport from roots to shoots in oilseed rape. *Plant Sci.*, 424–434. doi: 10.1016/j.plantsci.2018.10.018

Niu, X., Song, L., Xiao, Y., and Ge, W. (2017). Drought-tolerant plant growth-promoting rhizobacteria associated with foxtail millet in a semi-arid agroecosytem and their potential in alleviating drought stress. *Front. Microbiol.* 8 (1), 2580. doi: 10.3389/fmicb.2017.02580

Novoa, R., and Loomis, R. S. (1981). Nitrogen and plant production. *Plant Soil.* 58 (1-3), 177–204. doi: 10.1007/BF02180053

Ouyang, F., Mao, J. F., Wang, J., Zhang, S., and Li, Y. (2015). Transcriptome analysis reveals that red and blue light regulate growth and phytohormone metabolism in Norway spruce [Picea abies (L.) karst]. *PloS One* 10 (8), e0127896. doi: 10.1371/journal.pone.0127896

Pertea, M., Kim, D., Pertea, G. M., Leek, J. T., and Salzberg, S. L. (2016). Transcript-level expression analysis of RNA-seq experiments with HISAT, StringTie and ballgown. *Nat. Protoc.* 11, 1650–1667. doi: 10.1038/nprot.2016.095

Qaadt, R. (2020). Phytohormone signaling mechanisms and genetic methods for their modulation and detection. *Curr. Opin. Plant Biol.* 57, 31–40. doi: 10.1016/j.pbi.2020.05.011

Ren, H., and Gray, W. M. (2015). SAUR proteins as effectors of hormonal and environmental signals in plant growth. *Mol. Plant* 8 (8), 1153–1164. doi: 10.1016/j.molp.2015.05.003

Roberts, A., Pimentel, H., Trapnell, C., and Pachter, L. (2011). Identification of novel transcripts in annotated genomes using RNA-seq. *Bioinformatics* 27, 2325–2329. doi: 10.1093/bioinformatics/btr355

Ruan, J., Haerdter, R., and Gerendás, J. (2010). Impact of nitrogen supply on carbon/nitrogen allocation: a case study on amino acids and catechins in green tea [Camellia sinensis (L.) o. kuntze] plants. *Plant Biol.* 12, 724–734. doi: 10.1111/j.1438-8677.2009.00288.x

Ruan, L., Wei, K., Wang, L. Y., Cheng, H., Wu, L., and Li, H. (2019). Characteristics of free amino acids (the quality chemical components of tea) under spatial heterogeneity of different nitrogen forms in tea (Camellia sinensis) plants. *Molecules* 24, 415. doi: 10.3390/molecules24030415

Sathiyabama, M., Bernstein, N., and Anusuya, S. (2016). Chitosan elicitation for increased curcumin production and stimulation of defence response in turmeric (Curcuma longa l.). *Ind. Crops Prod.* 89, 87–94. doi: 10.1016/j.indcrop.2016.05.007

Shin, S. Y., Jeong, J. S., Lim, J. Y., Kim, T., Park, J. H., Kim, J. K., et al. (2018). Transcriptomic analyses of rice (Oryza sativa) genes and non-coding RNAs under nitrogen starvation using multiple omics technologies. *BMC Genom.* 19, 532. doi: 10.1186/s12864-018-4897-1

Shiponi, S., and Bernstein, N. (2021a). Response of medical cannabis (Cannabis sativa l.) genotypes to p supply under long photoperiod: functional phenotyping and the ionome. *Ind. Crops Prod.* 161, 113154. doi: 10.1016/j.indcrop.2020.113154

Shiponi, S., and Bernstein, N. (2021b). The highs and lows of p supply in medical cannabis: effects on cannabinoids, the ionome, and morpho-physiology. *Front. Plant Sci.* 12, 657323. doi: 10.3389/fpls.2021.657323

Sunkar, R., Chinnusamy, V., Zhu, J., and Zhu, J. K. (2007). Small RNAs as big players in plant abiotic stress responses and nutrient deprivation. *Trends Plant Sci.* 12 (7), 301–309. doi: 10.1016/j.tplants.2007.05.001

Sun, C. H., Yu, J. Q., and Hu, D. G. (2017). Nitrate: a crucial signal during lateral roots development. *Front. Plant Sci.* 8. doi: 10.3389/fpls.2017.00485

Tong, Y., Zhou, J. J., Li, Z., and Miller, A. J. (2005). A two-component high-affinity nitrate uptake system in barley. *Plant J.* 41 (3), 442–450. doi: 10.1111/j.1365-313X.2004.02310.x

Tyburski, J., and Tretyn, A. (2010). Glutathione and glutathione disulfide affect adventitious root formation and growth in tomato seedling cuttings. *Acta Physiol. Plant* 32 (2), 411–417. doi: 10.1007/s11738-009-0418-9

Venkatesan, S., Murugesan, S., Ganapathy, M. N., and Verma, D. P. (2004). Long–term impact of nitrogen and potassium fertilizers on yield, soil nutrients and biochemical parameters of tea. *J. Sci. Food Agr.* 84, 1939–1944. doi: 10.1002/jsfa.1897

Wang, H. V., and Chekanova, J. A. (2017). Long noncoding RNAs in plants. *Adv. Exp. Med. Biol.* 1008, 133–154. doi: 10.1007/978-981-10-5203-3_5

Wang, Y., Fan, X., Lin, F., He, G., Terzaghi, W., Zhu, D., et al. (2014). Arabidopsis noncoding RNA mediates control of photomorphogenesis by red light. *Proc. Natl. Acad. Sci. U S A.* 111 (28), 10359–10364. doi: 10.1073/pnas.1409457111

Wang, Y. Y., Hsu, P. K., and Tsay, Y. F. (2012). Uptake, allocation and signaling of nitrate. *Trends Plant Sci.* 17 (8), 458–467. doi: 10.1016/j.tplants.2012.04.006

Wan, S., Zhang, Y., Duan, M., Huang, L., Wang, W., Xu, Q., et al. (2020). Integrated analysis of long non-coding RNAs (lncRNAs) and mRNAs reveals the regulatory role of lncRNAs associated with salt resistance in camellia sinensis. *Front. Plant Sci.* 11, 218. doi: 10.3389/fpls.2020.00218

Wei, K., Wang, L. Y., Cheng, H., Zhang, C. C., Ma, C. L., Zhang, L. Q., et al. (2013). Identification of genes involved in indole-3-butyric acid-induced adventitious root formation in nodal cuttings of camellia sinensis (L.) by suppression subtractive hybridization. *Gene* 514 (2), 91–98. doi: 10.1016/j.gene.2012.11.008

Wei, C. L., Yang, H., Wang, S. B., Zhao, J., Liu, C., Gao, L. P., et al. (2018). Draft genome sequence of camellia sinensis var. sinensis provides insights into the evolution of the tea genome and tea quality. *Proc. Natl. Acad. Sci. U. S. A.* 115, E4151–E4158. doi: 10.1073/pnas.1719622115

Wiesel, L., Davis, J. L., Milne, L., et al. (2015). A transcriptional reference map of defence hormone responses in potato[J]. *Sci. Rep.* 5, 15229. doi: 10.1038/srep15229

Xiao, H. M., Yuan, Z. T., Guo, D. H., Hou, B. F., Yin, C. L., Zhang, W. Q., et al. (2015). Genome-wide identification of long noncoding RNA genes and their potential association with fecundity and virulence in rice brown planthopper, nilaparvata lugens. *BMC Genomics* 16 (1), 749. doi: 10.1186/s12864-015-1953-y

Xia, E. H., Zhang, H. B., Sheng, J., Li, K., Zhang, Q. J., Kim, C., et al. (2017). The tea tree genome provides insights into tea flavor and independent evolution of caffeine biosynthesis. *Mol. Plant* 10, 866–877. doi: 10.1016/j.molp.2017.04.002

Xu, G., Fan, X., and Miller, A. J. (2012). Plant nitrogen assimilation and use efficiency. *Annu. Rev. Plant Biol.* 63, 153–182. doi: 10.1146/annurev-arplant-042811-105532

Yu, G., Wang, L. G., Han, Y., and He, Q.-Y. (2012). clusterProfiler: an r package for comparing biological themes among gene clusters. *OMICS: A J. Integr. Biol.* 16, 284–287. doi: 10.1089/omi.2011.0118

Zhang, W., Han, Z., Guo, Q., Liu, Y., Zheng, Y., Wu, F., et al. (2014). Identification of maize long non-coding RNAs responsive to drought stress. *PloS One* 9, e98958. doi: 10.1371/journal.pone.0098958

Zhang, Q., He, K., and Huo, H. (2012). Cleaning china's air. *Nature* 484, 161–162. doi: 10.1038/484161a

Zhang, X., Liu, H., Pilon-Smits, E., Huang, W., Wang, P., Wang, M., et al. (2020). Transcriptome-wide analysis of nitrogen-regulated genes in tea plant (*Camellia sinensis* l. o. kuntze) and characterization of amino acid transporter *CsCAT9.1*. *Plants (Basel).* 9 (9), 1218. doi: 10.3390/plants9091218

Zhang, S., Zhu, L., Shen, C., Ji, Z., Zhang, H., Zhang, T., et al. (2021). Natural allelic variation in a modulator of auxin homeostasis improves grain yield and nitrogen use efficiency in rice. *Plant Cell.* 33 (3), 566–580. doi: 10.1093/plcell/koaa037

Zhao, X., Li, J., Lian, B., Gu, H., Li, Y., and Qi, Y. (2018). Global identification of arabidopsis lncRNAs reveals the regulation of MAF4 by a natural antisense RNA. *Nat. Commun.* 9 (1), 5056. doi: 10.1038/s41467-018-07500-7

Zhu, T., Zhang, J., Meng, T., Zhang, Y., Yang, J., Müller, C., et al. (2014). Tea plantation destroys soil retention of NO3– and increases N2O emissions in subtropical China. *Soil Biol. Biochem.* 73, 106–114. doi: 10.1016/j.soilbio.2014.02.016

Frontiers in Plant Science

Cultivates the science of plant biology and its applications

The most cited plant science journal, which advances our understanding of plant biology for sustainable food security, functional ecosystems and human health.

Discover the latest Research Topics

See more →

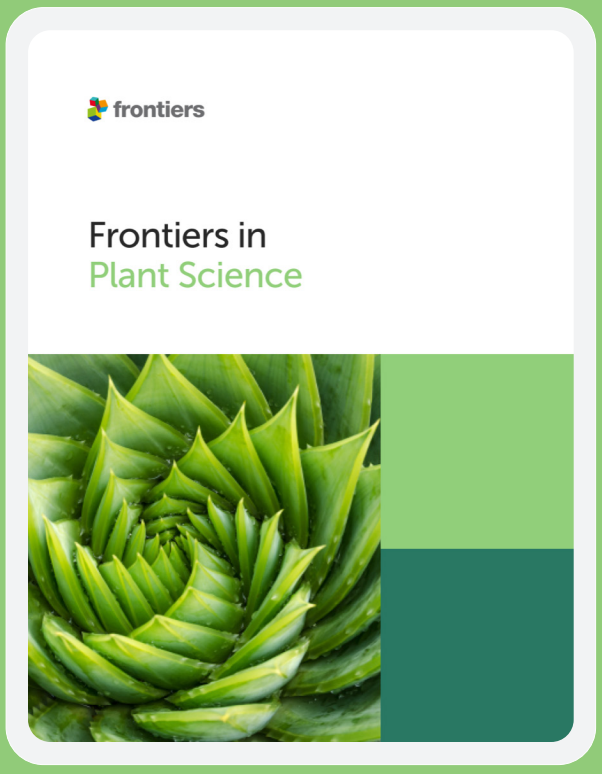

Frontiers

Avenue du Tribunal-Fédéral 34
1005 Lausanne, Switzerland
frontiersin.org

Contact us

+41 (0)21 510 17 00
frontiersin.org/about/contact